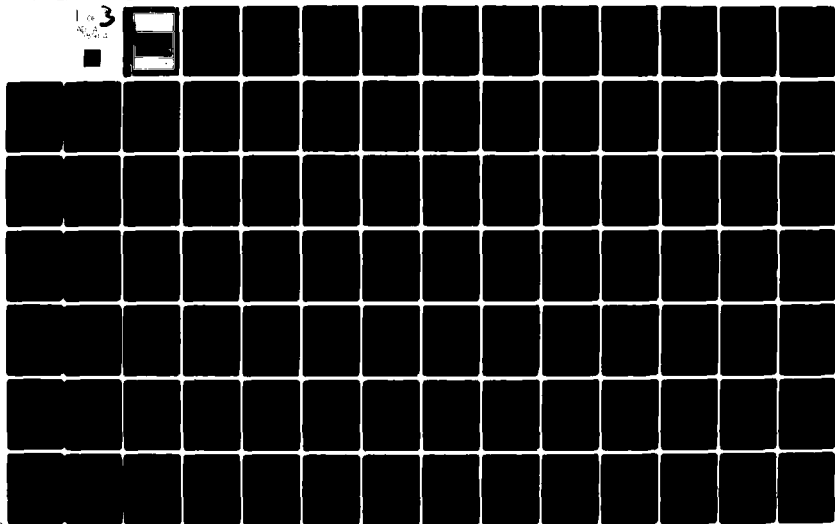


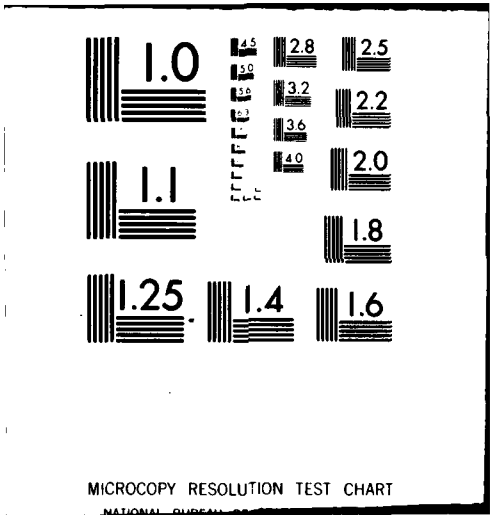
AD-A089 114 ADVISORY GROUP FOR AEROSPACE RESEARCH AND DEVELOPMENT--ETC F/6 1/1  
SPECIAL COURSE ON UNSTEADY AERODYNAMICS.(U)

UNCLASSIFIED AGARD-R-679

ML

1 of 3  
3  
10/2





MICROCOPY RESOLUTION TEST CHART  
NATIONAL BUREAU OF STANDARDS-1963-A

**LEVEL II** —

B.S. 

**AGARD-R-679**

**AGARD-R-679**

**AGARD**

ADVISORY GROUP FOR AEROSPACE RESEARCH & DEVELOPMENT

7 RUE ANCELLE 92260 NEUILLY SUR SEINE FRANCE

**AD A089114**

**AGARD REPORT No. 679**

**Special Course on  
Unsteady Aerodynamics**

**DTIC**  
**ELECTE**  
**S** SEP 12 1980 **D**  
**E**

**NORTH ATLANTIC TREATY ORGANIZATION**



**DISTRIBUTION AND AVAILABILITY  
ON BACK COVER**

NORTH ATLANTIC TREATY ORGANIZATION  
ADVISORY GROUP FOR AEROSPACE RESEARCH AND DEVELOPMENT  
(ORGANISATION DU TRAITE DE L'ATLANTIQUE NORD)

14 AGARD R-679

6 SPECIAL COURSE ON UNSTEADY AERODYNAMICS.

11 Jun 80

12/235

The material assembled in this book was prepared under the combined sponsorship of the Fluid Dynamics Panel, the von Kármán Institute and the Consultant and Exchange Program of AGARD and was presented as an AGARD Special Course at the von Kármán Institute, Rhode-St-Genèse, Belgium on 10-14 March 1980.

## THE MISSION OF AGARD

The mission of AGARD is to bring together the leading personalities of the NATO nations in the fields of science and technology relating to aerospace for the following purposes:

- Exchanging of scientific and technical information;
- Continuously stimulating advances in the aerospace sciences relevant to strengthening the common defence posture;
- Improving the co-operation among member nations in aerospace research and development;
- Providing scientific and technical advice and assistance to the North Atlantic Military Committee in the field of aerospace research and development;
- Rendering scientific and technical assistance, as requested, to other NATO bodies and to member nations in connection with research and development problems in the aerospace field;
- Providing assistance to member nations for the purpose of increasing their scientific and technical potential;
- Recommending effective ways for the member nations to use their research and development capabilities for the common benefit of the NATO community.

The highest authority within AGARD is the National Delegates Board consisting of officially appointed senior representatives from each member nation. The mission of AGARD is carried out through the Panels which are composed of experts appointed by the National Delegates, the Consultant and Exchange Programme and the Aerospace Applications Studies Programme. The results of AGARD work are reported to the member nations and the NATO Authorities through the AGARD series of publications of which this is one.

Participation in AGARD activities is by invitation only and is normally limited to citizens of the NATO nations.

The content of this publication has been reproduced directly from material supplied by AGARD or the authors.

Published June 1980

Copyright © AGARD 1980  
All Rights Reserved

ISBN 92-835-1364-9



Printed by Technical Editing and Reproduction Ltd  
Harford House, 7-9 Charlotte St, London, W1P 1HD

## INTRODUCTION

Unsteady aerodynamics play an important role in aircraft response, aircraft loads, vibration environments and flight systems analysis; this role is becoming more significant with the advent of active control technology (ACT). For internal flows in engines, turbomachinery and helicopter rotors, unsteady aerodynamics are dominant features.

The course was aimed at those either working in industry on dynamic problems in which there is an unsteady aerodynamic input or involved in research and development of unsteady aerodynamics and its applications. The course provided a basic understanding of a range of related unsteady flow phenomena relevant to aeronautical applications, an awareness of the current state-of-the-art of prediction methods and an appreciation of how unsteady aerodynamics are applied to contemporary practical problems.

The course covered the following areas:

- a qualitative understanding of the character of unsteady flows at subsonic, transonic and supersonic speeds, including viscous effects for both attached and separated flows.
- an outline of the contexts in which unsteady aerodynamics are required for aircraft stability and control, flutter, aircraft dynamics response, ACT, turbomachinery vibration and helicopter rotor operation.
- a survey of the state-of-the-art of the current prediction methods with particular emphasis on recent developments in unsteady transonics.
- a description of contemporary experimental techniques and apparatus.

The Director of the course was Professor G.J.Hancock of Queen Mary College University of London, UK. The local coordinator was Professor J.Sandford of the von Kármán Institute.

Accession For	
NTIS GRA&I	<input checked="" type="checkbox"/>
DDC TAB	<input type="checkbox"/>
Unannounced	<input type="checkbox"/>
Justification	
By _____	
Distribution/ _____	
Availability Codes	
Dist.	Avail and/or special
A	

### LECTURE SERIES STAFF

**LECTURE SERIES DIRECTOR:** Professor G.J.Hancock  
Dept. of Aeronautical Engineering  
Queen Mary College  
University of London  
Mile End Road  
London E1 4NS  
UK  
Tel: 01-980-4811 – Ext.364

### LECTURERS

Professor D.P.Telionis  
College of Engineering  
Virginia Polytechnic Institute  
and State University  
Blacksburg, Virginia 24061  
USA  
Tel: 703-961-7492

Dr T.S.Beddoes  
Aeromechanics Department  
Westland Helicopters  
Yeovil, Somerset BA20 2YB  
UK  
Tel: 0935-5222

Dr Wolfgang Geissler  
DFVLR – Institut für Aeroelastik  
Bunsenstrasse 10, 3400 Göttingen  
Germany  
Tel: 709-2353

Professor D.S.Whitehead  
University Engineering Department  
Trumpington Street  
Cambridge CB2 1PZ  
UK  
Tel: 0223-66466

Mr N.C.Lambourne  
65 Putnoe Lane  
Bedford  
UK  
Tel: 51405

Mr R.Doe  
Aerodynamics Department  
British Aerospace Aircraft Group  
P.O.B.77, Fulton House  
Bristol  
UK  
Tel: 693-831 – Ext.163

Dr J.O.Bridgeman  
NASA Ames Research Center  
Moffett Field, Ca.94043  
USA

### LOCAL COORDINATOR

Professor J.Sandford  
von Kármán Institute  
72 Chaussée de Waterloo  
1640 Rhode-St-Genèse  
Belgium  
Tel: 358-19-01

### AGARD REPRESENTATIVE

Mr R.H.Rollins II  
AGARD  
7 rue Ancelle  
92200 Neuilly-sur-Seine  
France  
Tel: 745-08-10

## CONTENTS

	Page
<b>INTRODUCTION</b>	iii
<b>LECTURE SERIES STAFF</b>	iv
	Reference
<b>SOME INTRODUCTORY CONCEPTS BASED ON THE UNSTEADY FLOW ABOUT CIRCULAR CYLINDERS</b> by G.J.Hancock	1
<b>INTRODUCTION TO UNSTEADY BOUNDARY LAYERS</b> by D.P.Telionis	2
<b>A QUALITATIVE DISCUSSION OF DYNAMIC STALL</b> by T.S.Beddoes	3
<b>SOME FEATURES OF LINEAR COMPRESSIBILITY</b> by G.J.Hancock	4
<b>METHODS FOR INVISCID SUBSONIC FLOWS ABOUT AIRCRAFT CONFIGURATIONS</b> by W.Geissler	5
<b>UNSTEADY AERODYNAMICS IN TURBOMACHINERY</b> by D.S.Whitehead	6
<b>UNSTEADY FLOWS ASSOCIATED WITH HELICOPTER ROTORS</b> by T.S.Beddoes	7
<b>ROLE OF UNSTEADY AERODYNAMICS IN AIRCRAFT RESPONSE</b> by G.J.Hancock	8
<b>APPLICATION OF INDICIAL AERODYNAMIC FUNCTIONS</b> by T.S.Beddoes	9
<b>EXPERIMENTAL TECHNIQUES IN UNSTEADY AERODYNAMICS</b> by N.C.Lambourne	10
<b>EXPERIMENTAL TECHNIQUES FOR UNSTEADY BOUNDARY LAYERS</b> by D.P.Telionis	11
<b>METHODS FOR INVISCID SUBSONIC FLOWS ABOUT UNSTEADY AEROFOILS</b> by G.J.Hancock and R.Doe	12
<b>ANALYTICAL METHODS FOR PREDICTION OF UNSTEADY LAMINAR BOUNDARY LAYERS</b> by D.P.Telionis	13
<b>ANALYTICAL METHODS FOR PREDICTION OF UNSTEADY TURBULENT BOUNDARY LAYERS</b> by D.P.Telionis	14
<b>PREDICTION METHODS FOR UNSTEADY SEPARATED FLOWS</b> by T.S.Beddoes	15
<b>NUMERICAL SOLUTION TECHNIQUES FOR UNSTEADY TRANSONIC AERODYNAMICS PROBLEMS</b> by W.F.Ballhaus and J.O.Bridgeman	16
<b>LINEARISED METHODS IN SUPERSONIC FLOW</b> by R.H.Doe	17



**SUPERSONIC FIELD EQUATION SOLUTIONS\***  
by R.H.Doe

**Reference**

**18**

**APPENDIX: LIST OF PARTICIPANTS**

**A**

---

\* Not available at time of printing.

**SOME INTRODUCTORY CONCEPTS BASED ON THE  
UNSTEADY FLOW ABOUT CIRCULAR CYLINDERS**

---

G.J. Hancock,  
Dept. of Aeronautical Engineering,  
Queen Mary College,  
University of London, U.K.

---

**1. RANGE OF UNSTEADY FLOW PHENOMENA**

---

To begin with, the various categories of unsteady flows which are of current interest in an aircraft context are briefly outlined.

At the relatively low response rates associated with aircraft controllability and manoeuvrability it is necessary to understand the unsteady aerodynamic flows about a whole aircraft configuration throughout its flight envelope of Mach number, altitude and range of manoeuvres, extending for combat aircraft to post-stall gyrations, following departure from controlled flight, where the aircraft motions are highly complicated. Combat aircraft can operate at high angles of attack where flow separation and flow breakdown inevitably occur hence it is necessary to understand the rates at which flow separations develop in both symmetric and asymmetric conditions, to be able to describe the separated flow fields, to understand how a separated flow field convects downstream aft of the main wing and forward fuselage in order to estimate the time-dependent interference effects on the horizontal and vertical tail units. Sometimes the separated flow field is well behaved as for strakes and delta wings but usually the separated flows break down and become indescribable. The development of understanding of such unsteady separated flows coupled with the highly non-linear behaviour of a compressible flow field at high subsonic and transonic speeds is a daunting prospect, especially when it is appreciated that combat aircraft have complex configurations, including variable sweep, closely coupled main wing and tail unit, and a range of store and missile attachments. In addition, it is necessary to be able to predict the aerodynamic loads due to time-varying deflections of control surfaces, spoilers, etc. from the point of view of control law design for manoeuvre demand systems, auto pilots, for terrain following, stabilisation of inherently unstable aircraft, spin prevention systems, etc.

Moving on to the faster response times associated with structural response, the problem is the consideration of structural dynamic motions superimposed on those of the overall aircraft motions described in the previous paragraph. The stability of the higher frequency structural modes, namely flutter, has been studied on the assumption that the problem is a linear one; at subsonic and supersonic speeds in attached flow there is some justification for this assumption but not at transonic speeds or when flow separation occurs. In broad terms, it is necessary to predict airloads on wings, fuselage, and tail unit, when the modes of structural deformation and their time behaviour are specified. The objective is to ensure adequate flutter margins and to ensure adequate structural strength in manoeuvres and in atmospheric turbulence, including structural fatigue assessment. Structural strength in atmospheric turbulence is particularly relevant to transport aircraft whose main wings are often gust designed.

It is not appropriate to attempt review the current state-of-the-art of unsteady aerodynamics at this stage. However, it may be appropriate to make one or two points. It is convenient to regard the wide range of areas of interest in unsteady aerodynamics into the following categories:

- i) attached flow in subsonic and supersonic streams
- ii) attached flow at transonic speeds
- iii) separated flows
- iv) self induced unsteady flows.

In the AGARD conference in 1977, on Unsteady Aerodynamics <sup>(1)</sup>, Ashley stated, and Bergh repeated in his summary <sup>(2)</sup>, that unsteady attached flows at subsonic and transonic speeds are sufficiently well understood on the basis of linearised theories. In relative terms, such a statement is uncontroversial, taken together with the follow up statement by Ashley <sup>(1)</sup> that it is inadvisable to continue with the refinement of linearised theories when there are more fundamental problems which need attention. However there are still areas of concern with the flow attached:

- i) at low frequencies, the so called dynamic stability derivatives, especially those involving interference, required to assess aircraft performance and aircraft handling qualities are not too well understood, prediction methods tend to be empirical and differences appear between flight and wind tunnel measurements;
- ii) very little work on lateral or asymmetric motions has been done and what has been done is not reassuring;
- iii) there is the effect of flow through engines, together with efflux interference effects, on steady or oscillatory loads, an area which has been neglected by the unsteady aerodynamics, and which could well be important in the context of vectored thrust;
- iv) while accepting that oscillatory linearised theories are satisfactory for the prediction of flutter, there is the element of doubt of whether the same prediction methods are adequate for control law design in ACT applications;
- v) only superficial attempts are made to modify theory by incorporating measured data.

Progress at transonic speeds is well documented and these aspects are given prominence in this Lecture Series.

Understanding of unsteady separated flows is still in its infancy; little can be said apart from the case dynamic stall in the context of two dimensional airfoils oscillating in and out of a separated flow regime, a problem of importance in helicopter rotor dynamics and discussed later in the Lecture Series.

Self induced flows, primarily buffeting, although of considerable importance are not given undue emphasis in this Lecture Series mainly because of the necessity to limit topics for inclusion.

## 2. WHAT IS 'UNSTEADY AERODYNAMICS'?

Unsteady aerodynamics can be said to be those flows whose character are time dependent. Such a statement, although factually correct, is neither instructive nor indicative of the various ways in which time variations can occur. However, in order to be more precise, it is necessary to invoke immediately mathematical concepts (this statement is made with a sense of apology since the apparent haste to present mathematics so early on an introductory paper is an admission of inadequacy).

Fluid velocities are normally defined in the sense of Euler where  $u(x,y,z,t)$ ,  $v(x,y,z,t)$  and  $w(x,y,z,t)$  refer to the fluid velocity components of elements of fluid which are instantaneously passing through the point(s)  $(x,y,z)$  at time  $t$ . Now the reference point  $(x,y,z)$  is itself defined relative to a specified axis system. A flow which is 'steady' relative to one axis system can be 'unsteady' relative to another axis system; for example for an aerofoil moving at a uniform velocity through air at rest, the flow is 'steady' relative to axes moving with the aerofoil but 'unsteady' relative to axes fixed in space, although in both treatments, the pressure distribution and the overall forces on the aerofoil are independent of time. If however the aerofoil is moving with a time dependent velocity then the problem is unsteady whatever axis system is taken.

It might be argued that a problem is unsteady if its solution involves time as one of the independent variables in all possible axis systems. Again, such a definition can introduce an element of doubt for it is not clear whether it is the answers being referred to or the mode of solution, for example, an aerofoil at zero incidence accelerating at a uniform rate in an inviscid, incompressible, fluid needs to be solved as an 'unsteady' problem yet the drag force is constant independent of time.

In general, a problem will be unsteady if the boundary conditions vary with time. However, the corollary is not true, a problem with steady boundary conditions can exhibit strong unsteady features,

for example, the steady stream of a real fluid past a stationary circular cylinder or buffet arising from shock wave - boundary layer interactions. This line of thought leads on to the observations that by far the main predominant unsteady aerodynamic phenomenon is turbulence itself, often associated with the generation and propagation of acoustic noise. In the Lecture Series, because of limitations in time, it is necessary to be selective on the topics discussed. The emphasis here is on those aspects of unsteady flows which affect response characteristics either of aircraft as a whole, or structural components, or compressor or turbine blades or rotors. Neither the nature of turbulence nor the generation and transmission of noise are discussed as primary topics, although reference will be made to the effects of turbulence and its modelling in unsteady boundary layers and separated regions. Acoustic radiation from deterministic (as distinct from random) sources is included because it is the basic ingredient of linearised compressible flow theory.

### 3. SOME INCOMPRESSIBLE INVISCID FLOWS ASSOCIATED WITH THE MOTION OF TWO DIMENSIONAL CIRCULAR CYLINDERS

#### 3.1 Basic Equations

This lecture is entitled 'some introductory concepts'; so to start at the beginning it is thought that a number of such concepts can be most simply illustrated by consideration of the motion of a two dimensional circular cylinder in an inviscid incompressible fluid. It is hoped that these illustrations give some insight; although inviscid flows around circular cylinders are of little direct practical value in their own right, transformation techniques can lead to results of practical usefulness for two dimensional aerofoils or slender wings.

Consider first the basic equations of an inviscid, incompressible fluid in a two dimensional motion. Let  $OXY$  represent a set of axes fixed in space and let  $u(X, Y, T)$ ,  $v(X, Y, T)$  denote the velocity components of an element of fluid as that element passes through the point  $(X, Y)$  at time  $T$  as shown in Fig. 1.

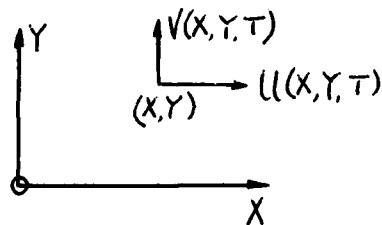


FIG. 1

The basic equations are:

$$\text{continuity} \quad \frac{\partial u}{\partial X} + \frac{\partial v}{\partial Y} = 0, \quad (1)$$

$$\text{motion} \quad \left. \begin{aligned} \rho \frac{Du}{Dt} &\equiv \rho \left[ \frac{\partial}{\partial T} + u \frac{\partial}{\partial X} + v \frac{\partial}{\partial Y} \right] u = -\frac{\partial p}{\partial X} \\ \rho \frac{Dv}{Dt} &= -\frac{\partial p}{\partial Y} \end{aligned} \right\} (2)$$

If the flow is irrotational, a velocity potential  $\Phi(X, Y, T)$  exists such that

$$u = \frac{\partial \Phi}{\partial X}, \quad v = \frac{\partial \Phi}{\partial Y}, \quad (3)$$

then from eqns. (2)

$$p + \frac{1}{2} \rho [u^2 + v^2] + \rho \frac{\partial \Phi}{\partial T} = F(T). \quad (4)$$

Next consider an axis system  $oxy$  moving with velocity  $U_0(T)$  in the positive  $X$  direction; denote  $u(x, y, t)$ ,  $v(x, y, t)$  as the velocity components of an element of fluid relative to the motion of the axis system as the element passes through the point  $(x, y)$  at time  $t$  (where  $t = T$ ).

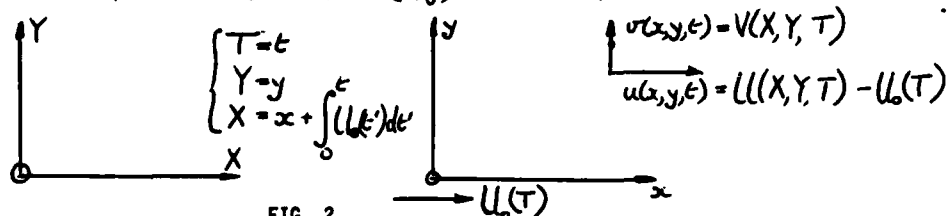


FIG. 2

On transformation eqns. (1,2) become:

$$\frac{\partial u}{\partial x} + \frac{\partial v}{\partial y} = 0 \quad (5)$$

$$\left. \begin{aligned} \rho \left[ \frac{\partial}{\partial t} (u + U_0) + u \frac{\partial u}{\partial x} + v \frac{\partial u}{\partial y} \right] &= -\frac{\partial p}{\partial x} \\ \rho \left[ \frac{\partial}{\partial t} v + u \frac{\partial v}{\partial x} + v \frac{\partial v}{\partial y} \right] &= -\frac{\partial p}{\partial y} \end{aligned} \right\} (6)$$

Thus, if  $\frac{dU_0}{dt}$  is zero (i.e.  $U_0(t)$  constant) the basic equations remain invariant under the transformation of axes even for unsteady flows, retaining the  $\frac{du}{dt}$  term. If  $U_0(t)$  is not uniform, eqns.(6) hold. And at infinity

$$u(x,y,t)_{x,y \rightarrow \infty} = U(X,Y,T) - U_0(t), \quad v(x,y,t)_{x,y \rightarrow \infty} = V(X,Y,T) \quad (7)$$

An example for the reader: derive the equations of motion relative to an axis system whose origin moves accordingly to the formula  $(X(t), Y(t))$  with the axes orientation varying as  $\theta(t)$ .

If  $\{U(X,Y,T), V(X,Y,T)\}$  is an irrotational field then  $\{u(x,y,t), v(x,y,t)\}$  is also an irrotational field, so a velocity potential  $\phi$  exists such that

$$u(x,y,t) = \frac{\partial \phi}{\partial x}, \quad v(x,y,t) = \frac{\partial \phi}{\partial y} \quad (8)$$

Integration of eqn.(6), using eqn.(8), leads to:

$$P + \frac{1}{2} \rho (u^2 + v^2) + \rho \frac{d}{dt} (\phi + x U_0(t)) = F(t) \quad (9)$$

### 3.2 Non-Circulatory Flows

Consider the flow past a stationary circular cylinder of radius  $R_c$  placed in a stream of velocity  $U_\infty(t)$ . The static pressure of the free stream decreases in the  $X$  direction to accommodate the accelerating free stream as shown in Fig. 3.

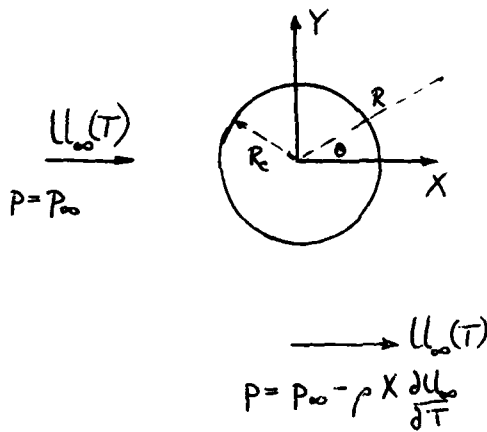


FIG. 3

Next consider a circular cylinder of radius  $R_c$  moving with velocity  $U_0(t)$  in fluid at rest with ambient pressure  $P_\infty$ , as shown in Fig. 4.



FIG. 4

This problem can be considered in two ways either, relative to  $OXY$  axes fixed in space, or relative to axes  $oxy$  moving with the cylinder.

Relative to fixed axes  $OXY$  the basic equation is again

$$\nabla^2 \phi = 0 \quad (15)$$

subject to the boundary condition

The basic equation, since the flow is irrotational, is, by combining eqns.(1,3)

$$\nabla^2 \phi = 0, \quad (10)$$

subject to the boundary condition

$$\frac{\partial \phi}{\partial R} \Big|_{R=R_c} = 0, \quad \frac{\partial \phi}{\partial X} \Big|_{R \rightarrow \infty} = U_\infty(t). \quad (11)$$

The solution of eqns.(10,11) is

$$\phi(R, \theta, T) = U_\infty(t) \left( R + \frac{R_c^2}{R} \right) \cos \theta. \quad (12)$$

On the surface of the cylinder, by reference to eqn.(4),

$$P + \frac{1}{2} \rho U_\infty^2 \sin^2 \theta + \rho \frac{dU_\infty}{dt} 2R_c \cos \theta = P_\infty + \frac{1}{2} \rho U_\infty^2 \quad (13)$$

Defining the force  $F_x$  acting on the cylinder in the  $X$  direction,

$$F_x = - \int_0^{2\pi} (P - P_\infty) \cos \theta R_c d\theta = \rho 2\pi R_c^2 \frac{dU_\infty}{dt} \quad (14)$$

$$\begin{aligned} [U \cos \theta + V \sin \theta] \\ X = \int_0^T U(\tau) d\tau + R_c \cos \theta = U_0(\tau) \cos \theta, \\ Y = R_c \sin \theta \end{aligned} \quad (16)$$

$$\Phi_{R \rightarrow \infty} = 0 \quad (17)$$

The solution to eqns.(14-17) is

$$\Phi(X, Y, T) = -\frac{U_0(\tau) R_c^2 (X - \int_0^T U_0(\tau) d\tau)}{[(X - \int_0^T U_0(\tau) d\tau)^2 + Y^2]} \quad (18)$$

On the surface of the cylinder, by reference to eqn.(4),

$$P + \frac{1}{2} \rho U_0^2(\tau) + \rho \left( -\frac{\partial \Phi}{\partial T} R_c \cos \theta + U_0^2(\tau) (1 - 2 \cos^2 \theta) \right) = P_\infty \quad (19)$$

Alternatively, relative to moving axes  $oxy$ , the basic equation is

$$\nabla^2 \phi = 0 \quad (20)$$

subject to the boundary condition

$$\frac{\partial \phi}{\partial r} \Big|_{r=R_c} = 0, \quad \frac{\partial \phi}{\partial x} \Big|_{x \rightarrow \infty} = -U_0(t) \quad (21)$$

The solution of eqns.(20,21) is

$$\phi(r, \theta, t) = -U_0(t) \cos \theta \left( r + \frac{R_c^2}{r} \right), \quad (22)$$

so that on the surface of the cylinder, by reference to eqn.(9)

$$P + \frac{1}{2} \rho U_0^2(t) \sin^2 \theta - \rho \frac{\partial \phi}{\partial t} R_c \cos \theta = P_\infty + \frac{1}{2} \rho U_0^2(t) \quad (23)$$

It can be seen that the pressure relationships given by eqns.(19,23) are identical.

The overall force  $F_x$  in the direction  $OX (=ax)$  is, on integration of either eqn.(19) or eqn.(23),

$$F_x = - \int_0^{2\pi} (P - P_\infty) \cos \theta R_c d\theta = -\rho \pi R_c^2 \frac{\partial U_0}{\partial T} \quad (24)$$

By comparison of eqns.(14) and (24) it is seen that the 'drag' force acting on a cylinder held in an accelerating stream is twice the 'drag' force acting on the cylinder when it is accelerating at the same rate in still air. This result is an important one, emphasising that, in general, the forces acting do not depend solely on relative motion of a cylinder and the outside air.

The drag force given by eqn.(24) is usually referred to as the apparent mass force.

It is noted that a sudden change in velocity from one steady forward velocity to another is accompanied by an impulsive drag force.

It follows from the preceding analysis that if the centre of cylinder has velocity components  $U_0(\tau), V_0(\tau)$  then the 'drag' forces proportional to  $\frac{\partial U_0}{\partial T}$  and  $\frac{\partial V_0}{\partial T}$  in the  $X$  and  $Y$  directions are simply superimposed.

Interesting compounded problems can be formulated. For example consider cylinder of radius  $R_c$  moving at velocity  $U_0(\tau)$  in the steady potential field associated with a source situated in a fluid otherwise at rest as shown in Fig.5; it is left to the interested reader to evaluate the forces (assume  $R_c \ll H$ ).

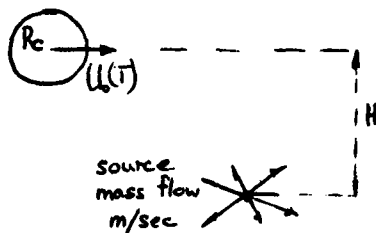


FIG. 5

Although in the example of Fig.5 there are non-linear pressure terms coupling the effects of the cylinder velocity and the relative time varying source velocities at the cylinder, the forces are linearly superimposed with the  $Y$  force due to this source field being twice the  $X$  force associated with the motion (i.e.  $U_0(\tau)$ ).

### 3.3 Circulatory Flows

Consider the flow about a circular cylinder which is moving with a steady velocity  $U_0$  in a fluid at rest such that a specified point  $S$  on the aft surface, defined by the angle  $\alpha$ , is designated a separation point as shown in Fig.6. This additional feature is represented by the introduction of a steady circulation  $\Gamma$ .

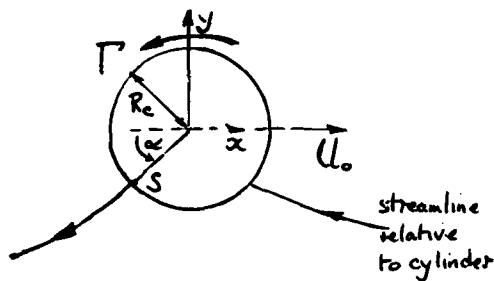


FIG. 6

Since the point S, defined by the angle  $\alpha$  is designated the separation point, it follows that

$$\Gamma = 4\pi U_0 R_c \sin \alpha \quad (26)$$

And on integration of the pressures around the surface the standard formulae

$$\text{Lift} = \rho U_0 \Gamma, \quad \text{Drag} = 0 \quad (27)$$

are obtained.

Next consider the case where the velocity of the cylinder varies with time, i.e.  $U_0(t)$ , with the specification that the same point S on the cylinder surface remains a separation point. It follows that the circulation  $\Gamma$  is now a function of time.

From Kelvin's theorem, the total circulation around a closed curve remains constant as that curve moves with the fluid, this result holds with stationary or moving axes. Thus if the circulation around the cylinder  $\Gamma$  increases with time then vorticity of the opposite sign is created, which is then convected downstream of the cylinder as shown in Fig. 7 where  $\frac{\partial U}{\partial t}$  and  $\frac{\partial \Gamma}{\partial t}$  are assumed to be positive. The total circulation around the shed vorticity will be  $-\Gamma(t)$ , assuming that the motion started from zero velocity.

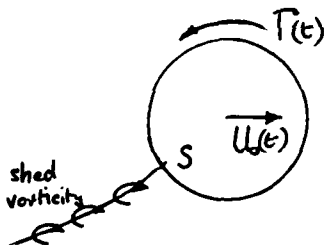


FIG. 7

It is this shed vorticity into the wake and its effect on the local flow about the cylinder which gives the so called history or hereditary effects in unsteady aerodynamics; what has happened in the past affects the present.

Since there is no static pressure discontinuity across the shed vorticity which is convected downstream along a streamline, from the unsteady Bernoulli equation (i.e. eqn.(9)):

$$q_m \Delta q + \frac{\partial}{\partial t} \Delta \phi = 0 \quad (28)$$

where  $\Delta q$  denotes the discontinuous change in tangential velocity  $q$  across the vortex sheet (i.e. upper value minus lower value),  $\Delta \phi$  denotes the discontinuity in velocity potential and  $q_m$  denotes the mean velocity of the tangential velocities on either side of the vortex sheet. It will be remembered that a  $\Delta \phi$  term also exists to make  $\phi$  single valued.

It is of interest to discuss the flow pattern in the neighbourhood of the separation point S. Now eqn.(28) holds at S. And at S, by reference to eqn.(25),  $\Delta \phi$  is equal to  $\Gamma$ ; it follows from eqn.(28) that there is a velocity discontinuity so  $\Delta q$  is finite and non-zero. Initially, it might be thought that the streamline along which the vorticity is shed leaves the cylinder at S at a finite angle as shown in Fig. 8(1); however such a postulated flow implies that the point S is a stagnation point thus  $\Delta q$  would be zero and there would be no mechanism for creating and shedding vorticity. In other words, eqn. (28) could not be satisfied.

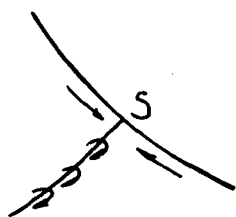


FIG. 8(i)

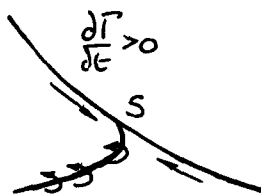


FIG. 8(ii)

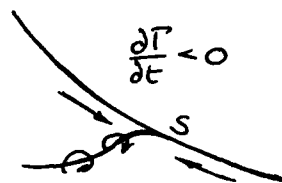


FIG. 8(iii)

In fact the shed vorticity must leave the cylinder surface tangentially as shown in Figs.8(ii,iii). The dividing streamline is a cusp, there is a stagnation point on one side of the separating streamline from the cylinder surface but not on the other. It is seen qualitatively in Figs.8(ii,iii) that if the arrows on the shed vorticity denote the sense of that vorticity the sketches are consistent. If the velocity difference at separation is  $q_s$  then from eqn.(28)

$$\left. \begin{aligned} \text{in Fig.8(ii)} \quad q_s^2 &= \frac{\partial \Gamma}{\partial t} ; \frac{\partial \Gamma}{\partial t} > 0 \\ \text{in Fig.8(iii)} \quad q_s^2 &= -\frac{\partial \Gamma}{\partial t} ; \frac{\partial \Gamma}{\partial t} < 0 \end{aligned} \right\} \quad (29)$$

An interesting point to note is that the sketches Fig.8(ii,iii) hold whenever  $\partial \Gamma / \partial t$  is non-zero, however small, yet in the limit where  $\partial \Gamma / \partial t$  is zero the separating streamline leaves normal to the surface and not tangential. This can be explained as follows: the curvature of the separating streamline from S as shown in Figs.8(ii,iii) depends on  $\partial \Gamma / \partial t$  and it is postulated that the radius of curvature tends to zero as  $\partial \Gamma / \partial t$  tends to zero; in this manner the conventional steady pattern emerges as an appropriate asymptotic limit.

As far as is known the general problem formulated in Fig.7 has not been solved, at least in the open literature. A numerical solution in successive time intervals would not be too difficult; an image vorticity system inside the cylinder would preserve the cylinder as a streamline; an iterative procedure would be needed at each time step to determine the proper shape of the shed vorticity streamline.

However, some trends can be described qualitatively.

Consider a circular cylinder which is accelerating at a uniform rate through air at rest keeping the same point S as the rear stagnation point as indicated in Fig.9.

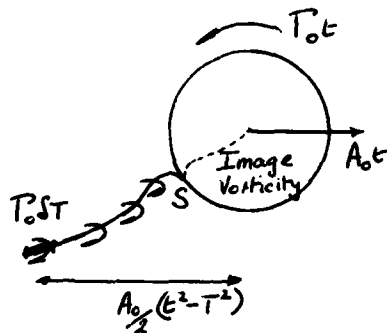


FIG. 9

The cylinder velocity in Fig.9 is denoted by  $A_0 t$  ( $t > 0$ ). Suppose that the circulation could be represented by  $T_0 t$  where  $T_0$  is a constant. Then the circulation shed between time  $T$  and  $T + \delta T$  is  $T_0 \delta T$ , and this circulation is left behind the moving cylinder. At time  $t$  the vortex of circulation  $T_0 \delta T$  is distance approximately  $A_0 (t^2 - T^2) / 2$  aft of the cylinder. Thus the induced flow field around the cylinder at time  $t$  is obtained by integrating the induced flow due to  $T_0 \delta T$  from  $T=0$  to  $T=t$ . It can be seen that this induced velocity field is approximately  $2T_0 A_0 t$  which is small compared with the other velocities in the neighbourhood of the cylinder which are  $O(t)$ . In physical terms the

circulation  $T_0 \delta t$  which is shed at time  $t$ , when  $t$  is large, is spread over an element of vortex sheet of strength  $T_0 / A_0 t$  which is small, i.e. the shed vorticity is convected away relatively quickly. To a first approximation, the flow can be represented by a doublet and vortex to ensure that the point S is a stagnation point, resembling the steady solution so  $T_0$  is proportional to  $A_0$ . The approximate forces acting are, referring to eqns.(9,24,26)



$$\text{Drag} \approx \rho \pi R_c^2 A_0 + \rho 2T_0^2 / A_0 \quad (30)$$

$$\text{Lift} \approx \rho A_0 T_0 U_c^2 + \rho R_c T_0 - \rho 2\pi R_c^2 T_0^2 / A_0 U_c$$

The terms in eqns.(30) arise in the following manner:

- $\rho \pi R_c^2 A_0$  - is the apparent mass term in the x direction.
- $\rho 2T_0^2 / A_0$  - is the coupling of the circulation with the induced velocity field due to the wake.
- $\rho A_0 T_0 U_c^2$  - is the coupling of circulation with forward speed.
- $\rho R_c T_0$  - arises from integrating  $\frac{\partial \psi}{\partial t}$  for the circulation term  $T_0 t$  around the cylinder surface.

There are additional terms but they are of lower order.

Next consider a cylinder moving with uniform speed  $U_1$  with steady circulation  $T_1$  with the point S as the rear separation point, so that steady lift  $\rho U_1 T_1$  acts. Let the cylinder velocity suddenly increase at  $t=0$  to  $U_2$  and the new speed is maintained for  $t>0$ , such that the same point S remains the separation point. It is expected that as  $t \rightarrow \infty$  a new steady state will emerge with a steady circulation  $T_2$  and a steady lift  $\rho U_2 T_2$ .

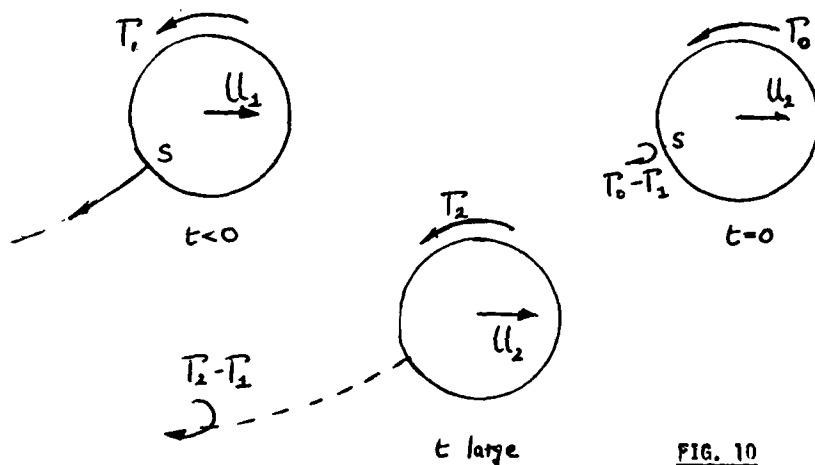


FIG. 10

As shown in Fig.10, immediately following the change in speed at  $t=0$  the circulation about the cylinder changes instantaneously to a value  $T_0$  and a starting vortex of initial strength  $T_0 - T_1$  is created. The value of  $T_0$ , obtained by satisfaction of the boundary conditions cannot be simply expressed. There is an impulse in the drag force due to the instantaneous velocity change of  $U_1$  to  $U_2$ , associated with the arguments presented in Section 3.2; and an instantaneous change in the lift associated with  $T_0$ .

However, as the time increases, in qualitative terms, the circulation around the cylinder approaches its steady circulation state  $T_2$  with a 'starting' vortex of approximate strength  $T_2 - T_1$  at a distance approximately  $U_2 t$  downstream of the cylinder. The 'starting' vortex induces a velocity  $V_2$  about the cylinder where

$$V_2 \sim \frac{T_2 - T_1}{2\pi U_2 t} \quad (31)$$

This flow field induces a negative lift force proportional to  $\frac{\partial V_2}{\partial t}$  and a drag force proportional to  $\rho V_2 T_2$ . There is a smaller additional drag force acting on the cylinder associated with the higher tangential velocities on the aft surface of the cylinder compared with those around the front surface of the cylinder induced by the shed vorticity and its image. Thus the lift force approaches its final steady state  $\rho U_2 T_2$  and the drag force approaches zero as

$$\text{Lift} = \rho U_2 T_2 - \mathcal{O}(V_2 t)$$

$$\text{Drag} = \mathcal{O}(V_2 t) \quad (32)$$

A similar argument can be applied to show that if a cylinder moving with velocity  $U_1$  for time  $t < 0$  suddenly moves with an additional transverse velocity  $V_1$  for time  $t > 0$  then again there would be a starting vortex which is shed downstream, and asymptotically, as  $t$  becomes large,

$$\text{Lift} = \text{final steady value} - O(\sqrt{t})$$

$$\text{Drag} = O(\sqrt{t})$$

(33)

Note that the drag is positive. This asymptotic behaviour ( $\sqrt{t}$ ) is an important factor which is featured in later discussions.

Much confusion has been caused in the literature by referring to the circulatory and non-circulatory contributions to overall forces and moments in unsteady incompressible flows. The impression given are that these effects are simply additive. This is not so, the so-called circulatory and non-circulatory contributions are closely interrelated. According to eqn.(25) albeit for a steady case, the first term can be referred to as the non-circulatory term while the second term, which depends on  $\Gamma$ , as the circulatory term; however eqn.(26) demonstrates immediately that if the separation point S is specified then the circulatory and non-circulatory parts are interrelated. In general, for any body in a time dependent motion in an incompressible fluid, if the correct boundary conditions are satisfied, then the resulting solution will be complete. Any attempt to distinguish between circulatory and non-circulatory contributions is pointless; in the author's experience errors have cropped up periodically over the years because of such attempts.

### 3.4 Circular Cylinders in Inviscid Shear Flow

The study of rotational flows about bodies is relevant to aeronautics in a number of areas. One concerns the estimation of gust loads which arise as an aircraft responds to atmospheric turbulence and by their very nature atmospheric gusts are rotational. Another area is concerned with tailplane or rear fuselage loads in the wake of a main wing and front fuselage, mostly when the flow over the main wing or front fuselage has separated. A third area concerns the dynamics of a smaller aircraft if it becomes entangled in the trailing vortices left behind a larger aircraft.

The solution of the flow about a body when the relative stream is a general rotational flow is extremely complicated. However, it is instructive to study some simple analytic solutions of a circular cylinder in a stream with uniform vorticity.

Consider first the steady problem of a stationary circular cylinder in a stream with uniform vorticity at infinity as shown in Fig.11.

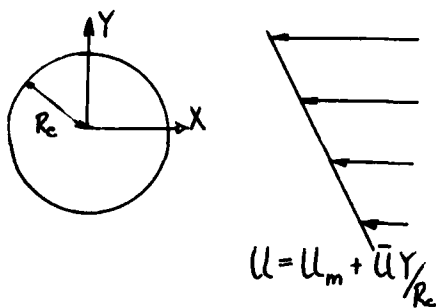


FIG. 11

The stream at infinity has velocity profile in the negative X direction given by  $u_m + \bar{u}Y/R_c$  so that the free stream has uniform vorticity  $\bar{u}/R_c$ .

In two dimensions vorticity is conserved along a streamline. Thus the case of uniform vorticity is relatively easy to deal with for the vorticity inevitably remains uniform throughout any perturbed field.

This problem can be solved analytically since the circular boundary conditions can be satisfied with:

- i) a dipole (i.e. doublet), to counteract the mean stream  $u_m$  (as used in eqn.(12)),
- ii) a quadrupole, to counteract the shear distribution  $\bar{u}Y/R_c$ ,
- iii) a vortex of strength  $(\bar{u}R_c)$  to represent the velocity induced on the surface of the cylinder by the perturbed fluid flow; this can be easily calculated since it is equivalent to fluid with uniform vorticity of strength  $(\bar{u}/R_c)$  situated inside the cylinder.

After some manipulation, the velocity on the cylinder surface becomes

$$Q_\theta |_{R=R_c} = 2u_m \sin\theta - \bar{u} \cos 2\theta \quad (34)$$

and the streamline pattern is shown in Fig.12.

A number of consequences arise from eqn.(34)

- i) although it was necessary to introduce a vortex into the solution, there is no net circulation around the cylinder surface,

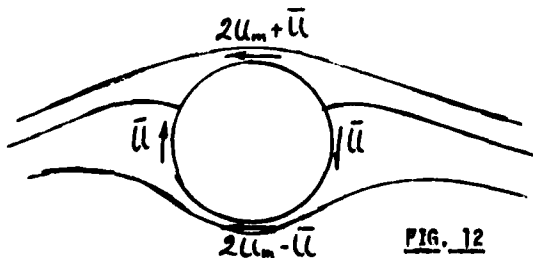


FIG. 12

ii) by Bernoulli's equation (i.e. eqn.(4)) for steady flow

$$p + \frac{1}{2} \rho Q^2 = \text{const}$$

along a streamline although the constant now varies from streamline to streamline, therefore there is a resultant lift ( in the positive Y direction) given by

$$\text{Lift} = \rho U_m \bar{U} R_c \pi \quad (35)$$

iii) although the lift is given by eqn.(35), the absolute pressure at any point is indeterminate because the pressure at the stagnation point(s) is indeterminate.

The last point (iii) is a most important one in shear flows. The difficulty is associated with the fact that the total pressure is constant along the streamline which passes through two stagnation points on the surface of the cylinder. But it is not possible to determine where that streamline originates from at infinity upstream because of the far field associated with the vortex introduced into the solution. This is a feature of all two dimensional shear flow problems, absolute pressures cannot strictly be calculated; many numerical solutions which appear in the literature which neglect these far field effects are suspect.

Next, it is possible to consider the time dependent problem of a cylinder moving at an arbitrary velocity in a shear flow as shown in Fig.13.

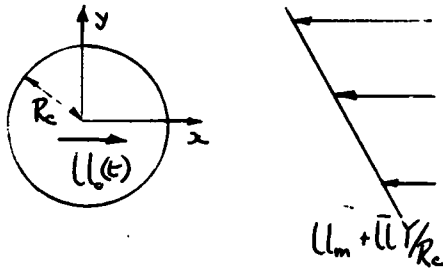


FIG. 13

By taking axes fixed in the cylinder, it follows directly from eqn.(34) that

$$q_0 |_{R=R_c} = 2(U_m + U(t)) \sin \theta - \bar{U} \cos 2\theta \quad (36)$$

Around the surface of the cylinder the pressure is given by reference to eqn.(6),

$$p = F(t) - \frac{1}{2} \rho q_0^2 - \int_0^\theta \rho \frac{\partial q_0}{\partial t} R_c d\theta + \int_0^\theta \rho \frac{\partial U_m}{\partial t} R_c \sin \theta d\theta \quad (37)$$

This result leads to the overall forces

$$\text{Drag} = \rho \pi R_c^2 \frac{dU_m}{dt} \quad (38)$$

which is the same as in irrotational flow, and

$$\text{Lift} = \rho (U_m + U(t)) \bar{U} R_c \pi \quad (39)$$

The more interesting problem from a practical point of view is the passage of the circular cylinder moving at a uniform velocity  $U_0$  across a transverse shear flow as shown in Fig.14.

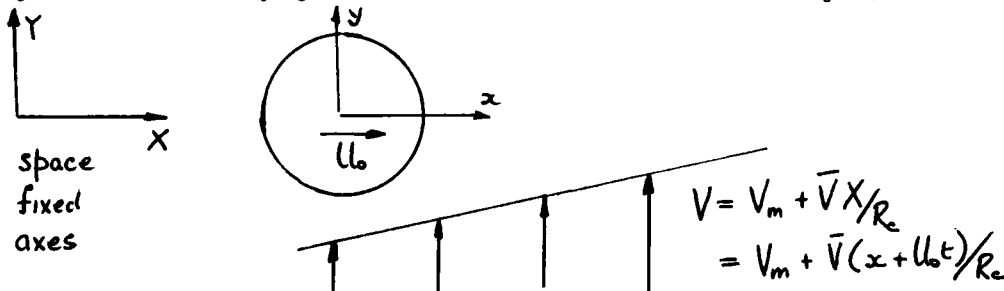


FIG. 14

The forces on the cylinder for the flow shown in Fig.14 can be built up from the previous results; i.e.

$$\left. \begin{aligned} \text{Thrust (i.e. force in the x direction)} &= \rho R_c V_m \bar{V} \\ \text{Lift} &= 2 \rho \pi R_c \bar{V} U_0 \end{aligned} \right\} \quad (40)$$

If the separation point is to be fixed at a particular point on the circular surface then an additional vortex of strength  $\Gamma(t)$  can be introduced, about the cylinder which in turn leads to a pattern of shed vorticity in exactly the same way as for the irrotational flow. To some extent the unsteady circulatory effects can be superimposed on the shear flow effects as above, although there is now coupling since  $\Gamma(t)$  will depend on  $V_m \bar{V}$  and on  $U_0 \bar{V}$ .

It is necessary to emphasise once again that only relative pressures can be calculated in two dimensional flows because it is not possible to identify which streamline at infinity is the one which becomes identical to the cylinder surface.

The limiting case of the flow shown in Fig.14 is the passage of a circular cylinder through sharp edged gust as shown in Fig.15, keeping the stagnation point fixed at point S. The sharp edged gust is essentially a vortex sheet normal to the motion of the circular cylinder.

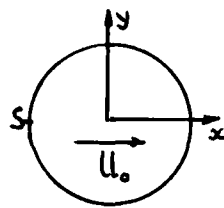
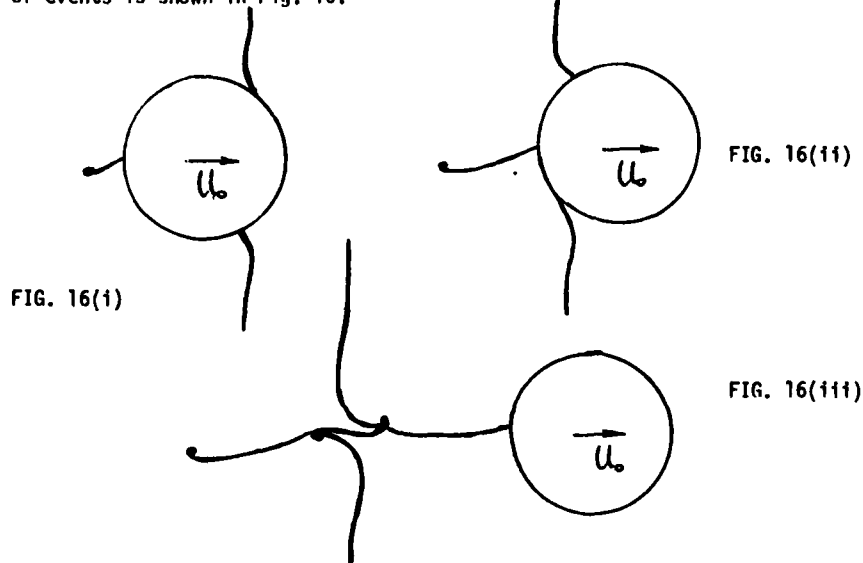


FIG. 15



A sequence of events is shown in Fig. 16.



Now

- Fig.16(i) shows the cylinder just entering the gust front, a lift will start developing so vorticity will be shed from the rear stagnation point.
- Fig.16(ii) shows the gust front passing over the cylinder surface; near the surface the sense of rotation of the gust front will cause retardation on the upper surface and acceleration on the lower surface, further away because of the induced circulation the opposite effect will occur.
- Fig.16(iii) shows the pattern when the cylinder has completely passed through the front, the two halves of the gust front are joined in a complicated manner (this is not entirely conjecture but based on a computer study of an aerofoil passing through a sharp edged gust, ref. 3).

### 3.5 Concluding Remarks on Inviscid Flows about Circular Cylinders

It should be recognised that the inviscid flow about a circular cylinder bears no resemblance whatsoever to the real flow past a circular cylinder.

However, by conformal transformation techniques, the ideal flow past a range of aerofoil sections can be obtained and an ideal flow past an aerofoil gives realistic results to a first approximation for the real flow past that on aerofoil when the real flow remains attached. Most of the qualitative features derived above are transferrable to aerofoils in incompressible fluid motions.

One feature of particular interest for an aerofoil is what happens in the neighbourhood of the trailing edge. According to the arguments given in Section 3.3, in an unsteady motion the separating streamline and shed vorticity leaves the cylinder surface tangentially. The same arguments apply to an aerofoil. Thus the flow leaves the trailing edge tangentially to either the upper surface or the lower surface, depending on the sign of the shed vorticity, as shown in Fig. 17.



FLOW ABOUT A TRAILING EDGE

FIG. 17

#### 4. REAL FLOWS ABOUT CIRCULAR CYLINDERS

##### 4.1 Circular Cylinders in Steady Stream

It seems appropriate to complete this first lecture by briefly reviewing the real low speed flow about a two dimensional circular cylinder because it illustrates another completely different but important area of unsteady aerodynamics, namely the creation of unsteady flows even though the boundary conditions are steady.

The various flow regimes around a circular cylinder depend on the Reynolds number, namely  $\rho U_{\infty} D / \mu$  where  $U_{\infty}$  is the velocity of the free stream,  $D$  is the cylinder diameter,  $\rho$  the fluid density and  $\mu$  the coefficient of viscosity.

Attached Flow Regime:  $Re < 5$

For  $Re < 5$  the flow is attached and steady. By definition Reynolds number expresses the ratio of inertial stresses to viscous stresses, so for  $Re < 5$  these two types of stress are the same order of magnitude throughout the flow. It is of interest to note that for  $Re < 1$  inertial stresses can be neglected, the equations become linear, and theoretical solutions are possible for such phenomena as the swimming of microscopic organisms.

Stable Range  $5 < Re < 40$

In this Reynolds number range the flow separates (at about  $80^{\circ}$  and  $280^{\circ}$ ) and the separated shear layers on either side of the cylinder curl inwards to form a symmetrical standing vortex pair on the rear side of the cylinder. As  $Re$  increases between 5 to 40, the vorticity in the separated shear layer increases so the vortex pair become elongated in the direction of the flow to provide a larger area for diffusion of the vorticity into the free stream to retain equilibrium.

Instability Range  $40 < Re < 90$

The wake for this range of Reynolds number is unstable, but this instability does not lead to flow breakdown. A regular asymmetric wake pattern is formed. The variations and developments in the various patterns for varying  $Re$  in this range have been admirably photographed by Zdravakovich<sup>(4)</sup>.

Vortex Shedding Range  $90 < Re < 150$

This is the well known range in which the flow separation occurs asymmetrically at the cylinder surface, shedding vortices alternate from each side of the cylinder, forming a wake consisting of a double row of laminar vortices for long distances aft of the cylinder.

The frequency of vortex shedding is usually expressed in terms of the non-dimensional Strouhal number

$$St = fD / U_{\infty} \quad (41)$$

where  $f$  is the frequency of vortex shedding (Hz),  $D$  is the diameter of the cylinder and  $U_{\infty}$  is the velocity of the free stream. With regular vortex shedding, the Strouhal number is somewhat less than 0.2.

The shedding of alternate vortices gives rise to an oscillatory lift component at the same frequency of the vortex shedding and an oscillatory drag force at twice that frequency. Because of experimental difficulties no experimental data appears to be available for the magnitude of the oscillatory lift and drag coefficients.

One interesting feature of the flow is that fluid in the centre of each upper vortex, emanates from the separating shear flow on the lower side of the cylinder and vice versa. It is this carry over and diffusion of vorticity from one side to another in the formative process of the vortices which is a distinctive feature of the flow characteristics. The introduction of a splitter plate down the axis of

symmetry effectively prevents the interaction of upper and lower surface shear flows thus destroying the formation of the vortex sheet.

Irregular Range  $150 < Re < 3 \times 10^5$

In this range the shed vortices contain turbulence resulting from transition in the vortices. Essentially, transition moves up the wake of vortices towards the rear end of the cylinder with increasing  $Re$  and the turbulent vortices diffuse rapidly. Close to the rear of the cylinder however, vortices continue to be shed regularly with  $Re < 3 \times 10^5$ .

Vortex shedding frequency is now defined as the frequency of the main peak in the frequency spectrum; in the irregular range the spectrum is a narrow band one and the wake is quasi-periodic. The Strouhal number through this range is about 0.2.

The level of amplitude of the oscillatory lift component  $C_L$  varies between 0.4 to 0.9 from different experiments, these variations are thought to be associated with different testing conditions. Oscilloscope traces of oscillating forces display a randomly modulated but basic single frequency signal. It is argued that these modulations are associated with three dimensional disturbances. Evidence exists that the flows divide into spanwise cell patterns and that these cells can move randomly across the span, evidence also exists that the shed vortices come off at a slight angle to the two dimensional ideal. Effectively, the spanwise correlation lengths decreases with increase in  $Re$ .

Critical Range  $3 \times 10^5 < Re < 1.5 \times 10^6$

The form of the main separation changes from laminar separation to turbulent separation. There is still a local laminar separation but transition in the separated shear layer causes the shear layer to reattach as a turbulent boundary layer, this turbulent boundary layer separates at a more aft location. In the subcritical range laminar separation occurs about  $82^\circ$  (measured from the nose); in the critical range the turbulent separation point moves back to about  $140^\circ$ . Because of the reduction in wake width, the base pressure on the cylinder is decreased so reducing mean drag. Fluctuations in the wake is no longer confined to a narrow frequency band.

Supercritical Range  $1.5 \times 10^6 < Re < 3.5 \times 10^6$

In this range, the separation point moves forward to about  $125^\circ$  and the laminar separation - turbulent reattachment bubble disappears. No dominant shedding frequency is found so the frequency spectrum retains the wide band random character, as in the critical range.

Transcritical Range  $Re > 3.5 \times 10^6$

At these higher values of  $Re$ , the separation moves forward to about  $115^\circ$  and narrow band 'vortex shedding' occurs once again with a Strouhal number about 0.25.

#### 4.2 Circular Cylinder in Unsteady Stream

A number of experiments have been carried out either on transverse oscillations of a two dimensional circular cylinder or with a stationary cylinder in an oscillatory flow field. A typical set of results of force measurements are shown in Fig.18 taken from reference 5.

For the steady cylinder in the irregular range, the spectrum is narrow band with a Strouhal frequency of 12.5 Hz, as shown in Fig.18(i).

An oscillatory stream component superimposed on the steady stream at a frequency of 10.5 Hz introduces as shown in Fig.18(ii), a peak at the input frequency in the spectrum but with a reduced peak at the Strouhal frequency, implying non-linear coupling between the input and natural Strouhal frequency responses.

At input frequencies of 11.5 Hz, 12.0 Hz and 12.5 Hz all of the energy in the spectrum is at the input frequency as shown in Fig.18(iii), this is the phenomena known as frequency 'lock-on'.

With input frequencies slightly higher than the Strouhal frequency, the input and Strouhal frequencies separate out as shown in Figs.18(iv). It is noted that at the higher input frequency of 14 Hz, although there is little evidence of the input at that frequency, the magnitude of the peak response at the Strouhal frequency is considerably reduced compared to the steady case as shown in Fig.18(i).

### 4.3 Concluding Remarks on Real Flows about Circular Cylinders

The above types of real flow about circular cylinders are relevant to two types of practical flows. The first concerns the flow about aerofoils, or cascades with round trailing edges; round trailing edges are preferred to sharp trailing edges because of cooling considerations; however, the main difference between the round aerofoil trailing edge and circular cylinder is in the relative thickness of the separating shear layers; nevertheless, narrow band frequency spectra have been observed. The second concerns the flow about slender fuselage noses which are typical of the front fuselage of recent combat aircraft and missiles; at high angles of attack flow separation occurs, forming discrete vortices induced by the effective cross flow normal to the nose; when separation first occurs two symmetric vortices are formed with axes lying along the fuselage but at higher angles the vortex pattern becomes asymmetric giving rise to asymmetric loading conditions.

### 5. Final Comment

The aim of the introductory lecture has been twofold. The first has been a presentation of the principles which underly methods of calculation of unsteady motions, albeit where the fluid is incompressible (as shown later this is not altogether the same as taking Mach number small), hopefully providing insight and understanding. And secondly, to introduce the complexities of real fluid behaviour and to bear such flow behaviour in mind when relating theory to experiment.

### REFERENCES

1. H. Ashley Unsteady Aerodynamics AGARD CP No. 227 (1977)
2. H. Berndt AGARD Advisory Report 128 (1978)
3. B.C. Basu & G.J. Hancock The Unsteady Motion of a Two Dimensional Aerofoil in Incompressible Inviscid Flow J. Fluid Mechanics Vol. 87 part I (1978)
4. M.M. Zhardorovitch Some Observations of the Formation of a Karman Vortex Sheet Fluid Mechanics Vol. 37 No. 3 (1969)
5. L.R. Wasserson On a Circular Cylinder in Oscillatory Flow Ph.D Thesis University of London 1971.

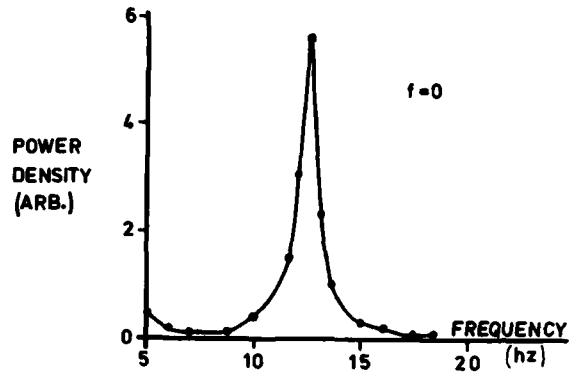


Fig 18 (i)

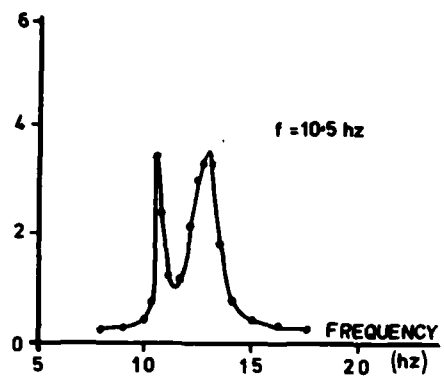


Fig 18 (ii)

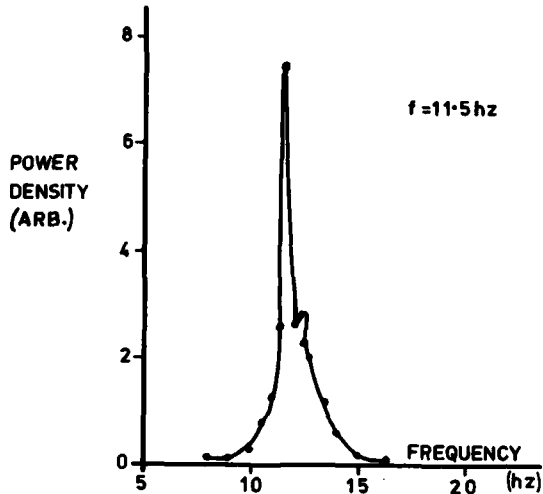


Fig 18 (iii)

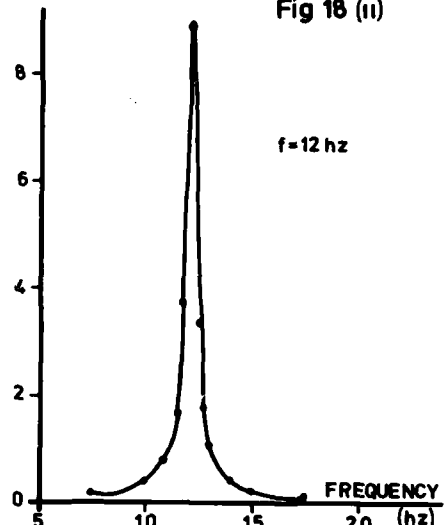


Fig 18 (iii)

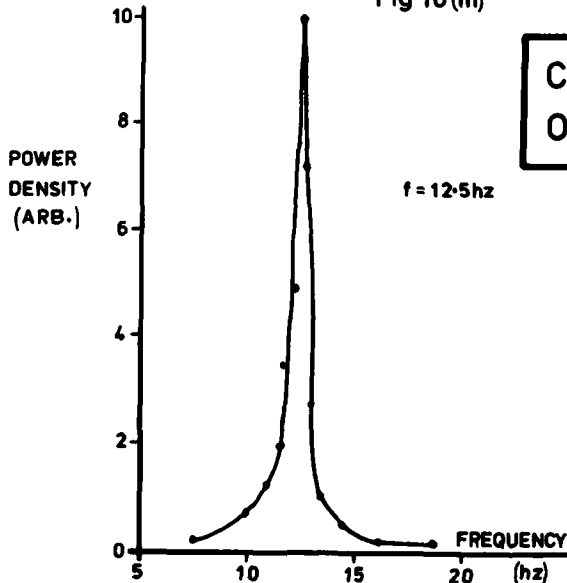


Fig 18 (iii)

CIRCULAR CYLINDER IN  
OSCILLATORY STREAM

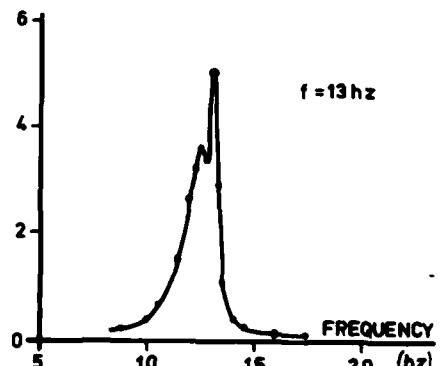


Fig 18 (iv)

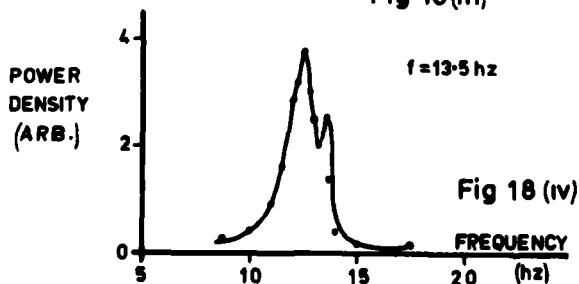


Fig 18 (iv)

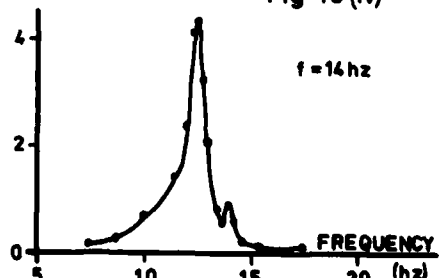


Fig 18 (iv)



## INTRODUCTION TO UNSTEADY BOUNDARY LAYERS

by

D. P. Telionis  
Virginia Polytechnic Institute and State University, Blacksburg, Virginia 24061 USA

The basic characteristics of transient and oscillatory boundary layers can be easily demonstrated in terms of elementary solutions of the Navier Stokes equations for idealized flow situations. Starting with such simple examples, this paper gives a qualitative description of the physics of unsteady boundary layers, briefly describing the response of skin friction, velocity profiles, the effects of nonlinearity on velocity and temperature fields, etc. Compressibility and three-dimensionability have only recently been addressed but unsteady turbulent boundary layers have been aggressively attacked both analytically and experimentally. The extension of turbulence models to unsteady flow is briefly discussed. Reversing boundary layers and unsteady separation are also briefly described as evidenced from a large number of contributions which in fact present conflicting views on the topic.

## 1. INTRODUCTION

It is our intention in this paper to present a brief and simplified overview of the physics of unsteady boundary layers. The description therefore should represent only the results of experimental or analytical investigations. The methods employed, experimental or analytical, should be the concern of subsequent papers in the present volume. However, results are inevitably biased by the method they were obtained. It is for example unavoidable to present data of oscillatory flows in terms of the mean and the amplitude of the oscillation, which implies the use of a signal analyzer or an asymptotic expansion. Moreover, concepts truly deriving from analysis, as for example "nonlinear characteristics" have already become part of the terminology in the description of physical phenomena.

The present paper represents a very short and very simplified description of a few classical phenomena of unsteady viscous flows. It is essentially an introduction to the material that will follow in the present volume. Inclusive reviews on special topics have appeared on different occasions<sup>1-3</sup>. In fact, the present author has just completed an extended monograph on the topic<sup>4</sup>, which will appear as a volume in the Springer series in Computational Physics. This paper is therefore served here as an appetizer. It will serve its purpose if it stimulates the interest of the reader.

Reviewing again material which can by now be considered classical, we decided here to reference mostly review articles and monographs. The reader will therefore have to resort to other articles in this volume or the review articles referenced here, for more information on the original contributions.

## 2. ATTACHED BOUNDARY LAYERS

Some very interesting characteristics of unsteady viscous flows are most conveniently demonstrated in terms of the well known Rayleigh and Stokes problems. The flow over an infinite flat plate (see Fig. 1) which is given either the velocity  $u_w$  impulsively, or the periodic velocity  $u_w \cos \omega t$ , is expressed in terms of the following two solutions of the Navier-Stokes equations

$$u = u_w \left( 1 - \operatorname{erf} \frac{y}{2\sqrt{\nu t}} \right) \quad (1)$$

$$u = u_w e^{-\sqrt{\frac{\omega}{2\nu}} y} \cos \left( \omega t - \sqrt{\frac{\omega}{2\nu}} y \right) \quad (2)$$

where  $u$  is the velocity parallel to the wall,  $y$  is the distance perpendicular to the wall,  $t$  is the time and  $\nu$  is the kinematic viscosity.

For the Rayleigh problem, the first solution, Eq. (1), indicates that for transient flows the effects of unsteadiness propagate away from the source of the disturbance, that is the flat plate, instantly and the extent of the contamination is scaled with the length  $\sqrt{\nu t}$ . Subsequent extensions<sup>5</sup> indicate that the character of impulsive changes of flows about bodies of arbitrary shapes is very similar. In fact for small times the changes are inviscid in character.

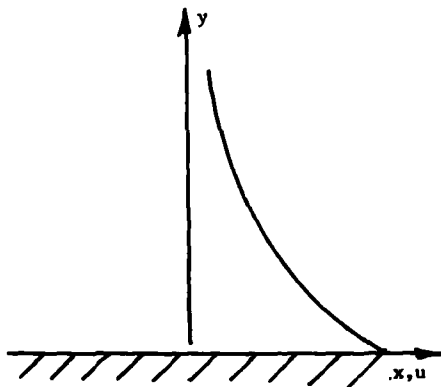


Fig. 1 System of coordinates for the Rayleigh and Stokes problems.

For a harmonically oscillating plate, Stoke's Solution, Eq. (2), indicates that the flow responds harmonically with a phase shift which varies with distance from the wall. An exponential decay of the amplitude is also present and distances from the wall are scaled by the factor  $\sqrt{\omega/2\nu}$ .

The problem of oscillations about a zero mean has interested a large number of investigators, because of a historical controversy of early experimental results. Such flows are rarely encountered in engineering applications. However, the simplicity of the problem permitted investigators already in the past century, to discover the phenomenon of steady streaming and the importance of nonlinearities. Consider for example the oscillatory motion of a circular cylinder, normal to its axis of symmetry, in a fluid which is otherwise at rest. The oscillations of the cylinder impart an oscillatory motion on the surrounding fluid. However, the fluid particles do not oscillate about a fixed position. They perform a combination of translation and oscillation. In the average, there is a net flow with streamlines shown schematically in Fig. 2. This phenomenon is familiar in literature<sup>6</sup> as "steady" or "acoustic" or "nonlinear" streaming. It is perhaps worth here to have a closer look in the vicinity of the oscillating wall. It was found that the oscillations of the wall impart an oscillatory motion in a layer of fluid with thickness approximately equal to  $\sqrt{\nu/\omega}$  as

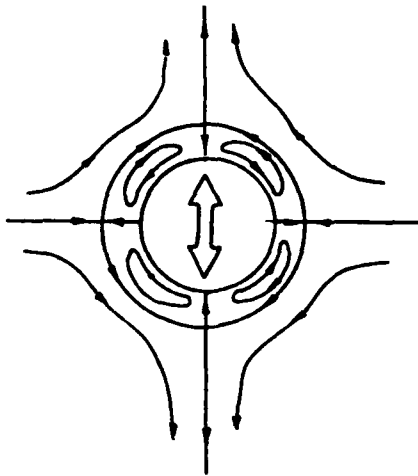


Fig. 2 Streamline pattern of steady streaming around an oscillating cylinder.

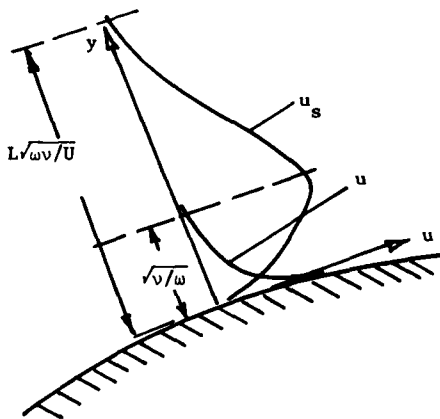


Fig. 3 The fluctuating and steady streaming boundary layers and their thicknesses.

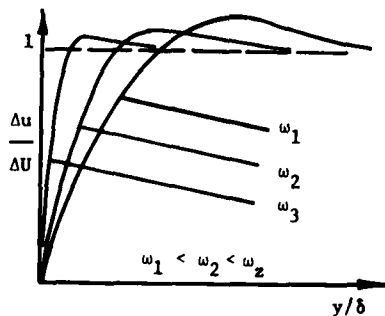


Fig. 4 Fluctuating velocity profiles for oscillations imposed on a boundary layer.

The other quantities in Eq. (3) are defined in terms of a "phase average".

$$\langle f(t) \rangle = \lim_{N \rightarrow \infty} \frac{1}{N} \sum_{n=0}^{N-1} f(t + nT) \quad (5)$$

shown schematically in Fig. 3. Within this layer, the Stokes layer, steady streaming starts building up. The strength of streaming increases with the distance from the wall and attains its maximum at the edge of the Stokes layer. The streaming layer extends further away from the wall and if the quantity  $U^2/\omega\nu$  is very large, it forms a second boundary layer of thickness  $L\sqrt{\nu\omega}/U$ . The most complete and critical reviews of the literature on this topic have been prepared by Riley<sup>5,10</sup>.

In engineering applications an external oscillatory disturbance is imposed on an already developed boundary layer. Three layers are then formed. The steady boundary layer, the Stokes Layer and the streaming layer. The first has thickness of the order of  $\sqrt{\nu/U}$ , the second is again of the order  $\sqrt{\nu/\omega}$  and the third is of the order of  $L\sqrt{\nu\omega}/U$  where now  $U_\infty$  is the velocity of the oncoming steady stream, and  $U$  is a typical velocity of the oscillation, as for example the product of the amplitude and the frequency. It should be emphasized that even with a harmonic excitation, higher harmonics are generated which may in turn give rise to higher order streaming effects.

One of the most interesting features of such flows is the fact that the amplitude of the outer flow, which is driving the boundary layer flow through viscosity, may be actually exceeded by the response of the boundary layer. A typical set of velocity amplitudes is shown in Fig. 4. This method of presenting the results is actually a little misleading as McCroskey<sup>11</sup> has recently pointed out. The response of the boundary layer always introduces a phase shift which in fact varies with distance from the wall. If instantaneous profiles are plotted, the velocity may never exceed the free stream value.

The phase differences are varying substantially across the boundary layer. For large frequencies, the flow right next to the wall leads the outer flow by an angle of  $45^\circ$ . Moving away from the wall, we encounter a region where the flow actually anticipates the motion of the outer flow as shown in Fig. 5.

Similar trends have been discovered for the behavior of temperature and therefore heat transfer. However, recent investigations indicate that overshoots and phase characteristics vary significantly with the pressure gradient, compressibility effects and dissipation. These variations are much larger than originally anticipated. Both analytical and experimental evidence indicate, for example, for flows with adverse pressure gradients, overshoots twice or ten times as large as the amplitude of the outer flow. As separation is approached, the percentage of overshoot grows even more wildly. In Fig. 6 and 7 we display the contours of constant amplitude for laminar and turbulent oscillatory flows respectively. We will return to these Figures in the next section to discuss the features of unsteady separation.

In the study of unsteady turbulent flows, the investigator encounters more difficulties. Turbulent flows are unsteady by definition. It is only in a statistical sense that we may measure and calculate profiles of velocity, temperature, Reynolds Stress, etc. Unsteady turbulent flows involve the random turbulent fluctuations which are in a sense "self-excited" as well as organized fluctuations which are induced by the outer flow. This point perhaps requires some clarification. The turbulent fluctuations are certainly excited by, and receive energy from the outer flow. Although some connection has been established between free stream turbulence and the turbulence within the boundary layer, it is very well possible to generate a wide spectrum of turbulence without any counterparts in the outer flow. The organized fluctuations, for which we will reserve in the sequel the term unsteady flow have the same frequency with the externally imposed fluctuations.

The need to investigate these problems analytically or experimentally led to the triple decomposition

$$f = \bar{f} + \tilde{f} + f' \quad (3)$$

where  $\bar{f}$  is the time average of a quantity

$$\bar{f} = \lim_{t_0 \rightarrow \infty} \frac{1}{t_0} \int_0^{t_0} f dt \quad (4)$$

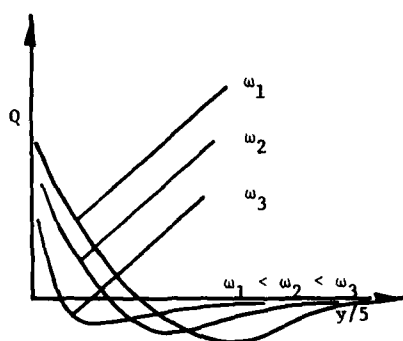


Fig. 5 Phase angle profiles for oscillations imposed on a boundary layer.

where  $T$  is the period of the driving oscillation. The process represented symbolically by Eq. (5) implies an ensemble average of values collected at a fixed phase within the period, i.e. the phase angle  $2\pi t/T$ .

In terms of the phase average, the organized and random fluctuations are defined as follows:

$$\tilde{f} = \langle f \rangle - \bar{f} \quad (6)$$

$$f' = f - \langle f \rangle \quad (7)$$

A schematic representation of a triple decomposition is shown in Fig. 8.

Governing equations have been derived for all three types of functions but the systems involve higher order moments of both time, ensemble and mixed average modes. Closure assumptions are necessary. Instead, theoreticians attempted to consider the unsteady form of the turbulent boundary-layer equations and search for closure methods based on more general modeling of the Reynolds stress. Numerical results provide some information about the behavior of unsteady turbulent boundary layers. However, there are still some unresolved discrepancies, essentially due to the lack of sufficient experimental data. Theoretical models have been shown to predict quite accurately the mean flow, do a poor job predicting the fluctuating component of the flow and totally disregard the characteristics of turbulence. Instantaneous profiles of turbulent energy were obtained only very recently and show a clear periodic displacement in the direction perpendicular to the wall as shown in Fig. 9.

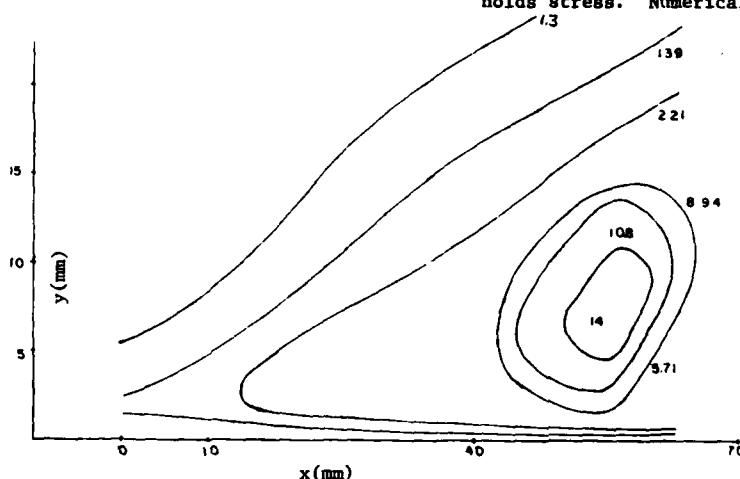


Fig. 6 Contours of constant amplitude of oscillation for laminar separation of an oscillating boundary layer.

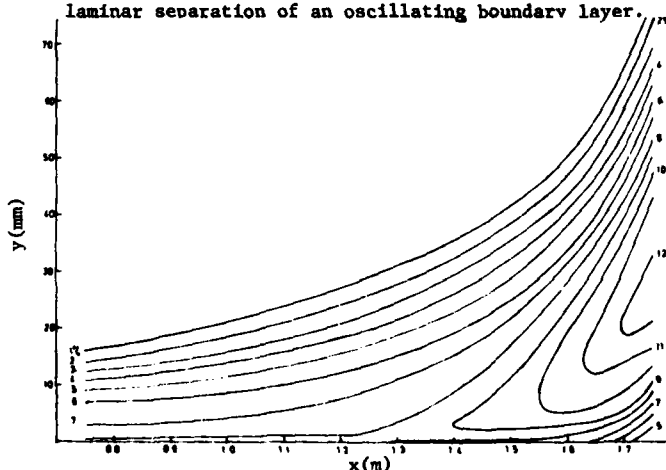


Fig. 7 Contours of constant amplitude of oscillation for turbulent separation of an oscillating boundary layer.

erates indeed a very thin layer of reversing flow which emanates from the point of separation and propagates rapidly upstream as shown schematically in Fig. 10. The region of partially reversed flow is led by a moving point of zero skin friction. Numerical and experimental evidence were provided only a few years ago. It was demonstrated indeed that this behavior is totally confined within the thickness of the boundary layer and no disturbances can be detected in the outer stream.

For oscillating flows it was recognized quite early that the flow may generate a thin layer of reversing flow during a time interval of the period. Experimental evidence became available for both laminar and turbulent boundary layers in the seventies.

Theoretical calculations of reversing unsteady boundary layers were obstructed by the separation singularity, or at least so it was believed. It was later demonstrated numerically that the point of zero skin friction is not necessarily accompanied by a singularity. This enabled numerical analysts to march their calculations through points of zero skin friction and into regions of partially reversed flow.

A problem almost untouched up to now is the possible interaction between the random and organized disturbances. Only very recently has it been demonstrated that a pulsating turbulent jet may allow the transfer of energy from the mean flow to the random turbulent motion. Interaction between the two fields may appear quite reasonable in view of modern descriptions of turbulent motion. It is now widely accepted that the bursting frequency has a deterministic character and that large and coherent structures can be detected within the turbulent boundary layer. If the discrete frequency of the external periodic disturbance is a multiple or close to a multiple to any of the above natural frequencies of the phenomenon, then it is very well possible that energy may be transferred from one field to the other.

### 3. REVERSING & SEPARATING BOUNDARY LAYERS

A number of investigators (Sears, Moore, Rott, Lin) independently recognized in the fifties that boundary layers may locally and for short periods of time, reverse without any evidence of separation. In the case of transient flows, an ever increasing adverse pressure gradient, gen-

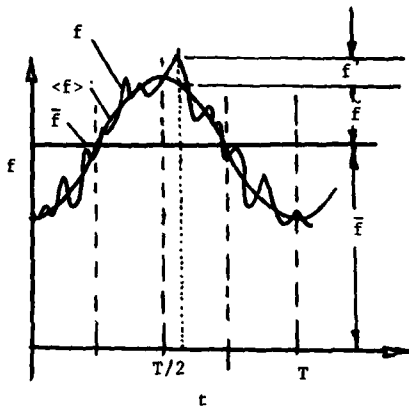


Fig. 8 The triple decomposition.

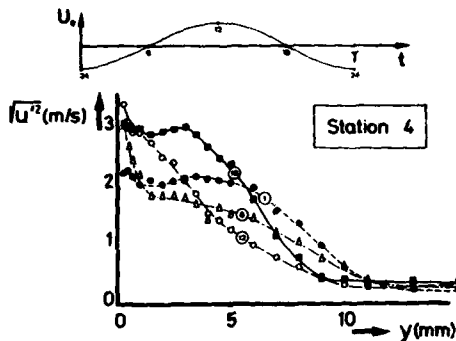


Fig. 9 The instantaneous profile of the turbulent energy for an oscillating turbulent boundary layer.

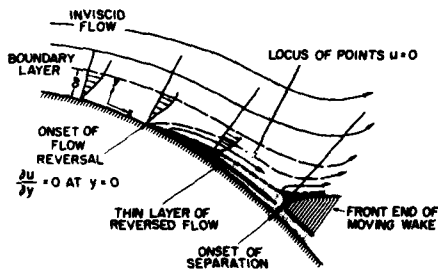


Fig. 10 Streamline pattern in the neighborhood of an upstream moving separation.

The second difficulty encountered has a mathematical character. The boundary-layer equations are parabolic. The variable  $x$  along the boundary is a time-like variable. The physical analog of parabolicity can be expressed in terms of the propagation of disturbances and equivalently zones of influence and dependence. For a steady boundary layer the zone of influence of a certain point extends to all downstream stations. If the flow is partially reversed, then the situation is more complex. Disturbances travel downstream with the speed of the outer flow and upstream, within the reversing portion of the boundary layer, with speed equal to the absolute maximum of the negative velocities as shown schematically in Fig. 11. The terms "downstream" and "upstream" we define here in terms of the direction of the outer flow. A straight-forward marching of the calculation in the downstream direction is now prohibited. For steady flows, special numerical tricks are introduced in order to march the calculations through narrow regions of reversing flows. For unsteady flows and under certain conditions it is possible to continue marching in the downstream direction if appropriate marching schemes are introduced. This is due to the fact that a second parabolic variable is introduced and the domain of influence extends in a three-dimensional domain, allowing the introduction of a differencing scheme which does not violate the Courant-Friedrichs-Levy condition.

One of the main reasons for calculating boundary layers is the need to determine the location of separation. Today we still know very little about separation, steady or unsteady. The present author feels that the features of separation control in a catalytic fashion the further development of the flow, the size and shape of the eddies in the wake, etc. However, even the definition of the phenomenon has been the source of disagreement and very rightfully so. Prandtl defines separation as the point where "a fluid-sheet projects into the free flow and effects a complete alteration of the motion". The most widely accepted definition of separation today is essentially the same. Separation is defined as the point along the solid boundary where the flow breaks away from the wall initiating a region of recirculating wake flow. The fact remains that the phenomenon is difficult to identify experimentally or analytically and there exist flow situations where one could not identify the point of separation with confidence. More on this point, the reader will find in subsequent contributions to this volume.

Interest in this area was revived in the late sixties as described in recent review articles<sup>12,13,14</sup>. It was argued that a singularity of the Goldstein type should accompany the point of separation and not the point of zero skin-friction. Numerical evidence in support of this argument were first based on calculations of steady flows over moving walls. It was demonstrated that calculations could proceed smoothly through the point of zero skin friction until the point where the MRS criterion was met, i.e.

$$\frac{\partial u}{\partial y} = 0, \quad \text{at } u = 0 \quad (8)$$

Typical features of the separation singularity were found at the point where condition (8) was met.

The MRS criterion of separation for steady flows over moving walls has been inadvertently accepted as a criterion for unsteady separation. Rephrasing the criterion proposed by Sears in the fifties, we can indeed now state that unsteady separation should be the point where the MRS criterion is met in a system of reference moving with the point of separation. In this frame the MRS point has the form of a saddle point as depicted schematically in Fig. 12.

Subsequent numerical calculations of truly unsteady flows have also indicated that the point of zero skin friction is free of any singularities and that the boundary layer behaves smoothly for a considerable distance downstream. A moving separation singularity was discovered but it was not possible to prove that the MRS criterion for unsteady separation was met. Similar numerical experiments have been carried out since then with conflicting results. In fact some authors maintain that a separation singularity will take an infinite time to appear if the flow is started from rest or if an adverse pressure gradient is suddenly or gradually imposed on an unseparated flow.

The analytical work of Williams and his associates<sup>13</sup> demonstrates that a transformation can map a certain class of unsteady separating flows over fixed walls to steady separating flows over moving walls, a case that has been well documented and understood both analytically and experimentally. In fact, most recently, Shen<sup>14</sup> proved that all unsteady separating flows can be transformed into steady flows over moving walls. These works have given more credibility to the theories connecting unsteady separation with a singularity.

Very recently some very refreshing approaches to the problem have appeared<sup>13,14</sup>. Shen<sup>14</sup> reviews extensively all earlier works and compares with the efforts of his group. It is well known by now that all

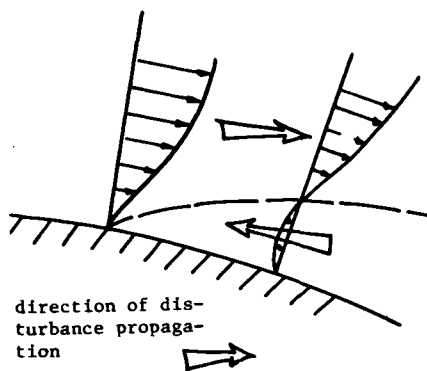


Fig. 11 Direction of propagation of disturbances in a partially reversed boundary layer.

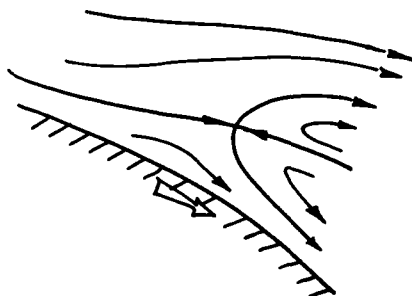


Fig. 12 Streamline pattern in the vicinity of separation over a downstream moving wall.

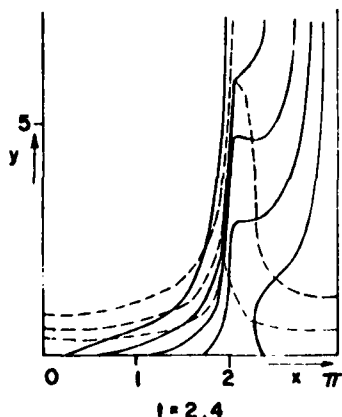


Fig. 13 Lagrangian evolution of an initially rectangular mesh.

numerical integration of the boundary-layer equations indicate the initiation of singular behavior in the form of rapid growth of the normal component of the velocity, the displacement thickness, etc. Shen and his associates therefore conclude that there should be no need to examine the boundary-layer profile in detail. Instead they propose to associate separation directly with the condition of "unmatchability". This is defined as the growth of the product  $\nu R^{1/2}$  until it violates the basic boundary layer assumption. Their investigations point out analytically that indeed it is possible that singular separation may emerge at a finite time under suitable conditions.

In an alternative approach<sup>14</sup>, the problem is recasted in Lagrangian terms. Numerical calculations then follow the particle paths. For convenience, Shen and his associates define a rectangular mesh at  $t = 0$  and follow its subsequent shape development as time progresses. Their results, for an outer flow distribution that corresponds to the flow around a cylinder and a uniform initial boundary layer are shown in Fig. 13. A clear singularity is emerging at a finite time which by extrapolation was found to correspond to a dimensionless time of 2.75. The topography of the distorted mesh is a beautiful visualization of the singular behavior appearing in the form of a vertical barrier, which eventually blocks the passage of particles at the point of separation.

Inspired by his work on three-dimensional boundary layers and the analogy between three-dimensional steady flow and two-dimensional unsteady flow, Wang<sup>15</sup> proposes to investigate the phenomenon by studying the topography of the "generalized skin friction" lines on the  $t$ - $x$  plane. Such lines are defined as the lines that are tangent at each point in the  $t$ - $x$  plane to the slope given by  $\partial u/\partial y$  at  $y = 0$ . Wang works out a few interesting examples which corroborate but also contradict earlier results. More details on these recent contributions the reader will find in the accompanying paper "Analytical Methods for Prediction of Unsteady Laminar Boundary Layers".

Finally a short comment is perhaps pertinent here with regard to recent experimental evidence on laminar or turbulent separation. The amplitude of externally imposed oscillations on both laminar and turbulent flows appears to grow violently as separation is approached. In fact if one proceeds beyond separation, one finds that the point of separation represents the peak of the amplitude amplification as shown in Figs. 6 and 7. Similar trends have been demonstrated by the random fluctuations of a turbulent boundary layer.

#### REFERENCES

1. Stewartson, K., "The Theory of Unsteady Laminar Boundary Layers" in *Advances in Applied Mechanics*, Vol. 6, pp. 1-37, Academic Press, New York, 1960.
2. Stuart, J. T., "Unsteady Boundary Layers" in *Laminar Boundary Layers*, L. Rosenhead (ed.), Oxford, pp. 349-406, 1964.
3. Rott, M., "Theory of Time-Dependent Laminar Flows", in *Theory of Laminar Flows*, F. K. Moore (ed.), Princeton University Press, Princeton, N.J., 1964.
4. Stuart, J. T., "Unsteady Boundary Layers" in *Recent Research of Unsteady Boundary Layers*, E. A. Eichelbrenner (ed.), Vol. 1, pp. 1-46, 1971.
5. Riley, N., "Unsteady Laminar Boundary Layers", *SIAM Review*, Vol. 17, pp. 274-297, 1975.
6. Wirz, H. J., "Computation of Unsteady Boundary Layers", *Lecture Notes in Physics*, No. 41, *Progress in Numerical Fluid Dynamics*, Wirz, H. J., ed., Springer-Verlag, Berlin, pp. 442-476, 1975.
7. Telionis, D. P., "Calculations of Time-Dependent Boundary Layers", in *Unsteady Aerodynamics*, ed. R. B. Kinney, Vol. 1, pp. 155-190, 1975.
8. Telionis, D. P., "REVIEW - Unsteady Boundary Layers, Separated and Attached", *Journal Fluids Engineering*, 101, pp. 29-43, 1979.
9. Telionis, D. P., *Unsteady Viscous Flow*, Springer, to appear.
10. Riley, N., "Oscillatory Viscous Flows, Review and Extension", *Journal Inst. Math. Appl.*, 3, pp. 419-434, 1967.

11. McCroskey, W. J., "Some current Research in Unsteady Fluid Dynamics - The 1976 FREEMAN SCHOLAR LECTURE", Journal of Fluids Eng., Vol. 99, pp. 8-38, 1977.
12. Sears, W. R. and Telionis, D. P., "Boundary Layer Separation in Unsteady Flow", SIAM J. Appl. Math., 28, pp. 215-235, 1975.
13. Williams, J. C., "Incompressible Boundary-Layer Separation" in Annual Review of Fluid Mechanics, eds. M. VanDyke, J. V. Wehausen, J. L. Lumley, 9, pp. 113-144, 1977.
14. Shen, S. F., "Unsteady Separation According to the Boundary-Layer Equation" in Advances in Applied Mechanics, 18, pp. 177-220, 1978.
15. Wang, K. C., "Unsteady Boundary Layer Separation", Martin Marietta Laboratories, Report MML TR 79-16c, April 1979.

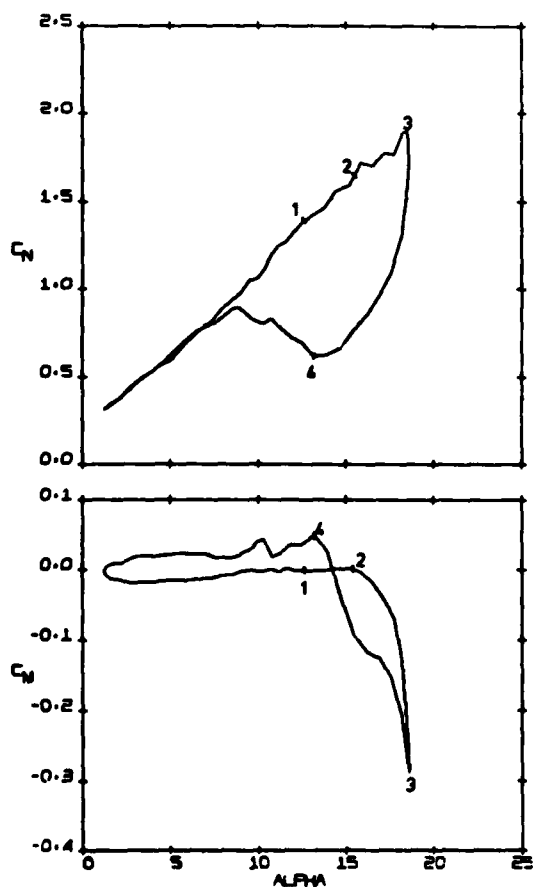
## A QUALITATIVE DISCUSSION OF DYNAMIC STALL

Dr T.S.Beddoes  
Aeromechanics Dept.  
Westland Helicopters  
Yeovil, Somerset BA20 2YB  
UK

### INTRODUCTION

Definition of the onset of stall is of fundamental importance in the design of flight vehicles. A large part of the flight boundary is defined by the phenomena that are associated with stall; i.e. limiting loads, stability and vibration. The precise behaviour of the stall is subject to many secondary aspects of a given configuration and in the last analysis is most often determined by direct or related wind tunnel tests on a static model. It has been recognised for some time that in a dynamic environment; i.e. gusts, manoeuvring flight, the statically determined loads are likely to be exceeded. Until recently however, it has been difficult to quantify the magnitude of the increase and to define precisely the significance of related parameters. Even though much has been learned of the gross behaviour during dynamic stall, it is apparent that in detail, much more needs to be defined experimentally, and that existing theory is quite inadequate.

For many aeroelastic studies, it is sufficient to include only linearised unsteady aerodynamics; this constitutes 'classical' flutter. A class of problems involving unsteady separation has been recognised and studied, mainly with reference to control surface design; i.e. buzz. Another set of nonlinearities is associated with stall flutter which involves more primary structure. This is associated with operation at or near the stall boundary as defined for the static case, but introduces a purely aerodynamic source of negative damping which can fundamentally alter the aeroelastic behaviour. The non-linearities associated with transient separation effects may introduce characteristics not simply interpreted in terms of linearised coupling, stability or instability, but never-the-less associated with periodic effects and come under the general classification of vibration. In this form, the phenomenon can be sufficiently severe to effectively constitute a limiting factor in the flight envelope; e.g. control load growth in the helicopter and allowable buffet penetration for manoeuvring aircraft. It would be desirable to form a distinction between dynamic stall effects and buffet. This may be done by assigning to buffet the field of flow separation phenomena which does not involve any major re-attachment.



FORCES AND MOMENTS	
1	EXCEEDS STATIC MAXIMUM LIFT. EXTRAPOLATE LINEAR RANGE.
2	PITCHING MOMENT DIVERGENCE. VORTEX LIFT PRESENT.
3	MAXIMUM LIFT, RAPID DECAY. MAXIMUM PITCHING MOMENT.
4	READJUST TO LINEAR RANGE.

FLOW STRUCTURE	
1	FLOW REVERSALS WITHIN BOUNDARY LAYER. FORMATION OF VORTEX
2	VORTEX DETACHES AND MOVES OVER AIRFOIL SURFACE.
3	VORTEX PASSES TRAILING EDGE. FULL STALL DEVELOPS.
4	REATTACHMENT OF FLOW.

FIG. 1. DYNAMIC STALL EVENTS

## 1. GROSS FEATURES OF DYNAMIC STALL

The gross features of dynamic stall as manifest during a cyclic variation of pitch angle are illustrated in figure 1. Four distinct phases of flow development may be discerned. The first and most fundamental consequence of an appreciable rate of increase of attack is that values of lift coefficient beyond the static stall are achieved whilst the gross changes in the boundary layer which precede stall are developing. Flow reversals within the boundary layer are observed to develop during this period without any gross changes in the flow external to the boundary layer and thus the force and moment characteristics appear as an extrapolation of the normal attached flow regime. The second phase is characterised by the re-organisation of the flow external to the boundary layer. Gross flow separation is observed to develop on the forward part of the airfoil, or behind the recompression shock wave if appropriate, and is associated with the shedding of a concentrated vortex. Subsequent motion of the vortex over the surface continues to generate increased lift, but gross changes in pitching moment result from re-distribution of the chordwise pressure. Passage of the vortex beyond the trailing edge of the airfoil initiates the third phase which constitutes the complete breakdown of the external flow. Lift decays rapidly and, correspondingly, the lift induced pitching moment. If and when, during the cycle, the angle of attack falls below the normal static stall angle, the flow will re-attach from the leading edge. This is the fourth phase during which the non-separated flow characteristics are resumed at an appropriate time-scale.

Based on observation of extensive test data for many different airfoils, it has been concluded that, to a first order, there is a common time-scale to be associated with the above events, and somewhat independent of airfoil geometry, intermediate motion and Mach Number. If time is non-dimensionalised by introducing the factor  $V/C$ , then the resulting parameter  $\tau$  is equivalent to the number of chord lengths travelled. Adopting this time base, two cycles of the example shown in figure 1 are re-plotted to form figure 2. The above events are noted, with the exception of the re-attachment phase, and two more parameters are introduced to illustrate the corresponding behaviour of the chordwise pressure distribution.

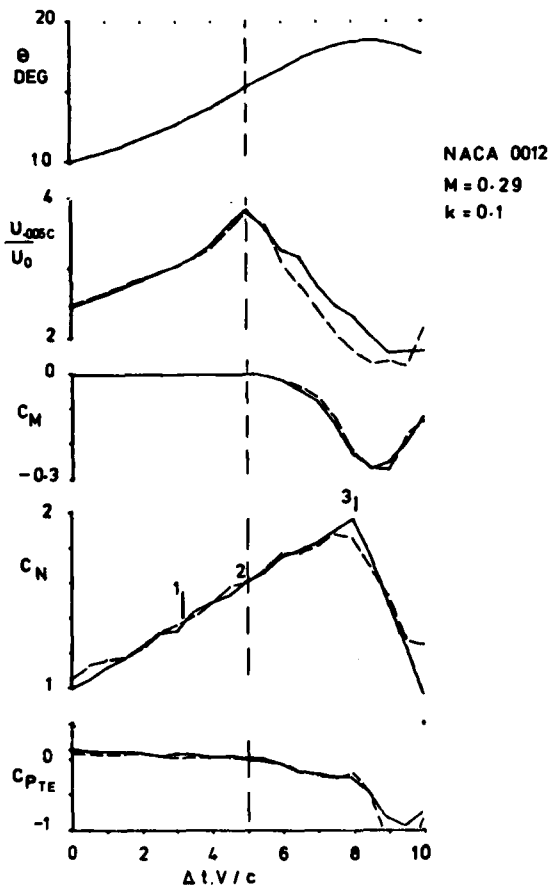


FIG.2. DYNAMIC STALL - TIME SCALE

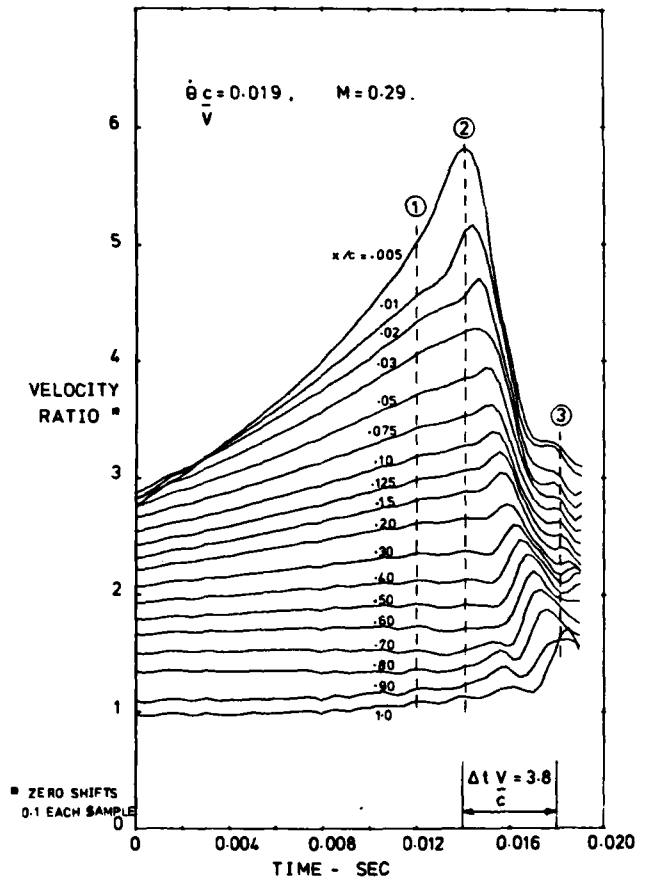


FIG.3. DYNAMIC STALL - CHORDWISE PROGRESSION

These are, leading edge ( $\frac{1}{2} c$ ) velocity ratio and trailing edge pressure. The first of these shows the continued growth of the leading edge suction peak and the detachment of the leading edge vortex which occurs approximately two chord lengths after the limiting static  $C_{l, max}$  has been achieved. Even after this event, the build-up of lift continues smoothly until the abrupt collapse associated with departure of the primary shed vortex. A mild progressive trailing edge pressure divergence is observed initially; it accelerates somewhat during motion of the vortex and collapses completely in conjunction with the lift. The second stage of development takes place during 3 or 4 chord lengths of travel.



A more complete picture of the build-up of local velocities and the progression of the vortex induced wave is shown in figure 3. This example is taken from the response time history to a ramp input thus angle of attack is increasing monotonically with time throughout. The local Mach Number corresponding to the highest observed leading edge pressure is 1.38 and the chordwise velocity gradient is so high that the presence of a shock wave is difficult to detect. A non-dimensional time-scale is included from which it can be seen that development of vortex shedding and separation corresponds to the example shown in figure 2.

With variations in the forcing parameters such as amplitude, mean angle and frequency, the events described above, shift around the cycle and produce significant changes in the characteristics of the lift and moment curves. For example, (from the tests of reference 1) figure 4 shows the effect of increasing frequency at nominally constant mean angle amplitudes and illustrates the highly negative pitch damping which may occur. Vortex shedding is delayed, with increasing frequency, until it finally occurs after the maximum angle has been reached and after the maximum value of lift has been achieved. It is apparent from figure 4 that finally a frequency has been reached which does not allow sufficient time for the somewhat simplified sequence of events discussed so far to be completed. Thus there is an upper limit beyond which the whole physical process must change.

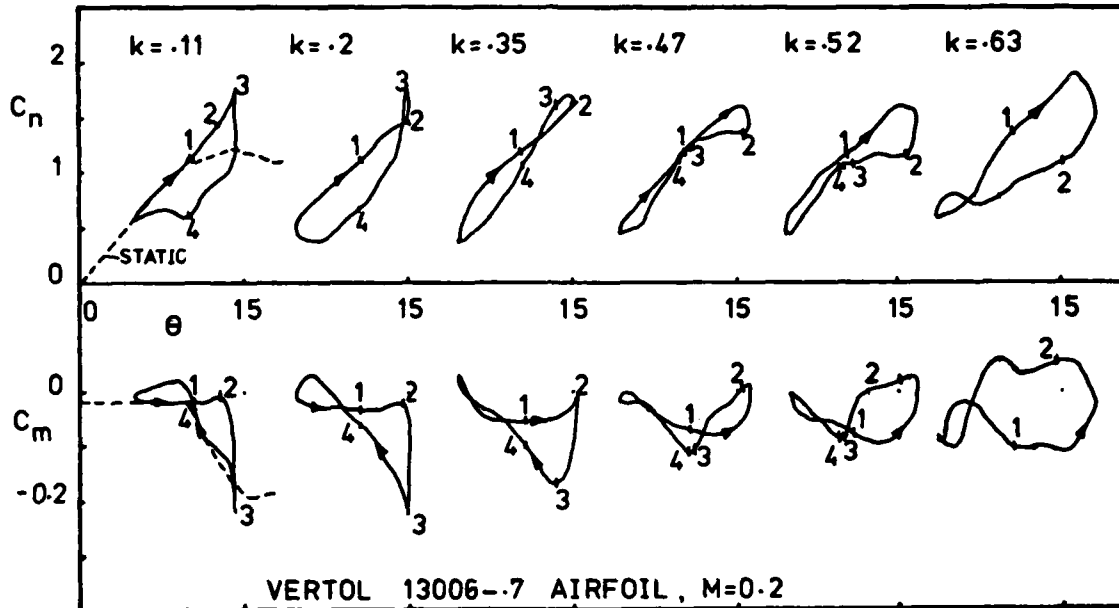


FIG.4. PHASING OF STALL EVENTS, INCREASING FREQUENCY

This reduced frequency appears to be around 0.6 and has a period which is equivalent to about 5 chord lengths of travel. It is possibly more than a coincidence that some tests (reference 2) designed to investigate the effect of increasing frequency on the validity of the Kutta condition determined a similar limit in spite of being confined to low amplitude around zero lift. Another region for which the conceptual model described above breaks down is generated when the minimum angle of attack exceeds the range required for re-attachment of the flow. In this case, depending on the degree of departure, partial re-attachment may occur and due to the early phasing of the subsequent separation, quite large positive values of damping may be generated.

An airfoil encounter with a gust or alternative form of discontinuity in the flow field produces a monotonically increasing angle of attack which may be idealised as a ramp function, and is most commonly initiated from the fully attached flow state. The same sequence of stall events is observed in this case and perhaps more clearly demonstrates the consistency of behaviour up to extremely high rates, as demonstrated in reference 3 in one of the first published accounts of such experiments.

Considerable variability in the details of behaviour during the first two phases of stall have been observed. For the first phase, at least, this is not surprising considering the variability exhibited by the static stall where determining factors must carry over to some extent, into the dynamic case. References 4, 5 and 6 present much information on this topic, particularly concerning the progression of reversed flow within the boundary layer. A common feature is the rapid acceleration of flow reversal as it extends into the forward part of the chord, culminating in the accelerated growth and detachment of the primary vortex shed at moment stall. Some less significant shedding of vortices may occur during this phase, particularly at low Reynolds Number.

It has been observed that the presence of the classical leading edge laminar separation bubble has only secondary effect on the dynamic stall process which subsequently occurs via re-separation of the turbulent boundary layer. Reynolds Number and airfoil profile appear to influence the location of the primary vortex within the forward 20% of the chord at low Mach Number. At higher Mach Numbers, the primary separation is associated with the region at the foot of the upper surface shock wave.

Contrary to the static case, Reynolds Number appears to have only minor effects on strongly dynamic stall. Some recent tests at constant Mach Number of 0.3 and R.N. of  $0.9 \times 10^6$  and  $2.5 \times 10^6$  showed very similar dynamic stall angles, although the static angles for pitching moment break differed by more than two degrees. The propagation rate of the primary vortex is consistently less than 50% of the free stream velocity; reference 7 provides data on this aspect, indicates some dependence on reduced frequency and observes that the initial rate is lower still.

As noted, for increasing angle, the lift continues to grow after the primary vortex has detached and the leading edge suction has collapsed. In many cases the lift slope increases above the value for attached flow; e.g. reference 5. This excess vortex lift is most apparent at low free stream Mach Number and seems to disappear with increasing Mach Number.

The final two stages are not only less consistent in detail but also much less repeatable under conditions of harmonic forcing. There is evidence of secondary vortex shedding which interacts strongly with the motion, and presumably has its own time scale. This raises the possibility of sub-harmonic occurrences. However, the gross features of abrupt decay in circulation and delayed resumption of unseparated characteristics are common.

A form of excitation not considered so far consists of plunge motion which is perhaps closer in nature to gust encounter, since it involves increase in angle of attack without pitch motion. Some test results have been presented in reference 8. The features of stall development in this instance are substantially the same as exemplified for pitch motion. Some slight differences in the onset of stall can be shown to result from pitch rate effects on the velocity and gradient in the leading edge region and the relative trajectory of the shed vortex is, of course, modified, but overall these effects are of secondary importance. Similar conclusions were reached in reference 10, which reports on tests utilising a sinusoidal gust generator.

The effect of sweep on dynamic stall has been investigated in reference 9. Results show an additional delay in the angle of attack for the collapse of leading edge suction, pitching moment divergence and maximum lift over and above that which would be anticipated from application of simple sweep laws. Harmonic forcing was used to generate the data and a characteristic of the test results for cycles of oscillation which include progressively more grossly separated flow was a failure to regenerate the unseparated lift at low angles where this would be anticipated. The result was an overall shift of the lift curve to higher angles, and consequent delays in occurrence of the dynamic stall events. In general, onset of separation effects occurred at the same or slightly lower values of  $C_N$  based on the appropriate normalisation. Thus it might be anticipated that for initial conditions for which simple sweep laws provide an adequate representation, then the dynamic behaviour may likewise prove similar. In the event of fully developed stall, the subsequent changes in re-attachment and persistence of trailing edge separation will have an effect on the resulting level of circulation, and hence effect the initial conditions for subsequent stall. This consideration is particularly relevant to the helicopter blade condition where sweep is increasing very rapidly and the steady state boundary layer behaviour typical of the swept condition may not have time to develop.

## 2. OPERATING LIMITS

To a large extent the operational limitations of any flight vehicle are determined by stall. The dynamic case constitutes a refinement of the boundaries established by static stall characteristics. Initially, structural and mass properties are selected so that the onset of flutter or instability as predicted by linearised analysis is not a limiting factor. Non-linearities associated with operation in the proximity of the stall introduce aeroelastic phenomena that, potentially, may prove disastrous.

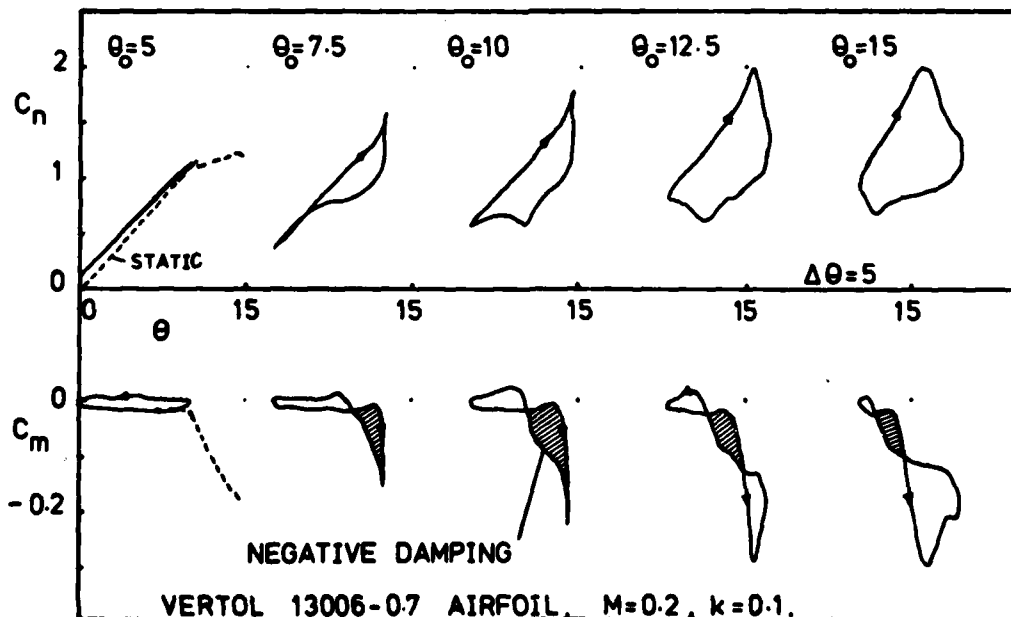


FIG.5. DEVELOPMENT OF NEGATIVE DAMPING

The least subtle and most easily labelled phenomena is stall flutter which occurs when negative aerodynamic damping converts an otherwise stable mode into a divergence or limit cycle oscillation. The growth and decay of negative damping in torsion, for a given amplitude and frequency of oscillation, as the mean angle is increased is illustrated in figure 5 (from reference 1). Positive pitch damping is represented by a negative value of the line integral  $\int C_m d\theta$ , which corresponds to a counter clockwise loop in the  $C_m$  diagram. Initial penetration of stall introduces an additional clockwise loop which may grow until it predominates. Further penetration produces a  $C_m$  break which is sufficiently early in the cycle that maximum  $C_m$  occurs whilst  $\theta$  is still increasing, thus introducing another loop of counterclockwise sense. By this mechanism, positive damping is re-instated when separation is present for a large part of the cycle. A particular case of increasing frequency acting to reduce negative damping is shown by figure 4. In this instance, the onset of the pitching moment break is delayed in the cycle thus restoring the positive potential damping. At a higher mean angle ( $20^\circ$ ), the opposite happens.

It can be seen from these examples that the phasing of the dynamic stall events throughout a cycle of oscillation completely determines the resultant damping. As Mach Number increases, these general characteristics are retained for a while, although for a specific structural frequency, by definition, the reduced frequency decreases in the inverse proportion, which may be a significant factor. The onset of reduced damping follows the trend defined by the pitching moment break from static data, but precedes this event by a margin determined primarily by the amplitude of the oscillation. An example stability boundary is shown in figure 6 (from reference 1); the two frequencies given, 48 Hz and 72 Hz, correspond at  $M = 0.2$  to reduced frequencies of 0.45 and 0.67.

A rapid increase in angle of attack near the stall results in maximum values of lift and pitching moment in excess of those obtained from static tests. Thus a singular event such as a discrete gust or rapid manoeuvre will produce maximum loads greater than anticipated on the basis of static stall. This may be simulated experimentally by forcing with a ramp function as demonstrated in reference 3.

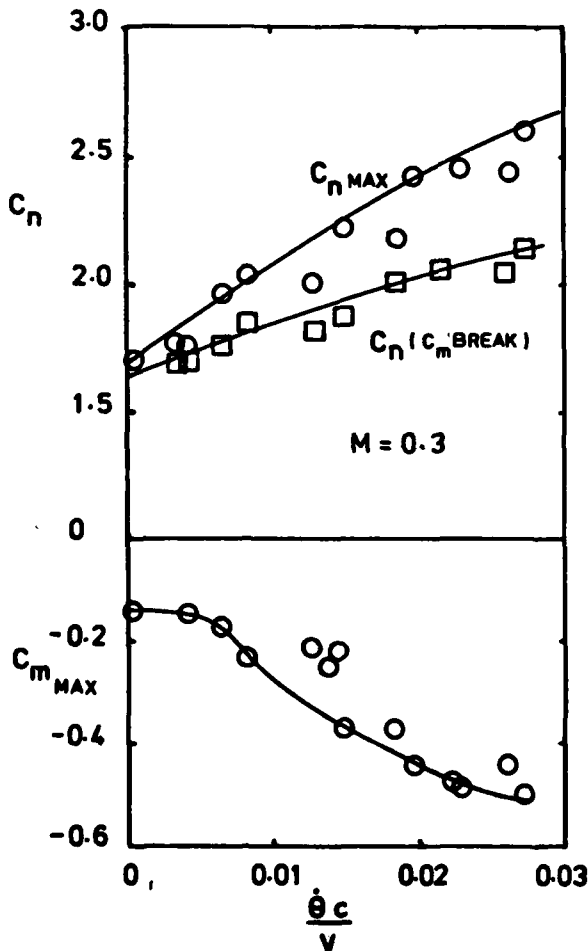


FIG.7. LIMITING VALUES FOR RAMP INPUT (CONSTANT PITCH RATE)

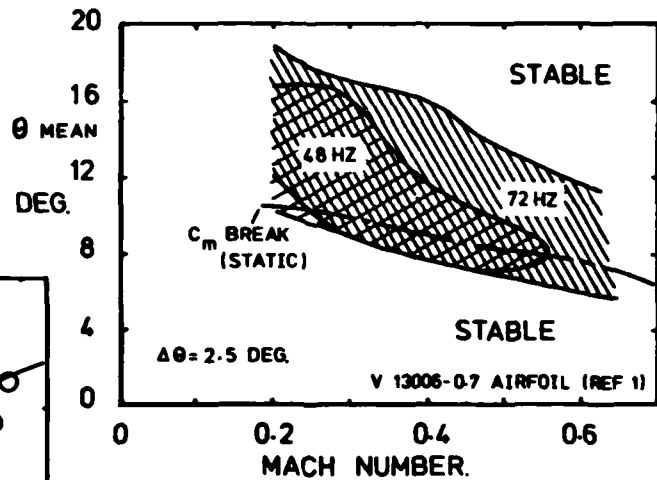


FIG.6. EXTENT OF UNSTABLE REGION

Some results of more recent tests are presented in figure 7. In addition to the maximum force and moment values, the onset of vortex shedding and the corresponding moment divergence are shown. As Mach Number increases, the drop in lift at the static stall becomes less pronounced until, at high subsonic  $M$ , the normal force continues to increase steadily through stall (gross separation). This characteristic persists into the dynamic case and modifies the pitching moment behaviour accordingly. Thus the pitching moment break assumes greater significance in denoting the onset of buffet. If structural response is significantly large, the possibility exists of initiating stall flutter.

Bending or flapping mode response is influenced by unsteady effects. In the event of stall being encountered, it is possible for the phase relationship between displacement and load response to shift by  $180^\circ$  thus producing a negatively damped or limit cycle form of oscillation.

A summary of some results from reference 8 is presented in figure 8. Co-incidentally large pitching moments may be generated, thus raising the possibility of coupled torsion-bending motion if the two natural frequencies are close.

In recent years, a large body of experimental data on dynamic stall has been accumulated. A full analysis in detail and identification of second order effects has not been completed. There is still much therefore, to be learned from existing test data. A qualitative understanding of dynamic stall phenomena has emerged, however, most emphasis has been placed on the low Mach Number range.

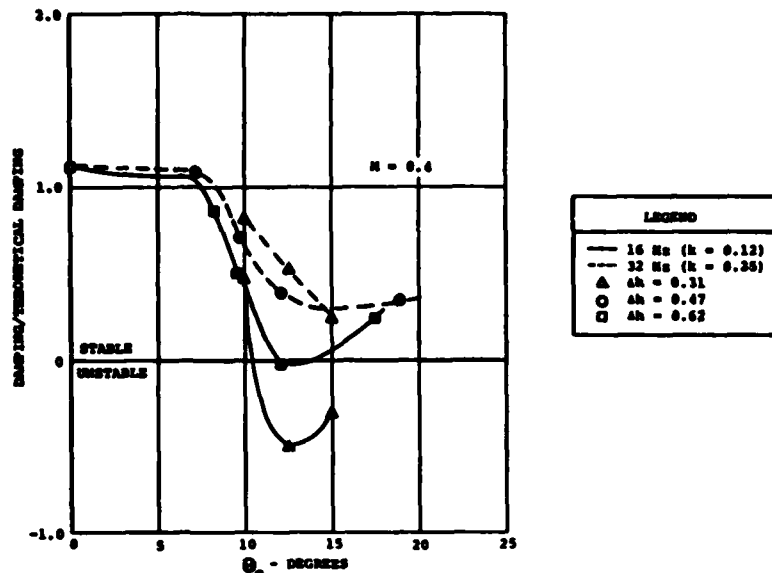


FIG. 8. Summary of Damping Data in Vertical Translation for NACA 0012 (Modified) Airfoil.

#### References

1. Gray L. et-al. Wind tunnel tests of thin airfoils oscillating near stall. USAAVLABS TR68-89 1969
2. Satyanarayana, B. Davis, S. Experimental studies of unsteady trailing edge conditions. AIAA Journal, Feb. 1978.
3. Häm, N.D., Garelick, M.S., Dynamic stall considerations in helicopter rotors. Journal of the American Helicopter Society, April 1968.
4. Carr, L.W., McAlister, K.W., McAlister, K.W., McCroskey, W.J., Analysis of the Development of Dynamic Stall based on oscillating airfoil experiments. NASA TN.D-8382 January 1977.
5. Authors as above; Dynamic Stall Experiments on the N.A.C.A.0012 Airfoil, NASA Technical Paper 1100, January 1978.
6. McAlister, K.W., Carr, L.W. Water Tunnel Experiments on an Oscillating Airfoil. NASA TM.78446. March 1978.
7. Carta, F.O., Chordwise Propagation of Dynamic Stall cells in an oscillating Airfoil. A.I.A.A. Preprint 75-25, 1975.
8. Liiva, J. et-al. Two Dimensional Tests of Airfoils Oscillating near stall. USA.VLABS, TR.68-13, 1968.
9. St. Hilaire, A.O. et-al. The influence of Sweep on the Aerodynamic loading of an Oscillating NACA.0012 Airfoil. Vol.1 - Technical Report, NASA CR.3092, 1979.
10. Parker, A.G., Bicknell, J., Some Measurements on Dynamic Stall. Journal of Aircraft, July 1974.

## SOME FEATURES OF LINEAR COMPRESSIBILITY

G.J. Hancock,  
Dept. of Aeronautical Engineering,  
Queen Mary College, University of London, U.K.

### 1. WAVE EQUATION

At subsonic Mach numbers, below the transonic Mach number range, most theoretical prediction methods for inviscid flows are based on linearised equations, which are equivalent to superimposing small disturbances on a uniform stream. Small disturbances are represented by the acoustic wave equation. The first part of this lecture is concerned with a description of some of the characteristic features of linear wave propagation in air at rest.

The basic wave equation, relative to space fixed axes, is

$$\nabla^2 \phi = \frac{1}{a_0^2} \frac{\partial^2 \phi}{\partial t^2}, \quad \nabla^2 \quad (1)$$

where  $\nabla$  is the Laplacian operator,

$a_0$  is the speed of sound, given by

$$a_0^2 = \gamma p_0 / \rho_0 = \frac{dp}{d\rho}, \quad (2)$$

$\gamma$  is the ratio of specific heats,  $p_0$  and  $\rho_0$  are the pressure and density of the undisturbed air.

The fluid velocity vector  $\underline{q}(u, v, w)$  is given by

$$\underline{q} = \text{grad } \phi \quad (3)$$

and

$$p - p_0 = -\rho_0 \frac{\partial \phi}{\partial t} \quad (4)$$

Eqn.(4) is essentially the unsteady Bernoulli equation with the  $\frac{1}{2}\rho_0 q^2$  term neglected.

The basis of eqns.(1-4) is that the magnitude of the velocity field is small compared with the speed of sound  $a_0$  so that the velocity squared terms can be neglected. It should be recognised that the speed of sound, which is the speed at which disturbances are propagated through the air, can only occur at a microscopic level by a molecular collision process; a high wave velocity is compatible with the small fluid velocities only because the assumption is made that the fluid can be regarded as a continuum.

In a one dimensional flow

$$\frac{\partial^2 \phi}{\partial x^2} = \frac{1}{a_0^2} \frac{\partial^2 \phi}{\partial t^2} \quad (5)$$

A general solution of eqn.(5) is

$$\phi(x, t) = f(x - a_0 t) + g(x + a_0 t) \quad (6)$$

where  $f, g$  are arbitrary functions; the function  $f$  represents waves which are moving in the positive  $x$  direction with velocity  $a_0$  while the function  $g$  represents waves moving in the negative  $x$  direction with velocity  $a_0$ . One dimensional waves are of relevance in wave propagation along pipes; this aspect is discussed further later in this lecture.

In a three dimensional radial flow which depends on  $r$  only, and not on any angles, then the basic eqn.(1) can be rearranged into the form

$$\frac{\partial^2 (\phi/r)}{\partial r^2} = \frac{1}{a_0^2} \frac{\partial^2 (\phi/r)}{\partial t^2}. \quad (7)$$

Thus the solution of eqn.(7) can be written in the form

$$\phi/r(t, t) = f(r - a_0 t). \quad (8)$$

Only outward travelling waves are indicated here, inward travelling waves arise with reflections. The velocity and pressure field follow by application of eqns.(3,4) so

$$q_r(r, t) = -f'(r - a_0 t)/r + f'(r - a_0 t)/r \quad (9)$$

$$p - p_0 = \rho_0 a_0 f'(r - a_0 t)/r \quad (10)$$

Note that in the far field, for  $r$  large, the velocity  $q_r$  and pressure  $p-p_0$  are in phase but not in the near field, for  $r$  small.

## 2. SOURCE TYPE FLOWS

Consider a three dimensional source type flow; take

$$\phi(r,t) = -\frac{m}{4\pi r} H(a_0 t - r) \quad (11)$$

where  $H(\tau)$  is the step function defined by

$$\left. \begin{aligned} H(\tau) &= 0 & \tau < 0 \\ H(\tau) &= 1 & \tau > 0 \end{aligned} \right\} \quad (12)$$

Note that the differential of the step function is the delta function,

$$\delta(\tau) = dH(\tau)/d\tau$$

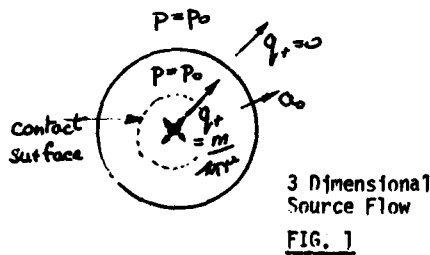
Eqn.(11) is the simplest solution of the general solution given by eqn.(8); eqn.(11) represents a uniform source flow which commences at  $t=0$ .

From eqns.(9,10)

$$q_r(r,t) = \frac{m}{4\pi r^2} H(a_0 t - r) + \frac{m \delta(a_0 t - r)}{4\pi r} \quad (13)$$

$$p - p_0 = \rho_0 a_0 \frac{m}{4\pi r} \delta(a_0 t - r) \quad (14)$$

Eqn.(13) states that as the wave front propagates outward from  $r=0$ , starting at  $t=0$ , as the source flow commences, there is an impulse in the velocity field as the wave passes radius  $r$ ; after the wave has passed the flow immediately takes up its steady state source flow velocity. Behind the wave front there is another spherical surface called the contact surface; the flow inside the contact surface comprises the fluid which has emanated from the source, the flow outside the contact surface is fluid which is moving outward due to passage of the compressive wave front as shown in Fig. 1. The fluid is



given its outward motion by the pressure pulse as the wave front passes. Eqn.(14) states that the pressure ahead and behind of the wave front is the same, namely the undisturbed air pressure  $p_0$ ; this is because  $q_r^2$  is assumed to be negligible. The corresponding source type flow in one dimension is from eqn.(6)

$$\phi(x,t) = (l(x-a_0 t) H(a_0 t - x)) \quad (15)$$

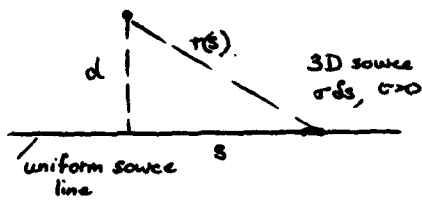
considering only waves travelling in the positive  $x$  direction; then, as shown in Fig.2

$$u = \frac{\partial \phi}{\partial x} = l H(a_0 t - x) \quad (16)$$

$$p - p_0 = \rho_0 a_0 l H(a_0 t - x) \quad (17)$$

For this one dimensional case, again as the wave front passes, the air immediately takes up its final steady flow velocity. Now, however, in distinction to the three dimensional flow, there is an increase in pressure in the entire flow behind the wave front. There are no impulses in either velocity or pressures associated with the wave front.

The two dimensional flow is somewhat different. Essentially, the velocity potential for a two dimensional source flow, commencing at  $t=0$  can be obtained by integrating the three dimensional solution. Consider a line of three dimensional sources of uniform strength  $q$ /unit length for  $t>0$ , then the flow represents a two dimensional situation. Referring to Fig.3, the velocity potential at a point  $d$  from the source line is, by integration of eqn.(11)



2D Source  
FIG. 3

$$\phi(d,t) = 0, \quad a_0 t < d$$

$$\phi(d,t) = -2 \int_{s=0}^{s^2=a_0^2 t^2 - d^2} \frac{\sigma ds}{4\pi(d^2+s^2)^{3/2}}, \quad a_0 t > d$$

Thus

$$\phi(d,t) = -\frac{\sigma}{2\pi} \sinh^{-1} \left\{ \frac{(a_0^2 t^2 - d^2)^{1/2}}{d} \right\} H(a_0 t - d) \quad (18)$$

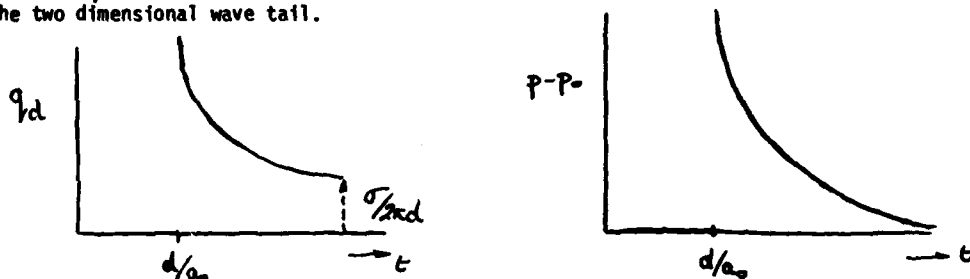
Note that  $\phi(d,t)$  becomes indeterminate as  $t \rightarrow \infty$ . However, the two dimensional velocity field and pressure field become

$$q_{rd}(d,t) = \frac{\sigma}{2\pi d} \frac{a_0 t}{(a_0^2 t^2 - d^2)^{1/2}} H(a_0 t - d), \quad (19)$$

and

$$p - p_0 = \frac{\sigma \rho_0 a_0}{2\pi} \frac{H(a_0 t - d)}{(a_0^2 t^2 - d^2)^{1/2}} \quad (20)$$

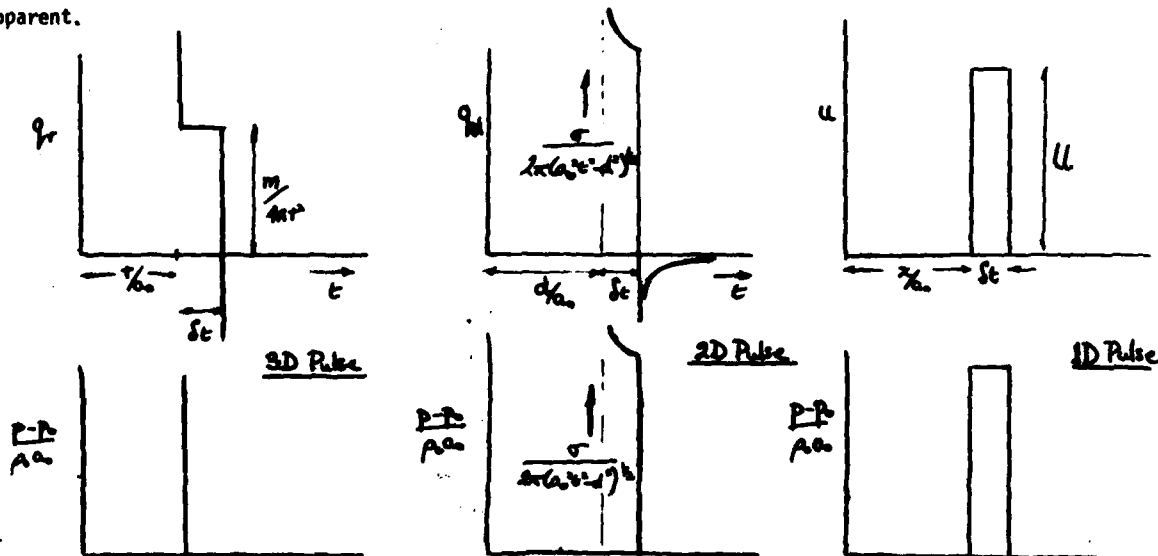
So in two dimensions the steady state is not immediately set up behind the wave front for neither the velocity field  $q_{rd}$  nor the pressure field  $p - p_0$ ; this phenomenon, as shown in Fig. 4, is sometimes referred to as the two dimensional wave tail.



2 D Source Characteristics  
FIG. 4

Although there appears to be an anomaly in the two dimensional case as shown in Fig. 4 compared with the one and three dimensional cases as shown in Figs. 2, 1, there is progression in the form of the pressure responses, from a pulse in three dimensions, a decreasing tail in two dimensions and a uniform pressure in one dimension.

A source pulse can be defined as a source which exists for a small time  $\delta t$  only; typical variations of the velocity fields and pressure fields are shown in Fig. 5. The two dimensional 'tail' is now more apparent.



Source Pulses  
FIG. 5

A more 'gentle' source pulse which builds up and decays continuously, like  $e^{-(t^2+T^2)}$  for example, essentially rounds off the discontinuities shown in Fig. 5, as shown in Fig. 6.

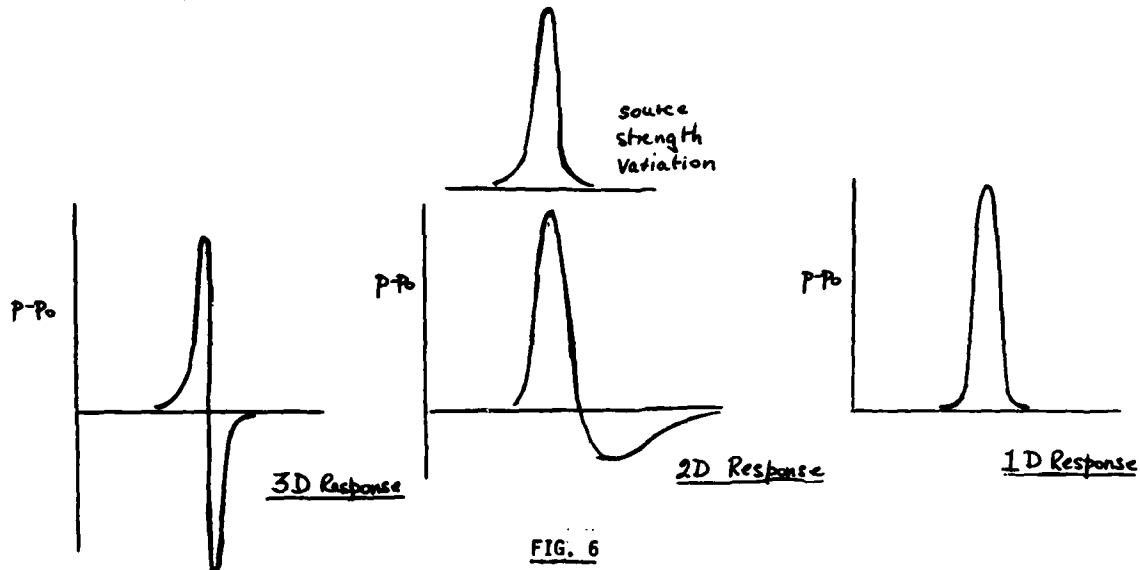


FIG. 6

To obtain the flow field for an arbitrary source strength varying with time; if  $m(T)$  is the source strength per unit time at time  $T$ , then a source of strength  $m'(T)dT$  is introduced into the flow at time  $T$ , where the dash denotes differentiation with respect to  $T$ . Thus the flow field and pressure field can be built up by superposition.

In 3 dimensions from eqn.(13)

$$q_r = \int_{T=0}^{T=t-r/a_0} \frac{m'(T)dT}{4\pi r^2} + \int_{T=0}^{T=t-r/a_0} \frac{m'(T) \delta(a_0 T - t) dT}{4\pi r} \quad (21)$$

$$= m(t-r/a_0)/4\pi r^2 + m'(t-r/a_0)/4\pi r$$

and similarly

$$p-p_0 = \rho_0 a_0 m'(t-r/a_0)/4\pi r \quad (22)$$

Eqns.(21,22) are of course identical with eqns.(9,10) we have gone round full circle. The fundamental point to emphasise from eqns.(21,22) is that what happens at radial point  $r$  at time  $t$  is simply related to what happened at the source at the earlier time of  $t-r/a_0$ , the time taken for the wave to pass from the source to the point  $r$ .

It is seen from eqns.(21,22) that there is a near field where  $r$  is small and a far field where  $r$  is large; in the far field, the velocity  $q_r$  and the pressure  $p-p_0$  are in phase; in the near field the flow behaves in a quasi-static manner.

For a source varying in a simple harmonic manner,  $m(t)$  is proportional to  $m e^{i\omega t}$ , the velocity and pressure fields follow directly from eqns.(21,22).

$$q_r(r,t) = \frac{m e^{i\omega(t-r/a_0)}}{4\pi r} \left\{ \frac{1}{r^2} + \frac{i\omega}{r} \right\} \quad (23)$$

$$p-p_0 = \frac{m e^{i\omega(t-r/a_0)}}{4\pi r} \left\{ \frac{i\omega}{r} \right\} \rho_0 a_0 \quad (24)$$

Thus  $q_r$  and  $p-p_0$  are harmonic in time at constant  $r$  and harmonic in  $r$  at constant time  $t$ . If there is a surface distribution of sources, then those sources distance  $2\pi a_0/\omega$  away from each other, if in phase, can amplify their local flow and pressure fields, hence additional modulations on the flow field characteristics can be introduced.

The field induced by a source in the presence of a plane boundary can be simulated by the method of images. For example, a wave front emanating from a point source pulse situated close to a solid planar boundary leads to a radiation field as indicated in Fig.7, the image source pulse 'gives' the reflected wave behaviour.



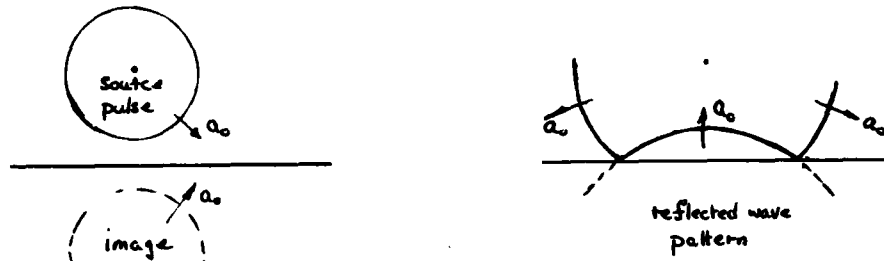


FIG. 7

The reflections of a wave system with a non-planar boundary, for example, a circular cylinder leads into the general area of diffraction which is too extensive to get involved with here.

Turning to 2 dimensions, by reference to eqns.(19,20) for an arbitrary source strength  $\sigma(\tau)$  per unit time the velocity and pressure fields are

$$q_{rd}(d,t) = \frac{a_0}{2\pi d} \int_{T=0}^{T=t-d/a_0} \frac{\sigma'(\tau)(t-T)dT}{(a_0^2(t-T)^2 - d^2)^{1/2}} ; \quad d^2 = x^2 + z^2 \quad (25)$$

$$p - p_0 = \frac{\rho_0 a_0}{2\pi} \int_{T=0}^{T=t-d/a_0} \frac{\sigma'(\tau) dT}{(a_0^2(t-T)^2 - d^2)^{1/2}} \quad (26)$$

The cases where  $\sigma(\tau)$  is a step function have been discussed.

When  $\sigma(\tau)$  is simple harmonic, i.e.

$$\sigma(\tau) = \sigma e^{i\omega\tau}$$

then the pressure perturbation becomes

$$(p - p_0)_{c \rightarrow \infty} = \frac{\rho_0 \sigma i \omega e^{i\omega t}}{2\pi} \int_{u=1}^{\infty} \frac{e^{-\lambda u} du}{(u^2 - 1)^{1/2}} ; \quad \lambda = \omega d / a_0 \quad (27)$$

This integral is a standard integral proportional to a Hankel function of second kind and zero order,

$$\int_{u=1}^{\infty} \frac{e^{-i\lambda u} du}{(u^2 - 1)^{1/2}} = -i\frac{\pi}{2} H_0^{(2)}(\lambda) \quad (28)$$

The induced velocity field for a simple harmonic source follows from eqn.(25) thus

$$q_{rd}(d,t) = \frac{\sigma i \omega e^{i\omega t}}{2\pi a_0} \int_{u=1}^{u=a_0 t/d} \frac{u e^{-i\lambda u} du}{(u^2 - 1)^{1/2}}$$

Without going through the mathematical niceties, on differentiation of eqn.(28) with respect to  $\lambda$ , then

$$\int_{u=1}^{\infty} \frac{(-iu) e^{-i\lambda u} du}{(u^2 - 1)^{1/2}} = \frac{d}{d\lambda} \left[ -i\frac{\pi}{2} H_0^{(2)}(\lambda) \right] = i\frac{\pi}{2} H_1^{(2)}(\lambda) \quad (29)$$

### 3. DIPOLE SOLUTIONS

Dipoles, or doublets, are formed by bringing together a positive source and a negative source. The line along which these sources are brought together denotes the axis of the doublet. Mathematically, the velocity potential for a dipole is obtained by differentiation of the velocity potential of a source in the direction of the negative dipole axis.

Thus in 3 dimensions with the axis of the dipole in the  $z$  direction, on differentiation of eqn.(8),

$$\phi_{\text{Dipole}}(x,y,z,t) = \left\{ +\frac{\mu(t-a_0 t)}{r^2} - \frac{\mu'(t-a_0 t)}{r} \right\} \frac{z}{4\pi r} \quad (30)$$

where  $\mu$  denotes the strength of the dipole. The pressure field is given by

$$p(x,y,z,t) - p_0 = \rho_0 a_0^2 \frac{z}{4\pi r} \left\{ \mu' \frac{(t-a_0 t)}{r^2} - \mu'' \frac{(t-a_0 t)}{r} \right\} \quad (31)$$

For a doublet there is a near pressure field and a far pressure field. When the strength of the doublet varies in a simple harmonic manner then the pressure in the far field is  $90^\circ$  out of phase with the pressure in the near field. In the far field, as can be seen by differentiation of eqn.(31), the velocity field is in phase with the pressure and along the  $z$  axis in the far field, the velocity and pressure

decrease as  $1/r$ , the same as for the source.

In two dimensions, the velocity potential for a dipole becomes

$$\phi_{\text{dipole}}(x, z, t) = \int_{T=0}^{T=t-(c^2+z^2)^{1/2}/a_0} \frac{(\partial \mu / \partial T) x a_0 (t-T) dT}{2\pi (x^2+z^2) (a_0^2(t-T)^2 - x^2 - z^2)^{1/2}} \quad (32)$$

the pressure field is best left in the form

$$p(x, z, t) - p_0 = \frac{\rho a_0}{2\pi} \frac{\partial}{\partial x} \int_{T=0}^{T=t-(c^2+z^2)^{1/2}/a_0} \frac{(\partial \mu / \partial T) dT}{(a_0^2(t-T)^2 - x^2 - z^2)^{1/2}} \quad (33)$$

#### 4. 'CIRCULATORY' FLOWS

To describe the motion of an incompressible fluid, it is convenient to explain phenomena primarily terms of vortices and vorticity, as outlined in the first lecture of this series. However, mathematically a vorticity distribution is equivalent to a doublet distribution. A two dimensional vortex sheet along the  $x$  axis say, of strength  $\gamma(x)$  (i.e. the difference in tangential velocities on both sides of the  $x$  axis) is equivalent to a doublet (or dipole) distribution of strength  $\mu(x)$  the doublet axis being normal to the  $x$  axis, where  $\mu'(x)$  is equal to  $\gamma(x)$ . In particular a finite length of uniform doublet distribution between  $x_1 \leq x \leq x_2$ , (i.e.  $\mu(x) = \mu = \text{constant}$ ) is equivalent to two equal and opposite vortices at  $x = x_1$  and  $x = x_2$ .

Hence the convection of shed 'vorticity' aft of a body in a compressible fluid can be regarded, not in terms of a distribution of vorticity, but of a doublet distribution.

Suppose that two equal and opposite 'vortices' are created at time  $t=0$  as shown in Fig. 8.

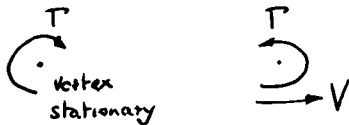


FIG. 8

One vortex remains fixed while the other convects downstream with  $V$ . This flow is equivalent to a sequence of doublets being formed; if the strength is  $\mu$  per unit length in the  $x$  direction then the distribution along the  $x$  axis at time  $T$  is given by

$$\mu dx (H(T) - H(x-VT)), \quad x > 0 \quad T > 0 \quad (34)$$

It is then possible to build up a picture of how the pattern of the flow field develops.

In general, denoting  $\mu(\xi, T)$  as the doublet strength between  $\xi=0$ ,  $\xi=c+Vt$  to represent the doublet associated with the starting process about a two dimensional aerofoil then the downwash  $w(x, t)$  is, from eqn.(32), on  $z=0$

$$w(x, t) = \int_{\xi=0}^{\xi=c+Vt} d\xi \int_{T=0}^{T=t-(x-\xi)/a_0} \frac{\partial \mu(\xi, T)}{\partial T} \frac{a_0(t-T) dT}{2\pi (x-\xi)^2 (a_0^2(t-T)^2 - (x-\xi)^2)^{1/2}} \quad (35)$$

where the finite part of the integral is taken. Eqn.(35) reduces to

$$w(x, t) = \frac{\mu(\xi, t - [c+Vt - \xi]/a_0)}{2\pi(x-\xi)} - \int_{\xi=0}^{c+Vt} \frac{\partial \mu(\xi, t - (t-\xi)/a_0)}{\partial \xi} \frac{d\xi}{2\pi(x-\xi)} + \int_{\xi=0}^{c+Vt} d\xi \int_{T=0}^{T=t-(x-\xi)/a_0} \frac{\partial \mu(\xi, T)}{\partial T} \left[ \frac{a_0(t-T)}{(a_0^2(t-T)^2 - (x-\xi)^2)^{1/2}} - 1 \right] \frac{dT}{2\pi(x-\xi)^2} \quad (36)$$

Eqn.(36) is essentially leading to the formation of the linearised integral equation for determining the doublet strength  $\mu(\xi, t)$  over a chord  $0 < x < c$  for a given downwash condition  $w(x, t)$  starting at  $t=0$ .

If  $\mu(\xi, T)$  is oscillatory in time so that

$$\mu(\xi, T) = \mu(\xi) e^{i\omega T} \quad T > 0, \quad 0 < \xi < \infty.$$

then from eqns.(35, 29)

$$w(x, t) = \left[ \int_{\xi=0}^{\infty} \left\{ \frac{-\mu(\xi) i\omega \sqrt{\frac{1}{2}} H_1^{(0)}\left(\frac{\omega(x-\xi)}{a_0}\right)}{2(x-\xi)} \right\} d\xi \right] e^{i\omega t} = \left[ \int_{\xi=0}^{\infty} \left\{ \frac{\partial}{\partial \xi} \left( \mu(\xi) i\sqrt{\frac{1}{2}} \frac{\omega(x-\xi)}{a_0} H_1^{(2)}\left(\frac{\omega(x-\xi)}{a_0}\right) \right) \frac{d\xi}{\xi-x} \right\} \right] e^{i\omega t} \quad (37)$$

Eqn.(37) is similar to the standard integral in linearised compressible oscillatory aerofoil theory.

The aim in the above analysis is to demonstrate the features of two dimensional and three dimensional sources and doublets and to show how their super position leads fairly directly to the types of integrals associated with standard linearised theory.

## 5. ONE DIMENSIONAL WAVE REFLECTIONS

It is of interest to discuss briefly one dimensional wave motions in pipes to illustrate resonance; this is of relevance to the measurement of unsteady pressures using tubes between the position where the pressure is required and a pressure transducer.

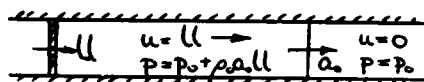


FIG.9(i)

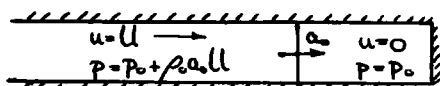


FIG.9(ii)



FIG.9(iii)

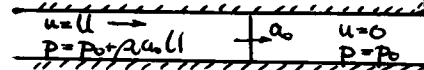


FIG.9(iv)

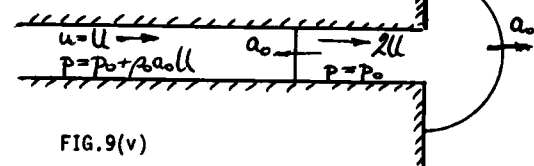


FIG.9(v)

Consider a one dimensional pipe as shown in Fig.9(i) with a piston moving in the positive  $x$  direction with velocity  $U$ , then a compressive wave passes down the tube inducing a uniform flow  $U$  and uniform pressure  $\rho_0 a_0 U$ . Now consider a compressive wave approaching a solid boundary as shown in Fig.9(ii), then, after reflection, a compressive wave is formed travelling in the negative  $x$  direction, as shown in Fig.9(iii), leaving stationary air behind the front but at a pressure  $2\rho_0 a_0 U$ . Thus by reflection, waves travelling in both positive and negative directions are possible.

Consider the case when

$$u(x,t) = \frac{U}{2} \sin \omega(t - x/a_0) + \frac{U}{2} \sin \omega(t + x/a_0) \quad (38)$$

$$= U \sin \omega t \cos \omega x/a_0$$

then

$$p(x,t) - p_0 = \rho_0 a_0 U \cos \omega t \sin \omega x/a_0 \quad (39)$$

If the piston situated at  $x=0$ , moves with velocity  $U \sin \omega t$ , then a solid reflecting boundary, where  $u=0$ , can be located at

$$\omega x/a_0 = \pi/2, 3\pi/2, \quad (40)$$

In this case, there is no input in energy since  $p$  is zero at the piston and so the system of waves continues unabated in so-called resonance.

According to this simple theory if

$$\omega x/a_0 = \pi, 2\pi, \quad (41)$$

then  $p$  is zero; in crude terms this represents wave patterns in an open ended tube where the outside air is at zero (relative) pressure;  $u(x,t)$  is not zero at the open end so air flows in and out but since the pressure is zero again, there is no work done, so resonance occurs.

However, with an open tube there is a loss of energy at the open end. Shown in Fig.9(iv) a compressive wave approaches an open end; now to reduce the pressure after reflection to zero an expansion wave must be formed which passes back down the tube with fluid being expelled out of the end of the tube with velocity  $2U$ . However, there is a compressive spherical pressure pulse as shown in Fig.9(v) which passes into the external ambient air, this situation resembles a uniform source of strength  $2UA\rho_0$ , all of the pressure variation is contained within the pressure pulse so the pressure behind the pulse is zero. Energy associated with the pressure pulse in the external air is lost. With simple harmonic waves the air passes in and out of the end of the tube but the wave field into the external air is always radiating outward, dissipating energy. But the energy loss is relatively small compared with the energy in the tube; the fractional decrease in energy is proportional to the cross sectional area but inversely proportional to the tube length and to the wavelength.

## 6. EFFECTS OF RELATIVE MOTION

Finally, consider an acoustic source situated in a free stream of uniform velocity  $U$ . Assuming that the perturbation velocity field is small compared with  $U$  then the equations of motion give

$$P - P_\infty = -\rho_\infty U \frac{\partial \phi}{\partial x} - \rho_\infty \frac{\partial \phi}{\partial t} \quad (42)$$

where  $P_\infty$  is the static pressure at infinity. Substitution of eqn.(42) into the continuity equation, neglecting second order terms, gives

$$\beta_\infty^2 \phi_{xx} + \phi_{yy} + \phi_{zz} - 2M_\infty \phi_{xt} - \frac{1}{a_\infty^2} \phi_{tt} = 0 \quad (43)$$

where  $M_\infty = U/a_\infty$ ,  $\beta_\infty^2 = 1 - M_\infty^2$

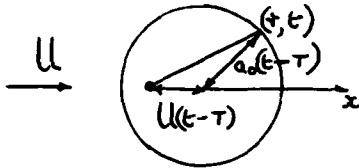


FIG. 10

To decide what happens at point  $r$  at time  $t$ : conditions at  $r$  at time  $t$  are essentially determined by what happens at the source at the earlier time  $T$  recognising that the acoustic wave is convected downstream with velocity  $U$ .

Thus by geometry as shown in Fig. 10, it is seen that

$$a_\infty^2(t-T)^2 = (x - U(t-T))^2 + y^2 + z^2 \quad (44)$$

which when solved gives the delay time

$$t_v = t - T = \left[ M_\infty x + (x^2 + \beta_\infty^2 y^2 + \beta_\infty^2 z^2)^{1/2} \right] / a_\infty \beta_\infty^2 \quad (45)$$

If the source strength varies as a function of time  $m(t)$ , then the velocity potential solution of differential equation (43) is

$$\phi(x, y, z, t) = \frac{m(t - t_v)}{4\pi (x^2 + \beta_\infty^2 y^2 + \beta_\infty^2 z^2)^{1/2}} \quad (46)$$

where  $t_v$  is given by eqn.(45). Again it is seen that if  $m(t)$  is of constant strength for  $t \gg 0$  (i.e.  $m(t) = m H(t)$ ) then the flow takes up its steady state behind the wave front. It is somewhat surprising that although the wave effects are convected downstream the actual perturbation flow behind the wave front is symmetric with respect to  $x, y$  and  $z$ . The reason is associated with the convective pressure term  $-\rho_\infty U \frac{\partial \phi}{\partial x}$ ; upstream of the source  $\frac{\partial \phi}{\partial x}$  will be negative while downstream  $\frac{\partial \phi}{\partial x}$  is positive so the convective pressure is compressive upstream and expansive downstream thus accelerating the perturbation forward flow and retarding the downstream rearward velocity.

The above analysis also holds for an acoustic source moving with uniform velocity in stationary air.

For an acoustic source moving with arbitrary velocity then the appropriate flows can be obtained by following the analysis described in the first lecture of this series.

It follows from eqn.(46) that the velocity potential for a dipole with its axis in  $z$  direction is

$$\phi_D(x, y, z, t) = \frac{\beta_\infty^2 z (t - t_v)}{4\pi (x^2 + \beta_\infty^2 y^2 + \beta_\infty^2 z^2)^{3/2}} + \frac{z \mu'(t - t_v)}{4\pi a_\infty (x^2 + \beta_\infty^2 y^2 + \beta_\infty^2 z^2)} \quad (47)$$

Turning now to the two dimensional case the velocity potential for a two dimensional source which commences at  $t=0$  in a relative uniform stream  $U$  can be determined by following the same arguments leading to eqn.(18) for the still air case (i.e.  $U=0$ ). By reference to Fig. 11, and to eqn. (46)

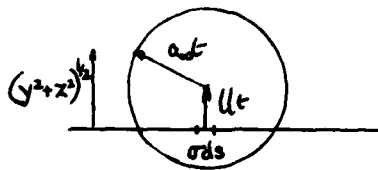


FIG. 11

$$\begin{aligned} \phi(x, z, t) &= 0 \quad \left\{ \begin{array}{l} \text{for } a_0^2 t^2 - (x - Ut)^2 - z^2 < 0 \\ \text{or } a_0 \beta_\infty^2 t + x M_\infty < (x^2 + \beta_\infty^2 z^2)^{1/2} \end{array} \right. \\ \phi(x, z, t) &= - \int_{s=0}^{s=a_0 t} \frac{\sigma ds}{4\pi (x^2 + \beta_\infty^2 y^2 + \beta_\infty^2 z^2)^{1/2}} \\ &= \frac{\sigma}{4\pi \beta_\infty} \sinh^{-1} \left( \frac{\beta_\infty^2 [a_0^2 t^2 - (x - Ut)^2 - z^2]}{[x^2 + \beta_\infty^2 z^2]} \right)^{1/2} \\ &= \frac{\sigma}{4\pi \beta_\infty} \cosh^{-1} \left( \frac{\beta_\infty^2 a_0 t + x M_\infty}{(x^2 + \beta_\infty^2 z^2)^{1/2}} \right) \quad (48) \end{aligned}$$

The velocity components and pressures can be simply obtained by differentiation.

The velocity potential for a uniform two dimensional dipole with its axis in x direction then follows

$$\phi_D(x,z,t) = \frac{\mu H(t-t_v)}{2\pi} \frac{\beta_0^2 a_0 t + xM}{[(\beta_0^2 a_0 t + xM)^2 + x^2 + \beta_0^2 z^2]^{3/2}} \cdot \frac{z\beta_0}{(x^2 + \beta_0^2 z^2)} \quad (49)$$

Eqn. (49) is of exactly the same form as the dipole in still air (see eqn.(32)) except that the time variable  $a_0 t$  in still air is replaced effectively by  $(\beta_0^2 a_0 t + xM)$  in moving air. Thus the analysis given in section 4, i.e. eqns.(36,37) leads directly into one form of the standard linearised lifting equation.

#### 7. CONCLUDING REMARKS

The aim of this lecture has been to introduce the basic acoustic singularities which arise in linearised subsonic unsteady aerodynamics and in particular to show the relationships between two dimensional and three dimensional singularities.

## METHODS FOR INVISCID SUBSONIC FLOWS ABOUT AIRCRAFT CONFIGURATIONS

by

W. Geissler

Deutsche Forschungs- und Versuchsanstalt für Luft- und Raumfahrt e.V.  
 - Aerodynamische Versuchsanstalt Göttingen -  
 Institut für Aeroelastik  
 Bunsenstraße 10, 3400 Göttingen, Germany

## SUMMARY

For the determination of unsteady airloads about complex aircraft configurations a variety of theoretical as well as experimental methods exist. For special aeroelastic application, like the determination of flutter boundaries, the measurement of unsteady airloads on harmonically oscillating configurations is required. In the following lecture some of the most important theoretical methods currently in frequent use to solve unsteady subsonic problems are discussed in some detail and compared with experimental results. Emphasis is also placed on the derivation of the final integral relations serving as the initial equations for special numerical approaches.

## 1. INTRODUCTION

Unsteady airloads on harmonically oscillating aircraft configurations are the necessary inputs into the dynamic aeroelastic equation for the determination of flutter boundaries. Due to the complexity of the governing time-dependent flow equations, the development of appropriate unsteady prediction methods is one of the major problems in aeroelastic investigations. Even if the time-dependence is simply harmonic, one has to deal with a wave-like problem which complicates the treatment of compressible subsonic and transonic flows, especially the latter.

Therefore several levels of simplification must be introduced in order to obtain sets of equations suitable for numerical solution. Analytical solutions are unavailable for nearly all unsteady problems of practical interest.

In the following lecture, which is a shortened and updated version of the lectures given in [1], various levels of simplification of the governing unsteady flow equations are briefly discussed. The different forms of integral relations are given which are the initial equations for numerical methods which are currently in frequent use. These methods are discussed in some detail and comparisons with experimental data are drawn. This detailed comparison between theory and experiment especially illustrates the problems to be investigated in the future.

The prediction methods for the determination of unsteady airloads on aircraft components do not include viscosity. In a few cases corrections can be made by using the boundary layer displacement concept, as will be discussed later. But if separation occurs, prediction methods based on potential theory obviously will fail. Careful measurement of unsteady pressures on the surfaces of oscillating configurations have proved to be a sensitive indicator of various types of three-dimensional separation. Measured unsteady pressures can signal separation much earlier than steady pressures.

## 2. BASIC EQUATIONS

Where problems of unsteady aerodynamics are investigated, especially the flutter problem, aeroelasticity is usually the initiator. Before detailing unsteady aerodynamic theory, it is therefore necessary to review briefly the governing dynamic aeroelastic equation. In generalized form this equation reads

$$(1) \quad M_r \ddot{q}_r(t) + \sum_{s=1}^{\infty} D_{rs} \dot{q}_s(t) + M_r \omega_r^2 q_r(t) - \sum_{s=1}^{\infty} A_{rs} q_s(t) = Q_r^D(t) ; \quad (r = 1, 2, \dots, \infty)$$

with the notations given in [1a].

Two types of aerodynamic forces are represented in (1).  $Q_r^D(t)$  are the generalized disturbance forces, which are independent of the aircraft motion and are regarded therefore as aerodynamic forcing functions. This type of unsteady airload occurs for instance during the flight through a turbulent atmosphere, or when the aircraft operates in the stall region, where fluctuations occur within the separated flow causing unsteady reacting forces on the wing surface. For aeroelastic investigations, this type of force may be assumed to be known. Without this non-homogeneous term  $Q_r^D(t)$ , one has to deal with a homogeneous dynamic aeroelastic stability problem such as flutter, in which the second type of aerodynamic force remains, which is caused by the time-dependent movement of the body. These forces are included in the aerodynamic coefficients  $A_{rs}$ . The motion-induced airloads are a function of the generalized coordinates  $q_r(t)$ .

In most aeroelastic investigations it is sufficient to assume simple harmonic time-dependence of the body motion. This usually leads to a response which is also harmonic in time. In this case, the aerodynamic coefficients can be expressed by

$$(2) \quad A_{rs} = \iint_S \vec{u}_r(x, y, z) \vec{p}_s^A(x, y, z) dS ,$$

where the term  $e^{i\omega t}$  is omitted and  $\vec{u}_r(x, y, z)$  is the amplitude vector of the  $r$ -th natural mode, and  $\vec{p}_s^A(x, y, z)$  is the unsteady aerodynamic pressure amplitude acting at a point  $(x, y, z)$  on the surface of the body which is oscillating harmonically in the  $s$ -th natural mode. Different from steady aerodynamic problems, aerodynamic coefficients are now complex quantities, which have a real part in phase with the body motion and an imaginary part in quadrature to the motion. This phase shift of the aerodynamic response, with respect to the displacement vector, is the physical reason why elastic structures exposed to an airstream may become dynamically unstable, which leads to self-sustained flutter vibrations.

## 2.1 EQUATIONS OF MOTION IN FLUID DYNAMICS

For the investigation of classical aeroelastic problems of flight vehicles with streamlined surfaces, it is sufficient to assume that the viscosity of the flow plays only a minor role, and thus may be initially neglected. Therefore, the parameter Reynolds number

$$(3) \quad \text{Re} = U_{\infty} \cdot l_0 / \nu \rightarrow \infty$$

is set equal to infinity. However, it must be proved later on whether this assumption is valid for special problems. In Eq.(3) the arbitrary time-dependent equations of motion of a viscous fluid, i.e. the Navier-Stokes equations, can be simplified considerably to another set of equations, i.e. the Euler equations (4)

$$(4) \quad d\vec{v}/dt + 1/\rho \text{ grad } p = 0$$

With the continuity equation

$$(5) \quad d\rho/dt + \rho \text{ div } \vec{v} = 0$$

together with the usual assumption of isentropic flow

$$(6) \quad \rho/\rho^{\gamma} = \text{constant}$$

Eqs.(4) to (6) are the governing equations of motion. They serve as the starting point for most unsteady aerodynamic problems associated with aeroelasticity. There are five equations for the solution of the five unknowns  $\vec{v}, p, \rho$  with  $\vec{v}$  as the arbitrary time-dependent velocity vector of a fluid particle. The assumption (6) is only valid for pure subsonic and supersonic flow. However, difficulties occur in the transonic flow regime where strong shock waves may appear. Eq.(6) must be replaced then by the energy equation together with the equation of state, thus involving the temperature  $T$  as an additional unknown.

The substantial time derivative  $d/dt$  in Eqs.(4) and (5) can be expressed by

$$(7) \quad d/dt = \partial/\partial t + \vec{v} \text{ grad}$$

Applying the differential operator  $d/dt$  to the velocity vector  $\vec{v}$  two different types of acceleration occur in a flow:

$$\partial\vec{v}/\partial t \cong \text{local acceleration} \quad \text{and} \quad \vec{v} \text{ grad } \vec{v} \cong \text{convective acceleration}$$

where the local term  $\partial/\partial t$  varies with transformation from a space-fixed to a moving frame of reference, whereas the convective term remains unchanged for such a transformation.

## 2.2 POTENTIAL EQUATION

A further and very important simplification of the equations of motion is obtained with the assumption of irrotationality of the flow, mathematically expressed by

$$(8) \quad \text{grad} \times \vec{v} = 0$$

With condition (8) the flow is called a potential flow

$$(9) \quad \vec{v} = \text{grad } \Phi$$

with  $\Phi$  as the velocity potential.

In Eqs.(8) and (9) the first integral of Eq.(4) leads to the Bernoulli equation

$$(10) \quad \frac{d\Phi}{dt} - \frac{1}{2} (\vec{v} \cdot \vec{v}) + \int_{P_{\infty}}^P \frac{dp}{\rho} = 0$$

With the introduction of the local speed of sound by the Laplace formula

$$(11) \quad dp/d\rho = a^2$$

and

$$(12) \quad \frac{d\rho}{dt} = \frac{d\rho}{dp} \cdot \frac{dp}{dt} = \frac{1}{a^2} \frac{dp}{dt}$$

combined with the continuity equation (5) and with Eq.(9) yields:

$$(13) \quad \frac{1}{a^2} \frac{dp}{dt} = -\rho \Delta \Phi$$

with  $\Delta$  as the Laplace operator. If the  $d/dt$  operator is again applied to Eq.(10) and the occurring time derivative of the pressure is replaced by Eq.(13), the final result yields

$$(14) \quad \frac{1}{a^2} \frac{d}{dt} \left[ \frac{d\Phi}{dt} - \frac{1}{2} \vec{v}^2 \right] - \Delta \Phi = 0$$

Eq.(14) is the arbitrary time-dependent potential equation, which is invariant with respect to rigid body transformations.

The potential equation can be expressed in two different coordinate systems, which are both of interest for the solution of problems in unsteady aerodynamics.

### 2.2.1 SPACE-FIXED FRAME OF REFERENCE

If the coordinate system is fixed in space corresponding to an observer standing on the ground and looking at a flight vehicle moving through the atmosphere which is at rest without the moving body, then the fluid particles influenced by the body have the induced velocity  $\vec{v}$  with respect to this fixed frame of reference. In this case the substantial time derivative yields

$$d/dt = \partial/\partial t + \vec{v} \cdot \text{grad} \quad ,$$

which can be applied to the potential equation (14) yielding

$$(15) \quad \frac{1}{\alpha^2} \left[ \frac{\partial^2 \Phi}{\partial t^2} + \frac{\partial}{\partial t} (\vec{v} \cdot \vec{v}) + \frac{1}{2} \vec{v} \cdot \text{grad} (\vec{v} \cdot \vec{v}) \right] - \Delta \Phi = 0 \quad .$$

Eq.(15) is the full potential equation in a space-fixed frame of reference.

In most applications in unsteady aerodynamics, however, it is more convenient to transform the potential equation into a body-fixed frame of reference, and thus, in arbitrary time-dependent cases, into an accelerated frame of reference.

### 2.2.2 MOVING (ACCELERATED) FRAME OF REFERENCE

Now the coordinates are fixed to the body and from the point of view of an observer in this system (a system which may be accelerated) the fluid particle has a velocity which is a combination of the induced velocity  $\vec{v}$  and the flight velocity  $\vec{V}_{kin}$  (kinematic velocity). The observer in a body-fixed frame of reference can only determine the relative movements of fluid particles with respect to the body. The relative velocity  $\vec{w}$  is obviously determined by

$$(16) \quad \vec{w} = \vec{v} - \vec{V}_{kin} \quad .$$

Now it is important that the substantial time derivative in body-fixed coordinates changes to

$$(17) \quad d/dt = \partial/\partial t + \vec{w} \cdot \text{grad}$$

where  $(\partial/\partial t)_{\text{space-fixed}}$  is transformed to  $(\partial/\partial t - \vec{V}_{kin} \cdot \text{grad})_{\text{body-fixed}}$  and the term  $\vec{v} \cdot \text{grad} \vec{v}$  remains unchanged in both systems.

By introducing (17) into Eq.(14), the corresponding potential equation in moving coordinates is obtained. After some lengthy reductions this equation reads

$$(18) \quad \frac{1}{\alpha^2} \left\{ \frac{\partial^2 \Phi}{\partial t^2} + \frac{\partial}{\partial t} (\vec{w} \cdot \vec{w}) + \frac{1}{2} \vec{w} \cdot \text{grad} (\vec{w} \cdot \vec{w}) + \vec{w} \cdot \frac{\partial}{\partial t} (\vec{V}_{kin}) - \frac{1}{2} \vec{w} \cdot \text{grad} (\vec{V}_{kin} \cdot \vec{V}_{kin}) - \frac{\partial}{\partial t} (\vec{V}_{kin} \cdot \vec{V}_{kin}) \right\} - \Delta \Phi = 0.$$

The first three terms in brackets are identical to the corresponding terms in Eq.(15) if  $\vec{v}$  is replaced by  $\vec{w}$ . However, there are three additional terms containing time-dependence and gradient of the kinematic velocity  $\vec{V}_{kin}$ , which in arbitrary cases are significant.

### 2.3 BERNOULLI EQUATION

Before the complicated time-dependent potential equations (15) and (18) are simplified further into expressions more suitable for solution, the Bernoulli equation (10) should also be expressed in a moving frame of reference. Using the substantial operator (17) Eq.(10) yields:

$$(19) \quad \frac{\partial \Phi}{\partial t} + \vec{w} \cdot \text{grad} \Phi - \frac{1}{2} (\vec{v} \cdot \vec{v}) = - \int_{P_{\infty}}^P dp/\rho$$

with  $\vec{v} = \vec{w} + \vec{V}_{kin}$  Eq.(19) changing to

$$(20) \quad \frac{\partial \Phi}{\partial t} + \frac{\vec{w} \cdot \vec{w}}{2} - \frac{\vec{V}_{kin} \cdot \vec{V}_{kin}}{2} = - \int_{P_{\infty}}^P dp/\rho \quad .$$

For the special case of incompressible flow ( $\rho = \rho_{\infty} = \text{constant}$ ) the pressure function on the right-hand side of Eq.(20) simply yields:

$$(21) \quad - \int_{P_{\infty}}^P dp/\rho = (p_{\infty} - p)/\rho_{\infty} \quad .$$

The condition  $\infty$  refers here to a point in the undisturbed atmosphere at an infinite distance from the body. With

$$(22) \quad c_p = (p - p_{\infty})/(\rho_{\infty} U_{\infty}^2/2)$$

and  $U_{\infty}$  as a (time-independent) reference velocity, Eq.(20) gives the pressure coefficient



$$(23) \quad c_p = -\frac{2}{U_\infty^2} \frac{\partial \Phi}{\partial t} + \frac{\vec{V}_{kin} \cdot \vec{V}_{kin}}{U_\infty^2} - \frac{\vec{w} \cdot \vec{w}}{U_\infty^2}$$

For compressible flow the pressure function yields

$$(24) \quad -\int_{p_\infty}^p \frac{dp}{\rho} = -\frac{p_\infty^{1/\gamma}}{\rho_\infty} \int_{p_\infty}^p p^{-1/\gamma} dp = -\frac{\gamma}{\gamma-1} \frac{p_\infty}{\rho_\infty} \left[ \left( \frac{p}{p_\infty} \right)^{\frac{\gamma-1}{\gamma}} - 1 \right]$$

and with

$$(25) \quad p/p_\infty = 1 + \gamma/2 Ma_\infty^2 c_p ; \quad Ma_\infty = U_\infty/a_\infty \quad \text{and} \quad p_\infty/\rho_\infty = a_\infty^2/\gamma$$

the final expression for compressible flow reads

$$(26) \quad c_p = \frac{2}{\gamma Ma_\infty^2} \left[ \left\{ 1 + \frac{\gamma-1}{2} Ma_\infty^2 \left[ \frac{\vec{V}_{kin} \cdot \vec{V}_{kin}}{U_\infty^2} - \frac{\vec{w} \cdot \vec{w} + 2 \frac{\partial \Phi}{\partial t}}{U_\infty^2} \right]^{\frac{\gamma-1}{\gamma}} \right\} - 1 \right]$$

## 2.4 LINEARIZATION

For most of the aeroelastic problems of interest it is necessary to reduce Eqs. (15) and (18) together with Eqs. (23) and (26) by a linearization procedure. For a fixed-wing flight vehicle moving with a time-independent translatory main velocity ( $\vec{U}_\infty$ ) and undergoing additional small amplitude oscillatory movements with the velocity vector  $\vec{V}(t)$ , it is assumed that  $\vec{U}_\infty$  is approximately aligned with the x-axis (small main incidence) and  $\vec{V}$  is of harmonic time-dependence

$$(27) \quad \vec{V} = \vec{\bar{V}} e^{i\omega t}$$

where the amplitude vector  $\vec{\bar{V}}$  is small compared to  $|\vec{U}_\infty|$ , such that quadratic and higher order terms of  $\vec{\bar{V}}$  can be neglected. Secondly, it is assumed that the induced velocities  $\vec{v}$  are small compared to  $|\vec{U}_\infty|$  (small disturbances), such that quadratic and higher order terms in  $\vec{v}$  also can be neglected.

If the preceding assumptions are taken into account in the potential equation (18) then the terms

$$(28) \quad \partial/\partial t (\vec{w} \cdot \vec{w}) \approx 2 U_\infty \Phi_{xt} \quad \text{and} \quad 1/2 \vec{w} \cdot \text{grad} (\vec{w} \cdot \vec{w}) \approx U_\infty^2 \Phi_{xx}$$

are simplified considerably.

The three terms containing the gradient and the time derivative of  $\vec{V}_{kin}$  in Eq. (18) can be neglected if an additional assumption is made: the body under consideration is a lift-producing wing- or tailplane configuration, which can be approximated by a thin lifting surface located in the plane of the main velocity (x, y-plane, Fig. 1). In this case the kinematic velocity vector is simplified further to

$$(29) \quad \vec{V}_{kin x} = -U_\infty \quad , \quad \vec{V}_{kin z} = -(U_\infty \partial z/\partial x + \partial z/\partial t)$$

( $z \triangleq$  time-dependent displacement of the lifting surface:  $z = \bar{z} e^{i\omega t}$  in the harmonic case) and the terms  $\text{grad} (\vec{V}_{kin} \cdot \vec{V}_{kin})$ ,  $\vec{w} \cdot \partial/\partial t (\vec{V}_{kin})$  and  $\partial/\partial t (\vec{V}_{kin} \cdot \vec{V}_{kin})$  in Eq. (18) are negligible. With this linearization for lifting surfaces, Eq. (18) reduces to the well-known linearized potential equation for sub- and supersonic flow, which is frequently discussed in the textbooks [2] and [3].

$$(30) \quad \frac{1}{\alpha_\infty^2} \left\{ \frac{\partial^2 \Phi}{\partial t^2} + 2 U_\infty \frac{\partial^2 \Phi}{\partial x \partial t} + U_\infty^2 \frac{\partial^2 \Phi}{\partial x^2} \right\} - \Delta \Phi = 0$$

In this equation a further assumption has been made corresponding to the local velocity of sound, which is approximated by its constant value at infinity. This latter assumption is no longer valid for transonic flows, in which case the linearization leads to a much more complicated nonlinear equation: the transonic small perturbation equation (TSP).

These assumptions are very limiting though in most cases sufficient for aeroelastic applications. Figs. 2 and 3, however, show two examples where the linearization procedure discussed previously does not lead simply to equation (30). Fig. 2 shows a body of considerable thickness moving with constant velocity vector  $\vec{U}_\infty$  inclined to the main axis by  $\alpha_s$  and oscillating with a small angular amplitude  $\alpha'$  about a pitching axis with an additional time-dependent velocity vector  $\vec{V}(t)$ . Here the kinematic velocity has the components

$$\vec{V}_{kin x} = -(U_\infty \cos \alpha + \bar{V}_x e^{i\omega t}) \quad , \quad \vec{V}_{kin z} = -(U_\infty \sin \alpha + \bar{V}_z e^{i\omega t})$$

with

$$\alpha = \alpha_s + \alpha' e^{i\omega t}$$

Although the amplitudes of oscillation again may be small and the assumption of small perturbations of the flow still may be applicable, some terms in Eq. (18) cannot be neglected. This can be easily proved. Further details of this case are given in section 4.3.

These difficulties are more obvious in Fig. 3 for a helicopter rotor blade, in which the kinematic velocity is prescribed by a translating, rotating and oscillating frame of reference. In this case, further simplifications must be taken into account if special solution procedures, such as singularity or integral methods, are to be applicable.

Corresponding to the potential equation, the linearization procedure can also be applied to the Bernoulli equations (23) and (26) yielding

$$(31) \quad c_p = -\frac{2}{U_\infty^2} \frac{\partial \Phi}{\partial t} - \frac{2}{U_\infty} \frac{\partial \Phi}{\partial x} ,$$

where a binomial expansion of Eq.(26) is used. Eq.(31) is also valid for incompressible flow.

## 2.5 ACCELERATION POTENTIAL

From the Euler equations (4) it can be deduced that

$$(32) \quad \frac{d\vec{v}}{dt} = -\frac{1}{\rho} \text{grad } p = -\text{grad} \int_{p_\infty}^p \frac{dp}{\rho} .$$

Thus the acceleration of a fluid particle is the gradient of a scalar function, i.e. the pressure function, which may be defined as the acceleration potential

$$(33) \quad d\vec{v}/dt = \text{grad } \psi .$$

Integrating Eq.(33) the potential equation (14) yields

$$(34) \quad 1/\alpha^2 \, d\psi/dt - \Delta \Phi = 0 .$$

Applying the substantial time derivative ( $d/dt$ ) on Eq.(34) and replacing the term

$$(35) \quad \Delta (d\Phi/dt) = \Delta (\psi + 1/2 v^2) ,$$

the final result is

$$(36) \quad \frac{1}{\alpha^2} \frac{d^2 \psi}{dt^2} - \Delta (\psi + 1/2 v^2) = 0 .$$

Linearizing Eq.(36) gives

$$(37) \quad \frac{1}{\alpha_\infty^2} \left( \frac{\partial^2 \psi}{\partial t^2} + 2 U_\infty \frac{\partial^2 \psi}{\partial x \partial t} + U_\infty^2 \frac{\partial^2 \psi}{\partial x^2} \right) - \Delta \psi = 0 ,$$

which has a form identical to the linearized potential equation (30) based on the velocity potential  $\Phi$ .

In the case of harmonic oscillations the linearized relation between  $\Phi$  and  $\psi$  is then given by

$$(38) \quad \bar{\psi} = i\omega \bar{\Phi} + U_\infty \partial \bar{\Phi} / \partial x .$$

For later application of the acceleration potential, the recalculation of the velocity potential from the acceleration potential is needed

$$(39) \quad \bar{\Phi} = \frac{e^{-i\omega x/U_\infty}}{U_\infty} \int_{-\infty}^x \bar{\psi} e^{i\omega x'/U_\infty} dx' ,$$

where the Sommerfeld radiation condition  $\bar{\Phi} = 0$  for  $x \rightarrow -\infty$  is fulfilled.

## 3. SOLUTION PROCEDURES

A large variety of solution procedures for the unsteady flow equations exists in literature today. These solution procedures may be summarized by finite difference, finite element and surface singularity methods. While finite difference methods are applicable for the solution of most of the partial differential equations discussed previously, surface singularity or integral methods are only applicable for linear equations. Thus, a more extensive simplification of the governing flow equations is necessary for linear equations. However, the computer cost and time involved in solving problems by finite difference methods is much higher than for the solutions of problems by singularity methods. As long as nonlinearities are not too severe, cheaper surface singularity methods will be favored for aircraft design problems, in which a large amount of parameters such as Mach number, frequency, mode shape, and geometry must be investigated.

### 3.1 FINITE DIFFERENCE AND FINITE ELEMENT METHODS

In general, all partial differential equations and even the Navier-Stokes equations may be solved by suitable finite difference or finite element techniques, taking into account appropriate stability and boundary conditions. However, large difficulties such as the turbulence problem or other highly nonlinear flow problems like separation occur, and the capacity of even the largest existing computers does not suffice.

In unsteady aerodynamics with respect to aeroelastic problems, the viscosity of the flow may be neglected as previously discussed. However, when regarding the important unsteady transonic flow problems involving shock-boundary layer interactions, this assumption is brought into question. Due to nonlinearities existing even in the nonviscous flow equations, unsteady transonic problems are mainly investigated by finite difference methods. Without going into detail about these methods (a survey of unsteady transonic flow phenomena is given in [4]), some of the existing calculation methods should be cited for completeness.

The most advanced finite difference methods existing today solve the two-dimensional unsteady Euler equations (4), for instance as in [5] and [6].

The preceding level of simplification is the full-potential equation (14) solved in [7] for harmonically oscillating airfoils. Linearizing the full-potential equation leads to the transonic small perturbation equation (TSP), which has been solved by a

number of investigators ([8] and [9]) for two-, as well as for three-dimensional problems.

Only a limited number of investigators use the alternative finite element approach. For this type of method the flow field is discretized in a suitable distribution of finite elements (2d-problems) or even finite volumes (3d-problems). The first attempt to solve the unsteady transonic small perturbation equation by a finite element procedure is shown in [10]. More examples and details of transonic flow problems together with a large list of references are given in [11].

### 3.2 SURFACE SINGULARITY METHODS

As long as the linearized unsteady potential equation (30) is applicable for problems in pure subsonic and supersonic flow, a different solution procedure can be applied by using the concept of surface singularities. The advantage of this type of method is that only the surfaces of the bodies under consideration need to be represented by singularities, such as sources, sinks, and doublets. The outer boundary condition (at infinity) is automatically fulfilled. The solutions include not only the flow quantities on the body surfaces, but also in the surrounding flow field. The corresponding methods can be based on the velocity potential  $\Phi$  (Eq.30), as well as on the acceleration potential or pressure function  $\psi$  (Eq.37). Both possibilities will be discussed in more detail in the following sections.

Firstly, the derivation of the governing integral equation together with the corresponding surface boundary condition and the Kutta condition will be outlined in the following sections using the example of the velocity potential in subsonic flow.

#### 3.2.1 INTEGRAL EQUATION

For the special problem involving large steady flight velocity  $|U_\infty|$  and additional small amplitude harmonic oscillations, the velocity potential  $\Phi$  can be represented by

$$(40) \quad \Phi(x, y, z, t) = \Phi_0(x, y, z) + \varphi(x, y, z, t) \quad ; \quad \varphi(x, y, z, t) = \bar{\varphi}(x, y, z) e^{i\omega t} \quad ;$$

i.e. by a steady term  $\Phi_0$  and a time-dependent unsteady term  $\varphi$ . Introduction of Eq.(40) into Eq.(30) yields for the unsteady part of the potential (with the term  $e^{i\omega t}$  omitted)

$$(41) \quad (1 - Ma_\infty^2) \frac{\partial^2 \bar{\varphi}}{\partial x^2} + \frac{\partial^2 \bar{\varphi}}{\partial y^2} + \frac{\partial^2 \bar{\varphi}}{\partial z^2} - 2i\omega \frac{Ma_\infty}{a_\infty} \frac{\partial \bar{\varphi}}{\partial x} + \frac{\omega^2}{a_\infty^2} \bar{\varphi} = 0 \quad ,$$

which is completely independent of the steady potential  $\Phi_0$ . Thus, for all unsteady flow problems based on the small perturbation equation, the steady solution of the problem is separated from the unsteady problem.

With the transformation

$$(42) \quad \varphi(x, y, z, t) = U_\infty \ell_0 \bar{\varphi}(X, Y, Z) e^{i(\lambda X + \omega^* T)} \quad ,$$

with  $\omega^*$  as the significant unsteady parameter defined by

$$(43) \quad \omega^* = \omega \cdot \ell_0 / U_\infty \quad ; \quad \lambda = \omega^* Ma_\infty^2 / \beta^2 \quad \text{and} \quad \beta = \sqrt{1 - Ma_\infty^2} \quad .$$

The coordinates and the time are made dimensionless by

$$(44) \quad X = x/\ell_0 \quad ; \quad Y = y \cdot \beta / \ell_0 \quad ; \quad Z = z \cdot \beta / \ell_0 \quad ; \quad T = t \cdot U_\infty / \ell_0 \quad ,$$

with  $\beta$  as the Prandtl-Glauert factor.

Introducing the transformation (42) into Eq.(41) yields

$$(45) \quad \frac{\partial^2 \bar{\varphi}}{\partial X^2} + \frac{\partial^2 \bar{\varphi}}{\partial Y^2} + \frac{\partial^2 \bar{\varphi}}{\partial Z^2} + \kappa^2 \bar{\varphi} = 0 \quad , \quad \text{with} \quad \kappa = Ma_\infty \omega^* / \beta^2 \quad .$$

Eq.(45) is the Helmholtz-wave equation for which fundamental solutions exist. One of these elementary solutions is the function:

$$f = e^{-i\kappa r} / r \quad , \quad r = \sqrt{(X - X')^2 + (Y - Y')^2 + (Z - Z')^2}$$

with  $r$  as the distance between a sending point  $(X', Y', Z')$  and a receiving point  $(X, Y, Z)$ .

Using Green's theorem, Eq.(45) can now be transformed into an integral equation for the unknown potential  $\bar{\varphi}$  [12]

$$(47) \quad 4\pi \cdot \bar{\varphi}(X, Y, Z) = \iint_S \left[ \bar{\varphi}(X', Y', Z') \frac{\partial}{\partial \zeta'} \left( \frac{e^{-i\kappa r}}{r} \right) - \frac{\partial \bar{\varphi}}{\partial \zeta'} \left( \frac{e^{-i\kappa r}}{r} \right) \right] d\xi' d\eta'$$

with  $\xi, \eta, \zeta$  as surface coordinates (Fig.2).

In the case of a lifting body, the surface integral of Eq.(47) must be taken over the surfaces of the body and the wake. The first term under the integral sign of Eq.(47) can be interpreted as the doublet term. The second part is the source term.

Differentiation of Eq.(47) with respect to  $\zeta$  (the outward normal direction in the control point) yields

$$(48) \quad \frac{\partial \bar{\varphi}}{\partial \zeta} = \vec{\zeta} \cdot \vec{\nabla}_{\text{kin}} = \frac{1}{4\pi} \iint_S \left[ \bar{\varphi} \frac{\partial^2}{\partial \zeta' \partial \zeta'} \left( \frac{e^{-i\kappa r}}{r} \right) - \frac{\partial \bar{\varphi}}{\partial \zeta'} \frac{\partial}{\partial \zeta} \left( \frac{e^{-i\kappa r}}{r} \right) \right] d\xi' d\eta' \quad ,$$

as the final integral equation for the determination of the unknown source and doublet strength on the body surface. Eq.(48) expresses the kinematic boundary condition, i.e. the normal component of the prescribed kinematic velocity must be cancelled by the induced normal velocities of the singularity system.  $\vec{\nabla}_{\text{kin}}$  must be of harmonic time-dependence consistent with Eq.(40). Therefore, Eq.(48) is complex with a real part in phase with the prescribed oscillating motion and an imaginary part in quadrature to the motion.

For the special case  $x = 0$  the integral equation is simplified considerably. Two different reasons may cause this simplification

1.  $Ma_\infty = 0$  for the incompressible unsteady problem
2.  $\omega^* = 0$  for the time-independent steady (compressible or incompressible) problem.

It should be pointed out here that for the incompressible unsteady case, the full potential equation reduces to the simple Laplace equation

$$(49) \quad \Delta \bar{\phi} = 0,$$

which is linear in itself, and still leads to the integral equation (48) with the exponential terms replaced by 'one.'

All unsteady integral methods based on the velocity potential can be derived from the general equation (48). A solution of the complete integral equation, however, is still difficult, and further simplification with respect to the body geometry must be accepted for practical applications.

In Eq.(48) one must always keep in mind that this integral formulation is based on the linear small perturbation equation (30), which has been derived with the assumption of small induced velocities and special limitations of the kinematic velocity involved.

### 3.2.2 KUTTA CONDITION

For lift-producing configurations, such as wings and tailplanes, the Kutta condition at the trailing edge of the wing must be applied in steady, as well as in unsteady, aerodynamics. This phenomenological condition expresses the main effect of viscosity, which is otherwise completely neglected in potential theory. When introducing the Kutta condition into the solution procedure of the integral equation, one has to consider the smooth flow off the trailing edge, which is identical to the condition of equal steady and unsteady pressures at two points, i.e. on the upper and lower wing surfaces adjacent to the trailing edge or Kutta point. For steady three-dimensional problems and for unsteady two- and three-dimensional problems, the wake flow behind the wing must be taken into account. Here exists a principle difference between methods applying the velocity potential and methods applying the acceleration potential. The velocity potential has a discontinuity crossing the surface of the wake. This discontinuity can be represented by a doublet sheet. The existence of the wake must be considered in solving the integral equation (48). In applying the acceleration potential, however, no discontinuity in the wake exists, due to the fact that the pressure through the wake is continuous, i.e. the wake is a free stream surface which cannot sustain any forces. Further details of these principle differences between the two concepts will be discussed later.

### 3.2.3 UNSTEADY PRESSURES, FORCES, MOMENTS

After the singularity distributions on the body surface have been calculated by solution of Eq.(48), the next step is to apply the Bernoulli equation in the nonlinearized (26) or linearized version, in order to calculate unsteady pressure distributions. The pressures then directly enter the aerodynamic coefficients  $A_{rs}$  (2) needed in the governing dynamic aeroelastic equation (1). The additional step of calculating unsteady pressures by means of the Bernoulli equation is avoided if the acceleration potential  $\bar{\psi}$  is used. This advantage will be outlined in a later section.

In the special case of a thin lifting surface (Fig.1) the pressure jump is needed across the surface instead of the local value on the surface, i.e. the local lift.

In the equations

$$(50) \quad \Delta p = p_\ell - p_u, \quad \Delta \bar{\psi} = \bar{\psi}_u - \bar{\psi}_\ell,$$

the index  $\ell$  refers to the lower and the index  $u$  refers to the upper surface of the wing.

Applying the linearized Bernoulli equation (31) together with the transformations (42) and (44) yields

$$(51) \quad \Delta c_p = \Delta p / (\rho_\infty U_\infty^2 C / 2) = 2 \left[ i\nu \Delta \bar{\psi} + \frac{\partial \Delta \bar{\psi}}{\partial X} \right] e^{i\lambda X} = \Delta c_p' + i \Delta c_p''$$

with  $\nu = \omega^* / \beta^2$  and  $C$  as the amplitude of the oscillatory motion.

If the structural deflection of a wing section can be neglected as in the case of high-aspect-ratio wings, then the integrated pressure coefficients in streamwise direction define the local lift and moment, which directly enter the aerodynamic coefficient  $A_{rs}$ . In addition, the spanwise lift and moment distributions are advantageous for comparison between different prediction methods and experimental data.

The local lift coefficient  $c_\ell$  is calculated by

$$(52) \quad c_\ell(y) = \frac{dL}{\frac{\rho_\infty}{2} U_\infty^2 \ell(y) C dy} = 2 \left[ \Delta \bar{\psi}_T e^{i\lambda X_T} + i\omega^* \int_{X_V}^{X_T} \Delta \bar{\psi} e^{i\lambda X} dX \right],$$

where the index  $V$  refers to the leading edge and the index  $T$  to the trailing edge of the wing section.  $\ell(y)$  is the local chord length of the section. In a similar way the local moment coefficient  $c_m$  and the local moment coefficient of the control surface  $c_n$  are defined.

It should be pointed out that in Eq.(52) the differentiation of  $\Delta \bar{\psi}$  with respect to  $X$  is avoided, and thus a numerical differentiation of the streamwise potential distribution necessary in Eq.(51) is unnecessary for the calculation of the unsteady local lift and moment.

## 4. THREE-DIMENSIONAL SUBSONIC METHODS

### 4.1 LIFTING SURFACE THEORIES

The starting points for all lifting surface theories are shown in Eqs.(30) or (37). These starting points depend on whether

the velocity potential  $\Phi$ , or the acceleration potential, or pressure function  $\psi$  is applied. In the first case, the corresponding aerodynamic influence function of the integral equation is relatively simple, but the wake behind the lifting surface must be considered, thus leading to semi-infinite wake integrals. However, the velocity potential concept can be applied also to bodies with complex geometries, thus accounting for the complete geometrical boundary condition, and possibly the Bernoulli equation.

In the case of the acceleration potential, however, the aerodynamic influence function is more complicated. This fact is due to a recalculation of the velocity potential from the pressure function Eq.(39) in formulating the kinematic boundary condition on the wing surface. The advantage of the acceleration potential concept is that the pressure difference on the lifting surface is already the solution function and no additional calculations have to be performed. Furthermore the wake behind the wing, in this case, does not have to be taken into account, due to zero pressure difference there.

#### 4.1.1 LIFTING SURFACE THEORY BASED ON THE VELOCITY POTENTIAL (PANEL METHOD)

For infinitely thin lifting surfaces, the general integral equation (48) can be simplified by the conditions in (50) with

$$(53) \quad \partial \Delta \bar{\varphi} / \partial \zeta = 0$$

(since  $\Delta \bar{\varphi}$  is an odd function of  $z \equiv \zeta$ ) to the form

$$(54) \quad \frac{\partial \Delta \bar{\varphi}}{\partial Z} = \frac{1}{4\pi} \lim_{Z \rightarrow 0} \iint_{S+W} \Delta \bar{\varphi}(X', Y') \frac{\partial^2}{\partial Z^2} \left( \frac{e^{-ix'r}}{r} \right) dX' dY'$$

The surface integral in Eq.(54) must be taken over the wing surface (S) and the wake (W). The linearized downwash on the wing surface, due to an oscillatory motion of the wing, is given by Eq.(29).

$$(55) \quad w = \partial z / \partial t + U_{\infty} \partial z / \partial x ; \quad z = \bar{z}(x, y) e^{i\omega t}$$

which can be transformed by Eq.(42) to

$$(56) \quad W = 1 / (U_{\infty} \beta) (\bar{z} i\omega + U_{\infty} \frac{\partial \bar{z}}{\partial x}) e^{-i(\lambda X + \omega^* T)}$$

The kinematic boundary condition on the wing surface is now given by

$$(57) \quad (\partial \Delta \bar{\varphi} / \partial Z)_{Z=0} = -\bar{W}$$

with the unknown potential jump  $\Delta \bar{\varphi}$  under the integral sign Eq.(54). After  $\Delta \bar{\varphi}$  has been calculated the linearized Bernoulli equation (51) can be applied. With  $\Delta c_p \equiv 0$  in the wake the latter equation gives the condition of  $\Delta \bar{\varphi}$  in the wake

$$(58) \quad i\nu \Delta \bar{\varphi} + \partial \Delta \bar{\varphi} / \partial X = 0$$

which can be integrated, thus leading to

$$(59) \quad (\Delta \bar{\varphi})_w = \Delta \bar{\varphi}(X_T, Y) e^{-i\nu(X - X_T)}$$

where  $X_T$  is the position of the trailing edge.

The integral equation (54) together with the boundary condition (56) is solved now by a panel method, which was first done by W.P. Jones and J.A. Moore in [13]. Fig.1 shows the lifting surface divided into small surface elements, which are distributed over the wing surface with element concentrations at the wing leading and side edges. Chordwise strips on the wing surface extend into the wake, thus forming semi-infinite wake strips emanating from the trailing edge. Corresponding to the integral expression in Eq.(54), the wing panels are represented by doublet distributions of constant doublet strength within each panel.

The kinematic boundary condition is now applied in the geometric midpoints of each panel, and thus Eq.(54) and (56) together with the wake condition (59) can be formulated in discretized form

$$(60) \quad -4\pi \bar{W}_m = \sum_{n=1}^{I \cdot J} \Delta \bar{\varphi} \iint_{\Delta S_n} \frac{\partial^2}{\partial Z^2} \left( \frac{e^{-ix'r}}{r} \right)_{Z=0} dX' dY' + \sum_{q=1}^J \Delta \bar{\varphi}(X_T, Y) \iint_{\Delta W_q} e^{-i\nu(X-X_T)} \frac{\partial^2}{\partial Z^2} \left( \frac{e^{-ix'r}}{r} \right)_{Z=0} dX' dY'$$

with  $m$  referring to the control point and  $n$  referring to the integral- or sending point.  $I \cdot J$  is the total number of wing surface panels. Eq.(60) still cannot be solved by means of a linear system of equations, because there are more unknowns than equations, due to the wake terms  $\Delta \bar{\varphi}_w$ . To remove these terms, it is assumed that the potential distribution in chordwise direction of the wing can be approximated by a parabolic curve through the trailing edge value and the values in the two wing panels adjacent to the trailing edge, having the indices  $i, j$  and  $(i-1), j$  (Fig.1). The wake integrals (second term in Eq.(60)), however, are much more complicated semi-infinite integrals, which must be calculated numerically by solving expressions like

$$(61) \quad A_{m,n} = \int_0^{\infty} e^{-i\nu s} f(s) ds ; \quad f(s) = \int_0^{\Delta s'} e^{-ix'r} \frac{(1+ix'r)}{r^3} ds'$$

( $s = X - X_{T,q}$ ,  $\Delta s' \cong$  strip-width).

Using the periodicity of the exponential function in (61), this formula can be rearranged to

$$(62) \quad A_{m,n} = \int_0^{\tau} e^{-i\nu s} (f(s) - f(s+\tau) + f(s+2\tau) - + \dots) ds ; \quad \tau = \pi/\nu$$

The infinite series in Eq.(62) are calculated up to the tenth member. The rest is approximated by a geometric series. The final integral in (62) is evaluated by means of Simpson's rule.

After the linear system of equations has been solved for the unknown coefficients  $\bar{\Delta\varphi}$ , the unsteady pressure coefficients  $\Delta c_p$  may be calculated by Eq.(51). In this case, the derivatives of  $\bar{\Delta\varphi}$  with respect to  $X$  are needed. They must be calculated numerically, using a spline fit to the functions  $\bar{\Delta\varphi}(X)$  or simply be finite differences. It has already been mentioned that for the calculation of local lift- and moment-coefficients, only the  $\bar{\Delta\varphi}$ -values are needed in Eqs.(52). Thus, the  $X$ -derivative in the Bernoulli equation is avoided in this case.

It should be mentioned that the number of control points on the wing, and thus the magnitude of the linear system of equations, is reduced considerably by symmetry conditions. Only one half of the wing must be represented by control points. Obviously, the influence of the symmetric half of the wing and wake must be taken into account by the influence of the corresponding doublet distributions there.

Fig.4 illustrates a typical result of the method for a rectangular wing with pitching oscillations about its midchord axis. Real and imaginary parts of the chordwise and spanwise pressure coefficients  $\Delta c_p^r$ ,  $\Delta c_p^i$  are represented for different numbers of panels. The results are compared with the kernel function method [15] based on the acceleration potential (section 4.1.2.1).

#### 4.1.2 LIFTING SURFACE THEORY BASED ON THE ACCELERATION POTENTIAL

In recent years much effort has been spent on the development of the alternative approach based on the acceleration potential, for which the linearized potential equation (37) serves as the starting point. Two different main concepts for the solution of this equation have been frequently investigated; the kernel function, and the doublet-lattice approach. The former works with prescribed functions for the unknown pressures. The latter uses a panel-type discretization procedure.

##### 4.1.2.1 KERNEL FUNCTION METHOD

The integral equation based on the linearized acceleration potential equation (37) and the boundary condition (55) has the general form

$$(63) \quad -\frac{\bar{w}(x,y)}{U_\infty} = \frac{1}{8\pi} \iint_S \bar{\Delta c}_p(x',y') K(x-x', y-y', Ma_\infty, \omega^*) dx' dy'$$

with  $K$  as the kernel function, expressing the influence of a single pressure doublet of unit strength located at  $x',y'$  on the wing surface  $S$  in a receiving point  $x,y$ . This function is illustrated in [15]. The idea of the kernel function approach is to approximate the unknown pressure distribution  $\Delta c_p(x',y')$  in the chordwise and spanwise direction by prescribed functions, where special known features of the pressure distributions are already included

$$(64) \quad \Delta c_p(x,y) = \sum_{i=1}^n \sum_{j=1}^m c_{i,j} f_i^{(n)}\left(\frac{x}{b}\right) g_j^{(m)}\left(\frac{y}{b}\right)$$

with  $f_i^{(n)}$  as the chordwise and  $g_j^{(m)}$  as the spanwise loading functions. The coefficients  $c_{i,j}$  are assigned now to favorably selected control points where the boundary condition must be satisfied. Thus Eq.(63) can be represented by a system of  $N = (n \times m)$  linear algebraic equations for the  $N$  unknown coefficients  $c_{i,j}$ . The loading functions  $f_i^{(n)}$  may be defined by the usual Birbaum-Achermann or Glauert functions from steady theory

$$(65) \quad f_i^{(n)}(X) = \begin{cases} [(1-X)/(1+X)]^{1/2} & \text{for } n=0 \\ \sin |n \cos^{-1} X| & \text{for } n>0 \end{cases}$$

with

$$X = (x - x_L) / \ell(y),$$

where  $x_L$  is the position of the leading edge at the spanwise position  $y$ .

These functions include the known square root singularity at the leading edge and the Kutta condition of zero pressure difference at the trailing edge of the wing. Thus a limited number of these functions is already sufficient for the appropriate representation of the  $\Delta c_p$  distributions.

The spanwise functions  $g_j^{(m)}$  are either determined directly with the aid of suitable interpolation functions as in the Multhopp-Truckenbrodt procedure [16] or they are expressed in terms of another set of pre-selected functions according to lifting-line load distribution.

The general formulation of the integral equation (63) using prescribed loading functions yields

$$(66) \quad -\{\bar{w}\} = \left[ \iint \bar{\Delta c}_p K dx' dy' \right] \{c\}$$

with  $\{\bar{w}\}$  and  $\{c\}$  as  $N$ -order column matrices of the prescribed downwash and load coefficients, respectively. After this system has been solved for the  $N$  unknowns  $c_{i,j}$ , the unsteady pressure differences  $\Delta c_p$  can be calculated by Eq.(64).

The analytical treatment of the integral expression in Eq.(66), i.e. the aerodynamic influence function, causes difficulties due to high order singularities included in this function.

The kernel function method has been used successfully for numerous unsteady flow problems including arbitrary wing planforms, Mach numbers, reduced frequencies and mode shapes. Fig.5 illustrates a typical example of unsteady airloads on a rectangular wing with pitching oscillations about the quarter-chord axis [15]. The analytical results are compared with corresponding experimental data. The agreement between theory and experiment is fairly good, although the measured wing configuration had a NACA - 0012 (12% thick) airfoil section, whereas a thin lifting surface was assumed for the theory.

An example of the applicability of the method for compressible subsonic flow is shown in Fig. 6. Unsteady airloads are illustrated on a rectangular wing oscillating in pitching mode about the quarter-chord axis. Up to Mach number 0.8 the agreement between theory and experiment is again quite good. Larger differences occur for the higher Mach numbers, where nonlinearities due to shock waves cause large differences between linearized theory and experiment.

The advantage of the kernel function method compared to the panel method discussed in the previous section is the limiting number of load functions necessary for a sufficient accuracy of the solution. Thus computer time and costs are minimal when using the kernel function approach. Difficulties, however, occur in cases where the pressure on the lifting surface has not only a singularity at the leading edge, but additional singularities at the hinge lines of control surfaces. Then the number of loading functions must be increased considerably to accommodate these more complicated pressure distributions, or special loading functions including the pressure singularity at the leading edge of the oscillating flaps must be used.

#### 4.1.2.2 DOUBLET-LATTICE METHOD

A different purely numerical approach based on the acceleration potential is known as the doublet-lattice method described in [17]. This method was applied more extensively by several authors. The governing equation is again the linearized potential equation (37) for the acceleration potential  $\psi$ . Similar to the velocity potential panel method of section 4.1.1, the wing surface is split up into small surface elements (Fig. 7). The quarter chord line of each element is represented now by a pressure doublet line of constant, yet unknown, strength. The corresponding control point of each panel is located at its 3/4-chord point. This assumption of the control point location was confirmed by numerical experimentation such that the Kutta condition is automatically fulfilled and no additional assumptions for this condition are necessary.

If the wing surface is represented by  $N$  surface elements the integral equation (63) may be given in discretized form

$$(67) \quad -\frac{\bar{w}_i(x, y)}{U_\infty} = \sum_{j=1}^N D_{i,j} \Delta \bar{c}_{pj} \quad ,$$

with the aerodynamic influence function  $D_{i,j}$  corresponding to the influence of a pressure doublet line of length  $\ell_j$  (Fig. 7) and strength 'one' in a control point  $i$ :

$$(68) \quad D_{i,j} = \frac{1}{8\pi} \Delta c_j \cos \varphi_j \int_{\ell_j} K(x_i, y_i, x_j(\ell), y_j(\ell), Ma_\infty, \omega^*) d\ell$$

with the geometric terms  $\Delta c_j$ ,  $\varphi_j$ ,  $\ell_j$  given in Fig. 7. The general expression for the function  $K$  is given in [17] even for the case of nonplanar lifting surfaces. Eq. (67) can be assumed again as a linear system of algebraic equations with  $\Delta \bar{c}_p$  as the solution vector. Identical to the velocity potential panel method, the number of equations is determined by the number of surface elements representing the wing.

The advantage of the method is again its flexibility, thus being applicable for arbitrary lifting surfaces including discontinuities of the normal wash at control surface-leading edges, fold lines or intersections of other surfaces (pylons, T-tails, etc.). The method has been proved for a large variety of unsteady flow problems including interference effects of bodies. Thus it is one of the standard methods in unsteady aerodynamics.

#### 4.2 UNSTEADY WING THEORY INCLUDING THICKNESS AND INCIDENCE

All methods discussed so far are based on the linearized potential equation in connection with linearized boundary conditions and the corresponding linearized Bernoulli equation. Thus, these methods are limited to lifting bodies which can be assumed to be infinitely thin. In most applications for aeroelastic problems, these assumptions may be sufficient. On the other hand, it is important to know the magnitude of the neglects due to all these linearizations.

It has been mentioned that for the limiting incompressible flow case the governing potential equation reduces to simple Laplace equation, which is already linear in itself. Therefore, the arbitrary integral equation (48) with the exponential terms replaced by 'one' serves as the governing equation for this case. This theoretical concept, which is again based on the velocity potential, can be applied thus to arbitrary body geometries including not only lift-producing configurations, but also bodies like fuselages, stores, and tanks.

The geometric conditions of the wing problem are shown in Fig. 8. Instead of a corresponding thin lifting surface, now the whole wing surface is split up into suitable distributed surface elements [18]. The wake is again represented by strips emanating from the trailing edge to infinity. These wake strips may be of arbitrary curved shape, however, it is assumed that the wake contour is known a priori.

Corresponding to the steady three-dimensional method for lifting bodies given in [19], the wing surface is now distributed by sources and sinks, and in addition, by doublets of constant strength within each element. The integral equation (48) is now modified with  $\Phi = \Phi_q + \Phi_d$  (source and doublet terms) to

$$(69a) \quad \partial \Phi_{q0} / \partial z = - \left( U_{z0} + \partial \Phi_{d0} / \partial z \right)$$

for the steady potential (index 0), and

$$(69b) \quad \partial \bar{\varphi}_{qi} / \partial z = - \left( \bar{U}_{zi} + \bar{V}_z + \partial \bar{\varphi}_{di} / \partial z \right)$$

for the unsteady potential (index 1), where the doublet terms  $\partial \bar{\varphi}_{di} / \partial z$  are shifted to the right-hand side of the integral equations and added to the prescribed kinematic velocity terms  $\bar{U}_z$  (normal component of the translatory motion) and  $\bar{V}_z$  (normal component of the oscillatory motion). Thus, the doublet terms are assumed to be known at the first step. Their final magnitudes are determined later by the suitable application of the Kutta condition. The source and doublet terms which are equivalent to the induced normal velocities of the surface source and doublet distributions can be calculated by

$$(70) \quad \frac{\partial \varphi_q}{\partial \zeta} = \frac{1}{4\pi} \iint_S \sigma_q \frac{\partial}{\partial \zeta} \left( \frac{1}{r} \right) dS \quad ; \quad \frac{\partial \varphi_d}{\partial \zeta} = \frac{1}{4\pi} \iint_S \sigma_d \frac{\partial^2}{\partial \zeta \partial \zeta'} \left( \frac{1}{r} \right) dS + \frac{1}{4\pi} \iint_W \Delta \varphi_{dw} \frac{\partial^2}{\partial \zeta \partial \zeta'} \left( \frac{1}{r} \right) dW \quad ,$$

where  $\Delta \varphi_{dw}$  is the doublet strength within the wake.

Both steady and unsteady potentials are calculated in Eqs. (69a and b), because in the nonlinearized boundary condition and Bernoulli equation (26), the relative velocity vector  $\vec{w}$  includes both steady and unsteady terms. Thus the problem can no longer be separated into independent steady and unsteady parts. The calculation of unsteady pressures by means of the complete Eq. (26) postulates the knowledge of the corresponding steady velocities. In incompressible flow the reduced frequency  $\omega^*$  is not included in the aerodynamic influence functions  $\partial \varphi_q / \partial \zeta$  (source terms, Eq. (70)), which are then identical for both steady and unsteady cases. Thus, both integral equations (69) can be solved by only one linear system of equations with several right-hand sides of the equation being represented by steady plus unsteady terms. The results of this solution procedure are two solution vectors: one source-strength distribution satisfying the steady boundary condition, and the second satisfying the unsteady boundary condition.

For the solution obtained so far the dipole strengths were assumed to have unit strength. Thus, for each chordwise strip of the wing an additional factor - the overall doublet strength of this section - is needed for the final solution. Here the Kutta condition, with the assumption of zero pressure difference between two control points on the upper and lower wing surface adjacent to the trailing edge, must be applied. This condition leads to a quadratic system of equations for the steady problem and to a linear system of equations for the unsteady problem. The number of equations is determined by the number of chordwise strips of the wing.

Applying the incompressible Bernoulli equation (23) in two adjacent points on the upper and lower sides of the thin wake, and assuming zero pressure difference there, the unsteady potential difference gives

$$(71) \quad (\Delta \bar{\varphi}_1)_w = (\Delta \bar{\varphi}_1)_T e^{-i\omega^*(s-s_T)}$$

where  $s$  is the unit tangential vector of the curved wake, and the index  $T$  refers again to the position of the trailing edge. The steady potential jump  $(\Delta \varphi_s)$  is constant within a wake strip. After all source and doublet strengths have been calculated, the general form of the Bernoulli equation (23) can be used finally to calculate steady and unsteady pressures on the wing surface.

Typical results obtained with this method are shown in Fig. 9 for a rectangular wing oscillating in pitching mode about its quarter chord axis. The wing has a NACA 0012 airfoil section. The results are obtained for the case of  $\alpha_s = 4^\circ$  main incidence and  $\omega^* = 0.14$ . Comparison with experiments [20] shows good agreement within the inboard sections of the wing. In the very tip region ( $y/l = 0.962$  in Fig. 9), however, deviations of the measured data from the theoretical results are largely due to the influences of the tip vortex there.

Fig. 10 shows unsteady pressures for a swept tapered wing oscillating again in pitching mode at its quarter chord. The wing has a NACA 0010 symmetric airfoil section in this case. Three theoretical curves are included in this plot

1. linear lifting surface theory,
2. nonlinear theory including thickness,
3. nonlinear theory including boundary layer corrections.

The theoretical curves are compared with corresponding experimental data [21]. To take into account first order boundary layer effects, a 2-d boundary layer calculation [22] has been carried out for each wing section using the steady pressures of the inviscid solution. Then the boundary layer displacement thicknesses have been added to the wing surface and a second calculation about the thickened wing was performed. The results show an improvement of the real parts of the unsteady pressures compared with experiment. Obviously, it is necessary to consider both thickness and boundary layer effects to obtain this improvement, a point which is extensively discussed in [11] for transonic flows, in which it plays a dominant role.

#### 4.3 UNSTEADY THEORY FOR OSCILLATING BODIES

A similar approach to that given in the previous section for finite thick wings can be applied to bodies (missiles, fuselages, tip-tanks etc.). For a configuration represented in Fig. 2 a linearization of the boundary condition is not obvious. Therefore, the exact geometric boundary condition, together with the complete Bernoulli equation (26) will be applied again in this case. A considerable simplification of the problem is obtained if the body is assumed to have no lift; thus, only a source-sink distribution is necessary, which is placed on the real body surface. Splitting up this surface again into surface elements and assuming constant source strength for each panel, the integral equation (48) - taking only the source terms - yields

$$(72a) \quad \frac{\partial \Phi_{q0}}{\partial \zeta} = -U_{\zeta 0}$$

for the steady and

$$(72b) \quad \frac{\partial \bar{\varphi}_{qi}}{\partial \zeta} = -(\bar{U}_{\zeta i} + \bar{V}_{\zeta})$$

for the unsteady potential (corresponding to Eqs. (69)), where again the aerodynamic influence functions  $\partial \Phi_{q0} / \partial \zeta$  and  $\partial \bar{\varphi}_{qi} / \partial \zeta$  are given by Eq. (70).

The right-hand sides of Eqs. (72) express the steady and unsteady normal components of the kinematic velocity in a body-fixed frame of reference. The determination of the kinematic velocity components in body-fixed coordinates (right-hand sides of Eqs. (72)) should be outlined at this point in more detail. If the case of pitching oscillations is assumed together with a time-independent translatory velocity of the body, then two different components of this motion can be observed on the body surface

1. Velocity  $\vec{V}$  due to harmonic oscillations of a surface point,
2. Velocity  $\vec{U}$  due to the translatory movement of the body.



Thus the kinematic velocity becomes

$$(73) \quad \vec{V}_{kin} = -(\vec{U} + \vec{V})$$

With the pitching axis parallel to the y-axis and with the vector  $U_{\infty}$  in the x,z-plane,  $\vec{V}_{kin}$  has the components

$$(74) \quad \vec{V}_{kin x} = -(U_{\infty} \cos \alpha + \bar{V}_x e^{i\omega^*T}) ; \quad \vec{V}_{kin z} = -(U_{\infty} \sin \alpha + \bar{V}_z e^{i\omega^*T})$$

with

$$(75) \quad \alpha = \alpha_s + \alpha' e^{i\omega^*T}$$

as the arbitrary time-dependent angle of incidence having a steady ( $\alpha_s$ ) and a time-dependent ( $\alpha' e^{i\omega^*T}$ ) part.

If  $d$  is the smallest distance between the surface point and the axis of rotation (Fig.2), then the velocity vector  $\vec{V}$  yields

$$(76) \quad \vec{V} = i\omega^* d \alpha' e^{i\omega^*T}$$

Substituting Eq.(75) into Eq.(74) gives the components of the vector  $\vec{U}$

$$(77) \quad \begin{aligned} U_{\infty} \cos \alpha &= U_{\infty} [\cos \alpha_s \cos(\alpha' e^{i\omega^*T}) - \sin \alpha_s \sin(\alpha' e^{i\omega^*T})] \\ U_{\infty} \sin \alpha &= U_{\infty} [\sin \alpha_s \cos(\alpha' e^{i\omega^*T}) + \cos \alpha_s \sin(\alpha' e^{i\omega^*T})] \end{aligned}$$

and for small oscillation amplitudes ( $\alpha'$ ) the quadratic and higher order terms in Eqs.(77) may be neglected. Thus Eq.(74) yields: (78)

$$\vec{V}_{kin x} = -U_{\infty} \cos \alpha_s + (U_{\infty} \sin \alpha_s \alpha' + \bar{V}_x) e^{i\omega^*T} ; \quad \vec{V}_{kin z} = -U_{\infty} \sin \alpha_s - (U_{\infty} \cos \alpha_s \alpha' + \bar{V}_z) e^{i\omega^*T} = \vec{V}_{kin s} + \vec{V}_{kin i}$$

where  $\bar{V}_x$  and  $\bar{V}_z$  are the corresponding components of  $\vec{V}$ .

By means of a simple coordinate transformation the components of  $\vec{V}_{kin}$  may be expressed also in surface or panel coordinates ( $\xi, \eta, \zeta$  in Fig.2) with  $\bar{V}_{\zeta}$  entering the right-hand side of the final integral equation (69) in the wing case or Eq.(72) in the body case. The term  $U_{\infty} \cos \alpha_s \alpha'$  is identical with the normal component  $\bar{U}_{\zeta j}$  in Eqs.(69) and (72).

If only small amplitude oscillations are assumed, the steady and the unsteady integral equation due to the first harmonic of the motion are sufficient. In [23] it is shown, however, that this linearization procedure with respect to the amplitude of oscillation is unnecessary if further terms in Eqs.(77) are retained, which leads to additional integral equations due to the second and higher harmonics of the motion. The solution procedure is simplified again because only one linear system, of equations with several right-hand sides, has to be solved. In correspondence to the treatment of the boundary condition and integral equation, the Bernoulli equation also can be formulated to give steady, first and higher harmonics of the pressure.

Carefully measured steady as well as unsteady pressure distributions are plotted in Figs.11-12 for an ellipsoid of axis ratio  $a/b = 3$  for three different steady incidences [25]. The solid curves in these plots are the results of the theoretical approach taking care of the exact geometrical boundary condition and Bernoulli equation. As long as viscosity is insignificant (front part of the body at low incidence), then the calculated curves fit extremely well with the experimental data. At the rear part of the body a separation region can be observed within the unsteady pressure distributions rather than in the steady pressures. With increasing incidence a pressure peak within the imaginary part of the unsteady pressures occurs, which must also be referred to as viscous effects. This peak is shifted forward with increasing incidence and may be caused by the two contra-rotating body vortices observed for such bodies of revolution. It is interesting to mention that the steady pressures in this region do not show any difference compared to the potential theoretical curve.

Methods for bodies of finite thickness have been discussed thus far only in the limiting case of incompressible flow. Large difficulties occur if compressibility effects are to be taken into account. Firstly, it must be kept in mind that the concept of linearization of the full potential equation (18) into Eq.(30) must still be used because a corresponding integral relation for the full potential equation does not exist. On the other hand, if the body under investigation cannot be approximated by a thin surface, one must try to use a surface singularity distribution and fulfill the boundary condition on the real body surface. In addition, one can try to solve the non-linearized Bernoulli equation for compressible flow. This concept is used in [24] for oscillating axisymmetric bodies in subsonic flow. Here Eq.(48) with the doublet terms neglected serves as the starting point. Difficulties occur in the numerical treatment of the surface integrals which now have the form

$$(78) \quad J = \iint_{\Delta S_j} \frac{e^{-ixr}}{r} ; \quad r = [(x-x')^2 + \beta^2((y-y')^2 + (z-z')^2)]^{1/2}$$

with  $x$  as the compressible reduced frequency. In [26] a series expansion of the exponential term in Eq.(78) and analytical integration of the single terms are described up to the sixth member of the series expansion.

A typical result of the method is given in Fig.13 for a spheroid with pitching oscillations about the midchord axis at  $Ma_{\infty} = 0.6$ . The results are compared with the corresponding incompressible curves and with results of a different solution procedure including compressibility effects [27]. The latter method solves the Helmholtz wave equation (Eq.(45)) directly by means of spheroid functions. Results of this quite different concept compared to surface singularity methods serve as a useful and necessary check on the reliability of the purely numerical concept. Fig.14 shows results for an ogive cylinder in compressible flow oscillating in pitching motion.

## 5. CONTROL SURFACES

Unsteady airloads on three-dimensional wings including one or more oscillating control surfaces can be calculated by one of the methods described in the previous sections. Only the normal wash on the oscillating flap must be modified, thus leading to a discontinuity along the leading edge of the flap. This discontinuity has already been investigated in [28], where a

logarithmic singularity in the pressure distribution was observed. Using the kernel function approach outlined in section 4.1.2.1, this special feature of the chordwise pressure distribution must be accounted for within the spanwise control surface region, whereas outside this region the usual loading functions are sufficient. Another possibility for applying the kernel function approach for wings with controls is described in [29] and [30]. Here the discontinuity in the normal wash distribution is subtracted, thus leading to smooth distributions, which can be solved easily by a standard kernel function approach. Although quite satisfactory results have been obtained with these modified kernel function approaches, tedious and time-consuming work is still required to determine the corresponding loading functions and to distinguish between the different regions where different functions must be applied.

Since surface discretization procedures such as the doublet-lattice or velocity potential panel methods are available, no special problems occur with the inclusion of oscillating controls. It is only necessary to represent the control surface leading and side edges by panel edges. Then the right normal wash within each panel control point is accounted for, regardless of the position of the panel, i.e. control or main wing surface. Using the velocity potential panel method it is advantageous to concentrate surface elements in front of and behind the control surface hinge lines due to the steep gradient of the chordwise potential distribution in this region.

Fig. 15 shows a comparison of calculated [14] and measured [31] pressure distributions for a swept wing with two control surfaces oscillating in anti-phase and the main wing remaining in a fixed position. The correspondence between calculated and measured results is quite good, except in regions close to the control hinge line. Here a small gap between the oscillating control surface and the main wing existed in the experimental case, which causes a reduction of the unsteady pressure on the main wing and increased pressures on the control. This behavior becomes obvious with increasing gap-width until the Kutta condition on the main wing and a square root singularity on the control leading edge is reached, yielding the limiting values for the single lifting surfaces.

Fig. 16 represents the situation for high subsonic flow for a two-dimensional wing with control surface. With increasing Mach number ( $Ma_\infty = 0.804$ ) additional deviations between calculated [14] and measured [32] results due to increasing nonlinearities in the flow can be observed. Interesting here is the change in sign of the real part pressure singularity at the leading edge of the wing, which is well-represented by the calculations.

Fig. 17 gives calculated and measured results for the case of a wing with a NACA 0012 airfoil section using the theoretical method with the inclusion of thickness [18].

Some special features of the measured pressure distribution are represented by the theory as the final pressure peak at the leading edge and lower real pressure parts on the control surface. But obviously the introduction of thickness effects alone is insufficient; viscous effects should be included, particularly in the gap region. This problem must be further investigated in future work.

## 6. UNSTEADY AERODYNAMIC INTERFERENCE

Up to this point prediction methods have been discussed to determine unsteady airloads on single oscillating wing or body surfaces. But the singularity distributions which have been calculated by means of the flow tangency condition on the surface also influence the surrounding flow field, in that they induce corresponding unsteady velocities. These velocity fields can be calculated easily in arbitrary field points off the surface once the singularity strengths have been determined. A flight vehicle has many different lifting surfaces (wings, tailplanes, etc.), and bodies (fuselage, tip-tanks, external stores, etc.). Each influences the others. Due to such aerodynamic interference, the aeroelastic stability of the flight vehicle is affected considerably. Special problems like T-tail flutter, wing-tailplane flutter for wings with variable wing geometry and wing-store flutter are some examples in which interference effects are of basic importance in aeroelastic investigation. Therefore, a number of prediction methods have been developed to investigate interference problems.

These methods are based on the same concepts discussed in the previous sections for lifting and non-lifting bodies in sub- and supersonic flows. In [33] a kernel function approach for interfering lifting surfaces is presented. [34] outlines a corresponding method based on the doublet-lattice concept, which includes the effects of bodies. A similar approach based on the velocity potential panel method is shown in [35]. Finally, a mixed doublet-lattice (for the lifting surface) and velocity potential panel (for the body) procedure has been applied in [36] for wing-store combinations. In the latter case, the body surface is represented by a velocity potential source distribution; the wing is assumed to be infinitely thin and is represented by acceleration potential doublets (NLR1-method).

In all calculation procedures using surface elements on the interfering surfaces, the only additional difficulty that occurs, compared to the single body cases, is a possible considerable increase in the number of surface elements and thus an increase in the number of linear algebraic equations. Special iteration procedures in solving the large systems of linear equations for interference problems are given in [36]. There the coefficient matrix is partitioned into wing- and body-submatrices having dominant main diagonals and into "interference matrices" containing the induced effects of the different bodies on each other.

One example of the application of the kernel function concept is given in Fig. 18 [37] for a wing-tailplane combination, where the sweep-angle of the wing and the chordwise location of the tailplane was varied. The calculated results are compared with corresponding wind tunnel measurements.

Fig. 19 shows the unsteady spanwise load distributions for a swept, tapered wing with and without tiptank, pylon and store, oscillating in pitching motion as obtained by the NLR1-method [36]. It can be observed from the plots that the tiptank has a lift-increasing effect like an endplate, whereas the store-eylon combination creates a jump in the spanwise load distribution. The calculated results are in fair agreement with corresponding experimental data.

Similar methods are presented for supersonic flows based on the kernel function concept [38] or on the velocity potential method [39]. But in the supersonic case, lack of experimental results makes it difficult to determine which of the methods gives sufficient results.

## 8. CONCLUSION

A large variety of reliable prediction methods for the determination of unsteady airloads on oscillating configurations exists today, and only some of the most important methods have been discussed in the foregoing sections. Although highly effective unsteady lifting surface theories have been computed for both sub- and supersonic flow regimes, many problems are still not solved satisfactorily, and thus further intensive investigation is needed. As outlined, the inclusion of profile geometry, i.e. thickness effects alone, is insufficient to improve the method, however additional viscous effects, which may be in the same order of magnitude, must also be taken into account to obtain a real improvement of the results compared to experiments. Therefore, the introduction of viscous effects either on the basis of boundary layer theory or on the basis of more complex viscous problems occurring within separated flow regions are necessary aims for future investigations. A special example with regard to these complex problems should be mentioned: the problem of wings with oscillating control surfaces. Viscous effects within the gap between the main wing and the control affect considerably the unsteady loads on the control surface. For this problem, both theoretical and experimental investigations are necessary. Another very difficult unsteady problem, in which viscous effects play a dominant role, is the dynamic stall problem occurring on retreating helicopter rotor blades. Here the cyclic separation and reattachment of the flow on the rotor blade influences the overall unsteady forces. Prediction methods to determine the correct unsteady airloads in this case are not available and approximate methods do not include all the complicated unsteady flow phenomena involved. Therefore, emphasis is placed on experimental investigations determining pressure distributions on blades oscillating with very high amplitudes about mean steady incidences, and measuring in a further step unsteady airloads on rotating and oscillating blades.

The whole transonic speed range still remains in the least satisfactory state. But transonic problems are of high importance for aeroelastic investigations.

## 9. REFERENCES

- [ 1 ] GEISSLER, W. Unsteady Aerodynamic Inputs for Aeroelastic Analyses.  
VKI-Lecture Series on "Aeroelastic Problems in Aircraft Design" 7. - 12. May 1979.
- [1a] FÖRSCHING, H. Modal Analysis of Aircraft Structures.  
VKI-Lecture Series on "Aeroelastic Problems in Aircraft Design" 7. - 12. May 1979.
- [ 2 ] BISPLINGHOFF, R. L., ASHLEY, H., HALFMAN, R. L. Aeroelasticity.  
Addison-Wesley Publ. Corp., Inc., Reading, Mass. (1962).
- [ 3 ] FÖRSCHING, H. Grundlagen der Aeroelastik. Springer-Verlag, Berlin/Heidelberg/New York (1974).
- [ 4 ] TIJDEMAN, H. Unsteady Airloads on Oscillating Lifting Systems at Transonic Flow.  
VKI-Lecture Series on "Aeroelastic Problems in Aircraft Design" 7. - 12. May 1979.
- [ 5 ] MAGNUS, R. J., YOSHIHARA, H. Calculations of Transonic Flow over an Oscillating Airfoil.  
AIAA-Paper 75-98, 13th Aerospace Sciences Meeting, Pasadena, Jan. 1975.
- [ 6 ] BEAM, R., WARMING, R. F. Numerical Calculations of Two-Dimensional Unsteady Transonic Flow with Circulation.  
NASA TN-D 7605 (1974).
- [ 7 ] ISOGAI, K. Calculation of the Unsteady Transonic Flow over Oscillating Airfoils Using the Full Potential Equation.  
AIAA-Paper 77-448, Dynamics Specialists Conference, San Diego, March 1977.
- [ 8 ] BALLHAUS, W. F., LOMAX, H. The Numerical Simulation of Low Frequency Unsteady Transonic Flow Fields.  
Proc. 4th International Conference on Numerical Methods in Fluid Dynamics, Univ. of Colorado, Boulder, June 1974.
- [ 9 ] KRUPP, J. A., COLE, J. D. Studies in Transonic Flow, IV-Unsteady Transonic Flow. UCLA-Eng-76104, Oct. 1975.
- [10] CHAN, S. T. K., BRASHEAR, M. R. Finite Element Analysis of Unsteady Transonic Flow.  
AIAA-Paper 75-875, 8th Fluid and Plasma Dynamic Conference, Hartford, Connecticut, June 1975.
- [11] TIJDEMAN, H. Investigations of the Transonic Flow around Oscillating Airfoils. Dissertation, T.H. Delft (1977).
- [12] WILLIAMS, D.E. Manual on Aeroelasticity Part II, Chapter 3. Three-Dimensional Subsonic Theory, Jan. 1961.
- [13] JONES, W.P., MOORE, J.A. Simplified Aerodynamic Theory of Oscillating Thin Surfaces in Subsonic Flow.  
AIAA-Journal 11, pp. 1305 - 1309 (1973).
- [14] GEISSLER, W. Ein numerisches Verfahren zur Berechnung der instationären aerodynamischen Druckverteilung der harmonisch schwingenden Tragfläche mit Ruder in Unterschallströmung.  
Teil I: Theorie und Ergebnisse für inkompressible Strömung. DLR-FB 75-37 (1975).  
Teil III: Theorie und Ergebnisse für kompressible Strömung. DLR-FB 77-15 (1977).
- [15] LASCHKA, B. Zur Theorie der harmonisch schwingenden tragenden Fläche bei Unterschallströmung.  
Z. Flugwiss. 11, pp. 265 - 292 (1963).
- [16] MULTHOPP, H. Methods for Calculating the Lift Distribution of Wings (Subsonic Lifting Surface Theory).  
ARC R & M 2884 (1955).
- [17] ALBANO, E., RODDEN, W.P. A Doublet-Lattice Method for Calculating the Lift Distribution on Oscillating Surfaces in Subsonic Flow. AIAA-Journal 7, pp. 279 - 285 (1969).
- [18] GEISSLER, W. Nonlinear Unsteady Potential Flow Calculations for Three-Dimensional Oscillating Wings.  
AIAA-Journal, Vol. 16, No. 11, Nov. 1978.
- [19] HESS, J. The Problem of Three-Dimensional Lifting Potential Flow and Its Solutions by Means of Surface Singularity Distributions. Computer Methods in Applied Mechanics and Engineering 4, pp. 283-319 (1974).
- [20] TRIEBSTEIN, H. Instationäre Druckverteilungsmessungen an angestellten Rotorblattspitzen in inkompressibler Strömung. DLR-FB 76-42 (1976).
- [21] TRIEBSTEIN, H. Instationäre Druckverteilungsmessungen an Flügel-Außenlastkombinationen in inkompressibler Strömung. DLR-FB 77-12 (1977).
- [22] ROTTA, J.C. FORTRAN IV-Rechenprogramm für Grenzschichten bei kompressiblen ebenen und rotationssymmetrischen Strömungen. DLR-FB 71-51 (1971).
- [23] GEISSLER, W. Berechnung der Druckverteilung an harmonisch oszillierenden dicken Rumpfen in inkompressibler Strömung. DLR-FB 76-48 (1976).

- [24] GEISSLER, W. Der harmonisch schwingende Rumpf in Unterschallströmung - Einfluß der Kompressibilität DFVLR-FB 78-24 (1978).
- [25] GEISSLER, W., KIENAPPEL, K. Investigations of the Incompressible Flow around an Oscillating Ellipsoid. XIV Biennial Fluid Dynamics Symposium "Advanced Problems and Methods in Fluid Mechanics" Blazejewko(Polen), 3. -8. 9. 1979.
- [26] HESS, J.L. Calculation of Acoustic Fields about Arbitrary Three-Dimensional Bodies by a Method of Surface Source Distributions Based on Certain Wave Number Expansions. Report No. DAC 66901, Douglas Aircraft Division, Long Beach, Calif. USA (1968).
- [27] CHAO, K.L. Analytische Lösung der verallgemeinerten Helmholtz-Wellengleichung für kompressible Unterschallströmung und Berechnung der instationären Druckverteilungen an harmonisch schwingenden rotationselliptischen Körpern. DLR.FB 77-11 (1977).
- [28] LANDAHL, M. On the Pressure Loading Functions for Oscillating Wings with Control Surfaces. AIAA-Journal 6, pp. 345 - 348 (1968).
- [29] ASHLEY, H., ROWE, W.S. On the Unsteady Aerodynamic Loading of Wings with Control Surfaces. Z. Flugwiss. 18, pp. 321 - 330 (1970).
- [30] ROWE, W.S., WINTER, B., REDMAN, M.C. Prediction of Unsteady Aerodynamic Loadings Caused by Trailing Edge Control Surface Motions in Subsonic Compressible Flow. NASA CR 2003 (1972).
- [31] TRIEBSTEIN, H., WAGENER, J. Druckverteilungsmessungen an einem harmonisch schwingenden Pfeilflügel mit zwei Rudern in inkompressibler Strömung. DFVLR-AVA-Bericht 70 J04 (1970).
- [32] TIJDEMAN, H., SCHIPPERS, P. Results of Pressure Measurements on an Airfoil with Oscillating Flap in Two-Dimensional High Subsonic and Transonic Flow (Zero Mean Incidence and Zero Mean Flap Position). NLR-TR 73078 U (1973).
- [33] LASCHKA, B. Interfering Lifting Surfaces in Subsonic Flow. Z. Flugwiss. 18, pp. 359 - 368 (1970).
- [34] GIESING, J.P., RODDEN, W.P., KALMAN, I.P. Subsonic Steady and Oscillatory Aerodynamics for Multiple Interfering Wings and Bodies. Journal Aircraft 9, pp. 693 - 702 (1972).
- [35] CHAN, L.T., SUCIU, E.O., MORINO, L. A Finite Element Method for Potential Aerodynamics around Complex Configurations. AIAA-Paper 74-107, Washington D.C. (1974).
- [36] ROOS, R., BENNEKERS, B., ZWAAN, R.J. A Calculation Method for Unsteady Subsonic Flow about Harmonically Oscillating Wing-Body Configurations. AIAA-Paper 75-864 (1975).
- [37] TRIEBSTEIN, H., BECKER, J. Untersuchung instationärer Interferenzeffekte an einem harmonisch schwingenden Flügel-Höhenleitwerks-Modell mit variabler Flügelgefeilung im niedrigen Unterschallbereich. DLR-FB 71-52(1971).
- [38] CUNNINGHAM Jr., A.M. Oscillatory Supersonic Kernel Function Method for Interfering Surfaces. Journal Aircraft 11, pp. 664 - 670 (1974).
- [39] GIESING, J.P., KALMAN, I.P. Oscillatory Supersonic Lifting Surface Theory Using a Finite Element Doublet Representation. AIAA-Paper (1975).

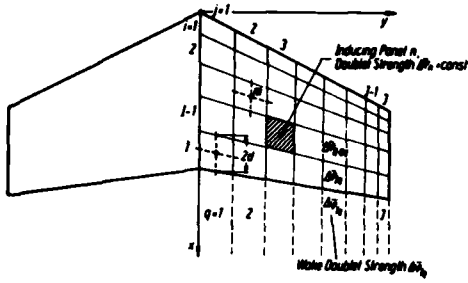
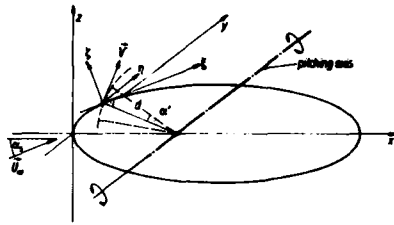


Figure 1: Velocity potential panel method. Coordinate system, panel arrangement.



$$\alpha(t) = \alpha_0 + \alpha' e^{i\omega t}$$

Figure 2: Oscillating body with incidence.

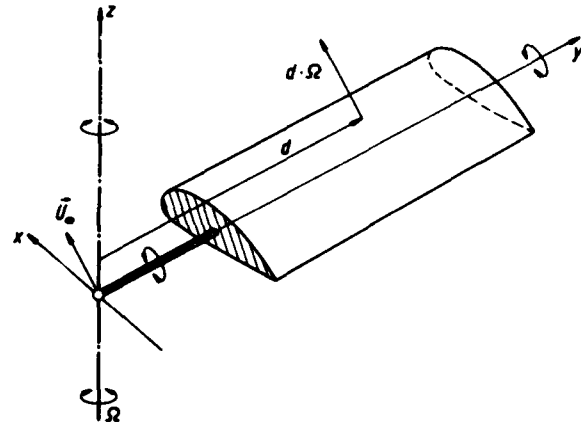


Figure 3: Helicopter rotor blade.

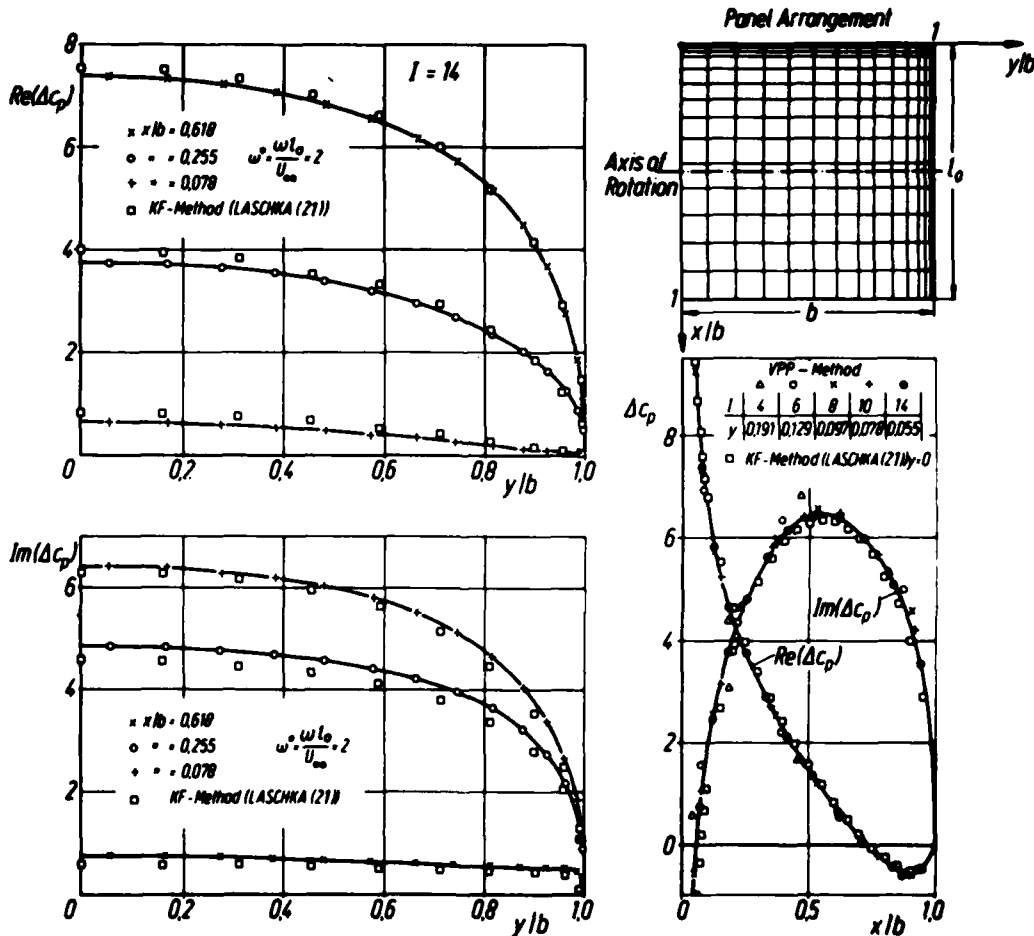


Figure 4: Unsteady pressure distributions for a rectangular wing with pitching oscillations.

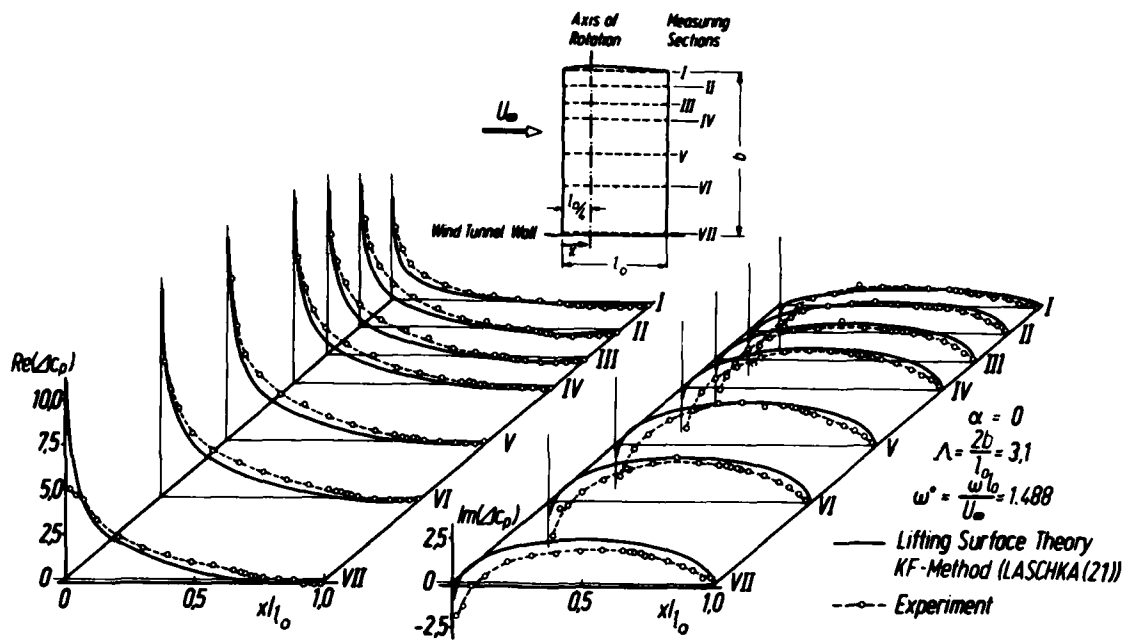


Figure 5: Unsteady pressure distributions for a rectangular wing with pitching oscillations in incompressible flow. NACA 0012 profile

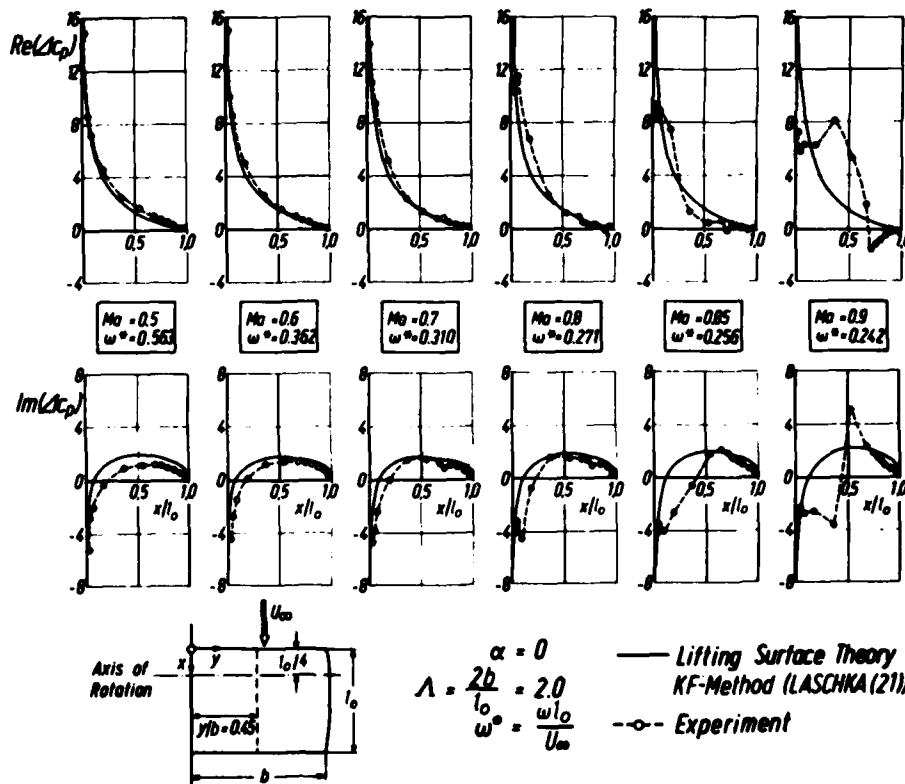


Figure 6: Unsteady pressure distributions for a rectangular wing with pitching oscillations in compressible subsonic flow. NACA 0008 profile

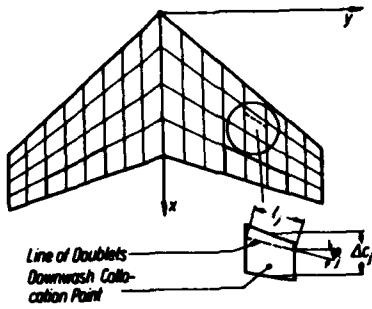


Figure 7: Doublet-lattice method. Lifting surface and panel geometry.

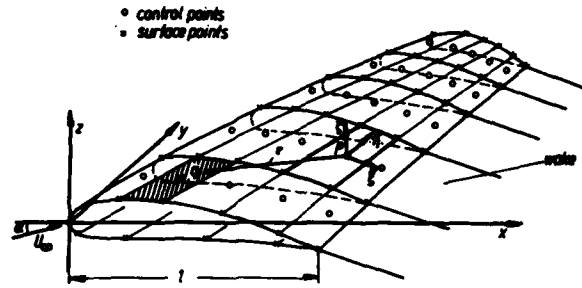


Figure 8: Wing with thickness and incidence. Geometry and panel arrangement.

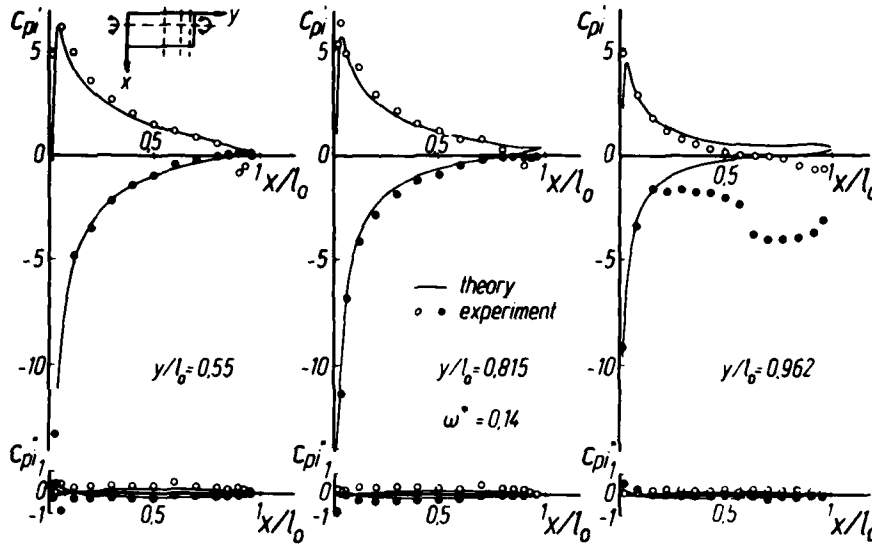


Figure 9: Unsteady pressure distributions for a rectangular wing.  $\Delta = 4$ ,  $\alpha_s = 60^\circ$ ,  $\omega^* = 0.14$  - NACA 0012 profile

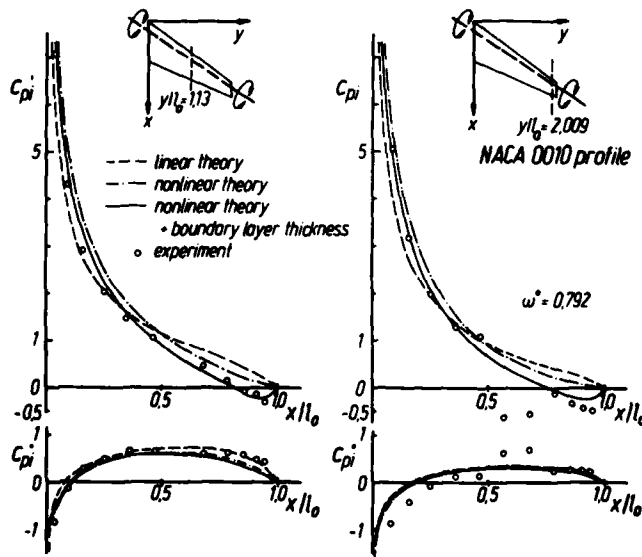


Figure 10: Unsteady pressure distributions for a swept-tapered wing with pitching oscillations. Influence of boundary layer thickness.  $\Delta = 2$ ,  $\alpha_s = 0^\circ$ ,  $\omega^* = 0.792$  - NACA 0010 profile

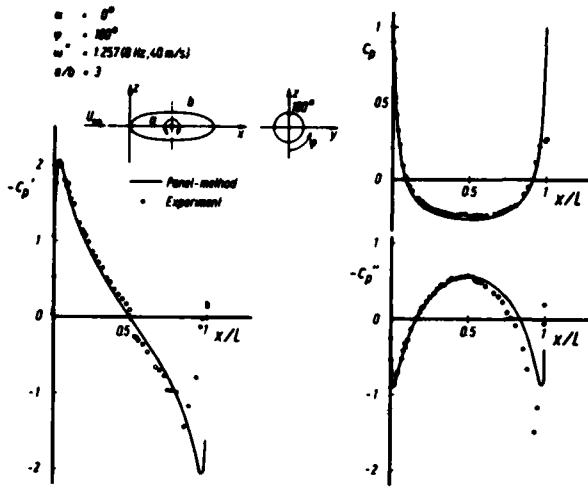


Figure 11 (left): Ellipsoid with pitching oscillations. Comparison between theory and experiment.  $\alpha_s = 0^\circ$ ,  $\omega^* = 1,257$

Figure 12 (right): Ellipsoid with pitching oscillations. Comparison between theory and experiment.  $\alpha_s = 20^\circ$

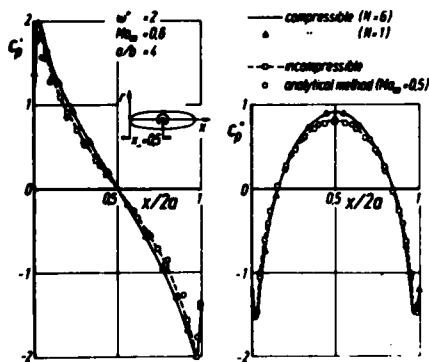
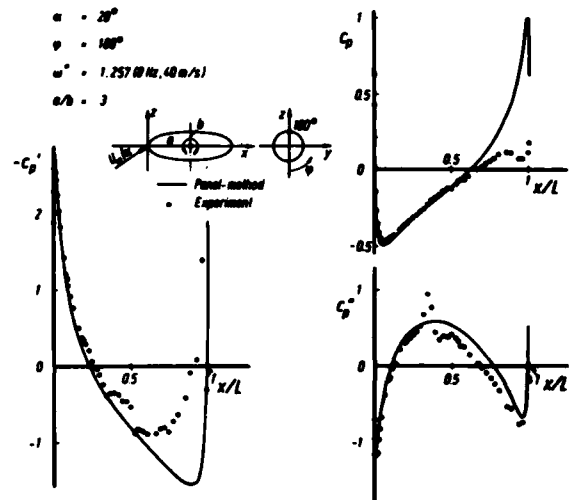


Figure 13: Unsteady pressure distributions for an ellipsoid with pitching oscillations in compressible flow.  $a/b = 4$ ,  $Ma_\infty = 0,6$ ,  $\omega^* = 2$

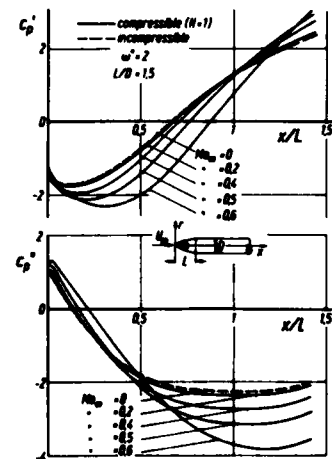


Figure 14: Unsteady pressure distributions for a pointed body with pitching oscillations in compressible flow.  $L/D = 1,5$ ,  $\omega^* = 2$



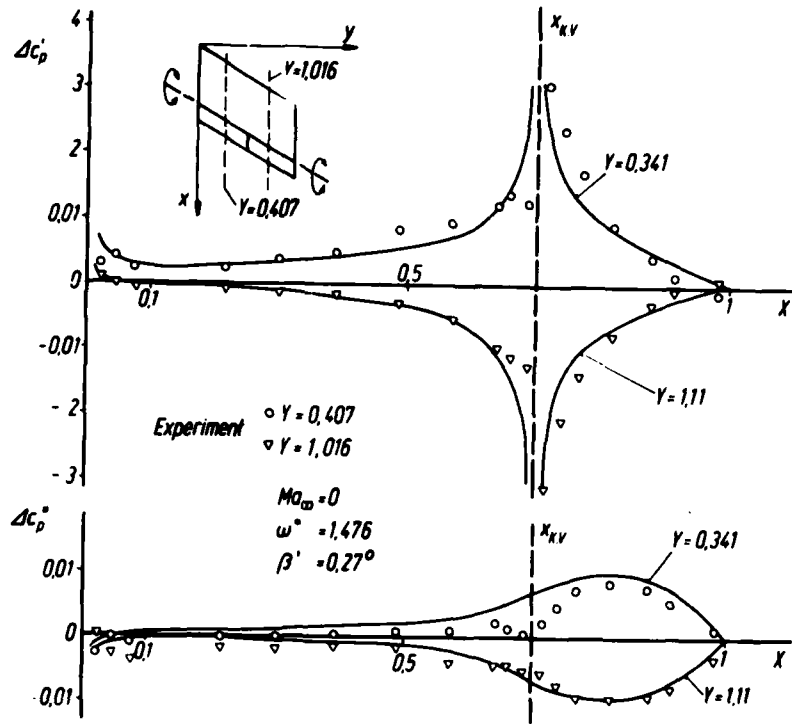


Figure 15: Unsteady pressure distributions on a swept wing with two controls oscillating in anti-phase.  
 $\Lambda = 2,94$ ,  $Ma_{\infty} = 0$ ,  $\omega^* = 1,476$

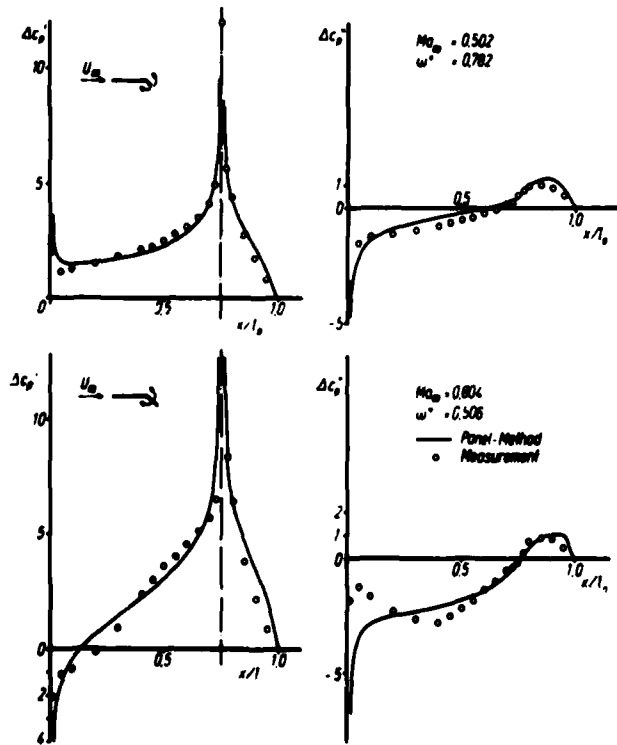


Figure 16: Wing section with oscillating control. Unsteady pressure distributions.

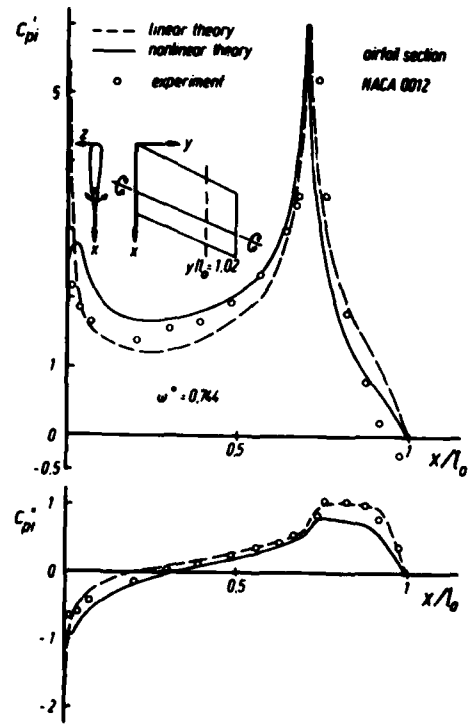


Figure 17: Unsteady pressure distributions for a swept wing with control surface in incompressible flow.  
 $\Lambda = 2,94$ ,  $\alpha_s = 0^\circ$ ,  $\omega^* = 0,744$

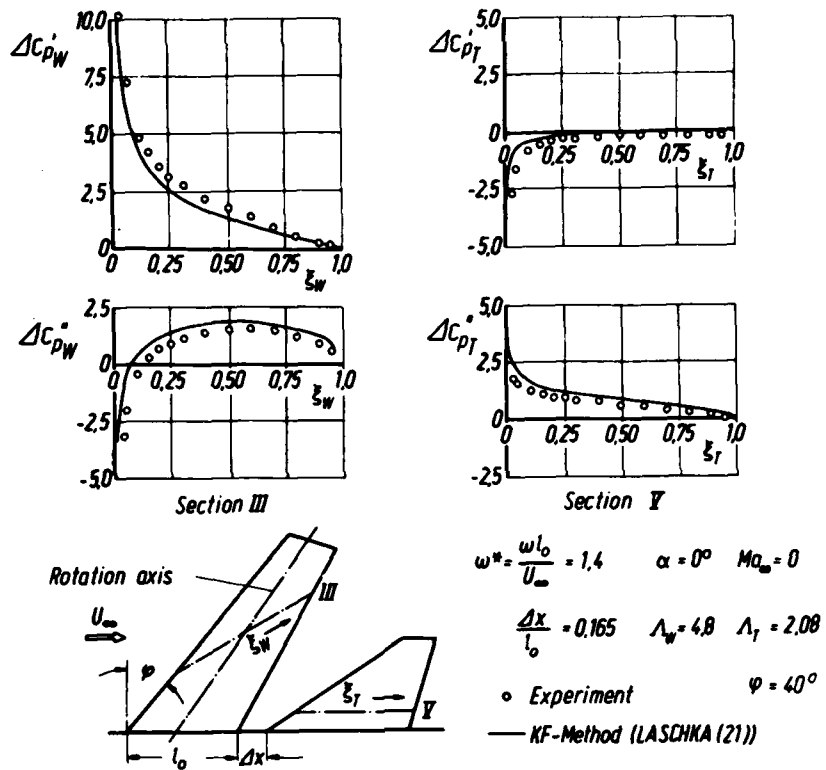


Figure 18: Unsteady pressure distributions for an interfering wing-tailplane configuration with pitching oscillations (Ref. [60]).  
 $\omega^* = 1.4$ ,  $Ma_\infty = 0$

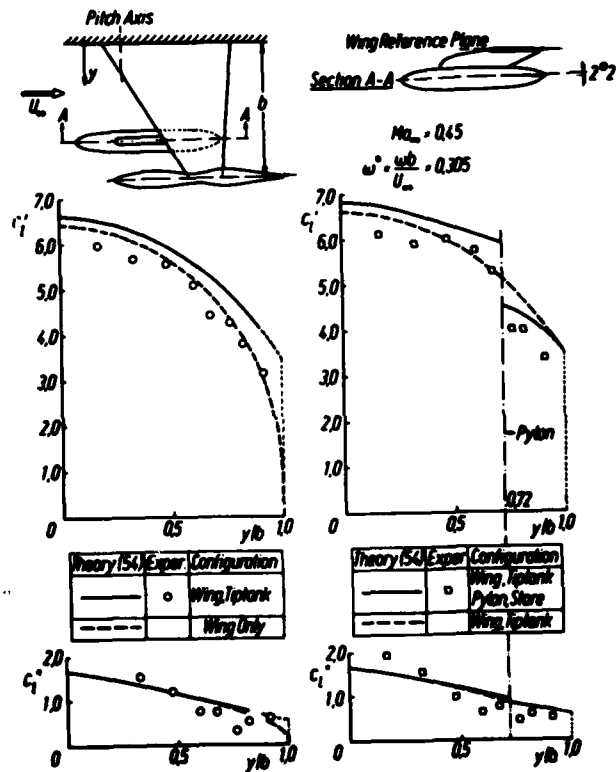


Figure 19: Spanwise lift distributions for a swept, tapered wing-tiptank (left) and wing-pylon-tiptank-store (right) combination (Ref. [59]).  
 $\omega^* = 0.305$ ,  $Ma_\infty = 0.45$

## UNSTEADY AERODYNAMICS IN TURBOMACHINERY

by  
 D.S. Whitehead  
 Reader in Engineering  
 Cambridge University Engineering Department  
 Trumpington Street  
 Cambridge CB2 1PZ  
 England

## SUMMARY

This series of three lectures considers unsteady flow phenomena in turbomachines, blade flutter, and methods for unsteady cascades.

The phenomena of inlet maldistribution, rotating stall, surge, blade vibration, and sound generation are described, and related to the requirements for unsteady aerodynamic theory.

The types of blade flutter and the modes in which it occurs are then described, a theoretical method of flutter prediction is discussed, and the effects of mechanical damping and mistuning evaluated.

A theory of linearized two-dimensional unsteady flow in cascades is outlined for both subsonic and supersonic flow, and the importance of the two different kinds of acoustic resonance which occur is discussed.

Unsteady Flow Phenomena in TurbomachinesIntroduction

There are a considerable number of manifestations of the effects of unsteady flow in turbomachinery. I shall start by giving a brief description of the main physical effects, and then go on to consider how some of these effects can be predicted by theoretical calculation. Correlations, although of great practical use, are generally specific to particular designs of machine, and these will not be given any significant treatment.

Inlet Maldistribution

If the flow at entry to a turbomachine is non-uniform, due for instance to the wakes from struts supporting the bearings, to the effects of a non-axisymmetric air intake, or to hot-spots from a combustion chamber, then the rotor blades will see an unsteady environment as they rotate. This can cause various unwanted effects, such as blade vibration, loss of efficiency, and compressor surge. It is therefore necessary to know how the non-uniformity develops as it progresses through the machine.

The simplest way to do this is to use the compressors-in-parallel theory. This assumes that each part of the annulus of the machine operates as a separate system in steady flow, independent of what is going on in all the other parts of the annulus. For small perturbations in incompressible flow this theory gives the result.

$$\frac{V_{x2}'}{V_{x1}'} = - \frac{\rho \bar{V}_{x1}}{f'}$$

where

$V_{x1}'$  is the inlet axial velocity perturbation  
 $V_{x2}'$  is the outlet axial velocity perturbation  
 $\rho$  is the fluid density  
 $\bar{V}_x$  is the mean inlet axial velocity  
 $f'$  is the slope of the characteristic of the blading, plotted in the form of the outlet static pressure minus inlet total pressure against axial velocity. This is illustrated for a compressor on figure 1. For a normal operating point such as A,  $f'$  is large and negative, and the disturbance is strongly attenuated as it goes through the machine. As the stall point at B of the compressor is approached,  $f'$  becomes small, and the disturbances grow as they go through the machine.

This very simple and elementary theory ignores the unsteady effects on the performance of the rotor blades, and it will be part of our task to consider how these unsteady effects can be assessed.

Rotating Stall

As the compressor is throttled past the point B on figure 1, very small non-uniformities at inlet can grow to large amplitude. The usual result is that "rotating stall" appears. This consists of one or more patches of stalled flow which rotate around the machine, usually at somewhat less than half the speed of rotation of the rotor. If rotors and stators were identical, then the speed of rotation would, by symmetry, be expected to be exactly half of the rotor speed.

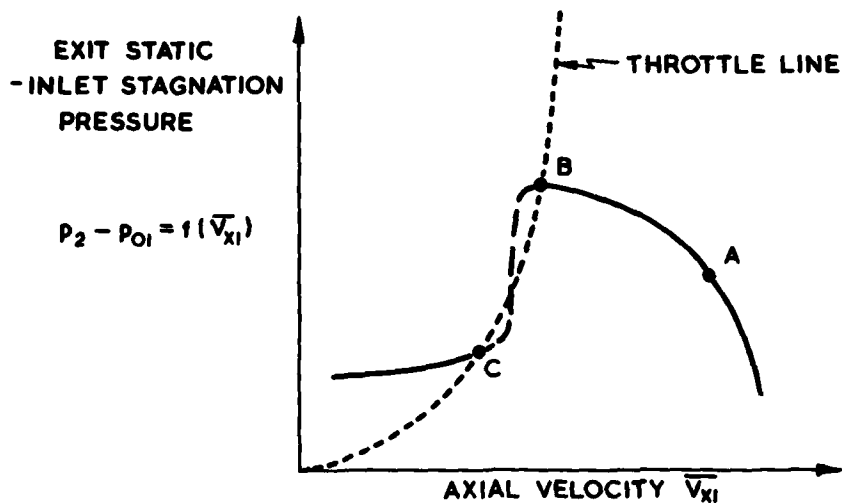


Fig. 1 Compressor Characteristics

At low speed the result of this is that the mean operating point suddenly drops to a point such as C, the efficiency becomes poor, and all the blades are subject to severe buffeting from the rotating stall patches.

#### Surge

At higher speed, instead of settling down at a point such as C, the compressor may go into a mode of operation in which the flow oscillates with large amplitude. This is surge, and the instantaneous flow reverses during part of the cycle. On a test facility the frequency is of the order of 1 Hz, but on a jet engine where the duct volumes are much less, the frequencies are of the order of 10 Hz. Note that these frequencies are much less than the rotating stall frequency, and in fact rotating stall may exist over part of the surge cycle.

Greitzer (1976) has shown that whether or not a compressor surges is determined largely by the parameter  $B = U/2\omega L_c$ , where  $U$  is the mean rotor velocity,  $\omega$  is the Helmholtz resonator frequency for the exit plenum volume and the duct in which the compressor is running, and  $L_c$  is the axial length of this duct. Greitzer found that one particular three-stage axial compressor surged when  $B$  exceeded 0.8.

#### Blade Vibration

One result of inlet maldistribution may be that the rotor blades are forced to vibrate at large amplitude. The blades on an axial-flow turbomachine are usually of solid metal, and they are therefore much more massive than the air or gas in their immediate vicinity. The unsteady aerodynamic forces and moments are therefore not strong enough to alter the modes of vibration of the blades significantly, and the situation is fundamentally different from that of an aeroplane wing. This means that the problem of predicting the amplitude may be split into first a calculation of the principal modes and natural frequencies of the bladed disc, and secondly a calculation of the unsteady forces and moments acting on the blades when they are vibrating in one of these modes. We shall only consider the second of these two problems.

It sometimes happens that the aerodynamic forces are such as to feed energy into a small amplitude vibration, and the vibration is then self-excited. This is flutter and will be considered in a later lecture.

#### Sound Generation

An important consequence of unsteady flow over blading is the generation of unwanted sound. This can arise due to the interaction of the pressure field or vorticity field due to one blade row interacting with a second blade row. For this reason the fans on fan-jet engines are usually designed with no inlet guide vanes, and with a large gap between rotor blades and stator blades. Sound can also be generated by the interaction of a rotor row with turbulence in the inlet air-stream, and by turbulence generated in the flow over blades. Sound generated by the rotation of the pressure field of the rotor alone can usually be arranged to be cut-off. (But this is the most important source of sound for propellers).

#### Requirements for Unsteady Aerodynamic Theory

In order to predict these various effects, it is necessary to know the unsteady characteristics of the blade rows. The frequencies involved in surge are so low that a quasi-steady approach is justified, but for all other cases an unsteady aerodynamic theory is really necessary.

The inputs to the theory are as follows:

- (a) bending vibration of the blades,
- (b) edgewise vibration of the blades,
- (c) torsional vibration of the blades,

- (d) stagnation pressure variations ("Vorticity Waves") at entry,
- (e) stagnation temperature variations ("Entropy Waves") at entry,
- (f) acoustic waves entering from upstream,
- (g) acoustic waves entering from downstream.

For each of these seven inputs, the following outputs from the theory are required:

- (a) Lift force on the blades,
- (b) chordwise force on the blades,
- (c) moment on the blades,
- (d) vorticity shed from the blades,
- (e) temperature variations downstream,
- (f) acoustic waves radiated upstream,
- (g) acoustic waves radiated downstream.

This information enables all the unsteady effects to be predicted. Unfortunately, however, it is in many cases not yet available. Stalled flow involving unsteady boundary layer separation has, so far as I know, only been applied to cascades in a rather rudimentary manner. Three dimensional linearized theories have been developed by Salaün (1974) and Namba (1977) and Graham (1970) has developed similarity laws for extending two-dimensional linearized aerodynamics, and these will be discussed in a later lecture. Two-dimensional theories in which the steady flow is not assumed to be a uniform flow (as in the linearized theories) are under active development in several places, but have not reached the stage at which it is appropriate to discuss them.

#### References

- Graham, J.M.R., 'Similarity rules for thin aerofoils in non-stationary subsonic flows'. J. Fluid. Mech. Vol. 43 (1970) p.253.
- Greitzer, E.M., 'Surge and Rotating Stall in Axial Flow Compressors. Part I: Theoretical Compression System Model. Part II: Experimental Results and Comparison Theory.' Trans. ASME, Journal of Engineering for Power, Vol. 98 (1976) pp. 190-217.
- Salaün, P., 'Pressions aerodynamique instationnaires sur une grille annulaire en écoulement subsonique.' ONERA Publications No. 158 (1974).
- Namba, M., 'Three-dimensional analysis of blade force and sound generation for annular cascade in distorted flows.' J. Sound Vib. Vol. 50 (1977) p.479.

### Blade Flutter

#### Types of Flutter

Blade flutter, or self-excited vibration of the blades, has been recognised as a major problem almost from the beginning of the development of the axial flow compressor. Established cases of flutter in turbine blades are very rare, and this is not normally recognised as a significant problem. Nevertheless, I have long suspected that many cases of blade failures in turbines which have been put down as forced vibration have in fact been due to a near approach to a flutter situation, in which the aerodynamic damping of the vibration has become very small. But this is an unconventional view, and I shall confine myself to compressor blading.

The most common type of flutter is stall flutter, which is sometimes observed near the peak of the compressor characteristic when at least part of the span of the blade is stalled. Amplitudes are usually large, and give rapid failure of the blades. There is no basic theory which can predict this type of flutter, but empirical rules such as that proposed by Armstrong and Stevenson (1960) are capable of controlling its occurrence. This rule states that for bending vibration the frequency parameter  $\omega c/V_1$  (where  $\omega$  = angular frequency,  $c$  = blade chord, and  $V_1$  = inlet flow velocity) should not be less than 0.33, and that for torsional vibration the frequency parameter should not be less than 1.6.

Choke flutter sometimes occurs when the blade passage is choked and there is a shock wave across the passage. The motion of the blades is associated with motion of the shock wave. Luckily the conditions under which it occurs are usually outside the normal range of operation of the compressor, so that it is not an important problem.

Turning to cases where the compressor is working near its design conditions, so that neither stalling nor choking occurs, it becomes possible to make a reasonable prediction of flutter using basic theory. The most important practical case is that of the fan blading on modern fan-jet engines. These fan blades operate with supersonic relative velocity into the tip sections, and they are found to be very close to a flutter condition, as reported, for instance, by Halliwell (1976).

#### Modes

Let us consider first a symmetric flexible disc fitted with a set of identical blades without snubbers, and suppose that each blade vibrates in its first bending mode slightly modified by the disc flexibility. One mode of such a system, having 3 nodal diameters, is illustrated in figure 1. In general, for  $r$  nodal diameters the deflection of the  $m$  th blade is

$$\sin(2\pi r m/N) e^{i\omega t}$$

where  $N$  is the number of blades. There is another mode with deflection

$$\cos(2\pi r m/N) e^{i\omega t}$$

When expressed in this way, the modes will be called "mechanical modes".

An alternative and equivalent way of specifying these two modes is to use

$$e^{i(\omega t + 2\pi r m/N)},$$

and

$$e^{i(\omega t - 2\pi r m/N)}.$$

This method is more convenient for aerodynamic calculations, and modes expressed this way will be called "aerodynamic modes". Each blade has the same amplitude, and there is a phase angle  $\beta = 2\pi r/N$  between each blade and the next. The complete set of  $N$  modes may then be obtained by taking  $0 \leq r \leq (N-1)$ , giving  $N$  equally spaced values of  $\beta$ .

There are further families, each of  $N$  modes, corresponding to the first torsion, second bending, second torsion, and other higher modes of individual blades.

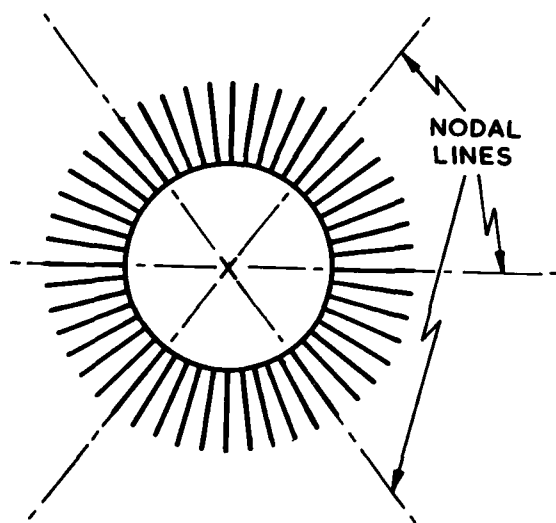


Fig. 1 Principal Mode of Bladed Disc

$$r = 3$$

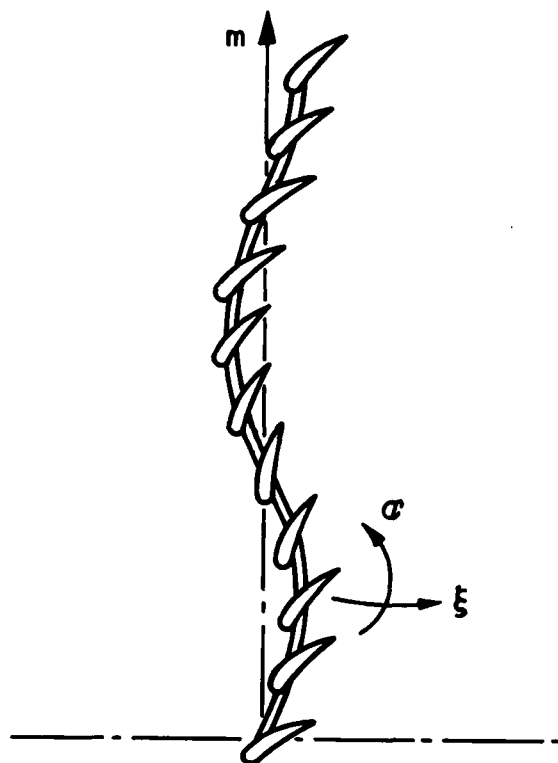


Fig. 2 Developed view onto tips of vibrating snubbed blade assembly

In order to alleviate the vibration problems, the blades are in many cases inter-connected by "snubbers" or part-span shrouds. These snubbers lock up tight under the centrifugal loading to give the effect of a continuous ring interconnecting the blades. As illustrated in figure 2, the effect on the modes is to link the bending and torsional motion of the blades, so that the axial deflection ( $\xi$ ) and torsional deflection ( $\alpha$ ) in a mechanical mode are given by

$$\xi = A \sin(2\pi r m/N) e^{i\omega t},$$

$$\alpha = -A(2\pi r/Ns) \cos(2\pi r m/N) e^{i\omega t}.$$

where  $s$  is the blade spacing. The complementary mode is

$$\xi = A \cos(2\pi r m/N) e^{i\omega t},$$

$$\alpha = A(2\pi r/Ns) \sin(2\pi r m/N) e^{i\omega t}$$

Note that the deflection and torsion are in quadrature spatially (but in phase in time).

These can also be expressed alternatively as aerodynamic modes

$$\xi = A e^{i(\omega t + 2\pi r m/N)}$$

$$\alpha = -iA(2\pi r/Ns) e^{i(\omega t + 2\pi r m/N)}$$

and the complementary mode is

$$\xi = A e^{i(\omega t - 2\pi r m/N)}$$

$$\alpha = +iA(2\pi r/Ns) e^{i(\omega t - 2\pi r m/N)}$$

These aerodynamic modes still have the property of constant phase angle between adjacent blades.

There will again be a number of families of modes of this type, each with  $N$  modes. These modes can be calculated with good accuracy.

#### Flutter Prediction

Suppose that the blades are vibrating in one of these "aerodynamic modes", with constant phase angle,  $\beta$ , between each blade and its neighbour. The problems of calculating the aerodynamic forces and moments will be considered in a later lecture, but one thing can be seen by symmetry and that is that these forces and moments will also have the property of constant phase angle,  $\beta$ , from each blade to the next. These forces and moments can therefore alter the frequency of vibration, and they may feed in or take out work, but they cannot introduce motion with any other value of  $\beta$ . If the net work is zero we have a marginal flutter situation, and we reach the important conclusion that the "aerodynamic modes" as previously defined are the flutter modes of the system. There may be a slight change to the radial variation of amplitude, but this will normally be negligible, and the difference between the flutter frequency and the mechanical natural frequency will be small.

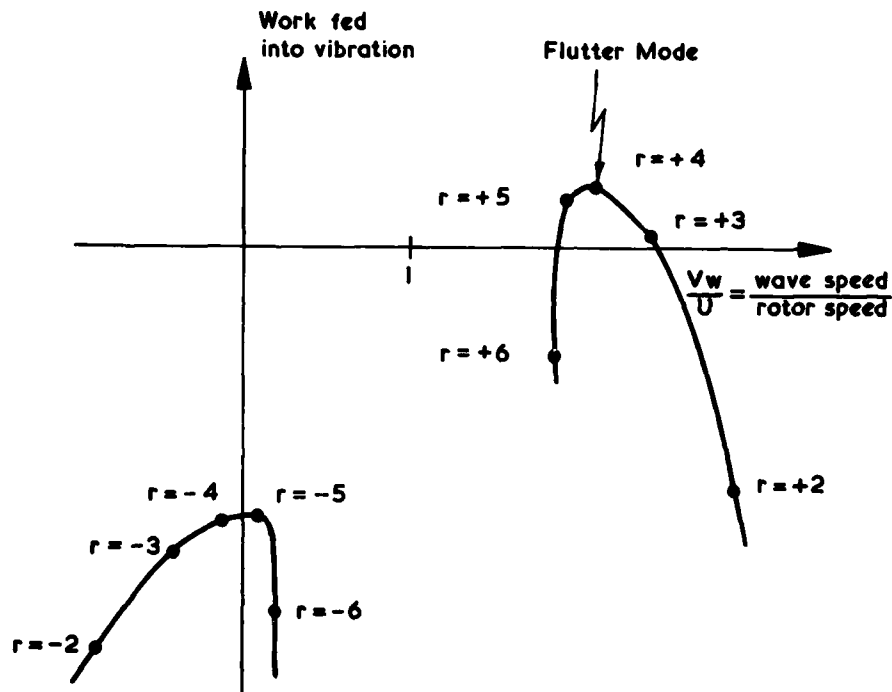


Fig. 3 Work fed into vibration by aerodynamic forces

$$\frac{Vw}{U} = \frac{\text{Wave speed relative to casing}}{\text{Rotor speed}} = 1 + \frac{1}{2\pi r} \frac{\text{Vibration frequency}}{\text{Rotation frequency}}$$

Figure 3, taken from the paper by Halliwell (1976), shows the work fed into the vibration by the aerodynamic forces plotted against the ratio wave speed/rotor speed, (or equivalently  $\beta$  or  $r$ ). The mode which will flutter is that which feeds most work into the vibration, and in this case is  $r = 4$ . It is therefore necessary to do the calculation for a number of different values of  $\beta$  (or  $r$ ), and find that which maximises the work. In the absence of mechanical damping, flutter is predicted if the maximum work is positive and the flutter mode is predicted.

#### Effect of Mechanical Damping

In practice it is likely that mechanical damping removes a significant amount of vibrational energy, and flutter will only occur if the aerodynamic work is greater than this. Whitehead (1964) found in a low Mach number experiment that the effect of mechanical damping was to roughly double the airspeed for flutter, but this is probably an extreme case. Mechanical damping is therefore always favourable, but since it is very variable in practice it is questionable whether it is wise to rely on it for safety of a machine.

#### Effect of Mis-Tuning

If the blades are not identical, but are, as is always the case in practice, mistuned, then the "aerodynamic modes" as defined above are no longer principal modes of the mechanical system. The flutter mode will therefore contain components of the other aerodynamic modes besides that which gives maximum work input. But as far as the aerodynamic forces are concerned the "aerodynamic modes" are orthogonal, so that the net work input is the sum of the work from each "aerodynamic mode" as if only that mode were present. These other aerodynamic modes will therefore feed in less work than would be obtained in the exactly tuned case. It is concluded that the effect of mistuning on flutter is always favourable. This argument can be made rigorous, (Whitehead 1964).

The effect of mistuning on flutter may be contrasted with the effect on forced vibration, where the effect can be to concentrate the energy into one blade and increase the amplitude by a factor of  $(1 + \sqrt{N})/2$ , (Whitehead 1966, 1976).

When the blades are connected by snubbers, the principal modes of the bladed disc are forced to correspond very closely with the "aerodynamic modes". The effect of mistuning on flutter of snubbed blades is therefore very small.

#### References

- Armstrong, E.K. and Stevenson, R.E., 'Some practical aspects of compressor blade vibration.' Journal Roy. Aero. Soc., Vol. 64, (1960), p. 117.
- Halliwell, D.G., 'The characteristics, prediction and test analysis of supersonic flutter in turbofan engines.' Proc. I. Mech. E. Conf. on "Vibrations in Rotating Machinery", Churchill College Cambridge, 1976.
- Whitehead, D.S., 'Torsion flutter of unstalled cascade blades at zero deflection.' R. & M. 3429, (1964).
- Whitehead, D.S., 'The effect of mistuning on the vibration of turbomachine blades induced by wakes.' J. Mech. Engng. Sci. Vol. 8, (1965), p. 15.
- Whitehead, D.S., 'Effect of mistuning on forced vibration of blades with mechanical coupling.' Journal Mech. Eng. Sci. Vol. 18, (1976), p. 306.

### Methods for Unsteady Cascades

#### Basic Equations

In this lecture it is proposed to give an outline of a few of the methods which are currently being used to provide unsteady aerodynamic data for cascades in both subsonic and supersonic flow. The methods to be described are two-dimensional and linearized, which means that the unsteady effects are small perturbations of a uniform flow. This of course limits the applicability of the methods quite severely. It is impossible to deal with the effects of camber, thickness, incidence, and of mean pressure rise or fall in the cascade. The model used is illustrated in figure 1.

The equations of continuity, momentum, and isentropic flow are then

$$\left. \begin{aligned} \frac{D\rho}{Dt} + \rho_o \nabla v &= 0 \\ \frac{Dv}{Dt} + \frac{1}{\rho_o} \nabla p &= 0 \\ \frac{p}{\rho} = \frac{\gamma p_o}{\rho_o} &= a_o^2 \\ \frac{D}{Dt} &= \frac{\partial}{\partial t} + U \frac{\partial}{\partial x} \end{aligned} \right\} (1)$$

where

and the suffix o indicates the uniform flow.



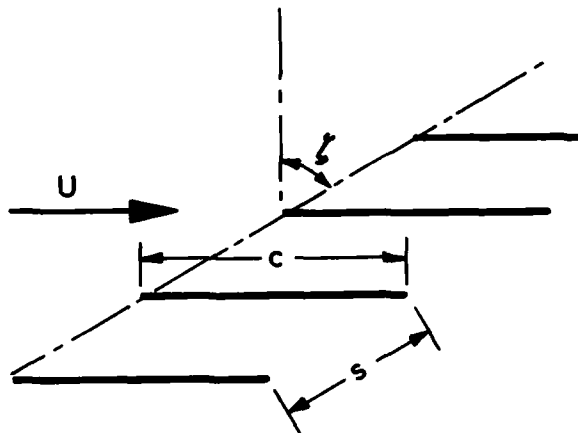


Fig. 1 Flat plate model

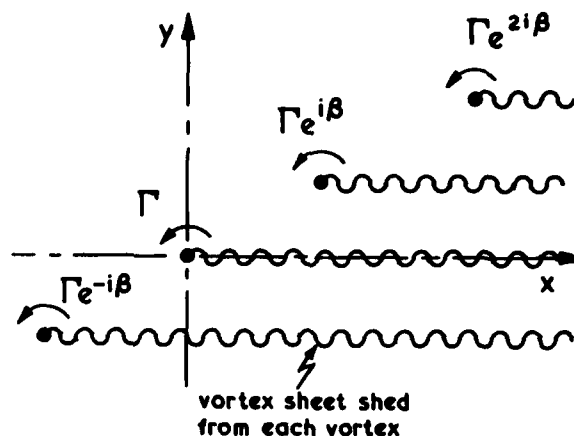


Fig. 2 Elementary row of vortices

### Methods of solution

The methods of solution which will be discussed here are the singularity methods, used in subsonic flow by Kaji and Okazaki (1970) and Smith (1972) and in supersonic flow by Verdon and McCune (1975), Nagashima and Whitehead (1977), Verdon (1977), and Ni (1979). An alternative approach is to use the Wiener-Hopf technique, which has been shown to work particularly well for closely spaced blades by Koch (1978).

First we consider two simple basic solutions.

### Vorticity and Pressure Waves

One solution of equation (1) is

$$\left. \begin{aligned} u &= -(aU/\omega) \bar{v} e^{i(\omega t - x/U - ay)} \\ v &= \bar{v} e^{i(\omega t - x/U - ay)}, \\ p &= a_0^2 \rho = 0 \end{aligned} \right\} (2)$$

This shows a velocity pattern which varies sinusoidally with time and is convected downstream at the main-stream velocity  $U$  and has wavenumber  $\alpha$  in the  $y$  direction. These are vorticity waves, and they involve no pressure or density perturbation.

The second basic solution is for acoustic waves, and is

$$\left. \begin{aligned} u &= (k/\alpha) \bar{v} e^{i(\omega t - kx - ay)} \\ v &= \bar{v} e^{i(\omega t - kx - ay)} \\ p &= a_0^2 \rho = \{(\omega - kU)\rho_0/\alpha\} \bar{v} e^{i(\omega t - kx - ay)} \end{aligned} \right\} (3)$$

where

$$(\omega - kU)^2 - a_0^2(k^2 + \alpha^2) = 0 \quad (4)$$

These acoustic waves have zero vorticity. For a given phase angle  $\beta$  between blades, the wavenumber must satisfy

$$as \cos \zeta + ka \sin \zeta = -(\beta + 2\pi n) \quad (5)$$

where  $s$  is the cascade spacing,  $\zeta$  is the stagger angle, and  $n$  is an integer.

Equations (4) and (5) may or may not have two real roots in  $k$  and  $\alpha$  for given frequency ( $\omega$ ), phase angle ( $\beta$ ), and integer ( $n$ ). If they do have real roots, then there exists a pair of acoustic waves, one of which carries energy upstream, and one carries energy downstream. If there are no real roots, then the solutions show exponential decay in the upstream and downstream directions, and the waves are said to be "cut-off".

The solution (2) forms the input to the system, when dealing with vorticity waves at inlet to the cascade. The solutions (3) form the input to the system, when dealing with acoustic waves entering the

system from upstream and downstream. These basic solutions will also be used to construct the complete solutions.

#### Solution for a Vortex Row

In order to construct the complete solution, each blade will be replaced by a number of singularities placed on the chord line. There is a choice here of working in terms of either velocity potential or pressure perturbation (which in linearized analysis is equivalent to acceleration potential). I think that pressure perturbation is much to be preferred, since there is then no need for singularities to be placed in the wakes of the blades to represent shed vorticity. We therefore require the solution for a row of unsteady pressure dipoles, or equivalently unsteady bound vortices, as shown on figure 2, having the required phase angle  $\beta$  between each vortex and the next.

In subsonic flow the solution for each vortex can be written down as the well-known Hankel function solution, and the solution for the complete row is then obtained as a summation over the complete row. This series converges very badly, and is unsuitable for numerical work.

In subsonic flow we therefore proceed to construct the solution upstream of the row of vortices as the sum of a number of upstream-going acoustic waves, as given by equation (3). The waves are specified by taking suitable positive and negative values of the integer  $n$  in equation (5).

Downstream of each vortex there exists a vortex sheet of which the strength varies sinusoidally with distance from the vortex. The amplitude of this vortex sheet is determined by the condition that in any time interval the circulation shed into the wake is equal in magnitude and opposite in sign to the change in circulation of the vortex. These vortex sheets may be represented by the sum of a number of vorticity waves as given by equation (2), all satisfying the required phase change from blade to blade. In addition there is the sum of a number of downstream going acoustic waves, as given by equation (3). Details of the way in which these waves are put together to represent a row of vortices are given in the paper by Smith (1972). Kaji and Okazaki (1970) achieve the same result mathematically by applying the Poisson summation formula to the series of Hankel functions.

The series obtained in this way converges rapidly, because the acoustic waves for large positive or negative values of  $n$  are all cut-off, and decay very rapidly with distance away from the row of vortices. This is true even for points which are quite close to one of the vortices.

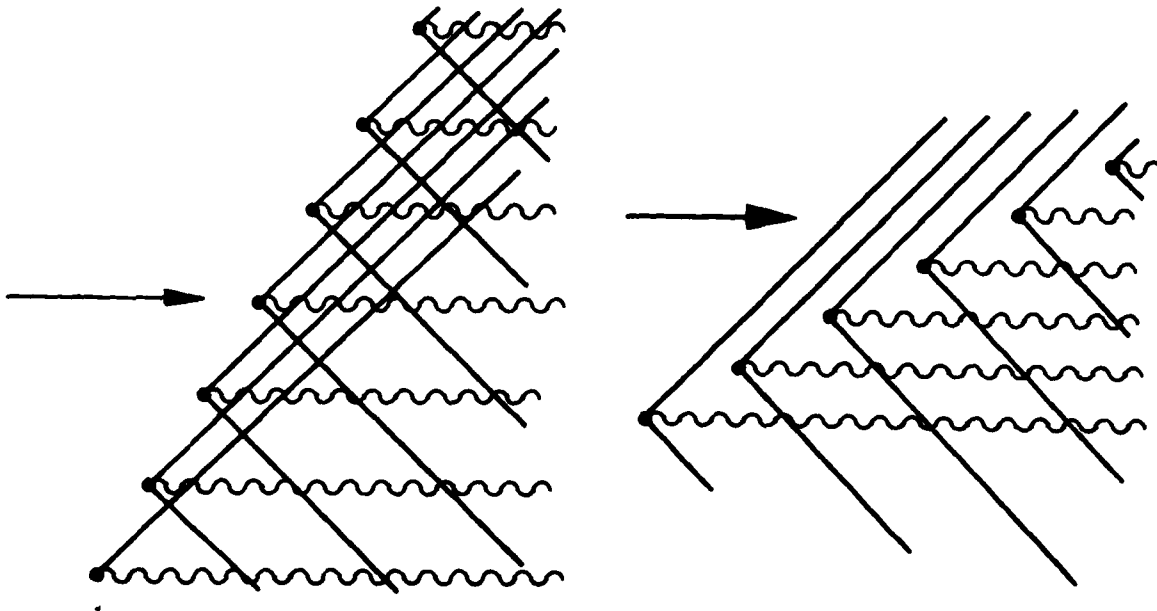


Fig. 3 Wave pattern for supersonic axial velocity

Fig. 4 Wave pattern for subsonic axial velocity

In supersonic flow things are more difficult. It is first necessary to distinguish between cases when the axial velocity is supersonic and when it is subsonic. If the axial velocity is supersonic, all disturbances generated by the row of vortices go downstream, as shown in figure 3, and there is no upstream effect. No turbomachine works in this regime, so that this case is of academic interest only and will not be further considered. When the axial velocity is subsonic, although the total velocity is supersonic, one set of waves goes upstream and one set goes downstream, as shown in figure 4. This case therefore combines some of the features of supersonic flow and some of the features of subsonic flow.

In order to compute the velocity field for the row of vortices in supersonic flow, the series of Bessel functions representing the individual vortices converges badly, and is unsuitable. If one transforms

this to a series of acoustic waves, in the way that works so well for subsonic flow, the resulting series does not converge at all, since the waves corresponding to large values of  $n$  all propagate and are all of comparable magnitude.

Nagashima and Whitehead (1977) overcame this problem by dividing the velocity field into two parts, a quasi-steady part and a remainder. The quasi-steady part can be expressed as a sum over individual vortices and summed analytically. The remainder can be transformed to a sum of acoustic waves which converges satisfactorily.

#### Solution of the Integral Equation

The complete solution for the cascade can now be constructed by distributing a number of these vortices (pressure dipoles) along the chord of the reference blade, and thereby implying the presence of similar vortices with the required phase on all the other blades. Figure 5 shows the vortices evenly distributed along the chord, and this is entirely satisfactory in supersonic flow. But in subsonic flow there is a big numerical advantage to be gained by crowding the points towards the leading and trailing edges, as is done in standard thin-aerofoil theory.

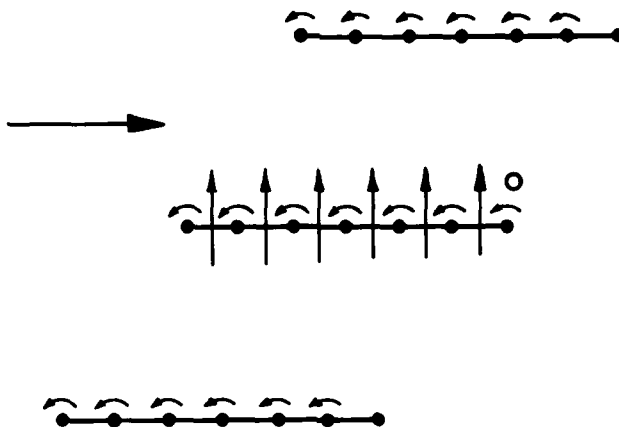


Fig. 5 Representation of cascade blades by a distribution of vortices

If the strengths of all the vortices were known, then the upwash velocity at all points along the chord of the blade could be calculated. This upwash velocity, plus the upwash velocity due to any incoming waves, must match the actual velocity of the surface of the blade, in the direction of the normal to the blade surface. If there are  $N$  unknown vortices, then this condition is applied at  $N$  points to give  $N$  linear equations which can be solved for the unknown vortex strengths.

In subsonic flow the Kutta condition, which states that the pressure jump across the blade must be zero at the trailing edge, must be applied. This means that the vortex at the trailing edge has zero strength. It is then convenient to match the upwash velocities at  $N$  points midway between the positions of the vortices.

In supersonic flow no Kutta condition is applicable, since waves of finite strength can propagate from the trailing edge, so that the pressures on each side of the wake are equalised. It is then convenient to match the upwash velocities at the same points as those at which the vortices are placed.

Once the strengths of the vortices (pressure dipoles) have been determined, since these are directly proportional to the pressure difference across the blade, they can be integrated along the chord to get the aerodynamic force and moment. They can also be summed, with the appropriate phasing, to give the strengths of the outgoing acoustic and vorticity waves.

Computer programs for doing these calculations therefore provide the unsteady aerodynamic data necessary for predicting forced vibration, flutter, and the acoustic performance of cascades. The programs are fast and can calculate one case in less than 0.5 seconds.

#### Acoustic Resonances

In the operation of these unsteady programs, there are certain points at which trouble occurs, and these correspond to acoustic resonances of the system. There are two kinds of resonance.

The first kind is associated with the upstream and downstream ducts, and has nothing to do with the particular geometry of the blades. It occurs in both subsonic and supersonic flow when the frequency and phase angle are such that equations (4) and (5) are just on the verge of having real roots in  $k$  and  $\alpha$  and corresponds to the acoustic waves being just on the point of cut-off. At this point the acoustic waves carry energy in a tangential direction. In a turbomachine the acoustic energy goes round the duct, and does not emerge, so there is no damping due to acoustic radiation. At these points the aerodynamic forces and moments, when plotted against, say, phase angle, show sudden discontinuities. An example is shown in figure 6. It is possible to find, theoretically, regions of "resonance flutter", close to this resonance condition (Whitehead, 1971).

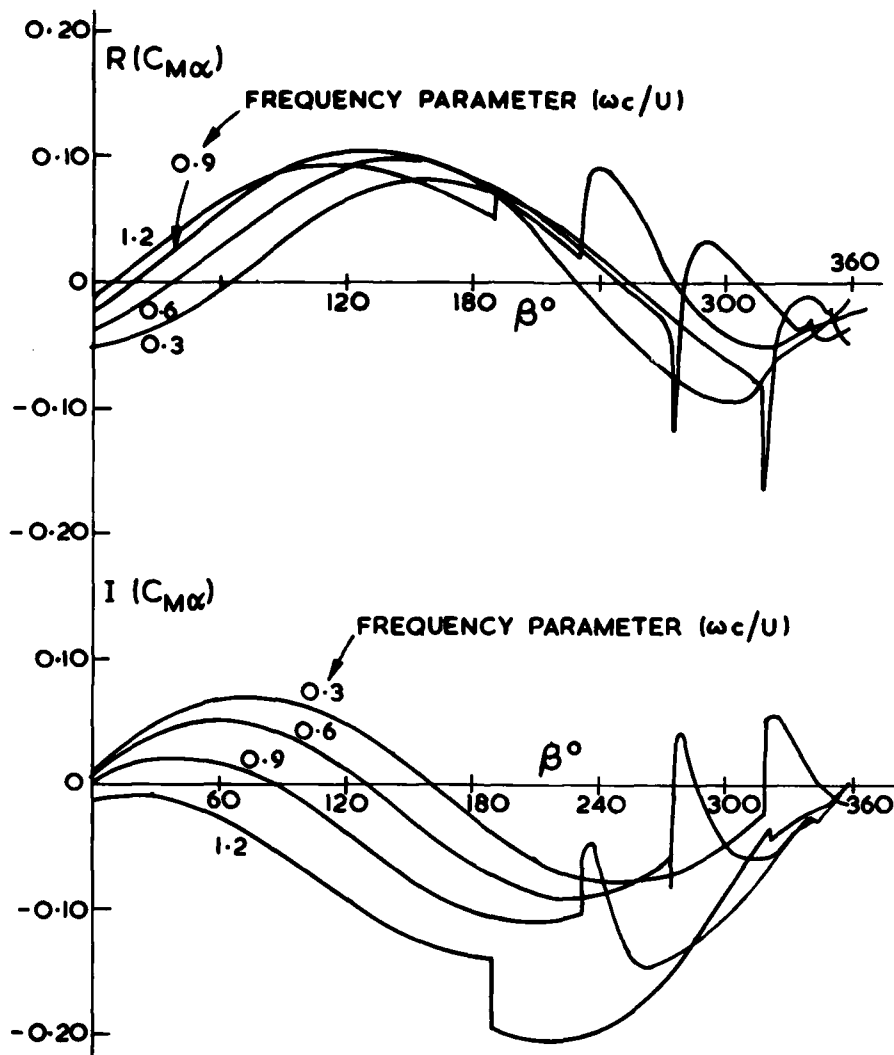


Fig. 6 Example of moment coefficients

$M = 1.35$ ,  $s/c = 0.79$ ,  $\zeta = 59.5^\circ$ , Axis at mid-chord

The practical importance of this resonance condition is in some doubt. Smith (1972) observed it in his experiment where he had a very long duct downstream of a rotor row. But in a vibration experiment (Whitehead, Watson, Nagashima and Grant, 1976), where the axial spacing between blade rows was only about 2 blade chords, the resonance was not seen. It appears that the resonance is only effective if there is a large space in which it can build up.

The second kind of acoustic resonance has been described by Parker (1976) and involves fluid moving in and out of the blade passages. One such mode is sketched in figure 7. At this condition there can be a large pressure change across the blade, with a large blade force for a small amount of blade motion. In the vibration context it might be more accurate to call it an anti-resonance.

This second type of resonance is often observed at low Mach number and high frequency parameter, excited by vortex shedding effects. It is not known whether it is important for blade vibration situations, and there is no evidence that it exists at supersonic speeds.

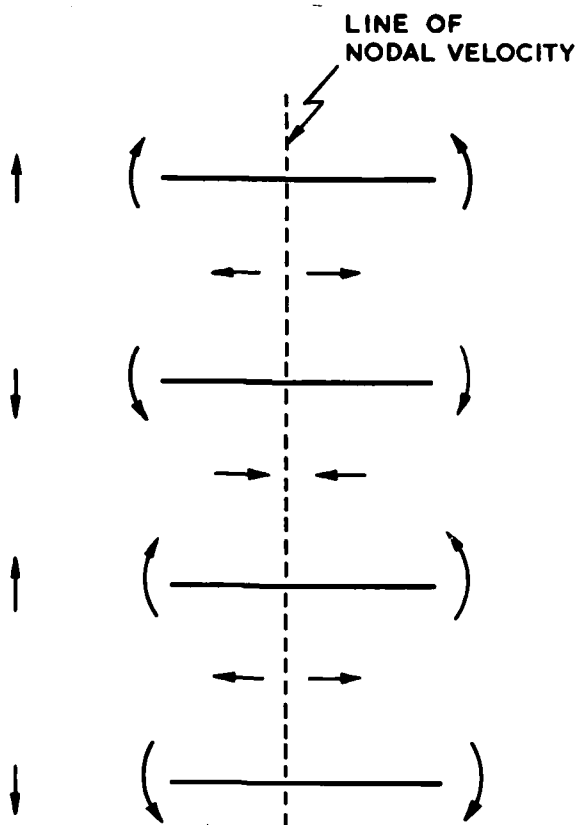


Fig. 7 Example of blade acoustic resonance

#### References

- Kaji, S. and Okazaki, T., 'Propagation of sound waves through a blade row. II Analysis based on the acceleration potential method.' *J. Sound. Vib.* Vol. 11, (1970), p. 355.
- Koch, W., 'Sound generation and blade vibrations of cascaded flat plates in subsonic flow.' DFVLR report IB, 251-78 A27, (1978).
- Nagashima, T., and Whitehead, D.S., 'Linearized supersonic unsteady flow in cascades.' R. & M. 3811, (1976).
- Ni R-H, 'A rational analysis of periodic flow perturbation in supersonic two-dimensional cascades.' *Trans. ASME* Vol. 101, (1979), pp. 431-439.
- Parker, R., 'Resonance effects in wake shedding from parallel plates: calculation of resonant frequencies.' *J. Sound Vib.* Vol. 5, (1976), p. 330.
- Smith, S.N., 'Discrete frequency sound generation in axial flow turbomachines.' R. & M. 3709, (1972).
- Whitehead, D.S., 'Vibration and sound generation in a cascade of flat plates in subsonic flow.' R. & M. 3685, (1971).
- Whitehead, D.S., Watson, R.J., Nagashima, T., and Grant, R.J., 'An experiment to measure moment coefficients for aerofoils oscillating in cascade.' *Revue Francaise de Mecanique. Numero Special 1976.* p. 123; IUTAM Symposium on Aeroelasticity in Turbomachines. Paris, October 1976.
- Verdon, J.M., and McCune, J.E., 'Unsteady supersonic cascade in subsonic axial flow.' *AIAA Journal* Vol. 13, (1975), p. 193.
- Verdon, J.M., 'Further developments in the aerodynamic analysis of unsteady supersonic cascades. Part I - The unsteady pressure field. Part II - Aerodynamic response predictions.' *Trans. ASME* Vol. 99, Ser. A, (1977), p. 509-525.

## UNSTEADY FLOWS ASSOCIATED WITH HELICOPTER ROTORS

Dr T.S. Beddoes  
 Aeromechanics Dept.  
 Westland Helicopters  
 Yeovil, Somerset BA20 2YB  
 UK

INTRODUCTION

The analytic treatment of helicopter performance and structural loading at any level of sophistication must incorporate a representation of the spatial and temporal variation of the local flow relative velocity and angularity. Quasi-steady aerodynamics in conjunction with simplified models of rotor inflow and structural characteristics have served to identify many of the fundamental problems which were encountered in the development of a practical vehicle. Reference 1, in particular, includes an extensive review of this stage of development. Exploitation of the potential usefulness of the helicopter has required a reduction in structural weight and an expansion of the flight boundary as limited by tolerable fatigue loading. Fatigue loading results from the interaction of structural dynamic characteristics and aerodynamic forcing which reflects the presence of many contributions to unsteady flow within the rotor disc. A summary of the various sources of unsteady forcing is presented in figure 1 as a breakdown of the two fundamental categories which consist of blade motion and the structure of the flowfield. The development of rotor wake models from theoretical consideration supported by experimental studies has occupied much effort for many years; an excellent review of this and an extensive bibliography is contained in reference 2.

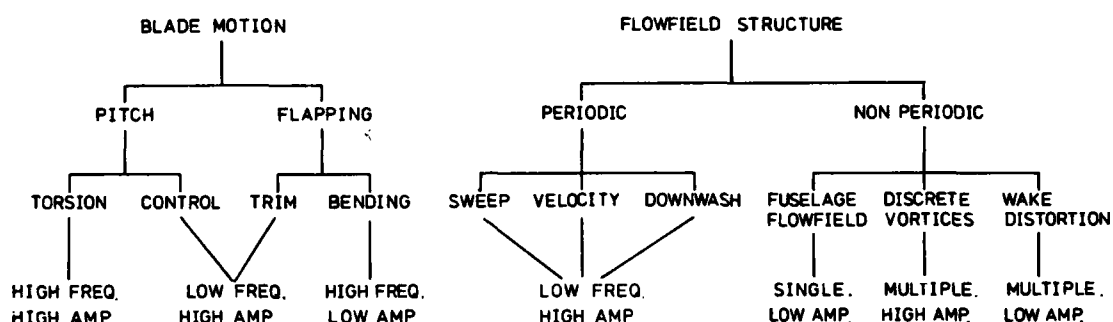


FIG.1. SOURCES OF UNSTEADY FORCING

BLADE MOTION

Relative to the rotating hub the helicopter blade has three degrees of freedom, pitch, flap and lag. The last of these, lag, does not contain motion of sufficient amplitude to warrant discussion as a source of flow unsteadiness. The pitch degree of freedom includes impressed motion from trim and control requirements which, conventionally, is large and applied at the basic rotor frequency ( $\Omega$ ). A large part of the resulting angle of attack variation is, however, cancelled out by disc attitude and coning effects and first harmonic flapping velocity. Torsional stiffness of the rotor blade is not high and is reduced further by the control system which reacts the net pitching moment at the blade root. Consequently, rotor airfoils are designed to minimise pitching moment, a requirement which is at variance with the desired use of camber to optimise maximum lift. In the normal working range torsional deflections are not large but when stall is encountered locally, which occurs as the flight boundary is approached, then pitching moments may suddenly increase by an order of magnitude. This results in significant structural response at the torsion natural frequency (typically  $4\Omega$ - $6\Omega$ ) and, if sufficiently severe, stall flutter may be excited. The first torsion natural frequency is usually the highest at which significantly large structural displacements occur and in terms of reduced frequency ( $\frac{h}{2V}$ ) typical values are shown in figure 2 which is illustrative only for medium size rotors. Less conventional, are proposals to modify helicopter inherent vibration characteristics by applying higher harmonic blade pitch. Model tests have been performed to examine this, see for example, reference 3.

For centrally hinged articulated rotors the natural frequency in flap is  $1\Omega$  and normally not more than 15% higher for offset or hingeless blades. In addition to response at  $1\Omega$ , as forward speed increases, there is significant  $2\Omega$  excitation and flapping response in this mode. The second bending mode has, typically, a natural frequency of around  $2.7\Omega$  and thus also responds significantly to the strong  $2\Omega$  forcing. The amplitude of response of the higher bending modes falls off rapidly and on this account are of less significance aerodynamically. It is not possible to generalise these frequencies adequately, bearing in mind the range of possible blade geometries and materials but figure 2 is included to give some idea of the spectrum of significant oscillatory perturbations in angle of attack resulting from blade motion.

FLOWFIELD STRUCTURE

Adopting a shaft axis system, the rotor disc reference forms a plane at right angles to the shaft. Tilt of this plane to contribute to the propulsive component of lift prod-

uces a uniformly distributed component of the free stream velocity in the axial or out-of-plane direction. In plane, at any given radial station ( $x = \frac{r}{R}$ ) the components of rotational and free stream velocity combine to produce a large first harmonic variation of relative velocity ( $U_t$ ) normal to the blade leading edge:

$U_t = U \cos \phi \cdot \sin \psi + x \cdot R \Omega$  where  $\phi$  = forward tilt of shaft and  $\psi = \Omega t$  = blade azimuth angle. Thus inboard on the retreating side the local velocity may reverse sign. This is obviously the dominant factor contributing to flow unsteadiness not only in terms of local dynamic pressure and Mach Number but also due to its influence on the resultant flow angularity for given out of plane components. The variability is illustrated by the contours of Mach Number shown in figure 3 for a high speed case,  $\mu = \frac{U}{R\Omega} = 0.4$ , and, in relation to local angle of attack near the tip, in figure 4. When the in-plane component of velocity in the radial direction,  $U_r = U \cos \phi \cdot \cos \psi$ , is taken into account the variation in local sweep ( $\Lambda$ ) may be deduced, figure 5. Depending on the method of formulation for the calculation of absolute local loading and implementation of airfoil section characteristics the primary effect of sweep may be eliminated from consideration via application of simple sweep laws but in terms of secondary effects it cannot be neglected entirely.

If the formulation for the unsteady aerodynamics is based on the parameter  $As = 2U\Delta t/c$  i.e. the distance travelled in time  $\Delta t$  in terms of the semi-chord, then for a sampled solution the effect of velocity variation on circulation is implicitly taken into account. Such treatment is not rigorous but available test data (see for example reference 5) indicate that quasi-steady characteristics are preserved up to and including the onset of dynamic stall. Considering that the local velocity variation is predominantly first harmonic and therefore of low reduced frequency the first order representation may be justified for the subsonic case. For substantially supercritical conditions as encountered by the advancing blade tip the flow development does not follow quasi-steady behaviour. Both theoretical and experimental studies have examined this problem, e.g. reference 6, and the characteristics that are encountered. Figure 6 taken from reference 6 shows some of the comparisons between experiment and theory that were obtained from the test programme. Of note is the distinct phase shift around the azimuth defining the movement of the shock wave across the 30% chordwise station. Correlation with the theoretical model is clearly very good at this radial station (approximately 10% in from the tip). At a station closer to the tip (0.946 radius) correlation with the azimuthal phasing of the shock wave remains good, although some differences appear in the variation of supercritical pressures ahead of the shock. A likely explanation for this is found in the development of a strong 3-dimensional character to the flow. Inboard from the tip the variations in sweep around the rotor can be largely accounted for by using only the component of flow normal to the leading edge. On an infinite wing the differences produced by sweep forward or sweep back on the pressure distribution over the front of the chord are small and

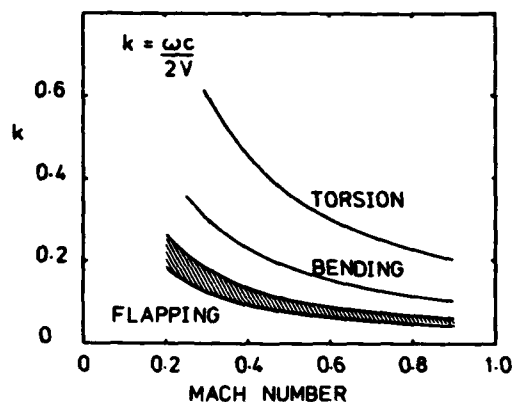


FIG. 2. SIMPLIFIED FREQUENCY SPECTRUM.

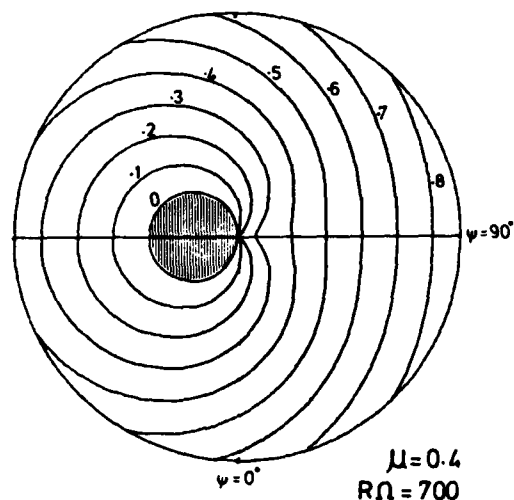


FIG. 3. MACH NUMBER CONTOURS.

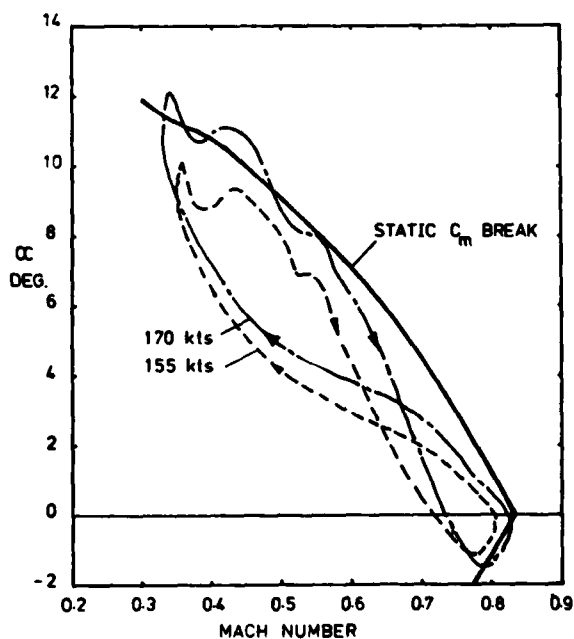


FIG. 4. LOCAL ANGLE OF ATTACK VERSUS MACH NUMBER, SECTION NEAR TIP.

such a model is representative. At the tip of the rotor (the .946 radius station in this case) strong end effects are present. At azimuths before zero sweep ( $\psi = 70^\circ$ ) a swept back condition will exist and isobars would concentrate towards the leading edge at the tip, whilst beyond  $\psi = 90^\circ$  sweep forward would exist and therefore the leading edge would see a relief in pressure gradients. This is clearly the trend of characteristics shown in figure 6 where at the later azimuth station the strength of the shock wave has clearly been reduced compared with the theory which is based on 2-D representation. It seems likely therefore that a combination of the time dependent characteristics with a 3-D model should reproduce more successfully the measured characteristics at the extreme tip of the rotor.

For detailed analysis of local and overall vibratory loading the induced effects of the rotor wake cannot be represented adequately in periodic terms because of the near singularities contributed by discrete vortices in the near wake. Before considering the wake in detail it is instructive to review the results of simplified treatment. From momentum considerations the mean induced velocity  $v_o$  normal to the plane of the rotor may be deduced.

$$v_o = T / 2\rho\pi R^2 [(U \sin \phi + v_o)^2 + U^2 \cos^2 \phi]^{1/2}$$

For the most elementary applications this may be considered distributed uniformly over the disc. If the rotor wake is represented by a skewed cylinder representing a system of vortex rings the induced velocity at the disc can be shown (reference 4) to include a component of upwash in the front and an additional downward component in the rear of the disc. The variation front to rear which increases with speed has been linearised for simplicity of application and produces a distribution which can be represented by:

$$\frac{v(x, \psi)}{v_o} = (1 + Kx \cos \psi), \text{ where } K = \frac{\tan^{-1}(U \cos \phi)}{U \sin \phi + v_o}$$

This representation, though by no means rigorous, gives a useful indication of the time averaged distribution of induced velocity within the disc and may be used where the complexity of the helical vortex wake is not required. Periodic variation of the flow normal to the blade element is also encountered during manoeuvring flight in addition to the consequences of encountering the previously generated wake.

Many mathematical models have been constructed of varying degrees of complexity to represent the true wake shed from the helicopter rotor, reference 2 reviews many of these. The most important feature to be considered is the rolled up vortex shed from each blade tip and for any given segment of a blade, away from the tip, the vortex having the most influence is frequently the one shed by the blade immediately ahead. To define the geometry of the various vortex paths, the natural starting point is the geometry established by the blade tip trajectories displaced downward from the tip path plane to convect at the mean downwash velocity. An idealisation such as this can be said to constitute an undistorted or helical wake. The plan view of the instantaneous helical wake from a four bladed rotor in the vicinity of the disc at an advance ratio  $\mu$  of 0.34 is shown in figure 7a. Immediately obvious are the various intersections which occur between each blade and the vortex paths from the other blades and sometimes from its own prior revolution. The actual proximity of the apparent intersection is determined by the vertical convection of each vortex and is obviously least for the vortex from the prior blade. Figure 7b shows the locus of this intersection and the abrupt change in character for a small change in  $\mu$  which may occur for certain critical values of  $\mu$  and is most marked in the fourth quadrant of the rotor disc.

In reality, each vortex trajectory is distorted by the induced effects of blade circulation and the resultant wake structure. Given adequate computational capability these effects may be assessed. In practice, certain simplifications may be made and the so-called

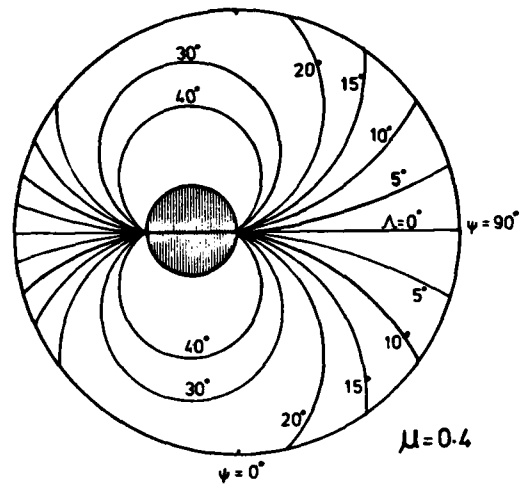
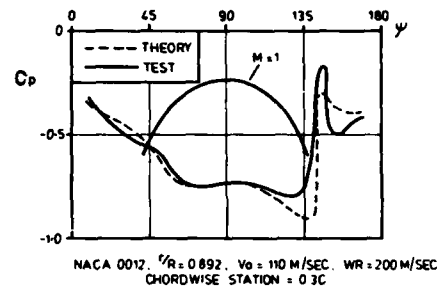
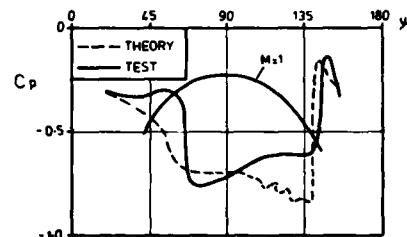


FIG. 5. CONTOURS OF LOCAL SWEEP.

THEORETICAL AND MEASURED PRESSURES ON A ROTOR BLADE.



NACA 0012,  $r/R = 0.892$ ,  $V_0 = 110$  M/SEC,  $WR = 200$  M/SEC  
CHORDWISE STATION = 0.3C



NACA 0010-5,  $r/R = 0.946$ ,  $V_0 = 110$  M/SEC,  $WR = 200$  M/SEC  
CHORDWISE STATION = 0.4C

FIG. 6. TIME DEPENDENT TRANSONIC FLOW.



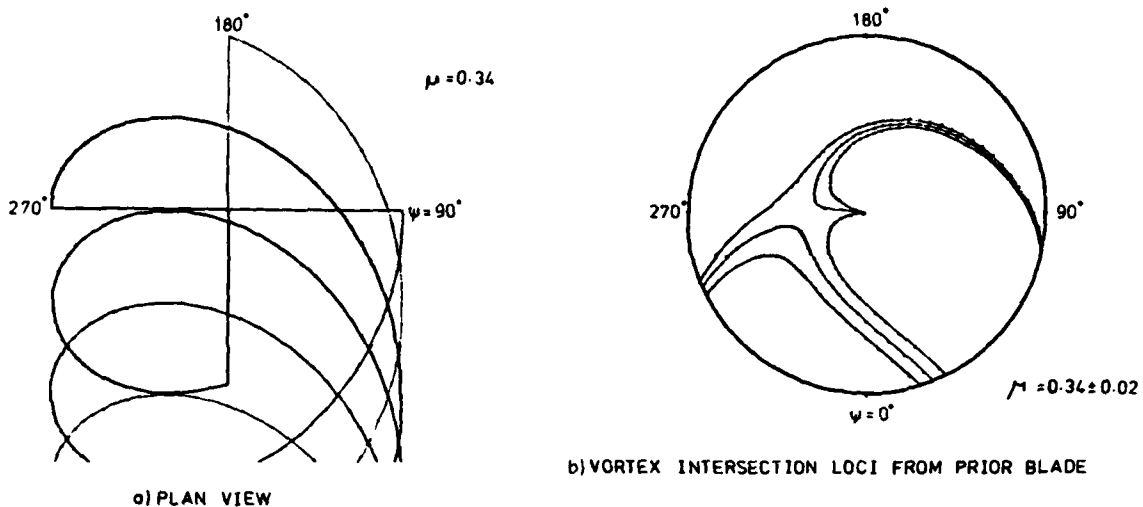


FIG. 7. HELICAL WAKE FROM A 4 BLADE ROTOR.

"free wake" computed without excessive time as presented in reference 7 from which figure 8 is reproduced to illustrate the nature of wake distortion. Figure 8a serves to make the point that within the rotor disc itself the distortions in the top view are small. The vertical distortion is seen in the side view to be much more significant and to demonstrate this more clearly the coordinates of the tip vortex were re-plotted, figure 8b, versus the wake azimuth angle,  $\psi_w$ , relative to the blade from which the vortex was generated. Most significant is the upward displacement of the vortex in the front half of the disc and the rapid downward displacement induced by the vortex shed from the following blade when it approaches closely. It may be recalled that the simplified cylindrical wake model produces

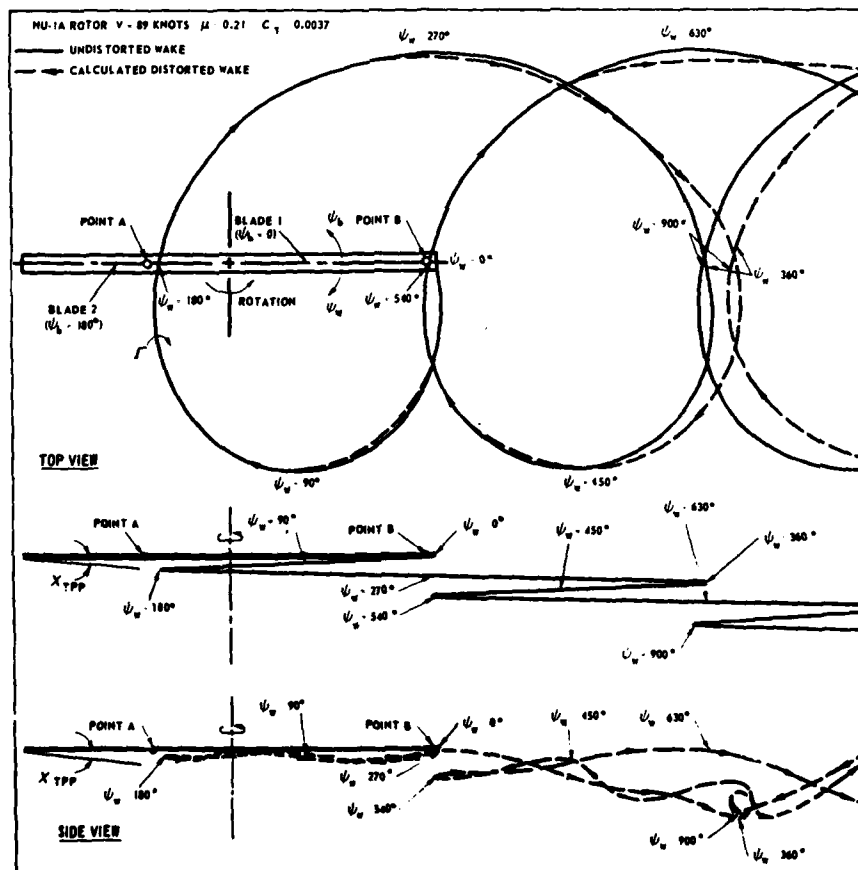


FIG. 8 a). TIP VORTEX PATTERNS, DISTORTED WAKE.

an integrated upwash component in the front of the disc which by analogy would have, qualitatively, such an effect on a free vortex in this region. In addition to these wake self induced effects, the flowfield around the fuselage produces further distortion of the tip vortex trajectory and additional localized induced velocities. More detailed description of wake structure, its calculation and interaction with other components may be found in references 8, 9 and 10.

From the above discussion it is apparent that, not infrequently, a trailed tip vortex may come into close proximity to a blade. When the separation becomes less than about one chord length strong three dimensional effects contribute to the nature of the interaction. References 11 and 12 present experimental results and theoretical discussion, for positioning of the vortex more or less normal to the blade span. For this relative geometry large spanwise pressure gradients are induced by both the spanwise variation of lift and the tangential velocity of the vortex. These gradients are sufficient to induce boundary layer separation but even in the absence of this induced separation it can be shown from potential theory that the chordwise distribution of pressure is significantly modified. This interaction geometry is directly relevant for the blade over the nose ( $\psi = 180^\circ$ ). At high speed and for blade azimuth angles beyond  $270^\circ$  a portion of the vortex may lie more or less parallel to the overtaking blade. Comparable studies of this configuration are not at present available.

#### THE COMBINED EFFECT

To validate the integrated effect of the features incorporated in rotor analytical methods, model and flight experiments are continually being performed. Reference 13 presents a coordinated flight test program and theoretical comparison for correlation purposes and it is appropriate in this context to present briefly some of the results.

The variation in local blade angle of attack around the azimuth is reflected to a first order by the response of the leading edge pressure coefficient. Figure 9 presents this information for 17 radial stations between 50% span and the tip. The presence of discontinuities in the flowfield is apparent and the relation to the geometry of the helical wake vortices is indicated by their superimposed loci. This geometry is re-plotted in figure 10 to illustrate the spatial relationship and again in figure 11 to show how, as thrust is increased, the areas of stall are aligned with the upwash field of vortices. A more direct comparison between the measured response as represented by leading edge pressure and the calculated forcing as represented by local angle of attack comprises figure 12, vortex crossings are signified by perturbations at azimuth angles of around  $90^\circ$ ,  $230^\circ$  and  $270^\circ$ .

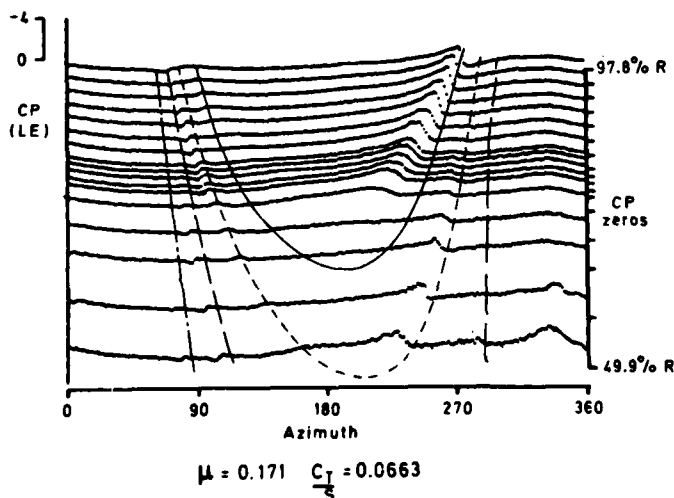


FIG. 9. LEADING EDGE PRESSURES AND PREDICTED VORTEX INTERSECTION LOCI.

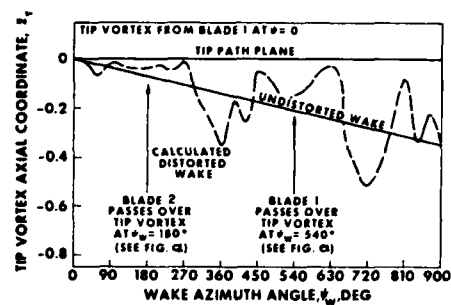


FIG. 8b). DISTORTED WAKE, AXIAL DISPLACEMENT.

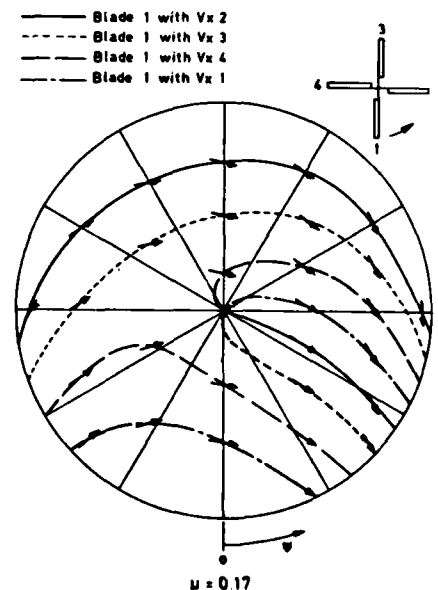


FIG. 10. LOCUS OF BLADE TIP VORTEX INTERSECTIONS

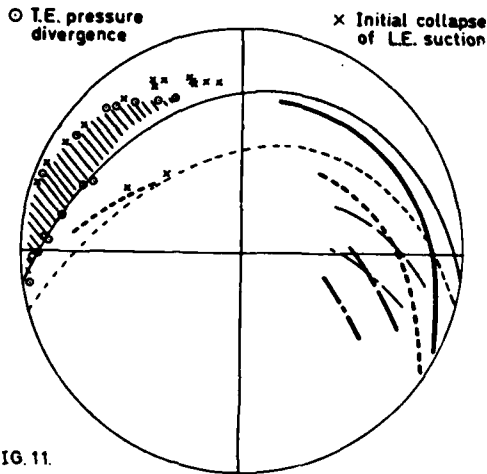


FIG. 11.

COMPARISON OF MEASURED AND PREDICTED BLADE-TIP VORTEX INTERSECTIONS,  $\mu = 0.17$ ,  $\frac{C_T}{S} = 0.12$   
(THICK LINE, FLIGHT. THIN LINE, PREDICTION)  
STALLED AREA ALSO SHOWN

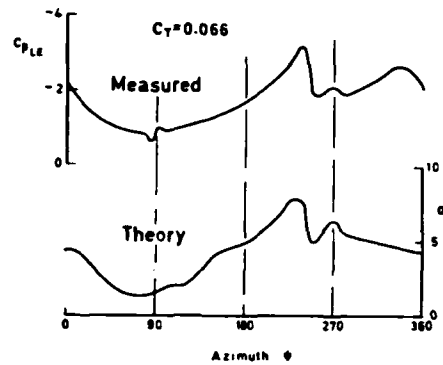


FIG. 12. LEADING-EDGE PRESSURE COEFFICIENT AND PREDICTED INCIDENCE VARIATION,  $\mu = 0.17, 0.8R$

As speed is increased the radial distribution of lift is modified significantly. One consequence of this is the increased excitation of higher bending modes and a change in character, around the azimuth, of flatwise bending moment, see figure 13. Some of the difference between calculated and measured bending moment around the front of the disc is attributed in reference 13 to the use of a non distorted wake and consequent under estimation of the effect of trailing vortex proximity.

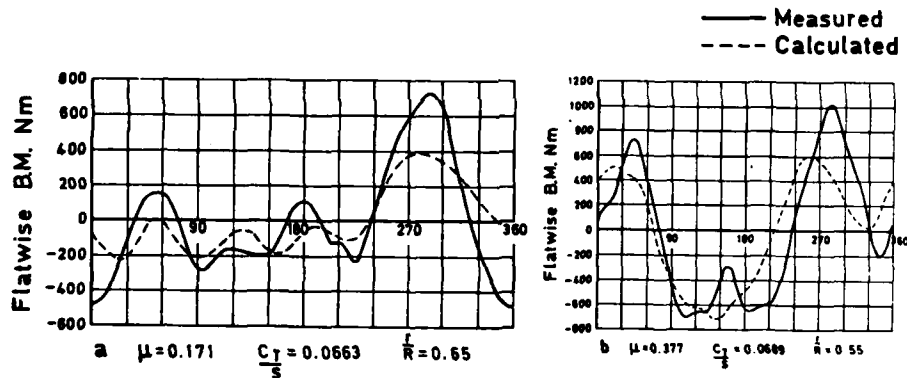


FIG. 13. MEASURED AND PREDICTED FLATWISE BENDING MOMENTS

The representation of dynamic stall in the rotor calculation has a significant effect on the ability to predict the limiting rotor loads defining the flight boundary. This is demonstrated in figures 14 a and b showing the effect of a 25% increase in blade loading coefficient, at high speed, on the blade torsion moment which in turn determines the loads transmitted to the control system. The presence of large stall related pitching moments excite the blade torsion natural frequency through several stall cycles, persisting for more than half a rotor revolution and producing a total elastic twist range of nearly  $8^\circ$ .

For some flight conditions the initiation of stall over the front of the disc is particularly sensitive to wake distortion. As discussed already there are two contributing factors to the displacement of the discrete vortices in this region. These are the wake induced velocities themselves and the presence of the helicopter fuselage.

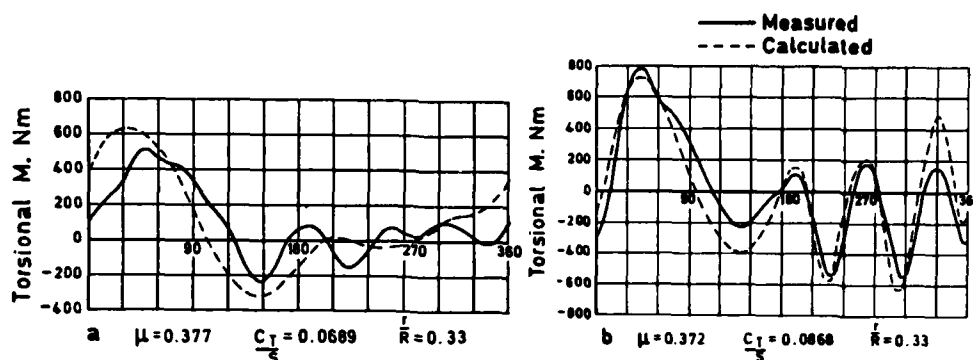


FIG.14. MEASURED AND PREDICTED TORSIONAL MOMENTS

The effect of the fuselage flowfield in modifying the already distorted wake is illustrated in figure 15 from an unpublished source. The baseline comparison is made including the wake distortion induced by wake itself to calculate the induced velocities at the rotor, to which are added the velocities induced by the fuselage flow. The improved comparison incorporates wake distortion induced both by the wake itself and the effect of the fuselage. This modification brings a trailing vortex in the front of the disc a little closer to the blade which is sufficient to induce separation around  $\psi = 180^\circ$  and initiate response at the torsion natural frequency. The resultant control load waveform reflects these events and reproduces the character observed from flight test.

#### CONCLUDING REMARKS

The successful design of advanced rotorcraft requires the ability to predict with confidence the large unsteady and vibratory loads generated and transmitted by the rotor. Capability to accomplish this has improved significantly in the last decade as a result of advances in the modelling of structural dynamics, unsteady aerodynamics and the rotor wake structure. The strong inter-relationship of these three areas cannot be overemphasised and further progress requires co-ordinated effort.

#### REFERENCES

1. Loewy, R.G. Review of Rotary Wing V/STOL Dynamic and Aero-Elastic Problems. Journal, American Helicopter Society, July 1969.
2. Landgrebe, A.J., Cheney, M.C. Rotor Wakes - Key to Performance Prediction. AGARD Conference Proceedings CP.111, Aerodynamics of Rotary Wings. September 1972.
3. McHugh, F.J., Shaw, J. Helicopter Vibration Reduction with Higher Harmonic Blade Pitch. Journal, American Helicopter Society, October 1978.
4. Coleman, R.P., Feingold, A.M., Stempin, C.W. Evaluation of the Induced Velocity Field of an Idealized Helicopter Rotor. NACA ARR L5E10, 1947.
5. Pierce, G.A., Kunz, D.L., Malone, J.B. The Effect of Varying Freestream Velocity on Dynamic Stall Characteristics. American Helicopter Society preprint 1036, 1976 Annual Forum.
6. Caradonna, F.X., Phillips, J.J. The Flow over a Helicopter Blade Tip in the Transonic Regime. 2nd European Rotorcraft Forum. September 1976.

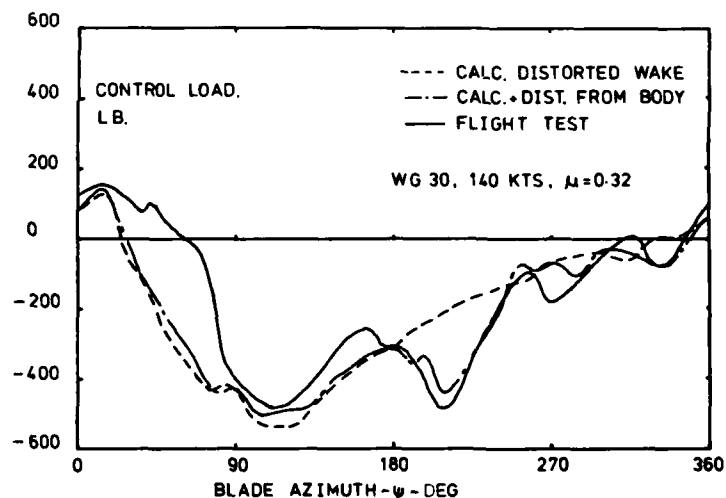


FIG.15. EFFECT OF INCREASE IN WAKE DISTORTION FROM FUSELAGE

7. Clark, D.R., Landgrebe, A.J. Wake and Boundary Layer Effects in Helicopter Rotor Aerodynamics. A.I.A.A. Paper No. 71-581, June 1971.
8. Tangler, J.L. Schlieren and Noise Studies of Rotor in Forward Flight. Preprint No. 77-33. American Helicopter Society, Annual Forum, May 1977.
9. Landgrebe, A.J., Egolf, T.A. Prediction of Helicopter Induced Flow Velocities Using the Rotorcraft Wake Analysis. Preprint 1002, American Helicopter Society, Annual Forum, May 1976.
10. Sheridan, P.F., Smith, R.P. Interactional Aerodynamics - A New Challenge to Helicopter Technology. Preprint 79-59, American Helicopter Society Annual Forum, May 1979.
11. Patel, M.H., Hancock, G.J. Some Experimental Results of the Effect of a Streamwise Vortex on a Two-Dimensional Wing. Journal of the Royal Aeronautical Society, April 1974.
12. Ham, N.D. Some Conclusions from an Investigation of Blade-Vortex Interaction. Journal of the American Helicopter Society, October 1975.
13. Brotherhood, P., Young, C. The Measurement and Interpretation of Rotor Blade Pressures and Loads on a Puma Helicopter in Flight. Paper No. 18. 5th European Rotorcraft Forum, 1979.

## ROLE OF UNSTEADY AERODYNAMICS IN AIRCRAFT RESPONSE

G. J. HANCOCK

(Dept. of Aeronautical Engineering, Queen Mary College, University of London, U.K.)

### 1. INTRODUCTION

Unsteady aerodynamics can be studied as a distinct discipline in which unsteady aerodynamic characteristics can be understood and determined for a wing or aircraft configuration or other body undergoing a specified time dependent motion. However, virtually all practical applications involving unsteady aerodynamics are associated with dynamic phenomena where inertial, structural stiffness, and (unsteady) aerodynamic forces interact; this means that the actual motion, for which the appropriate unsteady aerodynamics are required, cannot be postulated a priori. The purpose of this lecture is to illustrate some of the main dynamic situations which arise in aircraft response and to show how unsteady aerodynamics are used. It is important that any research worker in this field appreciates the role of unsteady aerodynamics for that role often dictates not only the form in which the unsteady aerodynamics is required but also the direction of research effort into unsteady aerodynamics. Although the illustrations outlined here are taken from aircraft response, the same theme underlines unsteady phenomena in helicopters and turbo-machinery.

In the design of an aircraft, there are two broad areas of response which need to be considered:

- |                         |  |
|-------------------------|--|
| overall aircraft motion | <ul style="list-style-type: none"> <li>- small perturbation longitudinal and lateral stability,</li> <li>- controls' effectiveness,</li> <li>- large perturbation asymmetric manoeuvres at low and high angles of attack,</li> <li>- handling characteristics,</li> <li>- departure from controlled flight,</li> <li>- post-stall gyrations, including spin, and spin recovery,</li> </ul> |
| structural response     | <ul style="list-style-type: none"> <li>- small perturbation symmetric and antisymmetric stability, i.e. flutter,</li> <li>- non-linear response, i.e. limit cycle instabilities,</li> <li>- buffeting,</li> <li>- structural loads due to manoeuvres and gusts.</li> </ul>   |

There is coupling between the overall aircraft modes of response and the structural modes of response. Structural flexibility affects the overall aircraft motion; similarly, overall aircraft motion affects some aspects of structural response, e.g. manoeuvre loads. In the past, this coupling has not been a strong one since typical response times of the overall aircraft motions were much slower than typical response times of the structural modes, hence fairly simple minded approaches to account for this coupling have been adequate. The advent of Active Control Technology has radically changed the scenario. With the feedback loops of modern control systems, the response times of the overall aircraft motions are more rapid becoming comparable to some of the structural mode response times, thus the coupling is complex and important; the successful design of a modern control system is critically dependent on ensuring that the above coupling effects are correctly incorporated.

Reference is made above to Active Control Technology. To be more specific, the main areas of current development are:

- i) relaxed stability in reducing the size of tailplane, or fin, but retaining overall controllability through feedback to the elevator (or rudder plus aileron);
- ii) 'carefree' manoeuvring by limiting the authority of control effectiveness in critical regimes of flight to prevent the aircraft going out of control or exceeding its structural strength limits;
- iii) gust load alleviation by reducing the gust loads on a main wing; when an aircraft enters a large gust, fast acting controls induce loads which counteract the gust loads; transport aircraft can have wings which are designed by gust load specifications so reductions in gust loads can save wing weight;
- iv) manoeuvre load alleviation by modifying the load distribution by introducing changes in control angles and overall incidence;
- v) flutter suppression by incorporating feedback with fast acting controls to extend the flutter speed beyond a specified flight envelope.

Areas (i), (ii), (iv) are primarily concerned with overall aircraft response, (iii), (v) are primarily concerned with structural response but, as already mentioned, the subdivision is not always clear cut.

This lecture will first discuss the unsteady aerodynamics associated with overall aircraft motions and then go on to discuss the unsteady aerodynamics associated with structural response. Finally, some remarks are made to consider the role of unsteady aerodynamics in control system design.

As a preamble, a word about steady and oscillatory aerodynamics. The steady aerodynamicist (this phrase denotes that the aerodynamics are steady; hopefully all aerodynamicists are steady) is concerned with the prediction of the aerodynamic load distribution on a specified aircraft configuration for a given steady flight condition (i.e. altitude, Mach number, incidence, control settings) to obtain overall lift, drag, and pitching moment, together with the appropriate steady lateral forces and moments when the steady flight condition is an asymmetric one (e.g. an engine out case). The steady flight condition might be a cruise condition or an almost steady manoeuvring condition; the flight condition might be assumed to be steady, when in fact it is not, for example, when conventional aircraft stability derivatives are estimated. It is important that the steady aerodynamicist appreciates that steady aerodynamics is in effect a limiting or asymptotic condition of an unsteady aerodynamic flow; setting up an aircraft configuration at a particular incidence and Mach number at time  $t = 0$  implies a transient flow as time  $t$  increases which settles down to a 'steady' state as time  $t$  becomes large. Unfortunately, many steady aerodynamicists, never having studied unsteady aerodynamics, do not appreciate this point, they tend to think that steady aerodynamics are 'instantaneous' aerodynamics; so the unsteady aerodynamicist often has an education job on his hands.

Now the unsteady aerodynamicist primarily deals with oscillatory aerodynamics, for reasons explained later. In this case, it is assumed that a mode of aircraft displacement (e.g. an overall aircraft mode, such as aircraft pitch, or alternatively a structural mode, such as the normal mode of primary wing bending) is oscillating in simple harmonic motion and that this oscillatory motion has been in existence for a long time. It is then often possible to make an estimate of the aerodynamic loads in-phase and in-quadrature to the displacement simple harmonic motion. Again, it should be appreciated that these oscillatory loads are asymptotic in the sense that the transient loads, which were initiated in the setting up of the oscillatory motion at zero time have decayed.

The essential ingredient of unsteady aerodynamics is the dependency of the loads at any instant of time on the past history of the motion; this statement is factually correct for even the most complicated of flows involving compressibility non-linearities and/or separated flows. Steady and oscillatory aerodynamics are two special 'motions' where past history effects can be most readily recognised and taken into account. Problems arise when the motions are general, arbitrary and non-steady. The current state-of-the-art of unsteady aerodynamics is to know how to use steady aerodynamics and/or oscillatory aerodynamics, possibly incorporating additional features of past history, in a design process.

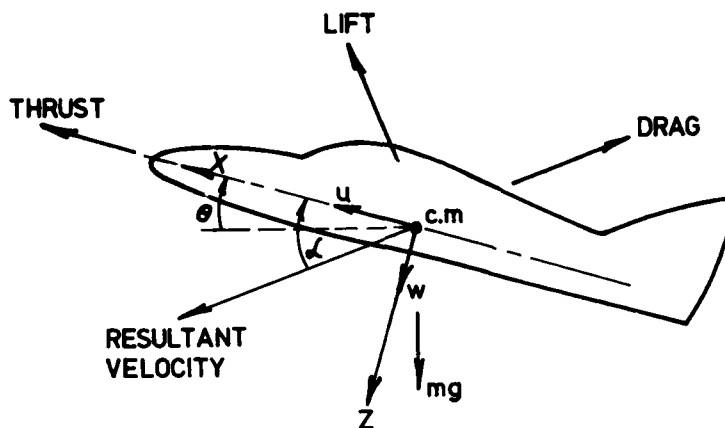
When describing unsteady aerodynamics one is interested in the degree of unsteadiness, which can be defined in terms of the rate at which the motion is changing. A convenient unit of aerodynamic time is the time taken for the air stream to pass over the mean wing chord; this datum unit is the one most usually taken although in some circumstances, the time taken for the air to pass the full length of the fuselage (to account for interference effects) might be more appropriate. Taking the unit of time therefore as  $c/V$ , where  $c$  is the mean wing chord and  $V$  is the forward speed of the aircraft, the response times of overall aircraft motions (e.g. the 'short period' motion) can be of the order of  $150 c/V$ , whereas the faster response time taken in flutter calculations is about  $4 c/V$  (i.e. the period of a higher frequency structural mode takes about 4 times the time for the air to travel one chord length). These figures indicate a typical range of 'unsteadiness'; fortunately the unsteadiness is not too rapid which should be remembered in the discussion of boundary layer effects.

## 2. AERODYNAMICS FOR OVERALL AIRCRAFT MOTIONS

### 2.1 Basic Equations.

Consider the equations of a rigid aircraft in symmetric motion:

$$\left. \begin{aligned} m \left( \frac{du}{dt} + qw \right) &= T + L \sin \alpha - D \cos \alpha - mg \sin \theta, \\ m \left( \frac{dw}{dt} - qu \right) &= -L \cos \alpha - D \sin \alpha + mg \cos \theta, \\ I_{yy} \frac{dq}{dt} &= M, \\ \frac{d\theta}{dt} &= q, \\ \tan \alpha &= w/u. \end{aligned} \right\} \quad (1)$$



## NOTATION FOR AIRCRAFT IN SYMMETRIC MOTION

FIG. 1

As shown in Fig. 1:

Oxz axes fixed in the aircraft with origin at centre of mass,  
Ox points forward, Oz points downward;

absolute velocity of centre of mass has components  $u$  along Ox and  $w$  along Oz;  
Ox, Oz are aerodynamic body axes which define the incidence  $\alpha$  such that  $\tan \alpha$   
is equal to  $w/u$ ;

pitch angle  $\theta$  is the angle which the Ox axis makes with the horizontal.

It is noted that  $\theta$  and  $\alpha$  are independent parameters.

Aircraft mass =  $m$ , aircraft moment of inertia =  $I_{yy}$ ,

Aircraft lift =  $L$ , drag =  $D$ , thrust =  $T$  (assumed along Ox direction),

Moment =  $M$ .

The thrust  $T$  depends on  $u, w$ , altitude and throttle setting. The aerodynamic forces  $L, D$  and aerodynamic moment  $M$  depend on the current values and past history of  $u, \alpha, d\theta/dt$  and density  $\rho$ , and also on the control angles and atmospheric gust inputs. Eqns. (1) are completely general for symmetric motion.

The problem is to solve eqns. (1) for  $u(t), w(t), \theta(t)$  for specified time changes in throttle setting, control angles and/or gust inputs.

It is not possible to express  $L(t), D(t)$  and  $M(t)$  as simple mathematical functions of  $u, \alpha, q$  over the past history prior to time  $t$ ; such a general relationship is known as a functional, following the terminology of Tobak (see for example ref. 1).

If there is an autostabilising unit, or other form of longitudinal control, there will be an additional equation of the form

$$\eta = \eta_p + F(\alpha, q, u), \quad (2)$$

where  $\eta$  is the elevator angle,  $\eta_p$  is the elevator angle input from the pilot, and  $F$  represents an operator on the feedback loops, involving possibly  $\alpha$  and/or  $q$  and/or  $u$ .

Only the longitudinal equations are shown here mainly for the purpose of illustration; in general the 6 degree-of-freedom set of equations, coupling longitudinal and lateral motions needs to be solved.

### 2.2 Quasi-Static Linearised Derivatives.

Traditionally, to study aircraft stability, eqns. (1) are linearised by introducing small perturbations in  $u, w, \theta$  about an initial trim (i.e. steady equilibrium) state, then

$$u(t) = u_s (1 + \bar{u}(t)), \quad w(t) = u_s (\alpha_s + \bar{\alpha}(t)), \quad \theta(t) = \theta_s + \bar{\theta}(t), \quad (3)$$

where subscript  $s$  denotes initial steady state and  $\bar{u}, \bar{\alpha}, \bar{\theta}$  are now small non-dimensional perturbation variables.



Correspondingly, the forces and moments are written in the form:

$$L = L_S(\rho, u_s, \alpha_s) + L_u \bar{u}(t) + L_\alpha \alpha(t) + L_q q(t) + L_{\dot{u}} \frac{d\bar{u}}{dt} + L_{\dot{\alpha}} \frac{d\alpha}{dt} + \dots, \quad (4)$$

with similar expansions for D and M.

Again traditionally,

- (i) all the remainder terms referred to as (+ ..... ) in eqn. (4) are ignored,
- (ii) all the derivatives  $L_u, L_\alpha, L_q, L_{\dot{u}}, L_{\dot{\alpha}}$  are regarded as independent of time, depending on  $\rho, u_s, \alpha_s$ ; variations in density with altitude are usually ignored.

Substitution of eqn. (4), and similar equations for D and M, into eqns. (1), neglecting second order quantities, leads to a set of ordinary differential equations in  $\bar{u}(t), \alpha(t), \theta(t)$  with constant coefficients, which can be solved by standard techniques.

Next, it is necessary to ascribe values to the derivatives. Now the steady aerodynamicist has the job of predicting the equilibrium state aerodynamic lift  $L_S(\rho, u_s, \alpha_s)$  on the basis of theory and wind tunnel measurements. It is conventionally assumed that the static derivatives  $L_u$  and  $L_\alpha$  are given by

$$L_u = u_s \frac{\partial L_S}{\partial u_s}, \quad L_\alpha = \frac{\partial L_S}{\partial \alpha}. \quad (5)$$

The dynamic or rotary derivatives  $L_{\dot{u}}, L_q, L_{\dot{\alpha}}$  are in a different category. By definition, these derivatives arise in an unsteady aerodynamic context, yet these derivatives are determined in a simple minded manner not altogether compatible with the corresponding unsteady aerodynamic behaviour. There is the further complication that it is not clear how such derivatives could, or should, be measured in a wind tunnel experiment.

There are a number of questions relating to the traditional approach of dealing with aircraft stability and control, these questions stem from the form of eqn. (4):

- (i) what is the basis of this expansion?
- (ii) what exactly are the derivatives?
- (iii) what are the remainder terms conventionally packaged as (+ .....); are they negligible and, if not, how are they calculated and incorporated into the equations of motion?

To partially answer these questions, consider the hypothetical situation whereby when the aircraft is in a steady equilibrium state at  $\rho, u_s, \alpha_s, \theta_s$ , the aircraft incidence is suddenly (instantaneously) changed to  $\alpha_s + \delta\alpha$ , where  $\delta\alpha$  is constant, at a reference datum time  $t = 0$ ; then for  $t > 0$  with the incidence constant at  $\alpha_s + \delta\alpha$ , keeping  $\rho, u_s, \theta_s$  unchanged, the change in lift as a function of time can be expressed as

$$\delta L(t) = L_{1\alpha}(t) \delta\alpha. \quad (6)$$

In eqn. (6)  $L_{1\alpha}(t)$  represents the transient (indicial) lift as a function of time due to a step change of unit  $\delta\alpha$  at  $t = 0$ ; in unsteady aerodynamic parlance this is known as the Wagner function. Physically  $L_{1\alpha}(t)$  is the change in lift associated with the creation and convection of downstream trailing vorticity. As  $t \rightarrow \infty$   $L_{1\alpha}(t)$  approaches a constant value associated with the new steady state of  $u_s, \alpha_s + \delta\alpha, \theta_s$ ; for a finite wing  $L_{1\alpha}(t)$  approaches its asymptotic state as  $O(1/t^2)$ . Because of the impulsive change in  $\delta\alpha$  there is a delta impulse in  $L_{1\alpha}(t)$  at  $t = 0$  when fluid is incompressible.

In general

$$L_{1\alpha}(t) \equiv L_{1\alpha}(\rho, u_s, \alpha_s, \delta\alpha, t) \quad (7)$$

since  $L_{1\alpha}(t)$  will depend not only on the initial starting condition but also on the actual magnitude of  $\delta\alpha$  itself. If  $\delta\alpha$  is not too large (this statement is best interpreted in terms of the flow conditions remaining the same as the incidence changes from  $\alpha_s$  to  $\alpha_s + \delta\alpha$ , for example, if the flow remains attached or if the type of flow separation remains the same) then  $L_{1\alpha}$  can be regarded as independent of  $\delta\alpha$ . If the flow is attached  $L_{1\alpha}$  is also independent of  $\alpha_s$ . If the flow is separated at the steady state  $\alpha_s$  but the degree of non-linearity of  $L_S$  with  $\alpha_s$  is small, then  $L_{1\alpha}$  will be a function of  $\alpha_s$ , but independent of  $\delta\alpha$ . The situation where  $L_{1\alpha}$  could be a function of  $\delta\alpha$  is when the flow is attached at a trim state  $\rho, u_s, \alpha_s$  but separated at the perturbed trim state  $\rho, u_s, \alpha_s + \delta\alpha$ .

When  $L_{1\alpha}(t)$  is independent of  $\delta\alpha$ , then for a general change in perturbation incidence  $\alpha(t)$  for  $t > 0$  the lift is given by

$$L(t) = L_S(\rho, u_s, \alpha_s) + \int_0^t L_{1\alpha}(\rho, u_s, \alpha_s, t-\tau) \frac{d\alpha(\tau)}{d\tau} d\tau \quad (8)$$

Strictly the limits  $0, t$  are included in the range of integration; this is important since in incompressible flow  $L_{1\alpha}(\rho, u_s, \alpha_s, t)$  includes a delta function at  $t = 0$ .

Eqn. (8) can be changed to the form

$$L(t) = L_s(u_s, \alpha_s) + L_{1\alpha}(\rho, u_s, \alpha_s, \infty)\alpha(t) + \int_0^t \left\{ L_{1\alpha}(\rho, u_s, \alpha_s, t-\tau) - L_{1\alpha}(\rho, u_s, \alpha_s, \infty) \right\} \frac{d\alpha(\tau)}{d\tau} d\tau, \quad (9)$$

where  $L_{1\alpha}(\rho, u_s, \alpha_s, \infty)$  is the incremental steady state lift associated with a unit increase in incidence.

Now introduce

$$g_{1\alpha}(\rho, u_s, \alpha_s, t, t-\tau) = \int_0^\tau \left\{ L_{1\alpha}(u_s, \alpha_s, t-\tau') - L_{1\alpha}(u_s, \alpha_s, \infty) \right\} d\tau'. \quad (10)$$

As  $\tau \rightarrow 0$  then the integrand in eqn. (10) is  $O((t-\tau')^2)$  which is integrable, so  $g_{1\alpha}(\rho, u_s, \alpha_s, t, t-\tau)$  is a finite function.

Substitution of eqn. (10) into eqn. (9) gives

$$L(t) = L_s(\rho, u_s, \alpha_s) + L_{1\alpha}(\rho, u_s, \alpha_s, \infty)\alpha(t) + \int_{1\alpha}(\rho, u_s, \alpha_s, t, 0) \frac{d\alpha}{dt} - \int_0^t \int_{1\alpha}(\rho, u_s, \alpha_s, t, t-\tau) \frac{d^2\alpha}{d\tau^2} d\tau. \quad (11)$$

By comparison of eqns. (11) and (4) it is seen that there is a correspondence between the derivatives as defined in eqns. (4) and the terms in eqn. (11), hence

$$\left. \begin{aligned} L_\alpha &= L_{1\alpha}(\rho, u_s, \alpha_s, \infty), \\ L_{\dot{\alpha}} &= \int_{1\alpha}(\rho, u_s, \alpha_s, t, 0) \rightarrow \int_{1\alpha}(\rho, u_s, \alpha_s, \infty, 0) \text{ for large } t, \end{aligned} \right\} \quad (12)$$

while the remainder of the series in eqn. (4) is expressed by the remainder integral in eqn. (11). The condition for large  $t$  is a reasonable one since an overall aircraft motion is a relatively slow one (relative to the unit of aerodynamic time, as explained earlier).

In these circumstances, the derivatives  $L_\alpha, L_{\dot{\alpha}}$  are constant derivatives independent of time

$$\begin{aligned} L_\alpha &= \partial L_{1\alpha}(\rho, u_s, \alpha_s, \infty) / \partial \alpha_s, \\ L_{\dot{\alpha}} &= \int_0^\infty \left\{ L_{1\alpha}(\rho, u_s, \alpha_s, \bar{\tau}) - L_{1\alpha}(\rho, u_s, \alpha_s, \infty) \right\} d\bar{\tau}. \end{aligned} \quad (13)$$

The derivative  $L_{\dot{\alpha}}$  is therefore simply the integral of the indicial response function.

It might be thought that the process leading to eqn. (11) can be extended to give a series expansion such as

$$L(t) = L_s(\rho, u_s, \alpha_s) + L_{\dot{\alpha}} \alpha(t) + L_{\ddot{\alpha}} \frac{d\alpha}{dt} + L_{\alpha''} \frac{d^2\alpha}{dt^2} + \dots \quad (14)$$

Such an expansion is most convenient for the dynamicist for then the solution of the equations of motion is straightforward. Unfortunately, such an expansion as eqn. (14) is not possible since it would imply that

$$L_{\ddot{\alpha}} = \int_0^t \int_{1\alpha}(\rho, u_s, \alpha_s, \tau', t-\tau') d\tau', \quad (15)$$

which is infinitely large for large  $t$  because  $\int_{1\alpha}$  is  $O(\tau')$  for small  $\tau'$  and finite for large  $\tau'$ . Similarly all the 'derivatives'  $L_{\alpha''}, \dots$  etc. are infinitely larger. Any attempt to formulate 'derivatives'  $L_{\ddot{\alpha}}, \dots$  etc., and then to separate these derivatives from the variable rates of change  $\ddot{\alpha}(t)$  etc., is completely unacceptable, in spite of many attempts to do so in the literatures.

More specific questions are now:

- (i) under what circumstances is the integral remainder time in eqn. (11) negligible?
- (ii) if the remainder integral term in eqn. (11) is not negligible, how are the dynamic equations to be solved?

As a partial answer to question (i) experience over the past 50 years seems to indicate that the remainder term as far as overall aircraft response is concerned is negligible, but question (i) is becoming more and more relevant as control systems tend to increase the frequency of the short period motions; further work is needed to answer the question (i). As a partial answer to (ii) standard step-by-step numerical procedures can be used if the indicial function is known but such methods do not necessarily lead to the qualitative understanding required for design purposes.

A more fundamental question is how a quantitative estimate of the transient function  $L_{1\alpha}(\rho, u_s, \alpha_s, t)$  could be obtained. Such a function is not normally determined at the present time although the numerical method of Morino named SOUSSA<sup>(2)</sup> incorporates such a procedure. Furthermore it is impossible to perform an experiment to determine  $L_{1\alpha}(\rho, u_s, \alpha_s, t)$  since it is impossible to build a mechanical device to change the incidence of a model instantaneously in a wind tunnel experiment, the fastest rise times would be comparable with the unit of aerodynamic time.

Remembering that the unsteady aerodynamicist aims at prediction of oscillatory derivatives, again by a reference to theory and experiment, it is of interest to relate the overall aircraft derivatives to oscillatory derivatives.

Now take the time dependent perturbation incidence to be a simple harmonic motion with real amplitude  $\delta\alpha$ , so

$$\alpha(t) = \delta\alpha e^{i\omega t} \quad (16)$$

Then as  $t \rightarrow \infty$  the lift force can be written in the form

$$L(t) = L_s(\rho, u_s, \alpha_s) + \tilde{L}_\alpha(\rho, u_s, \alpha_s, \omega) \delta\alpha e^{i\omega t}, \quad (17)$$

where  $\tilde{L}_\alpha \delta\alpha$ , the complex amplitude of the oscillatory incremental lift force, will have an in-phase and a quadrature component. For some regimes of flight  $\tilde{L}_\alpha$  could be a function of  $\delta\alpha$  but in this case it is highly probable that the lift force would include higher harmonics of the form  $e^{in\omega t}$  where  $n > 1$ ; this occurs in separated flows and in flows at transonic speeds. There are also special types of shear flows where half frequency effects appear.

When  $\tilde{L}_\alpha$  can be taken to be independent of  $\delta\alpha$ , on substitution of eqn. (16) into eqn. (8) it is seen that

$$\begin{aligned} \tilde{L}_\alpha(\rho, u_s, \alpha_s, \omega) \delta\alpha e^{i\omega t} &= \left\{ \int_0^t L_{1\alpha}(\rho, u_s, \alpha_s, t-\tau) \frac{d\alpha(\tau)}{d\tau} d\tau \right\}_{t \rightarrow \infty} \\ &= \left\{ \int_0^t \alpha(t-\tau) \frac{\partial}{\partial \tau} (L_{1\alpha}(\rho, u_s, \alpha_s, \tau)) d\tau \right\}_{t \rightarrow \infty}. \end{aligned} \quad (18)$$

Substitution of eqn. (16) into eqn. (18) gives

$$\tilde{L}_\alpha(\rho, u_s, \alpha_s, \omega) = \int_0^t e^{-i\omega\tau} \frac{\partial}{\partial \tau} (L_{1\alpha}(\rho, u_s, \alpha_s, \tau)) d\tau. \quad (19)$$

The real and imaginary parts of  $\tilde{L}_\alpha$  are known as oscillatory derivatives which are functions of  $\rho, u_s$  and  $\omega$ , usually independent of  $\alpha_s$  but not necessarily so. Note, from eqn. (19), as  $\omega \rightarrow 0$

$$\tilde{L}_\alpha(\rho, u_s, \alpha_s, 0) = L_{1\alpha}(\rho, u_s, \alpha_s, \infty), \quad (20)$$

which is the incremental steady state.

For small  $\omega$  it can be shown that

$$\tilde{L}_\alpha(\rho, u_s, \alpha_s, \omega) = \tilde{L}_\alpha(\rho, u_s, \alpha_s, 0) + i\omega A(\rho, u_s, \alpha_s) + \omega^2 B(\rho, u_s, \alpha_s) + \dots, \quad (21)$$

where A and B are real.

Relating eqn. (21) to eqn. (11) it is seen that the first two terms in eqn. (21) correspond to the second and third terms of eqn. (11), the remainder terms of eqn. (21) correspond to the integral remainder term in eqn. (11). Thus from eqns. (11, 12, 21)

$$\begin{aligned} L_{\alpha} &= (\text{Real Part } \{ \tilde{L}_{\alpha}(\rho, u_s, \alpha_s, \omega) \})_{\omega \rightarrow 0} , \\ L_{\dot{\alpha}} &= (\text{Imaginary Part } \{ \tilde{L}_{\alpha}(\rho, u_s, \alpha_s, \omega) \} / \omega)_{\omega \rightarrow 0} . \end{aligned} \quad (22)$$

The formula for  $L_{\dot{\alpha}}$  given in eqn. (22) is a convenient and proper method of estimation from either theory or experiment. Experimentally, both  $L_{\alpha}$  and  $L_{\dot{\alpha}}$  can be obtained from simple harmonic tests extrapolating the results to  $\omega \rightarrow 0$ . The remainder term in eqn. (11) can be obtained in terms of oscillatory derivatives, since from eqn. (19), taking the inverse Fourier transform,

$$L_{1\alpha}(\rho, u_s, \alpha_s, \tau) = \frac{1}{2\pi} \int_0^{\infty} \frac{\tilde{L}(\omega)}{i\omega} e^{i\omega\tau} d\omega \quad (23)$$

These relationships between quasi-steady and oscillatory derivatives do not help with the difficulty of including the remainder terms in a dynamic calculation.

All of the above analysis has been presented in terms of the indicial function  $L_{1\alpha}(\epsilon)$  for the lift following a sudden change in incidence. Reference to the basic equations of motion indicates that a number of such indicial functions would be required, namely

$$\begin{array}{ccc} L_{1\alpha}(\rho, u_s, \alpha_s, \epsilon) & L_{1u}(\rho, u_s, \alpha_s, \epsilon) & L_{1\theta}(\rho, u_s, \alpha_s, \epsilon) \\ D_{1\alpha}(\rho, u_s, \alpha_s, \epsilon) & D_{1u}(\rho, u_s, \alpha_s, \epsilon) & D_{1\theta}(\rho, u_s, \alpha_s, \epsilon) \\ M_{1\alpha}(\rho, u_s, \alpha_s, \epsilon) & M_{1u}(\rho, u_s, \alpha_s, \epsilon) & M_{1\theta}(\rho, u_s, \alpha_s, \epsilon) . \end{array}$$

(the subscript 1 denotes the transient due to a unit step input). The estimation of the drag derivatives via an indicial function would be an unnecessary refinement.

There are additional indicial functions associated with a step change in elevator angle, namely

$$L_{1\eta}(\rho, u_s, \alpha_s, \eta_s, \epsilon) \quad D_{1\eta}(\rho, u_s, \alpha_s, \eta_s, \epsilon) \quad M_{1\eta}(\rho, u_s, \alpha_s, \eta_s, \epsilon)$$

which serve as a reminder that strictly all indicial functions are functions of the trim elevator angle  $\eta_s$  in addition to  $\rho, u_s$  and  $\alpha_s$ .

There is need for further research into the relationship between conventional methods of calculating the dynamic derivatives  $L_{\dot{\alpha}}, L_{\dot{u}}, M_{\dot{\alpha}}, M_{\dot{u}}$  with the methods described above (i.e. eqn. (22)). Although the above analysis presents a formal method for estimating these dynamic derivatives the actual procedure is far from straightforward since the values of the derivatives are due primarily to wing-tailplane interference. An interesting project would be the calculation of the indicial functions for a wing-tailplane combination including the rolled up vortex sheet aft of the main wing, then estimating the dynamic derivatives to compare with standard methods.

This line of thought leads on to an alternative strategy, for if a method for calculating indicial functions could be formulated then the same method could be applied to give the loading during arbitrary changes  $\alpha(\epsilon)$  and  $q(\epsilon)$ ; it would then be possible to combine both the aerodynamic and dynamic calculations in a single step-by-step process in time. Such an approach, as yet at rather a superficial level, is being sought by Wells<sup>(3)</sup>.

### 2.3 Non-Linear Derivatives.

The arguments presented in Section 2.2 are based on the assumption that perturbation changes in  $\alpha(\epsilon)$  and  $q(\epsilon)$  do not significantly change the flow pattern. However, there are aircraft motions where the changes in  $\alpha(\epsilon)$  and  $q(\epsilon)$  are large, with the aircraft going in and out of separated flows or with rapid changes between different kinds of separated flows. So the question is how to represent such aerodynamic characteristics to calculate dynamic motions. No satisfactory answers are yet in sight.

Because of intrinsic difficulties in theoretical prediction methods for these types of flows the main emphasis at present is on deciding what wind tunnel experiments should be done to provide appropriate data for design purposes. Tobak<sup>(1)</sup> has made some significant observations on this aspect. It is possible to generalise the concept of the indicial functions as outlined in Section 2.2 essentially by recognising that the indicial function depends on the magnitude of the increment  $\delta\alpha$  (i.e.  $L_{1\alpha}(\rho, u_s, \alpha_s, \delta\alpha, \epsilon)$ ), in this case the representation for the lift for an arbitrary  $\alpha(\epsilon)$  is not a simple integral as in eqn. (8). For the relatively slow motions associated with overall aircraft motions, Tobak argues that for an arbitrary change in incidence  $\alpha(\epsilon)$  relative

to an initial state  $\rho, u_s, \alpha_s, \gamma_s$  the lift force can be expressed as

$$L(t) = L_s(\rho, u_s, \alpha_s + \alpha(t), \gamma_s) + L_{\dot{\alpha}}(\rho, u_s, \alpha_s + \alpha(t), \gamma_s) \frac{d\alpha}{dt}, \quad (24)$$

where the subscript  $s$  refers to steady state and  $\dot{\alpha}$  to a transient rate term. Eqn. (24) is seen to be a generalisation of eqn. (11), ignoring the integral 'remainder' term.

The crux of eqn. (24) is whether or not  $L_{\dot{\alpha}}$  is in fact independent of  $d\alpha/dt$  but dependent on  $\alpha(t)$ , and whether or not this single function  $L_{\dot{\alpha}}$  incorporates all of the past history effects for all possible motions  $\alpha(t)$ . There is no way at present of predicting such a function. Experimentally it would be necessary to perform a range of incidence motions. As far as is known such an experimental programme has not been done. Whether or not conventional simple harmonic tests for a range of amplitudes of  $\alpha$ , taking the quadrature term for  $L_{\dot{\alpha}}$ , is sensible or informative, is also not clear. Nevertheless, eqn. (24) suggests an approach which, if validated, could form the basis of a wind tunnel programme, to provide an entirely satisfactory form of aerodynamic input into dynamic equations.

However, this overall problem attains its zenith of complexity in the coupled longitudinal and lateral motions for an aircraft in post-stall gyrations, in transient and developed spins. For such motions Tobak<sup>(1)</sup> argues that for an aircraft in nearly rectilinear flight, involving perturbations in all degrees of freedom, the aerodynamic forces and moments can be made up from the following separate motions:

- i) steady incidence  $\alpha_s$  and sideslip  $\beta_s$ ,
- ii) a steady rate of coning (i.e. a steady state of rotation of the aircraft about an axis to the stream direction with the aircraft maintaining steady incidence and sideslip angles),
- iii) small pitching oscillations about a steady coning motion,
- iv) small yawing oscillations about a steady coning motion.

Thus a generalised force or moment coefficient could be expressed in the form

$$C_f = C_f(\alpha_s, \beta_s, cn) + C_{f_q}(\alpha_s, \beta_s, cn)q + C_{f_r}(\alpha_s, \beta_s, cn)r \quad (25)$$

where  $cn$  is a steady rate of coning,  $(q, r)$  are small perturbations in rate of pitch and rate of yaw about the steady  $(\alpha_s, \beta_s, cn)$  state. An appropriate wind tunnel programme would aim to measure  $C_f(\alpha_s, \beta_s, cn)$ ,  $C_{f_q}$ ,  $C_{f_r}$ . It is understood that attempts are being made in the U.S.A. to measure these parameters.

An approach in the U.K. is to assume that a generalised force, or moment, coefficient can be expressed in the alternative form,

$$C_f = C_f(\alpha(t), \beta(t)) + C_f(\alpha(t), p(t)) + C_{f_r}(\alpha(t))r + C_{f_q}(\alpha(t))q \quad (26)$$

where  $C_f(\alpha, \beta)$  is a static coefficient depending on incidence and sideslip,  $C_f(\alpha, p)$  incorporates the rate of roll  $p$ , and  $C_{f_r}(\alpha)$  and  $C_{f_q}(\alpha)$  are associated with small perturbations in rate of pitch and rate of yaw. Now  $C_f(\alpha_s, \beta_s)$  can be measured on any conventional six component balance,  $C_f(\alpha_s, p_s)$  can be measured on a rolling rig for a range of aircraft incidences, while  $C_{f_q}(\alpha_s)$  and  $C_{f_r}(\alpha_s)$  can be measured on a small amplitude oscillatory rig.

Both eqns. (25, 26) are pragmatic in the sense that they are made up from terms which can be measured in wind tunnel experiments. However, it is necessary to validate whether either or both of these equations represent the aerodynamics on an aircraft in high angle of attack motions. In the U.K. some answers are being provided by drop model tests, but there is a long way yet to go.

### 3. AERODYNAMICS FOR STRUCTURAL RESPONSE

The stability of structural response, namely flutter, is of fundamental importance. In the past, the primary task of the unsteady aerodynamicist has been to provide the appropriate aerodynamic data for flutter investigations where only the simple harmonic or oscillatory derivatives are required, as explained below.

Normally to study flutter, a modal analysis is undertaken. The  $n$ th mode ( $n=1, N$ ), either a normal mode or a branch mode, is denoted by  $q_n(t) f_n(x, y)$ , where  $f_n(x, y)$  represents the structural deformation and  $q_n(t)$  represents the amplitude and time variation. The basic stability equations can be written in the form

$$[M] \{\ddot{q}_n\} + [S] \{q_n\} = \begin{cases} \text{generalised} \\ \text{aerodynamic} \\ \text{forces} \end{cases} \quad (27)$$

where  $\{q_n\}$  is a column vector of all the modes,  $[M]$  is a square inertial matrix ( $N \times N$ ),  $[S]$  is the square structural stiffness matrix; the generalised aerodynamic forces are the aerodynamic inputs into each mode.

For a stability analysis it is reasonable to assume that the amplitude of deformation is small, and for attached flows, outside of the transonic region, linearisation of the aerodynamics is reasonable.

Eqn. (27) is to be solved to find the critical flutter condition where by definition the motion is simple harmonic. It is argued that at speeds below the flutter speed, any disturbance is damped out while at speeds above the flutter speed any disturbance will grow. Thus to determine the critical flutter condition, only oscillatory aerodynamics are required. Assuming a value of the frequency parameter  $\nu (= \omega c / u_s)$  the oscillatory loads associated with each modal oscillation can be calculated using methods described later in this Lecture Series. Representing the load distribution induced by the  $n^{\text{th}}$  mode by the expression

$$l_n(x, y, \nu) \bar{q}_n e^{i\omega t} = \{l_n'(x, y, \nu) + i\nu l_n''(x, y, \nu)\} \bar{q}_n e^{i\omega t}, \quad (28)$$

where the ' refers to the in-phase, '' to the out-of-phase,  $\bar{q}_n$  is the complex amplitude, the generalised aerodynamic force column matrix in eqn. (27) becomes

$$[A_{mn}] \{\bar{q}_n\} e^{i\omega t}, \quad (29)$$

where  $A$  is the square matrix with element  $A_{mn}$  given by

$$A_{mn} \equiv A_{mn}' + i\nu A_{mn}'' = \iint_{\text{aircraft}} f_m(x, y) l_n(x, y, \nu) dx dy, \quad (30)$$

$A_{mn}$  is a function of  $\rho, u_s, \nu$ , and possibly of  $\alpha_s$ , although this is usually neglected.

At the flutter condition eqn. (27) becomes of the form

$$[-\nu^2 [M] + [S] - [A'(\nu)] - i\nu [A''(\nu)]] \{\bar{q}\} = 0 \quad (31)$$

where  $[M]$ , and  $[S]$  are real but  $[A(\nu)]$  is complex. Eqn. (31) is a complex eigenvalue problem which when solved gives values for the two variables  $\nu$ , and  $\rho u_s^2$  for a non-trivial solution of  $\bar{q}_n$ .

An iterative method is required to solve eqn. (31) since  $\nu$ , and  $u_s$  (i.e. the Mach number) are not known to start with. Therefore the aerodynamic oscillatory derivatives are required over a range of frequency parameters and Mach number in order for the iterative solution to proceed. This procedure is numerically straightforward.

To study the severity of the onset of flutter, it is necessary to determine how rapidly the damping of structural response decays to zero as forward speed  $u_s$  approaches the critical flutter speed. Attempts are made to solve eqn. (27) at sub-critical speeds (there can be confusion in the use of this term; to the flutter dynamicist sub-critical implies speeds below the flutter speed, whereas sub-critical to the steady aerodynamicist implies speeds at subsonic Mach numbers below the transonic regime). The difficulty is that at sub-critical speeds the motions are not simple harmonic but decaying motions of some form and it is not easy nor straightforward to represent the unsteady aerodynamics of such decaying motions in the equations of motion. There are two main approaches, one originating from the U.K., the other from the U.S.A., both heuristic. In the U.K. the effect of the decay on the aerodynamic loads is neglected, the loads are assumed to depend only on the frequency; so eqn. (27) is solved in the form

$$[-\lambda^2 [M] + [S] - [A'(\rho, u_s, \alpha_s, \nu)] - i\lambda [A''(\rho, u_s, \alpha_s, \nu)]] \{q_n\} = 0 \quad (32)$$

for complex eigenvalues  $\lambda$ , where  $\nu$  is the complex part of  $\lambda$ . At sub-critical speeds a real positive part of  $\lambda$  exists, implying a rate of decay of the structural stability modes.

The U.S.A. approach is slightly different; here an artificial negative damping matrix is inserted into the basic equation and the value of this negative damping is determined by the condition that the motions are simple harmonic at a sub-critical speed. So the appropriate equation to be solved is

$$[-\gamma^2[M] + [S] + c\gamma[D] - [A(\rho, u_s, \alpha_s, \gamma)]] \{q_n\} = 0 \quad (33)$$

The eigen solution gives the values of  $\gamma$  and a damping coefficient  $d$  for given values of  $\rho, u_s, \alpha_s$ . There are a number of arbitrary ways of introducing  $d$  into the square damping matrix. The advantage of this approach is that oscillatory derivatives can be retained but the meaning of the resultant damping coefficient  $d$  is not clear.

An important problem of structural response is concerned with response to atmospheric gusts, then eqn. (26) can be formally rearranged

$$[M] \{\ddot{q}\} + [S] \{\dot{q}\} = \left\{ \begin{array}{l} \text{aerodynamic} \\ \text{load matrix} \\ \text{depending on} \\ \text{responses } q_n \end{array} \right\} + \left\{ \begin{array}{l} \text{aerodynamic load} \\ \text{matrix due to} \\ \text{gust inputs as} \\ \text{functions of time} \end{array} \right\} \quad (34)$$

There are two aerodynamic calculations to be done here, the first is the calculation of the loads due to response, secondly there is the calculation of the aerodynamic loads due to the gusts; on the whole the same methods can be applied to each set of calculations.

Assuming that the aerodynamics can be linearised, if the gust input is assumed to be oscillatory then the steady state response (i.e. response after the initial transients have died away) will be oscillatory, so standard oscillatory derivatives can be used. If the gust input is statistical in the sense that the range of gusts can be expressed by a random gaussian process with a prescribed spectral density, then the spectral density of the responses can be found from the frequency responses over the whole range of frequencies. If the gust input is deterministic, say to represent a discrete ramp type gust, then ideally the problem should be solved in the time domain using indicial functions (as outlined in Section 2.2); however in practice the Fourier transform is applied to both sides of the equation so that oscillatory derivatives can be used, and the final response in the time domain is obtained by the inverse Fourier transform. There are numerical difficulties at higher frequencies which are to some extent overcome if the limiting case of infinite frequency at any Mach number is taken to be piston theory.

Although the above procedures can be applied to calculate sub-critical response in attached flow at subsonic or supersonic speeds, there is some doubt on the accuracy of the results especially where the responses are associated with wing - tailplane interference. It is said that the comparison between flight measured results for sub-critical response compared with predicted results is not good, although it is accepted that there is better agreement between 'measured' and predicted flutter speeds. This lack of agreement at sub-critical speeds may be attributed to inaccuracies in either, or both, of the structural or aerodynamic models. Ashley comments on aerodynamic modelling of aircraft in his review paper<sup>(5)</sup> where he shows that with the same linearisation assumptions different methods can give substantially differing results for tailplane interference loads.

At the present time, the main problem area concerns those flows where the aerodynamics are non-linear, that is when the flows are separated at any Mach number or when the flows are attached at transonic speeds (separated flows at transonic speeds is the peak of complexity). It is necessary to predict the unsteady aerodynamic behaviour in a suitable form for calculating dynamic response, whether for flutter, which could well be of the limit cycle variety, or general response at speeds below the flutter speed.

If for a wing, or aircraft, which is performing a time dependent motion, the complete flow history is known for  $t < T$ , say, the unsteady aerodynamicist has the job of predicting what happens at  $T + \Delta T$  given the position of the wing or aircraft at  $T + \Delta T$ . If this can be done successfully, the combined dynamic/aerodynamics problem can be solved in principle in a step-by-step process. Such a procedure is a formidable undertaking, if one is solving a typical dynamics problem in  $N$  degrees of freedom by a 4th order Runge-Kutta process (or equivalent) it would be necessary to calculate the aerodynamic flows at  $8N$  different states at each time step in order to interpolate to the correct state. Anything less usually leads to unacceptable cumulative errors. Such an approach has actually been done by Rizzetta<sup>(4)</sup> for a flexibly supported two-dimensional airfoil at transonic speeds, solving the aerodynamics by a field solution method developed by Ballhaus, to be described later in this Lecture Series. As far as is known it is not possible to apply such an approach to separated flows because the methodology is not yet available.

There is a need for continuing research into these types of methods which combine the dynamic/aerodynamic interface directly in the solution process. Such methods, although extremely long in terms of contemporary computational time and complexity, can provide useful results for comparative purposes.

For design purposes, there is a need for research into methods for solving dynamic equations with approximate non-linear aerodynamics in such a way as to highlight the main dynamic response characteristics. There may be lessons to be learnt from our control system colleagues, for example, if the non-linear aerodynamics could be expressed in terms of 'describing functions' then the main features of dynamic response might be established, alternatively the possibility of obtaining solutions using integrated effects such as energy concepts needs to be further explored.

#### 4. CONTROL SYSTEM DESIGN

As stated earlier, aircraft are becoming more dominated by control systems in this era of ACT. Such advanced control systems inevitably bring problems. For example, reference 5 identifies three types of instability which arise on the YF-17; first limit cycle oscillations were induced at high system gain by an interaction between the control system and the overall rigid aircraft motions; secondly response of the control sensors to the structural mode deformation introduced a self-excited oscillation where the energy to sustain the oscillation was supplied in part by the control system; thirdly an instability arose in the absence of aerodynamic forces with the inertial forces acting as the exciting agency. Another consequence of advanced control systems is that they cause coupling between the overall aircraft degrees of freedom and the structural modes such that there is much less of a gap between the lower frequencies associated with overall aircraft motion and the higher frequencies associated with the structural modes, thus the concepts of quasi-static 'aerodynamic derivatives' become questionable.

The control engineer designs his control system by reference to the frequency plane (i.e. by plotting out the frequency response in either Bode or Nyquist plots), in the s plane (by plotting the eigenvalues  $s = \sigma + i\omega$  as a function of a parameter gain of the system, the so-called root locus plot), and in the time plane. Essentially the frequency response and s plane methods indicate the degree of stability of the system; the time plane is necessary to study response. A common starting point for all of these approaches is to express the various components of the overall system in terms of their transfer functions (i.e. the ratio of the Laplace transform of the output to the Laplace transform of the input). Therefore the control engineer would appreciate the aerodynamic inputs in the form of Laplace transforms. As already pointed out it is not easy to determine or represent linearised aerodynamics for general unsteady motions and so approximations are needed.

In the following summary of current developments the author wishes to acknowledge the help of D. L. Woodcock, R.A.E.

In the earlier sections the ideas have been built up on the basis of the indicial response to a step change since a step change is acceptable in physical terms. However mathematically the indicial response to an impulse or delta function is a more convenient base.

So define  $L_{\delta\alpha}(\tau)$  as the lift response to an impulsive change unit incidence at time  $\tau=0$  where  $\tau$  is non-dimensional time  $u_0 t/c$ . Thus for an arbitrary change in incidence  $\alpha(\tau)$  for  $\tau > 0$ , the lift  $L(\tau)$  is given by

$$L(\tau) = \int_0^{\tau} L_{\delta\alpha}(\tau - \tau_0) \alpha(\tau_0) d\tau_0 = \int_{-\infty}^{+\infty} L_{\delta\alpha}(\tau - \tau_0) \alpha(\tau_0) d\tau_0, \quad (35)$$

since  $L_{\delta\alpha}(\tau - \tau_0)$  is zero for  $\tau_0 > \tau$ , and  $\alpha(\tau_0)$  is zero for  $\tau_0 < 0$ .

Now  $L_{\delta\alpha}(\tau)$  can be expressed in the form

$$L_{\delta\alpha}(\tau) = k_0 \delta(\tau) + k_1 \delta'(\tau) + g(\tau) H(\tau), \quad (36)$$

where  $\delta(\tau)$  is the standard delta function, as defined by the integral property,

$$\int_{-\infty}^{+\infty} f(\tau) \delta(\tau - \tau_0) d\tau = f(\tau_0),$$

$\delta'(\tau)$  is the differential of the delta function, defined as

$$\int_{-\infty}^{+\infty} f(\tau) \delta'(\tau - \tau_0) d\tau = -f'(\tau_0),$$

$H(\tau)$  is the step function which is the integral of  $\delta(\tau)$

$$\int_{-\infty}^{\tau} \delta(\tau_0) d\tau_0 = H(\tau).$$



The values of  $k_0$  and  $k_1$  are associated with the behaviour at  $P$  close to zero and therefore associated with the behaviour for fast or high frequency motions.

Again there is a relationship between oscillatory motions and indicial motions, so in the notation of Section 2

$$\tilde{L}(\nu) = \int_{-\infty}^{\infty} L_{\alpha}(\tau_0) e^{-i\nu\tau_0} d\tau_0, \quad (37)$$

where  $\nu$  is the non-dimensional frequency parameter  $\omega c/u_0$ . In practice it is normally the oscillatory derivatives  $\tilde{L}(\nu)$  which are calculated directly, and the indicial function  $L_{\alpha}(\tau_0)$  obtained by Fourier inversion of eqn. (37).

Replacing  $\nu$  by  $(-i\rho)$  then eqn. (37) can be written as

$$\tilde{L}(-i\rho) = \int_0^{\infty} L_{\alpha}(\tau_0) e^{-\rho\tau_0} d\tau_0, \quad (38)$$

which can be regarded as a Laplace transform relationship.

Now at low frequencies  $\tilde{L}(\nu)$  can be expanded in the form

$$\tilde{L}(\nu) = \tilde{L}(-i\rho) \sim \sum_{r=0}^{\infty} \sum_{s=r}^{\infty} n_{rs} \rho^{r+s} \ln^s \rho, \quad (39)$$

whereas at high frequencies

$$\tilde{L}(\nu) = \tilde{L}(-i\rho) \sim k_1 \rho + k_0 + \sum_{r=1}^{\infty} \frac{a_r}{\rho^r}. \quad (40)$$

The limit of high frequency is piston theory, which gave expressions for  $k_0$  and  $k_1$ . If the fluid is assumed incompressible, piston theory is not the high frequency limit, thus there is a different limit between  $M \rightarrow 0$  (for which piston theory applies) and  $M \rightarrow \infty$  (for which it does not).

Because  $\tilde{L}(\nu)$  is complicated approximations are sought.

The crudest approximation is to write

$$\tilde{L}(\nu) \equiv \tilde{L}'(\nu_0) + i\nu \tilde{L}''(\nu_0) \approx \tilde{L}'(\nu_0) + i\nu \tilde{L}''(\nu_0) \quad (41)$$

where  $\nu_0$  is some chosen real value of  $\nu$ . For aircraft stability and control, as already explained,  $\nu_0$  is taken to be the limit as  $\nu_0 \rightarrow 0$ . For subcritical structural response, again as already described,  $\nu_0$  is taken to be the flutter frequency or a nearby frequency. The corresponding indicial response function is then

$$L_{\alpha}(\tau) \approx L'(\nu_0) \delta(\tau) + L''(\nu_0) \delta'(\tau). \quad (42)$$

A more common contemporary approximation is to assume

$$\tilde{L}(-i\rho) \approx k_0 + k_1 \rho + \frac{1}{(\rho + p_0)^m} \sum_{r=0}^{m-1} b_r \rho^r \quad (43)$$

which has the equivalent form

$$L_{\alpha}(\tau) \approx k_0 \delta(\tau) + k_1 \delta'(\tau) + e^{-p_0\tau} \left( \sum_{r=0}^{m-1} c_r \tau^r \right) H(\tau)$$

where there is a linear relationship between the coefficients  $b_r$ ,  $c_r$  and all the coefficients are real. The coefficients  $b_r$  ( $c_r$ ) are obtained from a least squares fit to a set of calculated values of  $\tilde{L}(-i\rho)$ . The choice of the single real pole  $p_0$  is arbitrary. The disadvantage of this expansion is that when used in a dynamic calculation a spurious dynamic root appears associated with  $p_0$ .

A generalisation of the above approximation which has been further developed recently by Vepa<sup>(8)</sup> and described as the use of Pade approximants is to assume

$$\hat{L}(-i\phi) \approx k_0 + k_1 p + \left\{ \frac{\sum_{r=0}^{m-1} u_r p^r}{\sum_{r=0}^m v_r p^r} \right\} \quad (44)$$

and its equivalent form

$$L_{\delta\alpha}(\tau) \approx k_0 \delta(\tau) + k_1 \delta'(\tau) + \sum_{r=1}^N e^{-p_r \tau} \sum_{s=0}^{n_r-1} c_{rs} \tau^s \quad (45)$$

where  $p = -p_r$  is an  $n_r$  multiple root of

$$\sum_{r=1}^N v_r p^r = 0$$

and so

$$\sum_{r=1}^N n_r = m$$

In eqn. (45)  $u_r, v_r$  are taken to be real, but the poles associated with the values of  $p$  to make  $(\sum v_r p^r)$  zero are now complex; this is the difference with the approximation in eqn. (43). All the poles  $p_r$  have negative real parts (i.e. the aerodynamic system is stable). But again spurious roots appear in the solutions to the dynamic equations. Current work is aimed at understanding whether or not these effects are significant when used in a control law analysis.

To avoid spurious dynamic roots (or in the parlance these days, undesirable augmented states) Edwards et al. have been developing an alternative approach. The basic problem to be solved is of the form

$$A \frac{d^2 q}{dt^2} + D \frac{dq}{dt} + E q = \int_{-\infty}^{+\infty} Q_{\delta q}(\tau - \tau_0) q(\tau_0) d\tau_0 + \int_{-\infty}^{+\infty} Q_{\delta \eta}(\tau - \tau_0) \eta(\tau_0) d\tau_0 + f(\tau) \quad (46)$$

where

$$\eta(\tau) = R \frac{dq}{dt} + S q$$

and

$q$  is a response variable  
 $A, D, E$  represent inertial, structural damping and structural stiffness  
 $\eta(\tau)$  is the elevator angle variation  
 $R, S$  represent rate, and direct, feedback  
 $f(\tau)$  is a disturbance input  
 $Q_{\delta q}(\tau)$  is the generalised load due to an impulse in  $q$   
 $Q_{\delta \eta}(\tau)$  is the generalised load due to an impulse in  $\eta$

Transforming to the  $p$  plane, eqn. (46) becomes

$$\{A p^2 + D p + E - \tilde{Q}_q(-i\phi)\} \hat{q}(p) = \tilde{Q}_\eta(-i\phi) (R p + S) \hat{q}(p) + \hat{f}(p) \quad (47)$$

The solution proceeds in two stages.

First Edwards determines the characteristic roots of the left-hand side of eqn. calculating the aerodynamic term(s)  $\tilde{Q}(-i\phi)$  from standard oscillatory programs but replacing the conventional frequency  $\omega$  by  $(\sigma + i\omega)$ . How far this process can be performed for finite wings at a general Mach number is not clear. It is argued that no spurious roots are introduced by this approach. The validity of such a procedure needs to be clarified.

If the characteristic roots of the left-hand side of eqn. (47) are denoted as  $p = p_r$  ( $r=1, \dots$ ), then the second stage is to expand the right-hand side about the poles  $p_r$  along the lines, but generalising, eqn. (43).

There are a number of questions which need to be resolved, for example:

AD-A089 114

ADVISORY GROUP FOR AEROSPACE RESEARCH AND DEVELOPMENT--ETC F/6 1/1  
SPECIAL COURSE ON UNSTEADY AERODYNAMICS.(U)

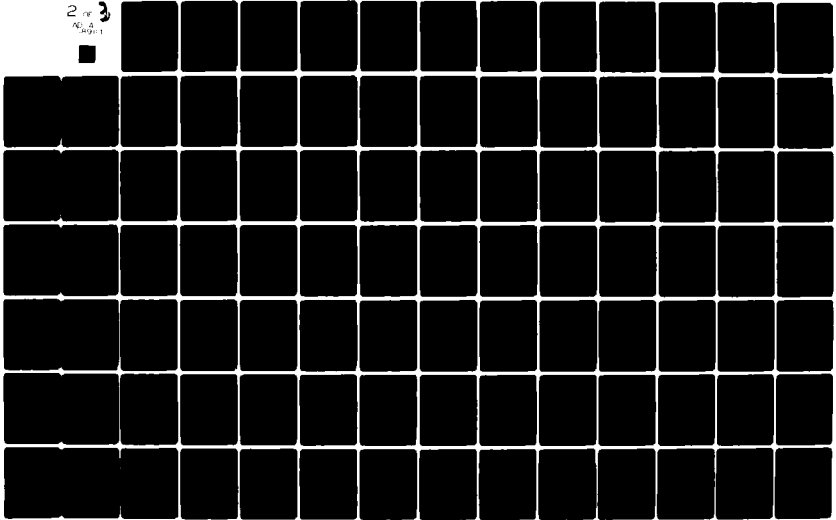
JUN 80

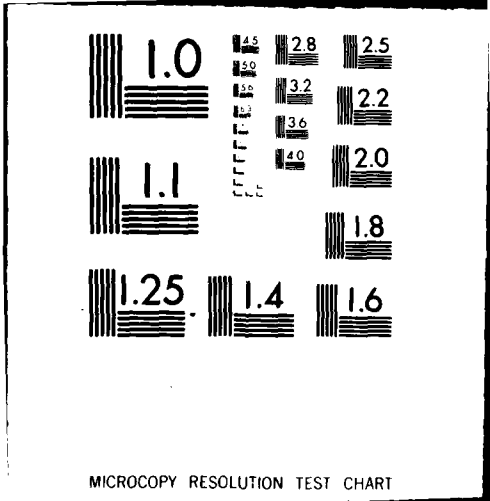
UNCLASSIFIED

AGARD-R-679

NL

2 of 3  
NL  
AGARD-1





MICROCOPY RESOLUTION TEST CHART  
NATIONAL BUREAU OF STANDARDS-1963-A

is the method effective for practical applications? how much computational effort is required?

It is seen from the above brief comments that aerodynamic modelling for control law design is one which needs and requires further attention.

#### 5. CONCLUDING REMARKS

The general theme of this presentation has been the appreciation that unsteady aerodynamics only have practical relevance in a dynamic context and that the mathematical modelling of the unsteady aerodynamic characteristics need to be compatible with the solution of the dynamic problem. In these days the solution of dynamic problems is crucial for estimation of design loads, aircraft response and control system design.

Even when the flow is attached at subsonic and supersonic Mach numbers conventional quasi-static derivatives for low frequencies and oscillatory derivatives for higher frequencies may not be adequate for modern requirements, it is becoming necessary to calculate the aerodynamic loads for arbitrary unsteady motions not only of wings but complete aircraft configurations. Such a specification operates at two levels; at one level relatively fast approximate but adequate methods are required for preliminary design purposes, while more thorough and exact methods are required to validate finalised designs.

Aircraft are operating more and more in non-linear aerodynamic regimes of flight involving separated flows and/or transonic Mach numbers. Although remarkable progress is being made with field solutions at transonic speeds the dynamic/aerodynamic interface remains a formidable challenge which even when overcome will provide methods which could be used only infrequently in a design process because of the large extensive programs involved, even recognising the advances in computer technology. Meantime, there is a real intermediate task for the theoretical unsteady aerodynamicist and dynamicist, namely, to inform the wind tunnel specialist what experiments are required and how the results can be used and incorporated into the solution of dynamic problems.

#### REFERENCES

1. M. Tobak & L.B. Schiff      On the Formulation of Aerodynamic Characteristics and Aircraft Dynamics - NASA TR 456, Jan. 1971.
2. W.R. Wells & D.A. Keskar      Relationship of Unsteadiness in Downwash to the Quality of Parameter Estimates - A.I.A.A. Paper 79 1639.
3. H. Ashley      Unsteady Subsonic and Supersonic Flow - AGARD CP 227, 1977.
4. D. P. Rizzetta      Time Dependent Response of a Two-Dimensional Airfoil in Transonic Flow - A.I.A.A. Journal No. 17, Jan. 1979.
5. T.D. Arthurs & J.T. Gallagher      Interaction between Control Augmentation System and Airframe Dynamics on YF 17 - A.I.A.A. Paper 75 824.
6. R. Vepa      On the Use of Pade Approximants to Represent Unsteady Aerodynamic Loads for Arbitrarily Small Motions of Wings - A.I.A.A. Paper 76 - 17, Jan. 1976.
7. J.W. Edwards      Applications of Laplace Transform Methods to Airfoil Motion and Stability Calculations - A.I.A.A. Paper 79 0772.

## APPLICATION OF INDICIAL AERODYNAMIC FUNCTIONS

Dr T.S. Beddoes  
Aeromechanics Dept.  
Westland Helicopters  
Yeovil, Somerset BA20 2YB, UK

INTRODUCTION

Numerous approaches have been used to calculate the aerodynamic loading in response to time varying motion. Even for the incompressible case the calculation is laborious but solutions have been obtained for idealised forcing such as harmonic motion (Theordorsen) or an instantaneous change between two steady state conditions (indicial response). Subsequently, by assuming suitably small perturbations the compressible flow equations were linearised and solutions again obtained for idealised motion. The theory for these two approaches has been presented, for example, in reference 2. More recently, using numerical methods, programs have been developed that can solve either the exact equations for steady compressible flow or the approximate equations of the non linear small disturbance theory of transonic flow and have been applied to the case of unsteady motion. The computational requirements for the latter approach are considerable and consequently application is largely limited to specific aspects of airfoil design and behaviour.

The objective here is to demonstrate relatively simple means for applying the theoretical results for idealised forcing to routine calculations of airloads and structural response. In this context non-linear system characteristics may be simulated and complex or arbitrary forcing may be included. Initially the aerodynamics are assumed to be more or less linear, that is, the flow is assumed to remain attached but the procedure is intended to provide the parameters required to define the onset of separation.

CHOICE OF AXIS

For convenience and simplicity in strip analysis application, motion is referred to the  $\frac{3}{4}$  chord location and pitching moments are related to the  $\frac{1}{4}$  chord. For steady state calculations specification of boundary conditions at the  $\frac{3}{4}$  chord is sufficient to define lift. This is true for both pitch and plunge motion. For sudden application of pitch rate about the  $\frac{3}{4}$  chord location it has been shown (reference 1) for subsonic flow that following an initial transient, the resulting lift decays rapidly to zero and the pitching moment degenerates with time to form a pure couple. As discussed later indicial lift response is comprised of two components, an impulsive force which is initially centred at the mid chord and which decays rapidly and a circulatory component which increases from zero, tends asymptotically to the steady state value, and maintains a centre of pressure at the  $\frac{1}{4}$  chord.

$$\text{Thus } \Delta C_l = C_{l\alpha} \phi_c(s) \cdot \Delta \alpha_{3/4} + C_{lq}(s) \cdot \frac{\dot{\theta}c}{V} \quad s = \frac{2V}{c} t$$

$$\Delta C_m = C_{m1}(s) \cdot \Delta \alpha_{3/4} \bar{x}_1(s) + C_{mq}(s) \cdot \frac{\dot{\theta}c}{V}$$

Where  $\phi_c(s)$  is the indicial lift response to angle of attack  
 $C_{lq}(s)$  is the indicial lift response to pitch rate about  $\frac{3}{4}c$   
 $C_{mq}(s)$  is the indicial moment response to pitch rate about  $\frac{3}{4}c$   
 $C_{l1}(s)$  is the impulsive component of  $\phi_c(s)$   
 $\bar{x}_1(s)$  is the centre of pressure variation corresponding to  $C_{l1}(s)$

and as noted  $C_{lq}(s)$  and  $\bar{x}_1(s)$  both tend to zero. The angle of attack at the  $\frac{3}{4}$  chord location is obtained by summing the contributions from the free stream velocity vector, plunge motion, pitch rate about an alternative axis location and the induced velocity field effects where appropriate.

INDICIAL LIFT AND MOMENT FUNCTIONS

The derivation of the indicial lift and moment functions for compressible flow have been presented by numerous sources e.g. references 1 and 2 which include numerical solutions for various Mach numbers. Two different approaches are used, one to solve for the initial loading which is impulsive in nature and another for the circulatory loading which builds up quickly in the first few chord lengths of travel and tends asymptotically to the steady state value. Considering first the indicial circulation, this has been shown (reference 6) to be proportional to that derived for the penetration of a sharp edge gust, which, for the incompressible case, was first solved by Kussner and for which the approximation

$$\psi(s) = 1 - 0.5e^{-13s} - 0.5e^{-s} \quad \text{has become accepted where } C_l(s) = 2\pi \frac{w}{V} \psi(s)$$

Solutions for the compressible case are presented in reference 2. The asymptotic values for  $C_{l1}(s)$  are given by the steady state lift curve slope values of  $2\pi/\sqrt{1-M^2}$  but for increasing Mach number the build up of lift is slower in terms of semi chord lengths travelled ( $s$ ). It can be shown that by scaling the ordinate  $C_l$  by  $\sqrt{1-M^2}$  and the abscissa  $s$  by  $1-M^2$  the compressible solutions for the Kussner function collapse to what is effectively a single solution. Correspondingly, then it is possible to utilise a simply modified Kussner function for use for compressible flow, i.e.

$$\psi_c(s) = (1-M^2)^{3/2} (1 - 0.5e^{-13s'} - 0.5e^{-s'}) \quad \text{where } s' = s(1-M^2)$$

$$\text{and } C_l(s) = 2\pi \frac{w}{V} \psi_c(s) \quad \text{or, alternatively, } C_l(s) = C_{l\alpha}(M) \frac{w}{V} \psi_c(s) \sqrt{1-M^2}$$

where  $C_{l\alpha}(M)$  is the best available value of lift curve slope for a given Mach number from theory or test. An application of the above expression is compared in figure 1 with the solutions presented by Bisplinghoff in reference 2. Similarly, it may be shown that a modified form of the above expression may be used to represent the circulatory response to indicial forcing i.e. an instantaneous change in angle of attack.

The impulsive forces which comprise the initial loading in response to an instantaneous change in angle of attack are generated by a compression wave on the lower and rarefaction wave on the upper surface. These produce an initial lift coefficient

$$C_l(0) = \frac{4\bar{\alpha}}{M}$$

Decay of this force with time is rapid, reference 2 presents a solution which is valid for a short period:

$$C_l = \frac{4\bar{\alpha}}{M} \left[ 1 - \frac{s}{2M} (1-M) \right], \quad 0 \leq s \leq \frac{2M}{1+M}$$

With the objective of producing an overall expression suitable for the application of Laplace transform methods it is not unreasonable to assume an exponential decay for the initial impulsive forces. Thus an indicial lift function may be generated which includes both the circulatory and impulsive lift terms:

$$\phi_c(s') = (1-M^2)^{3/2} (1-0.3e^{-0.08s'} - 0.7e^{-65s'}) + \frac{2}{\pi M} e^{-\frac{(37+.76M)}{M}s'}$$

such that  $C_l(s) = 2\pi \bar{\alpha} \phi_c(s)$  or  $C_{l\alpha}(M) \bar{\alpha} \phi_c(s) \sqrt{1-M^2}$

The above expression is compared to the solutions for the compressible indicial lift function presented in reference 2 for various Mach numbers (figure 2) and is shown to preserve the continuity between the initial, impulsive, loading and the succeeding circulatory loading. To examine more closely the time history for the first two semi chords of travel figure 3 shows a comparison of the above expression with the initial values from piston theory as quoted above.

### GENERALISED INDICIAL LIFT

Indicial Response to Step Change in Angle of Attack

$$C_l(s) = \frac{2\pi \kappa c_l}{\sqrt{1-M^2}} (1 - A_1 e^{-b_1 s'} - A_2 e^{-b_2 s'} - A_3 e^{-b_3 s'}) \quad \text{where} \quad s' = \frac{2Vt}{c} (1-M^2)$$

Thus  $C_l(t) = \frac{2\pi \kappa c_l}{\sqrt{1-M^2}} \left( 1 - \sum_{n=1}^3 A_n e^{-t/T_n} \right)$  where  $T_n = \frac{c}{2V b_n (1-M^2)}$

The Laplace transform of the response is  $C_l(p) = \frac{2\pi \kappa c_l}{\sqrt{1-M^2}} \left( \frac{1}{p} - \sum_{n=1}^3 \frac{A_n T_n}{1 + T_n p} \right)$

and the Laplace transform of the step input is  $\alpha(p) = \frac{\kappa c_l}{p}$

thus the transfer function for lift is  $\frac{C_l(p)}{\alpha(p)} = \frac{2\pi \kappa c_l}{\sqrt{1-M^2}} \left[ 1 - \sum_{n=1}^3 \frac{A_n T_n p}{1 + T_n p} \right] = \frac{2\pi \kappa c_l}{\sqrt{1-M^2}} \left[ \left( 1 - \sum_{n=1}^3 A_n \right) + \sum_{n=1}^3 \frac{A_n}{1 + T_n p} \right]$

For the linearised theory  $2\pi/\sqrt{1-M^2}$  represents the steady state lift curve slope, therefore for application, the measured two dimensional lift curve slope may be substituted.

Thus  $\frac{C_l(p)}{\alpha(p)} = C_{l\alpha}(M) \left[ \left( 1 - \sum_{n=1}^3 A_n \right) + \sum_{n=1}^3 \frac{A_n}{1 + T_n p} \right]$

Indicial Response to Step Change in Pitching Velocity about  $\frac{1}{2}$  Chord

$$C_{lq}(s) = -\frac{1}{M} e^{-s/M^2}, \quad \text{i.e.} \quad C_{lq}(t) = -\frac{1}{M} e^{-t/T_q}$$

where  $q = \frac{\dot{\theta} c}{V}$ ,  $T_q = \frac{c}{2V(1-M^2)}$  see fig. 4.

Hence the transfer function  $\frac{C_{lq}(p)}{q(p)} = -\frac{1}{M} \frac{T_q p}{(1 + T_q p)} = -\frac{1}{M} \left[ \frac{1}{(1 + T_q p)} \right]$

Thus for any form of motion comprising pitch and plunge referred to the  $\frac{1}{2}$  chord location

$$C_l(p) = \frac{C_l(p)}{\alpha(p)} \alpha(p)_{3/4} + \frac{C_{lq}(p)}{q(p)} q(p)_{3/4}$$

where  $\alpha(p)_{3/4}$ ,  $q(p)_{3/4}$  represent the Laplace transforms of the forcing  $\alpha(t)$ ,  $q(t)$

Thus  $C_l(t)$  is given by the inverse transform of  $C_l(p)$

### GENERALISED PITCHING MOMENT

Indicial Response to Step Change in Angle of Attack:

It has been established that the circulation of a flat plate plunging indicially is proportional to the lift of the plate entering a sharp-edged uniform gust. For the latter case it has also been established that the centre of pressure is at the  $\frac{1}{2}$  chord location throughout the motion. Therefore, having separated the indicial lift into circulatory and impulsive components, it is most convenient to treat the moment contributions independently. For a moment axis at the  $\frac{1}{2}$  chord, it follows that the pitching moment contribution of the circulatory lift component will be zero (neglecting camber).

The impulsive force is initially distributed uniformly along the chord thus its centre of pressure is, initially, at mid chord. The subsequent moment may be considered as the product of the impulsive

force component (which is decaying) and its effective center of pressure. Reference 2 presents the computed theoretical indicial pitching moment about the  $\frac{1}{4}$  chord. From these results and the expression for the variation of the impulsive force with time, the variation in centre of pressure may be deduced.

$$\bar{x}_1(t) = -0.25 \left[ 1 - \frac{(T_1 + t)}{T_1} e^{-t/T_1} \right]$$

where  $x_1(t)$  is the shift from the initial mid chord location. In the customary non dimensional form this becomes

$$\bar{x}_1(s) = -0.25 \left[ 1 - \frac{(T_1' + s)}{T_1'} e^{-s/T_1'} \right], \quad T_1' = T_1 \frac{2V}{c}$$

In Laplace form the indicial response is given by:  $\bar{x}_1(p) = \frac{1}{4p(1+T_1'p)^2}$

Since  $\alpha(p) = 1/p$ , the transfer function for the impulsive centre of pressure is  $\frac{\bar{x}_1(p)}{\alpha(p)} = \frac{1}{4(1+T_1'p)^2}$

A value for  $T_1'$  of  $4M^3$  produces the variation in total indicial pitching moment shown in figure 5.

For pitch rate about the  $\frac{1}{4}$  chord, as noted, the asymptotic value of lift is zero; the corresponding pitching moment is a pure couple. The initial impulsive loads generate a value of pitching moment about the  $\frac{1}{4}$  chord

$$C_m = -\frac{1}{12M} q$$

and the asymptotic value is  $C_m = -\frac{n}{8\sqrt{1-M^2}} q$

From the results presented in reference 1 the following expression for the timewise variation of  $C_m$  has been deduced:

$$C_{mq}(t) = -\frac{n}{8\sqrt{1-M^2}} (1 - e^{-t/T_q}) - \frac{1}{12M} e^{-t/T_q}$$

where  $T_q$  is the time constant derived for the decay of the impulsive lift. Thus the transfer function is:

$$\frac{C_{mq}(p)}{q(p)} = -\frac{1}{12M} - \frac{1}{1+T_q} \left[ \frac{n}{8\sqrt{1-M^2}} - \frac{1}{12M} \right]$$

#### APPLICATION OF THE LIFT TRANSFER FUNCTION

The existence of a lift transfer function implies that for any timewise variation of  $\alpha$  for which it is possible to derive a Laplace transform there will exist an explicit solution for the lift response. A simple and relevant example comprises the response to simple harmonic forcing at  $\omega$  rad./sec for which:-

$$\alpha(p) = \frac{1+Bp}{\omega(1+p^2/\omega^2)}, \quad q(p) = \frac{2k}{\omega^2} \frac{p}{(1+p^2/\omega^2)}$$

where  $B = \frac{c}{V} \Delta x$  and  $\Delta x =$  distance of  $\frac{1}{4}c$  aft of pitch axis,  $k = \frac{\omega c}{2V}$

Derivation of the expressions for the amplitude ratio and phase angle response are presented in Appendix 1. These expressions have been evaluated for a range of frequency and Mach Number and are compared in figure 6 with results obtained from linearised unsteady flow theory (reference 3).

The approach may be extended to the evaluation of experimental results. It would be desirable to verify experimentally the response to indicial forcing but this is in practice physically unrealisable. The nearest one can approach this condition is by applying ramps at an increasing rate until the limits of the apparatus are reached. Even then, finite mass and damping effects modify the ideal forcing. It is possible, however, to describe the characteristics of the equipment in terms of transfer functions and compare the airfoil force and moment response with that expected. This has been done for a recent set of experiments which incorporate an electro hydraulic actuator driving the airfoil through a tuned spring arrangement. This produces a transfer function of the form:-

$$\alpha(p) = \frac{1+Bp}{p^2(1+Fd)(1+2fp/\omega_n + p^2/\omega_n^2)}, \quad q(p) = \frac{1}{p(1+Fd)(1+2fp/\omega_n + p^2/\omega_n^2)}$$

Applying this forcing to the lift transfer function produces some rather lengthy expressions, but the results of such calculations are compared in figure 7 with test results.

These two examples illustrate that for an open or closed loop dynamic system for which the equations of motion may be expressed in operational form and which includes a lifting surface, the overall system response may be evaluated in explicit form. The examples given apply to 2 dimensional lifting surfaces, it should be possible to extend the procedure to the three dimensional case.

#### COMPARISON WITH NON LINEAR THEORY

The indicial lift and moment functions have been derived from the results of linearised unsteady flow theory. In recent years, with the growth of computational capacity, methods have been developed for the numerical solution of the non linear small disturbance equations for transonic flow. In addition to steady state solutions the methods have been applied to harmonic and indicial motion. Reference 4 presents an example, the response of a NACA 64A-410 at  $M = 0.72$  to an instantaneous increase of incidence from  $2^\circ$  to  $4^\circ$ . The resulting change in lift as computed by a finite difference procedure is compared with the indicial lift variation produced from the generalised indicial lift function (figure 8a).

The linear theory produces a centre of pressure at the  $\frac{1}{4}$  chord for the circulatory loading, thus the asymptotic value of pitching moment about the  $\frac{1}{4}$  chord is zero. For substantially supercritical flows incorporating shock waves this aspect of the theory in particular is inadequate. If, however, the centre of pressure location is derived for some finite perturbation of circulatory lift the resulting indicial pitching moment may be computed from the components of impulsive (1) and circulatory lift (2). The comp-



arison of pitching moment (figure 8b) shows the magnitude of these two components, their sum and the pitching moment from the finite difference calculation (the assumed centre of pressure was deduced from the asymptotes for lift and moment).

From the point of view of engineering applications these comparisons are quite encouraging. The discrepancies appear to be less than might be expected from experimental factors.

#### IMPLEMENTATION IN A SAMPLED SYSTEM

In many applications aerodynamic forces are required to be generated within what is effectively a closed loop solution involving structural and inertial responses. Furthermore, the problems may involve non linear forcing or response in which case a preferred form of solution is via digital simulation. This involves sampling at finite time steps and for this purpose the indicial response form is particularly appropriate. The previous expressions may be re-formulated for this purpose by considering an arbitrary variation of angle of attack with time  $\alpha(t)$  as being the summation of a series of step changes at each sampling. i.e.

$$\alpha(n) = \alpha(0) + \sum_1^n \Delta\alpha(n)$$

The general form of the indicial response to a change in attack of attack is  $\Delta C_l(s) = C_{l\alpha} \Delta\alpha \cdot \phi(s)$

where  $\phi(s)$  has the form  $\phi(s) = 1 - \sum_1^3 A_j e^{-b_j s}$

The combination  $\Delta\alpha \cdot \phi(s)$  may be considered as an effective angle of attack  $\Delta\alpha_E$  which differs from the instantaneous value by a decaying decrement.

$$\text{Thus } \Delta\alpha_E(n) = \Delta\alpha(0) - D(n) + \sum_1^n \Delta\alpha(n) \quad \text{where } D(n) = \sum_{j=1}^3 [D_j(n-1) e^{-b_j(1-M^2)2V\Delta t} + A_j \Delta\alpha(n)]$$

and  $\Delta t$  is the sample time. Included in the instantaneous value of  $\alpha_E$  is the component of pitch rate required to establish the boundary condition at the  $\frac{3}{4}$  chord location. The additional lift due to pitch rate about the  $\frac{3}{4}$  chord is given by:

$$\Delta C_{lq}(n) = -\frac{1}{M} \frac{c}{V} \dot{\theta}(n) + \Delta C_{lq}(n-1) e^{-\Delta t/T_q} \quad \text{where } T_q = \frac{c}{2V(1-M^2)}$$

As previously noted, the first two terms of the indicial lift function may be identified with the circulatory component and the third with the impulsive lift. Correspondingly, the appropriate contributions to the chordwise loading may be identified when required to determine the onset of stall. When stall has occurred the individual significance of these terms is lost but when re-attachment occurs they may be reconstituted via the concept of the lift decrement. That is, by assuming that  $\alpha_E(n) = C_l(n)/C_{l\alpha}$

bearing in mind that  $\alpha_E(n)$  has been generated for separated conditions, it follows that  $D(n) = \alpha(n) - \alpha_E(n)$

and assuming that the impulsive lift has decayed,  $D_1(n) = \frac{A_1 D(n)}{A_1 + A_2}$ ,  $D_2(n) = \frac{A_2 D(n)}{A_1 + A_2}$ ,  $D_3(n) = 0$ .

thus re-initialising the values required for the continuing attached flow calculations.

#### SOLUTION OF DYNAMIC RESPONSE TO ARBITRARY FORCING

There are many methods for the numerical solution of differential equations, they all have limitations which involve accuracy, stability or complexity. In this discussion application of the difference equations derived from the Z transform of a second order equation are presented. The Z transform is derived by the application of the Laplace transform to a sampled time function  $F(t)$ . Techniques for the derivation and manipulation of the Z transform have been expanded in response to requirements for the design of sampled data control systems, for example see reference 5.

For most aeroelastic problems the equations to be solved reduce to the form  $\ddot{\theta} + 2f\omega\dot{\theta} + \omega^2\theta = C(t)$  For closed loop and multiple degree of freedom problems  $C(t)$  may include external forcing plus coupling and feedback terms. An advantage of this formulation is that the structural characteristics may be linearised to produce the values of  $f$  and  $\omega$  for the appropriate modes whereas the overall problem remains non linear. If the forcing is effectively arbitrary, i.e. not conveniently expressed in moderately simple explicit form, then the above problem may be solved by a numerical procedure for evaluating the forcing and response at successive intervals. For convenience, equal intervals of time are used. Since the forcing is thus defined at discrete points in time, some representation of its intermediate value must be made. The most elementary representation is to hold the value of  $C(t)$  constant for the following interval and is commonly referred to as the 'zero order hold' implementation.

The continuous function is represented by  $\ddot{\theta} + 2f\omega\dot{\theta} + \omega^2\theta = C(t)$

for which application of the Laplace transform produces the solution

$$\Theta(p) = \frac{C(p)}{p^2 + 2f\omega p + \omega^2} \quad \Theta(p) = \frac{C(z)}{p^2 + 2f\omega p + \omega^2} \cdot \frac{1 - e^{-pt}}{p}$$

For the discontinuous sampled representation of the forcing (zero order hold)

From which the difference equation may be derived, where  $\omega' = \omega(1-z^2)^{1/2}$ ,  $f' = f/(1-z^2)^{1/2}$

$$\Theta(n) = \Theta(n-1) 2e^{-f'\omega'T} \cos \omega'T - \Theta(n-2) e^{-2f'\omega'T} + \frac{1}{\omega'^2} \left\{ [1 - e^{-f'\omega'T} (\cos \omega'T + f' \sin \omega'T)] C(n-1) + e^{-f'\omega'T} [-\omega'^2 \cos \omega'T - (\cos \omega'T - f' \sin \omega'T)] C(n-2) \right\}$$

Using the relation  $\dot{\theta}(p) = p\Theta(p)$  the following difference equation results

$$\dot{\theta}(n) = \dot{\theta}(n-1) 2e^{-f'\omega'T} \cos \omega'T - \dot{\theta}(n-2) e^{-2f'\omega'T} + \frac{1}{\omega'^2} \omega'^2 \sin \omega'T [C(n-1) - C(n-2)]$$

Thus for a constant time interval the solution reduces to a combination of constant coefficients and the two prior values of  $\theta$ ,  $\dot{\theta}$  and sampled forcing. The values of  $\theta$  and  $\dot{\theta}$  may then be used, if required, in evaluation of the new forcing.

It is of interest to evaluate the accuracy of the results obtained from application of the above procedure and to establish the minimum sampling interval that may be used. For this purpose the response to two idealised modes of forcing are examined. These are the indicial response (response to a step input) and the response to harmonic forcing  $c(t) = \sin \Omega t$ , starting initially from rest. For these two inputs the exact continuous response may be easily calculated for comparison. In the comparisons shown, time has been non dimensionalised by dividing by the period of the undamped natural frequency i.e.  $t' = t.2\pi/\omega$  and the sampling rate  $N$  is referred also to this base.

The indicial response is shown in figure 9 for both low and moderately high values of damping, it can be seen that quite satisfactory results can be obtained for a sample rate of  $N = 6$ . It is a characteristic of the zero order hold that, for harmonic forcing, a phase shift is introduced that is equivalent to half the value of the sampling interval. If this is acceptable, then, for values of the ratio of forcing frequency to natural frequency ( $\omega_c / \omega_n$ ) close to 1 the above sampling rate can be shown to be adequate.

For higher ratios of forcing frequency ( $\omega_c / \omega_n = 4$ , figure 10) it is necessary to increase the sample rate somewhat proportionally. In these examples, by defining explicitly the forcing, there is no possibility of errors arising from feedback of forcing terms derived from calculated response.

It was stated earlier that the method of formulation permitted the inclusion of feedback terms in the forcing that were not convenient to include in the characteristic equation. The implementation of this may be simulated (in the case of rate feedback) by assigning a low value of damping ( $\zeta = 0.02$ ) for the calculation of the coefficients of the difference equation and subtracting the appropriately scaled value of computed  $\dot{\theta}(n)$  from the forcing. As may be expected this degrades the solution both for indicial response (figure 11) and response to harmonic forcing (figure 12). It appears that, in order to regain the level of acceptability previously established, the sampling rate may need to be more than doubled. This depends of course on the relative values of the inherent and external damping. As a guide then, if significant damping effects are incorporated in the forcing, the sample frequency should be around 20 times the highest frequency present.

The above difference equations were derived employing the concept of a zero order hold. It is possible using the same techniques (reference 5) to implement alternative assumptions of the behaviour of the forcing function between samples. For instance the slope derived from the prior two samples may be projected into the following interval (first order hold) or an apparent half step lead may be introduced. Both of these schemes reduce the phase lag inherent in the zero order hold but, in the case of the first order hold, it is possible to introduce significant overshoot into the solution. In common with other approaches it is found that for each class of problems an optimum form of solution has to be determined. A feature of the above method is that the proper phase relationship between rate and displacement is maintained.

#### References

1. Lomax, H. et al. Two and three dimensional unsteady lift problems in high-speed. NACA Report 1077, 1952.
2. Bisphinghoff, R.L., Ashley, H., Halfman, R.L. Aeroelasticity. Addison-Wesley, 1955.
3. Minhinnick, I.T. Subsonic Aerodynamic flutter derivatives for wings and control surfaces RAE Report Structures 87, 1950.
4. Ballhaus, W.F., Magnus, R., Yoshihara, H. Some examples of unsteady transonic flows over airfoils. Proc. of a symposium held at the University of Arizona, March 1975.
5. Jury, E.I. Sampled data control systems Wiley, 1958.
6. Lomax, H. Indicial Aerodynamics, Part II, Chapter 6. AGARD Manual on Aeroelasticity.

#### APPENDIX 1 - FREQUENCY RESPONSE

The lift transfer function is given by:-

$$\frac{C_l(p)}{\alpha(p)} = C_{l\alpha}(M) \left[ \left( 1 - \sum_{n=1}^3 A_n \right) + \sum_{n=1}^3 \frac{A_n}{1 + T_n p} \right], \quad \frac{C_{lq}(p)}{q(p)} = -\frac{1}{M} \frac{T_q p}{(1 + T_q p)} = -\frac{1}{M} \left[ \frac{1 - 1}{(1 + T_q p)} \right]$$

For simple harmonic forcing,  $\theta = \sin \omega t$ ,  $q = \frac{\omega c}{V} \cos \omega t$

$$\alpha(p) = \frac{1 + Bp}{\omega(1 + p^2/\omega^2)} \quad \text{where} \quad B = \frac{c}{2V} \bar{x} \quad \text{and} \quad \bar{x} = \text{distance}$$

$$\text{of } \frac{1}{2} c \text{ aft of pitch axis in semi chords.} \quad q(p) = \frac{2k}{\omega^2} \frac{p}{(1 + p^2/\omega^2)} \quad \text{where} \quad k = \frac{\omega c}{2V}$$

Taking the  $\alpha$  terms first

$$\frac{C_l(p)}{C_{l\alpha}(M)} = \frac{1}{\omega} \left[ \left( 1 - \sum_{n=1}^3 \frac{A_n(1 + Bp)}{(1 + p^2/\omega^2)} \right) + \sum_{n=1}^3 \frac{A_n(1 + Bp)}{(1 + p^2/\omega^2)(1 + T_n p)} \right]$$

We obtain from the inverse transform after the initial transient has decayed.

$$\frac{C_1(t)}{C_{1c}(M)} = (1 - \sum_1^3 A_n |1 - k^2 \bar{x}^2|^{1/2}) \sin(\omega t + \phi) + \sum_1^3 A_n \left[ \frac{1 - k^2 \bar{x}^2}{1 + T_n^2 \omega^2} \right]^{1/2} \sin(\omega t + \phi_n)$$

where  $\phi = \tan^{-1}(k\bar{x})$ ,  $\phi_n = \tan^{-1}(k\bar{x}) - \tan^{-1}(T_n \omega)$

The above may be expressed in the form  $\frac{C_1(t)}{C_{1c}(M)} = N \sin(\omega t + \beta) = N(\sin \omega t \cos \beta + \cos \omega t \sin \beta)$

Equating the in phase and quadrature terms yields:

$$N \cos \beta = \left[ (1 - \sum A_n) \cos \phi + \sum \frac{A_n \cos \phi_n}{(1 + T_n^2 \omega^2)^{1/2}} \right] \cdot k\bar{x}^{1/2}, \quad N \sin \beta = \left[ (1 - \sum A_n) \sin \phi + \sum \frac{A_n \sin \phi_n}{(1 + T_n^2 \omega^2)^{1/2}} \right] \cdot k\bar{x}^{1/2}$$

Substituting

$$\cos \phi = \frac{1}{(1 + k^2 \bar{x}^2)^{1/2}}, \quad \sin \phi = \frac{k\bar{x}}{(1 + k^2 \bar{x}^2)^{1/2}}, \quad \cos \phi_n = \frac{1 + k\bar{x} T_n \omega}{[(1 + k^2 \bar{x}^2)(1 + T_n^2 \omega^2)]^{1/2}}, \quad \sin \phi_n = \frac{k\bar{x} - T_n \omega}{[(1 + k^2 \bar{x}^2)(1 + T_n^2 \omega^2)]^{1/2}}$$

We get:-

$$N \cos \beta = (1 - \sum A_n) + \sum \frac{A_n (1 + k\bar{x} T_n \omega)}{(1 + T_n^2 \omega^2)}, \quad N \sin \beta = (1 - \sum A_n) k\bar{x} + \sum \frac{A_n (k\bar{x} - T_n \omega)}{(1 + T_n^2 \omega^2)}$$

Considering the pitch rate term  $C_{1q}(p) = \frac{-2k}{\omega^2 M} \left( 1 - \frac{1}{1 - T_q p} \right) \left( \frac{p}{1 + p^2/\omega^2} \right)$

After the initial transient has decayed

$$C_{1q}(t) = \frac{-2k}{M} \left[ \frac{\cos \omega t - \cos(\omega t - \phi_q)}{(1 + T_q^2 \omega^2)^{1/2}} \right] \quad \phi_q = \tan^{-1} T_q \omega \quad \text{or} \quad C_{1q}(t) = \frac{2k T_q \omega}{M(1 + T_q^2 \omega^2)} (\sin \omega t - T_q \omega \cos \omega t)$$

Thus if the overall response is given by  $N' \sin(\omega t + \beta')$  then

$$N' \cos \beta' = (1 - \sum A_n) + \sum \frac{A_n (1 + k\bar{x} T_n \omega)}{(1 + T_n^2 \omega^2)} + \frac{2k T_q \omega}{M(1 + T_q^2 \omega^2)} C_{1q}(M)$$

$$N' \sin \beta' = (1 - \sum A_n) k\bar{x} + \sum \frac{A_n (k\bar{x} - T_n \omega)}{(1 + T_n^2 \omega^2)} - \frac{2k T_q^2 \omega^2}{M(1 + T_q^2 \omega^2)} C_{1q}(M)$$

Hence

$$N' = \left[ (N' \cos \beta')^2 + (N' \sin \beta')^2 \right]^{1/2} \quad \text{and} \quad \beta' = \tan^{-1} \left( \frac{N' \sin \beta'}{N' \cos \beta'} \right)$$

From the numerical values assigned to the generalised indicial lift function the following values for the above variables may be derived:-

$$T_1 \omega = \frac{12.5 k}{1 - M^2}, \quad T_2 \omega = \frac{1.5385 k}{1 - M^2}, \quad T_3 \omega = \frac{Mk}{(.37 + 76M)(1 - M^2)}, \quad T_q \omega = \frac{M^2 k}{(1 - M^2)}$$

$$A_1 = 0.3, \quad A_2 = 0.7, \quad A_3 = \frac{-k}{M C_{1c}(M)}$$

$$\Psi_C(s) = (1-M^2)^{1/2} (1-0.5e^{-13s'} - 0.5e^{-s'})$$

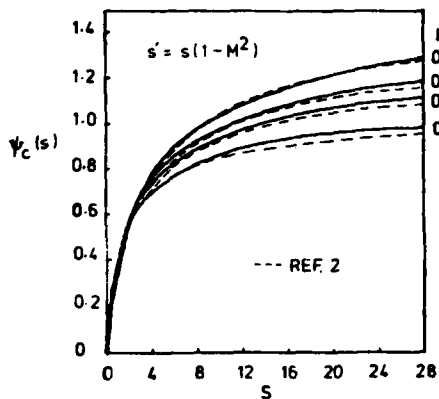


FIG. 1. COMPARISON OF GENERALISED KUSSNER FUNCTION.

$$\Phi_C(s) = (1-M^2)^{1/2} (1-0.3e^{-0.08s'} - 0.7e^{-65s'}) + \frac{2}{\pi M} e^{-(\frac{37+.76M}{M})s'}$$

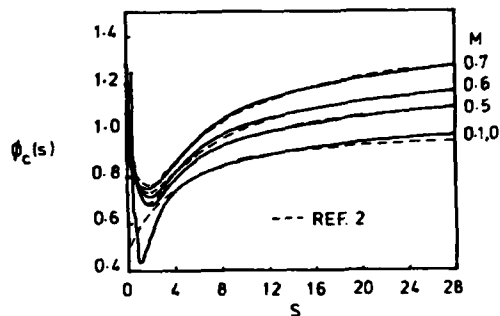


FIG. 2. COMPARISON OF GENERALISED WAGNER FUNCTION.

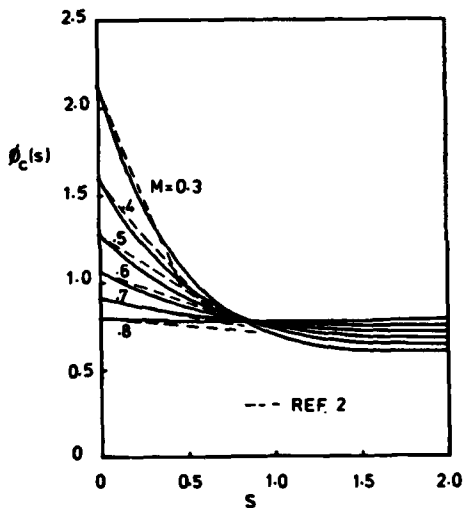


FIG. 3. INITIAL PORTION OF 'WAGNER' FUNCTION.

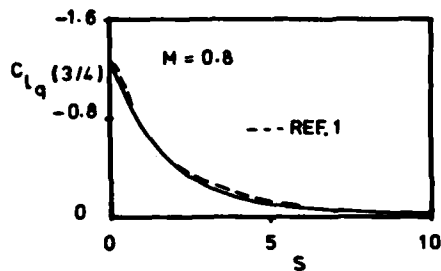


FIG. 4. INDICIAL LIFT RESPONSE TO PITCH RATE ABOUT 3/4 CHORD.

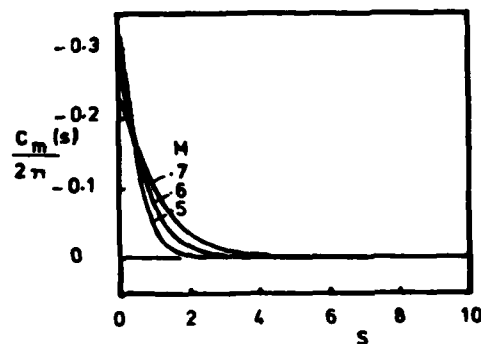


FIG. 5. INDICIAL PITCHING MOMENT RESPONSE.

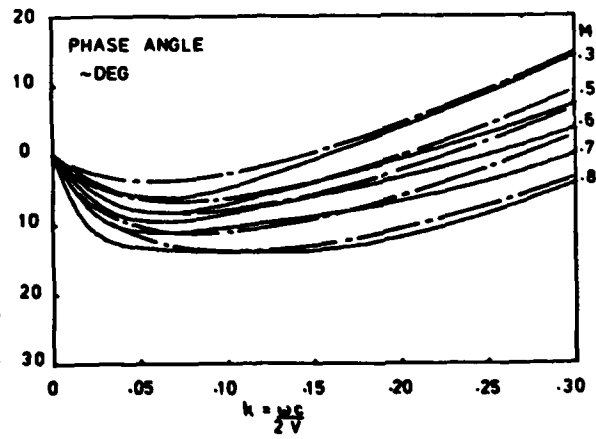
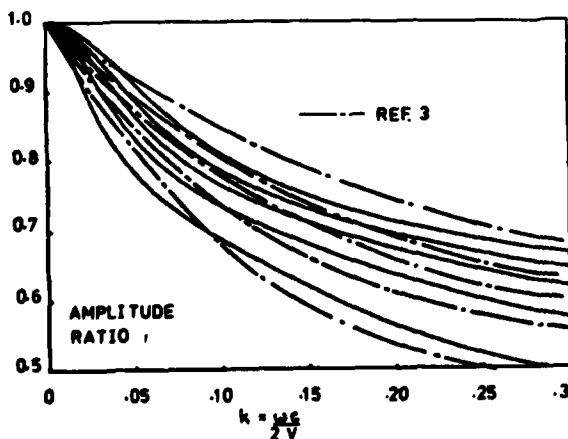


FIG. 6. FREQUENCY RESPONSE, COMPARISON WITH LINEARISED THEORY.

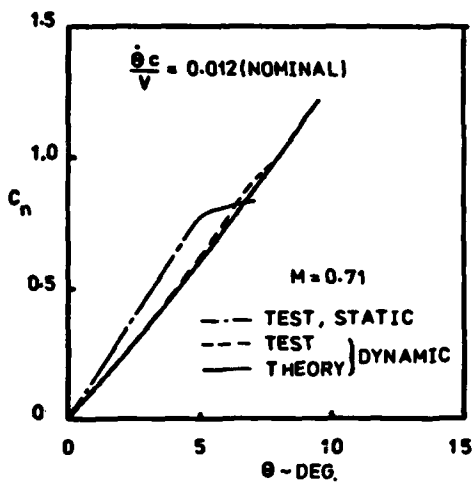


FIG. 7. RESPONSE TO RAMP FORCING, COMPARISON WITH TEST.

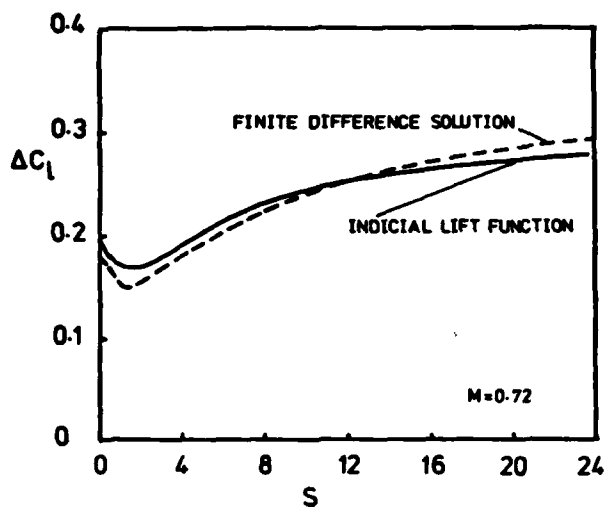


FIG. 8(a). GENERALISED INDICIAL LIFT, COMPARISON WITH NONLINEAR THEORY.

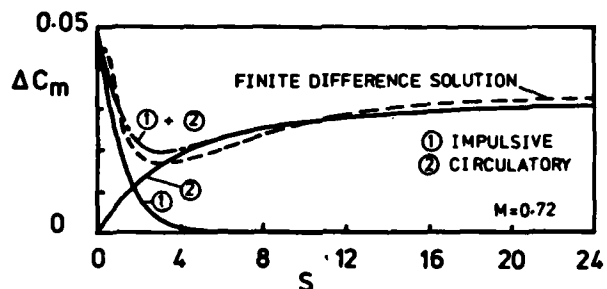


FIG. 8(b). PITCHING MOMENT RESPONSE, COMPARISON WITH NONLINEAR THEORY.

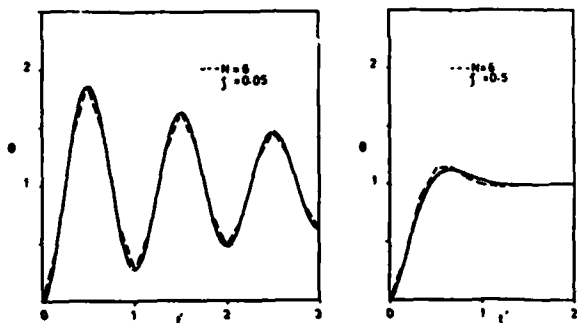


FIG. 9. INDICIAL RESPONSE, NUMERICAL SOLUTION.

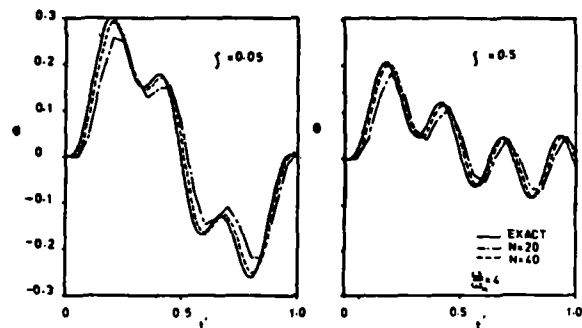


FIG. 10. HARMONIC FORCING, NUMERICAL SOLUTION.

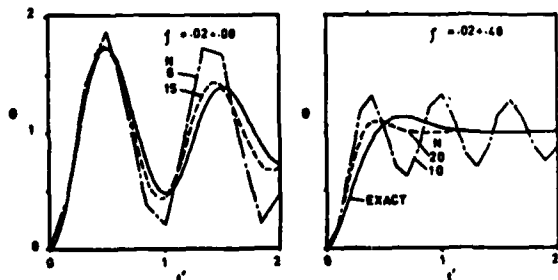


FIG. 11. INDICIAL RESPONSE, NUMERICAL SOLUTION WITH FEEDBACK.

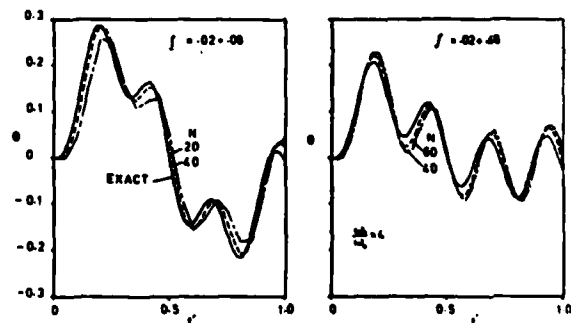


FIG. 12. HARMONIC FORCING, NUMERICAL SOLUTION WITH FEEDBACK.

## EXPERIMENTAL TECHNIQUES IN UNSTEADY AERODYNAMICS

N. C. Lambourne  
 Royal Aircraft Establishment  
 Structures Department, Bedford, UK

## SUMMARY

The role of experiments in the field of unsteady aerodynamics and the methods of simulating unsteady conditions with models in wind tunnels, or other facilities, are outlined. The techniques of measuring unsteady quantities such as aerodynamic force and pressure are described, attention being given to the part played by computers in the acquisition, processing and presentation of measured data. The choices facing the experimenter and some of the phenomena that may be encountered are discussed. Finally, specific examples of test rigs and test procedures are briefly described.

## 1 INTRODUCTION

Taken as a general class, experiments in unsteady aerodynamics embrace a wide range of procedures and measuring techniques. They depend on expertise in a diversity of subjects distinct from aerodynamics itself. For instance, most experiments use a variety of electrical equipment and require, in the end, the manipulation, measurement and processing of electrical signals. Often the person who will ultimately make use of the experimental results remains somewhat outside the actual measuring processes. There is thus a need for a common understanding of the procedures and their limitations.

The intention here is to provide an outline of the methods commonly used when dealing with subjects in which unsteady aerodynamics affects the behaviour of aircraft. Not all unsteady phenomena are included: turbulence (apart from atmospheric gusts), the unsteadiness within a boundary layer and aspects of unsteady aerodynamics peculiar to turbines and compressors are omitted.

Some subjects are treated more thoroughly than others. Indeed, those subjects adequately dealt with in readily available literature are given only cursory mention. Whilst the present document on its own should be sufficient to provide an introduction, a more complete picture could be obtained from the recommended references.

Within the present limits of time and space it is certainly not possible to give a complete coverage of methods and equipment. Apologies are offered to those who find their work unmentioned.

## 2 SUBJECTS OF EXPERIMENTS

The main aeronautical subjects that involve unsteady aerodynamics and which require experimental investigation are:

- buffeting;
- behaviour in gusts;
- flutter and other flow-induced oscillations;
- aircraft stability;
- rapid operation of controls;
- behaviour of helicopter blades.

In all these subjects there is interaction between the unsteady aerodynamic forces and the structural response. Some experiments aim at reproducing the whole unsteady phenomenon; the structural behaviour is then a principal objective. Other types of experiment are concerned only with the aerodynamic forces or pressures, the aim being to determine these for a prescribed unsteady situation.

Experiments are usually done only when the problem is not amenable to reliable theoretical treatment because one or more of the following elements are present:

- boundary layer and viscous effects;
- mixed subsonic and supersonic flows;
- shock wave;
- flow separation;
- cyclic changes of flow régime;
- complicated geometrical configuration.

The specification of the model and the test conditions relate to an aeroplane and a flight condition through the requirements for dynamical similarity. Sometimes the relationship is a rather loose one. The aim of the experiment is usually one or more of the following:

- (1) To provide data to be used directly in design;

- (2) To provide data for comparison with theoretical calculations; to validate a theoretical method;
- (3) To explore a phenomenon.

For aims (1) and (2) the relationship between the model test and the aeroplane is illustrated in Fig 1. The model and test specifications are more severe for (1) than for (2), because in the latter case the mathematical calculations can act as a buffer. The exploratory type of investigation allows the experimenter the greatest freedom.

### 3 CONDITIONS FOR SIMILARITY

The simulation of full-scale conditions requires that certain non-dimensional similarity parameters have the same values for the model and prototype systems. Mach number  $M$  and Reynolds number  $Re$  are familiar parameters important in steady tests. Unsteadiness leads to the introduction of a further similarity parameter which can be expressed in several alternative ways. If  $T$  is the duration of a definable event then kinematical similarity requires  $TV/L$  to be invariant, where  $V$  is a relative velocity and  $L$  a typical dimension. When the conditions are oscillatory,  $T$  is conveniently taken as the periodic time and, using frequency  $f$ , an alternative non-dimensional parameter is the frequency parameter  $fL/V$  which is often based on either the full-, or the half-chord of a wing. For non-oscillatory unsteady conditions, alternative similarity parameters based on a linear acceleration  $\ddot{z}$ , or an angular velocity  $\dot{\theta}$  are respectively  $\ddot{z}L/V^2$  and  $\dot{\theta}L/V$ . Thus for a rigid model undergoing a prescribed unsteady motion the test conditions can be specified by any one of the following unsteady parameters:

$$TV/L, \quad fL/V, \quad \ddot{z}L/V^2, \quad \dot{\theta}L/V.$$

When the experiment involves the dynamic response of an elastic model, three other similarity parameters become important:

stiffness parameter	$E/\rho V^2$
structural damping parameter	$D/\rho V$
mass, or density, ratio	$\sigma/\rho$

where  $EL$  = stiffness, force/unit linear deflection,  
 $DL^2$  = structural damping, force/unit linear velocity,  
 $\sigma L^3$  = structural mass (*ie* force/unit linear acceleration).

When gravitational forces enter into the problem, another similarity parameter is:

$$\text{Froude number} \quad V^2/gL$$

where  $g$  = acceleration due to gravity.

It is usually impossible for a scale model to achieve the correct Mach number and the correct Froude number simultaneously. The model is then built to satisfy one or other of the following types of modelling.

#### Mach modelling

Gravitational effects ignored.  
 Parametric conditions satisfied:  
 $M, \quad E/\rho V^2, \quad \sigma/\rho, \quad D/(\sigma E)^{\frac{1}{2}}$

where the structural damping  $D$  now relates to model mass and stiffness by the parameter  $D/(\sigma E)^{\frac{1}{2}}$ , which is proportional to the relative damping of the model.

In a tunnel where flow conditions are defined by Mach number, total pressure  $p_t$  and total temperature  $K_t$ , an alternative set of parameters is

$$M, \quad E/p_t, \quad \left(\frac{E}{\sigma}\right)/K_t, \quad D/(\sigma E)^{\frac{1}{2}}.$$

In words, the scaled stiffness of the model must relate to the tunnel total pressure, and a parameter  $(E/\sigma)$  representing structural efficiency must relate to the tunnel total temperature. The potential advantage offered by a cryogenic tunnel to the construction of aeroelastic models is hereby disclosed<sup>1</sup>.

#### Froude modelling

Mach number effects ignored.  
 Parametric conditions satisfied:  
 $V^2/gL, \quad E/\rho V^2, \quad \sigma/\rho, \quad D/(\sigma E)^{\frac{1}{2}}.$

Since  $g$  is constant, the linear scale of the model fixes the velocity scale which in turn, if  $\rho$  is constant, fixes the stiffness scale. That is,

$$V^2 \propto L, \quad E \propto L, \quad \sigma = \text{constant}.$$

Froude modelling is appropriate to free-flight models.

## Low-speed tunnel modelling

Mach number and gravitational effects ignored.  
Parametric conditions satisfied:

$$E/\rho V^2, \quad \sigma/\rho, \quad D/(\sigma E)^{1/2}$$

The linear and the velocity scale may then be chosen independently.

### 4 TEST FACILITIES

#### 4.1 Wind tunnels

Most unsteady experiments are made in conventional wind tunnels. The majority are made in a stream flow that is basically steady and uniform, the element of unsteadiness being introduced either by motion of the model or by the flow changes caused by the model. Usually a tunnel with an absence of flow fluctuations is preferred for unsteady experiments although sometimes their presence can be exploited as a means of model excitation.

Many experiments involve model flexibility either explicitly or implicitly. It is then an advantage for the tunnel total pressure to be variable since this allows variation of the similarity parameter  $E/\rho V^2$  whilst keeping Mach number constant.

Currently there is an interest in cryogenic tunnels not only for their ability to attain high Reynolds numbers but also because the low temperature and the capability of varying temperature have potential advantages for matching model dynamic properties with flow characteristics<sup>1</sup>.

#### 4.2 Tracks and free-flight facilities

Some experiments are made by moving a model through a stationary atmosphere or fluid. Unsteady motions can then be obtained by constraining the model to follow a prescribed path. Alternatively the model may move freely. A description has been given of a facility at the IMF Lille<sup>2</sup> in which a model with remotely operated control surfaces is catapulted and, whilst in free flight, its behaviour following control surface deflection is studied by photography. A track to simulate gust encounter will be mentioned in the next section.

#### 4.3 Gust facilities

Atmospheric gusts are simulated either by modifications to a conventional wind tunnel or by special facilities. Some arrangements are designed to reproduce an isolated gust, others to produce harmonically varying upwash. Fig 2 shows several schemes.

- (a) A two-dimensional jet is deflected by the movement of upper and lower flaps. The gust tunnel at Queen Mary College, London operates on this principle<sup>3</sup>.
- (b) A two-dimensional jet is deflected by transient or oscillatory motions of two or more aerofoils ahead of the model. Examples of this type of facility are located at the University of Salford<sup>4</sup> and the DFVLR<sup>5</sup>.
- (c) In an arrangement used at NASA Langley<sup>6,7</sup> one or more rotatable vanes are attached to the side walls of a conventional transonic tunnel at a suitable distance upstream of the model. A complete model centrally mounted is thus in the downwash field of the vanes and, when these are oscillated in synchronism, the model experiences an oscillatory downwash.
- (d) At Cambridge University<sup>8</sup> a two-dimensional facility with flexible walls at the top and bottom can be used to simulate either vertical or horizontal fluctuations in velocity and is mainly used in research on turbine and compressor blades. The walls can be distorted by mechanical means and a travelling wave motion imposed. Whether the velocity fluctuation is in the vertical or the horizontal direction depends on the phasing of the motion applied to the walls.
- (e) By using a gust track, a model is carried on a moving vehicle to pass through a transverse jet, thereby experiencing a single transient gust. A facility of this kind has been used by the RAE<sup>9</sup>.

In all gust facilities, as well as making force or pressure measurements on the model, it is necessary to make a thorough calibration of the device to determine the exact nature of the simulated gust flows. This is often more difficult than making the measurements on the model. As an example Fig 3 shows the flow field in the gust tunnel at QMC<sup>3</sup> in the test region downstream of the harmonically operated deflector plates.

Gust facilities tend to be used more for research than for routine testing.

### 5 EXPERIMENTAL ARRANGEMENTS

Most experiments in unsteady aerodynamics consist of a *model system* to which an *input* is supplied and an *output* measured. The model may be rigid or flexible. The input may be an imposed unsteady perturbation, an applied unsteady force, unsteadiness in the local flow over the model (as in buffeting) or a steady flow that causes an instability (as in flutter). The measured output may be aerodynamic forces or pressures or the



unsteady response of the model. Fig 4 identifies four of the possible types of experimental arrangement and relates these to various subjects of investigation. For simplicity a complete model is shown in each of the diagrams but more usually experiments are made with partial models, for example half-span wings.

The perturbation motion applied to the model may be some form of transient, such as a step or a ramp, but more often it is simple harmonic.

Note the difference between (a) imposing a known motion and measuring aerodynamic force or pressure and (b) applying a known harmonic force to a sprung model and measuring motion. The first is the direct way of measuring unsteady aerodynamic quantities. The second, the indirect method is often used to measure aerodynamic derivatives; then the aerodynamic properties are effectively regarded as combinations of stiffness, damping and inertia which add to the corresponding mechanical quantities. The procedures adopted to measure the aerodynamic derivatives are then the same as those used to determine the properties of a completely mechanical system. Finally, the aerodynamic contributions are obtained as differences of two sets of measurements, one obtained wind-on, the other in a vacuum (but more usually in still-air).

## 6 APPLICATION OF MOTION OR UNSTEADY FORCE

### 6.1 Motion

Periodic motions can be applied to the model by cams, cranks or other reciprocating mechanisms. High frequency oscillation can be obtained with electromagnetic vibrators but these really produce forces, not inexorable motions. For motion that can have any prescribed form the present tendency is to use an hydraulic actuator, or ram, controlled by a servo-loop. Such components are able to overcome very large forces but tend to be limited to frequencies not much above 100 Hz. Most actuators produce linear motion but types have recently been designed to produce rotary oscillation.

### 6.2 Force

Harmonic forces can be applied by mechanical out-of-balance exciters or by forcing through a spring. More usually they are generated by electromagnetic vibrators, the force being known from the current in the coil. These devices can operate at high frequencies but the amplitudes of the forces are small and often necessitate working near to a resonance of the system.

In flight impulsive forces can be applied by explosive charges, sometimes known as 'bonkers'.

### 6.3 Triggered release

A triggered release from a deflected position is a simple method of applying an input to a model. Measurement of the transient response can then be used to determine stiffness and damping of a system having a single degree of freedom.

## 7 MEASUREMENT OF UNSTEADY DISPLACEMENTS AND FORCES

### 7.1 Displacements

Various types of displacement transducers are available commercially, their operation usually depending on a relative displacement causing a measurable change in an electrical quantity. It is often difficult to obtain devices small enough to be installed within a model. Ref 10 describes a recently developed fibre-optic probe to measure the rotation of a control surface in a small model.

The fixed reference required by displacement transducers is not easily provided when model motions are to be measured in a tunnel. For this reason, in oscillatory measurements it is more usual to employ accelerometers; these operate satisfactorily as displacement sensors provided the frequency is not too low. If a measure of absolute displacement is required this can be obtainable by double integration of the signal.

Literature indicates that research continues into optical interferometric and holographic methods of measuring model deformation.

### 7.2 Forces

Almost all methods of determining an unsteady force depend on applying the force to a spring element, the deflection of which is measured, usually by some electrical device. Even in the ideal situation where all the other components are rigid, the introduction of a spring means attention must be given to the dynamic response of the system, and particularly to its natural frequency. The classic example - the response of a single degree of freedom system when harmonic force is applied is shown in Fig 5. The manner in which amplitude and phase vary with frequency illustrates the importance of keeping all natural frequencies high, the need for dynamic rather than static calibration and more generally the difficulties in measuring rapidly varying forces.

When the model itself is moving, the force being measured will include contributions from the model inertia which are usually much larger than the aerodynamic forces whose magnitudes are to be determined. It is possible to arrange to balance-out the

inertia contributions either mechanically, or electrically using signals from accelerometers, but such methods become less reliable as the working frequency increases.

## 8 MEASUREMENT OF UNSTEADY PRESSURES

An unsteady pressure consists of a steady level and a fluctuating component. In aerodynamic experiments the steady pressure may be as high as 1 (or more) bar whilst the amplitude of the fluctuating component to be measured may be as little as  $10^{-3}$  bar. To obtain adequate percentage accuracy in the measurement of the fluctuations requires the unsteady and steady components to be separately measured, although this need not mean two completely different systems.

### 8.1 Methods

Fig 6 illustrates three main methods of measuring unsteady pressure distributions on an aerodynamic surface.

#### *In situ* transducers

In this method small pressure transducers are installed so that their pressure sensitive areas form part of the aerodynamic surface. The great advantage of this arrangement is that, in principle at least, the pressure required to be measured is the pressure acting on the transducer. Usually however, this advantage is outweighed by the difficulty of achieving a flush and correctly contoured surface. Also, the sensitive areas of the transducers, being exposed, are liable to damage.

#### Tube system

This system, as pioneered by the NLR, uses small-bore tubing to transmit the aerodynamic pressures to a location, usually just outside the working section where they are measured. In this method it is economical to use one transducer and a pressure switch (a Scanivalve) to measure a number of pressures sequentially. The length of tubing means that the unsteady pressure measured by the transducer is not the same as the unsteady pressure acting at the orifice. The transfer function of such a typical system with a tube length of about 1 m is shown in Fig 7. There is usually good agreement between the transfer function calculated by theory<sup>11</sup> and that measured in a laboratory bench test. Unfortunately, as shown in Fig 8, the transmission characteristics change when there is a flow across the orifice and the effect increases with local Mach number. It is possible to make allowance for this effect<sup>12</sup> but it requires at least one transducer to be installed in the model to allow calibration to be made under the flow conditions. Use of a tube system allows a stiff and relatively simple construction for the model.

#### Recessed transducers

Transducers are installed in the model and connected to surface orifices by the shortest possible passage. Compared with the tube system, this method largely avoids problems of transmission, allows the pressures to be measured simultaneously and is better able to deal with pressure time-variations that are not sinusoidal.

The disadvantages are in the cost of the required number of transducers and the complication of having to install them in a manner that allows their eventual recovery.

### 8.2 Miniature pressure transducers

Most pressure transducers depend for their operation on the deflection of a flexible diaphragm the two sides of which are exposed to differing pressures. The deflection of the diaphragm is converted by some means into an electrical signal which is measured and from which using appropriate calibration factors the pressure is determined.

Many transducers have flush diaphragms; Fig 9a&b illustrate the differences between two classes, the absolute and the differential types.

In the absolute type the pressure on the inner side of the diaphragm is that obtained in a hermetically sealed volume, which can be a vacuum. In principle, provided the internal pressure remains constant, the output voltage from the transducer is proportional only to the pressure  $p$ , applied to the outer side of the diaphragm and it is not necessary to know explicitly the pressure in the enclosed volume.

As its name implies, the differential type is designed to measure the difference between two applied pressures, one the unsteady pressure  $p$ , to be measured, the other a steady reference pressure  $p_0$  usually brought to the transducer by a tube. The relative advantages of the two types for unsteady measurements is discussed later.

A large variety of both classes is available commercially. Shape and size are prime considerations when selecting a type to install within a model. Fig 9c&d gives some idea of two small types available from Kulite Semi-Conductor Products Inc. New Jersey, USA. The flat 'button' type could be useful where thickness is the limitation, but it is the cylindrical type that has found favour for model installation. It may be noted that other cylindrical transducers are available with diameters less than 1 mm.

In a type of transducer commonly used, the diaphragm is silicon on which a strain sensitive semiconductor material has been deposited to form an active four-arm Wheatstone bridge. The basic circuit of the transducer and its associated module to compensate for temperature changes is shown in Fig 9e. Because the diaphragm is vulnerable to damage by abrasion, the type of transducer that comes complete with a screened diaphragm is usually preferred. The natural frequency of the diaphragm is very high, 230 kHz or above which means the transducer can easily cope with the usual situation where the frequencies are no more than a few hundred Hz.

Although excellent for the measurement of unsteady components many small transducers suffer from temperature effects that make them unsuitable for accurate measurement of the steady component of pressure. In consequence it has been customary to use two separate systems, transducers for the unsteady components and a conventional tube system for the steady components, thereby complicating the design of the model. Recently, a promising scheme has been developed to use the same transducers for both unsteady and steady measurements<sup>13</sup>.

### 8.3 Installation of transducers

Fig 10 shows several methods of installing a transducer within a model and connecting it to an orifice at the surface. In all cases a coating of silicone rubber or other slightly resilient substance is used to seal the body of the transducer in a hole only slightly larger than its diameter. It is obviously preferable for the orifice plugs, but not the transducers to be inserted into the model before finally machining the surface. The main requirements for good installation are:

the block into which the transducer is inserted should protect it from mechanical stress;

the volume of air at the face of the transducer and the length of the connecting passage between transducer and orifice should be as small as possible.

It is usually difficult to keep the connecting passage short when the orifice is near a trailing edge. When an arrangement, such as that shown in Fig 10d is resorted to, it is important to test for unwanted transmission features.

### 8.4 Transducer and amplifier characteristics

Transducers, such as Kulites, that depend on change of resistance need to be supplied with a steady voltage, say 5 V, and then, depending on the pressure applied, they produce an output of several millivolts which will need to be amplified. Regarding the transducer and its associated signal conditioning as a whole, an ideal system for measuring unsteady pressures would be one in which:

the output voltage  $E$  is linear with applied pressure  $p$ , or pressure difference  $(p - p_R)$ ;

the sensitivity  $dE/dp$  is independent of oscillation frequency;

there is no phase lag between  $E$  and  $p$ , at least over the working range of frequency;

the output  $E$  is independent of all other environmental changes, such as temperature, acceleration, mechanical stress or electro-magnetic radiation.

As already mentioned, compensation for temperature change is usually made by additional circuitry. With Kulites any sensitivity to acceleration can be neglected for most applications. A sensitivity to light falling on the diaphragm has been reported, but when the transducer is recessed within the model this should not be a problem.

An absence of phase lag is achieved by the high natural frequency of the diaphragm and the design of the amplifier. A reasonable specification for the latter would require the phase change to be less than  $1^\circ$  for frequencies up to 1 kHz.

### 8.5 Calibration procedure

Calibration of the pressure measuring system is of the utmost importance because the final results and any comparisons with theory ultimately depend on it. The calibration should embrace the whole system as installed in the model, and, as far as possible, should be done under similar conditions to those obtaining during the actual measurements. Although it is possible for calibration to be based only on steady pressures it is preferable to make use of a device for generating oscillatory pressures. A hand-held instrument that can be moved across the model from orifice to orifice is shown in Fig 11. A rubber tube at the outlet allows the oscillatory pressure to be applied to the orifice of the transducer under test. Either a displacement transducer or a reference pressure transducer, as shown in the diagram, is used to define the phasing of the oscillatory pressure. As indicated in the diagram, the amplitude of the pressure depends on the thermodynamic behaviour of the enclosed air; this generally remains unknown so that the device cannot be regarded as an absolute standard. In practice the pressure generator itself is calibrated against an established reference transducer over a range of frequency. The reference transducer chosen for this task is judged to have a dynamic sensitivity identical to its static sensitivity which is measured against a pressure standard.

A motor-driven generator of the type described is suitable for frequencies up to 100 Hz and a pressure amplitude of  $10^{-2}$  bars.

The procedure used by one research team for calibrating transducer systems installed in models is now outlined. It involves selection of transducers and measurements of sensitivity. Firstly, no transducer is installed in a model unless it shows adequate linearity. When all the transducers have been installed, the model is placed in a pressure or vacuum chamber and subjected to the range of steady pressures that will be encountered later in the wind tunnel. By adjustment of the gain of the amplifiers, each transducer channel is brought to the same sensitivity (volt/bar) and this sensitivity is measured against a secondary standard of pressure (a Texas gauge). Temperature effects will be examined at this stage. Finally working in atmospheric conditions, the oscillatory pressure generator will be applied to each orifice: (a) to verify that the dynamic sensitivity over the relevant range of frequency is the same as the steady sensitivity; and (b) to see whether there are transmission phase lags which demand improvements in the installation or corrections in the data processing.

It will be appreciated from the foregoing account that the calibration procedure involves several cross checks, but ultimately it rests on the assumption that, for one transducer at least, the sensitivity is independent of the oscillation frequency. Also in none of the calibration tests is the effect of flow across the orifice represented. There is certainly scope for further investigation into both these matters.

#### 8.6 Relative merits of absolute and differential types of transducers

The relative merits for unsteady pressure measurements are summarized as follows.

##### Absolute type

###### Advantages:

- no need to supply a reference pressure;
- ability to determine steady pressure directly from voltage output.

###### Disadvantages:

- small-amplitude sensitivity must be determined over a range of steady pressure;
- non-linearity is more likely to occur because large deflections of the diaphragm may be caused by the steady pressure.

##### Differential type

###### Advantages:

- provided the reference pressure is always the mean of the oscillatory pressure, there is no need to determine the sensitivity at different steady pressures;
- linearity may be more easily achieved because diaphragm deflection remains small.

###### Disadvantages:

- a suitable steady pressure reference must be provided, and this may require additional tubing;
- the steady pressure component cannot be determined without knowledge of the reference pressure.

The potential advantage of the differential type in having only the unsteady component as the pressure difference across the diaphragm is often not easily realised without additional complication. One method is to connect the reference side of the transducer to the source of pressure through fine bore tubing of sufficient length to smooth out the fluctuations.

When differential transducers are installed in a hollow model, their reference pressures are sometimes obtained by venting each one through a short length of fine tubing to the inside of the model. The pressure inside a model is usually close to the static pressure of the stream, so that under lifting conditions those transducers at positions of high steady  $C_p$  will experience large differences in the steady pressure across their diaphragms. In that case some of the advantage of the differential type is lost.

## 9 TREATMENT OF TIME-DEPENDENT SIGNALS

Nearly all unsteady measurements require the analysis of electrical signals from transducers. These signals will either represent the response to a deterministic input to the model or be the result of some random-like process occurring at the model. In practice, the signals from deterministic inputs are likely to include other extraneous components including random 'noise' some of which may be generated in the instrumentation but some will come from fluctuations inherent in the flow over the model. Of all the signals to be dealt with, those from pressure transducers and accelerometers tend to be most affected by noise.

Various objectives of signal analysis are:

- 1 Determination of the harmonic components coherent with a sinusoidal input; measurement of harmonic transfer function. These often require the separation of the required components from noise.
- 2 Measuring the response of a quantity to a specific transient input (*eg* pressures due to a ramp displacement of the model).
- 3 Determination of system parameters (*eg* stiffness and damping) from response to a specified input.
- 4 Determination of system parameters from response to a random input.
- 5 Measuring the harmonic content of the signal.
- 6 Obtaining a statistical description of a random signal.

The subject of signal analysis is very large, and for an extensive treatment the reader is recommended to textbooks such as Refs 14 and 15. Only certain of the more commonly used procedures are mentioned in what follows.

#### 9.1 Determination of harmonic components due to a sinusoidal input

This is probably the most frequently used form of analysis in unsteady experiments.

The left hand side of Fig 12 shows examples of signals obtained from accelerometers and pressure transducers during an oscillatory experiment in a wind tunnel. Trace 1 approximates so closely to a sinusoid that amplitude and phase could be obtained by direct measurement of the trace. Trace 2 is periodic but evidently contains harmonic components above the fundamental. Traces 3 and 4 suffer from noise that prevents the making of direct measurements. Indeed Trace 4 might be thought to be completely random.

In all cases the treatment is to apply Fourier analysis to the signals to obtain time-averages for the fundamental components related to the input as follows:

$$\begin{aligned} \text{in phase} &= (2/mT) \int_0^{mT} f(t) \cos \omega t \, dt \\ \text{in quadrature} &= (2/mT) \int_0^{mT} f(t) \sin \omega t \, dt \end{aligned}$$

where  $f(t)$  is the signal,  $\cos \omega t$  is the sinusoidal input and  $T \equiv 2\pi/\omega$  is the periodic time.

Note that the integration extends over a period of time that coincides with a *whole number*,  $m$ , of cycles. The higher harmonics of order  $n$  are likewise obtained by realising the quantities:

$$(2/mT) \int_0^{mT} f(t) \begin{pmatrix} \cos n \omega t \\ \sin n \omega t \end{pmatrix} dt$$

In practice, separate reference signals corresponding to  $\cos \omega t$  and  $\sin \omega t$  are available from the primary electrical oscillator driving the model and the multiplication of each of these with  $f(t)$ , the signal to be measured, can be done by various methods either analogue or digital. For instance commercially available Transfer Function Analysers can be used to obtain the fundamental and in some cases the higher harmonic components. However, the present-day tendency is to use a computer for digital processing of the signals. The basic treatment is then to obtain digital samples of  $f(t)$  at a time rate that is an integral multiple of the fundamental frequency and from these to calculate the Fourier coefficients in the computer. The introduction of a computer offers efficient analysis using a Fast Fourier Transform algorithm to obtain a value of the discrete form of the Finite Fourier Transform

$$F(\omega) = \int_0^T f(t) e^{-i\omega t} dt$$

where  $T$  is now the total sampling time.

Provided  $T$  contains a whole number of cycles of the reference signal, the harmonic components determined in this way are identical to those obtained by the simple Fourier analysis. In addition, the calculation of the Fourier transform discloses the presence of other periodicities and gives information about the frequency content of the noise. The right hand side of Fig 12 shows the amplitude spectra for each of the time signals. The harmonic components coherent with the input can be obtained from the height of the spectral lines.

## 9.2 Analysis of transients

Aerodynamic damping and stiffness are sometimes determined from the transient response of the model after being released from a deflected position. In simple cases these quantities can be obtained from measurements of the time-history traces. But if noise is present, or there is coupling between two or more degrees of freedom, more elaborate methods involving signal processing and spectral analysis may be necessary.

When the unsteady pressures resulting from a prescribed transient input to the model are required it may be necessary to extract an average response from the noisy signals from several repeated transients. In such cases, it is sometimes advocated that the complex Fourier transform should be obtained for each transient, an average of these then taken and finally, using the inverse Fourier transform, to return to the time domain to obtain an averaged response.

## 9.3 Analysis of random signals

In some experiments such as those concerning buffeting, or the determination of system characteristics from the response to tunnel turbulence, it is necessary to find certain statistical properties of the excitation or response, for example the Power Spectral Density. The computer application of the Fourier transform occupies an important place in many of the methods. Textbooks need to be consulted for details.

## 10 EQUIPMENT FOR DATA ACQUISITION AND PROCESSING

Analogue instruments such as Transfer Function Analysers, Spectrum Analysers, RMS Meters and Phase Resolvers continue to find a place in unsteady measurements, but there is a growing tendency to employ computer-based systems for acquiring, recording and processing the data. The Fast Fourier Transform already mentioned, has placed digital methods in a pre-eminent position. Also the high speed of operation and the display capabilities associated with the computer have revolutionized experimental procedures.

Measurements of unsteady pressure distributions inevitably involve many measuring channels each producing a large number of time-wise samples. Data acquisition, processing and the final presentation of results are now planned as an integrated operation. Equipment for these tasks has already been described in Refs 16 and 17.

A data acquisition system known as PRESTO recently commissioned within the RAE, and described in Ref 18, was designed to a functional specification that required the results in non-dimensional form to be available as graphs and tables within a few minutes of initiating the test. For instance, in making measurements with an oscillating model, plots of the chordwise distributions of inphase and inquadrature pressures can be obtained almost immediately after the signals have been sampled. This overcomes problems associated with blind recording and post-experiment analysis of results.

A block diagram of the PRESTO system is shown in Fig 13. In essence  $N$  channels ( $N < 64$ ) are sampled simultaneously  $S$  times a second, and the blocks of data so obtained are stored on disc. At the same time the data can be processed in the required manner, a suite of programs providing great flexibility in application. Depending on the phenomena being investigated, the number of channels  $N$ , can be traded with frequency (which depends on  $S$ ), the main limitation being a maximum value of  $NS$  which for PRESTO is about  $0.25 \times 10^6 \text{ sec}^{-1}$ .

## 11 TUNNEL INTERFERENCE

Interference effects include all the differences between the results obtained in a tunnel and those which would be obtained with the *same model* in a free atmosphere. Various effects are:

- wall constraint on the flow around the model;
- reflection from the wall of pressure disturbances generated by model motion;
- tunnel resonance;
- termination of an unsteady wake by a turning corner of the tunnel, the fan, or a shock wave;
- tunnel turbulence or flow unsteadiness.

Whereas the first of these is familiar in steady testing, the others are more relevant to unsteady conditions. Also, only the first effect is directly relevant to the choice of model size.

### 11.1 Wall constraint effects

Corrections for interference effects on oscillatory measurements can be obtained by theory for some situations<sup>19</sup>, but it is often better to choose a model size for which the effects are small enough to be neglected.

In many instances the perturbation forces for an oscillating model are dependent on the steady flow over the model in its mean position. To obtain oscillatory measurements free from interference requires:

- (1) the mean flow to be free from interference, and
- (2) an absence of interference on the unsteady perturbations about the mean flow.

The first of these requirements can be satisfied by following the recommended practices of steady testing. So also can the second for changes that are quasi-steady, but for oscillatory conditions, consideration has to be given to the possibility of additional interference effects on both the inphase and inquadature components.

For low speed and transonic tests the choice of model size is a matter of judgement based on experience of steady and unsteady testing.

Current practice for three-dimensional transonic tests with oscillating wings tends to choose model spans and planform areas within the following limitations:

$$s/b < 0.4, \quad S/C < 0.15$$

where  $s$  = span and  $S$  = planform area of the model and  
 $b$  = breath,  $C$  = cross section area of the tunnel.

The effectiveness of these criteria is largely confirmed by recent tunnel-to-tunnel comparisons<sup>20</sup>. However, other results<sup>21</sup> suggest that a larger model ( $s/b \sim 0.5$ ,  $S/C \sim 0.25$ ) is acceptable when only a control surface is moving and when the main surface is near to its zero steady lift condition.

Transonic tunnels have walls that are ventilated either by slots or by perforations. The amount of ventilation provided in the design of the tunnel can influence the forces on a model and this becomes more important as the model-to-tunnel size ratio increases. It is possible to assess the correctness of the chosen wall-porosity from general experience of steady lift curve slopes obtained in the tunnel.

### 11.2 Reflections from the tunnel walls

Consider a small model situated centrally in a tunnel. Imagine at time  $t = 0$  the incidence of the model is suddenly changed. A pressure disturbance will travel outward from the model at the local speed of sound,  $a$ . The walls, if they are solid, will reflect the disturbance and eventually, with some attenuation, it will arrive back at the model. For a two-dimensional model the time for a disturbance to return to its point of origin is

$$\delta t = H/a(1 - M^2)^{1/2}$$

where  $M$  is the Mach number of the flow, assumed uniform,  $H$  is the tunnel height and  $a$  the speed of sound.

On this basis, if the initial steady flow were interference-free, the model would continue to be free of any wall-effect until time  $\delta t$  when the reflected disturbance returned. Unfortunately this interference-free time is too short to be of practical use except possibly in a very large tunnel close to  $M = 1$ . The idea of disturbances being reflected back from the walls does however lead into the subject of tunnel resonance.

### 11.3 Tunnel resonance

In theory, tunnel resonance can occur when a train of reflected disturbances from an oscillating model returns with a phase delay that tends either to cancel or to reinforce the pressure changes occurring at the model. For a tunnel with solid walls the lowest frequency, which corresponds to cancellation, is

$$f_r = a(1 - M^2)^{1/2}/2H.$$

Usually the resonance frequency is in the practical range of test frequencies only for transonic conditions, but the occurrence is then complicated by the ventilation at the walls of a transonic tunnel. For ventilated walls, theory predicts a lowest resonance frequency

$$f_r = na(1 - M^2)^{1/2}/H$$

where  $n$  depends on the degree of wall porosity varying between 0.5 for completely closed walls, and 1.0 for completely open boundaries, as for an open jet.

Resonance has been shown to occur under two-dimensional conditions. An early example was given by Runyan, Woolston and Rainey<sup>22</sup> who found a sudden decrease in the oscillatory lift when the oscillation frequency of the model coincided with the calculated tunnel resonance frequency. Resonance effects can be reduced by sound absorbing walls<sup>23,24</sup>. However, it is doubtful whether the phenomenon occurs at all with three-dimensional models.

### 11.4 Wake curtailment

In a free-atmosphere an oscillating model leaves behind a periodic wake. In theory, the flow at the model must be consistent with the distribution of wake vorticity. If, as in a tunnel, the natural wake is destroyed by a corner of the tunnel, a shock wave, or the driving fan, it is reasoned that the unsteady condition at the model will be affected. Theoretical calculations have shown this to be important in certain special cases, but usually the phenomenon is not regarded as important.

## 11.5 Tunnel turbulence

Unless tunnel turbulence is to be exploited as a means of model excitation, it is generally regarded as a nuisance not only because it can interfere with the aerodynamic measurements but also because it causes model vibration and consequently reduces fatigue life. Furthermore, its presence necessitates a longer sampling time in making the measurements, which in turn extends the time the model is exposed to vibratory conditions.

When the local flow at the model produces random-like disturbances as in buffeting, which themselves are the subject of the measurements, the presence of tunnel turbulence can only lead to difficulties in interpreting the results. On the other hand, in experiments where the input is deterministic and the effects of tunnel turbulence are linearly superposed on the response to the input, the required separation can be achieved by signal processing as already mentioned. If non-linearities between input and response are present, the effect of extraneous fluctuations can be more serious and an example will be discussed later in section 13.

Transonic tunnels, particularly those with perforated walls provide most of the examples of flow unsteadiness. In one case an improvement was obtained by covering the perforated walls with gauze<sup>23</sup>. More generally, the use of sound absorbing material at the tunnel walls has been shown to be beneficial<sup>23,24</sup>.

## 12 MATTERS FOR DISCUSSION

Previous sections have outlined the measuring techniques common to many experiments. Even after the objectives of an experiment have been settled, there is still the job of finding the most suitable course of action amongst the several possibilities. Much depends on equipment and funds to hand, and also on the expertise and experience that is available. Remarks on some questions that frequently arise now follow.

### 12.1 Half-model or complete span model

The two main advantages of a half-model mounted at the wall of the tunnel are the higher Reynolds number and the ability to have direct access to the root of the model. In unsteady experiments the second of these is the more important. Compared with sting-mounting, wall-mounting provides the root of the model with a firm attachment, and any motion-producing mechanism or measuring devices can be conveniently accommodated at the tunnel wall but outside the working section.

The disadvantages of a half-model stem from the presence of the tunnel wall boundary layer and the need for a root gap and some kind of seal if the model is to move relative to the wall. In cases where the aerodynamic forces on a fuselage are important, or where the wings are of low aspect ratio or highly swept, the half model is not appropriate. For the measurement of derivatives due to lateral motion it is obviously necessary to use a tip-to-tip model centrally mounted in the tunnel.

### 12.2 Boundary layer transition

At the low Reynolds numbers obtaining in model experiments the boundary layer remains laminar over much more of the chord than for the full-scale aeroplane. This may lead to unrepresentative flow separations or shock-wave boundary-layer interactions. Also if, because of the low Reynolds number, transition is delayed until mid-chord or beyond, the transition point could undergo much larger backwards and forwards movements as the model oscillates and this could lead to a spurious set of additional aerodynamic forces.

These considerations provide the reasons for fixing transition, usually by a band of roughness attached close to the leading edge of the model. However, the turbulent boundary layer so formed is usually much thicker than it should be for full-scale similarity. This is particularly serious for trailing-edge controls.

As described in Ref 26 pressure measurements for an oscillating control surface have been made with the model shown in Fig 14. The measured chordwise distributions of pressure amplitude and phase are shown in Fig 15 for two Mach numbers,  $M = 0.8$  and  $M = 0.9$ . For each Mach number, measurements are shown for free transition and for transition fixed by a roughness band at  $0.05c$ . For  $M = 0.8$ , fixing transition causes a reduction in the oscillatory lift and this is attributed to an increase in the thickness of the boundary layer as a consequence of the forward position of transition. At  $M = 0.9$  a shock wave is present in the vicinity of  $0.3c$ . The oscillatory motion of the shock causes the large oscillatory pressures measured downstream of this position where there are substantial differences between the results for transition-free and transition-fixed. It is considered that these differences in the form of the pressure distribution are not solely due to a change in the thickness of the boundary layer, but rather to the shock wave interaction with the laminar layer being different in character to its interaction with the turbulent layer.

Following the advice of Ref 27, it is probably best not to fix transition when working with control surfaces unless a surface shock wave is present. Then the requirement is to ensure, by locally added roughness or other means, that no unrepresentative shock-induced separation occurs.



### 12.3 The problem of model flexibility

The aim in many experiments, particularly those directed to measuring unsteady aerodynamic pressures for comparison with theoretical calculations, is to impose an oscillatory motion on a *rigid* model. For full-scale similarity appropriate values of frequency parameter will need to be reached. It is then often difficult to attain the specified working frequency whilst maintaining adequate rigidity in the model under dynamic conditions. This is another example of the problem illustrated by Fig 5. For a model to remain rigid under dynamic conditions, its stiffness should be high and all its natural frequencies well removed from, and preferably much higher than, the working frequency.

The model must therefore be designed and constructed not only to have a high stiffness, but also a high ratio of stiffness to mass. Since the latter is also an aim of full-scale design, it is soon obvious that when high rigidity is demanded at representative values of frequency parameter, the model designer is really being asked to do better than the aircraft designer. To be successful he will need to exploit new or unconventional materials and structural forms.

The idea of a rigid model undergoing oscillation in a simple mode makes for easy comparison with theory; but such motion is not representative of aircraft. Rather than strive for rigidity it may be better to accept that every model will be flexible when subjected to high frequency oscillation and to plan to make the measurements for motion in an elastic normal mode. Although the mode may not remain the same under wind-on conditions, it could be measured with sufficient accelerometers. The results will then be in the form of *measured* oscillatory pressures for a *measured* mode of distortion. Unfortunately the latter may consist of coupled motions included phase changes across the wing.

### 12.4 The choice between measuring forces or measuring pressures

Of the various forces acting during an oscillation, the aerodynamic force will usually be only a small proportion of the inertial force due to the model mass. Almost always an unsteady aerodynamic force is obtained as the difference between two measurements, one wind-on and the other wind-off. For the difference to accurately represent the aerodynamic force it is necessary for the motion of the model, including any elastic distortion to be the same for the two measurements; if not an additional inertial force will appear as a spurious aerodynamic force. Such changes in the mode of motion can be caused by the oscillatory aerodynamic forces if the model is less than rigid under dynamic conditions.

From this it should be clear that whilst the measurement of unsteady aerodynamic forces may not be too difficult at low frequencies, the extraction of the aerodynamic force from the inertial contributions becomes more difficult with increase of frequency. Although in principle the actual model motion could be sensed by accelerometers and appropriate inertial corrections deduced, or analogue signal cancellation arranged, it is likely to end up in a complicated and unsatisfactory procedure.

For high frequencies the measurement of pressures is more reliable. The main disadvantages are: (1) the construction of the model will be more complicated; (2) the model is likely to be more flexible because of the installation of transducers; and (3) a large number of measuring channels will be necessary to obtain pressure distributions in sufficient detail to establish the total forces acting on a model.

Measurement of the aerodynamic forces on rigid components, such as wing stores, even for high frequencies is, however, satisfactory. Unsteady *pressures* on the main lifting surface and unsteady *forces* on rigid control surfaces or stores may offer the best solution.

For some purposes there is no choice. The determination of the stability derivatives for a complete model by pressure measurements is unthinkable. It is fortunate that these measurements can be made at low frequencies.

## 13 NONLINEARITIES

The problems of unsteady aerodynamics are usually concerned with small perturbations, the effects of changes of shape, displacement or relative velocity. It is usually assumed that the perturbation forces and pressures are linear with the quantity that is changing and indeed, some of the experimental techniques are based on this assumption. Whereas overall forces tend to remain linear, the same is not always true for local pressures. Nonlinear features are often associated with vortices, shock waves or flow separation. In experiments in which a sinusoidal motion is applied to the model, nonlinearities, if present, will appear as higher-order harmonic components in the measured pressures.

The subject of the first example, taken from Ref 28 and shown in Fig 16, is a model of a slender delta wing at sufficient incidence to generate leading-edge vortices above its upper surface. The model is oscillating in a mode of longitudinal deformation and this causes the strength and spanwise position of the two vortices to oscillate, thus affecting the pressure distribution at the upper surface. Although the motions of the model and the vortices are sinusoidal, it is obvious that a point over which the suction peak oscillates will experience a minimum pressure twice during each cycle of the

oscillation. Thus the oscillation in the position of the suction peaks leads to additional harmonic components one of which is shown in the diagram.

The second example is the pressure variation in the vicinity of a shock wave at the upper surface of a wing which is undergoing a pitching oscillation<sup>29</sup>. An approximation to the actual behaviour is suggested by Fig 17 where the distribution of surface pressure is represented by three straight lines which oscillate because the shock responds to the wing motion and which are shown in their extreme and mean positions. The diagram illustrates how the time-histories of the pressures at some positions are non-sinusoidal. In an actual experiment measurement of the amplitudes of the first two harmonic components produced the following results:

x/c	Fundamental A1	Second harmonic A2	A2/A1
0.05	42 units	0 units	0
0.2	32	1	0.03
0.3	80	15	0.19
0.4	165	17	0.10
0.5	29	7	0.24
0.6	30	0	0

In the actual experiment, the deep troughs shown for position B in Fig 17 did not occur regularly. As shown in Fig 18, the waveform obtained at 0.3 chord seems to consist of a sinusoid which for some cycles has its trough drawn down into a steep valley corresponding to a large increase of pressure. This is due to extraneous fluctuations causing for different cycles a greater or lesser movement of the shock, so that for only some cycles does the shock reach the 0.3C position.

This is an example where, because of nonlinearity, the extraneous fluctuations or noise affect quantities that are measured as averages over a period of time. If *none* of the cycles during the measuring time experienced the shock, the average pressure amplitude would be smaller than if *every* cycle experienced the shock. A sample of mixed cycles would have an average amplitude between those two extremes. Thus, if the fluctuations were absent there would be a sharp distinction between the pressure amplitudes for those positions that do, and those that do not, experience the passage of the shock. In other words, the chordwise distributions of the oscillatory pressure distributions tend to be 'blurred' by the noise.

Fig 19 shows a simple illustration of the effect amplitude can have on the normalised pressure due to an oscillating shock wave.

#### 14 SPECIFIC INVESTIGATIONS

The previous sections have dealt with general techniques applicable to many different forms of experiment. The following sections describe certain procedures and test rigs currently in use for specific investigations. Each of the first two subjects, buffeting experiments and flutter testing, embraces a complete aeronautical phenomenon and some account is taken of the interactions between the aerodynamics and the aero-elastic and dynamic properties of the structure. The other subjects, stability derivatives, the aerodynamics of flutter and control surface motions, and the dynamic stalling of helicopter blades are concerned only with the measurement of aerodynamic forces or pressures for prescribed unsteady conditions.

#### 15 WING BUFFETING

Wing buffeting is usually associated with high incidences. It is the vibratory response of the structure to unsteady aerodynamic forces caused by flow separation.

The subject is very well exposed by recent literature and only a brief description will be given here. For general accounts the following should be consulted: John<sup>30</sup>, Butkewicz<sup>31</sup>, Mabe<sup>32</sup>.

Experiments with models in wind tunnels are almost invariably related to the design of new prototypes and are usually separately directed to:

Buffet onset - to determine the flight conditions at which buffet will first occur.

Buffet intensity - to predict the response of the aircraft after penetrating the buffet boundary (important in respect of structural fatigue, weapon aiming, pilot comfort).

##### 15.1 Buffet onset tests

Of the two types of experiment, this is by far the easiest, tests often being made with the kind of model normally used for steady tests. A popular method is to observe the output of strain-gauges attached near the wing root and as incidence is increased, to

note the point at which there is a sudden increase in the intensity of the unsteady strains. More accurate predictions can be obtained when the model has the correct (that is distorted) shape of the full-scale wing under the appropriate high-lift conditions.

## 15.2 Experiments to predict buffet intensity

Possible procedures are:

Measuring the response of a dynamically similar aeroelastic model, and deducing the response for the aeroplane by direct scaling. (Recommended reading: Hanson, Ref 33.)

Using a flexible (but not dynamically similar) model to measure buffet excitation and aerodynamic damping and, from these and estimates of the aeroplane structural damping, calculating the response of the aeroplane. (Recommended reading: Butler and Spavins, Ref 34.)

Measuring the buffet pressures on a rigid model, to obtain spectral content and spacial correlation, and from the results calculating the response of the aeroplane. (Recommended reading: Hwang, Ref 35.)

The Butler and Spavins technique is particularly interesting since two unsteady aerodynamic quantities, buffet excitation and model damping are determined by statistical means from one and the same signal representing model vibration. The underlying assumptions are that the buffet excitation is random and the model has only a single degree of freedom (although in principle the method could be extended to multi-freedom systems). Damping is obtained either from the width of the peak in the power spectrum of the response, or from the decay rate in the autocorrelation function or by the more recently developed Randomec method<sup>36</sup>. Once damping has been determined the excitation is obtained from the rms response.

## 16 FLUTTER TESTING

The aim is to determine the flutter characteristics of a model by exposing it to flow conditions of increasing severity. Flutter models vary from the simple plate-like structures used in research to the extremely elaborate and costly aeroelastic models of full scale aircraft such as that described in Ref 37. Similarity requirements are discussed in Ref 38. For tests in low-speed flow it is usual to increase stream velocity until flutter is imminent; for high-speed tests it is more usual to increase tunnel total pressure at constant Mach number. In some experiments, usually with the less costly models, an actual fluttering condition will be reached. In others, usually with the more costly models, the intention is not to reach the flutter condition but to predict the flutter boundary from a series of response measurements made with increasing flow severity.

Possible forms of the variation of frequency and damping for the modes of a system having two degrees of freedom are shown in Fig 20. The modal frequencies and damping can be obtained by analysis of the response of the model to some form of excitation applied either mechanically, or by tunnel turbulence<sup>39,40</sup>. In principle the excitation and analysis techniques for determining the flutter subcritical response of a model are similar to those used in flight flutter testing, for which the recommended reading is van Nunen and Piazzoli<sup>41</sup>.

Current problems requiring the flutter testing of aeroelastic models are mainly concerned with the effects of transonic conditions or the effects of stores added to the wings. Flutter tests are usually coupled with complementary theoretical predictions which are made both for the aeroplane and for the model since the two systems may not be exactly similar. Comparison between the results of the flutter test and theoretical prediction can sometimes throw light on the values of important unsteady aerodynamic quantities, but the relationship between an aerodynamic quantity and the flutter behaviour is not usually direct. Although the aerodynamic quantities would be obtained more directly by measurements of aerodynamic forces or pressures for imposed oscillatory motions, the flutter test has the ability to embrace the whole structural problem and to include complicated aerodynamic configurations.

## 17 MEASUREMENT OF STABILITY DERIVATIVES

An appreciation of the wide variety of rigs used in wind tunnels for the measurement of derivatives may be obtained from the review of Orlik Rückemann<sup>42</sup>. Also information on the basic principles may be obtained from an older account given by Bratt<sup>43</sup>.

By drawing on the descriptions of Fail<sup>44</sup>, brief mention is now made of two rigs illustrating different approaches to the problem.

### 17.1 A response-measuring multifreedom rig at RAE Bedford

This rig is suitable for tunnels up to 4 m wide and in the form described, is arranged to measure lateral derivatives, but the same principle could be adapted to the measurement of longitudinal derivatives. The rig provides the model with three degrees of freedom, the procedure being to apply a known oscillatory excitation force, to measure the responses in each of the three coordinates  $\psi$  yaw,  $y$  side slip and  $\phi$  roll and from these measurements, by using the equations of motion of the system, to determine the set of derivatives. Fig 21 shows the essential features of the sting supporting the

model. The two spring units provide the model with the three freedoms. The natural frequencies are about 4, 5 and 6 Hz and the normal modes are:

- yawing about an axis near the CG of the model;
- sideslipping mainly, but with some yawing about a far-forward axis;
- rolling.

An electromagnetic vibrator at the rear of the sting, not shown in the diagram, provides a known excitation force in each coordinate and the system is oscillated at, or near, each natural frequency in turn. Working near resonance means a reasonable amplitude can be obtained with a small exciter. The system when oscillating at frequency  $\omega$  is governed by three equations of motion relating to yawing moment  $N$ , side force  $Y$  and rolling moment  $L$ :

$$(\omega^2 I_{11} + i\omega N_{\dot{\psi}} + N_{\psi})\psi + (\omega^2 I_{12} + i\omega N_{\dot{y}} + N_y)y + (\omega^2 I_{13} + i\omega N_{\dot{\phi}} + N_{\phi})\phi + N_e = 0$$

$$(\omega^2 I_{21} + i\omega Y_{\dot{\psi}} + Y_{\psi})\psi + (\omega^2 I_{22} + i\omega Y_{\dot{y}} + Y_y)y + (\omega^2 I_{23} + i\omega Y_{\dot{\phi}} + Y_{\phi})\phi + Y_e = 0$$

$$(\omega^2 I_{31} + i\omega L_{\dot{\psi}} + L_{\psi})\psi + (\omega^2 I_{32} + i\omega L_{\dot{y}} + L_y)y + (\omega^2 I_{33} + i\omega L_{\dot{\phi}} + L_{\phi})\phi + L_e = 0$$

where the  $I$ s are inertial constants, the derivative coefficients,  $N_{\dot{\psi}}$ ,  $N_{\dot{y}}$ , etc include aerodynamic and mechanical contributions, and  $N_e$ ,  $Y_e$  and  $L_e$  are the excitation forces.

The complex amplitudes of the coordinates are obtained from strain gauges attached to the sting. The amplitudes are measured at each of the three oscillation frequencies yielding a total of nine complex equations which, with knowledge of the nine inertial constants, are sufficient to solve for the 18 unknown coefficients. The measurement procedure is carried out twice - once wind-on and once wind-off, so that the aerodynamic derivatives are obtained as differences. The reduction process depends on two assumptions: (1) that the derivatives are independent of frequency (justified by the low frequencies); and (2) that the model rigidity is sufficient for the mechanical properties of the system to be unaffected by the change in air loads between wind-off and wind-on.

The extraction of the derivatives requires that the equations be taken six at a time. Thus, for example, the single equation for yawing moment taken for each of three frequencies, and after separating inphase and inquadrature contributions, yields six equations from which the yawing moment derivatives can be obtained.

The accuracy of the results depends on a careful choice of system properties, on the determination of the inertial constants and on the calibration of the strain gauge units that are used to measure the displacements.

#### 17.2 A two-freedom force-measuring rig at Cornell Aeronautical Laboratory

This rig which is fully described in Ref 45, measures longitudinal derivatives. The main point of interest is that instead of applying force and measuring motion, as in the previous example, it operates by applying a known motion and measuring the forces.

The rig is designed for use in a 2.5 x 2.5 m transonic wind tunnel. The model can be oscillated at frequencies between 3 and 12 Hz with vertical amplitudes up to  $\pm 0.15$  m and pitching amplitudes up to  $\pm 5^\circ$ . The mechanical system is shown diagrammatically in Fig 22. The required motion, consisting of a combination of pitching  $\theta$  and heaving  $z$ , is obtained by adjusting the eccentric amplitudes and the phase angle between the flywheels. These adjustments are made by means of small hydraulic motors whilst the rig is oscillating. The forces and moments on the model are measured by a conventional strain gauge balance incorporated in the sting supporting the model. Instead of obtaining the aerodynamic contributions by differencing the readings obtained wind-on and wind-off, the inertial reactions appearing in the balance signals are cancelled by accelerometer signals. Indeed, any proportion of any signal can be added to any other signal so that all component interactions are eliminated. The compensated signals are finally analysed to give amplitude and phase referred to a reference signal obtained from the driving system.

The ability to provide a combination of two motions has interesting possibilities for reproducing certain basic types of motion of relevance to flight and measuring certain derivatives directly as illustrated in Fig 23.

#### 17.3 Comparison between response- and force-measurement rigs

An advantage of applying inexorable motion is the ability to control an unstable, or negatively damped, model. Also the model can be oscillated in a chosen motion and at any frequency and it is probably easier to detect and measure forces that are nonlinear. The principal disadvantage is the large excitation force that is needed and the massive construction that accompanies it.

The advantage of a response-measuring rig is that by working near resonance the exciter can be quite small and much more easily accommodated.

Both techniques have to solve the problem of separating the aerodynamic forces from the large inertial forces and resolving the aerodynamic forces into the various component derivatives but the methods of doing this are different in the two cases.

## 18 MEASUREMENT OF AERODYNAMIC RESPONSE TO CONTROLS

The unsteady aerodynamics of control surfaces are of interest in flutter calculations, but at the present time, the subject is of special interest to Active Control Technology.

A balance to measure the principal wing forces due to control surface motion is shown in Figs 24 and 25 and fully described in Ref 46. It supports a half-model at the wall of a tunnel, and an oscillatory motion can be imposed on the control surface by a vibrator connected to it through a push rod and shaft. The frame to which the model is attached is supported at three locations by strain gauge elements which measure the unsteady reactions. These, together with the measured excitation force, when operated upon by a set of dynamic calibration factors yield the oscillatory inphase and inquadrature components of lift, pitching moment and rolling moment. Hinge moment components are determined by a torque-measuring unit incorporated in the shaft driving the control surface (Fig 25).

The balance is suitable for tests in tunnels with working section areas up to about  $1 \text{ m}^2$ . It has operated satisfactorily at frequencies up to about 100 Hz using low aspect ratio models of rigid construction. Attempts to use the balance with a model of aspect-ratio 6 clearly showed the difficulty of measuring unsteady forces on a model not having sufficient rigidity.

The high aspect ratio model, already seen in Fig 14, is an example where the advantage lies with unsteady pressure, rather than force, measurements. For this model chord-wise distribution of oscillatory pressure have been measured at four sections as shown in the diagram and some results as described in Ref 26.

## 19 PITCH AND HEAVE RIG

This is a rig in use at the Aircraft Research Association, Bedford for tests on two-dimensional aerofoils in a transonic tunnel<sup>47</sup>.

In most other experimental arrangements the motion applied to the model is harmonic and of small amplitude. Linearity is often assumed. However, in this final example large amplitudes can be applied and the motion need not always be harmonic.

The rig was designed to test new aerofoil sections under the kind of dynamic conditions experienced by a section of a helicopter blade in forward flight. Whilst not attempting to reproduce the time-wise variation of Mach number, the rig can apply various combinations of harmonic heaving and pitching, or arbitrary time-wise changes of incidence. Its main use is in examining the dynamic stalling properties of newly designed sections.

The principles of the rig are shown in Figs 26 and 27. The constituent motions are supplied by separate components, the heave motor and the pitch hydraulic ram. The aerofoil is mounted eccentrically in large discs arranged to be flush with the side walls of the tunnel. When the discs are rotated by the heave motor, the aerofoil orbits about a transverse axis: but unless the pitch ram alters the length of the lowest link, the pitch angle of the aerofoil remains constant throughout. The motion of the aerofoil is then a combination of vertical translation and horizontal translation, but the latter is small and is not intended to simulate the variations in forward speed that are experienced by the helicopter blade.

Pitching motion is obtained by alteration of the length of the lowest link by operation of the hydraulic ram. This causes a rotation of the lower diamond-shaped component, which motion is transferred by push-rods to the upper diamond to which the model is attached. The ram can be phase-linked with the heave motion or driven independently. Pitch amplitudes up to  $\pm 20^\circ$  and pitch rates up to  $1300^\circ/\text{s}$  can be obtained with this equipment. The chord of the test aerofoils are usually 100 mm and the maximum frequencies are 20 Hz for heaving and 100 Hz for pitching.

Unsteady pressure distributions are measured by a number (usually up to 34) Kulite transducers installed within the aerofoil, and lift and pitching moment are obtained by integration of the pressures. The rig is complemented by a data acquisition system<sup>48</sup>, which is also used to programme and control the test runs.

Fig 28 shows an example of data obtained during a ramp change of pitch, in which incidence  $\alpha$  was increased from zero to about  $20^\circ$ . Separation occurs when the incidence reaches about  $15^\circ$ ; the time histories of the pressures show the progression across the chord. Also it can be seen that the break in the pitching moment precedes the break in the lift.

## 20 EPILOGUE

The previous sections have outlined methods of measurement and described specific experimental procedures.

When experimental results are to be used either for comparison with theory, or directly in design, it is necessary to make some assessment of their accuracy. This is dependent on:

- (1) the accuracy of the experimental representation, including such items as the adequacy of the model, the effects of wind tunnel interference and scale effects;
- (2) the precision of the measurements, which itself is dependent on the instrumentation and its calibration.

The first is usually difficult, if not impossible, to quantify and requires judgement in the particular circumstances. It is easier to attach a value to the second, although again, this depends on circumstances. To give an example, it is probably true for oscillatory pressures that amplitudes can be measured to an accuracy of a few percent and phase angles to a few degrees.

Sometimes experiments show large differences in comparison with available theory, clearly indicating that theory must be improved. In the meantime whilst the improvements are awaited, it may be difficult to apply the experimental results directly to the design problem. An example of this is contained in Ref 29 which shows the difficulty of trying to predict the effects of supercritical flow on wing flutter solely from measurements of pressure for one simple mode of wing motion.

Current experimental interests relate to one or more of the following items:

- transonic flow, and the flutter of supercritical wings;
- high incidence conditions for wings with some areas of separated or vortex flow;
- control devices in relation to ACT.

Looking into the future, it would seem that, apart from the measurement of stability derivatives, the trend in unsteady experiments will continue to be towards the measurement of pressures and not forces. It is easy to enthuse over the prospects for greater sophistication, including the measurement of pressure distributions for complicated modes of flexible distortion, faster and more efficient data processing and possibly computer-based interaction between experiment and theory. But measurements need to be justified; they are not an end in themselves but a means to improve the design of aircraft. Experimental work will continue only whilst the exploration of phenomena or the provision of measured data is seen to lead to better aircraft.

#### Acknowledgment

The help of various persons in supplying specialized information is gratefully acknowledged.

#### REFERENCES

No.	Author	Title, etc
1	N.C. Lambourne	Similarity requirements for flutter and other aeroelastic models in a cryogenic wind tunnel. RAE Technical Memorandum Structures 888 (1976)
2	W. Charon, R. Verbrugge	Nouvelle technique d'essais sur maquettes libres en laboratoire pour la détermination de caractéristiques aérodynamiques. AGARD CP 235 (1978)
3	M.H. Patel G.J. Hancock	A gust tunnel facility. ARC R & M No.3802 (1976)
4	R.A. Sawyer	Design and operation of a low-speed gust tunnel. AGARD-CP-174 (1975)
5	B. Krag	Gust-vehicle parameter identification by dynamic simulation in wind tunnels. AGARD CP 235 (1978)
6	C.F. Reid C.G. Wrestler	An investigation of a device to oscillate a wind tunnel airstream. NASA TN D-739 (1961)
7	J. Gilman R.M. Bennett	A wind tunnel technique for measuring frequency response functions for gust load analysis. AIAA Paper 65-787 (1965)
8	J.H. Horlock	An unsteady flow wind tunnel. <i>Aero Quarterly</i> , Vol.25, pp 81-90, May 1974
9	G.K. Hunt D.R. Roberts D. Walker	Measurements of transient pressures on a narrow delta wing due to an upward gust. ARC CP 624 (1961)

## REFERENCES (continued)

- | No. | Author  | Title, etc   |
|-----|---|--|
| 10  | B.L. Welsh  | A new angular displacement transducer.<br>RAE Technical Report 79026 (1979)  |
| 11  | H. Bergh<br>H. Tijdeman                                     | Theoretical and experimental results for the dynamic response of pressure measuring systems.<br>NLR-TR-F238 (1965)   |
| 12  | H. Tijdeman<br>H. Bergh                                     | The influence of the main flow on the transfer function of tube transducer systems used for unsteady pressure measurements.<br>NLR MP 72023U (1972)                                      |
| 13  | B.L. Welsh<br>C.R. Pyne                                     | A method to improve the temperature stability of semiconductor strain gauge pressure transducers.<br>RAE Technical Report 77155 (1977)   |
| 14  | J.S. Bendat<br>A.G. Piersol                                 | <i>Random Data: Analysis and measurement procedures.</i><br>Textbook. John Wiley (1971)  |
| 15  | K.G. Beauchamp  | <i>Signal Processing.</i><br>Textbook. George Allen & Unwin (1973)   |
| 16  | G.N. Malcolm<br>S.S. Davis                                  | New NASA-Ames wind tunnel techniques for studying airplane spin and two-dimensional unsteady aerodynamics.<br>AGARD CP 235 (1978)  |
| 17  | P.H. Fuijkschot   | Pharos, processor for harmonic analysis of the response of oscillating surfaces.<br>NLR MP 77012U (1977)   |
| 18  | B.L. Welsh<br>D.M. McOwat                                   | PRESTO - a system for the measurement and analysis of time-dependent signals.<br>RAE Technical Report 79135 (1979)   |
| 19  | W.E.A. Acum   | Interference effects in unsteady experiments.<br>Chapter IV AGARDograph 109, Subsonic wind tunnel wall corrections (1966)  |
| 20  | N.C. Lambourne<br>R. Destuynder<br>K. Kienaappel<br>R. Roos | Comparative measurements in four European wind tunnels of the unsteady pressures on an oscillative model (the NORA experiments).<br>AGARD Report (to be published)                       |
| 21  | N.C. Lambourne<br>K.C. Wight<br>B.L. Welsh                  | Measurements of control-surface oscillatory derivatives on a sweptback, tapered model wing in two transonic tunnels.<br>ARC R & M No.3806 (1977)   |
| 22  | H.L. Runyan<br>D.S. Woolston<br>A.G. Rainey                 | Theoretical and experimental investigation of the effect of tunnel walls on the forces acting on an oscillating airfoil in two-dimensional compressible flow.<br>NACA Report 1262 (1956) |
| 23  | D.G. Mabey  | The use of sound-absorbing walls to reduce dynamic interference in wind tunnels.<br>RAE Technical Report 76157, ARC R & M No.3831 (1976)   |
| 24  | D.G. Mabey  | The reduction of dynamic interference by sound absorbing walls in the RAE 3ft wind tunnel.<br>RAE Technical Report 77120, ARC R & M No.3837 (1977)                                       |
| 25  | X. Vaucheret  | Influence du niveau de bruit des souffleries transsoniques sur les caractéristiques aérodynamiques des maquettes.<br>AGARD CP 227 (1977)   |
| 26  | D.G. Mabey<br>D.M. McOwat<br>B.L. Welsh                     | Aerodynamic characteristics of moving trailing-edge controls at subsonic and transonic speeds.<br>AGARD CP 262 (1979)  |
| 27  | A.W. Moore  | Scale effects on oscillatory control-surface derivatives.<br>ARC CP 1151 (1969)  |
| 28  | N.C. Lambourne<br>D.W. Bryer<br>J.F.M. Maybrey              | Pressure measurements on a model delta wing undergoing oscillatory deformation.<br>ARC R & M No.3693 (1972)  |

REFERENCES (concluded)		
No.	Author	Title, etc
29	N.C. Lambourne B.L. Welsh	Pressure measurements on a wing oscillating in super-critical flow. RAE Technical Report 79074 (1979)
30	H. John	Critical review of methods to predict the buffet capability of aircraft. AGARD-R-623 (1974)
31	P.J. Butkewicz	Buffet analysis. Chapter 8 AGARD Advisory Report No.82 (1975)
32	D.G. Mabey	Limitations in the correlation of flight/tunnel buffeting tests. Chapter 10 AGARD Advisory Report No.82 (1975)
33	P.W. Hanson	Structural and aerodynamic quantities of the dynamic system, similarity laws, and model testing. Chapter 4.2, AGARD Advisory Report No.82 (1975)
34	G.F. Butler G.R. Spavins	Preliminary evaluation of a technique for predicting buffet loads in flight from wind-tunnel measurements on models of conventional construction. RAE Technical Memorandum Aero 1698 AGARD CP 204 (1976)
35	C. Hwang	Response analysis for random excitation. Chapter 4.3, AGARD Advisory Report No.82 (1975)
36	H.A. Cole Jr	On-line failure detection and damping measurement of aerospace structures by random decrement signatures. NASA CR 2205 (1973)
37	P. Esch T. Windeck	Design and construction of the Alpha jet flutter model. AGARD CP 174 (1975)
38	C. Scruton N.C. Lambourne also N.C. Lambourne C. Scruton	Similarity requirements for flutter model testing. Chapter 6 Part IV, Manual on Aeroelasticity, AGARD (1960)  On flutter testing in high-speed wind tunnels. ARC R & M No.3054 (1956)
39	D.R. Gaukroger K.H. Heron C.W. Skingle	On the processing of response data to obtain modal frequencies and damping ratios. <i>J. Sound &amp; Vibration</i> , 35(4), 559-571 (1974)
40	K.W. Newman C.W. Skingle D.R. Gaukroger	The development of rapid-testing techniques for flutter experiments. R & M ARC CP 1274 (1974)
41	J.W.G. van Nunen G. Piazzoli	Aeroelastic flight test techniques and instrumentation. AGARD Flight Test Instrumentation Series, Vol 9, AGARDograph No.160 (1979)
42	K.J. Orlik-Rückeffmann	Techniques for dynamic stability testing in wind tunnels. AGARD CP 235 (1978)
43	J.B. Bratt	Wind tunnel techniques for the measurement of oscillatory derivatives. Chapter 5, Part IV, Manual on Aeroelasticity, AGARD (1961), ARC R & M 3319
44	R. Fail	Experimental determination of stability and control aerodynamic characteristic. VIK Lecture Series 80, Aircraft Stability and Control (1979)
45	I.C. Statler O.B. Tufts W.J. Hirtreiter	A new capability for measuring dynamic air loads in a wind tunnel. <i>J. Aircraft</i> , Vol.3, No.5 (1966)
46	K.C. Wight N.C. Lambourne	A control-surface oscillatory derivative rig for use with half-models in high-speed wind tunnels. ARC CP 1353 (1976)
47	R.H. Landon	A description of the ARA two-dimensional pitch and heave rig and some results from the NACA 0012 wing. Aircraft Research Association Memo 199 (1977)
48	A. Pendleton	A high-speed data acquisition system for oscillatory aerodynamic studies. Aircraft Research Association Memo 198 (1977)



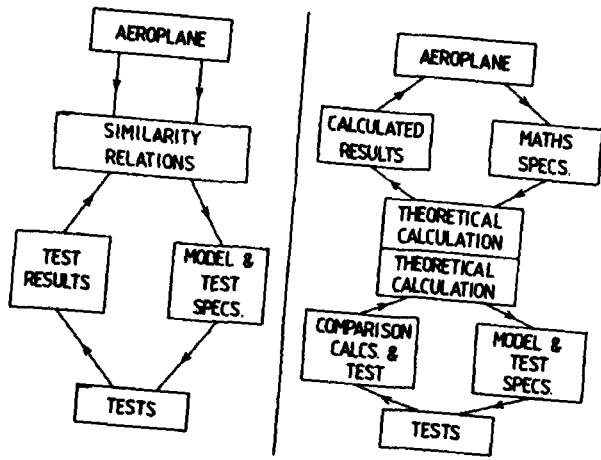


Fig 1 Role of model testing

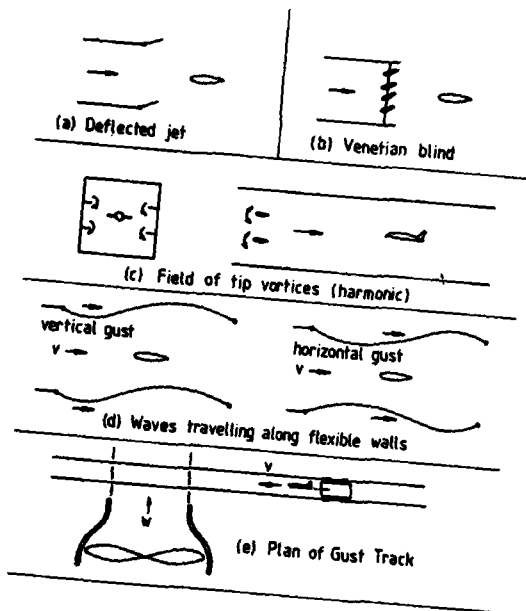


Fig 2 Gust facilities (schematic)

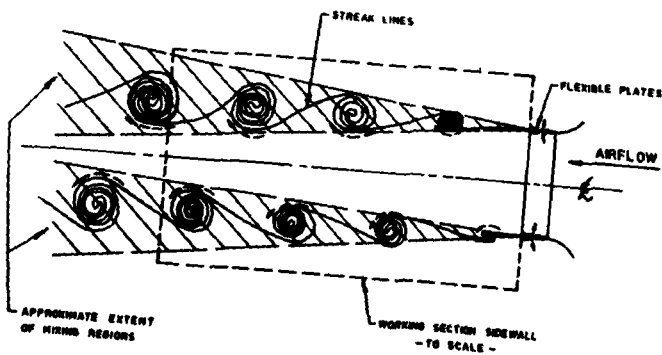
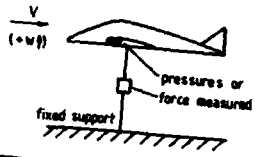
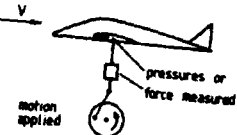


Fig 3 Sketch of flow field for high frequency nozzle oscillation in QMC gust tunnel (from Ref 3)

Rigid Model  
Buffet  
Gust aerodynamics



Rigid Model  
Stability derivatives  
Flutter aerodynamics

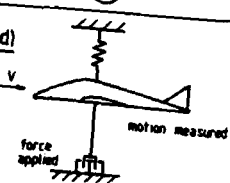


Rigid Model (spring supported)

Stability derivatives

Aeroelastic Model

Flutter subcritical response



Aeroelastic Model

Buffet  
Flutter

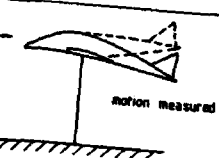


Fig 4 Some experimental systems

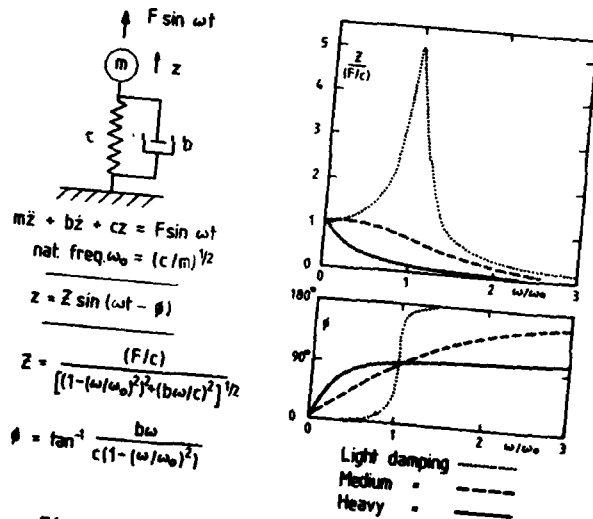


Fig 5 Dynamic response of system with one degree of freedom

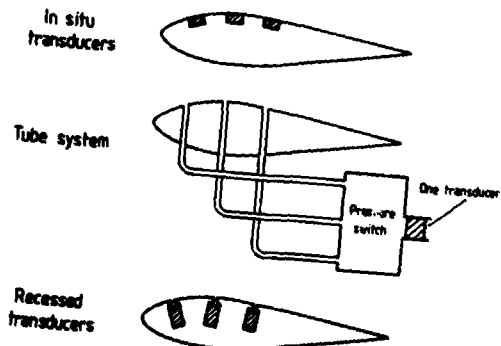
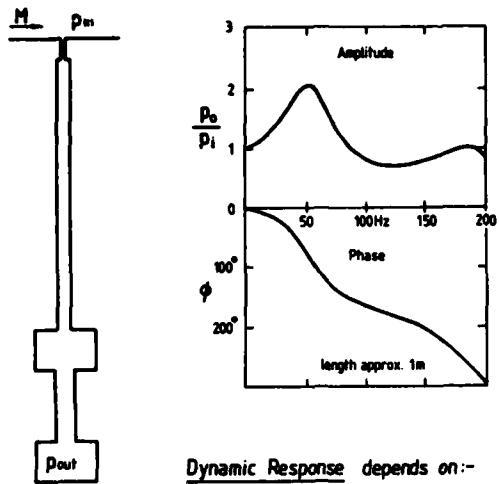


Fig 6 Methods of unsteady pressure measurement



Dynamic Response depends on:-  
 Tube length, diameter, volumes.  
 Air density, temperature.  
 Tangential flow Mach number.

Fig 7 Dynamic response of a long tube for small amplitudes

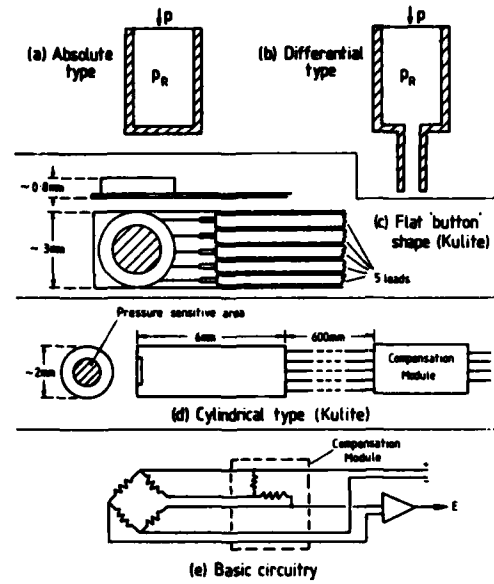


Fig 9 Pressure transducers

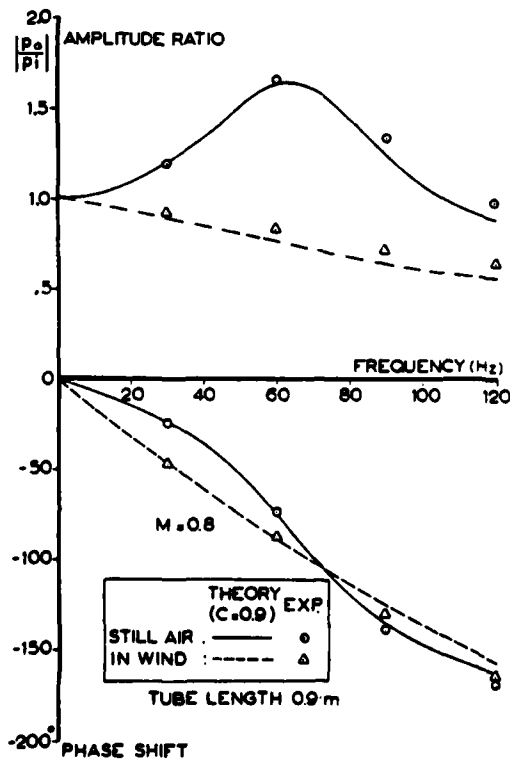


Fig 8 Effect of flow on transfer function of tube (from Ref 12)

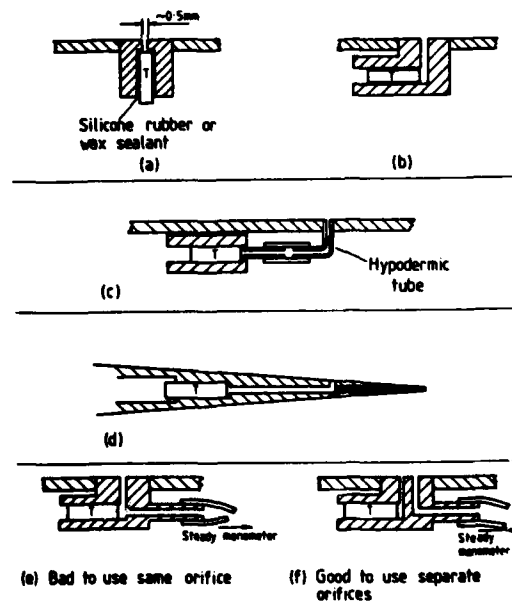
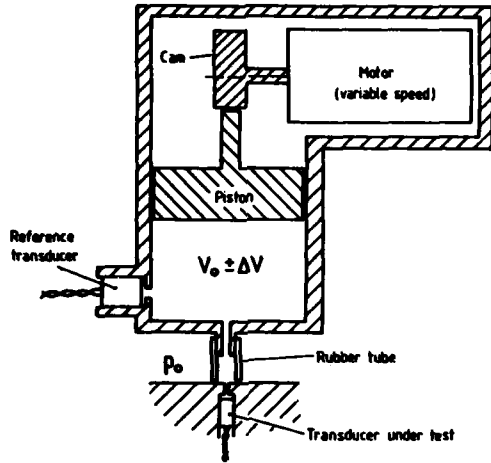


Fig 10 Installation of pressure transducers in model



Oscillatory pressure =  $\Delta p \sin \omega t$   
 $\Delta p \approx \frac{P_0 \Delta V}{V_0} \times \begin{pmatrix} 1.0 & \text{for isothermal} \\ 1.4 & \text{for adiabatic} \end{pmatrix}$

Fig 11 Oscillatory pressure generator

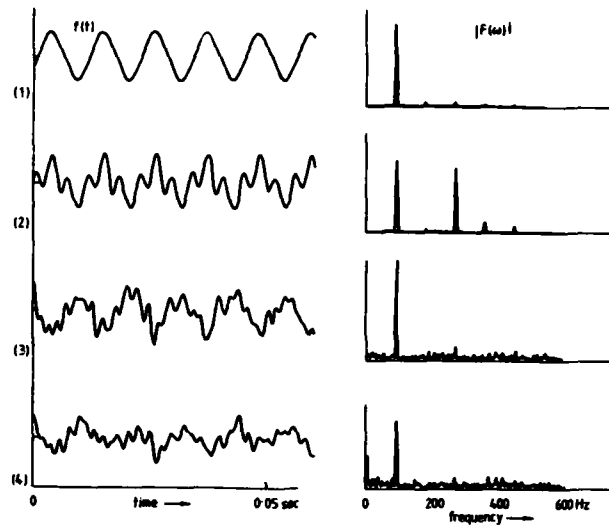


Fig 12 Time domain to frequency domain

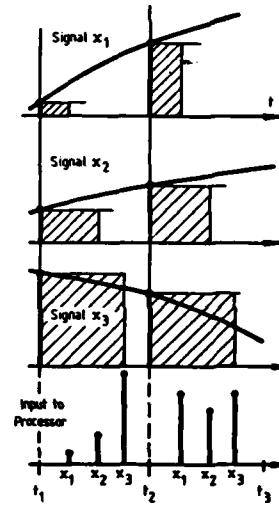
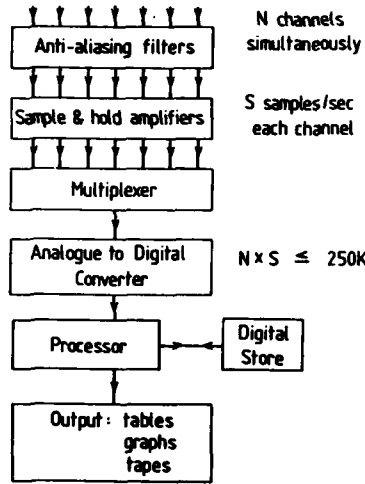


Fig 13 Data acquisition and processor

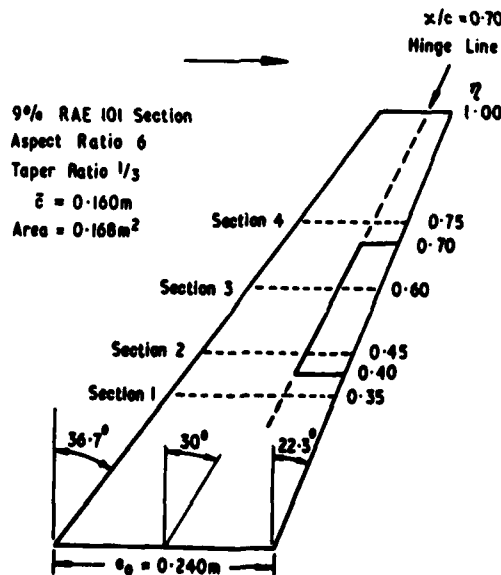


Fig 14 Model with control surface. Pressure distributions at sections 1 to 4 measured with oscillating control (from Ref 26)

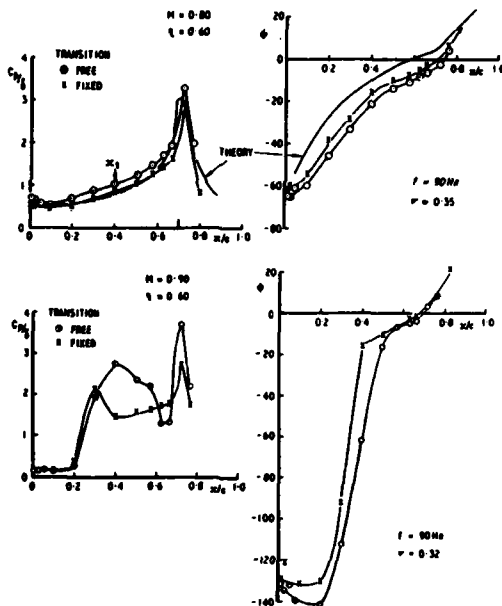


Fig 15 Effects of fixing transition for  $M = 0.8$  and  $M = 0.9$ . Pressure amplitude and phase at section 3 due to oscillating control (see Fig 14);  $\delta =$  control angle,  $\nu = \omega c/V$  (from Ref 26)

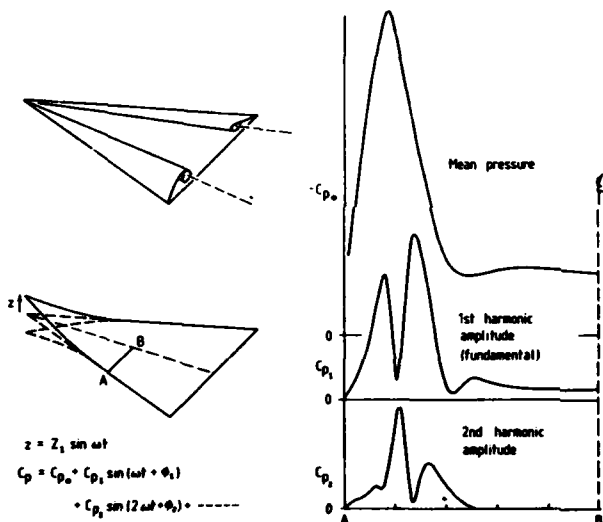


Fig 16 Pressure distributions from oscillating suction peak (from Ref 28)

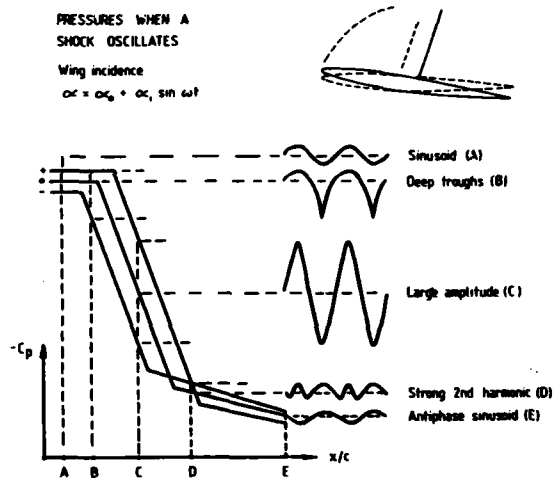


Fig 17 Schema showing production of pressure fluctuations by oscillating shock wave (from Ref 29)

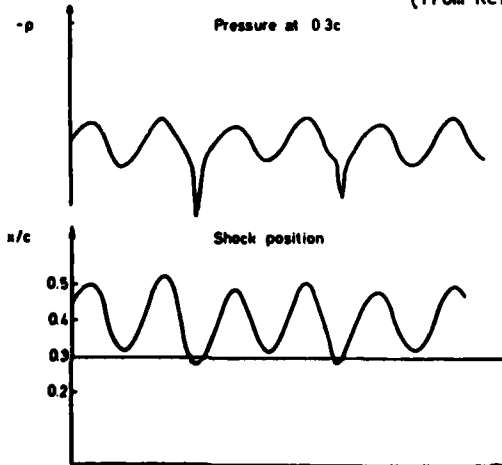


Fig 18 Oscillatory pressure related to small variations in amplitude of shock wave (from Ref 29)

Flutter Testing

Vibration properties of system :  $Ae^{(\mu+i\omega)t}$

Measure  $\mu$  and  $\omega$  with  $eV^2$  increasing

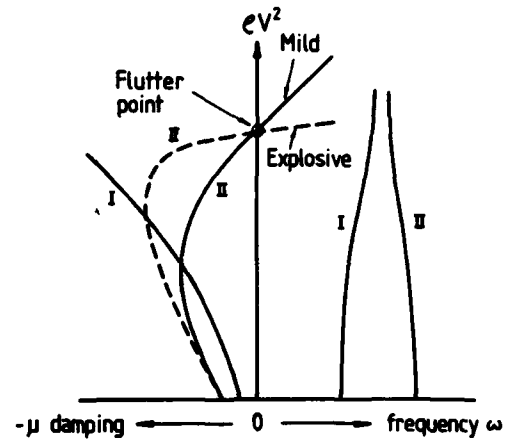
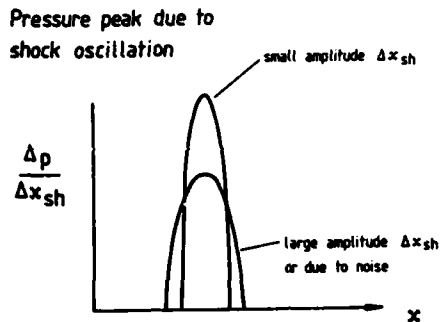
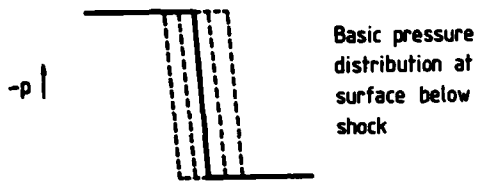


Fig 19 Pressure distribution due to shock oscillation. Effect of increasing amplitude or of addition of noise

Fig 20 Flutter diagram for two degrees of freedom (from Ref 41)

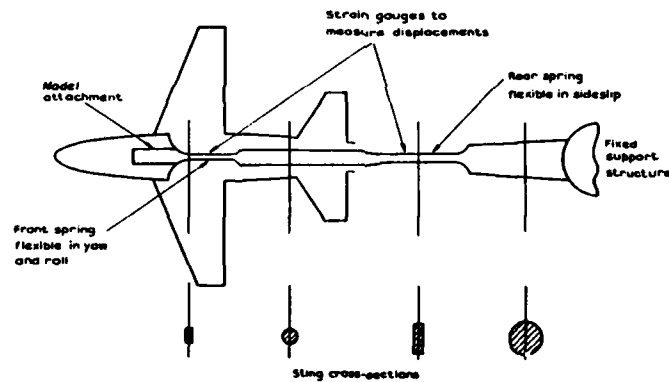


Fig 21 RAE derivative rig; spring arrangement (from Ref 44)

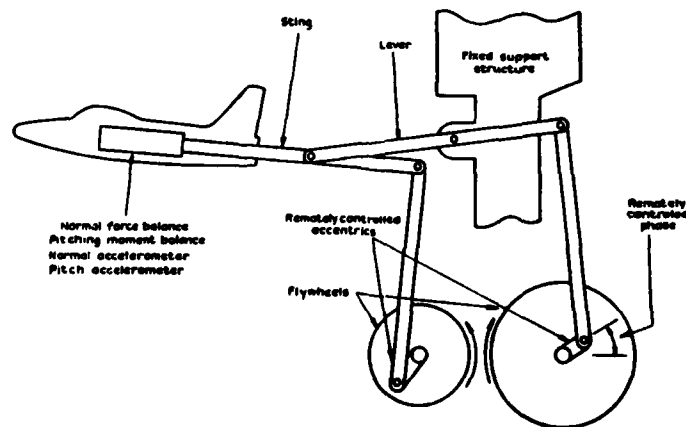


Fig 22 Cornell dynamic testing system (from Ref 44)

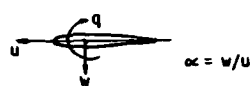
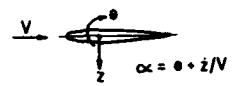

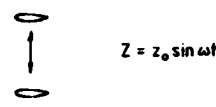



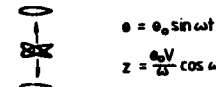
Flight Velocities	Wind Tunnel Displacements	Measurements
 <p><math>\alpha = w/u</math></p>	 <p><math>\alpha = \theta + z/V</math></p>	<p>Lift = Z Moment = M</p>
	 <p><math>Z = z_0 \sin \omega t</math></p>	<p><math>Z_z \rightarrow Z_{ac}</math>  <math>Z_z \rightarrow Z_{ac}</math>  <math>M_z \rightarrow M_{ac}</math>  <math>M_z \rightarrow M_{ac}</math></p>
	 <p><math>\theta = \theta_0 \sin \omega t</math></p>	<p><math>Z_\theta \rightarrow Z_{ac}</math>  <math>Z_\theta \rightarrow Z_q + Z_{ac}</math>  <math>M_\theta \rightarrow M_{ac}</math>  <math>M_\theta \rightarrow M_q + M_{ac}</math></p>
	 <p><math>\theta = \theta_0 \sin \omega t</math>  <math>z = \frac{a_0 V}{\omega} \cos \omega t</math></p>	<p><math>Z_\theta \rightarrow Z_q</math>  <math>M_\theta \rightarrow M_q</math></p>

Fig 23 Motions in flight and tunnel compared

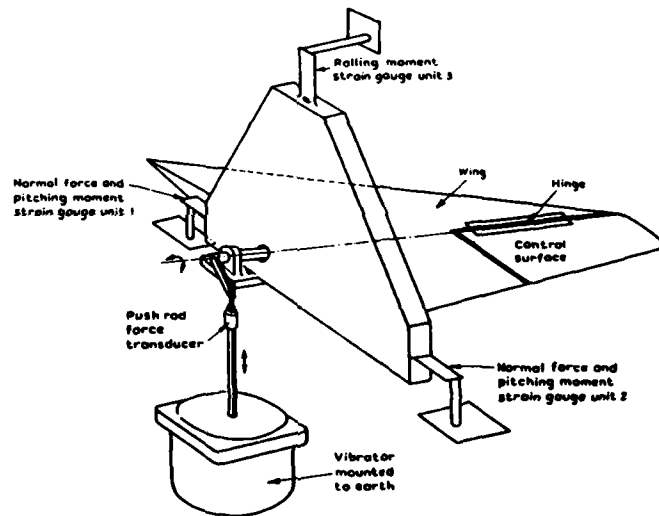


Fig 24 Force measuring system with oscillating control surface (from Ref 46)

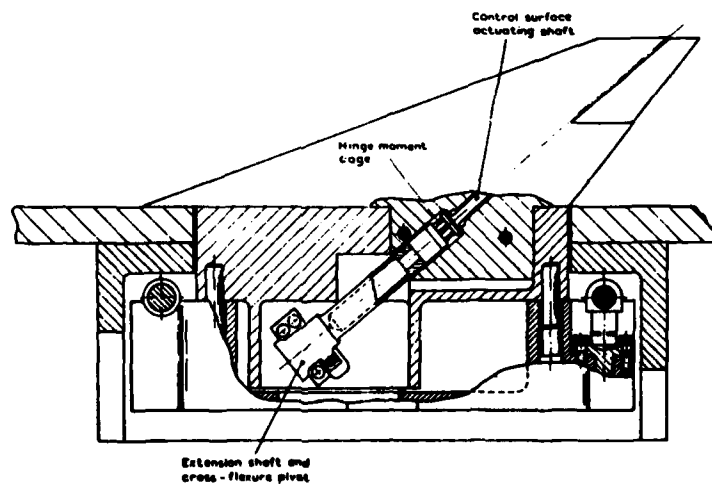


Fig 25 Details showing hinge-moment unit (from Ref 46)

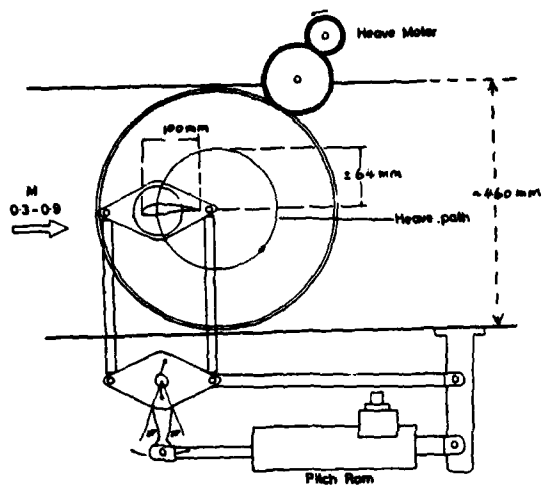


Fig 26 ARA pitch and heave rig, side view of tunnel mounting

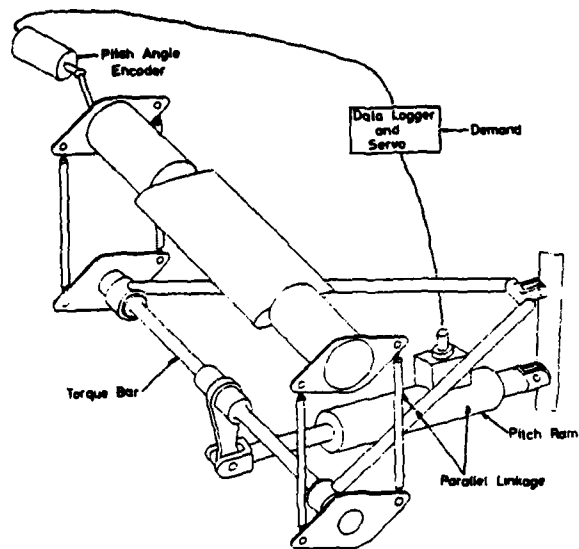


Fig 27 ARA pitch and heave rig, showing linkages of pitch drive

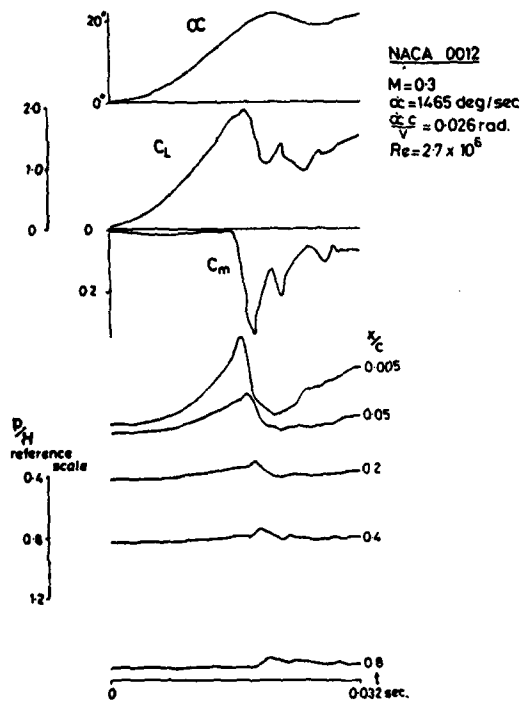


Fig 28 Results from ARA rig for ramp change of incidence

## EXPERIMENTAL TECHNIQUES FOR UNSTEADY BOUNDARY LAYERS

by

D. P. Telionis  
Virginia Polytechnic Institute and State University  
Blacksburg, Virginia 24061

This short paper concentrates on methods of measuring velocity distributions in unsteady viscous flows and techniques for analyzing and presenting the data. Unsteady pressure measurements are not included here. Both hot wires and laser-doppler velocimeters have been successfully used to investigate unsteady boundary layers. A variety of flow visualization methods ranging from smoke and tuft observation in air to hydrogen bubbles and solid particles in water, have been successfully used in the study of complex unsteady flows, as for example the formation and development of large scale vortices. Recently it has been attempted to obtain simultaneously velocity measurements at a point and instantaneous flow visualization. Both laminar and turbulent flows with or without pressure gradients have been investigated. Such flows, especially turbulent flows and separating flows require special averaging techniques to disclose their basic characteristics. Typical data from flat plate flows with adverse pressure gradients, separating flows and flows over oscillating airfoils are presented.

## 1. INTRODUCTION

Theory and experiment usually compete in the discovery and explanation of physical phenomena. A discovery is usually made by one method of investigation and then the other is called upon to corroborate and explain it. In the area of unsteady viscous flows, it is perhaps theory that preceded the experiment. In impulsive changes of the flow, interest was generated from the very first paper of Prandtl<sup>1</sup> on boundary layers, followed by classical contributions of Blasius<sup>2</sup> and Goldstein and Rosenhead.<sup>3</sup> Experimental verification of the properties of flows started impulsively from rest have followed later, as described in this article.

In the area of oscillating flows, experimental work of Faraday, Dvorak, Rayleigh in the nineteenth century and the work of Carriere, Andrade and Schlichting at the beginning of this century, followed by a large number of more recent experimental investigations, disclosed the basic features of oscillations with no mean and the phenomenon of acoustic streaming. References on the topic, the reader will find in Riley.<sup>4</sup> Attempts to explain analytically the physics of the problem and resolve the controversies of experimental data appeared much later and the problems were not clearly resolved until very recently (Stuart,<sup>5,6</sup> Riley<sup>4</sup>). Oscillating boundary layers with nonvanishing mean were considered first analytically by the pioneering work of Lighthill,<sup>7</sup> Moore<sup>8</sup> and Lin.<sup>9</sup> Initial efforts for experimental verification followed soon after<sup>10</sup> but only very recently, serious experimental work was undertaken and this was mostly concentrated on unsteady turbulent boundary layers as described in this short paper. The reader will find more details and more references in a very recent review article (Telionis<sup>11</sup>).

Interest in the area of unsteady viscous flows was for decades rather academic. After all, until very recently, the design of aerodynamic components was based essentially on empirical data of steady flows. It has been finally realized that real-life aerodynamics is for all practical purposes an unsteady phenomenon. Unsteady airfoil stall is a typical example of spectacular deviations of unsteady from steady flows. A closer look via analytical and experimental methods disclosed that such deviations are almost entirely due to unsteady viscous effects and in particular unsteady separation as described in recent review articles.

In this paper we decided to concentrate on two topics which are of great practical importance: Oscillating boundary layers and unsteady separation. Transient boundary layers and oscillation about a zero mean will not be discussed here. For information on these topics the reader is referred to Refs. 5, 6, 11, 12, 13 and 14. The spirit of the present review therefore, revolves essentially about applications to aeronautics.

More in tune with the title of this paper would be a grouping of the topics of interest according to the methods of investigation rather than the topic of interest. In this sense it is admitted here that the title of the paper is a little misleading. However, the experimental techniques described are not new. We describe here how, well established methods are employed in the investigation of specific problems of unsteady boundary-layer flows.

## 2. DATA ACQUISITION AND REDUCTION

Except for the work of Hill and Stenning,<sup>10</sup> most of the experimental work in the area of unsteady boundary layers deals with turbulent boundary layers. Investigation of unsteady turbulent flows hinges critically on the method of reducing and analyzing the data. The meaning of unsteady turbulent flows itself requires some clarification, since turbulent flows are inherently unsteady. A common practice in the experimental investigation of random phenomena is to average the signal at each point in space. Time averaging and ensemble averaging at a point  $\underline{r}$  in space are defined by the following equations

$$\overline{q(\underline{r})} = \lim_{T \rightarrow \infty} \frac{1}{T} \int_0^T q(\underline{r}, t) dt \quad (1)$$

$$\langle q(\underline{r}, t_0) \rangle = \lim_{N \rightarrow \infty} \frac{1}{N} \sum_{n=0}^N q_n(\underline{r}, t_0) \quad (2)$$

where  $q_n$  is the  $n$ th realization of the phenomenon. If the ensemble average is independent of time,  $t_0$ , then the variable  $q$  is stationary. It is weakly stationary if the ensemble average and the autocorrelation do not depend on time and strongly stationary if all higher moments are independent of time as well. If a random variable is stationary and the time averages do not depend on the particular realization, then the variable is ergodic and  $q = \langle q \rangle$ .



Consider now a random variable on which an external oscillation with discrete frequency is imposed. In particular, consider a turbulent boundary layer which is driven externally by a fluctuation of the outer flow velocity. For all practical applications, the frequency of externally imposed fluctuations is contained in the spectrum of frequencies of the turbulent flow. The discrete signal is therefore buried in the random signal. The organized part of the signal can be separated if the period,  $T$ , of the externally imposed discrete oscillation is known. A "conditional ensemble average" can then be defined:

$$\langle q(t) \rangle = \lim_{N \rightarrow \infty} \frac{1}{N} \sum_{n=0}^N q(t+nT) \quad (3)$$

Conditional sampling was introduced in periodic turbulent flows in the late fifties and early sixties<sup>15-18</sup> and is often also termed "phase" or "periodic" sampling. In terms of the conditional average, the organized part of the signal can be determined

$$\bar{q} = \langle q \rangle - \bar{q} \quad (4)$$

and the random fluctuations are defined accordingly

$$q' = q - \langle q \rangle \quad (5)$$

Acharya and Reynolds<sup>19</sup> provide a number of identities relating the quantities  $\bar{q}$ ,  $q$ ,  $q'$  and  $\bar{q}$  as well as governing equations of such quantities and their moments defined in terms of both the averaging methods described. The property under consideration can now be decomposed into three parts: the time averaged or mean, the organized fluctuation and the random fluctuation, as shown schematically in Fig. 1.

$$q(\underline{r}, t) = \bar{q}(\underline{r}) + \bar{q}(\underline{r}, t) + q'(\underline{r}, t) \quad (6)$$

Such decompositions have been proposed by Townsend,<sup>20</sup> Phillips,<sup>21</sup> Kovaszny et al.<sup>22</sup> for the investigation of similar problems.

A number of second or higher order moments can now be defined. Reynolds stresses that drive the mean flow are

$$\tau_a = \overline{u'v'} \quad , \quad \tau_b = \overline{u\bar{v}} \quad (7)$$

where  $u$  and  $v$  are velocity components parallel and perpendicular to the wall respectively. Ensemble averaging the product of the random fluctuations, yields a Reynolds stress which drives the organized fluctuations

$$\tau_c = \langle u'v' \rangle \quad (8)$$

Similarly we may define turbulent kinetic energy functions that depend on the random fluctuations, the organized fluctuations or both.

In practice, conditional averaging requires an external trigger at a specific instant within a period. This can be an electronic signal which is in turn activated by a mechanical signal. The electronic signal can easily be further delayed to allow the sampling to span the whole period. Very often, an analog signal itself can be used to control the periodic sampling. In this case a particular

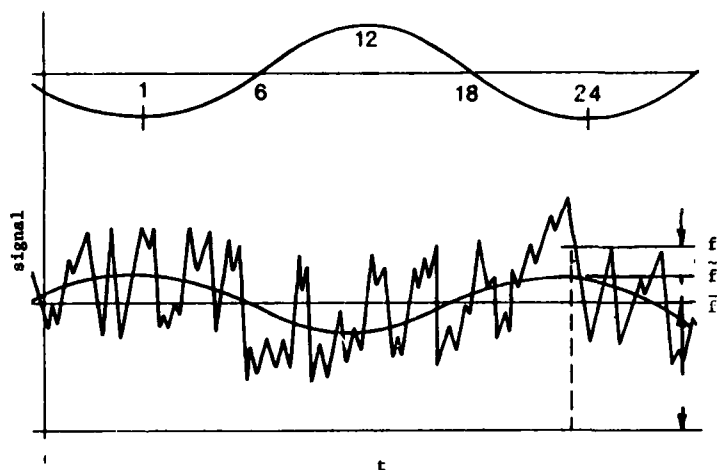


Fig. 1 Definition of averaging processes and the triple decomposition.

value of this signal, which Kovaszny<sup>22</sup> terms the "master signal", or a value of its slope can be used as a trigger to obtain one sample value. Most modern signal analyzers, as for example Hewlett Packard's HP-5420A or Zonic's DMS 5003, provide the capability of periodic sampling in any of the nodes described above.

Koraszny<sup>22</sup> describes a variety of other problems that require periodic sampling and averaging. A class of such problems is related to recurrent phenomena. These are phenomena that are initiated at random times, but the driving mechanism is always the same.

Most modern signal analyzers process signals digitally. This usually requires that the signal levels are as close to the peak of the dynamic range as possible, in order to minimize the error in digitizing.<sup>19</sup> However there are distinct advantages in digital operations. Most important of all, the same digital sample can be used to provide various ensemble averages, as for example  $\langle q \rangle$ ,  $q$  and higher moments like the turbulent energy or the Reynolds stress.<sup>19</sup> Acharya and Reynolds argue further that digital processing circumvents the problem of maintaining the delicate calibration of analog multipliers.

### 3. CONTROLLING PARAMETERS FOR TURBULENT BOUNDARY LAYERS

The earliest experiments on unsteady turbulent boundary layers were reported in Ref. 23. Karlsson<sup>23</sup> investigated the response of a tripped turbulent boundary layer developing on a flat plate and driven by a harmonic disturbance in the outer flow. Karlsson was able to vary his amplitudes and frequencies in a range unmatched by contemporary investigators. He considered amplitudes of the outer flow velocity up to 34% of the outer mean and frequencies from 0 to 48 Herz for a Reynolds number  $R^* = \bar{U}_\infty \delta^*/\nu = 3.6 \times 10^5$  where  $\bar{U}_\infty$  is the mean of the outer flow and  $\delta^*$  the displacement thickness. Karlsson reduced his data by analog operations. Comparing his boundary layer signal  $u$  with the outer flow signal  $U_e$ , he calculated the time averaged products

$$\overline{U_e^2(\omega t)}, \overline{u(t) U_e(\omega t)}, \overline{u(t) U_e(\omega t + \pi/2)}, \overline{U_e^2(\omega t + \pi/2)} \quad (9)$$

Combining these moments he was able to calculate the in-phase and the out-of-phase components of the organized fluctuation of the velocity

$$u_{in} = \sqrt{2} \frac{\overline{U_e(\omega t) u(t)}}{\overline{U_e^2(\omega t)}} \quad (10)$$

$$u_{out} = \sqrt{2} \frac{\overline{U_e(\omega t + \pi/2) u(t)}}{\overline{U_e^2(\omega t)}} \quad (11)$$

Any higher harmonics of the organized response are thus lumped together with the random fluctuations. The RMS of the higher harmonics and the random signals can be calculated by the formula

$$\overline{r^2} = \overline{u^2(t)} - \left[ \frac{(\overline{U_e(\omega t) u(t)})^2}{\overline{U_e^2(\omega t)}} + \frac{(\overline{U_e(\omega t + \pi/2) u(t)})^2}{\overline{U_e^2(\omega t)}} \right] \quad (12)$$

Karlsson measured and reported mean velocity profiles, profiles of  $u_{in}$  and  $u_{out}$  as well as profiles of  $\overline{r^2}$ . His data, for almost two decades, has been the only available data for testing theoretical models of unsteady turbulent boundary layers. His findings indicate that even for the largest amplitudes of fluctuation there is no influence on the mean profile. Karlsson's  $u_{in}$  and  $u_{out}$  profiles are qualitatively similar to their laminar counterparts.

Experimental investigations of oscillating turbulent boundary layers were attempted again with vigor in the seventies. Modern electronic hardware made the task of periodic sampling and digital processing of the data relatively easier. A large number of publications on the topic appeared almost simultaneously.<sup>16,17,18,24-32</sup> With all this information available, it soon became obvious that the problem is a lot more complex than the problem of laminar oscillations. For laminar flow, the Strouhal number  $S = \omega L/U_\infty$  is the only similitude parameter that would govern the flow and permit comparison between different experiments or experiment and theory. True, the Reynolds number controls the scaling in the direction normal to the wall. However, the appropriate stretching of the normal scale results in collapsing of data obtained with different Reynolds numbers. In turbulent flows the situation is entirely different. The history of the flow plays a much more important role. The situation is hopelessly confusing if natural transition to turbulence is allowed to control the flow. Even with artificial transition, the upstream history of turbulence controls the periodic response of the turbulent boundary layer and results in unexpected deviations. It has been suggested that the Reynolds number based on the displacement thickness or the momentum thickness would be the proper parameter for dynamic similarity. This would account for the alternative designs of the leading portion of models, since a good number of investigators simply study the boundary layer that develops on the tunnel walls. There is no doubt that a single parameter, like some Reynolds number, is not enough to characterize the turbulent boundary layer at a point, nor would for sure all such layers develop in an identical form further downstream. Moreover, other parameters, like the wall roughness, the free stream turbulence or even acoustic disturbances may influence the subsequent development of the boundary layer. All these well known difficulties are greatly amplified in the case of unsteady turbulent boundary layers.

An element of the problem that has not been attacked experimentally yet is the possible interaction between the random and the deterministic fields. Acharya and Reynolds<sup>19</sup> propose a comparison of the frequency of externally imposed oscillation to the frequency of the bursting process.<sup>33</sup>

$$f_b = \frac{U}{5\delta} \quad (13)$$

Investigating the response of internal, fully developed flows they found that the organized part of the Reynolds stress is considerably higher for a frequency very close to the bursting frequency. Thomas and Shukla<sup>34</sup> have looked into the wall region of fully developed fluctuating turbulent pipe flow. They report on the interaction between the bursting effect and the imposed fluctuations and compare their experimental results with the theoretical model based on the concept of surface renewal.

Binder and Didelle<sup>18</sup> and Soutif<sup>35</sup> investigated the response of a turbulent jet to fluidic lip disturbances that generate symmetric or antisymmetric periodic fluctuations. The authors presented instantaneous profiles and the downstream evolution of periodic and turbulent intensities. Most important of all, they indicated that the externally imposed fluctuation may transfer energy to the turbulent motion. Indeed 20 jet thicknesses downstream of the disturbance, the periodic fluctuations die out but the intensity of turbulence grows to a value 70 percent larger than the corresponding undisturbed jet intensity. In a later publication, Favre-Marinet and Binder<sup>36</sup> repeated careful measurements of the Reynolds stresses in the pulsating jet. They show that the Reynolds stress  $\tau_a = \langle u'v' \rangle$  oscillates with much larger amplitudes compared to normal stresses  $\langle u'^2 \rangle$  and  $\langle v'^2 \rangle$ . Moreover the ratio  $\langle u'v' \rangle / \langle q^2 \rangle$  with  $\langle q^2 \rangle$  the organized part of the turbulent kinetic energy, varies periodically between the values of 0 and 0.4. This clearly indicates the inadequacy of quasi-steady models which assume  $\langle u'v' \rangle$  to be proportional to the turbulent kinetic energy.

The evidence described clearly indicates that it is possible to transfer momentum and energy from an external organized oscillation to the random field of turbulence. The opposite, of course, would be an extremely interesting problem, since then it would be possible to quiet down a turbulent field. Except for the work of Karlsson and only for the highest frequency that he investigated, there is no other evidence of such deterministic-random field interactions for external turbulent boundary layers. Karlsson's data present the profile of the RMS random fluctuation essentially averaged through the cycle of oscillations, as defined by Eq. (12). The quantity  $\overline{r^2}/U_\infty$  varies from a value 0.10 near the wall, almost linearly, to 0.02 or 0.03 at the edge of the boundary layer. For  $f = 48$  Herz, the  $\overline{r^2}$ -profile behaves erratically with a scatter that perhaps is due to experimental inaccuracies. However, values of 0.13 or above seem to persist for at least 1/3 of the boundary layer thickness. Surprisingly, the mean profile as well as the organized fluctuation, i.e., the profiles of  $u_{in}$  and  $u_{out}$  indicate a normal behavior, in qualitative continuation of the trends established by lower frequency data.

One more parameter is widely accepted as a basic characteristic of an unsteady turbulent boundary layer: the relative amplitude of oscillation. Both reduced frequency and reduced amplitude have been repeatedly shown to have a negligible effect on the mean profile. This is in fact true for amplitude ratios of as much as 0.4 or even 0.5. The profiles of the reduced fluctuations change considerably with the frequency, but depend rather mildly on the amplitude ratio.

In an effort to present a clear picture of today's available experimental information, we collected in Table 1 the parameters that characterize the experimental data on unsteady turbulent boundary layers. This has been a very difficult task since each author chooses to provide the quantities that he feels are more representative of the flow under investigation. Many of the quantities presented in this table had to be calculated from data provided by the author. Quite often, quantities were calculated from scratch based on classical flat plate boundary layer theory. In cases of doubt, the figures are contained in a parenthesis. In some cases the authors provide general information about their initial station, but proceed to make detailed measurements at another station further downstream. It has been attempted to include here data pertaining to the station at which all the information was obtained. If this was not possible then initial station information were included. Some authors provide data for more than one station. In these cases it was attempted to single out the most characteristic station, usually the one closer to separation.

Reference		$R^* = \overline{u}_\infty \delta^*/\nu$	$S = \omega L/\overline{u}_\infty$	$f$ (Hz)	$f_b$ (Hz)	$e = \overline{u}_e/\overline{u}_\infty$
Karlsson <sup>23</sup>	†	$3.6 \times 10^3$	2.9 - 163.2	0.33 - 48	14	0.08 - 0.34
Houdeville et al <sup>16</sup>	†	$7 \times 10^4$	1.5	40	1750	0.330
Schachenmann et al <sup>18</sup>	†	$(1.16 \times 10^3)$ $(0.70 \times 10^3)$	1 7.33	7 30	(558) (337)	0.069 0.013
Cousteix et al <sup>24</sup>	†	$3.36 \times 10^4$	0.27	43	670	0.330
Patel <sup>25</sup>	†	$4 \times 10^3$	0.35 1.05	11	160	0.110
Charnay et al <sup>26</sup>	†	$(1.6 \times 10^4)$	1	36	(84)	0.260
Cousteix et al <sup>27</sup>	†	$7 \times 10^4$ $3.36 \times 10^3$	2.5 5	40 43	1750 670	0.330 0.370
Simpson <sup>28</sup>	*	$(1.5 \times 10^3)$	1.1	3.7	(93)	0.330
Kenison <sup>29</sup>	*	$4 \times 10^3$	0 - 3.0	0 - 6.0	44	0.035 - 0.102
Tomsho & Brown <sup>30</sup>	†	$(0.75 \times 10^3)$	1.05 6.28	5 30	(358)	0.100
Houdeville et al <sup>31</sup>	*	$3.6 \times 10^4$	3.0 - 10.0	38	350 - 70	0.19 - 0.13
Hayakawa <sup>32</sup>	†	$1.7 \times 10^4$	2.63 3.88	2.16 3.45	47	0.064 0.103

Table 1. Compilation of nominal parameters of available experimental data: † at entrance, \* near the point of separation, ‡ flat plate.

Table 1 should be considered only as an initial approximate compilation of data. It is felt that the only way of providing a complete and accurate set of nominal data is by direct contact with the authors of the referenced works and the time limits for the preparation of this paper did not allow such an ambitious undertaking. A similar compilation has been prepared by Ramaprian<sup>37</sup> who included fewer references but calculated more quantities characteristic of the average skin friction, the pressure gradient, etc.

#### 4. TYPICAL EXPERIMENTAL DATA

It should be interesting to plot data of different experiments on the same graph for comparison and in fact this should have been done in a critical review like the present. However, it is felt that no such comparison should be attempted since no two experimental riggings have the same parameters as described before. Such a comparison should be done only in terms of a theoretical model which could be used to transform the experimental data to match a set of nominal conditions. To be more precise, it is proposed here that an analytical model should be used to simply extrapolate experimental data to achieve the same values of the controlling parameters and facilitate comparison.

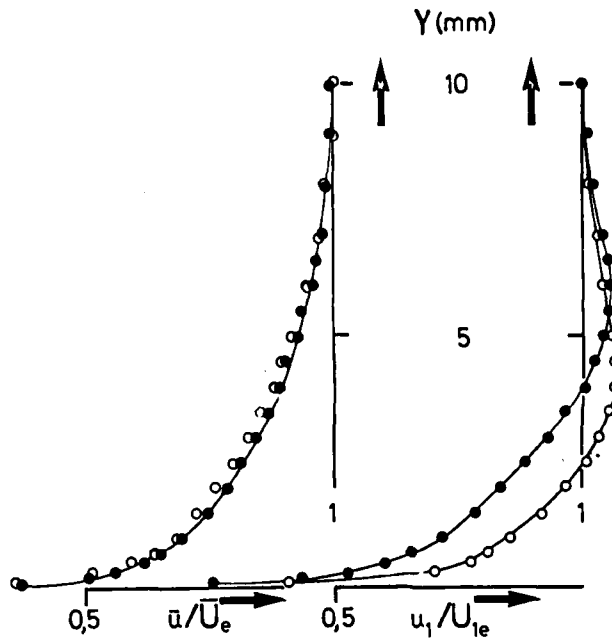


Fig. 2. The mean and the organized part of the velocity for flat plate flow from Ref. 27.  $\epsilon = 0.33$ ;  $\bullet, R^* = 7 \times 10^4, S = 2.5$ ;  $\circ, R^* = 3.36 \times 10^3, S = 5$ .

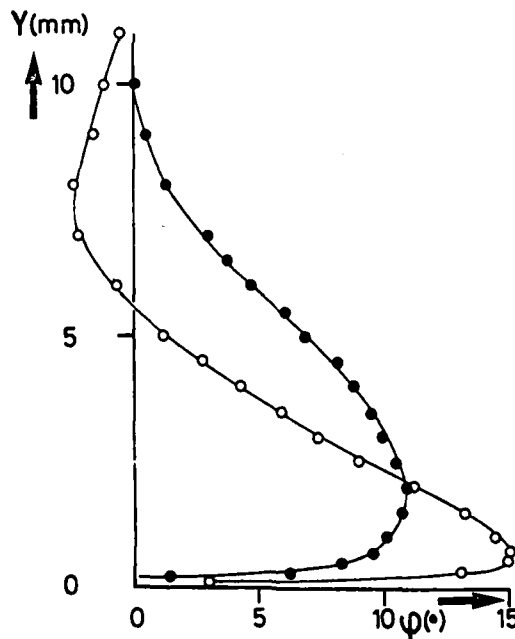


Fig. 3. The phase angle profile for flat plate flow from Ref. 27.  $\epsilon = 0.33$ ;  $\bullet, R^* = 7 \times 10^4, S = 2.5$ ;  $\circ, R^* = 3.36 \times 10^3, S = 5$ .

In the present discussion we will confine ourselves to descriptions of the physical phenomena. This will become easier if representative experimental data are presented.

It has been established that gross features like the mean of the boundary layer velocity is very little affected by the external fluctuations. At this moment we cannot claim that the same is true for the location of separation but this is the topic of the following section. The externally imposed deterministic oscillations generate an organized oscillation which depends strongly on the frequency and mildly on the amplitude of the oscillation.

For a flat plate, that is for an outer flow velocity given by

$$U_e(x, t) = U_{e0}(1 + \epsilon \sin \omega t) \quad (14)$$

The situation appears to be relatively straightforward and can be clearly seen in the data of Karlsson. The amplitude of the organized velocity component overshoots the outer flow value by up to 25%. Surprisingly, smaller amplitude ratios,  $\epsilon$ , generate larger overshoots. The effect of frequency is more dominant but the qualitative behavior is very similar to that of a laminar boundary layer. For larger frequencies, the thickness of the organized part of the fluctuation, often also called the Stokes layer, decreases and the peak of the profiles approaches the wall and the numerical value of 1.0. Typical example of velocity profiles for  $S = 2.5$  and  $5.0$  from Ref. 27 are shown in Fig. 2. In this figure the mean profile and the organized fluctuation are shown. The second quantity is the reduced amplitude of the in-phase fluctuation, assuming

$$\begin{aligned} \bar{u} &= u_1 \sin \omega t + u_2 \cos \omega t, \\ \tilde{u}_e &= U_{1e} \sin \omega t \end{aligned} \quad (15)$$

It should be mentioned here that the experimental rigging described in Ref. 27 dictates a mild acceleration over the flat plate.

The phase profiles corresponding to the flow described above are shown in Fig. 3. In this figure definite phase leads are shown, a dominant characteristic for flat plate flows, at least for the inner part of the boundary layer.

Experimental ambiguities are introduced in the immediate neighborhood of the wall. Most available data are widely scattered in this region. The present author and his associates averaged and extrapolated Karlsson's data to calculate the phase advance of the wall shear. The amplitude of the wall shear and the displacement thickness as well as the corresponding phases are plotted against the Strouhal number

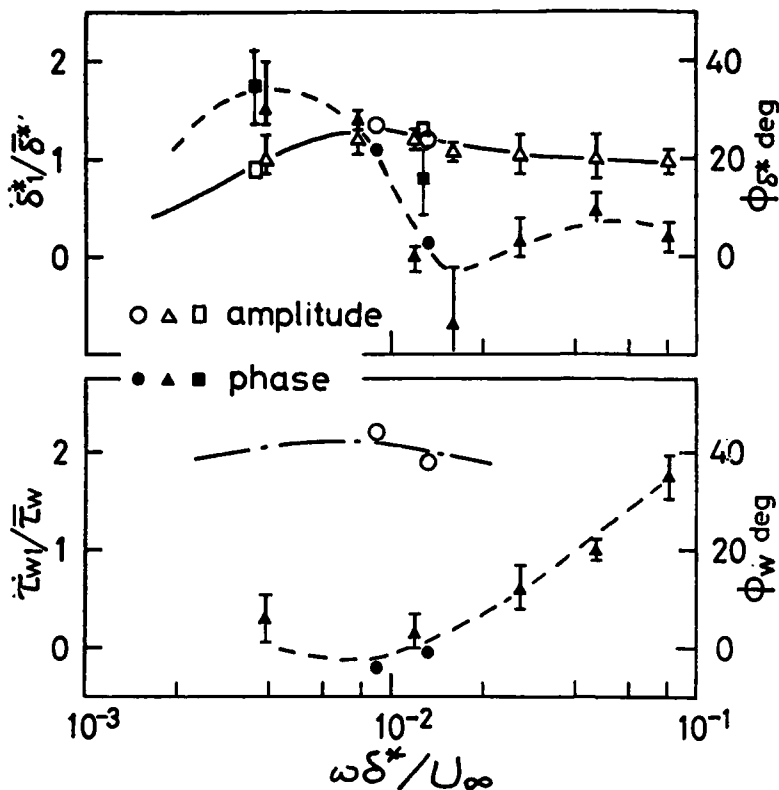


Fig. 4. Reduced displacement thickness and wall shear and the corresponding phase angles for a flat plate.  $\Delta, \triangle$ , Karlsson<sup>23</sup>;  $\square, \blacksquare$ , Houdeville et al.<sup>16, 24</sup>;  $\circ, \bullet$ , Hayakawa<sup>32</sup>. Open symbols: amplitude; closed symbols: phase.

a flat plate flow with  $S = 3.88$  and  $R^* = 1.7 \times 10^3$ . The deviation from the quasi-steady profile is most obvious in the lower half of the boundary layer.

##### 5. STABILITY AND TRANSITION

Early experimental investigations of parallel shear flows, external or internal, provide critical Reynolds numbers for either purely oscillatory flows or periodic flows that are steady in the mean. For the Stokes layer over a smooth flat plate, for example, the critical Reynolds number, based on the Stokes-layer thickness, is  $R_\delta = U_0 \delta / \nu = 565$ . In fact it was discovered that purely oscillatory flows are more stable than flows that have a nonvanishing mean. More experimental information on such classical problems and a long list of references can be found in recent publication<sup>38, 39</sup>. A complete account of analytical works on the topic the reader will find in Davis' review article<sup>40</sup>. All experimental evidence<sup>38, 39</sup> indicate that even for purely parallel flows, it is possible that transition may appear in the form of periodic bursts that emerge at a certain phase during the period, all across the streamlines and at all downstream distances. The phenomenon is similar to the appearance of turbulent patches in boundary layers developing in space.

Very little is known about the influence of uniform periodic disturbances on the problem of hydrodynamic stability, that is the development and growth of disturbances. It is recalled here that in many stability experiments, periodic disturbances are in fact introduced at a specific point in space. A ribbon with a specific frequency, for example, generates a disturbance whose subsequent growth is studied. The problem under consideration here is the transition characteristics of a boundary layer which is driven uniformly by an oscillating outer flow velocity. The periodic disturbances then take the form of standing waves as described extensively in the previous sections. Even then, it is sometimes necessary to seed the flow with short wave packets of arbitrary dominant frequency and arbitrary amplitude. The work in this area has been recently reviewed thoroughly by Loerke Morkovin and Fejer<sup>41</sup>. This section provides only a very short outline of elementary concepts on the topic.

The pioneering work of Miller and Fejer<sup>42</sup> disclosed that for an oscillating boundary layer, transition is organized in the form of turbulent patches very similar to the turbulent spots observed by Emmons<sup>43</sup> and Schubauer and Klebanoff<sup>44</sup> in steady flows. The main difference is that a turbulent patch appears at regular times and spaces and is actually a two-dimensional disturbance. Miller and Fejer note that the transition Reynolds number is influenced only by the amplitude of the free-stream oscillation whereas the transition length depends only upon the frequency of the free-stream oscillation.

based on the displacement thickness in Fig. 4. This figure, including our interpretation of Karlsson's data and Hayakawa's unpublished experimental information was put together by the second investigator.

Flows with pressure gradients reserve for the investigators unexpected surprises. Schachenman and Rockwell<sup>17</sup> report, for example, phase lags all across the boundary layer, double peaked velocity profiles, etc. Moreover, amplitude overshoots of 100% or even higher have been discovered by many recent experimentalists. The information at this point is fragmented and no definite trends can be identified.

To complete the physical description of the phenomenon we need information about the organized variation of higher moments. This is a difficult task and many experimentalists confined themselves to an average through the cycle of quantities like the turbulent kinetic energy, the Reynolds stress, etc. Instantaneous values of such quantities can be calculated by ensemble averaging and have been reported in Refs. 24, 26, 27 and 32. Such information will be valuable to theoreticians who pursue analytical modeling of unsteady turbulent boundary layers. Cousteix, Houdeville and Desopper<sup>27</sup> for example have reduced their data and estimated instantaneous profiles of the mixing length as shown in Fig. 5. The same group has reported<sup>26, 27, 31</sup> profiles of  $u'^2$ ,  $v'^2$ ,  $q^2$ ,  $\langle u'v' \rangle$ , etc. As a typical example of turbulence level variations through the cycle of deterministic fluctuations we present here in Fig. 6 the data of Hayakawa<sup>32</sup> for

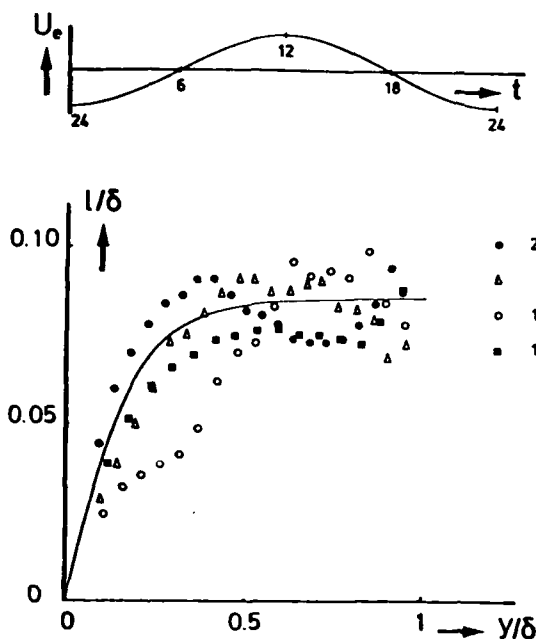


Fig. 5. Mixing length profiles at four instances within the period of oscillation, for flat plate flow (Ref. 27).

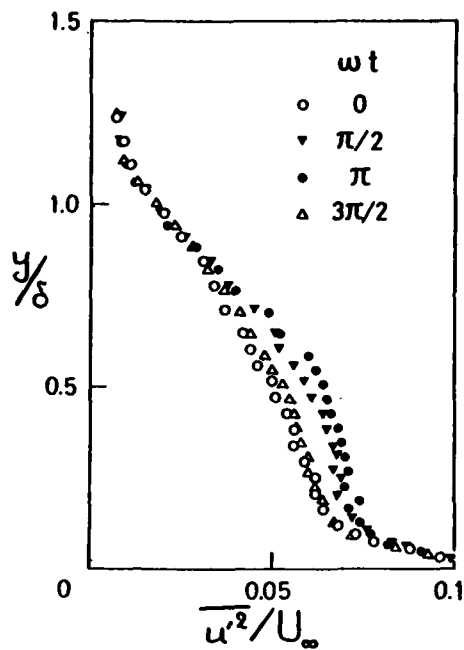


Fig. 6. Instantaneous reduced profiles of the RMS of random velocity fluctuations for a flat plate from Ref. 32.  $R^* = 1.7 \times 10^3$ ,  $S = 3.88$ .

Figure 7 presents the results of the work of Obremski and Fejer<sup>45</sup>. In this figure the boundaries of turbulent patches in the time-space plane are plotted for three periods of oscillation. A patch is preceded in time and space by a wave packet where minute turbulent disturbances grow.

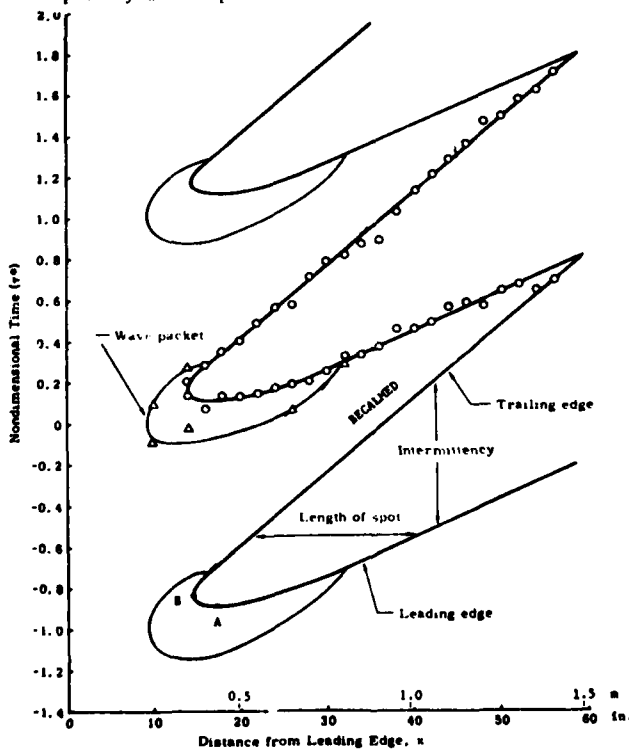


Fig. 7. The leading and trailing edges of turbulent patches (Ref. 45).

The leading and trailing edges of the patch are then traveling at a constant speed,  $0.88 U$  and  $0.51 U$  respectively, regardless of the amplitude and frequency of the externally imposed oscillation. Obremski and Fejer<sup>45</sup> experienced difficulties in estimations of transition Reynolds numbers and they attribute them to free stream turbulence and acoustic disturbances.

Kobashi et al<sup>46</sup> ran similar experiments indicating that increasing the unsteadiness of the flow makes the boundary layer more unstable and forces the unstable region in a narrow range of the phase of the oscillation. In a later publication<sup>47</sup>, the same authors employ a seeding mechanism, in this case a tripping wire, to control the initial steps of transition. This of course did not permit investigations of transition Reynolds numbers. However, they were able to study the development of a turbulent patch and its temporal evolution. They found that initially the turbulent patch emerges away from the wall, perhaps due to the mechanics of seeding, but soon it attaches to the wall and starts growing at a constant rate, keeping its shape almost self-similar.

Most recently, a similar investigation was undertaken by Consteix et al<sup>47</sup>. For the parameters of their experiments they actually found that the

phenomenon is controlled by the frequency of the external flow. Their measurements further indicate speeds of the leading and trailing edges of patches equal to  $0.89U_\infty$  and  $0.48U_\infty$  respectively.

## 6. SEPARATION

Interest in the problem of unsteady separation has been revived in the late sixties. Extensive historical accounts of the original ideas and early contributions the reader will find in recent review articles<sup>49-50</sup>. Despard and Miller<sup>51</sup> initiated the work by investigating laminar oscillating flows. For the frequencies and amplitudes that they examined they found that separation is displaced always upstream from its quasi-steady location but its position remains unaffected by the periodic disturbances. In fact they found that the initiation of the wake, as detected at the outer part of the boundary layer, coincides with a station at which the skin friction oscillates between zero and some negative value. This they proposed as a definition for separation in oscillatory flow.

More recent investigations<sup>52</sup> indicate that violent pressure gradient oscillations may eventually force drastic changes on the shape of the wake and the point of separation. This of course is the case for an airfoil that oscillates in and out of stall. Koromilas and Telionis<sup>53</sup> concentrated their interests in the immediate neighborhood of separation. Using a combination of Laser-Doppler-Velocimetry and flow visualization, they found that a turbulent wake organizes itself if the oncoming flow contains a periodic disturbance. This is true for a fully turbulent wake with a thickness not much greater than the thickness of the boundary layer and therefore a situation reminiscent of a thin airfoil at a small angle of attack. The situation is very similar to the intermittent but organized wakes generated by dynamic stall or the organized turbulent patches described in the previous section.

The findings of Reference 53 and the continuation of the same effort<sup>54</sup> are mostly in agreement with those of Despard and Miller<sup>51</sup>. However, it appears that for the lower frequencies examined in Refs. 53 and 54, the location of separation is actually displaced downstream instead of upstream. A more careful investigation of oscillating flows<sup>54</sup> indicated a new phenomenon characteristic of the point of separation. Inspecting the velocity amplitude profiles it was found that they increase monotonically as separation is approached. A characteristic peak appears at the station where the Despard and Miller criterion is met and simultaneously the flow visualizations indicate a more abrupt thickening of the boundary layer. Relative amplitude contours are shown in Figure 8. Similar contours have been reported by Kenison<sup>29</sup> but the quantity

plotted was the RMS of turbulent fluctuations. Kenison's measurements were actually terminated at separation as shown in Figure 9 and therefore the actual peak cannot be identified. However, the evidence of Figs. 8 and 9 seems to indicate that the growth of such disturbances is a characteristic of separation.

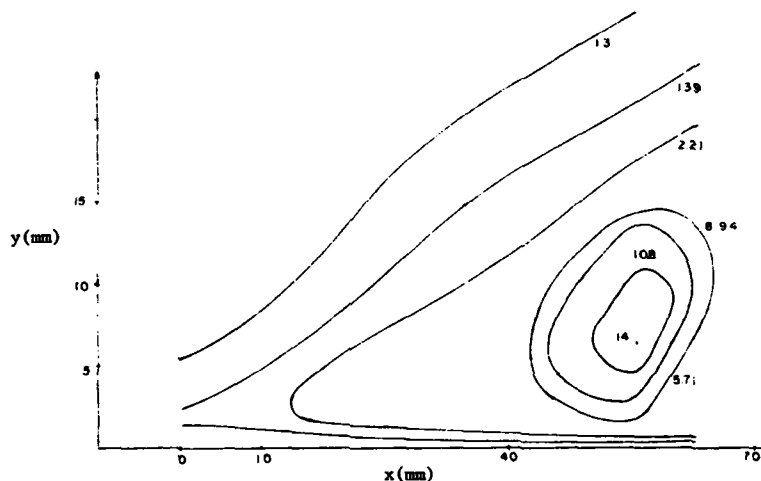


Fig. 8. Relative amplitude contours in the neighborhood of laminar separation (from Ref. 54).

shown in Figure 10. The opposite is true for decelerating flows.

The complexity of separating flows dictated the need for simultaneously sensing the entire flow field: This is possible only with methods of visualization. Very recently Taneda<sup>55</sup> published a tremendous amount of information on unsteady separating flows. Impulsive and transient starts and velocity changes of cylinders and ellipses were reported. Moreover, impulsive, transient and periodic changes of angles of attack were presented. This paper can simply serve as a lexikon of visualizations of unsteady separating flows. Taneda defines separation as the point at which the boundary layer is shed from the surface of the body. This is in agreement with earlier definitions of separation, i.e. the point at which the outer flow ceases to follow the contour of the body and breaks away into the flow. In both cases it is the interface of the viscous and inviscid flow that determines the phenomena. We usually view the flow from the outer side of the interface, whereas Taneda observes the inner side of the interface. However, it should be emphasized here that such definitions may become ambiguous in cases of mild adverse pressure gradients. The present author feels that the aerodynamic concept of separation as a catastrophic phenomenon with drastic consequences to pressure distributions can be unambiguously defined only in the limit of  $R_e \rightarrow \infty$ . In this case the interface between viscous and inviscid flow collapses on the skin of the body along the regions of attached boundary layers and actually separates from the body at the point of separation. Taneda<sup>55</sup> notes

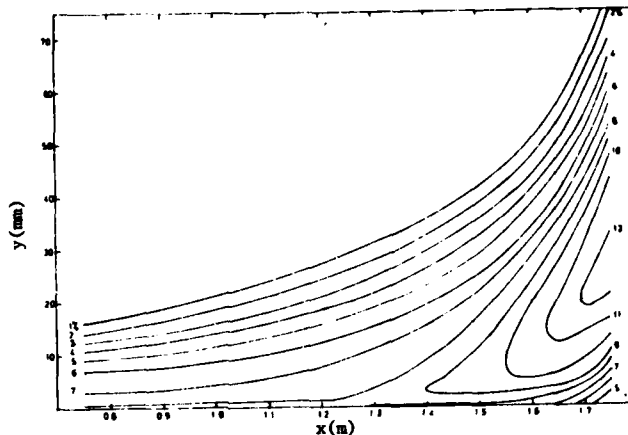


Fig. 9. RMS of random velocity fluctuations in the neighborhood of a separating turbulent boundary layer (from Ref. 29).

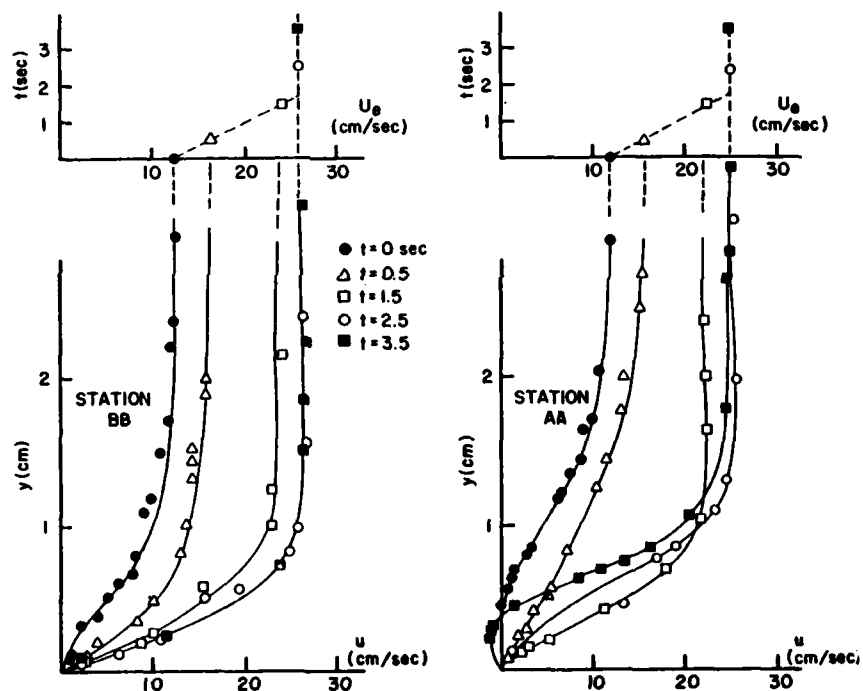


Fig. 10. Instantaneous velocity profiles and the outer flow velocity at two stations from Ref. 53. Station BB is 60mm upstream of steady separation, Station AA is approximately at steady separation. Symbols denote different instances of time and correspond to the  $U_e$ -temporal variations on top of the velocity profile.

that streakline patterns are invariant to the frame of reference and proposes that the determination of separation can be based on streakline observations. This is an interesting idea which may need further investigation.

A careful inspection of the flow visualization included in Ref. 53 and 54 indicates that some properties of separating flow are more or less global. For the small to medium values of adverse pressure gradients tested, it appears that steady flow separation is unambiguously defined by the vanishing of skin friction. The point at which this condition is met marks the beginning of a region of reversing flow and will be referred to in the sequel as the point of detachment. The detachment line forms a very small angle with respect



to the boundary of the body. In the flow visualization pictures the reversed flow region appears at first to be filled with extremely slow moving particles. The term "dead water" is indeed very appropriate for this region. A little further downstream the wake is activated and a few discrete large scale vortices appear. The generation of such vortices may be due to the instability of the free shear layer which emanates from the point of detachment. However, the present author feels that the exchange of momentum between the outer flow and the wake occurs much further downstream.

Two different types of separation have been distinguished in literature. Regular separation and "catastrophic" separation. The first has been extensively investigated analytically via the asymptotic analysis of the tripledeck. This theory holds for small disturbances of the flow with dimensions in both the streamwise direction and its perpendicular that vanish with powers of the inverse of the Reynolds number. Catastrophic separation, although not very well defined, in literature, is usually accepted as the point where the flow decisively leaves the solid boundary and generates a wake of finite width. The separation line in this case is finite even in the limit of  $Re \rightarrow \infty$ .

The data of Ref. 53 and 54 indicate that actually both types of separation are present in the neighborhood of wake formation. "Regular" separation for steady flow coincides with the point of zero skin friction followed by a small region of very slow flow which is rather controlled and almost steady. Further downstream the flow enters into a region of large scale vortices which could be identified as "catastrophic" separation. Considering the similarities of such flows with the description given by Sandborn and Liu<sup>56</sup>, we propose to use the term "pre-wake region" for the domain between the point of detachment and the point of catastrophic separation. In other words, pre-wake region is defined here as the region following the point of detachment, in which the flow is reversed and very slow with no evidence of discrete large scale vortices. For steady flow the pre-wake region is thin and has a length of not more than a few boundary layer thicknesses.

Moving over now to unsteady flows and inspecting the data obtained in Ref. 53 and 54, we can make the following observations. Basically the general flow patterns appear to be the same for steady and unsteady flow. Perhaps the most important difference is that in unsteady flow the "pre-wake region" appears quite often activated and usually much longer. In the thin separated region where the flow has decelerated to near stagnation, apparently the unsteady pressure distribution often generates momentum which results in well ordered reversing flow. For the impulsive changes tested by Koromilas and Telionis<sup>53</sup> the pre-wake region appears to be shooting upstream generating a very thin layer of reversed flow. This layer however is totally embedded in the boundary layer and does not generate disturbances in the outer flow. The pre-wake regions observed in Ref. 54 are not as elongated as those of Ref. 53. However, the excursions of the point of detachment are longer than their corresponding quasi-steady flow counterparts.

In view of the evidence provided up to now, it appears that the point of zero skin friction, that is Prandtl's criterion for separation, always signals the initiation of reversing flow and never the beginning of wake, that is "catastrophic" separation. For steady flow the two points are very close together. In fact it is possible that for very large Reynolds numbers, the two points coalesce and the extent of the pre-wake region tends to zero. However, for unsteady flow, the two points may be distinct.

#### REFERENCES

1. Prandtl, L., "Über Flüssigkeitsbewegung bei sehr kleiner Reibung" Proc. III International Math. Congress, Heidelberg, 484-491, 1904.
2. Blasius, H., "Grenzschichten in Flüssigkeiten mit kleiner Reibung", Zeit. Math. Phys., 56, 1-37 (1908).
3. Goldstein, S. and Rosenhead, L., "Boundary-Layer Growth", Proc. Comb. Phil. Soc., 32, 392-401 (1936).
4. Riley, N., "Oscillatory Viscous Flows, Review and Extension", J. of The Inst. of Math. and Its Appl., 3, 419-434 (1967).
5. Stuart, J. T., "Unsteady Boundary Layers", in Laminar Boundary Layers, ed., L. Rosenhead, Oxford, 349-406 (1964).
6. Stuart, J. T., "Double Boundary Layers in Oscillatory Viscous Flow", J. Fluid Mech., 24, 673-687 (1966).
7. Lighthill, M. J., "The Response of Laminar Skin Friction and Heat Transfer to Fluctuations in the Stream Velocity", Proc. Roy. Soc., 224A, 1-23 (1954).
8. Moore, F. K., "Unsteady Laminar Boundary-Layer Flow", NACA TN 2471 (1951).
9. Lin, C. C., "Motion in the Boundary Layer with a Rapidly Oscillating External Flow", Proc. 9th Int. Congr. Appl. Mech., Brussels, 4, 155-169 (1956).
10. Hill, P. G. and Stenning, A. H., "Laminar Boundary Layers in Oscillatory Flow", J. of Basic Eng., 82, 593-608 (1960).
11. Telionis, D. P., "Review - Unsteady Boundary Layers, Separated and Attached", J. Fluids Eng., 101, 29-43 (1979).
12. Stuart, J. T., "Unsteady Boundary Layers" in Recent Research of Unsteady Boundary Layers, ed. E. A. Eichelbrenner, 1, 1-46 (1971).
13. Riley, N., "Unsteady Laminar Boundary Layers", SIAM Review, 17, 274-297 (1975).
14. Knight, D. W., "Review of Oscillatory Boundary Layer Flow", J. of the Hydraulics Div. Proc. of ASCE, 104, No. HY6, 839-855 (1977).

15. Hussain, A. K. M. F. and Reynolds, W. C., "The Mechanics of an Organized Wave in Turbulent Shear Flow", Journal of Fluid Mechanics, 41, 241-258 (1970).
16. Houdeville, R., Desopper, A. and Cousteix, J., "Experimental Analysis of Average and Turbulent Boundary Layer", ONERA TP, No. 30, also Rech. Aerosp. No. 1976-4 (1976).
17. Schachenmann, A. A. and Rockwell, D. A., "Oscillating Turbulent Flow in a Conical Diffuser", ASME Journal of Fluids Engineering, 98, 695-702 (1976).
18. Binder, G. and Didelle, H., "Improvement of Ejector Thrust Augmentation by Pulsating of Flapping Jets", 2nd Symposium on Jet Pumps and Ejectors and Gas Lift Techniques, Paper No. E2 (1975).
19. Acharya, M. and Reynolds, W. C., "Measurements and Predictions of a Fully Developed Turbulent Channel Flow with Imposed Controlled Oscillations", Stanford University, Thermosciences Division, Technical Report TF-8 (1975).
20. Townsend, A., The Structure of Turbulent Shear Flow, Cambridge Univ. Press (1956).
21. Phillips, D. M., The Dynamics of the Upper Ocean, Cambridge Univ. Press (1967).
22. Kovaszny, L. S. G., "Measurement in Intermittent and Periodic Flow", Proc. Dynamic Flow Conference 1978 on Dynamic Measurements in Unsteady Flows, 133-160 (1978).
23. Karlsson, S. K. F., "An Unsteady Turbulent Boundary Layer", Journal of Fluid Mechanics, 5, 622-636 (1959).
24. Cousteix, J., Desopper, A. and Houdeville, R., "Structure and Development of a Turbulent Boundary Layer in an Oscillatory External Flow", ONERA TP 14, 1977; also presented at the Symposium on Turbulent Shear Flows, Penn. State Univ., PA (April 1977).
25. Patel, M. H., "On Turbulent Boundary Layers in Oscillatory Flow", Proceedings of the Royal Society of London, A353, 121-144 (1977).
26. Charnay, G. and Melinand, J. P., "Investigation of the Intermittent Region of Steady or Unsteady Turbulent Boundary Layer", EUROVISC Symposium on Unsteady Turbulent Boundary Layers and Shear Flows (January 1977).
27. Cousteix, J., Houdeville, R. and Desopper, A., "Resultats Experimentaux et Methodes de Calcul Relatifs aux Couches Limites Turbulentes en Ecoulement Instationnaire", in Unsteady Aerodynamics, AGARD-CP-227, Ottawa (1977).
28. Simpson, R. L., "Features of Unsteady Turbulent Boundary Layers as Revealed from Experiments", in Unsteady Aerodynamics, AGARD-CP-227, Ottawa (1977).
29. Kenison, R. C., "An Experimental Study of the Effect of Oscillatory Flow on the Separation Region in a Turbulent Boundary Layer" in Unsteady Aerodynamics, AGARD-CP-227 (1977).
30. Tomsho, M. E. and Brown, F. T., "The Oscillating Turbulent Boundary Layer in a Conical Diffuser", in Nonsteady Fluid Dynamics, ed. D. E. Crow and J. A. Miller, ASME, 3-12 (1978).
31. Houdeville, R. and Cousteix, J., Premiers Resultats d' une Etude sur les Couches Limites Turbulentes En Ecoulement Pulse avec Gradient de Pression Moyen Defavorable", 15th Colloquium on Aerodynamic Applications, Marseille (1978).
32. Hayakawa, M., private communication.
33. Offen, G. R. and Kline, S. J., "Experiments on the Velocity Characteristics of "Bursts" on the Interactions between the Inner and Outer Regions of a Turbulent Boundary Layer", Stanford University, Report No. MD-31 (1973).
34. Thomas, L. C. and Shukla, R. K., "Theoretical and Experimental Study of Wall Region Periodicity for Turbulent Pulsatile Flow", ASME Journal of Fluids Engineering, 98, (1976).
35. Soutif, M. "Diffusion et Structure Périodique des Jets Battants", Doctoral Thesis, Université Scientifique et Médicale de Grenoble, Institut National Polytechnique de Grenoble (1977).
36. Favre-Marinet, M. and Binder, G., "Quelques Caracteristiques Instationnaires des Moments Turbulents dans un Jet Pulsant", EUROVISC Workshop on Unstead Flows, Orleans, France (1978).
37. Ramaprian, B. R., private communication.
38. Merkli, P. and Thomann, H., "Transition to Turbulence in Oscillating Pipe Flow", J. Fluid Mech., 68, 567-575 (1975).
39. Hino, M., Masaki, S. and Shuji, T., "Experiments on Transition to Turbulence in an Oscillatory Pipe Flow", J. Fluid Mech., 75, 193-207 (1976).
40. Davis, S. H., "The Stability of Time-Periodic Flows", Annual Reviews of Fluid Mechanics, Vol. 8, 57-74 (1976).
41. Loerke, R. I., Morkovin, M. V. and Fejer, A. A., "Review-Transition on Nonreversing Oscillating Boundary Layers", J. Fluids Eng., 534-549 (1975).

42. Miller, J. A. and Fejer, A. A., "Transition Phenomena in Oscillating Boundary Layer Flows", J. Fluid Mech., 18, 438-449 (1964).
43. Emmons, H. W., "The Laminar-Turbulent Transition in a Boundary Layer", Part I, J. Aerospace Sci., 18, 490-503 (1951).
44. Schubauer, G. B. and Klebanoff, P. S., "Contribution on the Mechanics of Boundary-Layer Transition", NACA TR No. 1289 (1956).
45. Obremski, H. J. and Fejer, A. A., "Transition in Oscillating Boundary Layer Flows", J. Fluid Mech., 29, 93-111 (1967).
46. Kobashi, Y., Hayakawa, M. and Nakagawa, K., "Development of Disturbances in Unsteady Boundary Layers" in Unsteady Aerodynamics, ed. R. B. Kinney, University of Arizona, 2, 131-154 (1975).
47. Kobashi, Y. and Hayakawa, M., "Development of Turbulence Through Non-Steady Boundary Layer", in Structure and Mechanisms of Turbulence I, Lecture Notes in Physics, ed. H. Fieker, 75, 277-288 (1978).
48. Cousteix, J., Houdeville, R. and Desopper, A., "Transition d'une Couche Limite Soumise a une Oscillation de l'Écoulement Extérieur" Contributed to the AGARD Symposium on Laminar-Turbulent Transition, (May 1977).
49. Williams, J. C., "Incompressible Boundary-Layer Separation", in Annual Review of Fluid Mechanics eds. M. VanDyke, J. V. Wehausen, J. L. Lumley, 9, 113-144 (1977).
50. Shen, S. F., "Unsteady Separation According to the Boundary-Layer Equation" in Advances in Applied Mechanics, 18, 177-220 (1978).
51. Despard, R. A. and Miller, J. A., "Separation of Oscillating Boundary-Layer Flows", Journal of Fluid Mechanics, 47, 21-31 (1971).
52. Carr, L. W., McAlister, K. W. and McCroskey, W. J., "Analysis of the Development of Dynamic Stall Based on Oscillating Airfoil Experiments", NASA TN D-8382 (1977).
53. Koromilas, C. A. and Telionis, D. P., "Unsteady Laminar Separation: An Experimental Study", J. Fluid Mech.
54. Mezaris, T. B. and Telionis, D. P., "Visualization and Measurement of Separating Oscillatory Laminar Flow", AIAA Paper No 80-1420 (1980)
55. Taneja, S., "Visual Study of Unsteady Separated Flows Around Bodies", Prog. Aerospace Sci., 17, 237-348 (1977).
56. Sandborn, V. A. and Liu, C. Y., "On Turbulent Boundary-Layer Separation", J. Fluid Mech., 32, 293-304 (1968).

METHODS FOR INVISCID SUBSONIC FLOWS ABOUT UNSTEADY AEROFOILS

by

G. J. Hancock  
Dept. Aeronautical Engineering  
Queen Mary College  
University of London U.K.

R. Doe  
British Aerospace  
Filton Division  
Bristol U.K.

1. INTRODUCTION

This paper is intended to catalogue some of the numerical approaches which have been developed for subsonic flows about two dimensional aerofoils. Such solutions are useful in their own right, for aerofoil results are often used in strip theory approaches in early design stages, but primarily these methods lay down the language and framework for applications in three dimensions, to be described in later papers. In this paper the flow is assumed to be attached, the boundary layer effects are neglected so the inviscid equations are taken.

Although the distinction is artificial, if not misleading, this paper treats the case of incompressible fluid flow first, and then secondly introduces the effects of compressibility.

2. METHODS FOR INCOMPRESSIBLE FLUID MOTIONS

With incompressible fluids the velocity field equations separate from the pressure field equations, considerably simplifying the problem. Assuming inviscid flow, the basic equation is, taking fixed axes,

$$\nabla^2 \phi = \frac{\partial^2 \phi}{\partial x^2} + \frac{\partial^2 \phi}{\partial z^2} = 0 \quad (1)$$

where  $\phi$  is the perturbation velocity potential superimposed on a uniform free stream  $U$ ; the perturbation velocity components are

$$u = \frac{\partial \phi}{\partial x} \quad w = \frac{\partial \phi}{\partial z} \quad (2)$$

so  $u, w$  tend to zero as  $r$  tends to infinity. The static pressure  $P$  is then given by

$$P + \frac{1}{2} \rho [(U+u)^2 + w^2] + \rho \frac{\partial \phi}{\partial t} = P_\infty + \frac{1}{2} \rho U^2 + \rho \left( \frac{\partial \phi}{\partial t} \right)_{t \rightarrow \infty} \quad (3)$$

All methods for solution are made up from the superposition of singularity distributions. The basic singularity solutions of eqns. (1) are:

source	$\phi_s = \frac{\sigma}{2\pi} \ln r$	
doublet with axis in $z$ direction	$\phi_D = \frac{\mu}{2\pi} \frac{z}{z^2 + z'^2} = \frac{\Lambda}{2\pi} \frac{\cos \theta}{r}$	(4)
vortex	$\phi_V = \frac{\Gamma \theta}{2\pi}$	

Consider an aerofoil at incidence  $\alpha$  in stream of resultant velocity  $U$ .  
If the profile of a stationary aerofoil is given by

$$\left. \begin{aligned} z_s = \int_u(x_s) &= \int_c(x_s) + \int_t(x_s)/2 \\ &= \int_l(x_s) = \int_c(x_s) - \int_t(x_s)/2 \end{aligned} \right\} \quad (5)$$

on upper and lower surfaces, where suffices  $c$  and  $t$  refer to camber and thickness respectively and  $x_s$  is measured from aerofoil leading edge. For an arbitrary motion

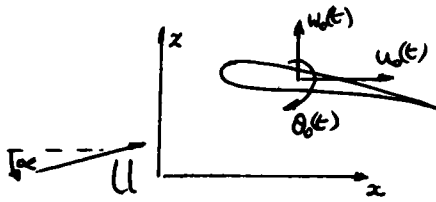


FIG. 1.

of the aerofoil defined by  $u_0(t)$  in the  $x$  direction,  $w_0(t)$  in  $z$  direction and pitch rotation  $\theta_0(t)$  about the chordwise location  $\bar{x}$  then the point  $(x_2, z_2)$  on the profile becomes  $(X, Z)$  where

$$\begin{aligned} X(x_2, t) &= \int_0^t u_0(t') dt' + (c_2 - \bar{x}) \cos \theta_0(t) + z_2 \sin \theta_0(t) \\ Z(x_2, t) &= \int_0^t w_0(t') dt' + z_2 \cos \theta_0(t) - (c_2 - \bar{x}) \sin \theta_0(t) \end{aligned} \quad (6)$$

the boundary condition of adjacent flow becomes

$$\frac{w(X, Z) - [w_0(t) - (c_2 - \bar{x}) \dot{\theta}_0(t)] + U \sin \alpha}{U \cos \alpha + u(X, Z) - [u_0(t) + z_2 \dot{\theta}_0(t)]} = \frac{\partial Z / \partial x_2}{\partial X / \partial x_2} \quad (7)$$

At the trailing edge a Kutta condition holds, so a time varying circulation will be set up about the aerofoil which in turn causes vorticity to shed and be convected downstream. At the trailing edge the flow velocities must be finite and the loading (i.e. pressure difference) must be zero. Downstream of the trailing edge there must be zero loading across the shed vorticity.

### 2.1 Steady Thin Aerofoil Theory

Linearised theory assumes that velocity perturbations are small compared with free stream, that thickness effects (i.e. symmetric part of the solution) are superimposable on camber and incidence (i.e. antisymmetric or lifting part of the solution).

For the lifting problem, according to linearised theory, singularities are placed on the  $x$  axis (i.e.  $z=0$ ,  $0 \leq x \leq c$ ) and the linearised form of the boundary condition of eqn. (7) is satisfied along the same line. Thus

$$U \left( \alpha - \frac{df_c}{dx} \right) = \int_0^c \frac{\gamma(\xi) d\xi}{2\pi(x-\xi)} \equiv \int_0^c \frac{\mu'(\xi) d\xi}{2\pi(x-\xi)} \equiv \int_0^c \frac{\Delta p(\xi) d\xi}{2\pi\rho U(x-\xi)} \quad (8)$$

where  $\gamma(\xi)$  represents a distribution of vorticity,  $\mu'(\xi)$  represents a distribution of doublets, and  $\Delta p(\xi)$  represents the loading (i.e. difference of pressure between lower and upper surfaces). The camber profile  $f_c(x)$  can include the deflection of a trailing edge control surface.

In eqn. (8)  $\mu'(\xi)$  can be regarded as  $(-\Delta\phi(\xi))$  the discontinuity in  $\phi$  across  $z=0$ , and so  $\mu'(\xi) (= \gamma(\xi))$  is equivalent to  $(-\Delta(\partial\phi/\partial\xi))$ . Note  $\Delta = \text{lower} - \text{upper}$ .

To obtain a unique solution of eqn. (8) the Kutta condition must be applied. In this case it is

$$\gamma(c) = \mu'(c) = \Delta p(c) = 0 \quad (9)$$

Listed below are some standard techniques of solution; all are collocation techniques, the unknown function  $\gamma(x)$  is expressed in terms of a finite number of arbitrary constants, eqn. (8) is then satisfied at a discrete number of (collocation) points along the chord; the number of collocation points is the same as the number of arbitrary constants and the locations of the collocation points are chosen to give an optimum solution.

(i) Superposition of continuous loadings<sup>(1)</sup>; assume

$$\gamma(x) \left\{ \text{or } \mu'(x) \text{ or } \Delta p(x) \right\} = \left( \frac{c-x}{x} \right)^{1/2} \sum_{I=1}^N A_I \gamma_I(x) \quad (10)$$

where  $\gamma_I(x)$  are orthogonal polynomials with respect to  $\left( \frac{c-x}{x} \right)^{1/2}$ . The assumed expression for  $\gamma(x)$  satisfies the correct form at the leading and trailing edges. Essentially

$$\gamma_I(\theta) = \sqrt{\frac{2}{\pi}} \frac{\cos(\frac{I+1/2}{2}\theta)}{\cos \frac{\theta}{2}} \quad \text{where } \frac{x}{c} = \frac{1 - \cos \theta}{2} \quad (11)$$

and the collocation points chosen to give the most accurate answer are located at

$$x(J) = \frac{c}{2} \left( 1 - \cos \left( \frac{2J-1}{2N+1} \pi \right) \right) \quad (12)$$

With control surfaces eqn. (10) can be extended to include the appropriate singular behaviour at the hinge line.

(ii) Superposition of piecewise linear functions; divide chord into N elements then assume

$$\gamma(x) = \gamma(I) + \left( \frac{x - x(I)}{x(I+1) - x(I)} \right) (\gamma(I+1) - \gamma(I)) \quad x(I) < x < x(I+1), I=1, N \quad (13)$$

where  $\gamma(I)$ ,  $I=1, N+1$  are unknown constants. To satisfy the Kutta condition  $\gamma(1/N)$  is zero, leaving N unknowns. And the N collocation points are (usually) chosen at mid-points of elements.

Substitution of eqn. (13) into eqn. (8) leads to simple analytic integrals which lead directly to the appropriate influence coefficients.

Method is reasonably accurate especially if non-uniform elements are taken with small elements concentrated about the nose and tail, or around the hinge line of control surfaces.

(iii) Standard vortex lattice method<sup>(2)</sup>; divide chord into uniform elements, assume that loading on each element can be represented by Dirac delta function placed at 1/4 (element length) from the leading edge of element, i.e.

$$\gamma(x) = \sum_{I=1}^N \gamma(I) \delta \left( x - \frac{c}{N} [(I-1) + 0.25] \right) \quad I=1, N \quad (14)$$

Collocation points  $x(J)$  are taken at 3/4 (element length) from leading edge of element, i.e.

$$x(J) = \frac{c}{N} [(J-1) + 0.75] \quad (15)$$

Substitution of eqn. (14) into eqn. (8) leads to trivial integration to give matrix of influence coefficients  $A(J, I)$  where

$$A(J, I) = \left[ 2\pi \frac{c}{N} (J - I + 0.50) \right]^{-1} \quad (16)$$

When  $f_c(x)$  is zero this method gives exact values for  $C_L$  and  $C_m$  for any number of elements, even when  $N=1$ . When  $f_c(x)$  is not zero a reasonable number of elements are required for acceptable accuracy.

For a trailing edge control surface the above method can be applied but the tangency flow condition in the element containing the control surface hinge line should be smoothed out over the element before taking the appropriate conditions at the collocation point.

(iv) Modified vortex lattice method due to Lan<sup>(3)</sup>, who shows that for the locations

$$\begin{aligned} x(I) &= \frac{1}{2} \left[ 1 - \cos \left( \frac{2I-1}{2N} \pi \right) \right] \\ x(J) &= \frac{1}{2} \left[ 1 - \cos \frac{J\pi}{N} \right] \end{aligned} \quad (17)$$

eqn. (8) can be integrated by trapezoidal rule

$$\left( \alpha - \frac{\partial f}{\partial x} \right)_{x=x(J)} = \frac{1}{2N} \sum_{I=1}^N \gamma(I) \frac{[x(I)(1-x(I))]^{1/2}}{x(J) - x(I)} \quad I=1, N \quad (18)$$

Furthermore the leading edge thrust is given by

$$\frac{\pi \rho}{4} \left[ \frac{U \left( u - \frac{d\Gamma}{dx} \right)_{x=0}}{N} + \frac{1}{2N^2} \sum_{I=1}^N \gamma(I) \left( \frac{1-x(I)}{x(I)} \right)^{1/2} \right]^2 \quad (19)$$

For  $N \geq 2$  and  $\gamma_c(x)$  equal to zero the values of  $\gamma(I)$ ,  $C_L$ ,  $C_M$  and leading edge thrust coefficient are exact.

There are solutions of eqns. (8)<sup>(4,5)</sup> which are not strictly collocation solutions but solutions based on variational principles. From a numerical analysis viewpoint all numerical solutions of eqn. (8) can be interrelated.

Perhaps it is pertinent to point out at this point an aspect of terminology; in structures, finite element methods are always via variational procedures whereas in aerodynamics finite element methods are invariably collocation methods.

## 2.2 Unsteady Thin Aerofoil Theory

On linearisation the unsteady lifting problem can be simply superimposed on the steady thickness and lifting problems; again with the linearisation approximations the singularity distribution and the boundary conditions are all placed on the  $x$  axis. Thus taking the linearised form of the boundary condition of eqn. (7), taking  $u_0(t)$  to be zero and extracting the steady condition, then

$$\begin{aligned} [-w(x, 0, t)] &= -w_0(t) + (x - \bar{x}) \dot{\theta}_0(t) + U \theta_0(t) \\ &= \int_0^{\infty} \frac{\gamma(\xi, t) d\xi}{2\pi(x - \xi)} \end{aligned} \quad (20)$$

Now, from Bernoulli's equation,

$$\Delta p(x, t) = -\rho U \left( \frac{d(\Delta \phi)}{dx} \right) - \rho \frac{\partial \Delta \phi}{\partial t} = \rho U \gamma(x, t) + \rho \int_0^x \frac{\partial \gamma(x', t)}{\partial t} dx' \quad (21)$$

Across the wake  $\Delta p$  is zero, hence for  $x > c$

$$\gamma(x, t) = \gamma(c, t - \frac{(x-c)}{U}) \quad (22)$$

Thus the basic equation to be solved for a motion commencing at  $t = 0$ , is

$$-w(x, 0, t) = \int_0^c \frac{\gamma(\xi, t) d\xi}{2\pi(x - \xi)} + \int_c^{c+Ut} \frac{\gamma(c, t - \frac{(\xi-c)}{U})}{2\pi(x - \xi)} d\xi \quad 0 \leq x \leq c; t > 0 \quad (23)$$

subject to the Kutta condition

$$U \gamma(c, t) + \frac{d}{dt} \int_0^c \gamma(x, t) dx = 0 \quad (24)$$

And where the loading is then given by eqn. (21).

Eqn. (23) can be solved by extending the methods of solution for the steady problem (listed (i)-(iv) in Section 2.1), solving eqn. (23) at successive intervals of time.

In particular:

- (i) the representation of  $\gamma(\xi, t)$  by piecewise linear distributions in  $N$  chordwise elements is numerically straightforward; the steady influence coefficient matrix still applies (for the first integral of eqn. (23)) while the integration of the second integral is direct based on values of  $\gamma(c)$  determined at earlier times;
- (ii) the vortex lattice method can be generalised; denoting the discrete bound vortex at station  $\xi(I)$ , and time  $t_n$ , as  $\Gamma_n(I)$ ; then taking the increments of time interval as  $(c/UN)$  (i.e. the time taken for the free stream to pass the length of one element) each bound vortex has a 'wake' of shed discrete vortices located at 1/4 point of each downstream element, both on the aerofoil chord and aft of the aerofoil as shown in Fig. 2.

$$\Gamma_n(\xi) \quad \left\{ \Gamma_{n-1}(\xi) - \Gamma_n(\xi) \right\} \quad \left\{ \Gamma_n(\xi) - \Gamma_{n-1}(\xi) \right\}$$

FIG 2

For oscillatory motions the problem simplifies. Taking

$$\gamma(\xi, t) = \bar{\gamma}(\xi) e^{i\omega t}, \quad w(x, 0, t) = \bar{w}(x) e^{i\omega t}, \quad \Delta p(\xi, t) = \bar{\Delta p}(\xi) e^{i\omega t}$$

then

$$-\bar{w}(x) = \int_0^c \frac{\bar{\gamma}(\xi) d\xi}{2\pi(x-\xi)} + \bar{\gamma}(c) \int_c^\infty \frac{e^{-i\omega(x-\xi)/U} d\xi}{2\pi(x-\xi)} \quad (25)$$

subject to the Kutta trailing edge condition of zero loading

$$U \bar{\gamma}(c) + i\omega \int_0^c \bar{\gamma}(x) dx = 0 \quad (26)$$

The integral from  $c$  to  $\infty$  on right hand side of eqn. (25) can be reduced to standard Si and Ci functions.

Now, from eqn. (21),

$$\bar{\Delta p}(x) = \rho U \bar{\gamma}(x) + \rho i\omega \int_0^x \bar{\gamma}(x') dx' \quad (27)$$

thus

$$\rho U \bar{\gamma}(x) = \bar{\Delta p}(x) - \frac{i\omega}{U} \int_0^x e^{-i\omega(x-\xi)/U} \bar{\Delta p}(\xi) d\xi \quad (28)$$

Hence eqn. (25) can be written in the form

$$-\bar{w}(x) = \int_0^c \frac{\bar{\Delta p}(\xi)}{\rho U} K(x, \xi, i\omega) d\xi \quad (29)$$

where  $K(x, \xi, i\omega)$  is the Kernel function given by

$$K(x, \xi, i\omega) = \frac{1}{2\pi(x-\xi)} - \frac{i\omega}{U} \int_{\xi'}^{\xi} \frac{e^{-i\omega(\xi'-\xi)/U} d\xi'}{2\pi(x-\xi')} \quad (30)$$

The various methods listed for the steady solutions in Section 2.1 can be extended to the oscillatory case.

- (i) Superposition of continuous modes for  $\bar{\Delta p}(\xi)$ , applied to eqn. (29); the same modes are chosen as those given by eqn. (10); the integration of the influence coefficients needs to be done numerically;
- (ii) Assumption of piecewise linear variation in elements; if eqn. (25) is to be solved, the influence coefficients derived for the steady case can be applied directly to the oscillatory case; if eqn. (29) is to be solved, the integrations are not so straightforward.
- (iii) Unsteady vortex lattice method is the representation of the aerofoil vorticity and wake vorticity in terms of discrete vortices; for each bound vortex at the 1/4 point of each element there is a wake of vortices, applying the arrangement of vortices as shown in Fig. 2 to the oscillatory case;
- (iv) Vortex doublet method assumes that  $\bar{\Delta p}(\xi)$  is represented by discrete Dirac delta functions, i.e.



$$\bar{\Delta p}(\xi) = \sum_{I=1}^N \Delta p(I) \delta(\xi - \xi(I)) ; \quad \xi(I) = \frac{c}{N} ((I-1) + 0.25), \quad I=1, N \quad (31)$$

which when substituted into eqn.(29) gives

$$\{-\bar{w}(x(\eta))\} = [K(x(\eta), \xi(I), \omega)] \left\{ \frac{\bar{\Delta p}(I)}{\rho U} \right\} \quad x(\eta) = \frac{c}{N} ((\eta-1) + 0.75), \quad \eta=1, N \quad (32)$$

In this case the Kernel function can be evaluated in terms of  $S_i$  and  $C_i$  functions.

### 2.3 Steady Thick Aerofoil Solutions

The problem is to solve the perturbation velocity potential equation

$$\nabla^2 \phi = 0 \quad (33)$$

subject to the adjacent flow boundary condition

$$\left( U \sin \alpha + \frac{\partial \phi}{\partial z} \right)_{x=x_s} = \left( U \cos \alpha + \frac{\partial \phi}{\partial x} \right) \frac{\partial f}{\partial x} \Big|_{x=x_s} \quad (34)$$

$$z = f(x_s) \quad z = f(x_s)$$

Again a Kutta condition at the trailing edge is required.

Essentially singularities are distributed over the aerofoil profile and the condition of tangential flow, eqn. (34), satisfied at discrete points on that profile. Different combinations of source and vorticity (i.e. doublet) distributions can be taken.

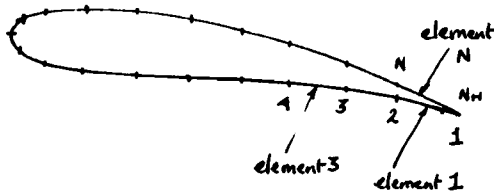


FIG. 3

The standard numerical approach is associated with A.M.O. Smith and his co-workers<sup>(6)</sup>. A variant of the method is shown in Fig. 3. The profile is divided into  $N$  elements; on each element is placed a uniform source distribution  $\sigma(I)$ ,  $I=1, N$  which varies from element to element, and a uniform vorticity distribution  $\gamma$  which is the same for all elements. Thus there are  $N+1$  unknowns; there are  $N$  linear equations of tangential flow (i.e. eqn. (34)) which are satisfied at the mid-point of each element and the Kutta condition

usually taken to be equal pressures at the mid-point of the trailing edge elements 1 and  $N$ . Alternative forms of the Kutta condition have been taken, e.g. that the flow leaving the trailing edge follows a bisector of the trailing edge angle.

There are improved versions of the above A.M.O. Smith method incorporating polynomial variations in the source distributions in the elements.

The A.M.O. Smith method gives reasonable results but loses accuracy for thick highly cambered aerofoils and the method tends to break down as the thickness of the aerofoil becomes small.

Alternatively singularities can be placed along the mean camber surface<sup>(7)</sup>. Such an approach is powerful, and recommended; for comparable accuracy with the standard A.M.O. Smith method, the number of elements can be reduced; furthermore the answers are not sensitive to the location of collocation points on the surface. Interior singularity distributions can be applied to thin aerofoils.

### 2.4 Unsteady Thick Aerofoil Solutions

The problem is now the full problem initially postulated, solving the Laplace differential equation, eqn. (1), for the velocity potential  $\phi$  to satisfy the boundary condition expressed by eqn.(7). The A.M.O. Smith has been extended to this unsteady motion.

There are three approaches depending on the degree and type of unsteadiness.

If the unsteady perturbations are small about some mean state (e.g. small amplitude oscillations about a mean state), then following the A.M.O. Smith technique a uniform steady and uniform oscillatory source distribution are assumed on each element  $(\sigma_s(\Gamma), \sigma_o(\Gamma)e^{i\omega t}, \Gamma=1, N)$  the strength varying from element to element, and a uniform steady and oscillatory vorticity distribution  $(\gamma_s, \gamma_o e^{i\omega t})$  which are the same for each element. A known distribution of shed vorticity is placed along the mean streamline emanating from the trailing edge; the steady and oscillatory boundary conditions are satisfied at the mid-point of each element. The oscillatory equations involve the steady solution and so there is coupling between the steady and oscillatory solutions. There is some ambiguity in the application of the Kutta condition. Only one condition is required to make the oscillatory solution unique. One solution is obtained by making the velocities at the trailing edge finite; another solution is obtained making the loading at the trailing edge zero; the difference between these two solutions arises mainly in the neighbourhood of the trailing edge. Results of this approach are given in reference 8.

An extension of the above approach when the aerofoil is again oscillating with small amplitude about some steady state, is to place all of the singularities on the steady profile, but expressing the boundary conditions on the steady profile in terms of a Taylor expansion from the boundary conditions on the actual displaced surface. Such an approach would be consistent with the inclusion of a boundary layer calculation using the so-called surface transpiration boundary condition to estimate the outer inviscid flow.

The third approach is for the general unsteady motion. At any instant of time a source distribution and uniform vorticity distribution can be placed on the instantaneous profile. The modelling of the wake needs care especially if both conditions of finite velocity and zero loading are to be satisfied (and lead to the accuracy of the numerical modelling). Giesing<sup>(9)</sup> modelled the wake by discrete (convecting) vortices but only satisfied the trailing edge condition of finite velocities; Basu and Hancock<sup>(10)</sup> again modelled the main wake by discrete vortices except for the wake just downstream of the trailing edge, there the wake was represented by an element of uniform vorticity but the element length and its direction were estimated as part of the calculation to ensure both finite velocities and continuity of the zero loading condition from the trailing edge of the aerofoil into the immediate wake.

### 3. EFFECTS OF COMPRESSIBILITY

At speeds below the critical Mach number, the flow outside of the boundary layer remains isentropic and irrotational and a perturbation velocity potential  $\phi$  exists. Compressibility causes the differential equation for  $\phi$  to become non-linear. If however second order terms are neglected then the standard linearised form emerges,

namely

$$\beta_{\infty}^2 \frac{\partial^2 \phi}{\partial x^2} + \frac{\partial^2 \phi}{\partial z^2} - \frac{2M_{\infty}^2}{a_{\infty}} \frac{\partial \phi}{\partial x \partial t} - \frac{1}{a_{\infty}^2} \frac{\partial^2 \phi}{\partial t^2} = 0 \quad (35)$$

where the coefficient of  $\partial^2 \phi / \partial x^2$ , namely  $\beta_{\infty}^2 = (1 - M_{\infty}^2)^4$  is valid as long as

$$M_{\infty}^2 \frac{\partial \phi / \partial x}{U} \ll \frac{\beta_{\infty}^2}{(3 - 2(1 - \gamma) M_{\infty}^2)}; \quad (36)$$

there are slightly different versions depending on how the linearised eqn. (35) is derived. Eqn. (36) indicates how close to the transonic regime eqn. (35) can be applied before eqn. (35) becomes invalid.

Compatible with eqn. (35) there are first order expressions for pressure and density, namely

$$p - p_{\infty} \approx -\rho U \frac{\partial \phi}{\partial x} - \rho \frac{\partial \phi}{\partial t} \quad (37)$$

$$\rho - \rho_{\infty} \frac{p - p_{\infty}}{a_{\infty}^2} \approx \rho_{\infty} \left( -M_{\infty}^2 \frac{\partial \phi}{\partial x} - \frac{\partial \phi}{\partial t} \right) \quad (38)$$

It should be recognised that a first order variation in density exists, this fact can cause difficulties not so much in the calculation of linearised lift distributions as in the calculation of induced drag which is a second order quantity<sup>(11)</sup>.

### 3.1 Steady Motions

For the steady lifting problem the basic equation is for the perturbation velocity potential

$$\beta_{\infty}^2 \frac{\partial^2 \phi}{\partial x^2} + \frac{\partial^2 \phi}{\partial z^2} = 0 \quad (39)$$

The consistent boundary condition is the linearised boundary condition (i.e. linearised to the same extent as eqn. (39)) applied on the plane  $x=0$ ,

$$\frac{\partial \phi}{\partial x} \Big|_{x=0} = -U \left( \alpha - \frac{d f_c}{dz} \right) \quad 0 < z < c \quad (40)$$

The solution of eqn. (39) satisfying eqn. (40) is obtained by a trivial transformation to an incompressible problem.

However it is fairly common for solutions to be obtained to eqn. (39) satisfying boundary conditions of tangential flow on a thick aerofoil profile. Such a solution is not altogether satisfactory because of the inconsistencies in level of approximation between the basic differential equation and the boundary conditions. In fact there are two possible boundary conditions. One boundary condition is to take the velocity component normal to the aerofoil surface equal to zero, the other boundary condition is to take a linearised form of the component of mass flow normal to the aerofoil surface equal to zero, taking into account the variation in density; these two boundary conditions differ somewhat especially around the nose region. For the thick profile eqn. (39) can be solved either by transformation to an incompressible problem with a transpiration boundary condition on the transformed profile, or directly by superposition of 'compressible source and vorticity' distributions (these are of interest in that a 'compressible vorticity' distribution, i.e. one which satisfies eqn. (3), at a general angle of inclination to the  $x$  axis induces both circulatory and source-like motions.

### 3.2 Oscillatory Motions

The problem is to solve the unsteady eqn. (35) subject to a boundary condition such as

$$[-\bar{w}(x) e^{i\omega t}] = [(1 + i\omega(x-x_0))] \bar{\theta} e^{i\omega t} \quad (41)$$

for an aerofoil pitching in simple harmonic motion with amplitude  $\bar{\theta}$  about an axis located at  $x=x_0$ .

The basic linearised solution then follows directly from the earlier lecture 'Some Features of Linear Compressibility' combining eqns. (37, 39) from that lecture to give

$$\bar{w}(x) = \frac{\beta_{\infty}}{2\kappa} \int_0^{\infty} \frac{d\xi}{\xi-x} \frac{d}{d\xi} \left\{ -\mu(\xi) e^{-\frac{iM_{\infty}\omega(\xi-x)}{\alpha_{\infty}\beta_{\infty}^2}} \frac{1}{2} i H_1^{(0)} \left( \frac{\omega(x-\xi)}{\beta_{\infty}^2 \alpha_{\infty}} \right) \left( \frac{\omega(x-\xi)}{\beta_{\infty}^2 \alpha_{\infty}} \right) \right\} \quad (42)$$

The doublet distribution  $d\mu/d\xi$  is simply related to the loading distribution via eqn. (28). Substitution into eqn. (42) leads to the standard Possio equation.

$$\left( \frac{-\bar{w}(x)}{U} \right) = \int_0^1 \frac{\Delta p(\xi')}{\rho U^2} K(x-\xi', \gamma, M_{\infty}) d\xi' \quad \xi' = \frac{\xi}{c}, x' = \frac{x}{c}, \gamma = \frac{\omega c}{U} \quad (43)$$

where

$$K(\xi, \gamma, M_{\infty}) = e^{-i\gamma\xi} \left[ e^{i\gamma\xi} \left\{ \frac{i\gamma M_{\infty} \xi}{4\beta_{\infty} |\xi|} H_1^{(0)} \left( \frac{\gamma M_{\infty} |\xi|}{\beta_{\infty}^2} \right) - \frac{\gamma}{4\beta_{\infty}} H_0^{(0)} \left( \frac{\gamma M_{\infty} |\xi|}{\beta_{\infty}^2} \right) \right\} \right. \\ \left. + \frac{i\gamma}{2\kappa} \ln \left( \frac{1+\beta_{\infty}}{M_{\infty}} \right) + \frac{i\gamma\beta_{\infty}}{4} \int_0^{\gamma\xi/\beta_{\infty}^2} e^{iu} H_0^{(0)}(\gamma M_{\infty} |u|) du \right]$$

Numerical methods of solution again follow those outlined previously

- (i) Eqn. (42) has been solved, assuming linear piecewise variation for in each chordwise element, satisfying the appropriate Kutta condition.
- (ii) Eqn. (43) has been solved by superposition of continuous modes for  $(\Delta p(x)/\rho U^2)$
- (iii) Eqn. (43) has been solved by representing  $(\Delta p(x)/\rho U^2)$  by a number of discrete Dirac delta functions at the 1/4 point of chordwise elements (i.e. vortex doublet method).

### 3.3 Arbitrary Motions

For arbitrary motions the basic equations are essentially evaluated in the lecture 'Some Features of Linear Compressibility' simply modifying eqn. (32) (in that lecture) to account for the free stream according to eqn. (49) (in that paper) leading to an equation similar to eqn. (36) (in that paper). Little numerical work appears to have been done on general arbitrary motions although a fair amount was done on indicial functions some time ago<sup>(11)</sup>:

REFERENCES

1. (i) H.Multhopp                           Methods for Calculating the Lift Distribution of Wings.  
ARC R & M 2884, 1950.  
     (ii) D.E. Davies                       Calculation of Unsteady Generalised Air Force on a  
Thin Wing Oscillating Harmonically in Subsonic Flow.  
ARC R & M 3409, 1965.
2. R.M. James                              On the Remarkable Accuracy of the Vortex Lattice  
Discretization in Thin Wing Theory.  
Rept. DAC 67211, Feb.1969, Douglas A/C Corp., California.
3. C.E. Lan                                A Quasi Vortex Lattice Method in Thin Wing Theory.  
Journal Aircraft, September 1974.
4. D.E. Davies                             An Application of Flax's Variational Principle to  
Lifting Surface Theory.   ARC R & M 3564.
5. R. D. Milne &                          Application of Projection Methods to Linearised Unsteady  
Sheikh Niaz                               Lifting Surface Theory. Ph. D. Thesis, Queen Mary  
College, University of London, 1971
6. Hess J.L. & Smith A.M.O.              Calculation of Potential Flow about Arbitrary Bodies.  
Progress in Aero. Sciences 8,1. 1967.
7. B.C. Basu                               A Mean Camberline Singularity Method for Two Dimensional  
Steady and Oscillatory Aerofoils and Control Surfaces  
in Inviscid Incompressible Flow.  
ARC Current Paper 1391, 1978.
8. B.C. Basu & G.J. Hancock            Two Dimensional Aerofoils and Control Surfaces in Simple  
Harmonic Motion in Incompressible Inviscid Flow.  
ARC Current Paper 1392, 1978.
9. Giesing J.P.                            Non-Linear Two Dimensional Unsteady Potential Flow with  
Lift.   Journ. Aircraft 5(2), 1968.
10. B.C. Basu & G.J. Hancock            Unsteady Motion of a Two Dimensional Aerofoil in  
Incompressible Inviscid Flow.  
Journ. Fluid Mechanics Vol.81, part 1, 1978.
11. G.J. Hancock & H.C. Garner        On the Application of Subsonic Linearised Wing Theory  
to Second Order Forces and Moments.  
ARC R & M 3758.
12. H. Lomax                                Indicial Aerodynamics.            Manual on Aeroelasticity,  
Part II, Chapter 6.

## ANALYTICAL METHODS FOR PREDICTION OF UNSTEADY LAMINAR BOUNDARY LAYERS

by

D. P. Telionis  
Virginia Polytechnic Institute and State University  
Blacksburg, Virginia 24061

Oscillatory boundary layers have been investigated at first via asymptotic expansions in terms of small parameters like the amplitude or the frequency of oscillation. The pioneering work of Lighthill, Moore, Lin and others is reviewed and subsequent more sophisticated expansions are described. In the last decade a large number of numerical investigations have appeared. Explicit, implicit methods as well as the well known box-method are described and their relative performance is evaluated. Typical examples are compared with classical experimental data. The definition of unsteady separation and criteria for its prediction have generated a lot of interest in the last decade. Analytical methods will be discussed for the prediction of unsteady separation. There is still some disagreement on this point with respect to the appearance of the separation singularity. The arguments of both points of view will be presented.

## 1. INTRODUCTION

For many decades, the analytical investigation of fluid mechanics was essentially a mathematical exercise with no significance whatsoever to practical applications and engineering. In fact, at that time most design engineers were not even aware of the results of potential theory, the theory of sound, etc. More careful theoretical modeling and in particular the development of boundary layer theory at the turn of our century have allowed the theoretician to consider more realistic problems. For many more decades to go, analytical investigations had rather academic character.

The need for convergence between experiment, practice and theory was at that time becoming obvious. Indeed, the development of boundary-layer theory has helped to decipher many of the peculiar effects of viscous flows, and essentially contributed in the education of generations of experimentalists and practical engineers. Still, and until very recently, the mathematical tools have prohibited theoreticians from calculating realistic flows immediately applicable in practice. Only in the last decade or two it became clear that modern computing machines can be used to calculate complicated flow fields, perhaps replace the wind tunnel with numerical experiments and become an important tool in design.

A breakthrough in the theoretical investigation of complex models like the Navier-Stokes equations was the development of asymptotic methods. Rayleigh's<sup>1</sup> and Prandtl's<sup>2</sup> pioneering works represent early versions of perturbation methods. Such methods have been used extensively since then and most recently were formalized into theories.<sup>3,4,5</sup> Perturbation methods have also proved invaluable tools in numerical analysis. They provide simple test cases for comparison, they are available to explain the sometimes erratic behavior or the computational results and usually provide data in such regions where numerical calculations are prohibitive. Finally, perturbation methods have been used quite extensively in combination with numerical methods.

The first part of this paper contains a short description of perturbation methods used in the development of unsteady boundary layer theory. This is followed by basic concepts in the application of numerical methods to unsteady viscous flow problems. A very interesting and novel approach of calculation based on a Lagrangian formulation is also briefly outlined. Finally, in the conclusions, some general comments are included and in particular, the results of many recent developments in the theory of unsteady separation are discussed.

This paper is only a short outline of material which has been extensively reviewed very recently. For the sake of brevity it was even decided to omit in most cases the explicit expression of initial and boundary conditions. The reader is referred to Refs. 6-17 for a more detailed description of different topics and a more complete list of references. A monograph on the same subject is also about to appear.<sup>18</sup>

## 2. ASYMPTOTIC THEORIES

There are two basic methods of perturbations by expansion in fluid mechanics: coordinate expansions and parameter expansions. The first is perhaps more common in the early developments but the second appears to have gained the trust of many investigators and has essentially dominated the field in recent years.

A typical example of a parameter expansion and historically the most significant is nothing else but boundary-layer theory. The boundary layer equations

$$\frac{\partial u^*}{\partial x^*} + \frac{\partial v^*}{\partial y^*} = 0 \quad (1)$$

$$\frac{\partial u^*}{\partial t^*} + u^* \frac{\partial u^*}{\partial x^*} + v^* \frac{\partial u^*}{\partial y^*} = \frac{\partial U_e^*}{\partial t^*} + U_e^* \frac{\partial U_e^*}{\partial x^*} + \nu \frac{\partial^2 u^*}{\partial y^{*2}} \quad (2)$$

can be considered as the approximate form of the Navier-Stokes equations in regions next to solid boundaries. In Eqs. (1) and (2)  $u^*$ ,  $v^*$ ,  $x^*$ , and  $y^*$  are velocity components and coordinates parallel and perpendicular to the wall, respectively,  $U_e^*$ ,  $t^*$  and  $\nu$  are the outer flow velocity, time and viscosity respectively. Alternatively this set can be viewed as the set of equations that the first term of a coordinate expansion satisfies:

$$q(x, y, t) = q_0(x, y, t) + R^{-1/2} q_1(x, y, t) + O(R^{-1}) \quad (3)$$

In Eq. (3), the Reynolds number  $R$  is assumed to be large and  $R^{-1/2}$  has proved to be the appropriate parameter in the asymptotic expansion. Inner and outer expansions and stretched coordinates are introduced as described in any classical text.

A typical example of a coordinate expansion can be found in the theory of unsteady boundary layers. Blasius<sup>19</sup> and later Goldstein and Rosenhead<sup>20</sup> and others, investigating the early stages of an impulsively started flow, seek a solution to Eqs. (1) and (2) in the form of an expansion in powers of a dimensionless coordinate  $t$ , the time.

$$u = u_1 + t u_1 + t^2 u_2 + \dots \quad (4)$$

$$v = t^{1/2} R^{-1/2} (v_1 + t v_2 + t^2 v_3 + \dots) \quad (5)$$

where the quantities  $u_i, v_i, i = 1, 2, \dots$ , depend on  $x$  and  $y$  alone. The idea of course is to eliminate one of the independent variables and this is indeed accomplished. The only difference in these solutions is that the problem is worked out in terms of similarity variables. The analysis indicates that the convective terms of the momentum equation are negligible for small times and that the Lagrangian acceleration balances directly with the diffusion terms. It is interesting to note that the problem can be formulated also in terms of a parameter expansion. To this end it is necessary to identify a small time scale  $t_0$ , perhaps characteristic of the duration of the early stages of the motion. Two dimensionless parameters can then be identified: the Strouhal number and the Reynolds number.

$$S = \frac{L}{U_\infty t_0}, \quad R = \frac{U_\infty L_0}{\nu} \quad (6)$$

where  $U_\infty$  is a typical velocity and  $L$  a typical length of the problem. If dimensionless and stretched variables are introduced

$$x = \frac{x^*}{L}, \quad Y = \frac{y^*}{\sqrt{\nu t_0}} \quad (7)$$

$$u = \frac{u^*}{U}, \quad V = \frac{v^*}{U_\infty} \frac{L}{\sqrt{\nu t_0}} \quad (8)$$

$$t = \frac{t^*}{t_0} \quad (9)$$

then Eqs. (1) and (2) can be written as follows

$$\frac{\partial u}{\partial x} + \frac{\partial V}{\partial Y} = 0 \quad (10)$$

$$\frac{\partial u}{\partial t} + \frac{1}{S} \left( u \frac{\partial u}{\partial x} + V \frac{\partial u}{\partial Y} \right) = \frac{\partial U_e}{\partial t} + \frac{1}{S} U_e \frac{\partial U_e}{\partial x} + \frac{1}{RS} \frac{\partial^2 u}{\partial Y^2} \quad (11)$$

The scaling of the different terms now is brought out and expansion in powers of the constant parameter  $S^{-1}$  yields essentially the same set of equations derived by Blasius.

Another classical example of coordinate expansion is the solution to the problem of oscillations with no mean. If the outer flow oscillates harmonically,

$$U_e^* = U_0^* e^{i\omega t^*} \quad (12)$$

then the boundary layer response is again a harmonic oscillation. In this case, if the quantities  $U, \omega^{-1}$  and  $L$  with  $U$  say equal to  $U_0^*(L)$ , are used to render velocities, time and length dimensionless respectively, then Eq. (2) becomes

$$\frac{\partial u}{\partial t} + \epsilon \left( u \frac{\partial u}{\partial x} + v \frac{\partial u}{\partial y} \right) = - \frac{\partial p}{\partial x} + \frac{1}{R_\omega} \frac{\partial^2 u}{\partial y^2} \quad (13)$$

where

$$\epsilon = \frac{U}{\omega L}, \quad R_\omega = \frac{\omega L^2}{\nu} \quad (14)$$

Riley<sup>21</sup> proposes a solution in the form of a double expansion

$$q(x, y, t; \epsilon, R_\omega) = q_0(x, y; R_\omega) e^{it} + \epsilon q_1(x, y; R_\omega) e^{2it} + \epsilon q_2(x, y; R_\omega) + O(\epsilon^2) \quad (15)$$

where  $q$  stands for any dependent variable and each term may in turn be expanded:

$$q_0(x, y; R_\omega) = q_{00}(x, y) + R_\omega^{-1} q_{01}(x, y) + \dots \quad (16)$$

The original analysis of course is much more involved and Riley identifies four different categories depending on the magnitude of the dimensionless parameters. For each case stretching of the coordinates and introduction of inner and outer variables is necessary. In fact the original analysis is based on the full Navier-Stokes equations and at each step approximate equations are derived. In this short presentation we confine ourselves to a few basic remarks:

Expansions of the form given by Eqs. (15) and (16) require special attention because the relative magnitude of the small parameters  $\epsilon$  and  $R_\omega^{-1}$  must be defined before one could proceed to collect terms of powers of such parameters. One of the most interesting features of the expansion of Eq. 15 is the steady term  $q_2$ . The nonlinearity of the governing equations gives rise to steady terms of order  $\epsilon$  which generate a steady flow familiar to investigators as "steady streaming" or "acoustic streaming." The streaming flow is characterized by a streaming Reynolds number which Stuart has recently identified:  $R_s = U^2/\omega\nu$ . For a large streaming Reynolds number, two thin layers can be identified. The Stokes layer and the streaming layer with thicknesses of order  $\sqrt{\nu/\omega}$  and  $L(\omega\nu)^{1/2}U^{-1}$ , respectively. The Stokes layer drives the steady streaming via the nonlinear terms. What is most interesting is the fact that at the edge of the Stokes layer the streaming velocity does not vanish. Its value matches in the sense of inner and outer expansions with the inner solution of the outer flow. A second and thicker boundary layer thus develops as shown in Fig. 1.

Moving on to oscillations about a nonvanishing mean, consider an outer flow velocity distribution given by

$$U_e^* = U_0^* + \epsilon U_1^* e^{i\omega t^*} \quad (17)$$

where  $\epsilon$  is a small dimensionless parameter representing the relative amplitude of the oscillations. Lighthill<sup>23</sup> expands in powers of  $\epsilon$  and derives a set of equations that govern the steady and unsteady part of the motion. To solve the equations thus generated, Lighthill expands again in powers of frequency or its inverse. The problem is therefore again formulated in terms of a double expansion. The joining of the two Lighthill solutions for large and small values of the frequency have been investigated by Rott and his co-workers and later by Ackerberg and Phillips.<sup>24</sup> It was identified that a basic similarity characteristic we can combine in one variable the frequency and the coordinate  $x$ . Introducing dimensionless variables

$$t = \omega t^* \quad , \quad x = \omega x^*/U_\infty \quad , \quad y = (\omega/\nu)^{1/2} y^* \quad (18)$$

$$u = u^*/U_\infty \quad , \quad v = v^*(\omega\nu)^{-1/2} \quad (19)$$

we can rewrite Eqs. (1) and (2) in the forms

$$\frac{\partial u}{\partial x} + \frac{\partial v}{\partial y} \quad (20)$$

$$\frac{\partial u}{\partial t} + u \frac{\partial u}{\partial x} + v \frac{\partial u}{\partial y} = \frac{\partial U_e}{\partial t} + U_e \frac{\partial U_e}{\partial x} + \frac{\partial^2 u}{\partial y^2} \quad (21)$$

It is noted that large values of  $x$  now correspond to either large values of the physical distance  $x^*$  or the frequency  $\omega$ . Solutions are sought in the form

$$q = q_0 + \epsilon q_1 e^{it} \quad (22)$$

where for a flat plate  $q_0 = q_0(\eta)$  and  $q_1 = q_1(\xi, \eta)$  with

$$\xi = x \quad , \quad \eta = y/\sqrt{2x} \quad (23)$$

For small values of  $\xi$ , an expansion in powers of  $\xi$  is introduced:

$$q_1 = q_{10}(\eta) + (2i\xi)q_{11}(\eta) + O(i\xi)^2 + \dots \quad (24)$$

For large  $\xi$  the situation is more involved. Ackerberg and Phillips identify the necessity for two layers, one next to the wall and one away from the wall. They further expand in powers of  $\xi^{-1/2}$  and appropriately match the inner and outer solutions.

A more straightforward approach is to combine asymptotic methods with numerical computations. Retaining the expansion in powers of  $\epsilon$  we essentially reduce the number of independent variables from 3 to 2. The resulting set of dimensionless equations has the form<sup>23</sup>

$$\text{order } \epsilon^0: \quad \frac{\partial u_0}{\partial x} + \frac{\partial v_0}{\partial y} = 0 \quad (25)$$

$$u_0 \frac{\partial u_0}{\partial x} + v_0 \frac{\partial u_0}{\partial y} = U_0 \frac{\partial U_0}{\partial x} + \frac{\partial^2 u_0}{\partial y^2} \quad (26)$$

order  $\epsilon^1$ :

$$\frac{\partial u_1}{\partial x} + \frac{\partial v_1}{\partial y} = 0 \quad (27)$$

$$iu_1 + u_0 \frac{\partial u_1}{\partial x} + u_1 \frac{\partial u_0}{\partial x} + v_0 \frac{\partial u_1}{\partial y} + v_1 \frac{\partial u_0}{\partial y} = U_0 \frac{\partial U_1}{\partial x} + U_1 \frac{\partial U_0}{\partial x} + \frac{\partial^2 u_1}{\partial y^2} \quad (28)$$

These equations can now be solved numerically in the two-dimensional space. Ackerberg and Phillips<sup>24</sup> have carried out such calculations and later Telonis and Romaniuk<sup>25</sup> have extended the work to include the effects of temperature and heat transfer. The method is only restricted to small amplitudes of oscillations. However arbitrary body shapes and frequencies can be considered since the equations are solved numerically in the  $x$ - $y$  space. Moreover, the method is readily available for three-dimensional calculations.

Figure 2 displays the amplitude of the velocity fluctuation for a moderate  $\xi$ . It is true that this quantity exceeds the amplitude of the driving external flow. However, this does not mean that the instantaneous boundary-layer velocity exceeds the corresponding outer flow value as McCroskey (private communication) pointed out to the author. In Fig. 3 we have plotted the phase of the velocity as a function of the parameter  $\xi$ .

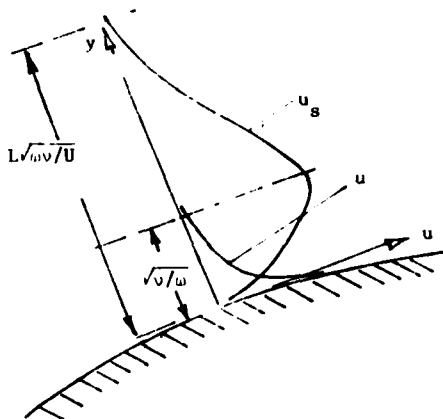


Fig. 1 Schematic sketch of Stokes and streaming layers.



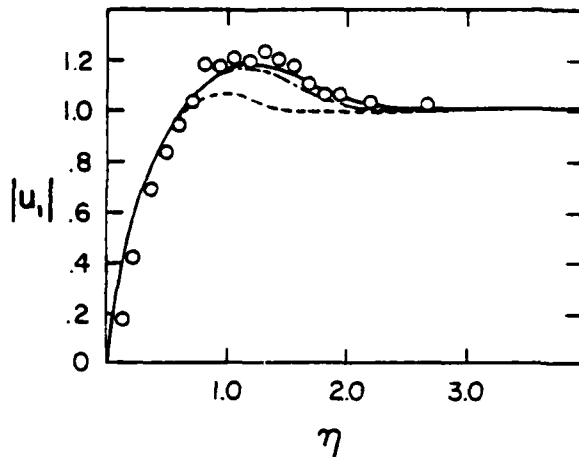


Fig. 2 Amplitude of the velocity fluctuations at  $\xi = 2.844$ ,  $U_e = 1 - 0.0035 \xi$ : —, Ref. 25, o; experimental and ---, numerical results of Ref. 26; - · - · - calculated by the method of Lighthill.<sup>23</sup>

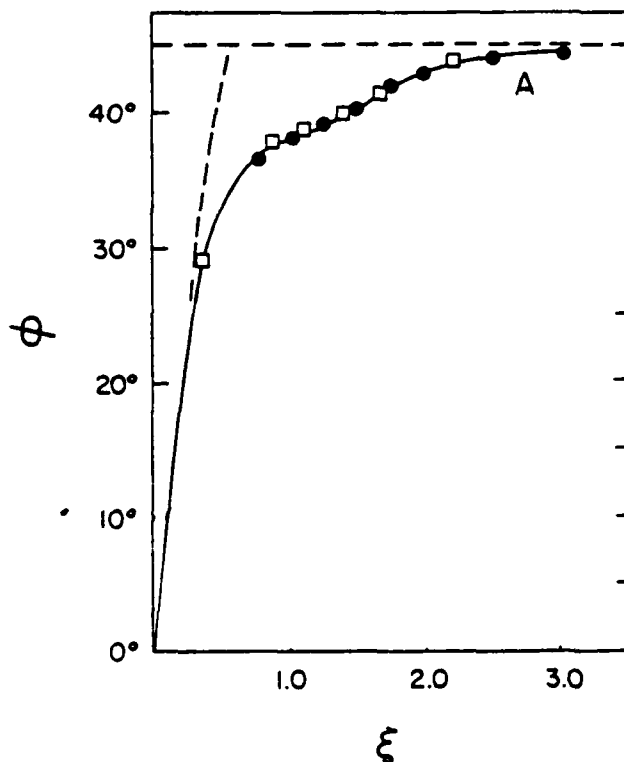


Fig. 3 The skin friction phase as a function of the frequency parameter  $\xi$ : ---, Lighthill;<sup>23</sup> □, exact numerical; for references, see Ref. 25, —, asymptotic expansion.<sup>25</sup>

### 3. NUMERICAL METHODS

Purely numerical computations of unsteady boundary layers are straightforward extensions of steady flow methods, with the exception of reversing boundary layers or, separating flows. The well-known difficulties due to nonlinearities are still present but this is not the topic of the present paper. In most cases the nonlinear effects are treated by linearization and iterations. Established methods of solution as for example implicit and explicit finite difference algorithms or the box method have been extended to unsteady flow.

The unsteady two-dimensional boundary-layer equations are parabolic in character, with time  $t$  and axial distance  $x$  as parabolic variables. The domain of influence<sup>27,28</sup> of a point  $x_0, t_0$  is extended in a downstream wedge with side walls defined by

$$\frac{dx}{dt} = u(x_0, y_m, t_0) \quad , \quad t = t_0 \quad (29)$$

where  $u(x_0, y_m, t_0)$  is the maximum velocity at the point  $x_0, t_0$ . Disturbances propagate in the direction perpendicular to the wall instantly. The message from a point therefore travels instantly up to the edge of the boundary layer, then convects downstream with the speed of the outer flow and moves again down to reach any point at an  $x$ -station instantly. The speed of propagation therefore is equal to the speed of the outer flow.

A stable algorithm should satisfy the Courant-Friedrichs-Lewy criterion. This criterion states that the local net of numerical influence at each grid point of the numerical scheme should contain the domain of influence of the point.

The most common method for the numerical calculation of unsteady flows is to convert the system to a set of steady flow equations and then use a steady flow algorithm. This is easily accomplished by writing the time derivative in a finite difference form

$$\frac{\partial u}{\partial t} \approx \frac{u - u_0}{\Delta t} \quad (30)$$

where  $u_0$  is the value of the variable at the previous time plane. The method fails in regions of reversed flow. At such points the unsteady boundary layer equations are free of singularities. However a straightforward extension of steady flow algorithms runs into a "forbidden" region. For two-dimensional steady flow the Courant-Friedrichs-Lewy criterion is violated in such a region. A more careful consideration of the three-dimensional grid indicates that an appropriate differencing scheme can be devised to permit the integration through regions of partially reversed flow. In terms of the notation of Fig. 4, two finite difference schemes suggested and tested are as follows:<sup>13,18</sup>

$$\frac{\partial u}{\partial x} \approx \frac{u_{m+1,k}^{n-1} - u_{m,k}^{n-1}}{2\Delta x} + \frac{u_{m,k}^n - u_{m-1,k}^n}{2\Delta x} \quad (31)$$

$$\frac{\partial u}{\partial x} \approx \frac{u_{m+1,k}^{n-1} - u_{m,k}^n}{\Delta x} \quad (32)$$

In the above equations  $u_{i,j}^s$  denotes the value of the function at the grid point

$x_i, y_j, t_s.$

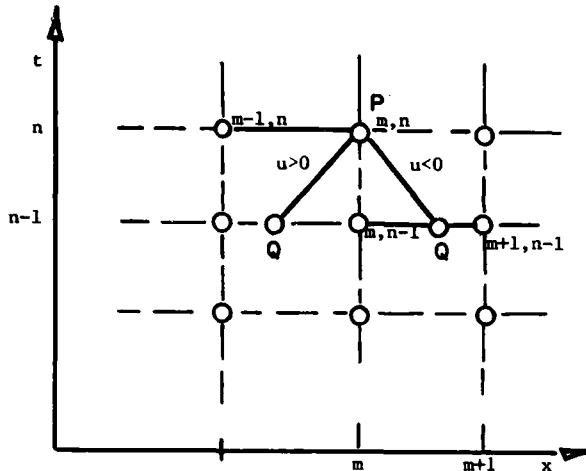
Keller<sup>28</sup> proposes a more direct method integrating directly along the subcharacteristics, that is along the boundary of the domain of influence. Based on the definition of the Eulerian operator he suggests that

$$\frac{\partial u}{\partial t} + u \frac{\partial u}{\partial x} = \frac{u_{m,n,k} - u_{m,n-1,k}}{\Delta t} + \frac{\Delta x_t}{\Delta t} \frac{u_{m,n-1,k} - u_{Q,n-1,k}}{\Delta x_t} = \frac{u_{m,n,k} - u_{Q,n-1,k}}{\Delta t} \quad (33)$$

where  $m$  and  $n$  denote grid points as shown in Fig. 4, and  $Q$  is the intersection of a backward subcharacteristic with the mesh. In this way the box method can be modified for calculations of unsteady reversing flows. It is recalled here that the method is based on the idea of reducing the problem to a set of ordinary differential equations by introducing a new dependent variable, the velocity gradient  $\tau = \partial u / \partial y$ . All derivatives can then be expressed in terms of values on the sides of a three-dimensional box. Keller evaluates the convective derivative at the mid-plane  $k - 1/2$  of the box and writes the finite differencing form of the momentum equation as follows

$$\frac{u_{m,k-1/2}^n - u_{Q,k-1/2}^n}{\Delta t} = - \left[ \frac{\partial p}{\partial x} \right]_m + \left[ \frac{\partial \tau}{\partial y} \right]_{PQ/2} - [v]_{k-1/2} \left[ \frac{\partial u}{\partial y} \right]_{PQ/2} \quad (34)$$

Fig. 4 Grid notation for the plane  $y = y_k$  of the three-dimensional domain  $x, y, t$ .



where  $PQ/2$  denotes evaluation at the midpoint of the segment  $PQ$ . In the above equation, brackets denote a difference between evaluations at the upper and lower index.

#### 4. DISCUSSION - UNSTEADY SEPARATION

The methods described in the previous sections have been quite successful in predicting fluctuating laminar flows. Controversies only arose with respect to the accuracy and efficiency of the methods or perhaps their mathematical rigor. The reader can find extensive accounts of numerical results in the review articles referenced here. In this section we will be concerned with a specific problem which most investigators tested their method against: unsteady separation.

There is significant difference between unsteady separation and other problems in unsteady viscous flows. Separation is by definition the point at which the boundary layer approximation breaks down, since the actual flow breaks away from the wall and ceases to follow the solid boundary. The problem of unsteady separation therefore is not just another problem to be considered by a new method. The difficulty lies in the fact that correct interpretation of the results of an inappropriate model, the boundary layer equation, may give information about the actual fluid flow or equivalently the behavior of the full Navier-Stokes equations. Whether this is possible altogether, is not yet proven. However, most investigators accept the fact that the boundary-layer equations contain information about the extent of their validity, for steady as well as unsteady flows.

The early work on unsteady separation hinged around two basic ideas due to Moore, Rott and Sears.<sup>15,16</sup> The first was a conviction that steady separation over a moving wall could be mapped to an unsteady separation over a fixed wall. The second idea was the criterion of separation for the first case, the MRS criterion

$$\frac{\partial u}{\partial y} = 0 \quad \text{at } u = 0 \quad (35)$$

Details on this material, the reader will find again in the review articles referenced here. The discussion in this section will favor the more recent analytical developments on the topic.

It is well known that the boundary-layer equations exhibit a singular behavior at the point of vanishing skin friction. Since the actual flow turns sharply away from the wall at the point of separation, the normal component of the velocity should be indeed expected to blow up as separation is approached. It was argued that the singular behavior is in fact a property that accompanies unsteady separation<sup>29</sup> and not the point of zero skin friction. In fact, Sears and Telionis propose as criterion for separation the appearance of this singular behavior. It is emphasized here that numerical instabilities are encountered as the point of the Goldstein singularity is approached. However, the progressive inability of the numerical scheme to converge is well ordered and it increases as the point of separation is approached. Moreover, it is accompanied by substantial growth of quantities like the normal component of the velocity, the displacement thickness, etc.

Numerical calculations<sup>30-32</sup> of unsteady flows based on an implicit finite-differencing scheme indicated that in unsteady flows, integration can proceed through the point of zero skin friction without any evidence of singularity. For flows that become progressively more adverse, a traveling singularity was discovered<sup>30-32</sup> further downstream of the point of zero skin friction. The box-method was also employed<sup>33</sup> in numerical calculations of laminar separating flows but with contradictory results. These methods of

computation were briefly described in Section 2.

Quite often numerical codes developed and extensively tested for steady three-dimensional calculations were converted to an unsteady two-dimensional form.<sup>34-36</sup> This is easily accomplished by setting the third velocity component equal to one, dropping the second momentum equation and interpreting the third space coordinate as time. Some modifications are also necessary on the pressure gradient terms and the boundary conditions.

New methods were introduced recently, especially for the purpose of studying unsteady separation. The first is due to Williams<sup>16,37,38</sup> and his co-workers and is essentially a self-similar method. A new coordinate system that travels with the speed of separation is introduced. In its most simple version, the dependent and independent variables are transformed according to the expressions

$$x = \bar{x} + \int U_s(t) dt, \quad y = \bar{y}, \quad t = \bar{t} \quad (36)$$

$$u = \bar{u} + U_s, \quad v = \bar{v}, \quad U_e = \bar{U}_e + U_s \quad (37)$$

where  $U_s(t)$  is the velocity of separation and the transformed quantities are denoted by an overbar. Williams and Johnson<sup>37,38</sup> discovered a class of outer flow velocity distributions, that under the transformation (36), (37), result in a problem of steady flow over a moving wall. Shen's more recent work<sup>17</sup> proved that the class of problems discovered by Williams and Johnson contains in fact all possible unsteady separating flows. With steady separating flow over downstream moving walls well understood and documented,<sup>37,38,39</sup> the significance of the contribution of Williams, Johnson and Shen is obvious. It proves that all unsteady separations are accompanied by a singularity.

In an alternative approach Shen and Nenni<sup>40</sup> approach the problem from an asymptotic point of view focusing attention on the behavior of the  $v$ -component of the velocity at the outer edge of the boundary layer. They base their definition of separation to the unmatchability condition and apply their method to weakly unsteady flows. These arguments,<sup>17,37,38,40</sup> although mathematically sound, may not be as convincing as engineers may expect. It remains to demonstrate that this is the behavior of an unsteady boundary-layer solution integrated step by step from a leading edge or a stagnation point. This has been attempted by quite a few investigators and their results will be outlined here.

Two basic types of problems have been considered. In the first, it is assumed that steady separating flow has been established and the point of separation is therefore characterized by a vanishing skin friction and a Goldstein singularity. At  $t = 0$  a disturbance on the outer flow distribution, impulsive or transient, is introduced that would force the point of separation to move to a new position. The problem is then to follow separation as it moves from its initial position and travels towards its final position. In the second problem the initial flow is free of separation. A change in the outer flow distribution is then introduced such that separation is induced. In the first problem separation and its classical steady flow properties are the starting point of the calculation and its subsequent unsteady development is sought. In the second problem, the initial flow field is not separating and the emergence of separation and the singular behavior is investigated.

#### a. The Displacement of Separation

This problem was considered first by Buckmaster<sup>41</sup> who introduced an asymptotic analysis around the point of zero skin friction. In an attempt to investigate the development of the separation singularity in time, Buckmaster further assumed a small time approximation. He found that at least for small times, the point of zero skin friction moves upstream but the position of the singular behavior is unaffected. Thus, a traveling point of zero skin friction leaves the initial singularity behind.

A direct numerical calculation of such a problem was reported by Telionis, Tsahalis and Werle<sup>30</sup> who consider as an initial steady flow the Howarth flow which involves a linear deceleration of the outer flow velocity and separation at the station  $x = -0.120 dU_e/dx$ . The outer flow distribution is assumed to switch impulsively from one linear distribution to another:

$$U_e = 1 - C_1 x \quad \text{for } t < 0 \quad (38)$$

$$U_e = 1 - C_2 x \quad \text{for } t \geq 0 \quad (39)$$

with  $C_2 > C_1$ . Numerical calculations indicate that the point of zero skin friction is displaced very quickly upstream, moves slower downstream and eventually starts propagating again upstream towards the final position of separation (see Fig. 5). In contrast, the position of the singularity is not affected at all by the drastic changes of the outer flow, in qualitative agreement, at least for small times with the analytical results of Buckmaster.<sup>41</sup> This inertia-like behavior of unsteady separation has been verified experimentally as described in Ref. 42. At later times, the calculations indicate that the singularity starts moving, very slowly at first, preceded always by the classical symptoms of separation, as for example, gradual but decisive growth of quantities like  $v$ ,  $\partial u/\partial x$ ,  $\delta$ , etc. According to the spirit and definitions of Ref. 29, the physical interpretation of these results is the following. Immediately after the impulsive change of the outer flow conditions, a thin layer of reversed flow shoots upstream, beneath the attached boundary layer and then downstream again, until eventually it begins a slower propagation towards the final position of separation. At about that time, separation begins to move upstream slowly at first, and then at a moderate rate, until eventually both points merge smoothly but asymptotically to the point where separation is calculated for the steady flow that corresponds to the outer flow given by Eq. (39).

The same problem was considered most recently by Wang<sup>36</sup> who converts his computer code from a three-dimensional to an unsteady two-dimensional computational scheme. In three-dimensional boundary-layer flows it has been argued and numerically demonstrated that a separating line on the skin of the body is also the envelope of skin friction lines. In a coordinate system  $x, y, z$ , where  $y = 0$ , defines the skin of the body, the family of skin-friction lines are given by

$$\frac{h_z dz}{h_x dx} = \lim_{y \rightarrow 0} \frac{w}{u} = \frac{\partial w / \partial y}{\partial u / \partial y} \Big|_{y=0} \quad (40)$$

where  $h$  is the scale factor for the coordinate system.

Wang<sup>36</sup> proposes to search for similar topographical patterns in the plane  $x-t$  for unsteady two-dimensional flows and defines separation as the line in time,  $t$ , and space,  $x$ , which is the envelope of curves defined by a formula analogous to Eq. (40)

$$\frac{h_x dx}{dt} = \frac{\partial u}{\partial y} \Big|_{y=0} \quad (41)$$

Results for the unsteady Howarth problem are shown in Fig. 5. There is an unacceptable discrepancy in the scale of time between the results of Refs. 30 and 36. This is indeed puzzling, since calculations by the same authors of other problems, as for example the impulsive start of a circular cylinder, are in excellent agreement, at least with respect to the location of the point of zero skin friction and its upstream displacement in time. Moreover, discrepancies are also obvious in the location of the initial and final positions of separation. The first group of discrepancies may be due to errors in the definition of the dimensionless time scale. The second group of discrepancies is not as disturbing and may be due to inaccuracies in the actual numerical calculations.

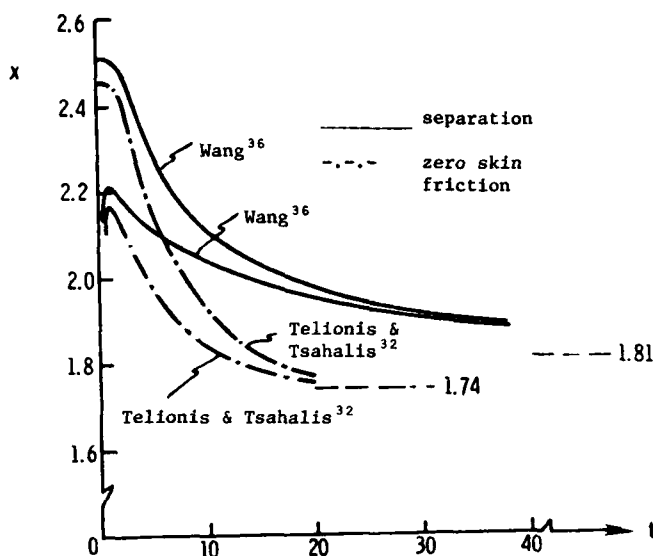


Fig. 5 The excursions of the point of zero-skin friction and unsteady separation as defined by Sears and Telionis<sup>15,29</sup> and Wang,<sup>36</sup> for an impulsively changed Howarth flow.

#### b. The Emergence of Separation

A more popular problem has been the emergence of separation in a flow which stays attached up to a certain time. This is possible for example, if the flow about a blunt body is started impulsively from rest, or alternatively, if with an established flow, the configuration of the body changes to generate regions of adverse pressure gradients. A classic case which belongs to the first category is the impulsive start of a circular cylinder which has been studied by almost all investigators working on unsteady boundary layers.

Blasius<sup>19</sup> and Goldstein and Rosenhead<sup>20</sup> recognized the fact that immediately after the impulsive start, the flow around the cylinder is potential and calculated the early stages of the boundary-layer development and the upstream displacement of the point of zero skin friction which at the time was believed to accompany separation. It was Proudman and Johnson<sup>43</sup> who clearly demonstrated with their asymptotic analysis that reversing flow may have absolutely no effect on the outer flow and that a reversing layer is compatible with attached external flow at the rear stagnation point of an impulsively started cylinder.

A number of contributions based on exact solutions of the Navier-Stokes equations appeared in the late sixties and their results are reviewed adequately by Collins and Dennis.<sup>38</sup> In the present paper we will concentrate more on recent contributions, addressing specifically the problem of unsteady separation for rather large values of the Reynolds number. Belcher et al.<sup>45</sup> describe two methods of numerical calculations of the boundary-layer equation: the first is a straightforward implicit method; the second employs data from two previous stations of  $t$  and neighboring points on the  $x$ -grid both upstream and downstream, much like, perhaps, in Eqs. (31) and (32).

Collins and Dennis<sup>44</sup> extend their method for solving the full Navier-Stokes equations to compute the impulsively started flow around a circular cylinder for different values of the Reynolds number. Their method is based on expansions of the form

$$\psi = \sum_1^{\infty} f_n(\xi, \tau) \sin n\theta \quad (42)$$

$$\zeta = \sum_1^{\infty} g_n(\xi, \tau) \sin n\theta \quad (43)$$

where  $\psi$  is the stream function,  $\zeta$  is the vorticity,  $\theta$  is a polar angular coordinate,  $\xi$  is the logarithm of a dimensionless radial coordinate and  $\tau$  is the dimensionless time. In this way, the problem reduces to a system of partial differential equations with only two independent variables which are solved numerically by a Crank-Nicolson scheme.

Telionis and Tsahalis<sup>32</sup> integrate the boundary-layer equations by an implicit method using a zig-zag scheme for partially reversed flows to study the impulsive start of a circular cylinder and an ellipse at

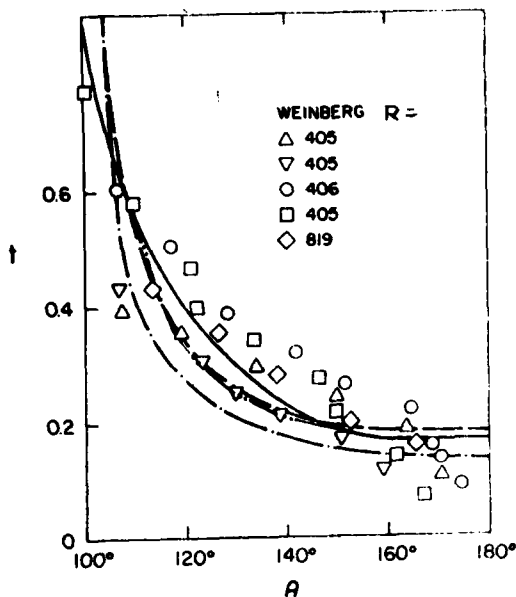


Fig. 6 The excursions of the point of zero skin friction for a circular cylinder started impulsively from rest ( $Re \rightarrow \infty$ ). ---, Presz et al.<sup>48</sup>; —, Thoman et al.<sup>49</sup>; - - -, Telionis et al.<sup>32</sup>; - · - · -, Cebeci.<sup>47</sup>

character of the flow is the appearance of secondary vortices at a dimensionless time of  $t \sim 1.00$  and  $\theta = 135^\circ$  where  $\theta$  is measured from the forward stagnation point. Collins and Dennis<sup>44</sup> calculated the flow for various values of the Reynolds number. Their vorticity plots indicate a kink in the region of  $\theta = 130^\circ$ - $150^\circ$ , a clear indication of the anticipation of secondary vortices. Such vortices were observed for as low Reynolds numbers as 550. Collins and Dennis<sup>44</sup> reported that their calculations break down at a finite time  $t_m$  which is progressively smaller for larger Reynolds numbers. For their largest Reynolds number, calculations are terminated at  $t_m = 1.25$ . Boundary-layer calculations reported in Ref. 45 were unsuccessful beyond  $t = 0.45$ , however more refined differencing schemes, similar to those given by Eqs. (31) and (32), permitted the computation up to  $t = 2$ , although inaccuracies appeared near the point of zero skin friction already at  $t = 1$ .

The mesh-configuration used by Cooke and Robins<sup>45</sup> was rather crude, containing 18 stations in the downstream direction. Boundary-layer calculations were repeated by Telionis and Tsahalis<sup>32</sup> who used a much more refined mesh configuration with 400 stations and 100 to 150 points at each station. Employing a zig-zag scheme, Telionis and Tsahalis found that the unexpected violent behavior of the flow is initiated approximately at  $t = 0.65$  and for  $\theta = 135^\circ$ . However this behavior does not seem to become organized before approximately  $t = 0.95$ . At this moment the abrupt growth of the u-component of the velocity seems to follow the pattern of a separation singularity. On any time plane, the behavior of all singular quantities is monotonic and the number of iterations required for convergence grows also monotonically until a station is reached at which no convergence is possible. A clarification is necessary here with respect to Fig. 4 of Ref. 32. In this figure the authors have actually plotted their modified v-component of the velocity which they define by their Eq. (12). This is a poor choice because this quantity by definition blows up at the rear stagnation point and behaves erratically in its neighborhood. However, its properties are qualitatively similar to those of the true v-component, away of the rear stagnation point.

Using inner and outer expansions, Bar-Lev and Yang<sup>46</sup> solved the full Navier-Stokes equations and obtained results in agreement with those of Collins and Dennis. However, their calculations for  $Re = \infty$  indicate no peculiar behavior in the range  $0.6 < t < 0.8$ .

Cebeci<sup>47</sup> undertook to repeat careful boundary-layer calculations. Using the standard box method with 41 stations and 100 points at each station, Cebeci discovered far from the wall unacceptable behavior of the velocity gradient reminiscent of the unmatchability condition of Shen.<sup>17</sup> This behavior was encountered first at  $t = 0.65$ ,  $\theta = 153^\circ$  and propagated upstream with a rate comparable with the rate of propagation of the singularity found by Telionis and Tsahalis.<sup>32</sup> However, Cebeci found that introduction of a zig-zag scheme completely eliminates any singularities at least up to a dimensionless time of  $t = 2.8$ , thus contradicting the findings of Telionis and Tsahalis.<sup>32</sup>

The problem of whether a singularity will appear in a finite time in a domain which started with no singular behavior, Cebeci has addressed before,<sup>33</sup> investigating a Howarth type of flow which is initiated as a Blasius flat plate flow. In this case as well, the numerical analysis was marched with a zig-zag scheme through a region of continuously growing reversed flow with no evidence of singularity. Most recently, Dwyer and Sherman<sup>51</sup> imposed an unsteady Howarth-like edge condition on the boundary-layer equation

$$U_e = 1 - Ax + x^2$$

an angle of attack. Bar-Lev and Yang<sup>46</sup> solve the full vorticity equation by the method of matched asymptotic expansions while Wang<sup>36</sup> and Cebeci<sup>47</sup> employ again their numerical schemes to solve the boundary-layer equations in a three-coordinate space. Van Dommelen and Shen<sup>50</sup> introduce a novel method for the calculation of unsteady viscous flows based on a Lagrangian formulation.

All results are in good agreement with respect to the excursions of the point of zero skin friction and the properties of the reversing layer as shown in Fig. 6. Some minor discrepancies exist in the estimation of the time when the point of flow reversal departs from the rear stagnation point, but soon after, the results appear to merge together. Collins and Dennis<sup>44</sup> and Bar-Lev and Yang<sup>46</sup> present data for the temporal variation of the point of zero skin friction for a wide range of finite Reynolds numbers.

Having established that the point of zero skin friction is not connected with unsteady separation, some questions of great significance are now posed to the investigator. Where and when will separation emerge in boundary-layer calculations, if at all it appears in finite times?

The exact solutions of the Navier-Stokes equations (see Reviews in Ref. 6-13) indicate that the recirculating bubbles grow smoothly without any extraordinary behavior. The first indication of major changes in the

This flow generates a small recirculating bubble which grows with time but is fully contained within the domain of integration. They found that the behavior of all properties is very smooth for a while and the recirculating bubble grows slowly until at a certain instant a singularity appears in the skin friction, accompanied by an erratic oscillatory behavior of the velocity profile at this station. Dwyer and Sherman found that the "unphysical growth" is independent of the size of the reversed flow region. Moreover, they argue that Cebeci<sup>33</sup> may have missed the singular behavior because he did not consider large enough values of dimensionless time, confining his calculations to  $t < 0.5$ .

Intrigued by the controversy over the specific case of the impulsively started cylinder, Shen<sup>17</sup> and Wang<sup>36</sup> decided to reconsider the problem, the first through a novel method and the second using a new definition of separation. Van Dommelen and Shen<sup>50</sup> recasted the boundary layer equations in Lagrangian coordinates. In this system of coordinates there is no distinction between steady and unsteady flow and therefore no difficulty should arise in interpreting the results. With  $\xi, \eta$  the fixed coordinates attached on the body and  $x(\xi, \eta, t), y(\xi, \eta, t)$  the coordinates of the particle which was found at  $\xi, \eta$  at time  $t = 0$ , Van Dommelen and Shen studied the distortion in time of the  $x, y$  grid and searched for a singularity which appears as a blow-up of quantities like  $\partial y / \partial \xi, \partial y / \partial \eta$  and  $\partial u / \partial x$  while quantities like  $x$  and  $u$  remain finite. They noted further that the singular behavior is accompanied by vanishing of  $(\partial x / \partial \xi)^2 + (\partial x / \partial \eta)^2$ , which implies the vanishing of both terms in this expression. This, in turn, implies the formation of an envelope of the  $x = \text{const}$  curves in the  $x, y$  plane which appears as a physical barrier or as a vertical wall in Fig. 7. No evidence of singular behavior was found in Ref. 50 until  $t = 2.4$ . The formation of the singularity became obvious in the next time step and at the point  $\theta = 110^\circ$ .

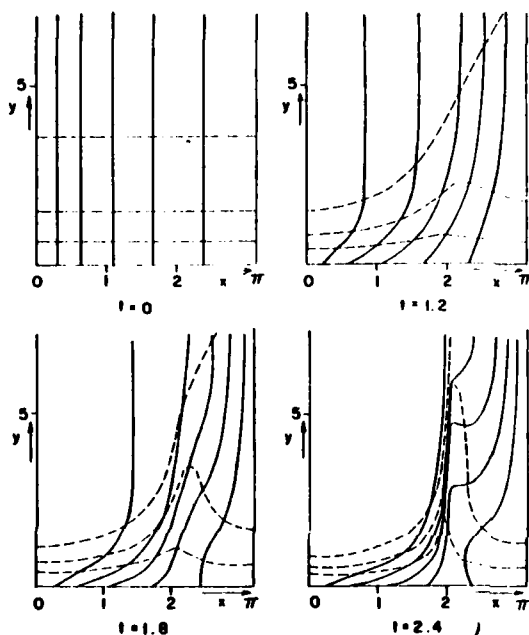


Fig. 7 The deformation in time of an initially rectangular mesh attached to the fluid particles (Ref. 51).

singularity reported by Tselionis and Tsalhis.<sup>32</sup> The first few points, about which the authors expressed some hesitation, cut across some of Wang's limiting streamlines. However after  $t = 1.0$ , it appears that the temporal path of the separation singularity is aligned with the neighboring curves and seems to be directing itself towards the initiation of the separation envelope.

The idea of envelope formation in an  $x, t$  plane is not actually new. Concepts of unsteady separation and the ideas of a moving separation singularity have been considered by investigators of unsteady turbulent flows as well. Cousteix et al.<sup>52</sup> presented a very similar pattern of limiting streamlines, indicating the formation of an envelope, almost two years before the publication of Ref. 36, a fact that the author of the latter seems to be unaware of. In Ref. 54 the results are compared with calculated trajectories of the separation singularity. Convincing qualitative agreement is evident but it is not possible to claim that the two definitions give identical results.

Studying the behavior of a single rectilinear vortex over a flat plate, Walker<sup>53</sup> was able to draw some conclusions quite pertinent to the problem of unsteady separation. In the neighborhood of the leading edge of the separated bubble, Walker discovered an overshoot in the velocity which appears to grow with time; while the number of iterations required for convergence increased and eventually the integration could not be continued past  $t = 0.675$ . Walker<sup>54</sup> expected the Proudman and Johnson model to apply in his problem but his numerical integration did not support this idea. This suggests that a singularity occurs at a finite time in accordance with the model of Refs. 15 and 29.

Williams,<sup>55</sup> Wang<sup>36</sup> and Dwyer and Sherman<sup>51</sup> extended their work on unsteady separation to three-dimensional flows. Information on this difficult problem is at this point fragmented and its discussion should be postponed until more information becomes available.

Wang employed his classical numerical scheme for the calculation of unsteady boundary layers but introduced a new definition of separation. In analogy to the case of steady three-dimensional flow, whereby separation is defined as an envelope of skin friction lines, Wang searched for similar geometrical configurations in an  $x-t$  plane. The analogy to "skin-friction" lines, or equivalently "limiting streamlines" are the curves defined by the equation

$$\frac{dx}{dt} = \frac{\partial u}{\partial y} \Big|_{y=0}$$

Wang considered again the problem of the impulsively started cylinder and calculated the limiting streamlines which are shown in Fig. 8. The formation of an envelope is clearly shown in this figure although it may not be possible to define the time of its initiation. On the same figure we plot the trace of the traveling

## 4. DISCUSSION

The evidence presented in this paper is critically interpreted and discussed in this section. The main interest is on unsteady separation as revealed from the boundary-layer equation. There is no doubt that this approximate model is not at all appropriate for the investigation of the actual phenomenon. To find how the real flow behaves, one should rather resort to the full Navier-Stokes equations, or to experiments. It is only because the boundary-layer equation is still a valuable predictive tool, that we are interested to learn what it can reveal about separation. Unfortunately, little information is available about the actual behavior of unsteady separation and this makes the investigation of the boundary-layer equation response even more difficult.

A fact that has been established both experimentally and numerically is that the vanishing of the wall shear does not signal separation in unsteady flow. A definition originally proposed by Sears became well-known recently as the MRS criterion because of the contributions of Moore and Rott to the original ideas.<sup>15,16,17</sup> Sears argued that separation should be accompanied by the vanishing of the shear somewhere within the flow but in a frame moving with separation. Since the speed of the point of separation is not known a priori, it is not possible to use this property as a criterion for separation.

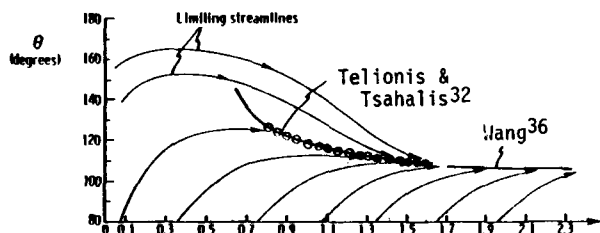


Fig. 8 Limiting streamlines for a cylinder started impulsively from rest, (Ref. 36).  $\circ$ , numerical calculations from Ref. 32.

Moore argued that the point of unsteady separation should be accompanied by the Goldstein singularity and later Sears and Telionis<sup>15,29</sup> suggested that the appearance of such a singularity could serve as a criterion for separation. This has been a very controversial point and many contributions have offered evidence in favor or against it. The main questions are: (1) Is it possible at all for a singularity to develop in the solution of the boundary-layer equation, if the domain of integration is free of such singularities at earlier times? Furthermore, (2) is such a singularity related to separation and, if so, could it be tracked and recorded to provide information on unsteady separation? Finally, (3) if the answer to the last question is negative, is there any other criterion that would signal unsteady separation? In other words, does the boundary-layer equation contain information about the extent of its validity? Most of the authors believe that the answer to the last question is YES. If the boundary-layer equation can be used to predict separation in steady flow, it should contain enough information to predict separation in unsteady flow as well.

The most controversial of the issues is centered around the first question and at this time the evidence points also to the answer YES; it is indeed possible that a singularity may develop in the solution of the unsteady boundary layer at a point in space which was free of singularities at earlier times. Such a singularity can be convected to the point of interest from downstream, as pointed out by Telionis et al.<sup>30</sup> and Wang.<sup>36</sup> This has not been disputed up to now. But then going one step further, is it possible for a singularity to emerge at a certain instant at a point in space if the domain of integration was free of singularities at earlier times and at all neighboring points? Evidence that this is again true is provided by a variety of methods: the numerical calculations of Telionis et al.<sup>32</sup> and Dwyer et al.,<sup>51</sup> as well as a large number of turbulent-boundary-layer calculations;<sup>12,13</sup> the analytical investigation of Shen and Nenni;<sup>40</sup> the numerical investigations in a Lagrangian system of coordinates of Van Dommelen and Shen.<sup>51</sup> Wang<sup>36</sup> reports no evidence of singular behavior, however the formation of an envelope in the  $x-t$  plane certainly implies infinite variation of a property with distance at a fixed time. The singularities discovered by the above investigators cannot be identified as separation singularities for sure. However, they emerge at the point where separation is expected to appear and after some time is elapsed, they displace themselves to the point of steady state separation. In another case, not directly related to external flow separation, Bodonyi and Stewartson<sup>56</sup> present a solution to the boundary-layer equation which is initially well behaved but breaks down after a finite interval of time.

Riley groups in the category of works presenting the opposite view References 43, 57, 44, and 45. He argues that the results presented in these references are at variance with those of Refs. 15, 29 and 32. The asymptotic work of Proudman and Johnson<sup>43</sup> and Robins and Howarth<sup>59</sup> is essentially an asymptotic expansion about the rear stagnation point. The flow field analyzed is a magnification of the region in the immediate neighborhood of the rear stagnation point. Proudman and Johnson<sup>43</sup> point out that large scale changes to the external flow cannot occur in a finite time if  $Re \rightarrow \infty$ . Separation and its possible singular behavior, however, is known to emerge far upstream, in a neighborhood which is located an infinite distance away from the point of the rear stagnation point. The findings of Refs. 43 and 59 therefore simply state that separation may not occur in the vicinity of the rear stagnation point in agreement with Refs. 32, 40, 50 and 51.

Collins and Dennis<sup>44</sup> solve the full Navier-Stokes equations whose solution is free of any singularities at the point of separation. Their results, therefore, even for the largest value of the Reynolds number, could not contribute to the understanding of the boundary-layer separation singularity. It is interesting

though that Collins and Dennis encounter some difficulties with their calculations, at times that are smaller and smaller for larger values of the Reynolds number. For  $Re = \infty$ , their procedure breaks down at  $t = 1.25$ . They hint that this behavior may be related to transition and it is felt that alternatively it may not be unrelated to the formation of a secondary vortex and separation.

Belcher et al.<sup>45</sup> using a zig-zag type of numerical integration carry their integration until  $t = 2$ , but do encounter inaccuracies near the position of steady separation. The experience of the present author indicates that with a coarse mesh, numerical integration may go through a station of singularity without any evidence of instability. In fact calculations can proceed sometimes beyond the point of separation into a region of well behaved and non-reversing flow, which bears no connection to the correct solution. In the calculations reported in Ref. 45 the upper surface of the cylinder, from  $\theta = 0$  to  $180^\circ$  was divided into only 18 increments. Each increment is therefore  $\Delta\theta = 10^\circ$ . More recent calculations<sup>47</sup> of the same problem using 41  $\theta$ -stations spaced by  $\Delta\theta = 4.5^\circ$  around the circular cylinder indicate no difficulties at all for much larger times. It is felt that such mesh configurations are very coarse. The work of Telionis and Tsahalis<sup>32</sup> with 400 stations within the same domain of integration, that is with  $\Delta\theta$  approximately equal to  $0.45^\circ$ , indicates that the singular behavior usually develops within a domain of  $2^\circ$  to  $2.5^\circ$ . The calculations of Refs. 45 and 47 could therefore easily "jump over" the singularity. It appears that until today the finest by far mesh used for the numerical solution of this problem is the one employed in Ref. 32. In Ref. 33 it is argued that a flow with a progressively growing adverse pressure gradient was found with no evidence of singular behavior. It is possible that the mesh of Ref. 33 is not fine enough to capture the singular behavior. It is emphasized therefore that the results of a numerical calculation could never be considered as a proof that a specific solution is free of singularities since with a coarse mesh the solution may appear perfectly normal in the entire domain of integration.

It has been argued that the appearance of the separation singularity is perhaps the creation of the particular numerical scheme under consideration. This may be true. However, the numerical results of Telionis and Tsahalis,<sup>32</sup> for  $t > 0.901$  seem to be very well behaved. In other words, what was identified in this reference as a separation singularity, is not just a disturbance with oscillating values of the properties like  $v$ ,  $\partial u/\partial x$  or even the velocity profile. At each instant  $t > 0.901$ , the calculations of Ref. 32 indicate a well ordered monotonic growth, until at a point, convergence becomes impossible. This singular behavior seems to propagate upstream, again in a well behaved fashion. The domain of influence of the singular station based on the differential equation or the differencing scheme, do not contain the point at which the separation singularity appears at the subsequent time step. The formation of each singularity therefore is totally independent of the earlier history of singularities.

The present author feels that the past decade has seen a large number of significant contributions to the problem. Unfortunately, some of the major difficulties remain unsurpassed and basic questions remain unanswered. It is believed that one of the main reasons of our inability to make positive progress in this area is the fact that we still understand very little about the actual phenomenon of unsteady separation. Only then will it be possible to give a meaningful answer to the second question posed in this section. However, recent experimental data seems to indicate that the classical concept of a single station of separation may be misleading. Each problem perhaps has its own characteristic features and should be examined independently. In this sense, the problem of the impulsively started circular cylinder is perhaps not a "good" problem for consideration, because the recirculating bubbles grow far beyond the domain of the validity of the boundary layer before a secondary vortex and a turbulent wake can be developed.

#### REFERENCES

1. Lord Rayleigh, "On the Motion of Solid Bodies Through Viscous Liquids," *Philos. Mag.* 21, 697-711 (1911).
2. Prandtl, L., "Über Flüssigkeitsbewegung bei sehr kleiner Reibung," III Intern. Congress of Mathematics, Heidelberg, 484-491 (1904).
3. Van Dyke, M., Perturbation Methods in Fluid Mechanics, Academic Press, 1964.
4. Cole, J. D., Perturbation Methods in Applied Mathematics, Blaisdell, 1968.
5. Nayfeh, A. H., Perturbation Methods, Wiley, 1973.
6. Stewartson, K., "The Theory of Unsteady Laminar Boundary Layers," in Advances in Applied Mechanics, Vol. 6, pp. 1-37, Academic Press, New York, 1960.
7. Stuart, J. T., "Unsteady Boundary Layers," in Laminar Boundary Layers, ed., L. Rosenhead, Oxford, 1964, pp. 349-406.
8. Rott, M., "Theory of Time Dependent Laminar Flows," in Theory of Laminar Flows, ed. F. K. Moore, Princeton University Press, Princeton, N.J., 1964, pp. 395-495.
9. Stuart, J. T., "Unsteady Boundary Layers" in Recent Research of Unsteady Boundary Layers, ed. E. A. Eichelbrenner, Vol. 1, 1971, pp. 1-46.
10. Riley, N., "Unsteady Laminar Layers," SIAM Review, Vol. 17, 1975, pp. 274-297.
11. Wirz, H. J., "Computation of Unsteady Boundary Layers," Lecture Notes in Physics, No. 41, Progress in Numerical Fluid Dynamics, Wirz, H. J., ed., Springer-Verlag, Berlin, 1975, pp. 442-476.
12. McCroskey, W. J., "Some Current Research in Unsteady Fluid Dynamics--The 1976 Freeman Scholar Lecture," ASME Journal of Fluids Eng., Vol. 99, 1977, pp. 8-38.
13. Telionis, D. P., "Calculations of Time-Dependent Boundary Layers," in Unsteady Aerodynamics, ed. R. B. Kinney, Vol. 1, 1975, pp. 155-190.



14. Knight, D. W., "Review of Oscillatory Boundary-Layer Flow," *J. Hydraulics Div.*, 104, 839-855 (1978).
15. Sears, W. R., and Telionis, D. P., "Boundary-Layer Separation in Unsteady Flow," *SIAM Journal of Applied Mathematics*, Vol. 28, 1975, pp. 215-235.
16. Williams, J. C., "Incompressible Boundary-Layer Separation," in *Annual Review of Fluid Mechanics*, eds. M. VanDyke, J. V. Wehausen, J. L. Lumley, Vol. 9, 1977, pp. 113-144.
17. Shen, S. F., "Unsteady Separation According to the Boundary-Layer Equation," in *Advances in Applied Mechanics*, 18, 177-220 (1978).
18. Telionis, D. P., *Unsteady Viscous Flow*, Springer, to appear.
19. Blasius, H., "Grenzschichten in Flüssigkeiten mit kleiner Reibung," *J. für Math. und Phys.* 56, 1-37 (1908).
20. Goldstein, S., and Rosenhead, L., "Boundary-Layer Growth," *Proc. Camb. Phil. Soc.* 32, 392-401 (1936).
21. Riley, N., "Oscillatory Viscous Flow, Review and Extension," *J. Inst. Math. Appl.*, 3, 419-434 (1967).
22. Stuart, J. T., "Double Boundary Layers in Oscillatory Viscous Flow," *J. Fluid Mech.* 24, 673-687 (1966).
23. Lighthill, M. J., "The Response of Laminar Skin Friction and Heat Transfer to Fluctuations in the Stream Velocity," *Proc. Roy. Soc.*, 224A, 1-23 (1954).
24. Ackerberg, R. C., and Phillips, J. H., "The Unsteady Laminar Boundary Layer on a Semi-Infinite Plate Due to Small Fluctuations in the Magnitude of the Free-Stream Velocity," *J. Fluid Mech.* 51, 137-157 (1972).
25. Telionis, D. P., and Romaniuk, M. S., "Velocity and Temperature Streaming in Oscillating Boundary Layers," *AIAA Journal*, 16, 488-495 (1978).
26. Hill, P. G., and Stenning, A. H., "Laminar Boundary Layers in Oscillatory Flow," *J. of Basic Eng.* 82, 593-608 (1960).
27. Wang, K. C., "Aspects of Multitime Initial-Value Problem Originating from Boundary-Layer Equations," *Physics of Fluids*, 18, 951-955 (1975).
28. Keller, H. B., "Numerical Methods in Boundary-Layer Theory," in *Annual Review of Fluid Mechanics*, 10, 417-433 (1978).
29. Sears, W. R., and Telionis, D. P., "Unsteady Boundary-Layer Separation," in *Recent Research of Unsteady Boundary Layers*, ed. E. A. Eichelbrenner, Vol. 1, 1972, pp. 404-447.
30. Telionis, D. P., Tsahalis, D. Th. and Werle, M. J., "Numerical Investigation of Unsteady Boundary Layer Separation," *Physics of Fluids*, 16, 968-973 (1973).
31. Telionis, D. P., and Tsahalis, D. Th., "The Response of Unsteady Boundary-Layer Separation to Impulsive Changes of Outer Flow," *AIAA Journal*, 12, 614-619 (1974).
32. Telionis, D. P., and Tsahalis, D. Th., "Unsteady Laminar Separation over Impulsively Moved Cylinders," *Acta Astronautica*, 1, 1487-1505 (1974).
33. Cebeci, T., "An Unsteady Laminar Boundary Layer with Separation and Reattachment," *AIAA Journal*, 16, 305-306 (1978).
34. Dwyer, H. A., "Calculation of Unsteady Leading Edge Boundary Layers," *AIAA Journal*, 6, 2447-2448 (1968).
35. Dwyer, H. A., "Some Characteristics of Unsteady Two- and Three-Dimensional Reversed Boundary Layer Flows," *AIAA Paper No. 79-1518*, 1979.
36. Wang, K. C., "Unsteady Boundary Layer Separation," *Martin Mariette Report*, MML TR 79-16C, April 1979.
37. Williams, J. C., III, and Johnson, W. D., "Semi-similar Solutions to Unsteady Boundary-Layer Flows Including Separation," *AIAA Journal*, 12, 1388-1393 (1974).
38. Williams, J. C., III, and Johnson, W. D., "Note on Unsteady Boundary-Layer Separation," *AIAA Journal*, 12, 1427-1429 (1974).
39. Telionis, D. P., and Werle, M. J., "Boundary Layer Separation from Downstream Moving Boundaries," *ASME Journal of Applied Mechanics*, 40, 2, 369-374 (1973).
40. Shen, S. F., and Nenni, J. P., "Asymptotic Solution of the Unsteady Two-Dimensional Incompressible Boundary Layer and Its Implications on Separation," in *Unsteady Aerodynamics*, R. B. Kinney, ed., 1, 245-259 (1975).
41. Buckmaster, J., "The Unsteady Evolution of the Singularity at Separation," *Journal of Engineering Mathematics*, 7, 223-230 (1973).
42. Telionis, D. P., "Experimental Techniques for Unsteady Boundary Layers," contribution to the present volume.

43. Proudman, I., and Johnson, K., "Boundary-Layer Growth near a Rear Stagnation Point," J. Fluid Mech., 12, 161-168 (1962).
44. Collins, W. M., and Dennis, S. C. R., "Flow Past an Impulsively Started Circular Cylinder," J. Fluid Mech., 60, 105-128 (1973).
45. Belcher, R. J., Burggraf, O. R., Cooke, A. J., Robins, A. J. and Stewartson, K., "Limit-less Boundary Layers," in Recent Research of Unsteady Boundary Layers, E. A. Eichelbrenner, ed., 2, 1444-1466 (1972).
46. Bar-Lev, M., and Yang, H. T., "Initial Flow Field Over an Impulsively Started Circular Cylinder," J. Fluid Mech., 48, 33-55 (1975).
47. Cebeci, T., "The Laminar Boundary Layer on a Circular Cylinder Started Impulsively from Rest", J. Comp. Phys., 31, 153-172 (1979).
48. Presz, W. M., and Heiser, W. H., "Unsteady Boundary-Layer Analysis for Two-Dimensional Laminar Flow," A. f. Flugwiss. 16, 33-39 (1968).
49. Thoman, D. C., and Szewczyk, A. A., "Time Dependent Viscous Flow Over a Circular Cylinder," Phys. Fluids, Supplement II, 76-86 (1969).
50. Van Dommelen, L. L., and Shen, S. F., "The Laminar Boundary Layer in Lagrangian Description", 13th Bienn. Fluid Dyn. Symp., Olsztyn, Poland.
51. Dwyer, H. A., "Some Characteristics of Unsteady Two- and Three-Dimensional Reversed Boundary Layer Flows", AIAA Paper No. 79-1518 (1979).
52. Cousteix, J., Houdeville, R. and Desopper, A., "Resultats Experimentaux et Methodes de Calcul Relatifs aux Couches Limites Turbulentes en Ecoulement Instationnaire", in Unsteady Aerodynamics, ABARD-CP-227, Ottawa (1977).
53. Walker, J. D. A., "The Boundary Layer Due to Rectilinear Vortex", Proc. Royal Soc., A359, 167-189 (1978).
54. Walker, J. D. A., private communication.
55. Williams, J. C., "On the Nature of Unsteady Three-Dimensional Laminar Boundary-Layer Separation", J. Fluid Mech., 88, 241-258 (1978).
56. Bodonyi, R. J. and Stewartson, K., "The Unsteady Laminar Boundary Layer on a Rotating Disk in a Counter-Rotating Fluid", J. Fluid Mech., 79, 669-688 (1977).
57. Robins, A. J. and Howarth, J. A., "Boundary-Layer Development at a Two-Dimensional Rear Stagnation Point", J. Fluid Mech., 56, 161-171 (1972).

## ANALYTICAL METHODS FOR PREDICTION OF UNSTEADY TURBULENT BOUNDARY LAYERS

by

D. P. Telionis  
Virginia Polytechnic Institute and State University  
Blacksburg, Virginia 24061

Almost all of the models for the closure of the turbulent boundary layer equations have been extended for the calculation of unsteady flows. The advantages and disadvantages of introducing more governing equations and, therefore, more arbitrary functions and constants are discussed. Algebraic models prove to be quite successful and very attractive since they involve the most simple procedures for the calculation of turbulent flows. One-equation and two-equation models have been extensively used with a variety of generalizations to account for the unsteadiness of the outer flow. Depending on the specific closure assumption, the character of the equation becomes either parabolic or hyperbolic. Numerical schemes for the solution of such equations have been introduced and will be referenced in this short review.

## 1. INTRODUCTION

The mathematical models that describe unsteady turbulent boundary layers are very similar in character with the equations of laminar boundary layers. New terms that model the Reynolds stresses and perhaps new equations are introduced but the equations usually remain parabolic. In one of the original formulations of the turbulent energy method, actually, the problem was reduced to first-order differential equations<sup>1,2</sup> hyperbolic in character. The method of characteristics or equivalent methods were then proposed for solution. However, since then, most investigators prefer alternative formulations which essentially retain the parabolic character of the differential equations<sup>3,4,5</sup>. Numerical methods developed for laminar flows can therefore be directly applied to turbulent flows. More details on the numerical schemes of integration can be found in the accompanying paper on laminar flows. Emphasis will be given here on the modeling of turbulent flows.

A natural classification of methods is based on the number of differential equations used in modeling the Reynolds stress<sup>7</sup>. If the Reynolds stress is related algebraically to mean flow quantities, then the model is considered a "zero-equation" model. If the differential equation that governs the Reynolds stress or if the turbulent energy equation with appropriate closure assumption is used, then the model is considered a "one-equation" model. Bringing into play the differential equation that governs the dissipation rate upgrades the model to a "two-equation" model. All methods have been used for the calculation of unsteady turbulent boundary layers and some modifications and additions have been proposed to account for special unsteady effects.

Modeling of the Reynolds stresses is a somewhat arbitrary process based on theoretical results of very special and simplified problems, or, qualitative experimental trends. In fact as the sophistication of the model increases, the number of necessary arbitrary assumptions increase as well. The final test of such methods is the comparison of theoretical results with experimental data. Unfortunately, at least until very recently, there was very little experimental information available and only for the special case of a flat plate<sup>8</sup>. In the past few years a few experimental projects were undertaken some of which are still under way, as reported by the present author in a recent review article<sup>9</sup>. At the present, work on modeling of unsteady turbulent flows is being continued in the light of the recent experimental information. This short paper gives a quick account of the methods and their relative success. More details the reader will find in Refs. 7, 9 and 10.

## 2. GOVERNING EQUATIONS

Consider the differential equations that govern two-dimensional incompressible turbulent boundary-layer flow:

$$\frac{\partial U}{\partial x} + \frac{\partial V}{\partial y} = 0 \quad (1)$$

$$\frac{\partial U}{\partial t} + U \frac{\partial U}{\partial x} + V \frac{\partial U}{\partial y} = \frac{\partial U_e}{\partial t} + U_e \frac{\partial U_e}{\partial x} + \nu \frac{\partial^2 U}{\partial y^2} + \frac{\partial \tau}{\partial y} \quad (2)$$

where  $U$  and  $V$  are the ensemble averaged velocity components parallel and perpendicular to the wall respectively,  $x$ ,  $y$  and  $t$  are the distances parallel and perpendicular to the wall and time respectively,  $\nu$  is the kinematic viscosity and  $\tau$  is the Reynolds stress.

The quantity  $\tau$  depends on the definition of the averaging process. According to the classical definition a random quantity,  $q$ , can be ensemble averaged as follows

$$\bar{q}(\underline{r}) = \lim_{N \rightarrow \infty} \frac{1}{N} \sum_{n=1}^N q(\underline{r}, t_n) \quad (3)$$

where the values  $q$  are sampled at arbitrary fixed or even random intervals of time. If an organized signal is buried in  $\bar{q}$ , then this process is averaging it out. The quantity  $q$  can be decomposed as follows

$$q(\underline{r}, t) = \bar{q}(\underline{r}) + \dot{q}(\underline{r}, t) \quad (4)$$

where by definition  $\bar{\dot{q}} = 0$ . If a conditional averaging process is adopted, that is if the sampling of the quantities  $q$  is controlled then it is possible to isolate an organized variation. Experimentally, the periodic or transient process provides an external trigger for the sampling process as described in more detail in Refs. 7, 9, 10, 11 and 12. The same mathematical expression given by Eq. (3) can be used to define

the conditional averaged quantities

$$Q(\underline{x}, t) = \lim_{N \rightarrow \infty} \sum_{n=1}^N q(\underline{x}, t + n\Delta t) \quad (5)$$

where now  $\Delta t$  is the period of a periodic oscillation. For a transient phenomenon the appropriate formula is

$$Q(\underline{x}, t) = \lim_{N \rightarrow \infty} \sum_{n=1}^N q_n(\underline{x}, t) \quad (6)$$

where  $q_n$  is the value of  $q$  of the  $n$ th realization after a time  $t$  has elapsed from a specified time station. The symbols  $U, V$  in Eqs. (1) and (2) denote conditionally averaged velocity components.

A random quantity can be decomposed now in terms of the conditional average and the random fluctuation

$$q(\underline{x}, t) = Q(\underline{x}, t) + q'(\underline{x}, t) \quad (7)$$

Note that  $q' \neq \dot{q}$ . For an unconditional sampling the Reynolds stress is given by

$$\tau = - \overline{p u \dot{v}} \quad (8)$$

For conditional averaging, the Reynolds stress in Eq. (2) contains ensemble averages of products of  $\dot{u}, \dot{v}$  and  $u', v'$ . We should conclude that the extension of models developed for steady flow to periodic or transient flows may not be straight forward. In other words, there is no justification at all to assume that the Reynolds stress,  $\tau$ , of Eq. (2) depends on conditionally averaged  $U$  and  $V$  in the same way that the Reynolds stress of the steady state equation depends on the ensemble averages  $\bar{u}$  and  $\bar{v}$ . Nevertheless, such an assumption may and has been used as a first engineering approximation to the problem and as a stepping stone in the development of more complete unsteady flow models.

The Reynolds stress may be related directly to the averaged flow or to the instantaneous turbulent energy. In the latter case the equation that governs the turbulent energy is needed to close the system

$$\frac{D}{Dt} (\overline{q^2/2}) - \frac{\tau}{\rho} \frac{\partial U}{\partial y} + \frac{\partial}{\partial y} \left[ \overline{v \left( \frac{p}{\rho} + \frac{q^2}{2} \right)} \right] + e \quad (9)$$

where  $e$  is the turbulent dissipation and  $q$  is defined by the equation

$$q^2 = \dot{u}^2 + \dot{v}^2 + \dot{w}^2 \quad (10)$$

In two-equation models a differential equation that governs the dissipation is added.

### 3. ALGEBRAIC MODELS

"Zero-equation models" are more familiar to investigators as "algebraic models". The Reynolds stress according to these models is assumed to depend algebraically on the mean flow and its derivatives. According to the most widely accepted model,

$$\tau = \epsilon \frac{\partial U}{\partial y} \quad (11)$$

A two-layer eddy viscosity model is then introduced. In the inner layer the eddy viscosity is proportional to the velocity gradient

$$\epsilon_t = \rho \lambda^2 |\partial U / \partial y| \quad (12)$$

where  $\lambda$  is the mixing length given by

$$\lambda = k_\lambda y [1 - \exp(-\frac{y}{A})] \quad (13)$$

with  $k_\lambda = 0.41$  and  $A$  the Van Driest damping factor<sup>13</sup>. The latter quantity is traditionally assumed to be inversely proportional to the friction velocity  $u_\tau = (\tau_w/\rho)^{1/2}$ , where  $\tau_w$  is the skin friction at the wall

$$A = A^+ v / u_\tau = A^+ v (\tau_w/\rho)^{-1/2} \quad (14)$$

and  $A^+ = 26$ .

To account for flows with pressure gradients as well as flows with heat transfer, Cebeci<sup>14</sup> assumed that a characteristic velocity in the Stokes flow that models the inner part of the turbulent boundary layer is the friction velocity at the edge of the viscous sublayer,  $\tau_s$ . The damping factor then becomes

$$A = A^+ v (\tau_s/\rho)^{-1/2} \quad (15)$$

This assumption permits a straightforward extension to unsteady flows. An estimate of the shear stress  $\tau_s$  can be derived by solving the approximate form of the momentum equation in the viscous sublayer. Integrating across the viscous sublayer from the wall to  $y_s^+ = y_s u_\tau / \nu = 11.8$ , yields

$$A = \frac{\nu A^+}{u_\tau} \left[ 1 - 11.8 \frac{\nu}{\rho u_\tau} \frac{\partial p}{\partial x} \right] \quad (16)$$

The acceleration effects of the outer flow now enter via the pressure gradient. Cebeci and his associates propose for the outer layer

$$\epsilon_0 = \frac{0.0168}{1 + 5.5(y/\delta)} \left| \int_0^\infty (U_e - U) dy \right| \quad (17)$$

Telionis and Tsahalis<sup>15</sup> (1975) adopted the same inner model for the eddy viscosity but used in the outer region the velocity defect law

$$\epsilon_0 = \frac{k_2 U_e}{\nu} \delta^* \gamma \quad (18)$$

where  $k_2 = 0.0168$ ,  $\delta^*$  is the displacement thickness and  $\gamma$  is intermittency factor

$$2\gamma = 1 - \operatorname{erf} \left[ 5 \left( \frac{y}{\delta} - 0.78 \right) \right] \quad (19)$$

In a later publication Telionis<sup>16</sup> attempted a comparative study of algebraic models for unsteady turbulent flows. In this paper the models of Kays<sup>17</sup> and Alber<sup>18</sup> were also extended to account for unsteadiness.

Cebeci and Keller<sup>19</sup> limited their calculations to spatially one-dimensional flows and compared their results to those of Bradshaw<sup>20</sup>. Dwyer et al.<sup>21</sup> also developed a technique based on the quasi-steady model of the mixing-length type and integrated the boundary-layer equations by a finite difference method. McCroskey and Philippe<sup>22</sup> later used this method, checked it against previous theoretical and experimental results and calculated the flow fields about airfoils. The quasi-steady mixing-length model was also used by Gupta and Trimpi<sup>23</sup>, who computed the development of a compressible turbulent boundary layer on a semi-infinite flat plate after the passage of a shock wave and a trailing driver-gas, driven-gas interface. Most recently Cebeci<sup>24</sup> employed this model again to calculate oscillatory flows over a flat plate and compare with experimental data.

It is well known that the laminar shear stress is very small compared to the Reynolds stress and outside the viscous sublayer, the term  $\nu \partial^2 U / \partial y^2$  in Eq. (2) is one order of magnitude smaller than the term  $\partial \tau / \partial y$ . With all algebraic models however, the Reynolds stress is proportional to the square of the velocity gradient. As a result the dominant derivative on the right hand side of Eq. (2) remains the second derivative with respect to  $y$ . The differential equation is parabolic and its numerical integration can be implemented by any of the methods described in the previous chapter. The investigations referenced in this section are based on straightforward numerical integrations in the three-coordinate space:  $x$ ,  $y$  and  $t$ .

An alternative formulation based on asymptotic expansion in powers of the amplitude, permit the reduction of the independent variables from three to two. This method however is confined to small amplitudes of oscillation and nearly harmonic flows. For an outer flow distribution given by

$$U_e(x, t) = U_0(x) + \alpha U_1 e^{i\omega t} \quad (20)$$

where  $\alpha$  is a small dimensionless number and  $\omega$  is the frequency of the imposed oscillation, we seek solutions in the form

$$u(x, y, t) = u_0(x, y) + \alpha u_1(x, y) e^{i\omega t} + \dots \quad (21)$$

$$v(x, y, t) = v_0(x, y) + \alpha v_1(x, y) e^{i\omega t} + \dots \quad (22)$$

Substituting expansions of this form in Eqs. (1), (2) and (11) and collecting powers of the quantity  $\alpha$  we derive sets of differential equations that can be solved seriatim for the quantities of order zero, one, etc.

Expanding in this fashion Eq. (12), Patel<sup>25</sup> estimates the Reynolds stresses that govern the mean,  $(u_0, v_0)$ , and the oscillatory part  $(u_1, v_1)$  of the flow

$$\tau_0 = \rho \ell^2 \left( \frac{\partial u_0}{\partial y} \right)^2 \quad (23)$$

$$\tau_1 = 2\rho \ell^2 \frac{\partial u_0}{\partial y} \frac{\partial u_1}{\partial y} \quad (24)$$

This expansion is therefore equivalent to the assumption that the total Reynolds stress is decomposed into a mean part,  $\tau_0$ , and an oscillatory part,  $\tau_1$ , in a way determined by the governing equation. Physically, it implies that the oscillatory Reynolds stress,  $\tau_1$ , is proportional to the gradient of the organized oscillations,  $\partial u_1 / \partial y$  but the eddy viscosity of the oscillatory motion is proportional to the gradient of the mean flow. Clearly, all these assumptions may be an optimistic initial attempt to solve the problem but bear no physical justification and yield poor results.

The simplest possible model that represents decoupling of the Reynolds stresses  $\tau_0$  and  $\tau_1$  is the quasi-laminar model which assumes that  $\tau_1 = 0$ . This assumption is essentially equivalent to a laminar oscillatory correction on a steady turbulent boundary-layer. It is well known that the boundary layer, laminar or turbulent, responds to local disturbances in an almost inviscid manner. The hypothesis here is that the outer flow pressure fluctuations are instantly carried across the turbulent boundary layer, without interaction with the random fluctuations. Or equivalently, that the turbulent eddies undergo an oscillatory deformation that does not affect their entity and the process of their mutual interaction. However, quasilaminar models did not prove successful if compared with experimental data of internal flows<sup>26</sup> or external boundary layer flows<sup>27</sup>. The next step would be to attempt independent modeling of the quantities  $\tau_0$  and  $\tau_1$ . In Ref. 27, for example, it is assumed that the oscillatory Reynolds stress is proportional to the square of the

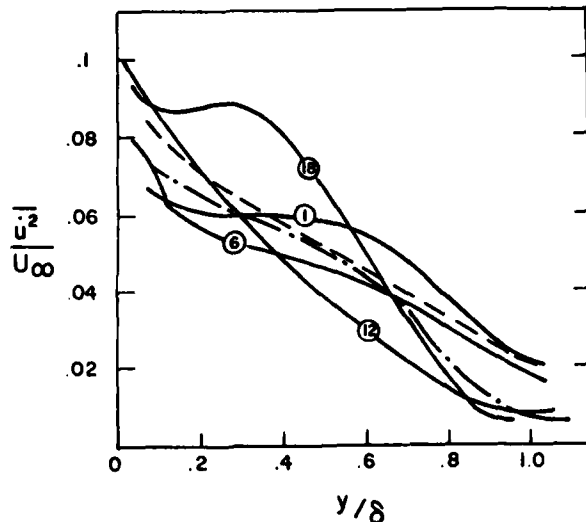


Fig. 1 Profiles of instantaneous levels of turbulence: —, four characteristic instances from Ref. 28, curves 1, 6, 12 and 18 correspond to Eq. (20) for  $\omega t = -\pi, -\pi/2, 0$  and  $\pi/2$  respectively; ---, from Ref. 25 averaged through the cycle; -.-.-, steady flow.

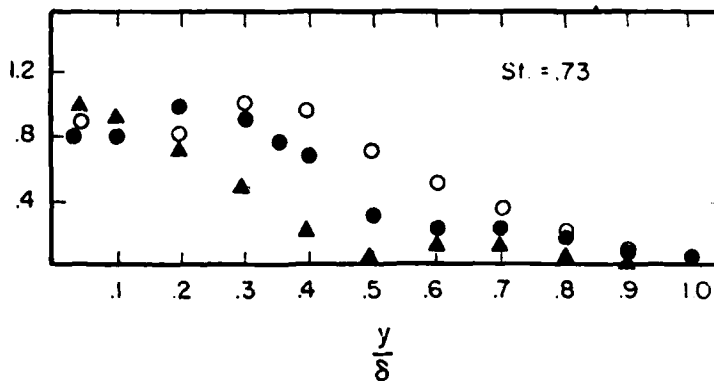


Fig. 2 Distribution of the normalized amplitude of the oscillatory part of the Reynolds stress,  $(\tau_1)$ , across the boundary layer for a Strouhal number equal to 0.073.  $\circ$ , rough estimate derived from Ref. 28;  $\bullet$ , Ref. 27;  $\blacktriangle$ , quasi-steady model.

successfully the velocity profiles as shown in Fig. 4. For a larger frequency the discrepancies appear to be smoothing out again.

gradient of the oscillatory part of the velocity.

Equations (23) and (24) represent the asymptotic form of the classical eddy viscosity model given by Eq. (12) which was originally proposed and extensively used in steady boundary layer flows. Solutions based on such expressions could therefore be classified as "quasi-steady" models, although they do depend on time implicitly, through the mean flow  $U_e(x, t)$ . Methods based on independent modeling of the steady and fluctuating part of the Reynolds stress may be considered as truly unsteady models. Evidence that unsteady models are more accurate representations of actual unsteady turbulent flow is provided by comparison of predicted velocity profiles with experimental data. Most recently, the actual variations in time of turbulent kinetic energy and the Reynolds stress were measured<sup>28,29</sup>. In Fig. 1 we plot profiles of instantaneous and averaged dimensionless values of one term of the turbulent energy as obtained from Refs. 25 and 28. It should be emphasized that the conditions for which these data have been obtained are quite different. Therefore, plotting the data on the same graph may be misleading and the reader is alerted to this fact. The reduced amplitude of the fluctuating component of the Reynolds stress as inferred from the measurements and calculated by an unsteady and a quasi-steady model are shown in Fig. 2.

The data is very limited and no definite information at this time can be extracted to guide the theoretical modeling of the Reynolds stress. The reported instantaneous profiles of Reynolds stress<sup>28</sup> correspond only to four values of the phase. As a result it is very difficult to obtain phase difference variation. However, a careful inspection of the experimental data is enough to convince that the Reynolds stress varies in phase with the outer flow only in the immediate neighborhood of the wall. Further away from the wall and for the most part of the boundary layer, it appears that the Reynolds stress leads the outer flow by approximately  $90^\circ$ . It should be noted that in quasi-steady models, the Reynolds stress is essentially and tacitly assumed to vary in phase with the outer flow.

A number of experimental projects have resulted in valuable experimental information in the last few years as described in Refs. 9 and 12. However, most theoreticians have tested their results against the classical data of Karlsson<sup>8</sup>. In Fig. 3 we show the amplitudes of the "in-phase" and "out-of-phase" velocity profiles for the lowest available frequency. It should be noted that quasi-steady models fail to predict the overshoot of the in-phase velocity component. At  $\omega/2\pi = 1.0$  which has been shown for laminar flows to correspond to the intermediate regime between high and low frequencies, the situation changes drastically and no analytical method has been shown up to now to predict

## 4. ONE-EQUATION MODELS

To close the system of Eqs. (1) and (2) by virtue of the energy equation, one needs to model the Reynolds stress in terms of the turbulent kinetic energy. According to one of the original models<sup>1</sup> it may be assumed that  $\tau$  is simply proportional to  $q^2$

$$\tau_o = \rho a_1 L^2 \left( \frac{\partial u_o}{\partial y} \right)^2 \quad (25)$$

where  $a_1$  is a universal constant equal to 0.15. The triple product and the energy dissipation are also modeled

$$\overline{v'(p'/\rho + q^2/2)} = \frac{1}{U_e} (\overline{q^2})_{\max} \overline{q^2} a_2 \quad (26)$$

$$e = (\overline{q^2})^{3/2} / L \quad (27)$$

where  $a_2$  and  $L$  are universal empirical functions of  $y$ . Here  $a_1$  and  $a_2$  are dimensionless but  $L$  has units of length.

Bradshaw et al<sup>1</sup> note that in most applications, the convection and diffusion terms are negligible and Eq. (9) reduces to

$$-\frac{\tau}{\rho} \frac{\partial U}{\partial y} + e = 0 \quad (28)$$

It can be readily seen then that the assumption (27) is equivalent to

$$\tau = \rho a_1 L^2 \left( \frac{\partial U}{\partial y} \right)^2 \quad (29)$$

which is essentially Prandtl's mixing length formulation. The present author feels that a straightforward extension of Eq. (28) to unsteady flow should include the local acceleration of the turbulent kinetic energy, which may not be small if large frequency oscillations are imposed. The equivalent simplified but unsteady version of Eq. (9) then is

$$\frac{\partial \overline{q^2}}{\partial t} - \frac{\tau}{\rho} \frac{\partial U}{\partial y} + e = 0 \quad (30)$$

One may conclude, that for unsteady flow, the functional dependence of  $\tau$  on  $L$  and  $\partial U/\partial y$  given by (29) is not sufficient. It is very interesting to solve this equation in order to arrive at the generalization of Prandtl's mixing length formula for unsteady flow, as dictated by the turbulent energy equation and the closure assumptions of Ref. 1. Assume that the mean flow oscillates harmonically

$$U = u_o + u_1 e^{i\omega t} \quad (31)$$

Assuming further that the Reynolds stress also fluctuates about a mean

$$\frac{\tau}{\rho} = \frac{\tau_o}{\rho} + \frac{\tau_1}{\rho} e^{i\omega t} \quad (32)$$

we can bring Eq. (30) to the form

$$\begin{aligned} \frac{i\omega}{2a_1} \frac{\tau_1}{\rho} e^{i\omega t} - \left( \frac{\tau_o}{\rho} + \frac{\tau_1}{\rho} e^{i\omega t} \right) \times \\ \left( \frac{\partial u_o}{\partial y} + \frac{\partial u_1}{\partial y} e^{i\omega t} \right) \\ + \left( \frac{\tau_o}{\rho a_1} + \frac{\tau_1}{\rho a_1} e^{i\omega t} \right)^{3/2} \frac{1}{L} = 0 \quad (33) \end{aligned}$$

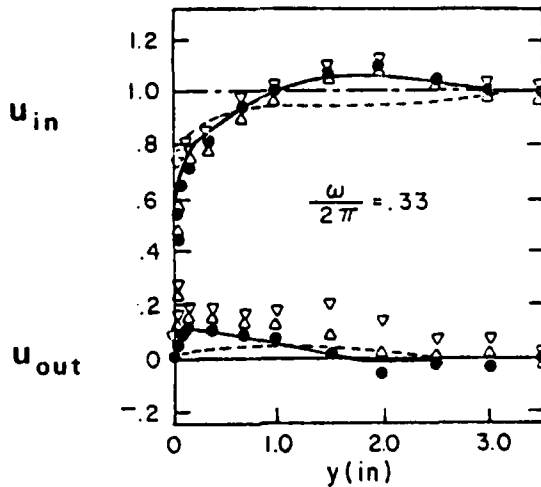


Fig. 3 In-phase and out-of-phase velocity profiles for  $\omega/2\pi = 0.33 \text{ sec}^{-1}$ , —, Ref. 27; - - -, Ref. 24;  $\nabla$ ,  $\Delta$ ,  $\bullet$ , experimental points from Ref. 8 for low, medium and high amplitudes respectively.

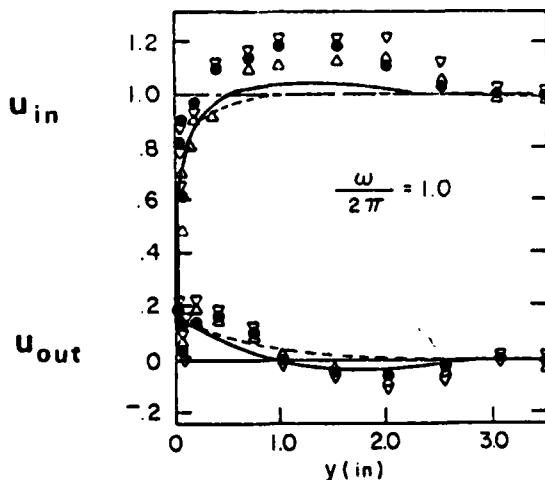


Fig. 4 In-phase and out-of-phase velocity profiles for  $\omega/2\pi = 1.00 \text{ sec}^{-1}$ , —, Ref. 27; - - -, Ref. 24;  $\nabla$ ,  $\Delta$ ,  $\bullet$ , experimental points from Ref. 8, for low, medium and high amplitudes respectively.

No perturbation principles are invoked here and the expansion in Eqs. (31) and (32) is simply decomposition to mean and oscillatory parts. The steady terms in Eq. (33) reduce to Eq. (29) expressed in terms of mean quantities

$$\tau_o = \rho a_1 L^2 \left( \frac{\partial u_o}{\partial y} \right)^2 \quad (34)$$

This may be considered as yet another indication that the mean part of an oscillating turbulent boundary layer is not influenced by nonlinear effects. Physically, this is due to the fact that the nonlinear terms in the turbulent energy equation, that is the convection terms usually represent a negligible contribution and can be omitted.

Neglecting the higher harmonics in Eq. (33), we can solve for the fluctuating part of the Reynolds stress

$$\frac{\tau_1}{\rho} \left[ -\frac{\partial u_o}{\partial y} + \frac{3}{2a_1 L} \left( \frac{\tau_o}{\rho a_1} \right)^{1/2} + \frac{4\omega}{2a_1} \right] = \frac{\tau_o}{\rho} \frac{\partial u_1}{\partial y} \quad (35)$$

Some qualitative characteristics can now be identified. Dividing through by  $(\tau_o/\rho a_1)^{1/2}$  renders the factor in the brackets dimensionless and indicates that  $\tau_1$  is proportional to the product of the gradients of the mean and the oscillatory velocity components

$$\tau_1 \propto \left( \frac{\partial u_o}{\partial y} \right) \left( \frac{\partial u_1}{\partial y} \right) \quad (36)$$

It is very interesting to note that a straightforward expansion of the algebraic models described in the previous section resulted in a similar equation. Such a closure model therefore has the potential of further development. The coefficient of proportionality, however, is complex and this implies that the Reynolds stress does not oscillate in phase with the velocity field, in agreement with the experimental findings of Ref. 28. The departure from the in-phase variation grows with frequency.

Assuming that the term  $\partial^2 U/\partial y^2$  in Eq. (2) is negligible, changes the character of the problem from parabolic to hyperbolic. Hyperbolic systems of equations are conveniently integrated by the method of characteristics<sup>1</sup>. The mesh is aligned with the characteristics and the system reduces to ordinary differential equations. Singleton and Nash<sup>30</sup> propose instead to march downstream, essentially following the traditional method of solution of the boundary layer equation. They introduce a transformation to account for the thickening of the boundary layer

$$t = t, \quad x = \xi, \quad y = S(x,t)\eta^\beta \quad (37)$$

where  $S$  is taken to be equal to  $1.25 \delta$ . They then account for three-dimensionality effects by considering the flow about an infinite yawed cylinder. A third velocity and Reynolds stress component is thus introduced but the problem can still be solved in two space dimensions and time. The equations are rewritten in the form

$$\frac{\partial F}{\partial t} = A \frac{\partial F}{\partial \eta} + B \frac{\partial F}{\partial x} + C \quad (38)$$

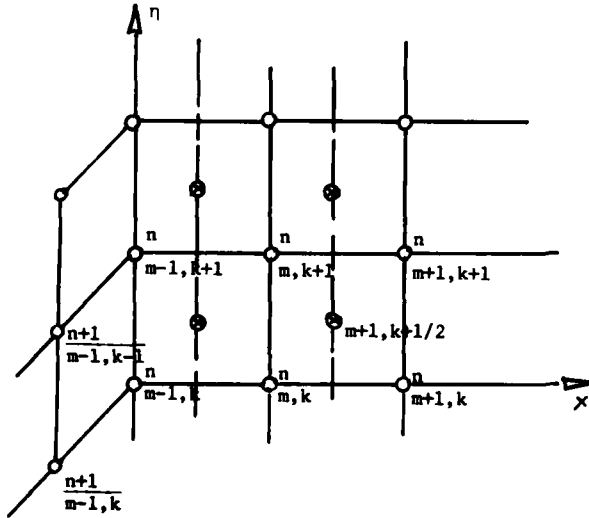


Fig. 5 Uniform grid for the numerical scheme of Ref. 30. ○, primary points; ●, secondary points.

the formula

$$F_{m,k+1/2}^{n+1} = \frac{1}{2} (F_{m,k}^n + F_{m,k+1}^n) + \frac{1}{8} \Delta \eta \left[ \left( \frac{\partial F}{\partial \eta} \right)_{m,k}^n + \left( \frac{\partial F}{\partial \eta} \right)_{m,k+1}^n \right] + \frac{1}{2} \Delta t \left[ \left( \frac{\partial F}{\partial t} \right)_{m,k}^n + \left( \frac{\partial F}{\partial t} \right)_{m,k+1}^n \right] \quad (41)$$

where  $F$  represents a dependent variable,  $A$ ,  $B$  and  $C$  are functions of the dependent variables and in addition  $C$  contains derivatives of  $U$  and  $V$  with respect to  $\eta$ . Following the work of Nash<sup>31</sup> a mesh pattern is introduced with primary and secondary points as shown in Fig. 5. Fourth-order differences in the  $\eta$ -direction are written

$$\begin{aligned} \left( \frac{\partial F}{\partial \eta} \right)_{k,m}^n &= \frac{1}{\Delta \eta} \left[ \frac{1}{12} F_{k-2,m}^n - \frac{2}{3} F_{k-1,m}^n \right. \\ &\quad \left. + \frac{2}{3} F_{k+1,m}^n - \frac{1}{12} F_{k+2,m}^n \right] + O(\Delta \eta)^4 \end{aligned} \quad (39)$$

except for the point  $k = K-1$  at the edge of the boundary layer where

$$\begin{aligned} \left( \frac{\partial F}{\partial \eta} \right)_{k,m}^n &= \frac{1}{\Delta \eta} \left[ \frac{1}{6} F_{K-3,m}^n - F_{K-2,m}^n \right. \\ &\quad \left. + \frac{1}{2} F_{K-1,m}^n + \frac{1}{3} F_{K,m}^n \right] + O(\Delta \eta)^3 \end{aligned} \quad (40)$$

For the calculations of unsteady flow, Singleton and Nash use an explicit second-order accurate, finite difference scheme. New time points are calculated at secondary points in the new time plane according to



These expressions are then used to derive more accurate values at the primary mesh points. With appropriate boundary and initial conditions, information is derived in the two dimensional space for time  $t$ . Time then is incremented to  $t + \Delta t$  and information on a new time plane is obtained. Marching therefore proceeds first in the  $x$ -direction sweeping the two-dimensional physical space and then in time, progressing in the future.

Nash, Carr and Singleton<sup>32</sup> employ the method described above to calculate the response of a turbulent boundary layer to oscillatory fluctuations of the outer stream. They investigate flow fields with adverse pressure gradients and proceed until the point of flow reversal. In these investigations and due to the neglect of the laminar shear stress, the calculations cannot be extended to the wall. Instead the solution is matched at  $y/\delta = .05$  with  $\delta$  the boundary-layer thickness, to an approximate solution. The same group (Patel and Nash<sup>33</sup>, Nash and Scruggs<sup>34</sup>) later extended their work by introducing a refinement in the neighborhood of the wall, to meet the inner boundary condition. This is essentially the law of the wall with appropriate modifications in order to handle regions of partially reversed flow.

A comparison of the relative performance of different methods (Singleton and Nash<sup>30</sup>, Nash, Carr and Singleton<sup>32</sup>, Kuhn and Nielsen<sup>35</sup>, Telionis and Tshahalis<sup>15</sup>) has been attempted by Cousteix, Desopper and Houdeville<sup>36</sup> who employ a two-equation model. Oscillating flows over a flat plate and a configuration that imposes an adverse pressure gradient were examined. In particular outer flows were chosen according to the formulas

$$U_e = U_0(1 + \alpha \sin \omega t) \quad (42)$$

$$U_e = U_0[1 + (\alpha_0 + \alpha_1 \sin \omega t)x] \quad (43)$$

where  $\alpha_1$  are dimensionless amplitudes,  $x$  and  $t$  are dimensionless downstream distance and time respectively and  $\omega$  is the reduced frequency,  $\omega = \omega L/U_0$ . All quantities were calculated at the point  $x = 1.0$ , for two different frequencies,  $\omega = 1.57$  and  $15.7$  and different values of the amplitude parameters.

Figure 6 and 7 show the periodic variation of the displacement thickness and the skin friction for a small amplitude ( $\alpha = 0.125$ ) and two different frequencies, ( $\omega = 1.57$  and  $15.7$ ). Unexpected discrepancies appear in the displacement thickness for low frequency and amplitude. Similar calculations for higher amplitudes indicate only some departure from the harmonic response of both quantities. The maxima of all curves appear to be more pointed but very little change in the phase angles can be observed. All methods indicate that the skin friction phase lead does not exceed  $10^\circ$ , although the displacement thickness phase lead may reach values of  $30^\circ$  or  $40^\circ$ . Moreover, large departures from the quasi-steady values are indicated in the plots of displacement thickness.

In Fig. 8 calculated and measured values of the skin friction phase lead are plotted versus the frequency parameter  $\omega$ . The case of laminar flow is also indicated and values of the skin friction phase lead are widely dispersed in the neighborhood of the wall. Karlsson actually measured only the in-phase and out-of-phase of the velocity components. An estimate of the phase angle from these data can be derived by extrapolation followed by calculation of the ratio of the out-of-phase to the in-phase components. The dispersion of the analytical results shown in this figure is equally disheartening.

Fig. 6 Displacement thickness and wall shear outer flow given, by Eq. (28) with  $\alpha = 0.125$ ,  $\omega = 1.57$ ;  $x/L = 1$ ,  $Re = 10^7$ , —, Ref. 36; ---, Ref. 32; -·-·-, Ref. 35; - - -, Ref. 15.

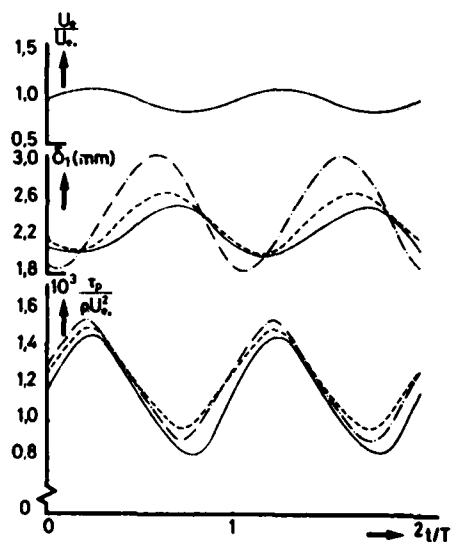
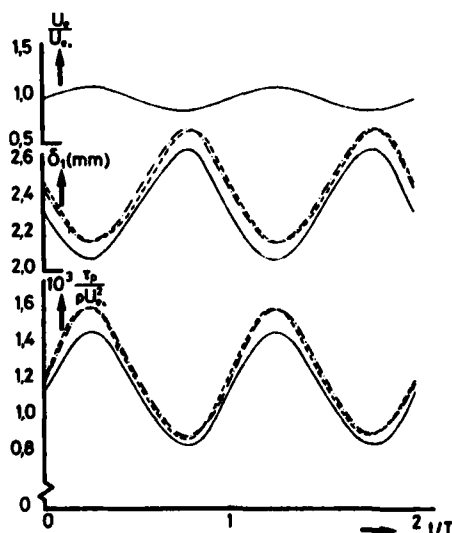


Fig. 7 Displacement thickness and wall shear for  $\alpha = 0.125$ ,  $\omega = 15.7$ ,  $Re = 10^7$ ,  $x/L = 1$ . —, Ref. 36; ---, Ref. 32; -·-·-, Ref. 35.



Quasi-steady calculations with outer flow distributions of the type given by Eq. (29) indicate that the wall shear may vanish during a portion of the period. In fact it is probable that separation is in the

neighborhood of this point as indicated by the large values of the displacement thickness. Calculated results with the quasi-steady models and the corresponding unsteady models are shown in Figs. 9 and 10 for small and large frequencies respectively. It is most interesting to note that the unsteady boundary layer remains attached and well behaved for a pressure gradient which, if averaged, would induce separation. It is noted further that the larger frequencies and therefore much larger pressure gradients that the boundary layer experiences periodically do not seem to affect the phenomenon. In other words, the strong but periodic pressure gradients due to the term  $\partial U_e / \partial t$ , which in fact grow larger with frequency, do not induce separation. The results indicate that the point of flow reversal is displaced downstream, at least for the range of frequencies investigated.

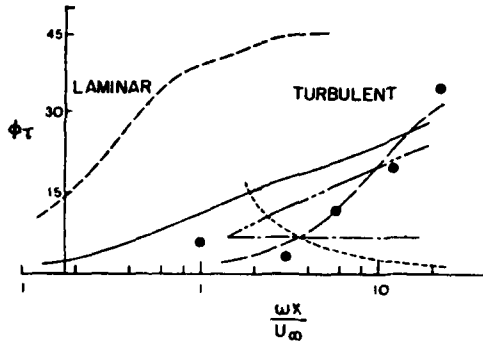


Fig. 8 The skin friction phase angle. Theoretical results: ---, Ref. 35; -.-.-, Ref. 32; ———, Ref. 15; - - - - -, Ref. 14; ———, Ref. 22. Experimental data derived approximately from Ref. 8.

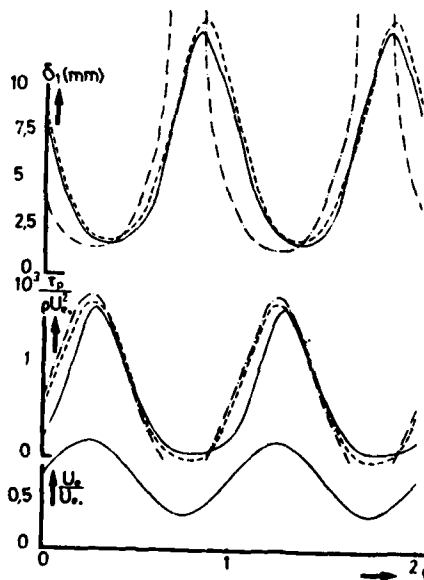


Fig. 9 Displacement thickness and wall shear for Eq. (29) with  $\alpha_0 = -0.2$ ,  $\alpha_1 = 0.4$ ,  $\bar{\omega} = 1.57$ ,  $x/L = 1$ ,  $Re = 10^7$ . ———, Ref. 36; -.-.-, Ref. 32; - - - - -, Ref. 35.

acter of the closure models is not necessarily different in the reversing flow region. In other words, the Reynolds stress effect is equivalent to shear stresses opposing the motion and pushing towards deceleration of the local flow, regardless of the direction of the outer flow. For models based on the turbulent energy method, Patel and Nash<sup>33</sup> propose a modification of Eq. (9) and (25)

$$\frac{D\tau}{Dt} + 2a_1 |\tau| \frac{\partial U}{\partial y} + 2a_1 \phi + 2a_1 \frac{\partial}{\partial y} (a_2 \tau) + 2a_1 \frac{\tau}{L} |\tau|^{1/2} = 0 \quad (49)$$

where

Nash, Carr and Singleton<sup>32</sup> calculated unsteady boundary layers and the upstream propagation of flow reversal but terminated their calculations at the point of zero wall shear. Turbulent boundary layers that remain attached, even over a thin recirculating region, have been calculated by Telionis and Tsahalis<sup>15</sup>, Patel and Nash<sup>33</sup> and others. In these references transient flows with ever steepening adverse pressure gradients are investigated. Telionis and Tsahalis<sup>15</sup> chose a linearly decelerating flow which eventually separates. In such calculations it is necessary that flow reversal propagates upstream faster than other disturbances as described in detail in the earlier chapter with regard to laminar flows. It is then necessary to drop a few of the mesh points at the downstream end of the domain. To avoid this, Patel and Nash<sup>33</sup> and later Nash<sup>32</sup> and Nash and Scruggs<sup>34</sup> chose an outer flow with a linear decrease followed by a linear increase of the velocity

$$U_e(x, t) = U_0 \text{ for } t \leq 0, \text{ all } x \quad (44)$$

$$U_e/U_0 = 1 - \frac{x}{x_1} [1 - f(t)] \quad \text{for } t \geq 0, 0 \leq x \leq x_1 \quad (45)$$

$$U_e/U_0 = 1 - \frac{x_2 - x}{x_1} [1 - f(t)] \quad \text{for } t \geq 0, x_1 \leq x \leq C \quad (46)$$

where  $C$  is the downstream extend of integration,  $x_1, x_2$  are prescribed values of  $x$  and  $f$  is an arbitrary function of time. Nash and Scruggs proposed

$$f = 1 - (1 - f_f)t/t_f \quad \text{for } 0 \leq t \leq t_f \quad (47)$$

$$f = f_f \quad \text{for } t_f \leq t \quad (48)$$

with  $f_f$  and  $t_f$  some prescribed constants. Such flows and their equivalent oscillatory variations were essentially proposed for investigation of the relationship between unsteady flow reversal and separation. Of interest in this section is the modeling of turbulent boundary layers with partially reversed velocity profiles.

To integrate through such regions, the basic assumption made by all the investigators is that for negative  $\partial U / \partial y$  the eddy viscosity also changes sign. However, it was further assumed that the basic char-

$$\phi = \Gamma \left[ \left| \tau \frac{\partial U}{\partial y} + \tau \left| \frac{\partial U}{\partial y} \right| \right] \quad (50)$$

with  $\Gamma$  some large number. The inclusion of the last term does not have any effect on the resultant shear stress and essentially serves to maintain the proper direction of the shear stress vector according to the equation

$$\tau = a_1 \bar{q}^2 \operatorname{sgn} \left( \frac{\partial U}{\partial y} \right) \quad (37)$$

In a later publication<sup>34</sup> Nash and Scruggs propose an alternative assumption for closing the turbulent energy equation

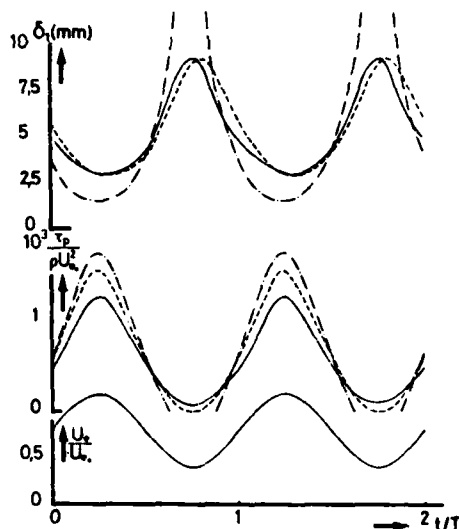
$$\tau = -k(\bar{q}^2)^{1/2} L \frac{\partial U}{\partial y} \quad (38)$$

This assumption results in a drastic change of the character of the differential equations. A second derivative of the mean velocity  $U$  reappears and the system becomes again parabolic.

It should be emphasized that according to the models described, the Reynolds stress in the neighborhood of a vanishing  $\partial U/\partial y$ , are zero. This occurs at the point of zero skin friction and from then on, there may exist further downstream, a point where  $\partial U/\partial y$  vanishes within the flow.

#### REFERENCES

Fig. 10 Displacement thickness and wall shear for Eq. (29) with  $\alpha_0 = -0.2$ ,  $\alpha_1 = 0.4$ ,  $\tilde{\omega} = 15.7$ ,  $x/L = 2$ ,  $Re = 10^7$ . —, Ref. 36; ---, Ref. 32; -.-.-, quasi steady calculation.



1. Bradshaw, P., Ferris, D. H. and Atwell, N. P., "Calculation of Boundary Layer Development Using the Turbulent Energy Equation", *J. Fluid Mech.*, **28**, 593-616 (1967).
2. Patel, V. C. and Nash, J. F., "Some Solutions of the Unsteady Turbulent Boundary Layer", in *Recent Research on Unsteady Boundary Layers*, E. A. Eichelbrenner (ed.), **1**, 1106-1164 (1971).
3. Norris III, H. L. and Reynolds, W. C., "Turbulent Channel Flow with a Moving Wavy Boundary", Stanford University Technical Report, No. TF-7, (May 1975).
4. Launder, B. E. and Spalding, D. B., "The Numerical Computation of Turbulent Flows", *Comp. Methods in Appl. Mech. and Eng.*, **3**, 269-389 (1974).
5. Nash, J. F., "Further Studies of Unsteady Boundary Layers with Flow Reversal", NASA CR-2767 (1976).
6. Telionis, D. P., "Analytical Methods for Prediction of Laminar Boundary Layers", contribution to the present volume.
7. Reynolds, W. C., "Computation of Turbulent Flows", in *Annual Review of Fluid Mechanics*, Vol. 8, pp. 183-208 (1976).
8. Karlsson, S. K. F., "An Unsteady Turbulent Boundary Layer", *J. Fluid Mech.*, **5**, 622-636 (1959).
9. Telionis, D. P., "Review - Unsteady Boundary Layers, Separated and Attached", *J. Fluids Eng.*, **101**, 29-42 (1979).
10. Telionis, D. P., *Unsteady Viscous Flow*, Springer, to appear.
11. Kovaszny, L. S. G., "Measurement in Intermittent and Periodic Flow", *Proceeding of the Dynamic Flow Conference*, 1978, 133-160 (1978).
12. Telionis, D. P., "Experimental Techniques for Unsteady Boundary Layers", contribution to the present volume.
13. Van Driest, E. R., "On Turbulent Flow Near a Wall", *J. Aero. Sci.*, **23**, 1007-1010 (1956).
14. Cebeci, T., "The Behavior of Turbulent Flow Near a Porous Wall with Pressure Gradient", *AIAA J.*, **8**, 2152-2156 (1970).
15. Telionis, D. P. and Tsahalis, D. Th., "Unsteady Turbulent Boundary Layers and Separation", *AIAA J.* **14**, 468-474 (1975).
16. Telionis, D. P., "On the Dynamics of Eddy Viscosity Models for Turbulent Boundary Layers", *Arch. of Mechanics*, **28**, 997-1010 (1976).
17. Kays, W. M., ASME Paper No. 71-HF-44 (1971).

18. Alber, I. E., "Similar Solutions for a Family of Separated Turbulent Boundary Layers", AIAA Paper No. 71-203, (1971).
19. Cebeci, T. and Keller, H. B., "On the Computation of Unsteady Turbulent Boundary Layers", in Recent Research on Unsteady Boundary Layers, E. A. Eichelbrenner (ed.), II, 1072-1105 (1972).
20. Bradshaw, P., "Calculation of Boundary Layer Development Using the Turbulent Energy Equation, VI. Unsteady Flow", NPL AERO Rept. 1288 (1969).
21. Dwyer, H. A., Doss, E. D. and Goldman, A. L., "A Computer Program for the Calculation of Laminar and Turbulent Boundary-Layer Flows", NACA CR 114366 (1970).
22. McCroskey, W. J. and Philippe, J. J., "Unsteady Viscous Flow on Oscillating Airfoils", AIAA J. 13, 71-79 (1975).
23. Gupta, R. N. and Trimpi, R. L., "An Eddy-Viscosity Treatment of the Boundary Layer on a Flat Plate in an Expansion Tube", Heat Transfer 1974, The Japan Soc. of Mech. Eng. and the Soc. of Chem. Eng., Japan, 2, 339-343 (1974).
24. Cebeci, T., "Calculation of Unsteady Two-Dimensional Laminar and Turbulent Boundary Layers with Fluctuations in External Velocity", Proc. Royal Soc., London, A355, pp. 225-238 (1977).
25. Patel, M. H., "On Turbulent Boundary Layers in Oscillatory Flow", Proc. Royal Soc. London, A353, pp. 121-144 (1977)..
26. Acharya, M. and Reynolds, w. C., "Measurements and Predictions of a Fully Developed Turbulent Channel Flow with Imposed Controlled Oscillations", Stanford University Technical Report, No. TF-8, (May 1975).
27. Romaniuk, M. S. and Telionis, D. P., "Turbulence Models for Oscillating Boundary Layers", AIAA Paper No. 79-0069 (1979).
28. Cousteix, J., Desopper, A. and Houdeville, R., "Structure and Development of a Turbulent Boundary Layer in an Oscillatory External Flow", Proceedings of Symposium on Turbulent Shear Flows, Penn. State University, University Park, PA (1977).
29. Cousteix, J., Desopper, A. and Houdeville, R., "Résultats Expérimentaux et Méthodes de Calcul Relatifs aux Couches Limites Turbulentes en Écoulement Instationnaire", AGARD Symposium on Unsteady Aerodynamics, Ottawa, Paper #17 (1977).
30. Singleton, R. E. and Nash, J. F., "A Method for Calculating Unsteady Turbulent Boundary Layers in Two- and Three-Dimensional Flow", Proc. AIAA Computational Fluid Dynamics Conference, 84-91 (1973).
31. Nash, J. F., "An Explicit Scheme for the Calculation of Three-Dimensional Turbulent Boundary Layers", J. Basic Eng., 131-141 (1972).
32. Nash, J. F., Carr, L. W. and Singleton, R., "Unsteady Turbulent Boundary Layers in Two-Dimensional Incompressible Flow", AIAA J. 13, 167-172 (1975).
33. Patel, V. C. and Nash, J. F., "Unsteady Turbulent Boundary Layers with Flow Reversal", in Unsteady Aerodynamics, ed. R. B. Kinney, Vol. 1, 199-220, 1975.
34. Nash, J. F. and Scruggs, R. M., "Unsteady Boundary Layers with Reversal and Separation", AGARD Symposium on Unsteady Aerodynamics, Ottawa, Paper No. 18 (1977).
35. Kuhn, G. D. and Nielsen, J. N., "Studies of an Integral Method for Calculating Time Dependent Turbulent Boundary Layers", Nielsen Engineering and Research, Inc., Rept. NEAR TR 57 (1973).
36. Consteix, J., Desopper, A. and Houdeville, R., "Recherches Sur Les Couches Limites Turbulentes Instationnaires", ONEPA TP No. 147 (1976).

## PREDICTION METHODS FOR UNSTEADY SEPARATED FLOWS

by

Dr T.S.Beddoes  
Aeromechanics Dept.  
Westland Helicopters  
Yeovil, Somerset BA20 2YB  
UK

### 1. Introduction

Experimental investigations have provided an understanding of the phenomena associated with separated flows, both unsteady and quasi steady. To apply this understanding to engineering problems requires the development of quantitative analytical methods to enable the importance of geometric and flow parameters to be evaluated. Unfortunately, the potentially more rigorous theories require very considerable computational effort, and, to compliment their usefulness for airfoil applications methods for the simulation or synthesis of experimentally derived characteristics have been developed for routine use. A wide field has been well covered by existing literature, for example, a previous AGARD lecture series (No. 94) in 1978 was devoted entirely to this topic. A comprehensive review and extensive bibliography has been compiled by Dr. McCroskey of NASA Ames in reference 19 covering unsteady flows, attached and separated, for airfoils and bodies. In addition, as a contribution to the above lecture series, Dr. McCroskey has already reviewed the 'state of the art' for prediction methods for unsteady separated flows on two dimensional airfoils at subsonic speeds (reference 1). A similar review (in French) has been presented by Dr. Phillippe of ONERA (reference 2). Much of this presentation, then, constitutes a repetition of these two references.

### 2. Theoretical Methods

#### a) Solutions to the Navier Stokes equation

The most fundamental formulation of the equations of motion for a viscous, compressible fluid constitute the Navier Stokes equations. Exact solutions for practical applications are not available but the development of finite difference and numerical techniques has enabled numerical solutions to be obtained. These solutions provide a means for overcoming the limitations resulting from the simplifications of 'classical' aerodynamics which allow the separate treatment of the boundary layer and external flow. This is particularly relevant for the process of unsteady separation where distinction between the two regimes is quite artificial. Three references (10, 11, 15) from the same conference proceedings, are quoted as examples of numerical techniques applied to the Navier Stokes equation. The specific problem of dynamic stall during harmonic forcing is treated by Mehta (Reference 10) and some of the graphical results constitute figure 1 which shows a sequence of pictures of streamlines and equi-vorticity lines synchronised with the pressure distribution. The physical features of bubble and vortex formation and motion are represented in great detail and were shown to correlate with flow visualisation pictures obtained for matching parameters.

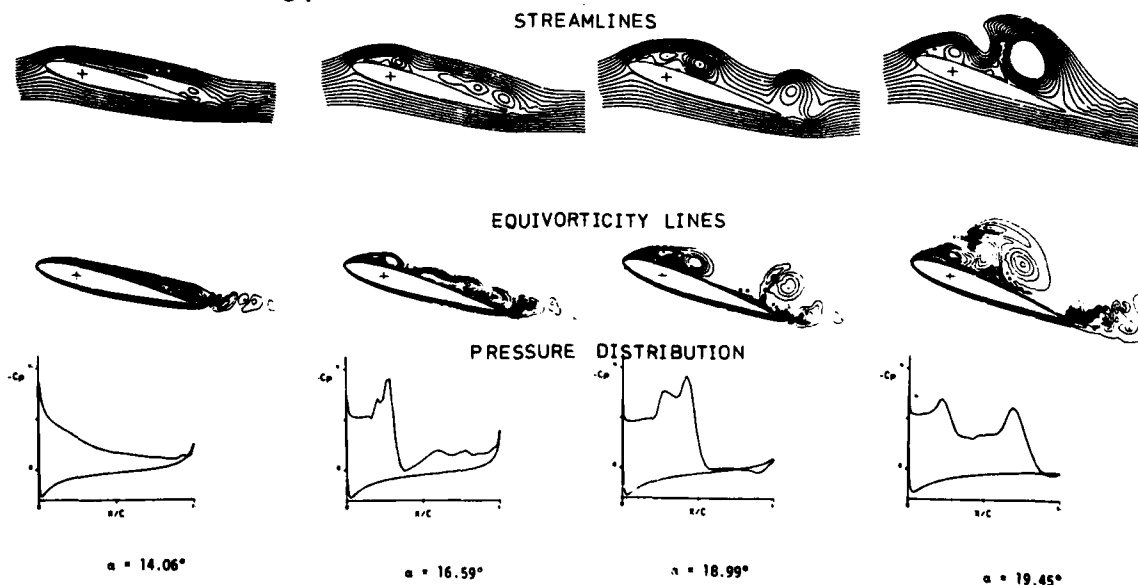


FIG.1. SOLUTION OF NAVIER STOKES EQUATIONS,  $k=0.25$

The inability to solve for the turbulent boundary layer has limited the solution to low Reynolds numbers ( $10^4$ ). Consequently the multiple vortex shedding from the aft and mid-section of the airfoil is not representative of the range of current practical interest (say  $3 \times 10^6$ ) where visualisation has indicated the dominance of the leading edge vortex. Compressibility effects are ignored; these are significant even at low free stream Mach number and need to be included to provide reliable predictions. These reservations are common to the two other treatments cited but should not detract from the significant accomplishment represented by these studies. To add some perspective to the computational requirements, for the computer used (CDC.7600) the total core storage was required and a CPU time of nearly 900 minutes quoted for one complete cycle of airfoil motion.

In reference 15, Kinney applies some of the techniques of 'classical' aerodynamics including representation of the body (airfoil) by bound-vortex singularities and solves for the forcing represented by an impulsive gust and a periodic gust. Wu et.al. in reference 11, present their experience in applying various approaches to formulating and solving the Navier Stokes equation. In due course it is to be hoped that current limitations will be overcome and a sufficiently rigorous solution obtained to provide further insight into the details of the development of separated flow. When this is accomplished, it should provide a basis for the development of more tractable solutions.

b) Discrete Vortex Potential Flow Model

Based on flow visualisation observations and pressure measurements from experiment, a conceptual model of dynamic stall was constructed by Ham (reference 12) in a form amenable to analysis by potential flow methods. The procedure is illustrated by figure 2. In the physical plane bound vorticity is shed from the leading and trailing edges of a thin airfoil in the form of free vortex elements which convect under the influence of the resultant local velocity. The strength of the vortices is adjusted to ensure stagnation points on the airfoil which include those required to define the forward separation point and the extent of the reverse flow region. The geometry is transformed into the  $\zeta$  plane, in which the airfoil becomes a circle, for solution by potential theory.

This approach has been extended by the Bertin Company for an airfoil with finite thickness and combined with a boundary layer analysis to provide definition of the forward separation point. The flow field and local velocities are calculated by an adaptation of the numerical potential flow technique of Geising (reference 20). Although this approach provides a fairly realistic representation of the developing flow-field during the onset of separation, crucial assumptions have to be made in order to perform the calculation. Thus pending further development the procedure cannot be used in an entirely predictive manner for arbitrary profiles.

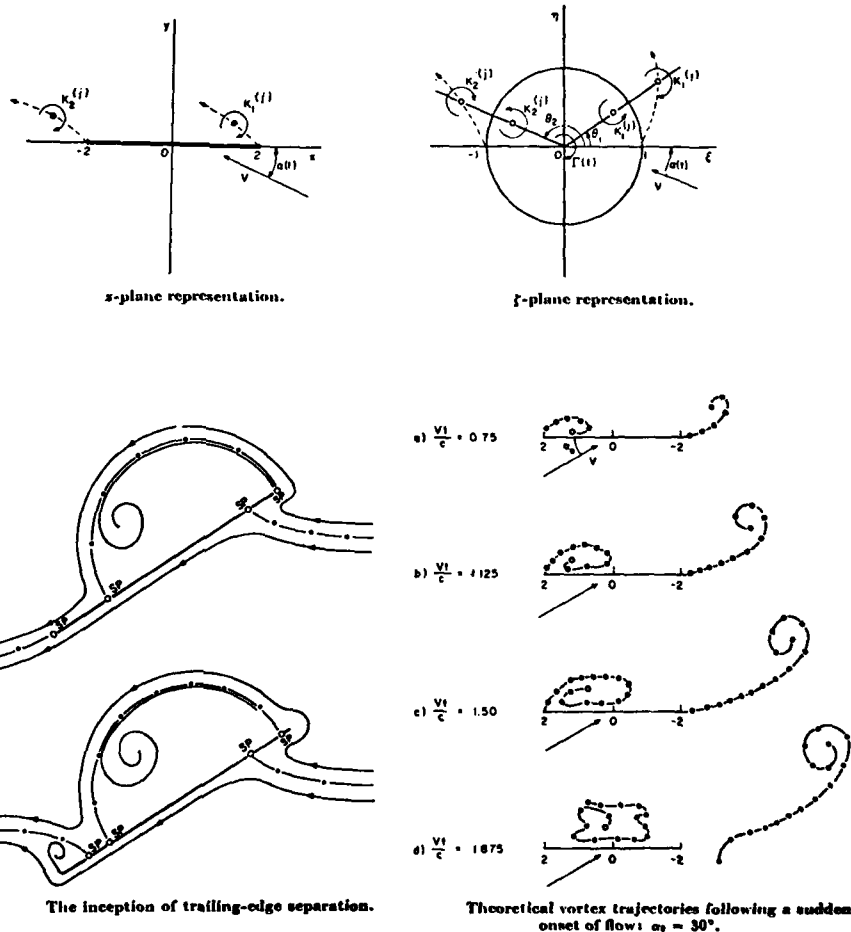


FIG.2. DISCRETE POTENTIAL VORTEX

c) Boundary Layer Calculations

For the steady state condition the application of boundary layer theory has been used with some success to determine flow behaviour near maximum lift; by including unsteady terms in the boundary layer equations the dynamic case may be examined. Development of the theory is treated elsewhere in this lecture series and application discussed in references 19 and 21. In physical terms the important distinction between the two regimes is that whereas, for the steady case, zero shear at the surface heralds flow reversal and hence separation, it can be shown that both theoretically and experimentally, flow reversals within the boundary layer whilst the airfoil is in motion take time to develop and may not immediately result in gross changes to the external flow. Reference 17 suggests that at high lift flow reversal within the laminar boundary layer is dominated by the spatial gradient but for turbulent flow toward the trailing edge the temporal gradient may assume as much significance.

Using the unsteady potential flow method of reference 20 to calculate the external flow, reference 18 presents an examination of dynamic effects on turbulent flow reversal. Figure 3 shows some of the results obtained by introducing unsteady effects into calculation of the boundary layer and external flow, independently and in conjunction, for uniform pitching velocity. For the combined effect, the progression of flow reversal from the trailing edge is fairly steady until the region of high adverse chordwise velocity gradient is reached, whereupon the reversal moves forward almost instantaneously toward the leading edge. This behaviour is characteristic of observed hot film measurements on the NACA.0012. Figure 3 also shows the effect of pitch rate on the angle at which the flow reverses at 50% chord, which coincides with the above phenomenon.

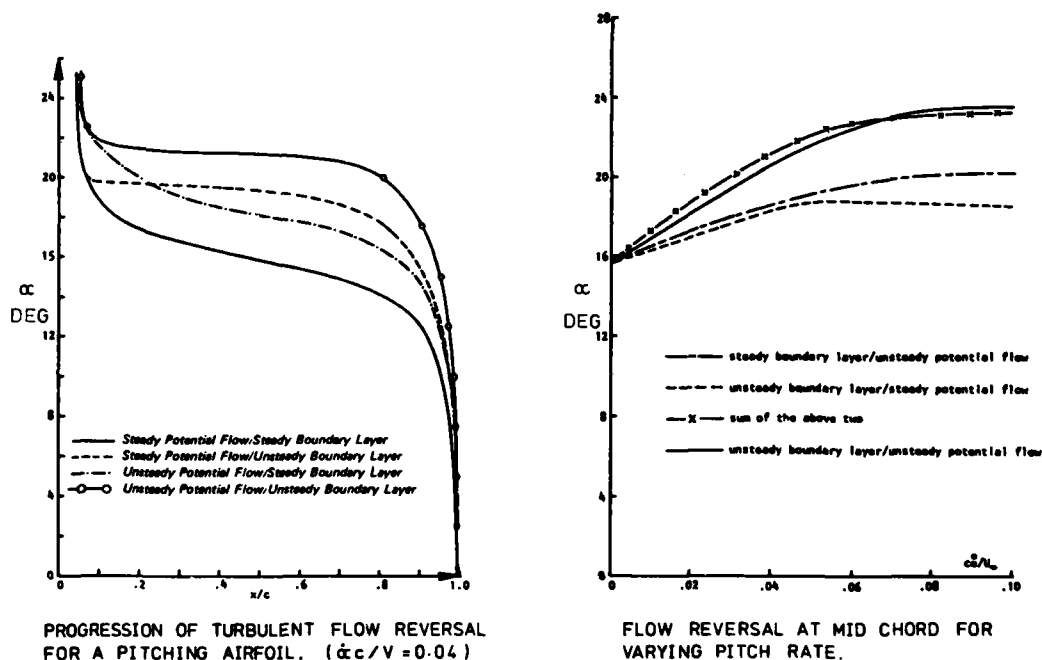
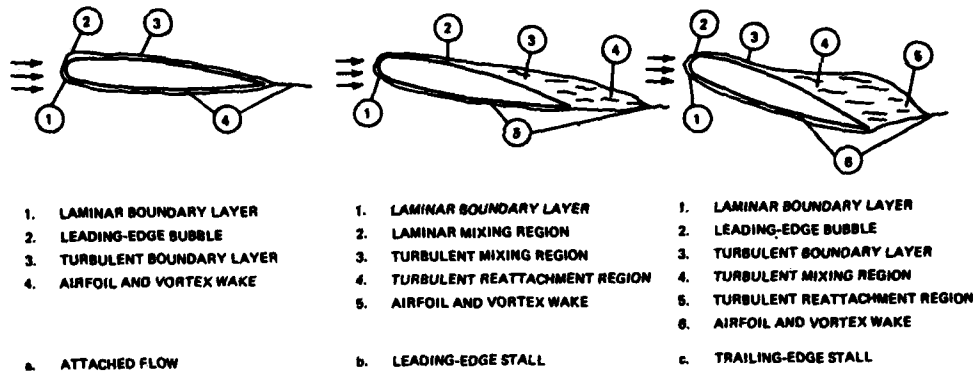


FIG.3. UNSTEADY BOUNDARY LAYER CALCULATIONS

For values of  $\dot{\alpha}c/u_{\infty} < 0.05$  which encompasses much of the range of practical interest, the delay in flow reversal is linear with  $\dot{\alpha}$  which infers a constant value of non-dimensional time delay ( $\Delta t u/c$ ) of about 2 which correlates again with observations of the delay in the collapse of leading edge suction. Reference 21 discusses further, the procedures and implications of this approach and conjectures on the connection between the boundary layer reverse flow and growth of the leading edge vortex. For many configurations at high lift, a leading edge bubble is present which means that transition to a turbulent boundary layer has occurred following laminar separation and prior to re-attachment. Reproduction of these initial conditions present an obstacle in the application of this promising approach to determining the onset of separation.

Unsteady Potential Solution

The process of developing separation requires an interaction between the external flow and the surface of the airfoil. References 13 and 14 present attempts at this interaction, using the classical aerodynamic tools of potential flow and boundary layer theory. The regions where boundaries are to be determined (figure 4). The analysis is applied and the respective calculations are obtained whereupon the process is repeated to evaluate the flow. Bubble formation is calculated using a finite difference method. Bubble formation is calculated using a finite difference method. Bubble formation is calculated using a finite difference method.



FLOW REGIONS - REF.14

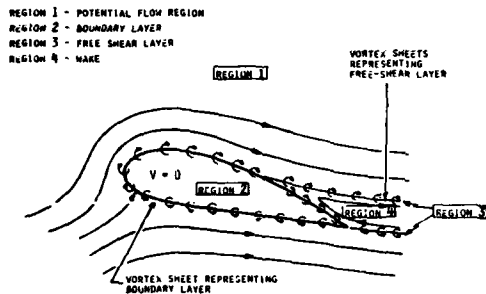
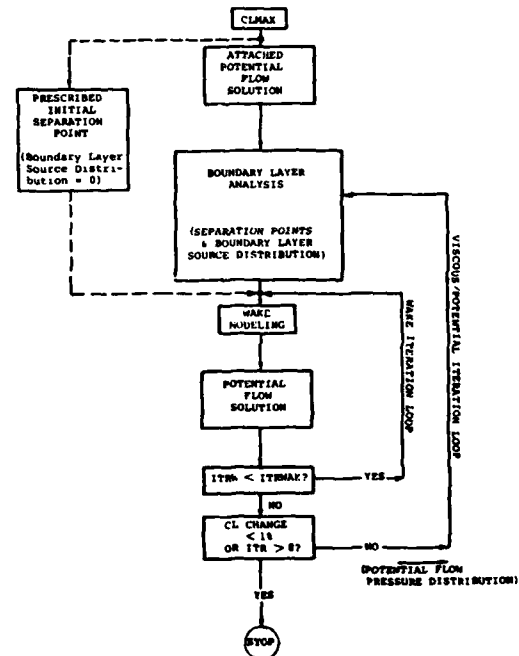
FLOW REGIONS AND  
CALCULATION PROCEDURE  
REF. 13

FIG.4. VISCOUS-POTENTIAL SOLUTION

In reference 13, integral methods are applied to boundary layer development and separation determined by zero shear. The potential flow is derived from a distribution of sources and vortices representing the airfoil and a vortex sheet represents the free shear layer. The method of reference 13 was developed for steady conditions and extended in reference 22 to accommodate dynamic effects by inclusion of time dependant circulation and an empirical lag in separation. Although all the elements required for flow development are present, many assumptions are still implicit in their application, and published results so far are not as convincing as might be desired. Nevertheless, the method represents the nearest approach of 'classical' aerodynamics to the rigour offered by solution to the Navier Stokes equations and at a more practical level of computing requirements. Refinement of this approach might be facilitated by the availability of results from the Navier Stokes solution.

### 3. Empirical Methods

Airfoil testing under dynamic conditions has been going on for more than twenty years motivated by recognition that local maximum lift levels on helicopter rotors are in excess of those attainable under static conditions. Having substantiated this phenomenon under controlled conditions engineering requirements dictate that a reasonable representation should be incorporated into any design analysis. At present conventional theory is incapable of qualitative prediction of dynamic stall, hence the reliance on empirically derived procedures for applying the information obtained from test. From the body of theory for unsteady aerodynamics applicable to attached flow conditions, certain parameters emerge which allow generalisation and scaling of the dependent forces and moments. These form the basis for the generalisation of test data involving penetration of the separated flow regime.



Thus events are transferred from the time domain and expressed as distance non-dimensionalised by semi-chord length,  $\Delta t \cdot 2V/c$ ; likewise, pitch rate becomes  $\dot{\theta} c/2U_\infty$ . Since dynamic effects generally delay the onset of separation, initial behaviour is observed as an extension of normal airfoil characteristics, and hence measured static data may be used as the most reliable representation of airfoil geometry and flow parameters (Reynolds number and Mach number) upon which to superimpose the appropriate modification. Current methods are reviewed briefly with one exception which reflects the author's interest.

a) UTRC  $\alpha$ , A, B Method

At the United Technologies Research Centre, an extensive program of oscillatory testing was performed on the NACA 0012 airfoil at low Mach numbers. On the basis that, for harmonic motion and attached flow, the instantaneous lift and moment can be expressed in terms of  $\alpha, \dot{\alpha} c/2V$ , (A) and  $\dot{\alpha} c/4 V^2$ , (B), these parameters were used to generalise the results for the entire program. By cross-plotting and interpolating for given values of the parameters, tables of  $C_L$  and  $C_M$  were constructed (reference 23). The tables and associated look-up routines were then incorporated within a rotor analysis program. Assumptions were made to permit application of the data to higher Mach numbers. Subsequently, the computational procedure has been streamlined (reference 24) by substituting for the table look-up routine, a series of coefficients derived from curve fitting. Not surprisingly, when the method is used to regenerate the test conditions, correlation appears to be good. When the implicit relationship between  $\alpha, \dot{\alpha}, \ddot{\alpha}$ , are violated and distinction between the first and second derivatives of pitch angle and angle of attack become important; for example, when approaching a wake vortex, the accuracy of the method may be less certain.

b) Boeing-Vertol Gamma Function Method

Boeing-Vertol have generated and published a large body of experimental data covering several airfoils, a significant Mach number range and for both pitch and plunge motion. To model the influence of motion on stall behaviour, the measured airfoil characteristics under static conditions are used as a basis and manipulated through use of an effective angle of attack. Firstly, the influence of pitching and plunging below stall is accounted for by applying a correction derived from the Theodorsen function, thus producing a quasi static blade element angle of attack ( $\alpha_{BE}$ ). From this is subtracted a correction term  $\Delta\alpha = \gamma (\dot{\alpha} c / 2V)^2 \cdot \dot{\alpha} / |\dot{\alpha}|$ , thus  $\alpha_{REF} = \alpha_{BE} - \Delta\alpha$  which is used to obtain  $C_L$  from the static data. The lift coefficient is then factored by  $\alpha_{BE} / \alpha_{REF}$  to restore its full value. This has the effect of delaying the appearance of stall by  $\Delta\alpha$ . Pitching moment is obtained via an empirical shift of centre of pressure when the flow is separated. The value of  $\gamma$  is determined empirically as a function of Mach number from tests of the appropriate airfoil. A consequence of this formulation is an inability to delay stall beyond the point at which  $\dot{\alpha}$  becomes less than zero when  $\alpha_{BE}$  is beyond the static stall angle.

Comments on the two following methods from M.I.T. and Lockheed are copied virtually verbatim from reference 1.

c) M.I.T. Method (Reference 25)

This method is basically an empirical representation of the forces and moments due to the vortex-shedding phenomenon for ramp changes in angle of attack. The actual angle of dynamic stall must be specified separately; the value  $\alpha_{DS} = \alpha_{SS} + 3^\circ$  has normally been used. For  $\alpha_{SS} < \alpha < \alpha_{DS}$ , the data below static stall are extrapolated. Starting at  $\alpha = \alpha_{DS}$ ,  $C_L$  and  $C_M$  are assumed to increase linearly with time, over a specified time interval, from inviscid to peak values that depend on  $\dot{\alpha} c/U_\infty$  at the instant of dynamic stall. If this is attained before  $\alpha = \alpha_{max}$ , then  $C_L$  and  $C_M$  remain constant until  $\alpha_{max}$ . They decay exponentially with preassigned time constants thereafter, until the static-stall values are attained. These new values are retained until  $\alpha = \alpha_{SS}$  on the downstroke, when the unstalled static section characteristics are resumed.

d) Lockheed Method (References 26, 27)

This combined analytical and empirical modelling of dynamic stall incorporates phase lag time constants and pitch-rate-dependent stall angle delay increments into a fictitious effective angle of attack. This effective angle is used to construct  $C_L$  and  $C_M$  from static airfoil characteristics and a linear combination of a number of separate dynamic stall elements. Some of these elements are assumed to be analogous flow phenomena that have been treated elsewhere in the literature, such as leading edge jets, the lag in circulation build-up on a pitching airfoil in potential flow, separation over moving walls, fluctuating pressure propagation in turbulent boundary layers, and the vortex lift due to leading-edge vortices on delta wings. Other elements are modelled directly from dynamic-stall measurements on oscillating airfoils. In this sense, the method has more degrees of freedom than any of the others, and information from many sources has been utilised.

At low frequency, the phase lag of the effective incidence is linearly proportional to  $\omega c/U_\infty$ . The latest version (Reference 29) includes increments of  $C_L$  and  $C_M$  due to the vortex shedding phenomenon, that are proportional to  $\sin^2 \alpha$ . Compressibility corrections are developed from various applications of the Prandtl-Glauert rule.

A comparison of the application of the above methods plus an early version of the time delay method was included in reference 1 and reproduced here as figure 5.

e) The Time Delay Method

Rather than regenerate the results of a specific programme of dynamic airfoil tests, this approach attempts to model, in a simplified manner, the physics of the separation process as deduced from many sources. What is, in essence, a time base, is generalised in the form of distance travelled in chord lengths.

Thus  $\tau = t \cdot V/c$ , which may be identified with the parameter  $s = 2 \cdot t \cdot V/c$  fundamental to the development of the expressions for the indicial aerodynamic response for the attached flow regime. Continuity between attached and separated flow calculations is thus provided. The basic features of dynamic stall have been described elsewhere in a qualitative manner. Within the context of rapid and repetitive closed loop rotor response calculation, the process has been idealised and quantified. It is applicable nevertheless to any two-dimensional or strip analysis airfoil response to forcing of a totally arbitrary nature.

The key feature of this method is the use of two non-dimensional time delays  $\tau_1$  and  $\tau_2$ , which have been identified based on observation of many series of tests of different airfoils. They represent the periods of time required for changes between idealised flow states. The first observable gross change in overall flow structure is the detachment of a vortex from the forward part of the airfoil. This may be preceded by flow reversals within the boundary layer and, obviously, the formation and growth of the vortex.  $\tau_1$  represents the time required for this initial stage of separation to take place and is initiated by the attainment of local velocities and gradients which cannot be sustained. When the vortex detaches, leading edge suction collapses and the distribution of suction reflects the passage of the vortex over the surface which takes place at a velocity of 30% - 40% of free stream velocity. During this period, total lift is sustained at a level associated with attached flow conditions, but when the vortex departs from the region of the trailing edge, the lift decays very rapidly to the level associated with fully separated flow as measured statically. Values of  $\tau_1$  and  $\tau_2$ , on the basis of observations, appear to be relatively insensitive to a first order to variations in Mach number and independent of airfoil geometry. From initiation, the value of  $\tau_1$  has been identified as approximately 2 and the value of  $\tau_2$  as approximately 5.5, which allows a period of 3.5 for vortex traverse of the airfoil.

For adequate reproduction of the characteristics of any specific airfoil throughout the Mach number range it is desirable to incorporate a representation of measured forces and moments obtained from static wind tunnel testing. As separation is delayed by dynamic effects, it is necessary to extrapolate the range of measured attached flow, and as separation effects are generated independently on an idealised basis, it is relatively easy to construct a simple curve fit representation of measured attached flow characteristics throughout the Mach number range. For example,  $C_l$  may be represented simply by a zero lift angle and slope,  $C_m$  and  $C_d$  by quadratic expressions with suitable breakpoints.

The procedure for implementing the model for dynamic stall is illustrated in the form of a flow chart (figure 6), which may constitute a subroutine to handle the force and moment characteristics of the airfoil throughout the complete range of attached and separated flow. The boxes are numbered for identification for further discussion.

1. Initialization

To initialize the procedure requires current values for the independent variables, velocity,  $\Delta\tau$ , Mach number, etc. In addition, to implement the indicial aerodynamic response, values from the prior calculation must be known, together with the logic which signifies the current flow state and a record of the time expired ( $\tau$ ) since the initiation of separation, if appropriate. Only information from the immediately prior calculation need be retained for the indicial method.

2. Criteria for Separation

From observation of experimental data, a model of separation for the dynamic case has been postulated; i.e. that having attained a high level of lift, sufficient to precipitate separation, then the subsequent process of boundary layer flow breakdown and vortex

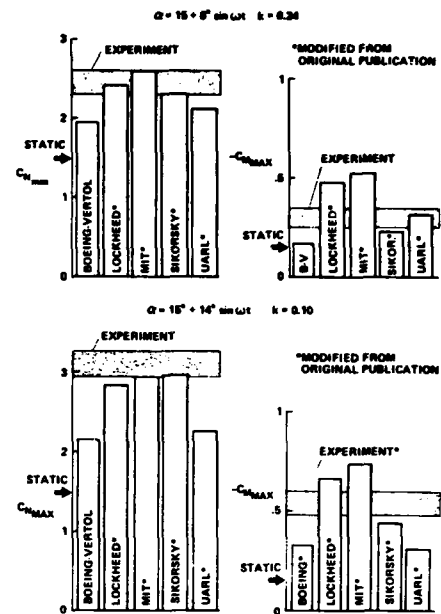


FIG. 5. COMPARISON OF DYNAMIC STALL PREDICTION METHODS

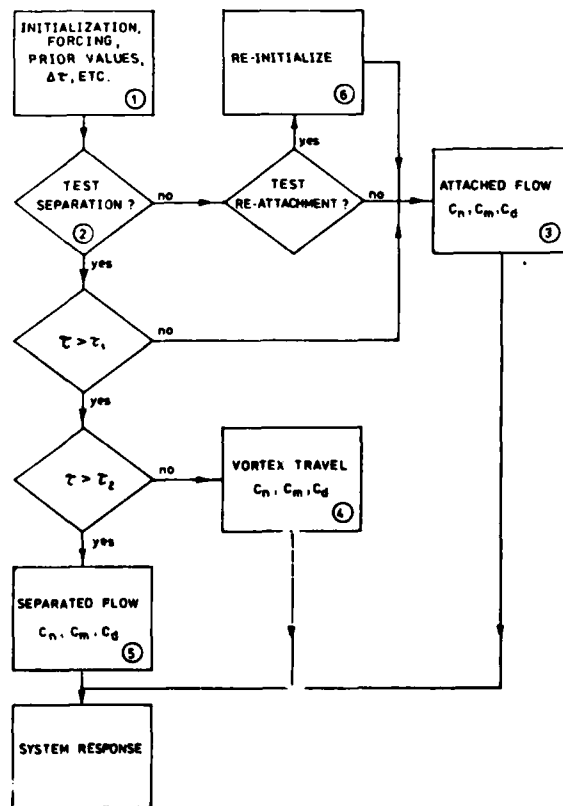


FIG. 6. CALCULATION PROCEDURE

formation will occupy a set period of time. During this period, which is assumed to be nominally constant (in non dimensional form) the gross features of the flow external to the boundary layer are assumed to be unmodified, to a first order. It remains then, to determine the limiting conditions for attached flow. Whatever criteria is used, it is obviously desirable that it should, when dynamic effects are negligible, be compatible with the observed static measurements of airfoil behaviour. This objective suggests that the static measurements themselves could be used as a criterion, in particular, the most consistently and clearly defined event which is the sudden break in pitching moment at the stall. Such a criterion identifying the angle of attack for  $C_m$  break and labelling it  $\alpha_s$ , was used in the initial development of the model (references 3 and 4). This parameter is strongly dependant on Mach number and its application for a range of airfoils and Mach numbers has produced fairly satisfactory results.

At low Mach number in particular, there is considerable variability in the development of flow separation at static stall and much has been written on this topic; for example, reference 5. Two basic categories may be constructed; i.e. 'trailing edge stall' in which the dominant feature is a progressive growth of separation from the trailing edge and 'leading edge' or 'nose' stall in which separation first appears in the front part of the airfoil. Within these categories, there are many identifiable variations in behaviour and it is common, for a given airfoil, for the stall characteristics to progress from one category to the other with a change in Reynolds Number. It is even possible for features from both categories to be present at the same time; e.g. the NACA.0012 at a Reynolds number of around  $3 \times 10^6$ . In reference 6, a criterion for leading edge stall for the dynamic case is presented as an extension of correlation studies by NASA on static stall (reference 7). A limiting value of peak velocity in the leading edge region in combination with a level of adverse velocity gradient forms the basis of the criterion. For a given airfoil and Mach number, this can be reduced to a sampled leading edge velocity alone. Use of the leading edge criterion has several implications:-

- a) If trailing edge separation is limiting in the static condition, an increment in limiting lift will be realised on application of the leading edge criterion to the dynamic case. It follows that transition between the two conditions must be dependant on achieving some significant rate of change.
- b) Since peak velocity is dependant on circulation, then the prior motion of the airfoil will become a factor and instantaneous angle of attack is no longer sufficient.
- c) Compressibility effects will become significant up to the point where shock waves are formed which are sufficiently strong to modify the shape of the velocity distribution.
- d) Pitch rate terms must be incorporated into the determination of peak velocity and gradient.
- e) If account of the persistence or limited growth of trailing edge separation is included in the calculation, it will modify the peak velocity.
- f) The leading edge criterion may be used in a predictive manner for a hypothetical airfoil geometry prior to fabrication and test.

Application of the leading edge criterion for a range of airfoils and tests (reference 6 for example), indicates that these implications are in fact realised. For use in repetitive dynamic calculations, the criterion may be simplified so that the local velocity at a single location near the leading edge needs only be monitored, the relationship between the critical local velocity and the peak value having been established in advance. The local velocity may be constructed from the contributions from the thickness distribution, camber, time dependent circulation and pitch rate; i.e.  $v_x(t) = v_0 + dv_x/d\alpha_e \alpha_e(t) + dv_x/d(\dot{\theta}c/2V) \dot{\theta}c/2V$

Where  $v_0$  represents the zero lift local velocity ratio,  $dv_x/d\alpha_e$  represents the variation of local velocity ratio with the effective circulatory lift angle and  $dv_x/d(\dot{\theta}c/2V)$  represents the variation with pitch rate. The effective circulatory lift angle (relative to the zero lift angle),  $\alpha_e(t)$ , is obtained from application of indicial aerodynamic response functions to the forcing time history and since the calculation at this stage utilises incompressible terms the appropriate value of  $\alpha_e(t)$  should reflect this. The above coefficients may be derived from application of incompressible two-dimensional, finite thickness airfoil theory. Compressibility effects may be assessed via the expression (from reference 8)  $v_c = 1 + v_x \{1 - M^2 [1 - M^2 (1 - v_x^2)]\}^{-1/2}$  and the resultant velocity  $v_c$  compared with the maximum allowable value which corresponds (for that station) to the predetermined maximum peak velocity. In some cases (reference 6) it may be found that the local critical value is only weakly dependant on Mach number. An example correlation of leading edge velocity up to and including dynamic stall is presented in figure 7.

Depending mainly on the shape of the component of the velocity distribution due to additional lift, it is found that for a freestream Mach number of around 0.3, then the allowable peak velocity is supersonic. This means that, for further increases in Mach number, the presence of significantly strong shock waves will modify the pressure distribution and invalidate the criterion. Reference 9 includes a correlation of maximum lift with the corresponding values of maximum upper surface suction from which an upper limit of 0.7 vacuum is deduced. This limit may be used to extend the range of applicability of the leading edge criterion but, until further research provides a foundation for a revised procedure, the upper limit of applicability for the leading edge criterion is within the range of 0.3 to 0.4 Mach number.

For the time being, above a Mach number of around 0.35, the criterion for initiation of separation remains the value of  $\alpha_s$  established from static test.

3. Calculation of forces and Moment for attached Flow

If logic dictates that gross separation is absent then lift and moment are calculated using the generalised indicial aerodynamic functions as outlined in the paper on that topic. Drag is calculated on a quasi static basis from the curve fitted airfoil test data (extrapolated as required). If the criterion for separation has been exceeded but the ensuing value of  $\tau$  does not exceed  $\tau_1$ , then the calculation proceeds as for attached flow.

4. Calculation during Vortex Traverse

If  $\tau_1 < \tau < \tau_2$  a detached vortex is assumed to be located over the airfoil. In this period additional lift may still be generated and is calculated as though the assumptions relevant to the indicial lift function had not been violated. At low Mach numbers an additional vortex lift has been observed and may be simulated by magnification of the calculated circulatory lift if required. As a consequence of the loss of leading edge suction and redistribution of lift the centre of pressure moves aft over the airfoil. From static tests with separation the instantaneous centre of pressure may be related to the angle of attack and in most cases the variation may be linearised between the first departure at  $\alpha$ , and an ultimate equilibrium reached at an angle which may be labelled  $\alpha_2$ . At any given angle the transition between the c.p. for attached flow and the appropriate value for separated flow may be taken to a function of time. A function analogous to a second order lag has been assumed; it is illustrated in figure 8 and may be implemented by a numerical method similar to that used for the indicial lift. The resultant pitching moment may be calculated from this centre of pressure and the current value of lift.

Loss of leading edge pressure simplifies the calculation of pressure drag which tends to the value of  $C_N \sin \alpha$ . This value may be refined by using the centre of pressure calculation as a measure of the severity of separation. An appropriate value of friction drag may be included.

5. Calculation for Separated Flow

In the present context it is assumed that if the angle of attack is greater than  $30^\circ$ , in either forward or reverse flow, then the flow must be separated; i.e. there is an upper limit for the application of unsteady aerodynamic. In these circumstances the airfoil characteristics can be simply represented by a curve fit derived from test; e.g.  $C_N = 2.2 \sin \alpha$ ,  $C_m/C_N = -0.15 - 0.001875 (\alpha - 30)$  and  $C_d = C_N \sin \alpha$ . For the angle of attack range below  $30^\circ$ , it is assumed that when the lift collapses ( $\tau > \tau_1$ ) the decline follows an exponential variation with time ( $e^{-0.7\tau}$ ) and the lower limit may be determined from an envelope of the observed data. This lower limit can be represented simply by the expression  $C_N = 1.1 \sin 3\alpha / (1-M^2)^{1/2}$ ,  $C_m$  can be derived from the centre of pressure location which is modelled as per the previous section and, again,  $C_d = C_N \sin \alpha + \text{friction drag}$ . During the 'separated' phase, an account is kept of the equivalent  $\alpha_E$  which is thus an indirect measure of circulation. When the flow re-attaches this value of  $\alpha_E$  is used to re-initialise the calculation of lift. In a similar manner, the centre of pressure location is monitored.

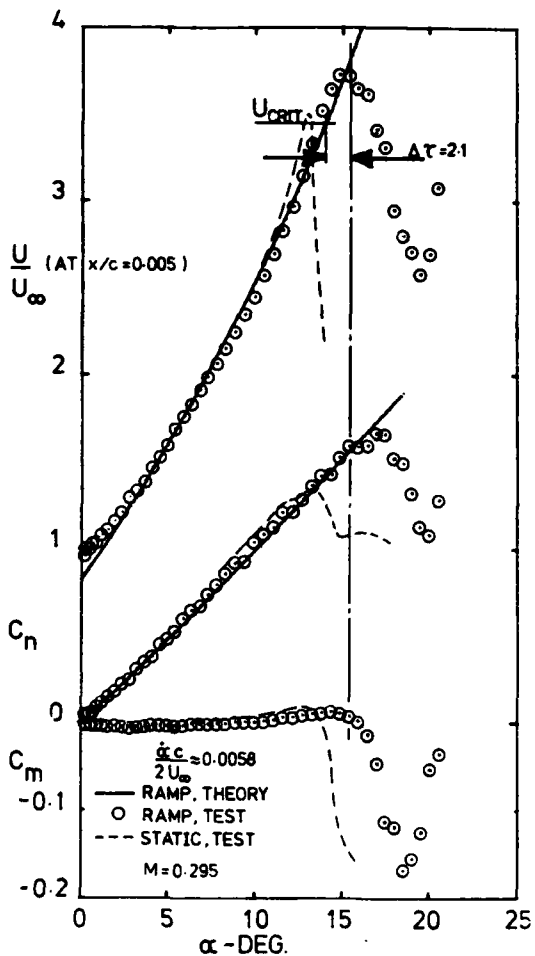
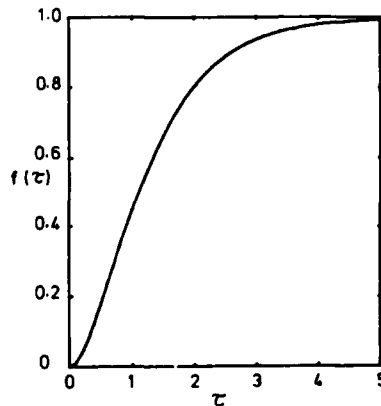


FIG. 7. LEADING EDGE VELOCITY DURING DYNAMIC STALL



FUNCTIONAL REPRESENTATION

$$f(p) = \frac{1}{(1+T_1 p)(1+T_2 p)}$$

RESPONSE TO STEP INPUT

$$f(\tau) = \Delta (1 + 3e^{-1.75\tau} - 4e^{-1.3125\tau})$$

STEP INPUT

$$\Delta = C_{P_{new}} - C_{P_{old}}$$

FIG. 8 CENTRE OF PRESSURE TRAVEL

## 6. Re-attachment

When the angle of attack is reduced below  $\alpha_c$ , following separation, then it is assumed that the flow will re-attach. At this point, the value of  $C_l$  will be lower than would have been computed for attached flow. This deficiency may be treated in the same way as any other which occurs in the process of constructing the time history for attached flow; i.e. via the indicial functions for attached flow. Thus the re-attachment is not instantaneous. Re-adjustment of the centre of pressure is handled via the time constants utilised for separated flow.

The equations used to implement the calculation of force and moment for separated flow are extensions of those used for attached flow; i.e. indicial functions, thus not only may continuity of calculation be maintained but the numerical methods are the same. In rotor calculations, during any cycle of oscillation or perturbation, the airfoil relative velocity will change significantly. By using a time base which is related to airfoil distance travelled through the air then, to a first order, the effects of varying velocity may be simulated, taking into account the prior history of circulation. Having assessed the aerodynamic forcing, system response may be calculated via the numerical procedures outlined for the application of indicial aerodynamic functions.

To construct a formulation suitable for routine, rapid inner loop calculation and at the same time preserve a generality that will accommodate any non-prescribed combination of independent variables requires considerable simplification of the physical processes involved. To examine these processes in more detail and under more controlled conditions than encountered in flight, a considerable amount of airfoil wind tunnel testing is currently in progress. In interpreting the results of test, it is often difficult to isolate the effect of any single variable, particularly when results are not exactly repeatable. In this context, use of the model described here for correlation purposes is helpful in identifying variations in behaviour, second order effects and inconsistencies in the test data. At the same time, confidence in the model may be assessed and areas for improvement identified.

Some results of a recent programme of tests on the RAE 9644 airfoil are included to show the degree of correlation currently obtained. (figures 9 and 10). Data for a Mach number of 0.3 are shown and the theoretical comparison incorporates the leading edge criterion. The lowest rate ramp illustrates the influence of trailing edge separation; i.e. a rounding of maximum lift and nose up pitching moment just prior to stall. This influence is not so apparent for increased rate. At higher Mach Numbers the  $\alpha_c$  criterion is used, comparisons are presented in reference 4.

## References

1. McCroskey, W.J. Prediction of unsteady flows on oscillating airfoils. Paper 12, AGARD Lecture Series No. 94. Three dimensional and unsteady separation at high Reynolds Numbers. February 1978.
2. Philippe, J.J. Le décrochage dynamique: un exemple d'interaction forte entre écoulements visqueux et non-visqueux. Paper 21 AGARD. Conference Proceedings No. 227. Unsteady Aerodynamics. Sept 77.
3. Carlson, R.G. et al. Dynamic stall modelling and correlation with experimental data on airfoils and rotors. NASA SP-352, Rotorcraft Dynamics, Paper 2. February 1974.
4. Beddoes, T.S. A synthesis of unsteady aerodynamic effects including stall hysteresis. Proc. 1st European Rotorcraft Forum. September 1975.
5. McCulloch, G.B. Gault, D.E. Examples of three Representative types of airfoil-section Stall at low speed. NACA TN.2502. 1951.

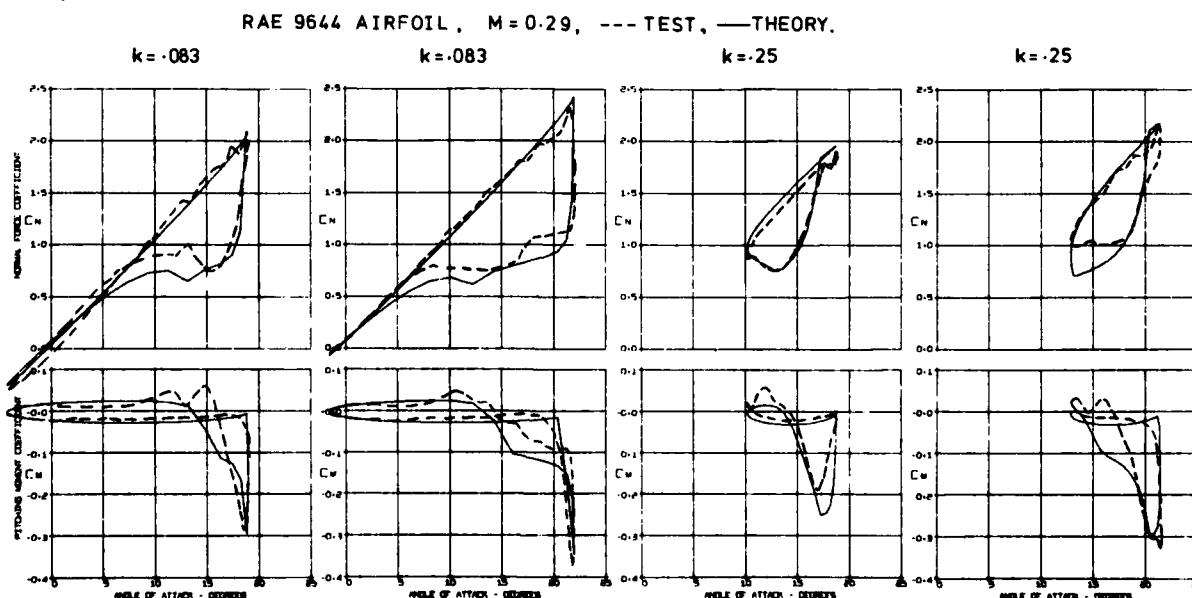


FIG.9. HARMONIC FORCING COMPARISON

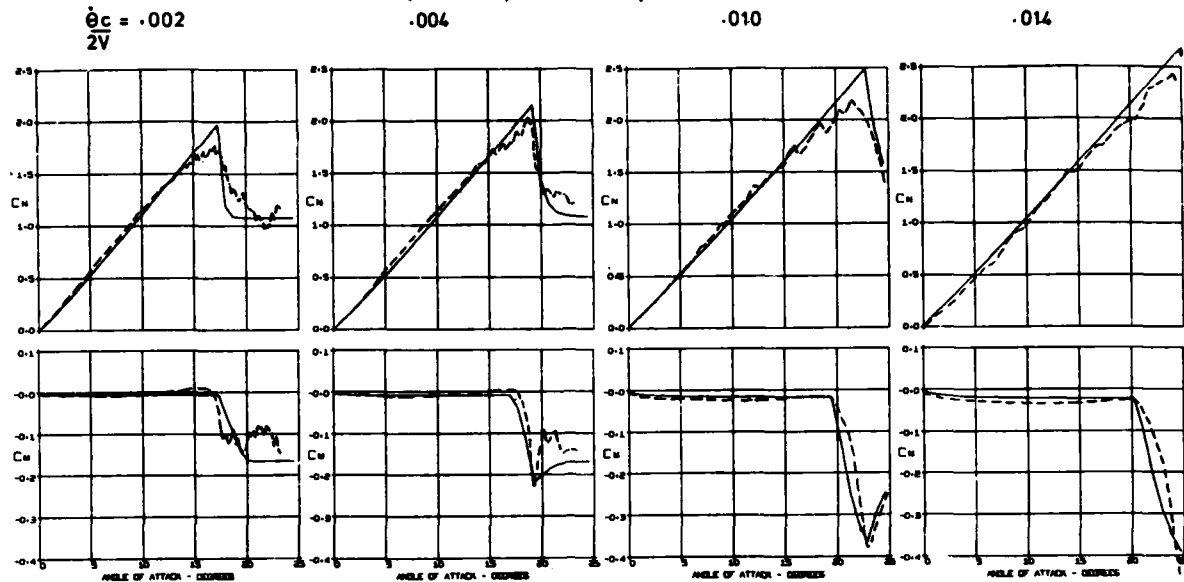
RAE 9644 AIRFOIL,  $M=0.3$ , ---TEST, —THEORY.

FIG. 10. RAMP FORCING COMPARISON

6. Beddoes, T.S. Onset of leading edge separation effects under dynamic conditions and low Mach number. *American Helicopter Society Annual Forum 1978, pre-print 78-63.*
7. Evans, W.T. and Mort, K.W. Analysis of computed flow parameters for a set of sudden stalls in low speed two-dimensional flow. *NASA TN D-85, 1959.*
8. Wilby, P.G. The Calculation of sub-critical pressure distribution on symmetric aerofoils at zero incidence. *N.P.L. Aero Report 1208, 1967.*
9. Smith, A.M.O. High lift Aerodynamics. *Journal of Aircraft.* June 1975.
10. Mehta, U.B. Dynamic stall of an Oscillating airfoil. Paper 23, AGARD Conference Proceedings No. 227. *Unsteady Aerodynamics, September 1977.*
11. Wu, J.C. et al. A numerical Study of unsteady viscous flows around airfoils. Paper 24, AGARD Conference Proceedings, No. 227, *Unsteady Aerodynamics, September 1977.*
12. Ham, N.D. Aerodynamic Loading on a two-dimensional airfoil during Dynamic stall. *A.I.A.A. Journal.* October 1968.
13. Maskew, B. Dvorak, F.A. Investigation of Separation Models for the prediction of  $C_{lmax}$ . *A.H.S. Annual Forum. Paper 77.33-01. May 1977.*
14. Crimi, P. Reeves, B.L. A Method for analysing Dynamic Stall of Helicopter Rotor Blades. *NASA CR-2009. May 1972.*
15. Kinney, R.B. Two-dimensional viscous flow past an airfoil in an unsteady airstream. Paper 26, AGARD Conference Proceedings No. 227, *Unsteady Aerodynamics. September 1977.*
16. Phillippe, J.J. Sagner, M. Calcul et mesure des forces aerodynamique sur un profil oscillant, avec et sans dechrochage. *AGARD CP.111. Paper No. 11. 1972.*
17. McCroskey, W.J. Phillippe, J.J. Unsteady viscous flow on oscillating airfoils. *AIAA Journal.* Jan.75.
18. Scruggs, R.M. et al. Analysis of dynamic stall using Unsteady Boundary Layer Theory. *NASA CR-2467. October 1974.*
19. McCroskey, W.J. Some current research in unsteady fluid dynamics. *Trans. of the ASME, Journal of Fluids Engineering.* March 1977.
20. Giesing, J.P. Non-linear two-dimensional potential flow with lift. *Journal of Aircraft.* March 68.
21. Nash, J.F. and Scruggs, R.M. Unsteady Boundary Layers with Reversal and Separation. *AGARD Conference Proceedings. CP-227, Paper 18. September 1977.*
22. Rao, B.M. Maskew, B. Dvorak, F.A. Theoretical Prediction of Dynamic Stall on Oscillating Airfoils. *A.H.S. Annual Forum Reprint 78-62. May 1978.*
23. Arcidiacono, P.J. Carta, F.O. Casellini, L.M. Elman, H.L. Investigation of Helicopter Control Loads induced by stall flutter. *USAAVLABS. TR.70-2. March 1970.*

24. Bielewa, R.L. Synthesised Unsteady airfoil data with applications to stall flutter calculations. A.H.S. Annual Forum, Reprint 935. May 1975.
25. Johnson, W. The Effect of Dynamic Stall on the Response and Airloading of Helicopter Rotor Blades. Journal A.H.S. April 1969.
26. Ericsson L.E. Reding, J.P. Dynamic Stall Analysis in the Light of Recent Numerical and Experimental Results. Journal of Aircraft. April 1976.
27. Ericsson, L.E. Reding J.P. Quasi-Steady and Transient Dynamic Stall Characteristics. AGARD CP-204. Paper No. 24. 1976.

## NUMERICAL SOLUTION TECHNIQUES FOR UNSTEADY TRANSONIC AERODYNAMICS PROBLEMS

William F. Ballhaus  
Aeromechanics Laboratory, U.S. Army R&T Laboratories (AVRADCOM)  
Ames Research Center, Moffett Field, California 94035

and

John O. Bridgeman  
Ames Research Center, NASA, Moffett Field, California 94035 U.S.A.

### I. INTRODUCTION

During the last decade, there has been a truly remarkable improvement in computational aerodynamics capability. This has resulted from the continuing availability of larger, faster computers and from rapid advances in the development of numerical methods. For example, the first useful numerical solution procedure for steady transonic flows about wings was reported in 1972 (Ref. 1). Solutions required about 12 hr of processor time on the IBM 360-67. By 1975 the numerical method had been improved, and with the availability of the CDC 7600, solutions could be obtained in 5-30 min of processor time (Ref. 2). The pilot computer code based on this method has been used for a number of practical aerodynamics applications, including the redesign of the HiMAT RPRV wing (Ref. 3) and the development of the Sabreliner Mark Five wing (Ref. 4), which is now in production. There is a danger in the widespread proliferation of aerodynamics computer codes, however, because many aerodynamicists have not had time to adjust to the rapid progress that has been made in computational aerodynamics. As a result, they are using computer codes based on numerical solution procedures with which they are unfamiliar.

The modern aerodynamicist must become as aware of the sources of error in these codes as he is of errors in experiments. Now, most aerodynamicists understand that there are differences in the inherent errors associated with computational methods and experiments. For this reason, one of the principal uses of computations has been to provide an alternative data source to supplement and verify experimental data. The computational data are free of wind-tunnel wall and support interference, Reynolds-number scaling limitations, and aeroelastic model distortions, unless of course they are included to determine how they influence the experimental results.

But, to use aerodynamic computer codes most effectively, an aerodynamicist must understand the characteristics of the formulational and numerical errors inherent in computational data. Formulational errors result from mathematical modeling of the fluid physics. Size and speed limitations of current computers preclude solution of the complete Navier-Stokes equations, including computation of all the scales in turbulent boundary layers and separated regions, for practical aerodynamic flow fields. Hence, mathematical formulations of the flow-field physics are solved that are approximations to the complete equations. These approximations are the source of formulational or physical modeling errors. For transonic flows, these formulations are nonlinear and must be solved using numerical techniques, such as finite-difference or finite-element methods. These approximate solution procedures are the source of numerical errors.

Most aerodynamicists have a much better understanding of formulational errors, which are associated with physical modeling, than of numerical errors. For example, most aerodynamicists would understand and be able to account for the difference between exact inviscid airfoil pressures and those obtained from a wind-tunnel test. This requires an understanding of the physics. Few would understand the differences between an implicit and a semi-implicit method and how these differences affect the accuracy of the solution and the efficiency of the method for a given problem. This requires an understanding of the numerics.

One of the principal purposes of this paper is to provide aerodynamicists with an understanding of some of the basic concepts of finite-difference solution techniques for unsteady transonic flows. The discussion begins in Sec. II with a review of the hierarchy of mathematical formulations that approximate the Navier-Stokes equations. Section III deals with the basic concepts involved in constructing numerical algorithms to solve these formulations. In Sec. IV semi-implicit and implicit schemes are constructed and analyzed. The discussion focuses primarily on techniques for solving the low-frequency transonic small-disturbance equation. This is the simplest formulation that contains the essence of inviscid unsteady transonic flow physics. The low-frequency formulation is emphasized here because codes based on this theory can be run in minutes of processor time on currently available computers. Furthermore, numerical techniques involved in solving this simple formulation also apply to the more complicated formulations. Extensions to these formulations are briefly described.

A second purpose of this paper is to provide an indication of the present capability for solving unsteady transonic flows. Example applications of the methods described in Sec. IV are presented in Sec. V. Finally, Sec. VI deals with important areas of future research for the advancement of computational unsteady transonic aerodynamics.

### II. MATHEMATICAL FORMULATIONS

#### Reynolds-Averaged Navier-Stokes Formulation

The Navier-Stokes equations are generally accepted as the basic equations governing most fluid dynamic phenomena of interest to aerodynamicists. The equations are capable of representing mathematically the physical phenomena encountered in transonic flows, including mixed subsonic-supersonic flow, shock waves, boundary layers, and separation. They also apply to turbulence, a random, dissipative, three-dimensional phenomenon that involves many characteristic scales. Since present computer speed and capacity do not permit resolution of all of these scales for practical aerodynamics problems, some type of averaging must be used. The commonly used Reynolds time-averaging procedure averages the equations over a time interval that is long compared with turbulent eddy fluctuations, but small compared with macroscopic flow-field changes. This process introduces new terms, called "Reynolds stresses," that represent time-averaged transport of turbulent momentum and energy. Thus, there are more unknowns in the averaged equations than there are equations. This is commonly referred to as the closure problem. The process of expressing the Reynolds stress terms in terms of empirical functions and constants or transport equations is referred to as turbulence modeling.

The unsteady, compressible Navier-Stokes equations for a perfect gas can be written in the conservation form:

$$\frac{\partial \rho}{\partial t} + \frac{\partial}{\partial x_j} (\rho u_j) = 0 \quad (\text{continuity}) \quad (1a)$$



$$\frac{\partial}{\partial t} (\rho u_i) + \frac{\partial}{\partial x_j} (\rho u_i u_j) = - \frac{\partial p}{\partial x_i} + \frac{\partial}{\partial x_j} \tau_{ij} \quad (\text{momentum}) \quad (1b)$$

$$\frac{\partial}{\partial t} (\rho h) + \frac{\partial}{\partial x_j} (\rho h u_j) = \frac{\partial p}{\partial t} + u_j \frac{\partial p}{\partial x_j} + \tau_{ij} \frac{\partial u_i}{\partial x_j} - \frac{\partial q_j}{\partial x_j} \quad (\text{energy}) \quad (1c)$$

where the stress tensor  $\tau_{ij}$  and the heat flux vector  $q_j$  are given by

$$\tau_{ij} = \lambda \delta_{ij} \frac{\partial u_k}{\partial x_k} + \mu \left( \frac{\partial u_i}{\partial x_j} + \frac{\partial u_j}{\partial x_i} \right) \quad (1d)$$

$$q_j = -k \frac{\partial T}{\partial x_j}$$

the bulk viscosity  $\lambda = -(2/3)\mu$  and where  $\mu$  is the dynamic viscosity;  $\rho$ ,  $u$ ,  $h$ ,  $p$  are the density, velocity, specific enthalpy, and pressure;  $k$  is the thermal conductivity; and  $\delta_{ij}$  is unity when  $i = j$  and zero when  $i \neq j$ . A summation is applied when indices are repeated.

The equations can be Reynolds-averaged in the following way. The flow variables are expressed in the form

$$u_i(x_i, t) = \overline{u_i(x_i)} + u'_i(x_i, t) \quad (2)$$

where the bar denotes the time average of  $u_i(x_i, t)$ . The time average is obtained from

$$\bar{Q} = \lim_{\Delta t \rightarrow \infty} \int_{t_0}^{t_0 + \Delta t} Q(t) dt \quad (3)$$

Here  $\infty$  means a time interval that is large compared with the scale of turbulent fluctuations; note that  $\bar{u}'_i = 0$ . Introducing this concept into the continuity and momentum equations gives

$$\frac{\partial \bar{\rho}}{\partial t} + \frac{\partial}{\partial x_j} (\bar{\rho} \bar{u}_j + \overline{\rho' u'_j}) = 0 \quad (4a)$$

$$\frac{\partial}{\partial t} (\bar{\rho} \bar{u}_i + \overline{\rho' u'_i}) + \frac{\partial}{\partial x_j} (\bar{\rho} \bar{u}_i \bar{u}_j + \overline{\bar{u}_i \rho' u'_j}) = - \frac{\partial \bar{p}}{\partial x_i} + \frac{\partial}{\partial x_j} (\bar{\tau}_{ij} - \overline{\bar{u}_j \rho' u'_i} - \overline{\rho u'_i u'_j} - \overline{\rho' u'_i u'_j}) \quad (4b)$$

Very often a different type of averaging is used called "mass-weighted averaging" (Ref. 5). The mass-weighted velocity is  $\bar{u}_i = \overline{\rho u_i} / \bar{\rho}$ . The instantaneous velocity can then be written  $u_i(x_i, t) = \bar{u}_i(x_i) + u'_i(x_i, t)$ . After a sequence of manipulations, the continuity and momentum equations can be expressed in a form similar to that of Eqs. (1) with  $\bar{\rho}$  and  $\bar{u}_i$  replacing  $\rho$  and  $u_i$ . The only difference is a Reynolds stress term  $-(\partial/\partial x_j) \overline{(\rho u'_i u'_j)}$  on the right-hand side of Eq. (1b). This is the term that must be modeled. Additional terms to be modeled also appear in the averaged energy equation.

#### Inviscid-Flow Equations

The Euler equations, the "exact" inviscid flow equations, result from setting  $\tau_{ij} = 0$  in the Navier-Stokes equations. In the case of one-dimensional flow they reduce to

$$\rho_t + (\rho u)_x = 0 \quad (\text{continuity}) \quad (5a)$$

$$(\rho u)_t + (\rho u^2)_x + p_x = 0 \quad (\text{momentum}) \quad (5b)$$

$$(\rho h)_t + (\rho u h)_x = p_t + u p_x \quad (\text{energy}) \quad (5c)$$

By definition,  $dh = T ds + \rho^{-1} dp$ , where  $s$  is the specific entropy. This expression can be combined with the continuity and energy conservation equations to give

$$\frac{Ds}{Dt} \equiv \frac{\partial s}{\partial t} + u \frac{\partial s}{\partial x} = 0$$

which is often used in place of the energy equation. This states that entropy is constant along particle paths.

The continuity and momentum equations can be combined and rewritten in the form

$$\left[ \frac{\partial}{\partial t} + (u + a) \frac{\partial}{\partial x} \right] (u + \sigma) = 0 \quad (6a)$$

$$\left[ \frac{\partial}{\partial t} + (u - a) \frac{\partial}{\partial x} \right] (u - \sigma) = 0 \quad (6b)$$

where  $d\sigma \equiv dp/\rho a$  (for a perfect gas  $\sigma = 2a/(\gamma - 1)$ ). These expressions state that the quantity  $u + \sigma$  is constant along curves defined by  $dx/dt = u + a$ , and the quantity  $u - \sigma$  is constant along curves defined by  $dx/dt = u - a$ . The two families of curves  $dx/dt = u \pm a$  are called characteristic curves.

The physical meaning of the characteristic curves is indicated in Fig. 1. Consider the case of a one-dimensional flow with uniform velocity  $u$  and speed of sound  $a$ . Suppose that at  $x = x_0, t = 0$  there is a disturbance of infinitesimal strength. The wavefront generated by this disturbance travels upstream (assuming subsonic flow) along the path  $x = (u - a)t + x_0$ . A wavefront propagates downstream along  $x = (u + a)t + x_0$ . At some subsequent time  $t = t_1$ , the region influenced by the original disturbance is BC. For transonic flows,  $u \sim a$  so that the downstream wave propagation rate is substantially greater than the upstream propagation rate.

The full potential equation is obtained from the Euler equations under the assumptions of irrotational and isentropic flow. A velocity potential can then be defined  $\bar{q} = \nabla \phi$ , where  $u = \phi_x$  and  $v = \phi_y$ . The x momentum equation can be integrated with respect to  $x$  to give Bernoulli's equation

$$\phi_t + \frac{1}{2} (\phi_x^2 + \phi_y^2) + \frac{a^2}{\gamma - 1} = \frac{1}{2} u_\infty^2 + \frac{a_\infty^2}{\gamma - 1} \quad (7)$$

where the free-stream velocity  $u_\infty$  has been assumed to be steady and uniform. The free-stream speed of sound is  $a_\infty$ . Here,  $a^2 = \gamma p \rho^{-1}$  and the isentropic relation  $p \rho^{-\gamma} = \text{constant}$  have been used. The speed of sound can be eliminated using  $a^2 = a_\infty^2 (\rho/\rho_\infty)^{\gamma-1}$  to provide a system of two equations in the two unknowns  $\rho, \phi$

$$\rho_t + (\rho u)_x + (\rho v)_y = 0 \quad (\text{continuity}) \quad (8a)$$

$$\frac{p}{\rho_\infty} = 1 + \frac{\gamma - 1}{a_\infty^2} \left[ \frac{1}{2} u_\infty^2 - \phi_t - \frac{1}{2} (\phi_x^2 + \phi_y^2) \right]^{1/(\gamma-1)} \quad (\text{Bernoulli}) \quad (8b)$$

The unsteady transonic small-disturbance equation can be written

$$A \phi_{tt} + 2B \phi_{xt} = C \phi_{xx} + \phi_{yy} \quad (9)$$

where  $A = k^2 M_\infty^2 / \delta^{2/3}$ ,  $B = k M_\infty^2 / \delta^{2/3}$ ,  $C = (1 - M_\infty^2) / \delta^{2/3} - (\gamma + 1) M_\infty^m \phi_x$  and where  $\phi$  is the disturbance velocity potential,  $M_\infty$  is the free-stream Mach number, and  $\delta$  is the airfoil thickness-to-chord ratio. The choice of the exponent  $m$  is somewhat arbitrary. The parameter  $k$  is the reduced frequency. For an airfoil of chord length  $c$ , traveling with speed  $u_\infty$ , and executing some unsteady oscillatory motion of frequency  $\omega$ ,  $k \equiv \omega c / u_\infty$ . The reduced frequency is given in terms of radians of oscillatory motion per chord length of airfoil travel. The quantities  $x, y, t, \phi$  in Eq. (9) have been scaled by  $c, c/\delta^{1/3}, \omega^{-1}, c\delta^{2/3}u_\infty$ , respectively. The right-hand side of Eq. (9) is the familiar two-dimensional, transonic, small-disturbance equation for steady flows. The pressure coefficient is given by  $C_p = -2\delta^{2/3}(\phi_x + k\phi_t)$ .

The characteristic equation for Eq. (9) is (Ref. 6):

$$Ct^2 - Ax^2 - (AC + B^2)y^2 + 2Bxt = 0 \quad (10)$$

Hence, the disturbance front for  $t > 0$  that results from an instantaneous disturbance of infinitesimal strength at the point  $x = y = 0$  at  $t = 0$  is

$$\left(x - \frac{Bt}{A}\right)^2 + \left(\frac{AC + B^2}{A}\right)y^2 = \left(\frac{AC + B^2}{A}\right)t^2 \quad (11)$$

Dropping the scaling on  $t, \phi$ , and  $y$ , and replacing  $M_\infty$  by  $u/a$  gives

$$(x - ut)^2 + y^2 = a^2 t^2 \quad (12)$$

The disturbance front propagates at the speed of sound relative to the fluid. It is a circle with radius  $(a \cdot t)$  and center at  $x = ut, y = 0$ , as shown in Fig. 2. The disturbance center corresponds to the location of the fluid particle that was at the point of the disturbance at  $t = 0$ , and it moves with velocity  $u$ . In the plane  $y = 0$ , the effect of the disturbance propagates upstream, for  $u < a$ , with velocity  $(u - a)$ , and downstream with velocity  $(u + a)$ . The characteristic surfaces for an infinitesimal disturbance are the same for the Euler and full-potential equations as for the small-disturbance equation.

An approximation to Eq. (9), valid for low reduced frequencies, is

$$2B \phi_{xt} = C \phi_{xx} + \phi_{yy} \quad (13)$$

where  $B$  and  $C$  are defined in Eq. (9). This equation can be derived from the unsteady Euler equations under the assumptions  $k \sim \delta^{2/3} \sim 1 - M_\infty^2 \ll 1$ . The pressure coefficient expression consistent with Eq. (13) is  $C_p = -2\delta^{2/3}\phi_x$ .

The characteristic surfaces for the low-frequency equation are given (Ref. 6) by taking the limit  $A \rightarrow 0$  in Eq. (10). The equivalent to Eq. (12) then is

$$y^2 = \frac{2a^2 t}{u} \left[ x + \frac{a+u}{2u} (a-u)t \right] \quad (14)$$

The disturbance front is a parabola, as illustrated in Fig. 3. Note that the disturbance propagation rate in the downstream direction is infinite. In the low-frequency approximation, the sound and particle speeds are infinite. Hence, the downstream propagation rate, which is the sum of the two, is also infinite. However, the upstream propagation rate, the difference of the two, is finite and equal to  $(u - a)(u + a)/2u$ . Since  $u \sim a$  for transonic flows, this is a good approximation to the upstream propagation rate  $(u - a)$  corresponding to Eq. (9).

#### Some Characteristics of Inviscid Unsteady Transonic Flows

In transonic flight, the unsteady motion of a body strongly affects the resultant aerodynamic forces acting on that body. The reason is that surface pressures, and hence aerodynamic forces, are extremely sensitive to perturbations in boundary conditions. For example, the well-known expression from linear theory relating the lift coefficient  $C_L$  to the angle of attack  $\alpha$  for a flat plate,  $C_L \sim \alpha / \sqrt{1 - M_\infty^2}$ , indicates that changes in  $C_L$  due to changes in  $\alpha$  become more pronounced as the free-stream Mach number  $M_\infty$  approaches unity. Similarly, changes in airfoil velocity or shape (e.g., flap deflection) can be expected to produce large changes in the magnitude of aerodynamic forces, especially for motions that induce large excursions of embedded shock waves.

Another characteristic of transonic flows is the large phase differences that often occur between the motion of an aerodynamic body and the flow-field response to that motion; that is, transonic flows are relatively slow to adjust to unsteady perturbations. This is to be expected, since disturbances generated on or near the body must travel upstream at the local speed of sound against a nearly sonic oncoming flow and, should they encounter a supersonic region, they must propagate around it. The slow upstream propagation rate allows a disturbance to affect the flow field near the airfoil for a period of time that is large compared with that in either a purely subsonic or supersonic flow.

For the problem of an airfoil of chord length  $c$  oscillating in pitch or plunge at a frequency  $\omega$ , four time scales can be identified:

$$\tau_U \sim \frac{c}{u-a}, \quad \tau_D \sim \frac{c}{u+a}, \quad \tau_C \sim \frac{c}{u}, \quad \tau_M \sim \frac{1}{\omega} \quad (15)$$

The four scales are associated with upstream disturbance propagation, downstream disturbance propagation, convection, and airfoil motion, respectively. For transonic flows,  $u \sim a$ , so that  $\tau_U \gg \tau_D \sim \tau_C$ . Because of the large difference between  $\tau_U$  and  $\tau_D$ , the flow downstream of a disturbance adjusts much more rapidly than the flow upstream of the disturbance. Low-frequency cases are those for which  $\tau_M \gg \tau_D$ . That is,  $k \equiv \omega c/u \sim 1 - M \ll 1$ , where  $M = u/a$ .

### III. SOME FUNDAMENTAL CONCEPTS OF FINITE-DIFFERENCE METHODS

The objective of the computational aerodynamicist is to first select a mathematical formulation that describes the significant physics of the flow and then solve the governing equation(s) numerically as efficiently as possible. For the transonic flow regime, nonlinear formulations are required to predict the proper mixed (subsonic-supersonic) character of the flow, including the presence of embedded shock waves. The most efficient solutions to these formulations have been generated using computational algorithms based on finite-difference methods. The successful construction of such algorithms is strongly dependent on the researcher's understanding of the fundamental concepts involved in finite-difference techniques.

#### Finite-Difference Approximations

A general second order quasi-linear partial differential equation for initial boundary value problems, representative of currently solved transonic potential formulations, can be written symbolically as

$$a \frac{\partial^2 \tilde{\phi}}{\partial t^2} + 2b \frac{\partial^2 \tilde{\phi}}{\partial x \partial t} + c \frac{\partial^2 \tilde{\phi}}{\partial x^2} + F(x, t, \tilde{\phi}, \frac{\partial \tilde{\phi}}{\partial t}, \frac{\partial \tilde{\phi}}{\partial x}) = 0 \quad (16)$$

where  $a$ ,  $b$ , and  $c$  are functions of  $\tilde{\phi}$ ,  $\partial \tilde{\phi} / \partial t$ ,  $\partial \tilde{\phi} / \partial x$ ,  $F$  is an arbitrary function, and  $\tilde{\phi}$  is the dependent variable which is a function of the spatial variable  $x$  and the temporal variable  $t$ . For simplicity only one space dimension is considered.

To solve the differential equation using finite-difference techniques, a grid of mesh points is introduced in  $x, t$  space with increments  $\Delta x$  and  $\Delta t$  and with indexing defined by  $t^n = n\Delta t$ ,  $x_j = j\Delta x$ . The exact solution to the governing equation,  $\tilde{\phi}(x, t)$ , is approximated on the grid by the solution to the numerical scheme,  $\phi(x_j, t^n) = \phi_j^n$ .

The idea, then, is to replace the partial differential equation with a system of algebraic equations for the values of the dependent variable at the mesh points. In the finite difference method, this is accomplished by replacing each partial derivative term in the governing equation with a finite-difference approximation. The resulting finite-difference equation is valid at each discrete point in the computational domain.

A finite-difference approximation to any derivative term can be derived by expanding the dependent variable at neighboring points about the point  $(x_j, t^n)$ . By forming appropriate linear combinations of these expansions, formulas are obtained that involve local values of the dependent variable. For example, formulas for the  $\partial \tilde{\phi} / \partial x$  term in Eq. (16) are readily obtained using Taylor series expansions for two neighboring points; they can be written as

$$\phi_{j\pm 1}^n = \phi_j^n \pm \Delta x \left( \frac{\partial \phi}{\partial x} \right)_j^n + \frac{\Delta x^2}{2} \left( \frac{\partial^2 \phi}{\partial x^2} \right)_j^n \pm \frac{\Delta x^3}{6} \left( \frac{\partial^3 \phi}{\partial x^3} \right)_j^n + \dots$$

Using this equation, three different finite-difference approximations for  $\partial \tilde{\phi} / \partial x$  can be derived; they are (1)  $(\phi_{j+1} - \phi_j) / \Delta x$  (forward), (2)  $(\phi_{j+1} - \phi_{j-1}) / 2\Delta x$  (central), and (3)  $(\phi_j - \phi_{j-1}) / \Delta x$  (backward).

Using Taylor series expansions for  $\phi_j^{n\pm 1}$ ,  $\phi_{j\pm 1}^{n-1}$ , and  $\phi_{j\pm 1}^{n+1}$  yields various formulas for the other derivative term in Eq. (16).

Since these finite-difference approximations are not unique, the question naturally arises: Which approximation is best to use in a given case? The answer is that there is usually no "cookbook" approach for constructing an optimum algorithm. The algorithm developer must rely on experience and on an understanding of basic concepts of accuracy, stability, convergence, and computational efficiency.

#### Modified Partial Differential Equation

Given a finite-difference approximation to the partial differential equation (16) and assuming the existence of a continuously differentiable function  $\phi(x, t)$  that coincides with the exact solution to the difference equation at the mesh points, then  $\phi(x, t)$  can be viewed as an approximation to  $\tilde{\phi}(x, t)$ , the exact solution to the differential equation. An alternative interpretation is that  $\phi(x, t)$  is the exact solution to a different partial differential equation that approximates the governing equation. This approximate differential equation is called the modified partial differential equation (mpde). The modified equation can be derived by expanding each term in the finite-difference algorithm in a Taylor series about the point  $(x_j, t^n)$ . The result is a partial differential equation containing an infinite number of space and time derivatives. This mpde contains the original ode plus higher order terms. In order to obtain an equation amenable to physical interpretation, the higher order time-derivative terms can (in some cases) be eliminated, as shown in Ref. 7. In general, for a given finite-difference analog of the governing equation, the modified equation will have the form

$$L(\phi) = \sum_{k=3}^{\infty} C_k \frac{\partial^k \phi}{\partial x^k} \quad (17)$$

where  $C_k$  denotes the coefficient of the  $k$ th spatial derivative and  $L(\phi)$  is the linearized form of Eq. (16).

As an example, consider the following finite-difference approximation to the model equation  $2\phi_{xt} = \beta\phi_{xx}$ .

$$\phi_j^{n+1} - \phi_{j-1}^{n+1} = \phi_j^n - \phi_{j-1}^n + c(\phi_{j+1}^n - 2\phi_j^n + \phi_{j-1}^n) \quad (18)$$

where  $c$  is the Courant number  $\beta\Delta t/2\Delta x$ . Substituting in the Taylor series expansions for each term and eliminating the higher order terms involving time derivatives yields the modified equation

$$2\phi_{xt} - \beta\phi_{xx} = \beta\left(\Delta x - \frac{\beta\Delta t}{2}\right)\phi_{xxx} + \frac{\beta}{4}\left(\Delta x^2 - \beta\Delta x\Delta t + \frac{\beta^2\Delta t^2}{3}\right)\phi_{xxxx} + \text{higher order terms} \quad (19)$$

Hence, the modified equation is equal to the governing equation with the addition of the truncation error terms (the right-hand side). The physical significance of these additional terms is investigated subsequently.

#### Consistency

A finite-difference approximation is said to be consistent with a given partial differential equation if it reduces to that equation in the limit of vanishing mesh spacings. From the modified equation viewpoint, a finite-difference scheme is consistent with the governing equation if the right-hand side of Eq. (17) tends to zero as  $\Delta t$  and  $\Delta x$  approach zero in an arbitrary manner. The satisfaction of the consistency condition ensures that the difference equation is approximating the correct differential equation. The difference scheme for the model equation given by Eq. (18) yields a consistent approximation as can be seen from the modified equation, Eq. (19).

Another finite-difference scheme for the model equation is given by

$$\phi_j^{n+1} - \phi_{j-1}^{n+1} = \phi_j^{n-1} - \phi_{j-1}^{n-1} + \frac{\beta\Delta t}{\Delta x} (\phi_{j+1}^n - 2\phi_j^n + \phi_{j-1}^n)$$

Introducing the approximation

$$\phi_j^n = \frac{1}{2} (\phi_j^{n+1} + \phi_j^{n-1})$$

yields the difference equation

$$\phi_j^{n+1} - \phi_{j-1}^{n+1} = \phi_j^{n-1} - \phi_{j-1}^{n-1} + \frac{\beta\Delta t}{\Delta x} (\phi_{j+1}^n - \phi_j^{n+1} - \phi_j^{n-1} + \phi_{j-1}^n)$$

The modified equation for this finite-difference scheme is given by

$$2\phi_{xt} - \beta\phi_{xx} = -\frac{\beta\Delta t^2}{\Delta x^2}\phi_{tt} + \frac{\beta\Delta x^2}{12}\phi_{xxx} - \frac{\Delta x^2}{3}\phi_{xxx} - \frac{\Delta t^2}{6}\phi_{xtt} + \frac{\beta\Delta t^4}{12\Delta x^2}\phi_{ttt} \quad (20)$$

Clearly, this scheme is in general inconsistent with the model linear equation due to the  $(\Delta t^2/\Delta x^2)\phi_{tt}$  term. It would be a consistent approximation if  $\Delta t \sim \Delta x^2$ . If  $\Delta t \sim \Delta x$  then this scheme approximates the equation  $A\phi_{tt} + 2\phi_{xt} - \beta\phi_{xx} = 0$  where  $A = \beta\Delta t^2/\Delta x^2$ .

#### Order of Accuracy

The order of accuracy of a finite-difference scheme is defined by the lowest order powers of the mesh spacings  $\Delta x$  and  $\Delta t$  appearing in the error terms of the modified equation. For example, the finite-difference scheme given by Eq. (18) is first-order accurate in both space and time as indicated by the fact that the truncation errors in the modified equation, Eq. (19), are proportional to the mesh spacings  $\Delta x$  and  $\Delta t$  to the first power.

A more accurate finite-difference approximation can be obtained by using central-spatial differences on the  $\phi_{xt}$  term. This scheme is given by

$$\phi_{j+1}^{n+1} - \phi_{j-1}^{n+1} = \phi_{j+1}^n - \phi_{j-1}^n + \frac{\beta\Delta t}{\Delta x} (\phi_{j+1}^n - 2\phi_j^n + \phi_{j-1}^n)$$

for which the modified equation is

$$2\phi_{xt} - \beta\phi_{xx} = -\frac{\beta^2\Delta t}{2}\phi_{xxx} + (-\Delta x^2 + \beta^2\Delta t^2)\frac{\beta}{12}\phi_{xxxx} + \dots$$

This scheme is first-order accurate in time and second-order accurate in space.

#### Stability

The stability of a finite-difference scheme pertains to its ability to prevent errors introduced in the numerical solution from becoming unbounded as the number of time steps  $n$  approaches an arbitrarily large number. The essence of stability is that there should be some limit to the extent that any component of the initial function may be amplified by the sequence of difference equations.

A commonly used technique for analyzing the stability of finite-difference schemes is the Von Neumann method. Denote the theoretical and numerical solutions to the difference equation by  $\phi_j^n$  and  $\hat{\phi}_j^n$ , respectively, and let the error be given by  $E_j^n = \hat{\phi}_j^n - \phi_j^n$ . In the Von Neumann method it is assumed that the error can be represented by a Fourier series

$$E_j^n = \sum_k \phi(k, t^n) e^{ikx_j}$$

where  $i = \sqrt{-1}$  and it is assumed that the boundary conditions are periodic. This tacitly implies a linear constant coefficient difference equation, which in general will not be the case. Fortunately, there is numerical evidence to support the contention that in many cases the method can be applied locally with the expectation that the stability characteristics will be roughly the same.

The error propagation can be investigated by substituting one arbitrary component of the Fourier series,  $\phi^n e^{ikx_j}$ , into the difference equation and solving for the amplification factor  $G(k)$ , where  $G(k) = \phi^{n+1}/\phi^n$ . The error component will not grow with time if  $|G(k)| \leq 1$ , and this is the Von Neumann stability condition.

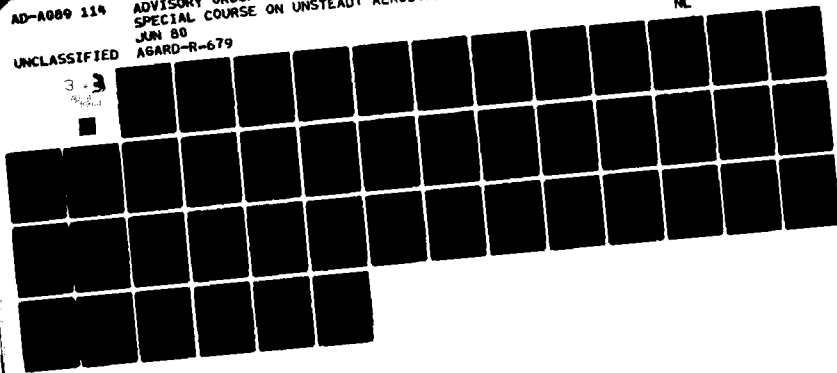
AD-A089 114

ADVISORY GROUP FOR AEROSPACE RESEARCH AND DEVELOPMENT--ETC F/G 1/1  
SPECIAL COURSE ON UNSTEADY AERODYNAMICS. (U)  
JUN 80  
AGARD-R-679

ML

UNCLASSIFIED

3



A  
9114

For the finite-difference scheme of Eq. (18) the amplification factor is given by

$$G(k) = \frac{(1 - e^{-ik\Delta x}) + c(e^{ik\Delta x} - 2 + e^{-ik\Delta x})}{(1 - e^{-ik\Delta x})} = \frac{(1 - 2c)(1 - \cos \theta) + i \sin \theta}{(1 - \cos \theta) + i \sin \theta} \quad (21)$$

where  $c = \beta\Delta t/2\Delta x$  and  $\theta = k\Delta x$ . The stability condition yields, after some algebra  $0 \leq c \leq 1$  or  $0 \leq \Delta t \leq 2\Delta x/\beta$ . For  $\beta < 0$  (supersonic flow) the stability condition cannot be satisfied and the scheme is said to be unconditionally unstable. For  $\beta > 0$  (subsonic flow) the stability condition places a restriction on the size of the time step and the scheme is said to be conditionally stable. Schemes that always satisfy the stability condition are said to be unconditionally stable.

#### Convergence

In any finite-difference approximation, a desired property is the ability to systematically reduce the difference between the solutions of the difference and differential equations. If the solutions to a difference scheme, upon successive refinement of the mesh, approach the exact solution, then the scheme is said to be a convergent approximation to the differential equation and hence maintains this property.

The fact that a finite-difference scheme produces stable solutions does not necessarily imply that these solutions will converge to the exact solution. Lax studied the relation between consistency, stability, and convergence of finite-difference approximations to initial value problems, the result of which is termed the Lax equivalence theorem (see, for example, Ref. 8):

Given a properly posed initial boundary value problem and a finite-difference approximation to it that satisfies the consistency condition, then stability is the necessary and sufficient condition for convergence.

Thus, for any consistent approximation, the question of convergence reduces to a stability consideration.

#### Dispersive and Dissipative Errors

There are many sources of error involved in the approximate solution of transonic flows. Formulation errors due to the approximations involved in the choice of mathematical formulation (e.g., inviscid, irrotational isentropic) and round-off errors due to machine-accuracy limitations are independent of the numerical scheme. Two types of errors that can be directly attributed to the finite-difference algorithm are dispersive and dissipative errors.

The numerical solution of a finite-difference equation will generally exhibit amplitude and phase errors due to dissipation and dispersion, respectively. The effect of these errors on the physics of the flow can be determined from an examination of the modified equation. For the model equation and finite-difference scheme of Eq. (18) the modified equation was shown to be of the form

$$2\phi_{xt} - \beta\phi_{xx} = \mu\phi_{xxx} + \gamma\phi_{xxxx} + \dots \quad (22)$$

The effects of each of the two lowest order truncation terms can be determined by examining three model equations and their solutions; they are obtained by assuming a general solution of the form  $\phi = e^{\alpha t} e^{ikx}$  and solving for  $\alpha$ :

$$\begin{aligned} \text{Low frequency:} \quad 2\phi_{xt} - \beta\phi_{xx} &= 0 & ; & \quad \phi = e^{ik[x+(\beta/2)t]} \\ \text{Burgers:} \quad 2\phi_{xt} - \beta\phi_{xx} &= \mu\phi_{xxx} & ; & \quad \phi = e^{-k^2(\mu/2)t} e^{ik[x+(\beta/2)t]} \\ \text{Korteweg-deVries:} \quad 2\phi_{xt} - \beta\phi_{xx} &= \gamma\phi_{xxxx} & ; & \quad \phi = e^{ik[x+(1/2)(\beta-k^2\gamma)t]} \end{aligned}$$

The exact solution to the equation with  $\mu = \gamma = 0$  is a traveling wave with constant amplitude and a speed  $\beta/2$ . The effect of the  $\phi_{xxx}$  term is to add to the exact solution an amplification factor that dissipates the solution for  $\mu > 0$  or causes exponential growth for  $\mu < 0$ . In fact, the stability of a finite-difference scheme can be determined by examining the sign of the lowest-order dissipative term. The  $\phi_{xxxx}$  term does not affect the amplitude but changes the wave speed to  $[\beta/2 - k^2(\gamma/2)]$ . Since the wave speed is now a function of wave number, each wave travels with a different speed, thus causing dispersion.

The dispersive and dissipative properties of a particular finite-difference scheme can be analyzed using the amplification factor  $G(k)$  obtained from the Von Neumann method. Since the amplification factor is complex, it can be written  $G(k) = |G|e^{i\psi}$ . If  $\psi_e$  is the exact phase shift per time increment  $\Delta t$  then  $\psi/\psi_e$  represents the relative phase shift error or velocity dispersion per time step. The scheme will be dissipative if  $|G| < 1$ . The dispersive and dissipative errors of various difference schemes can be compared using polar plots of  $|G|$  and  $\psi/\psi_e$ . For the model equation, the exact phase shift is given by  $\psi_e = k\beta\Delta t/2 = c\theta$  where  $\theta = k\Delta x$  and  $c$  is the Courant number  $\beta\Delta t/2\Delta x$ . Polar plots for exact, purely dispersive and purely dissipative schemes for the model equation are shown in Fig. 4. For the exact solution, both plots are semicircles of radius 1. The plot of  $\psi/\psi_e$  for the purely dispersive scheme indicates that the wave speed increases with the wave number. For the purely dissipative case the plot of  $|G|$  shows that the dissipation increases with wave number.

Figures 5 and 6 show the numerical solutions to the model equation for an upstream traveling wave using each of the above schemes. Solutions for both high- and low-frequency waves are shown that graphically illustrate the dispersive and dissipative properties indicated by the polar plots.

#### Implicit versus Explicit Schemes and Time Step Selection

Consider the equation  $2\phi_{xt} = \beta\phi_{xx}$  written in the form  $2u_t = \beta u_x$ , where  $\phi_x$  has been replaced by  $u$ . A general two-time-level finite-difference approximation to this equation is

$$u_i^{n+1} - u_i^n = \frac{\beta\Delta t}{2} \delta_x [ \theta u_i^{n+1} + (1 - \theta) u_i^n ] \quad (23)$$

where  $\delta_x u_i$  is an approximation to  $u_x$ , and  $\theta = 0, 1/2, 1$  correspond to explicit Euler, trapezoidal, and implicit Euler time-differencing, respectively. Notice that for  $\theta = 0$ ,  $u_i^{n+1}$  depends solely on values of  $u_i$  at time-level  $n$ . This is a characteristic of explicit schemes.

A scheme is said to be implicit if  $\theta \neq 0$ . Then the solution at the point  $i$  at time-level  $n+1$  depends on the solution at every other point at time-level  $n+1$ . Hence, a system of equations must be solved to advance the solution one time step. In one-dimensional problems, this system is usually solved directly. For two- and three-dimensional problems, the solution is complicated substantially; this is a deficiency of implicit algorithms. However, implicit schemes can often be constructed to be unconditionally stable, permitting selection of an integration time step  $\Delta t$  that is determined based on accuracy rather than stability considerations. A Von Neumann stability analysis applied to Eq. (23) with  $\delta_x u_i = (u_{i+1} - u_i)\Delta x^{-1}$  indicates that trapezoidal ( $\theta = 1/2$ ) and implicit Euler ( $\theta = 1$ ) are unconditionally stable, provided  $\beta \geq 0$  and that explicit Euler ( $\theta = 0$ ) has the stability restriction  $\Delta t \leq 2\Delta x/\beta$ .

The integration time increment  $\Delta t$ , chosen for a computation should, for reasons of computational efficiency, be the largest one that will adequately resolve the unsteady physical phenomena of interest. For disturbances with spatial wavelength  $\lambda$  propagating with speed  $v$ ,  $\Delta t \sim \lambda/v$ . In transonic flows the wave propagation velocities of interest are  $v_U = u - a$  for upstream propagation and  $v_D = u + a$  for downstream propagation. The smallest spatial wavelength that can be resolved on a finite-difference grid with spacing  $\Delta x$  is  $\lambda \sim 2\Delta x$ .

Consider the case of an oscillating airfoil. The number of time increments per cycle of oscillation is  $n = T/\Delta t = 2\pi/(\omega\Delta t)$ , where  $T$  is the period and  $\omega/2\pi$  is the frequency. Using  $k \equiv \omega c/u$  to eliminate  $\omega$  and letting  $\Delta t = \lambda/v$  provides an estimate of the number of time steps required per cycle of oscillatory motion in terms of the flow velocity  $u$ , airfoil chord length  $c$ , reduced frequency  $k$ , and spatial wavelength  $\lambda$  and propagation speed  $v$  of disturbances to be resolved:  $n = 2\pi cv(u\lambda k)^{-1}$ . There are three cases of interest: (1) high-frequency disturbances traveling downstream ( $\lambda \sim 2\Delta x$ ,  $v = u + a$ ); (2) high-frequency disturbances traveling upstream ( $\lambda \sim 2\Delta x$ ,  $v = u - a$ ); and (3) low-frequency disturbances traveling upstream ( $\lambda \sim c$ ,  $v = u - a$ ). For a computation with 50 mesh points on the airfoil chord,  $\Delta x = c/50$ ; and for typical values of Mach number and reduced frequency  $M = 0.8$ ,  $k = 0.05$  we obtain: (1)  $n_1 = 7,000$ , (2)  $n_2 = 700$ , and (3)  $n_3 = 30$ . Hence, substantial differences result in the number of time steps required per cycle, depending on the degree of resolution desired.

The three cases just described can be related to the use of explicit and implicit finite-difference schemes. Case 1 resolves high-frequency disturbances traveling downstream, and the time-step restriction for accuracy is  $\Delta t \sim 2\Delta x/(u + a)$ . This is the same form as the time-step restriction required for stability with explicit schemes. Hence, adequate resolution for Case 1 can be expected using an explicit scheme with a time step chosen to maintain stability.

Semi-implicit schemes have been developed that are implicit on downstream propagating disturbances and explicit on upstream propagating disturbances, so that the stability restriction is  $\Delta t \sim 2\Delta x/(u - a)$ . This corresponds to the time step required to resolve high-frequency disturbances traveling upstream, Case 2. Note that for the example described above, an order of magnitude fewer iterations per cycle would be required for Case 2, using a semi-implicit scheme, than for Case 1 with either an explicit or semi-implicit method.

For Case 3, in which only large wavelength disturbances are generated, substantially fewer time steps are required for accuracy than would be required for stability with either an explicit or semi-implicit scheme — as might be expected when the reduced frequency is small. For Case 3, an unconditionally stable implicit scheme should be used. A question naturally arises: Why not always use an implicit scheme and then adjust  $\Delta t$  for the required accuracy? Because implicit methods are usually more difficult to construct and code than explicit or semi-implicit methods, and because for a given  $\Delta t$  (within the stability bounds), explicit and semi-implicit methods usually provide better resolution of high-frequency disturbance propagation.

#### IV. SEMI-IMPLICIT AND IMPLICIT METHODS FOR UNSTEADY TRANSONIC FLOWS

Many unsteady transonic flow problems of practical importance occur in the reduced frequency range  $k = \omega c/u_\infty \ll 1$ . The time scale of the motion for these reduced frequencies is of the same order as the time scale corresponding to upstream disturbance propagation (along "receding" waves). As shown in the previous section, explicit schemes have a time-step restriction for stability based on downstream disturbance propagation (along "advancing" waves). The associated time scale is much smaller than that of the motion, hence the time-step restriction is much more severe than that required for adequate flow-field resolution. For this reason, explicit finite-difference methods applied to these flows have been notoriously inefficient. The standard approach to increasing computational efficiency is to introduce some degree of implicitness into the solution procedure. Several such methods have been developed for the efficient solution of these flows.

##### Semi-Implicit Schemes

Semi-implicit schemes have been developed for both the small-disturbance Eq. (9) and its low-frequency approximation Eq. (13) by Ballhaus and Lomax (Ref. 9). The schemes were designed to (1) have a time-step restriction for stability based on the receding rather than the advancing-wave-propagation time scale, (2) be as consistent as possible with the characteristics of the corresponding partial differential equation, and (3) reduce to the Murman scheme (Ref. 10) in the steady-state case. These schemes are illustrated schematically in Fig. 7. Both schemes are implicit in the  $y$  direction, thus avoiding a severe time-step restriction due to the shallowness of the characteristic traces in the  $y, t$  plane. The differencing in the  $x, t$  plane is implicit in the upstream direction and explicit in the downstream direction.

A semi-implicit scheme for the linearized low-frequency equation, namely,

$$2\phi_{xt} = \beta\phi_{xx} + \phi_{yy} \quad (24)$$

can be constructed using the differencing of the model linear equation of the previous section given by Eq. (18). Combining this scheme with the general two-time-level temporal difference approximation for  $\phi_{yy}$  yields

$$2\delta_x(\phi_{ij}^{n+1} - \phi_{ij}^n) = \Delta t \left\{ \beta\delta_{xx}\phi_{ij}^n + \delta_{yy} [\theta\phi_{ij}^{n+1} + (1-\theta)\phi_{ij}^n] \right\} \quad (25)$$

where  $\delta_x\phi_{ij} = (\phi_{ij} - \phi_{i-1,j})/\Delta x$ ,  $\delta_{yy}$  is a second-order central-difference approximation, and  $\delta_{xx}$  is a general-difference operator given by



$$\delta_{xx}\phi_{ij} = \left[ \frac{\Gamma}{2}(\Gamma-1)\phi_{i-2,j} + (1+\Gamma-2\Gamma^2)\phi_{i-1,j} + (-2+3\Gamma^2)\phi_{ij} + (1-\Gamma-2\Gamma^2)\phi_{i+1,j} + \frac{\Gamma}{2}(\Gamma+1)\phi_{i+2,j} \right] / \Delta x^2 \quad (26)$$

where  $\Gamma = -1, 0, 1$  corresponds to backward, central, and forward differencing, respectively.

The modified partial differential equation is given by

$$2\phi_{xt} = \beta\phi_{xx} + \phi_{yy} + \left[ \Delta x - \frac{\beta\Delta t}{2} \right] \phi_{xxt} + \left( \theta - \frac{1}{2} \right) \Delta t \phi_{yyt} + \beta\Gamma\Delta x \phi_{xxx} + \text{higher order terms} \quad (27)$$

A Von Neumann stability analysis indicates that the scheme is stable for  $\theta \geq 1/2$  and  $\Delta t \leq 2\Delta x/\beta$  provided that  $\Gamma = 0$  for  $\beta > 0$  (subsonic flow) and  $\Gamma = -1$  for  $\beta < 0$  (supersonic flow). Note that for  $\theta = 1/2$ , the truncation error term containing  $\phi_{yyt}$  is eliminated.

The difference equations must be solved by marching both in  $x$  (the free-stream direction) and  $t$ . For a given time level, tridiagonal equations are solved for  $\phi$  along  $y$  lines ( $x = \text{constant}$ ), successively marching in the  $x$ -direction. This procedure is similar to the successive line overrelaxation (SLOR) schemes used to solve steady transonic flows.

Now consider the nonlinear low-frequency equation written in the form

$$2kM_\infty^2\phi_{xt} = \left[ (1 - M_\infty^2)\phi_x - \frac{\gamma+1}{2}M_\infty^2\phi_x^2 \right]_x + \phi_{yy} \quad (28)$$

Equation (28) can be written in difference form as  $2kM_\infty^2\delta_x(\phi_{ij}^{n+1} - \phi_{ij}^n) = \Delta t [D_x f_{ij} + (\delta_{yy}/2)(\phi_{ij}^{n+1} + \phi_{ij}^n)]$  where  $f_{ij} = f(\phi_{xij}^n) = [(1 - M_\infty^2)\phi_{xij}^n - [(\gamma+1)/2]M_\infty^2(\phi_{xij}^n)^2]$  and  $\phi_{xij} = [\phi_{i+1/2,j} - \phi_{i-1/2,j}]/\Delta x$ .  $D_x$  is Murman's mixed-difference operator required to maintain stability in both subsonic and supersonic regions. As shown by Murman (Ref. 10), care must be taken in switching from one difference operator to another, otherwise the conservative form and its correct weak solution may not be maintained. Switched differences can be used while maintaining proper conservation form by expressing  $D_x$  in the form

$$D_x f_{ij} = \left\{ (1 - \epsilon_i)[f_{i+1/2,j} - f_{i-1/2,j}] + \epsilon_{i-1}[f_{i-1/2,j} - f_{i-3/2,j}] \right\} / \Delta x \quad (29)$$

where  $\epsilon_i = 0$  or  $1$  for  $[1 - M_\infty^2 - (\gamma+1)M_\infty^2(\phi_{i+1/2,j} - \phi_{i-1/2,j})/2\Delta x] > 0$  or  $< 0$ , respectively. Each point in the computational domain is classified according to the test for  $\epsilon_i$ . In Murman's terminology

$$\begin{aligned} \epsilon_{i-1} = 0, \quad \epsilon_i = 0 &\Rightarrow \text{subsonic point} \\ \epsilon_{i-1} = 1, \quad \epsilon_i = 1 &\Rightarrow \text{supersonic point} \\ \epsilon_{i-1} = 1, \quad \epsilon_i = 0 &\Rightarrow \text{shock point} \\ \epsilon_{i-1} = 0, \quad \epsilon_i = 1 &\Rightarrow \text{parabolic (or sonic) point} \end{aligned}$$

This differencing strategy amounts to using central differences in subsonic regions, backward differences in supersonic regions, a combination of both at shock points, and zero at sonic (parabolic) points. The effect of improper mixed differencing on shock speeds is described in the discussion on implicit methods.

Using the finite-difference approximations in Eq. (25) for  $\delta_x$  and  $\delta_{yy}$  along with the mixed-differencing scheme (29) results in a conditionally stable, conservative finite-difference scheme for Eq. (28). The scheme is consistent with both the differential equation and the shock-jump conditions associated with the integral form of the equation. Failure to include the shock-point transition operator, as in the original Murman-Cole scheme (Ref. 11), results in erroneous computed shock-jump conditions that depend on nonphysical considerations, such as mesh spacings. In the unsteady case, failure to maintain conservation form can result in erroneous computed shock speeds, as demonstrated later in this section.

The stability restriction for the semi-implicit scheme applied to the low-frequency Eq. (28) is

$$\Delta t \leq \min_{i,j} \frac{2kM_\infty^2\Delta x}{|1 - M_\infty^2 - (\gamma+1)M_\infty^2\phi_x|}$$

An unnecessarily severe time-step limitation is imposed with the semi-implicit scheme near singular points, such as the airfoil leading- and trailing-edges, where the small-disturbance assumptions break down (i.e.,  $\phi_x$  becomes large). This restrictive time step is used in updating every point in the flow field. This can be overcome by patching in a fully implicit method in these singular regions. However, it is usually easier to use an implicit method for the entire flow field.

### Implicit Schemes

The deficiencies of the semi-implicit schemes can be overcome and the computational efficiency substantially increased with the use of fully implicit methods. It was shown in Sec. III that an unconditionally stable method should be used for low-frequency motions to allow the largest possible time step that adequately resolves the flow field. In general, the implicit schemes are constructed to be unconditionally stable. In principle, relatively large time steps can be taken with these schemes if the flow-field response to some motion has only low-frequency content. In practice, however, the time step for accuracy (and, in some cases, even stability) is limited by high-frequency content in the solution due to the motion of shock waves (Ref. 12), although this restriction is much less severe than the one associated with the semi-implicit schemes.

The construction of an implicit scheme for Eq. (28) can be illustrated by considering the model linear equation, Eq. (24). An implicit, two time-level differencing of Eq. (24) is given by

$$2\delta_x(\phi_{ij}^{n+1} - \phi_{ij}^n) = \frac{\Delta t}{2}(\beta\delta_{xx} + \delta_{yy})(\phi_{ij}^{n+1} + \phi_{ij}^n) \quad (30)$$

where  $\delta_x$ ,  $\delta_{xx}$ , and  $\delta_{yy}$  are finite-difference operators to be defined. Trapezoidal temporal differencing has been chosen to provide second-order time accuracy.

Solution of Eq. (30) for  $\phi_{ij}^{n+1}$  requires the inversion of a nonbanded matrix to advance the solution each time step. To avoid this costly procedure an alternating direction implicit (ADI) technique, originally

introduced by Douglas and Gunn (Ref. 13) for the heat equation is used. The ADI scheme "factors" the difference equation into a sequence of equations, each of which requires only a simple tridiagonal inversion. The consistency, stability, and convergence properties of the original-difference algorithm are unaltered.

The ADI algorithm for Eq. (30) is given by

$$2\delta_x(\bar{\phi}_{ij}^{n+1} - \phi_{ij}^n) = \frac{\Delta t}{2} \left[ 2\beta\delta_{xx}\phi_{ij}^n + \delta_{yy}(\bar{\phi}_{ij}^{n+1} + \phi_{ij}^n) \right] \quad (31a)$$

$$2\delta_x(\phi_{ij}^{n+1} - \bar{\phi}_{ij}^{n+1}) = \frac{\Delta t}{2} \left[ \beta\delta_{xx}(\bar{\phi}_{ij}^{n+1} + \phi_{ij}^n) + \delta_{yy}(\bar{\phi}_{ij}^{n+1} + \phi_{ij}^n) \right] \quad (31b)$$

where  $\bar{\phi}_{ij}^{n+1}$  is an intermediate solution that is a consistent, first-order time-accurate approximation to the solution at time-level  $n+1$ . The first sweep through the grid treats  $\phi_{xx}$  explicitly; the reverse is true on the second sweep. Subtracting Eq. (31a) from (31b) and rearranging, yields

$$\left(2\delta_x - \frac{\Delta t}{2}\beta\delta_{xx}\right)\phi_{ij}^{n+1} = 2\delta_x\bar{\phi}_{ij}^{n+1} - \frac{\Delta t}{2}\beta\delta_{xx}\phi_{ij}^n$$

which is normally used in place of Eq. (31b). The difference-operators  $\delta_x$ ,  $\delta_{xx}$ , and  $\delta_{yy}$  can be chosen to be the same as those used in the semi-implicit scheme. The  $y$ -sweep then becomes identical to the semi-implicit method, which is conditionally stable. The addition of the  $x$ -sweep provides unconditional stability for the ADI scheme. Incidentally, the ADI scheme generalizes to three dimensions in the usual Douglas-Gunn-like fashion.

The shock-capturing properties of the implicit finite-difference scheme can be investigated using the model nonlinear equation

$$(\phi_x)_t + (\phi_x^2)_x = 0 \quad (32)$$

along with boundary conditions  $\phi(0,t) = 0$ ,  $\phi_x(0,t) = \phi_{xL}$ , and  $\phi_x(l,t) = \phi_{xR}$ , and initial conditions as shown in Fig. 8. The weak solution to the model problem can be found by deriving the shock-jump conditions. The model equation can be written in the divergence form  $\vec{v} \cdot \vec{v} = 0$ , where

$$\vec{v} = \left[ \frac{\partial}{\partial t}, \frac{\partial}{\partial x} \right]^T \quad \text{and} \quad \vec{V} = [\phi_x, \phi_x^2]^T.$$

Using the divergence theorem

$$\int_V \vec{v} \cdot \vec{v} \, dv = \int_S \vec{V} \cdot \vec{n} \, ds = 0$$

where  $\vec{n}$  is a vector normal to the shock surface in  $x$ - $t$  space as shown in Fig. 9. Substituting in for  $\vec{V}$  and  $\vec{n}$  gives the shock-jump condition  $-(\phi_{x2} - \phi_{x1})dx_s + (\phi_{x2}^2 - \phi_{x1}^2)dt = 0$  which yields the shock speed

$$v_s = \frac{dx_s}{dt} = (\phi_{x2} + \phi_{x1}) = (\phi_{xL} + \phi_{xR}) \quad (33)$$

The solution to the model problem is  $\phi_x = \phi_{xL}$  for  $x < x_s$ , and  $\phi_x = \phi_{xR}$  for  $x > x_s$ , where  $x_s$  is the instantaneous shock-wave location given by  $x_s = x_{s0} + (\phi_{xL} + \phi_{xR})t$ .

The implicit finite-difference scheme for Eq. (32) is written in the form

$$\delta_x(\phi_j^{n+1} - \phi_j^n) + \Delta t D_x f_j = 0 \quad (34)$$

where  $f_j = f(\phi_{xj}^n, \phi_{xj}^{n+1})$ ,  $\delta_x$  is a backward difference operator, and

$$\phi_{xj} = [\phi_{j+1/2} - \phi_{j-1/2}]/\Delta x \quad (35)$$

The operator  $\delta_x$  can be written in the form

$$\delta_x \phi_j = [(2+\lambda)\phi_j - 2(1+\lambda)\phi_{j-1} + \lambda\phi_{j-2}]/2\Delta x \quad (36)$$

which is first- or second-order accurate for  $\lambda = 0$  or  $1$ , respectively. The quantity  $f_j$  is some difference approximation for  $(\phi_x^2)$ , and the difference-operator  $D_x$  remains to be specified. To avoid iteration at the  $n+1$  level,  $f_j$  is linearized by expanding in terms of  $\phi_{xj}^{n+1}$ . Using a Taylor series expansion,

$$(\phi_{xj}^{n+1})^2 = (\phi_{xj}^n)^2 + 2\phi_{xj}^n(\phi_{xj}^{n+1} - \phi_{xj}^n) + O(\Delta t^2) \quad (37)$$

For trapezoidal temporal differencing,  $\phi_x^2$  is averaged at the  $n$  and  $n+1$  time levels; this gives

$$f_j = \frac{1}{2} [(\phi_{xj}^{n+1})^2 + (\phi_{xj}^n)^2] = \phi_{xj}^n \phi_{xj}^{n+1} + O(\Delta t^2) \quad (38)$$

which maintains the second-order time accuracy of the difference scheme.

As mentioned in the previous section, central and backward differences for  $\phi_{xx}$  are required to maintain stability for the cases  $\beta > 0$  (subsonic) and  $\beta < 0$  (supersonic), respectively. In differencing Eq. (34) then, central and backward differences should be used for  $f$  when  $\phi_x < 0$  (subsonic) and  $\phi_x > 0$  (supersonic), respectively. Murman's mixed difference operator as defined in Eq. (29) is used for  $D_x$ . Combining Eqs. (34)-(38), then gives first- and second-order accurate implicit difference equations for (32)

$$\phi_j^{n+1} - \phi_{j-1}^{n+1} = -\Delta x \Delta t D_x (\phi_{xj}^n \phi_{xj}^{n+1}) + \phi_j^n - \phi_{j-1}^n \quad (\text{first order}) \quad (39a)$$

$$3\phi_j^{n+1} - 4\phi_{j-1}^{n+1} + \phi_{j-2}^{n+1} = -2\Delta x \Delta t D_x (\phi_{xj}^n \phi_{xj}^{n+1}) + 3\phi_j^n - 4\phi_{j-1}^n + \phi_{j-2}^n \quad (\text{second order}) \quad (39b)$$

The term "second-order" in (39b) applies only for locally subsonic regions because the upwind difference used in  $D_x f_j$  for locally supersonic flows is only first-order accurate.

The procedure outlined here maintains proper conservation form by following a three-step procedure: (1) write the difference equation in conservation form, as in Eq. (32), (2) linearize, as in Eq. (38), and (3) apply the switching operator  $D_x$ , as in Eq. (29). Failure to maintain proper conservation form can result in erroneous shock speeds. For example, consider Eq. (32) written in the nonconservation form  $\phi_{xt} + 2\phi_x \phi_{xx} = 0$ . Now introduce a mixed spatial difference approximation to  $\phi_x \phi_{xx}$  in the form  $(1 - \epsilon_j)(\delta_x \phi_j)(\delta_{xx} \phi_j) + \epsilon_{j-1}(\delta_x \phi_{j-1})(\delta_{xx} \phi_{j-1})$  where  $\epsilon_j$  is defined as before and  $\delta_x$  and  $\delta_{xx}$  are first and second central differences, respectively. Coincidentally, it can be shown that this scheme is conservative; in fact, it is exactly equivalent to the Murman conservative scheme. Now, we can apply trapezoidal time differencing to this term and time-linearize to avoid nonlinear matrix operations in advancing the solution one time step. Two obvious linearizations for  $2\phi_x \phi_{xx} = \phi_x^{n+1} \phi_{xx}^{n+1} + \phi_x^n \phi_{xx}^n$  are: (1)  $2\phi_x \phi_{xx} = \phi_x^n (\phi_{xx}^{n+1} + \phi_{xx}^n)$  and (2)  $2\phi_x \phi_{xx} = (\phi_x^n + \phi_x^{n+1}) \phi_{xx}^n$ . Both of these linearizations are first-order accurate, and they produce the erroneous shock speeds

$$(1) \quad V_s = \frac{V_E}{1 + \frac{\Delta t}{2\Delta x} (\phi_{x_L} - \phi_{x_R})} \quad (2) \quad V_s = \frac{V_E}{1 - \frac{\Delta t}{2\Delta x} (\phi_{x_L} - \phi_{x_R})} \quad (40a,b)$$

where  $V$  is the correct shock speed given by Eq. (33). The shock speed can be derived by summing the difference expressions over all the points at a given time level to obtain the change at the downstream boundary during one time step and then relating this change to the shock displacement. Figures 10 and 11 show the variation of shock speed with  $\Delta t/\Delta x$  for each case for  $\phi_{x_L} = 1.0$  and  $\phi_{x_R} = -0.5$ . For both cases, the shock speed approaches zero as  $\Delta t/\Delta x$  becomes large. The shock speed becomes infinite in the second case when  $\Delta t/\Delta x = 2/(\phi_{x_L} - \phi_{x_R})$ . The numerical solutions to the model equation with  $\Delta t/\Delta x = 2/3$  are shown in Fig. 12 along with the exact solution. Erroneous shock speeds resulted here because we time-linearized a quantity ( $2\phi_x \phi_{xx}$ ) that is not the flux conserved in the physical formulation ( $\phi_x^2$ ).

Another way to accidentally generate a nonconservative scheme is to improperly include transition operators in mixed difference schemes. This problem went undetected in the early 1970s after the original Murman-Cole scheme was reported. Their scheme used the subsonic (central) difference operator at the first mesh point downstream of a shock ( $\epsilon_{j-1} = 1, \epsilon_j = 0$ ) instead of the shock point operator. In the unsteady case, it can be shown that this produces a shock speed that depends on the location of the shock within the grid. When the shock is located at a grid point the shock speed is zero, and the shock will remain stationary for all time thereafter.

A more subtle error that can result in a nonconservative scheme occurs with nonuniform grid spacings. The differencing of Eq. (32) for nonuniform grids remains in the form of Eq. (34) where the finite-difference operators are defined by

$$\begin{aligned} \delta_x \phi_j &= (\phi_j - \phi_{j-1})/\Delta x_{b_j} \\ \phi_{x_j} &= (\phi_{j+1/2} - \phi_{j-1/2})/(x_{j+1/2} - x_{j-1/2}) \\ D_x f_j &= \left\{ (1 - \epsilon_j)[f_{j+1/2} - f_{j-1/2}] + \epsilon_{j-1}[f_{j-1/2} - f_{j-3/2}] \right\} / \Delta x_{c_j}/2 \end{aligned} \quad (41)$$

and where  $\Delta x_{c_j} = (x_{j+1} - x_{j-1})$  and where  $\Delta x_{b_j}$  is yet to be defined; the natural choice is to let  $\Delta x_{b_j} = (x_j - x_{j-1})$ , since  $\delta_x$  is a backward difference operator. However, for a supersonic to subsonic shock case ( $\phi_{x_L} > 0, \phi_{x_R} < 0$ ) the shock speed for the above difference scheme is given by  $V_s = [2(\Delta x_{b_j}/\Delta x_{c_j})]V_E$  and is a function of the mesh stretching. To maintain conservation form and hence produce the correct shock speed the mesh spacing in the  $\delta_x$  operator must be chosen as  $\Delta x_{b_j} = \Delta x_{c_j}/2 = (x_{j+1} - x_{j-1})/2$ .

To investigate the shock-capturing characteristics of the conservative implicit scheme, four types of shock motions are considered; they are summarized in Table 1. The terms "subsonic" and "supersonic" are relative to the coordinate system and not to the moving shock.

TABLE 1.- CLASSIFICATION OF SHOCK MOTIONS

Shock	Characteristic	Spatial differencing
1. Supersonic-to-supersonic	$\phi_{x_L} > 0, \phi_{x_R} > 0$	Backward
2. Subsonic-to-subsonic	$\phi_{x_L} < 0, \phi_{x_R} < 0$	Central
3. Supersonic-to-subsonic (downstream moving)	$\phi_{x_L} + \phi_{x_R} > 0, \phi_{x_R} < 0$	Mixed
4. Supersonic-to-subsonic (upstream moving)	$\phi_{x_L} + \phi_{x_R} < 0, \phi_{x_R} < 0$	Mixed

A parameter that has a significant effect on the shock-capturing properties of the scheme is the number of  $\Delta x$  increments the shock wave travels in a time  $\Delta t$ ,  $T = (\Delta t/\Delta x)(dx_s/dt)$ , where the correct shock speed is  $dx_s/dt = (\phi_{x_L} + \phi_{x_R})$  and a uniform grid is assumed. A value  $T = 1$  corresponds to the case where the shock moves a distance of one  $x$ -grid point per time step. Another parameter of interest is the Courant number  $v = 2|\phi_x|(\Delta t/\Delta x)$ , and the stability restriction for the semi-implicit scheme is  $|v| \leq 1$ .

Now consider the implicit schemes (39) applied to the model problem Eq. (32) for the four types of shock motion listed in Table 2. The analysis of the resulting shock profiles is aided by examining the modified equation for the locally-linearized form of the model governing equation which is given by Eq. (19) with  $\beta = 4\phi_x$ . The modified equation can be put in the general form

$$2\phi_{xt} = \beta\phi_{xx} + [2\tau + (1 - \lambda)] \frac{\beta\Delta x}{2} \phi_{xxx} + \left\{ -1 + 3(1 - \lambda^2) + 6\tau[\tau + (1 - \lambda)] \right\} \frac{\beta\Delta x^2}{12} + \frac{\beta^3\Delta t^2}{48} \phi_{xxxx} + \dots \quad (42)$$

where for subsonic or supersonic flow,  $\tau = 0$ , or 1, respectively, and  $\lambda$  is defined as in Eq. (36). The coefficients of the dissipative term  $\phi_{xxx}$ , for both implicit schemes in the supersonic and subsonic cases, are shown in Table 2.

TABLE 2.- DISSIPATIVE COEFFICIENT

Scheme	Supersonic ( $\beta < 0$ )	Subsonic ( $\beta > 0$ )
First-order $\phi_{xt}$	$-\frac{\beta\Delta x}{2}$	$\frac{\beta\Delta x}{2}$
Second-order $\phi_{xt}$	$-\beta\Delta x$	0

The shock profiles for the first-order (39a) and second-order (39b) schemes for the supersonic-to-supersonic case are shown in Fig. 13 for different values of  $\tau$  and  $\nu$  at the same time. In this case, the  $(\phi_x^2)_x$  term is approximated by backward differences throughout. The shock is smeared over five grid points for the first-order scheme and over approximately twice as many points for the second-order scheme. This trend is indicated by the magnitudes of the dissipation shown in Table 2 for this case (i.e., the dissipative coefficient for the second-order scheme is twice as large as that for the first-order scheme). For each scheme, the shock profiles are similar in appearance at the different values of  $\tau$  and  $\nu$ .

Results for the second type of shock motion, the subsonic-to-subsonic case, are shown in Fig. 14. In this case, the term  $(\phi_x^2)_x$  is central-differenced throughout. The first-order results are similar in appearance to those for the supersonic-to-supersonic case. From Table 2 it can be seen that the dissipative terms for the first-order scheme in the supersonic and subsonic cases are identically equal (provided the  $\beta$ 's are the same magnitude). The second-order results contain oscillations that increase with  $\tau$  and  $\nu$ . For this case there is no first-order dissipation and the velocity dispersion at the shock is not sufficiently damped.

A sequence of shock profiles for a downstream-moving, supersonic-to-subsonic shock is shown in Fig. 15. For the supersonic-to-subsonic cases, mixed differences are used for  $(\phi_x^2)$ . The sequence of shock profiles is periodic, repeating every fifth time step, because  $\tau = 0.2$ . Both the schemes capture the shock sharply. Similar shock profiles result for the upstream moving supersonic-to-subsonic case.

The first-order results of Fig. 15 are replotted in terms of  $\phi$  versus  $x$  in Fig. 16. The dashed lines indicate the exact solution at different time steps. The exact shock location at time-level  $n$  is indicated by the intersection of two dashed lines and is marked by  $x_{S_n}$  on the abscissa. The location of the shock relative to the mesh at  $n = 19$  is repeated at  $n = 24$ , and that at  $n = 20$  is repeated at  $n = 25$ , etc. Points identified as shock points at level  $n$  according to (29) are denoted by  $S_n$ . The solution to the difference equation (39) for the case treated in Fig. 16 is  $\phi_j^{n+1} = \phi_j^n$  for  $x_j < x_{S_n}$  and  $\phi_j^{n+1} = \phi_j^n - \Delta x_S (\phi_{x_R} - \phi_{x_L})$  for  $x_j \geq x_{S_n}$ , where  $\Delta x_S$ , the distance the shock travels in time  $\Delta t$ , is given by  $\Delta x_S = \Delta t(\phi_{x_L} + \phi_{x_R})$ . Hence, in updating  $\phi$  from time-level  $n$  to  $n + 1$ , the solution remains unchanged for all (supersonic) points to the left of the shock point. The shock point, and all (subsonic) points to the right of it, move to the dashed line that is the exact solution for  $n + 1$ . The test to determine  $S_n$  ensures that the shock point remains downstream of the solution of  $\tau$  used here.

For large values of  $\tau$ , however, the shock-capturing procedure breaks down, and an instability occurs, as illustrated in Fig. 17. Here the solution downstream of the exact shock location is correct for each  $n$ ; because of the test for  $S_n$ , however, the shock point can move only one grid point downstream per time step, while for  $\tau = 2$ , the exact shock location moves downstream at a rate of two grid points per time step. An increasingly large discontinuity in  $\phi$  develops, which appears as a growing overshoot in  $\phi_x$ , and the process diverges.

For this type of switched-differencing-induced overshoot to occur, two conditions must be met: (1) the point immediately downstream of the shock must be a shock point, and (2) the (downstream moving) shock must move past this point in the next time step. Referring to Fig. 8, these conditions can be expressed

$$\phi_{j_{S+1}} - \phi_{j_{S-1}} < 0 \Rightarrow x_{j_S} - x_{S_0} > \Delta x \left\{ \frac{\phi_{x_L} + \phi_{x_R}}{\phi_{x_L} - \phi_{x_R}} \right\}$$

$$x_{j_S} - x_{S_0} < \Delta t (\phi_{x_L} + \phi_{x_R})$$

or, equivalently

$$\frac{\tau(\Delta x/\Delta t)}{\phi_{x_L} - \phi_{x_R}} < \frac{x_{j_S} - x_{S_0}}{\Delta x} < \tau.$$

This indicates that the occurrence of overshoots depends on the speed of the shock and its location relative to the mesh. As the shock propagates through the grid, the inequality may be satisfied at some time levels and not at others. It follows that these overshoots can never occur if

$$\tau = \frac{\Delta t}{\Delta x} (\phi_{x_L} + \phi_{x_R}) < \left\{ \frac{\phi_{x_L} + \phi_{x_R}}{\phi_{x_L} - \phi_{x_R}} \right\}$$

This is a more restrictive condition than the  $\tau \leq 1$  requirement for stability. Equivalent inequalities can be derived from the upstream-moving shock case in a similar way.

The ADI technique for maintaining implicitness in two dimensions and the treatment of the nonlinear term just described form the basis for a computer code, LTRAN2, designed to solve low-frequency unsteady transonic flows past thin airfoils. Further details, including the treatment of boundary conditions and lift, are described in Ref. 6. This basic technique has also recently been extended (Ref. 14) to solve the unsteady full potential equation.

#### An Implicit Method for the Euler and Navier-Stokes Equations

Efficient, noniterative, implicit finite-difference algorithms for nonlinear, hyperbolic and mixed hyperbolic-parabolic conservation laws have been constructed by Beam and Warming (Refs. 15, 16). The two-dimensional compressible Navier-Stokes or Euler equations can be written in the form

$$\frac{\partial U}{\partial t} = \frac{\partial}{\partial x} [-F(U) + V_1(U, U_x)] + \frac{\partial}{\partial y} [-G(U) + W_2(U, U_y)] + \frac{\partial}{\partial x} V_2(U, U_y) + \frac{\partial}{\partial y} W_1(U, U_x) \quad (43)$$

where  $U$  is an unknown  $p$ -component vector and  $F$ ,  $G$ ,  $V$ , and  $W$  are given vector functions. Let  $U(t) = U(n\Delta t) = U^n$ , where  $\Delta t$  is the integration time step. A general three-time-level, at least second-order accurate temporal differencing of Eq. (43) is given by

$$(1 + \epsilon)U^{n+2} - (1 + 2\epsilon)U^{n+1} + \epsilon U^n = \Delta t \left[ \theta \frac{\partial U^{n+2}}{\partial t} + \left( \frac{3}{2} - 2\theta + \epsilon \right) \frac{\partial U^{n+1}}{\partial t} - \left( \frac{1}{2} - \theta + \epsilon \right) \frac{\partial U^n}{\partial t} \right] + O(\Delta t^3) \quad (44)$$

where the parameters  $\theta$  and  $\epsilon$  are arbitrary real numbers. For  $\theta \neq 0$ , the scheme is implicit. Equation (44) can be written in the convenient form

$$\rho(E)U^n = \Delta t \sigma(E) \frac{\partial U^n}{\partial t} \quad (45)$$

where

$$\begin{aligned} \rho(E) &= (1 + \epsilon)E^2 - (1 + 2\epsilon)E + \epsilon \\ \sigma(E) &= \theta E^2 + \left( \frac{3}{2} - 2\theta + \epsilon \right)E - \left( \frac{1}{2} - \theta + \epsilon \right) \end{aligned} \quad (46)$$

and  $E$  is the shift operator defined by  $E^j U^n = U^{n+j}$ . Substituting in Eq. (45) for  $\partial U/\partial t$  from Eq. (43) yields

$$\rho(E)U^n = \Delta t \sigma(E) \left\{ \frac{\partial}{\partial x} [-F + V_1] + \frac{\partial}{\partial y} [-G + W_2] + \frac{\partial V_2}{\partial x} + \frac{\partial W_1}{\partial y} \right\}^n \quad (47)$$

The mixed spatial derivative terms  $\partial V_2/\partial x$  and  $\partial W_1/\partial y$  on the right-hand side of Eq. (47) preclude the construction of an efficient implicit algorithm by a spatial factorization into a product of one-dimensional operators. This difficulty is avoided by treating the mixed derivative terms explicitly by splitting the right-hand side in the form

$$\rho(E)U^n = \Delta t \sigma(E) \left\{ \frac{\partial}{\partial x} [-F + V_1] + \frac{\partial}{\partial y} [-G + W_2] \right\}^n + \Delta t \sigma_e(E) \left\{ \frac{\partial V_2}{\partial x} + \frac{\partial W_1}{\partial y} \right\}^n \quad (48)$$

where  $\sigma_e(E) = (3/2 + \epsilon)E - (1/2 + \epsilon)$ . Equation (48) can be written in the form

$$\rho(E)U^n - \omega \Delta t \sigma_e(E) \left\{ \frac{\partial V_2}{\partial x} + \frac{\partial W_1}{\partial y} \right\}^n = \Delta t [\sigma(E) - \omega \sigma_e(E)] \left\{ \frac{\partial}{\partial x} [-F + V_1] + \frac{\partial}{\partial y} [-G + W_2] \right\}^n + \Delta t \sigma_e(E) \left\{ \frac{\partial V_2}{\partial x} + \frac{\partial W_1}{\partial y} \right\}^n \quad (49)$$

where  $\omega$  is defined by  $\omega/(1 + \epsilon)$  such that the right-hand side only involves explicit terms.

The nonlinearity introduced by the functions  $F$ ,  $G$ ,  $V_1$ , and  $W_2$  presents an obvious difficulty in solving for  $U^{n+2}$ . This difficulty is overcome while maintaining the order of accuracy through the use of a proper local linearization. By using Taylor series expansions and the consistency condition for Eq. (44), it can be shown that

$$\rho(E) \frac{\partial F^n}{\partial x}(U) = \frac{\partial}{\partial x} [A^n \rho(E)U^n] + O(\Delta t^2) \quad (50)$$

$$\rho(E) \frac{\partial V_1^n}{\partial x}(U, U_x) = \frac{\partial}{\partial x} \left\{ [(P - R_x)^n + \frac{\partial}{\partial x} R^n] \rho(E)U^n \right\} + O(\Delta t^2)$$

where  $A$ ,  $P$ , and  $R$  are the Jacobian matrices  $\partial F/\partial U$ ,  $\partial V_1/\partial U$ , and  $\partial V_1/\partial U_x$ . Similar expressions can be derived for the terms  $\partial G/\partial y$  and  $\partial W_2/\partial y$ . Using these linearizations, Eq. (49) can be rewritten as a linear equation for  $\rho(E)U$ , namely,

$$\begin{aligned} & \left\{ I + \omega \Delta t \left[ \frac{\partial}{\partial x} (A - P + R_x)^n - \frac{\partial^2}{\partial x^2} R^n + \frac{\partial}{\partial y} (B - Q + S_y)^n - \frac{\partial^2}{\partial y^2} S^n \right] \right\} \rho(E)U^n \\ & = \Delta t [\sigma(E) - \omega \sigma_e(E)] \left\{ \frac{\partial}{\partial x} (-F + V_1) + \frac{\partial}{\partial y} (-G + W_2) \right\}^n + \Delta t \sigma_e(E) \left\{ \frac{\partial V_2}{\partial x} + \frac{\partial W_1}{\partial y} \right\}^n + O(\Delta t^3) \end{aligned} \quad (51)$$

The numerical evaluation of the right-hand side of Eq. (51) may represent a significant amount of computation. The number of evaluations of each nonlinear function (and its spatial derivatives at each time step) can be reduced to one using the quasi-one-leg approximations

$$\text{RHS} = \Delta t \left\{ \frac{\partial}{\partial x} [-F(\bar{U}) + V_1(\bar{U}, \bar{U}_x) + V_2(\bar{U}, \bar{U}_y)] + \frac{\partial}{\partial y} [-G(\bar{U}) + W_2(\bar{U}, \bar{U}_y) + W_1(\bar{U}, \bar{U}_x)] \right\}^n + O(\Delta t^3) \quad (52)$$

where  $\bar{U}^n = [\sigma(E) - \omega \sigma_e(E)]U^n$  and  $\bar{U}^n = \sigma_e(E)U^n$ .

To avoid the inefficient inversion of the formidably large system of algebraic equations generated by Eq. (51), an alternating-direction implicit algorithm is used. An ADI form can be obtained by approximately factoring the left-hand side of (51), namely,

$$\left\{ I + \omega \Delta t \left[ \frac{\partial}{\partial x} (A - P + R_x)^n - \frac{\partial^2}{\partial x^2} R^n \right] \right\} \left\{ I + \omega \Delta t \left[ \frac{\partial}{\partial y} (B - Q + S_y)^n - \frac{\partial^2}{\partial y^2} S^n \right] \right\} \rho(E)U^n = \text{RHS} + O(\Delta t^3) \quad (53)$$

where RHS is given by (52); the additional cross-product term introduced by the factorization is  $O(\Delta t^3)$  and hence does not upset the formal order of accuracy of the algorithm.

An obvious computational sequence to implement Eq. (53) as an ADI method is

$$\left. \begin{aligned} \left\{ I + \omega \Delta t \left[ \frac{\partial}{\partial x} (A - P + R_x)^n - \frac{\partial^2}{\partial x^2} R^n \right] \right\} \rho(E)U^* &= \Delta t \left\{ \frac{\partial}{\partial x} [-F(\bar{U}) + V_1(\bar{U}, \bar{U}_x) + V_2(\bar{U}, \bar{U}_y)] \right. \\ &\quad \left. + \frac{\partial}{\partial y} [-G(\bar{U}) + W_2(\bar{U}, \bar{U}_y) + W_1(\bar{U}, \bar{U}_x)] \right\} \\ \left\{ I + \omega \Delta t \left[ \frac{\partial}{\partial y} (B - Q + S_y)^n - \frac{\partial^2}{\partial y^2} S^n \right] \right\} \rho(E)U^n &= \rho(E)U^* \\ U^{n+2} &= [\rho(E)U^n + (1 + 2\epsilon)U^{n+1} - \epsilon U^n] / (1 + \epsilon) \end{aligned} \right\} \quad (54)$$

where  $\rho(E)U^*$  is a dummy temporal variable.

If the spatial derivatives in (54) are approximated by three-point central differences, then the  $x$  and  $y$  operators on the left-hand side of (54) each require the solution of a block-tridiagonal system of equations with each block having dimension  $p \times p$  ( $p = 4$  for the two-dimensional compressible Navier-Stokes and Euler equations). To improve the resolution of shock waves, upwind (backward) and central spatial differences are used in supersonic and subsonic regions of the flow field, respectively. Transition operators are required to maintain proper conservation form of the difference scheme when switching between upwind and central spatial differences.

## V. EXAMPLE APPLICATIONS

The algorithms described in Sec. IV have all been tested by comparing computed results with existing standard solutions or experimental data. These comparisons demonstrate new ways in which the algorithms can be used to solve practical aerodynamics problems, and they help verify accuracy and establish limitations.

### Oscillating Flap

One of the most useful experimental studies to provide insight into the physics of unsteady transonic flows was conducted at the National Aerospace Laboratory (NLR), The Netherlands, by Tijdeman and his associates (Refs. 17, 18). They recorded surface pressures and forces, along with flow visualizations, for transonic flow about an NACA 64A006 airfoil with a harmonically oscillating trailing-edge control surface.

One of the first steps in evaluating LTRAN2 was to solve the linear version of Eq. (13), obtained by setting  $\gamma = -1.0$ , for the airfoil with oscillating flap. The resulting computed surface pressures were then compared with exact linear theory computations provided by NLR. The linear theory results were obtained by solving the linear version of Eq. (9) using a solution technique of verified accuracy. Hence, any discrepancy between the linear theory and LTRAN2 results can be attributed to either numerical error in the LTRAN2 finite-difference scheme or to the low-frequency approximation on which LTRAN2 is based, or to both. The comparison is presented in Fig. 18 in terms of magnitude and phase of the pressure coefficient differentials across the airfoil surface. The reasonably good agreement indicates that the numerical accuracy and low-frequency approximation are adequate for this case.

An important feature of unsteady transonic flows is the motion of shock waves. NLR researchers observed and classified three types of shock-wave motion induced by the harmonically oscillating control surface.

In Type A, sinusoidal shock-wave motion, the shock moves nearly sinusoidally (only the lowest harmonic was measured) but with a phase shift relative to the flap motion. There also exists a phase shift between the shock motion and its strength; that is, the maximum shock strength is not encountered when the shock reaches its maximum downstream location, as in the steady case, but at a later time during its upstream motion.

In Type B, interrupted shock-wave motion, the shock moves as in Type A, but now the oscillatory shock strength is of the same magnitude as the mean steady shock strength. Hence, the shock weakens so that it disappears during the downstream moving portion of its cycle.

Type C, upstream propagating shock waves, occurs at slightly supercritical conditions. Shock waves are formed periodically that do not oscillate in displacement but continue to propagate upstream as the embedded supersonic region vanishes during the flap motion cycle.

LTRAN2 computations illustrating these three types of shock-wave motion were reported in Ref. 6 and some of these are also presented here. Surface pressures for motion Types A and B were also computed by Magnus and Yoshihara, who solved the Euler equations using an explicit finite-difference scheme. The Magnus-Yoshihara results serve here as a standard to help assess the accuracy of LTRAN2 computations. Their approach required nearly 200 times as much computer time to generate a solution as LTRAN2.

Type B motion is illustrated in Fig. 19. The shock reaches its maximum downstream extent at time D, increases in strength at time E, and then weakens at times F and A so that it totally disappears at time B. The shock reappears at time C and strengthens as it moves again downstream to its location at time D. LTRAN2 and Magnus-Yoshihara results agree reasonably well throughout the cycle.

The LTRAN2 and Magnus-Yoshihara results agree better than might be expected for the high reduced frequency involved ( $k = 0.358$ ). A possible explanation is that the characteristic length used in the expression for reduced frequency is incorrectly, in this case, taken to be the chord length  $c$ . Fluctuations in the flow field occur primarily in the region between the shock wave and the trailing edge, a distance that is more nearly equal to the flap length,  $c/4$ , than to the chord length. Including  $c/4$  as the proper length scale in the expression for reduced frequency gives  $k = \omega c/4u_\infty = 0.0895$  for the case shown in Fig. 19. This value is well within the low reduced frequency range, which, from our experience, is bounded by  $k = 0.2$ .

Type C motion is illustrated in Fig. 20. A shock wave forms at some time between C and D, then strengthens and propagates upstream. The forward motion of the shock wave entirely eliminates the embedded supersonic region at some time between E and F. The upper surface flow is entirely subsonic from this time until some time just before C. The shock wave continues to propagate upstream as shown at times G, H, and I.

At time J, it has disappeared, probably dissipated by numerical viscosity. A fine x-grid spacing of 1% chord was used to improve the resolution of the shock wave in this case. Type C shock motion has been computed for a different airfoil motion in Ref. 12 (also reported in Ref. 19). In this case, the shock was clearly resolved as it traveled several chord lengths upstream from the airfoil after having propagated off the leading edge.

The Type A, B, and C cases shown were all computed for free-stream Mach numbers that were lower than the corresponding Mach numbers in Tijdeman's experiments. Wind-tunnel interference effects and viscous effects would have to be modeled for the computations to reliably reproduce the experimental results for the same Mach numbers. Computed results reported in Ref. 20 indicate that wind-tunnel wall interference could have significantly altered the shock-wave motion type for a given  $M_\infty$  in the experiments.

#### The Indicial Approach

One of the primary applications of the methods described here is the prediction of flutter boundaries in the transonic regime. Usually, flutter boundaries are calculated from a linear system of equations of the form

$$[M]\ddot{q} + [C]\dot{q} + [K]q = F(q) \quad (55)$$

where M, C, and K are mass, damping, and stiffness matrices, respectively; q is a vector that is a measure of the structural response; and F(q) is a vector of applied forces. The aerodynamic response to the motion F(q) can be computed in several different ways. For example, the structural motion equation, Eq. (55), could be integrated in time simultaneously with the governing equations for transonic flow. The airfoil motion and aerodynamic forces would be free to drive each other. Flutter boundaries could then be determined by varying appropriate parameters such as the free-stream velocity, a procedure very similar to experimental determination of flutter boundaries. Two examples of this approach are presented subsequently. First we consider an alternative approach — time linearization.

For very small amplitude motions, an approximation can be made in which unsteady effects are treated as linear perturbations about nonlinear steady-state solutions. Since in many aeroelastic applications one need consider only infinitesimal amplitude motions, time-linearization methods can be very useful. To begin with, assume that the airfoil motion and force response are simple harmonic. Substituting expressions  $q(t) = qe^{i\omega t}$  and  $F(t) = [A]q$  into Eq. (55) leaves

$$[K + i\omega C - \omega^2 M]\bar{q} = [A]\bar{q} \quad (56)$$

The matrix A represents the dependence of the aerodynamic forces on the motion of structure. For subsonic or supersonic cases governed by linear aerodynamic equations, these forces are independent of the body shape and mean aerodynamic conditions, and there is no amplitude restriction. The unsteady component of the solution therefore represents the unsteady motion of a flat plate. Furthermore, the forces corresponding to different modes of structural motion can be superposed. The forces for each motion mode are tabulated as functions of  $M_\infty$  and k.

The equations governing transonic aerodynamics are nonlinear, and the superposition principle cannot be applied so generally. In the transonic case, a more limited form of superposition is used in which unsteady aerodynamic solutions are given as linear perturbations about nonlinear steady-state solutions. Then, the forces corresponding to different types of body motions can be superposed, and the forces for each motion can be tabulated as functions of  $M_\infty$  and k, as in the subsonic and supersonic cases. However, these forces are not independent of either the body shape or the mean aerodynamic conditions, and they are valid only for very small oscillation amplitudes.

When oscillation amplitudes are sufficiently small that time linearization is valid, surface pressures and aerodynamic forces can be computed using the indicial method (Ref. 21), an implementation of Duhamel's principle. For example, consider some arbitrary variation of angle-of-attack  $\alpha$  as a function of time and suppose that the indicial lift coefficient response to a unit change in  $\alpha$ ,  $C_{L\alpha}(t)$ , is known. Then the lift coefficient response to the arbitrary variation of  $\alpha$  is

$$C_L(t) = C_{L\alpha}\alpha(0) + \int_0^t C_{L\alpha}(\tau) \frac{d}{dt} \alpha(t - \tau) d\tau \quad (57)$$

That is, once the indicial response to a given motion mode is known, then the lift-coefficient response to an arbitrary variation of that type of motion is given by Eq. (57). Multiple-motion-mode problems can be treated by considering each mode separately and then superposing solutions. For a given mode, the integral in Eq. (57) must be evaluated for each motion frequency of interest. The indicial responses can easily be computed using the transonic solution methods described in Sec. IV.

Example calculations using the indicial method to compute unsteady moment coefficients as a function of  $M_\infty$  are shown in Fig. 21 for oscillatory plunging motion of an airfoil at  $k = 0.1$ . Several observations can be made. First, the purely linear (flat plate) results show only a weak dependence of moment coefficient on Mach number. They do not properly represent the physics of the flow field because flat-plate theory does not account for the motion (or even the existence) of shock waves. The nonlinear results, obtained by time-accurately integrating the governing equation for periodic oscillation of the airfoil until the pitching moment becomes periodic, clearly indicate significant variations in the real and imaginary parts of  $C_m$  with  $M_\infty$  for  $M_\infty$  greater than about 0.86. LTRAN2 can be used to obtain the indicial response to a step change in angle of attack and  $C_m$  evaluated by solving a Duhamel expression similar to Eq. (57). Results are shown for a sequence of step changes. Clearly the time linearization approximation is significantly in error for step changes as large as 1° and 1.5°.

#### Aeroelastic Computations

Here, a simple aeroelastic problem is devised and solutions computed to demonstrate that flow-field and structural-motion equations can be integrated simultaneously in time. Consider an NACA 64A006 airfoil with moment of inertia I free to pitch about midchord. The pitching motion is restricted by a torsion spring of stiffness K and structural damping g. The governing equation is

$$I\ddot{\alpha} + g\dot{\alpha} + K\alpha = M(\alpha) \quad (58)$$

where  $M(\alpha)$  is the aerodynamic moment and  $I$ ,  $g$ , and  $K$  are all positive constants.

We can construct a neutrally stable system (i.e., a system that will flutter) by properly choosing the structural constants. For example, from an indicial method computation for  $M_{\alpha} = 0.88$  and  $k = 0.1$ , we obtain  $|C_{m_{\alpha}}| = 0.8617$  and  $\phi = -68.87^\circ$ . Assuming the motion can be expressed in the form  $\alpha = \alpha_0 e^{i\omega t}$  and substituting this into Eq. (58) results in two expressions (the real and imaginary parts of Eq. (58)) relating the aerodynamic and structural constants:

$$A_1 = -A_3 |C_{m_{\alpha}}| \sin \phi$$

$$A_2 = 1 + A_3 |C_{m_{\alpha}}| \cos \phi$$

where  $A_1 = g/I\omega = 1.072$ ,  $A_2 = K/I\omega^2 = 1.414$ ,  $A_3 = Qc^2/I\omega^2 = 1.333$ , and  $Q$  = dynamic pressure. The equations are satisfied for the values shown.

Figure 22 shows aeroelastic responses for a series of computations in which the structural damping  $A_1$  was varied parametrically. These computations were obtained using LTRAN2 coupled with a simple ordinary differential equation integration procedure for Eq. (58). The aerodynamic and airfoil motion equations were integrated simultaneously. The motion was forced for the first few cycles until the pitching moment became periodic, after which the airfoil motion and aerodynamic response were left free to drive each other. The first cycle shown in Fig. 22 is forced for all cases. The initial motion amplitude is  $\alpha_0 = 0.5^\circ$ . For  $A_1 = 1.072$ , that is, the neutral stability point obtained from the indicial method and Eq. (58), the motion is very nearly sinusoidal. The small deviations from sinusoidal behavior can be attributed primarily to nonlinear unsteady effects and truncation errors in the numerical integration schemes. For other choices of  $A_1$ , the motion is either damped or unstable for values greater than or less than the value corresponding to the neutral stability (flutter) point. For this system to flutter, it is necessary that the moment variation lead the motion, which it does in the nonlinear case for  $M_{\alpha} \geq 0.88$ . Linear (flat-plate) theory does not predict a phase lead and thus could not be used in this case to predict the flutter point.

A similar calculation is shown in Fig. 23. The initial amplitude in this case is considerably larger,  $\alpha_0 = 1.5^\circ$  and the Mach number is smaller,  $M_{\infty} = 0.87$ ; the structural constants differ from those in the previous case. This example is presented mainly to illustrate the nonsinusoidal pitching-moment behavior that can result from the large shock-wave excursions encountered at larger airfoil motion amplitudes.

The aeroelastic computations presented here demonstrate that the nonlinear aerodynamic equations and the equations governing the motion of a structure can be integrated simultaneously to provide solutions to aerodynamic problems. Additional work in this area has been reported in Ref. 22. The further development of the simultaneous integration approach may eventually lead to the development of computational aeroelastic models from which flutter boundaries could be predicted in a manner similar to existing experimental methods; that is, the structural model could be perturbed and the response surveyed for disturbances that produce instabilities. Such an approach might prove advantageous for systems with many degrees of freedom, for which multiple indicial response computations would otherwise be required.

#### Aileron Buzz Computations

In 1947, during wind-tunnel tests of a semi-span wing from the P-80, it was discovered (Ref. 23) that severe aileron vibrations that had been encountered in flight were manifestations of a one-degree-of-freedom flutter. This phenomenon was characterized by shock-wave motion that produced a phase shift in the response of the hinge moment to the aileron motion. Aileron buzz was observed for certain combinations of Mach number and angle of attack.

Recently, Steger and Bailey (Ref. 24) simulated aileron buzz computationally using an approach similar to the one used in the aeroelastic computations just described. They simultaneously integrated in time both the thin-layer Navier-Stokes equations governing the flow field and a simple differential equation for the motion of the aileron,  $\delta I = H$ , where  $\delta$  and  $I$  are the aileron deflection angle and moment of inertia and  $H$  is the hinge moment. The thin-layer Navier-Stokes equations neglect the streamwise diffusion terms in the stress tensor. These equations were solved using the Beam-Warming algorithm described in Section IV. The computed and experimental buzz boundaries are in close agreement (Fig. 24). Computed results in terms of aileron deflection angle as a function of time are also shown in Fig. 24 for  $M_{\infty} = 0.79$ ,  $\alpha = -1.0^\circ$ . For this combination of Mach number and angle of attack, an initial deflection ( $4^\circ$  in this case), causes the aileron to oscillate, but it eventually returns to zero deflection. However, for a free-stream Mach number of 0.82 at the same angle of attack, a limit cycle oscillation results. The comparison of the (2-D) results with experimental data indicates that the (3-D) buzz frequency and negative deflection are accurately predicted, while the positive deflection is overpredicted. It is also interesting to note that when the viscous terms in the Navier-Stokes equations were neglected, either stable or divergent oscillations results; no aileron buzz was observed in the inviscid case.

#### VI. RESEARCH OPPORTUNITIES

Computational aerodynamicists generally are trying to improve the physical modeling in their simulations, extend present capability to treat more complex configurations, improve computational efficiency, and find better ways to apply codes to aerodynamic design and analysis. There are a number of specific research opportunities to support these overall objectives.

First, for the rate of progress to continue, it is essential that there be a continuing availability of larger, faster computer systems. This point is well addressed elsewhere (Refs. 25, 26) and will not be belabored here. However, it is important for the computational aerodynamicist to understand that the large computer systems of the next decade will meet the speed requirements by use of vector processing. This will require the algorithm developer to devote more attention to computer architecture and compiler characteristics in constructing efficient numerical solution procedures.

A number of other challenges provide significant research opportunities to solution algorithm developers. The computational efficiency of implicit algorithms can be improved by improving their stability characteristics. The potential for improvement is far greater for the Euler and Navier-Stokes solution procedures,



which still suffer from relatively severe time-step limitations, than for those applicable to the potential formulations (Ref. 27). A second obvious extension is to the treatment of three-dimensional flow fields. Very little work has been done in three-dimensional, unsteady transonic flows. Such extensions are complicated significantly in applications involving multiple component configurations. No suitable (automatic) grid-generation procedure yet exists even for steady flows about complex configurations. For unsteady applications, the grid must distort as the boundary locations change as, for example, in the case of a wing oscillating in bending and torsion. Work also is required in the development of solution adaptive grids, concentrating grid points in regions where flow variable variations are large. This is a dynamic process requiring that the grid evolve along with the solution. Finally, techniques must be found to eliminate reflections at far-field grid boundaries. Preliminary work on nonreflecting boundary conditions has been reported in Refs. 28 and 29. The use of nonreflecting boundary conditions allows placement of these boundaries much closer to the airfoil, reducing computation time and storage.

Presently, viscous effects can be properly modeled only for attached or mildly separated flows. However, the capability to accurately predict aerodynamic performance near performance boundaries requires proper treatment of massively separated flows. This is feasible using the Reynolds-averaged form of the Navier-Stokes equations with turbulence models. Considerable research is required, combining the talents of experimental as well as theoretical fluid dynamicists, to develop suitable turbulence models for separated flows.

Two principal advances are required in the area of applications. To begin with, appropriate standards must be adopted to improve the state of applications software. Currently available codes are often difficult to modify, do not run reliably, and are very costly to develop. In the future, as the scope and size of aerodynamics codes increase, teams of programmers will be required and the development management task will increase enormously. Software development concepts used routinely in other technology areas should be investigated and adapted for use in aerodynamics. Production codes must also be thoroughly tested and certified before widespread release. At the same time, aerodynamics researchers must find more effective ways of applying these new computational tools in design and analysis. For example, no clearly optimum manner of using nonlinear unsteady transonic codes for predictions of flutter boundaries has yet emerged. However, we anticipate substantial progress in this area during the next decade as a result of continuing improvements in unsteady transonic codes and increasing interest on the part of aeroelasticians.

#### REFERENCES

1. Ballhaus, W. F. and Bailey, F. R., "Numerical Calculation of Transonic Flow About Swept Wings," AIAA Paper 72-677, June 1972.
2. Bailey, F. R. and Ballhaus, W. F., "Comparisons of Computed and Experimental Pressures for Transonic Flows About Isolated Wings and Wing-Fuselage Configurations," NASA SP-347, 1975, pp. 1213-1231.
3. Gingrich, P. B., Child, R. D., and Panageas, G. M., "Aerodynamic Configuration Development of the Highly Maneuvering Aircraft Technology Remotely Piloted Research Vehicle," NASA CR-143841, 1977.
4. Timmons, L. M., "Improving Business Jet Performance: The Mark Five Sabreliner," SAE Paper 790582, Apr. 1979.
5. Marvin, J. G., "Turbulence Modeling for Compressible Flows," NASA TM X-73,188, 1977.
6. Ballhaus, W. F. and Goorjian, P. M., "Implicit Finite-Difference Computations of Unsteady Transonic Flows About Airfoils, Including the Treatment of Irregular Shock-Wave Motions," AIAA Paper 77-205, AIAA 15th Aerospace Sciences Meeting, Los Angeles, January 1977; also AIAA Journal, Vol. 15, No. 12, Dec. 1977, pp. 1728-1735.
7. Warming, R. F. and Hyett, B. J., "The Modified Equation Approach to the Stability and Accuracy Analysis of Finite-Difference Methods," Journal Computational Physics, Vol. 14, No. 2, Feb. 1974.
8. Richtmyer, R. D. and Morton, K. W., "Difference Methods for Initial Value Problems," John Wiley & Sons, New York, 1967.
9. Ballhaus, W. F. and Lomax, H., "The Numerical Simulation of Low Frequency Unsteady Transonic Flow Fields," Lecture Notes in Physics, No. 35, Proceedings of the Fourth International Conference on Numerical Methods in Fluid Dynamics, Springer-Verlag, 1975, pp. 57-63 (also published in Russian).
10. Murman, E. M., "Analysis of Embedded Shock Waves Calculated by Relaxation Methods," Proceedings of the AIAA Computational Fluid Dynamics Conference, July 1973, pp. 27-40.
11. Murman, E. M. and Cole, J. D., "Calculation of Plane Steady Transonic Flows," AIAA Journal, Vol. 9, No. 1, Jan. 1971, pp. 114-121.
12. Ballhaus, W. F. and Steger, J. L., "Implicit Approximate-Factorization Schemes for the Low-Frequency Transonic Equation," NASA TM X-73082, 1975.
13. Douglas, J. and Gunn, J., "A General Formulation of Alternating Direction Methods," Numer. Math., Vol. 6, p. 428, 1964.
14. Goorjian, P. M., "Computations of Unsteady Transonic Flow Governed by the Conservative Full Potential Equation Using an Alternating Direction Implicit Algorithm," NASA CR-152274, 1979.
15. Beam, R. M. and Warming, R. F., "An Implicit Factored Scheme for the Compressible Navier-Stokes Equations," AIAA Journal, Vol. 16, No. 4, Apr. 1978, pp. 393-402.
16. Beam, R. M. and Warming, R. F., "An Implicit Factored Scheme for the Compressible Navier-Stokes Equations II: The Numerical ODE Connection," AIAA Paper 79-1446, July 1979.
17. Tijdeman, H., "Investigations of the Transonic Flow Around Oscillating Airfoils," Ph.D. Thesis, National Aerospace Laboratory (Netherlands) TR 77090, Oct. 1977.
18. Tijdeman, H., Schippers, P., and Persoon, A. J., "Unsteady Airloads on an Oscillating Supercritical Airfoil," AGARD CP-226, Unsteady Airloads in Separated and Transonic Flow, Apr. 1977.
19. Ballhaus, W. F., "Some Recent Progress in Transonic Flow Computations," VKI Lecture Series: Computational Fluid Dynamics, von Karman Institute for Fluid Dynamics, Rhode-St-Genese, Belgium, March 15-19, 1976. Chapter 3 of Numerical Methods in Fluid Dynamics, H. J. Wirz and J. J. Smoldren, eds.

20. Ballhaus, W. F. and Goorjian, P. M., "Efficient Solution of Unsteady Transonic Flows About Airfoils," AGARD Specialists Meeting on Unsteady Airloads in Separated and Transonic Flow, Lisbon, Portugal, Apr. 1977. AGARD Conference Proceedings No. 226, Paper No. 14.
21. Ballhaus, W. F. and Goorjian, P. M., "Computation of Unsteady Transonic Flows by the Indicial Approach," AIAA Paper 77-447, AIAA Dynamics Specialists Meeting, San Diego, Mar. 1977. Included in A Collection of Technical Papers on Dynamics and Structural Dynamics, Vol. B. AIAA Journal, Vol. 16, No. 2, Feb. 1978, pp. 117-124.
22. Rizetta, D. P., "Time-Dependent Response of a Two-Dimensional Airfoil in Transonic Flow," AIAA Journal, Vol. 17, No. 1, Jan. 1979, pp. 26-32.
23. Erickson, A. L. and Stephenson, J. D., "A Suggested Method of Analyzing for Transonic Flutter of Control Surfaces Based on Available Experimental Evidence," NACA RM-A7F30, Dec. 1947.
24. Steger, J. L. and Bailey, H. E., "Calculation of Transonic Aileron Buzz," AIAA Paper 79-0134, Jan. 1979.
25. Chapman, D. R., "Computational Aerodynamics Development and Outlook," AIAA Journal, Vol. 17, No. 12, Dec. 1979, pp. 1293-1313.
26. Ballhaus, W. F. and Bailey, F. R., "Computational Aerodynamics on Large Computers." Invited paper to be published in Journal of Computers and Fluids and presented at the Symposium on Computers in Aerodynamics, Polytechnic Institute of New York, June 1979.
27. Ballhaus, W. F., Holst, T. L., and Steger, J. L., "Implicit Finite-Difference Simulations of Steady and Unsteady Transonic Flows," Lecture Notes in Physics, No. 90, Proceedings of the Sixth International Conference on Numerical Methods in Fluid Dynamics, Tbilisi, USSR, June 1978, Springer-Verlag, 1979, pp. 73-78.
28. Engquist, B. and Majda, A., "Absorbing Boundary Conditions for the Numerical Simulation of Waves," Math. Comp., Vol. 31, July 1977, pp. 629-651.
29. Engquist, B. and Majda, A., "Numerical Radiation Boundary Conditions for Unsteady Transonic Flow," Journal of Computational Physics, to appear.

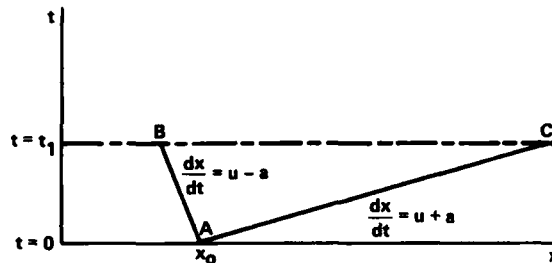


Fig. 1 Wave propagation from a disturbance at  $x = x_0$  at time  $t = 0$ .

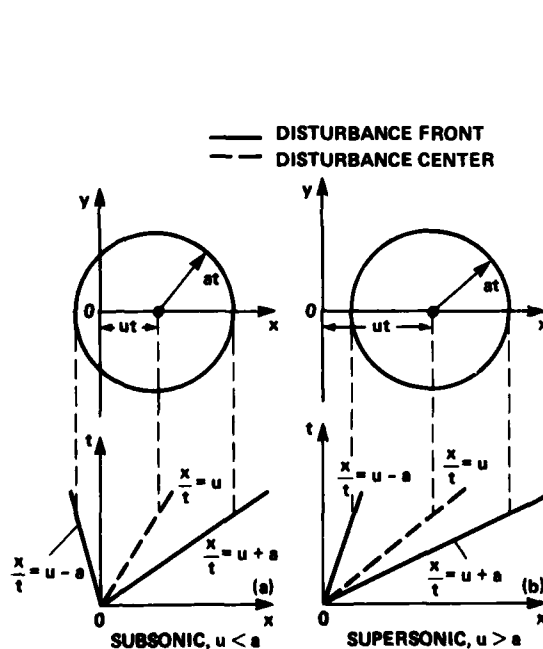


Fig. 2 Characteristic surfaces for the small disturbance equation.

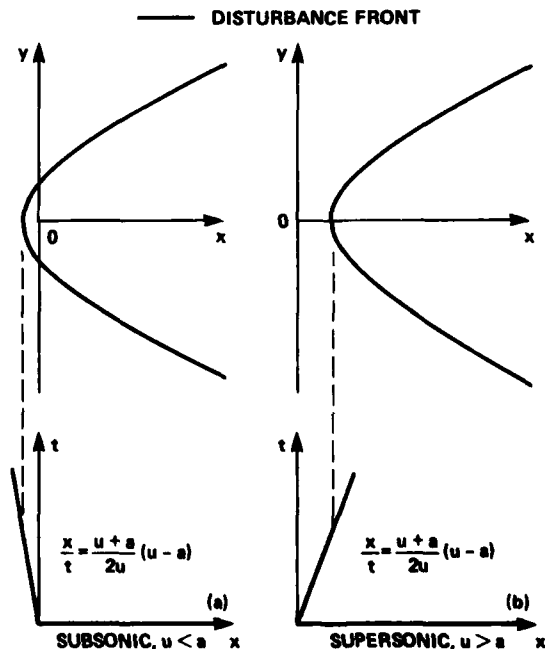


Fig. 3 Characteristic surfaces for the low-frequency approximation.

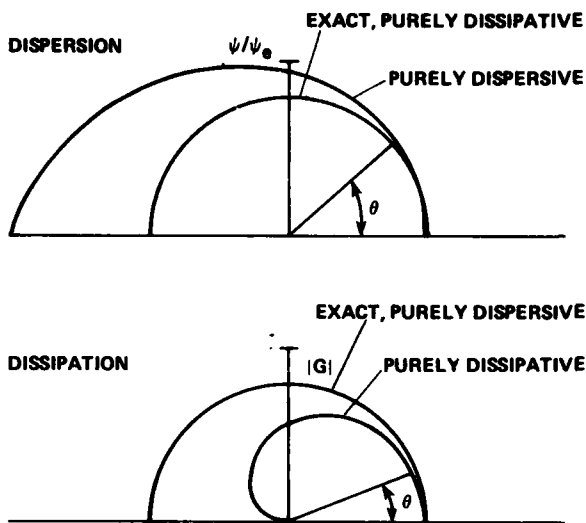


Fig. 4 Dispersive and dissipative properties.

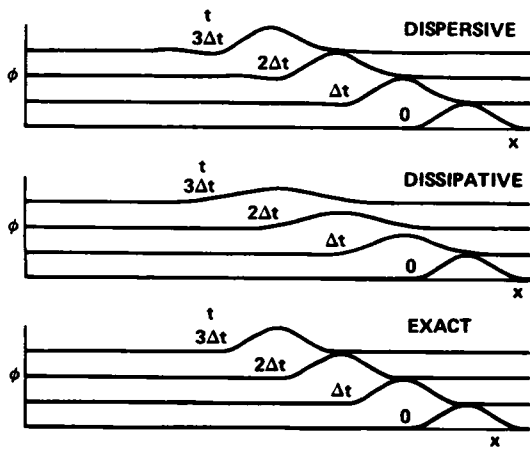


Fig. 5 Numerical solutions for a low-frequency traveling wave.

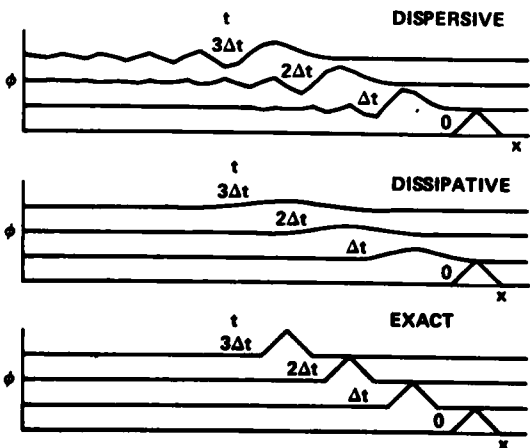


Fig. 6 Numerical solutions for a high-frequency traveling wave.

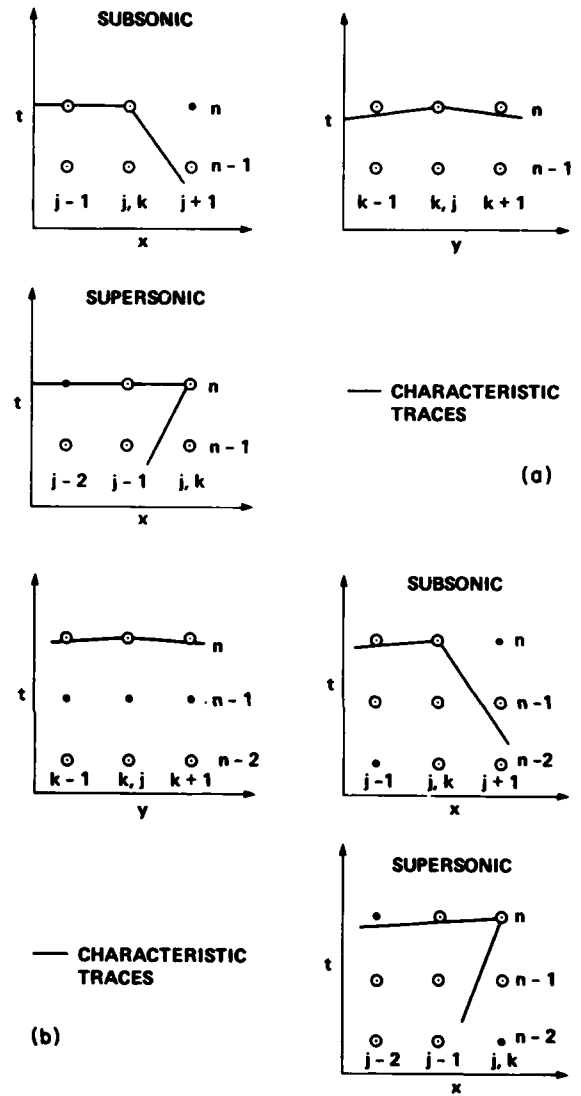


Fig. 7 Difference schemes. (a) Low frequency equation. (b) Small-disturbance equation.

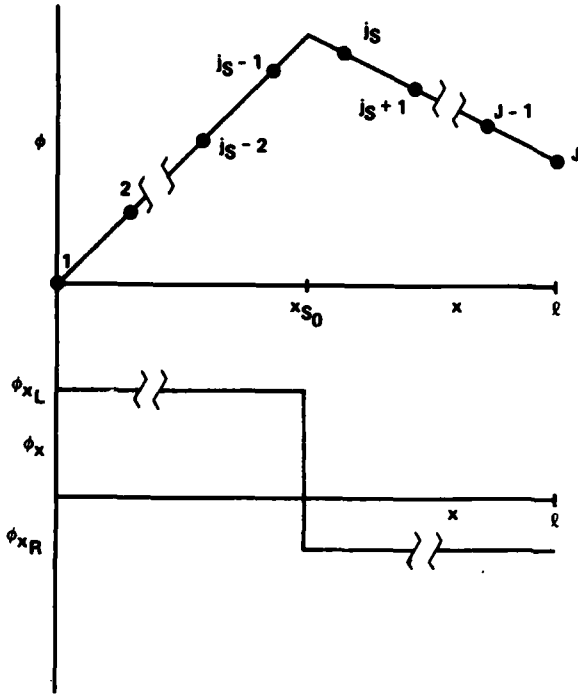


Fig. 8 Sketch of initial data for model one-dimensional problem.

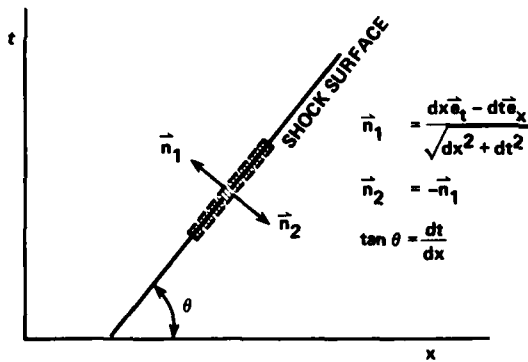


Fig. 9 Shock surface in  $(x,t)$  space.

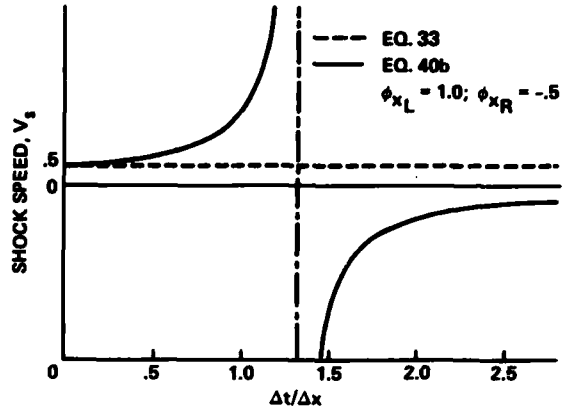


Fig. 11 Shock speed versus  $\Delta t/\Delta x$ .

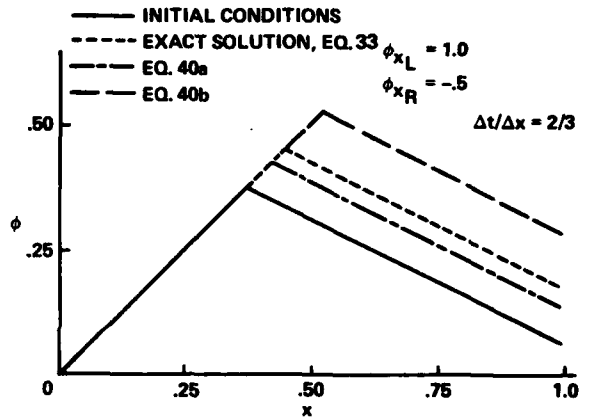


Fig. 12 Numerical solutions producing incorrect shock speeds ( $t = 9.t$ ).

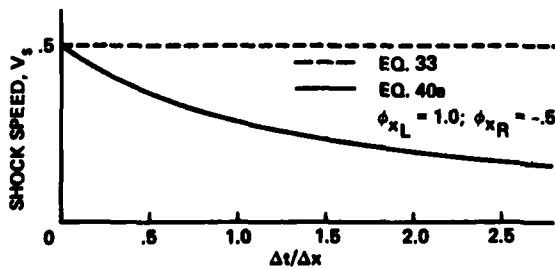


Fig. 10 Shock speed versus  $\Delta t/\Delta x$ .

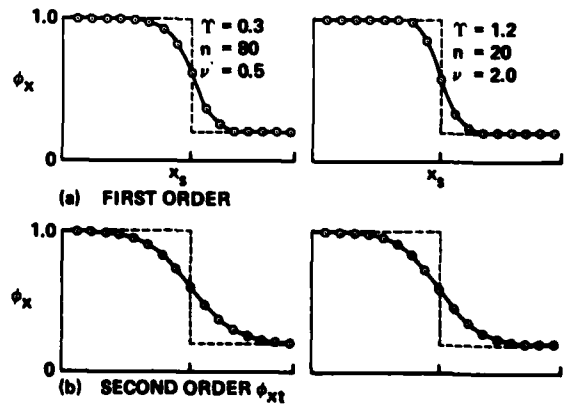


Fig. 13 Shock profiles for supersonic-to-supersonic case.

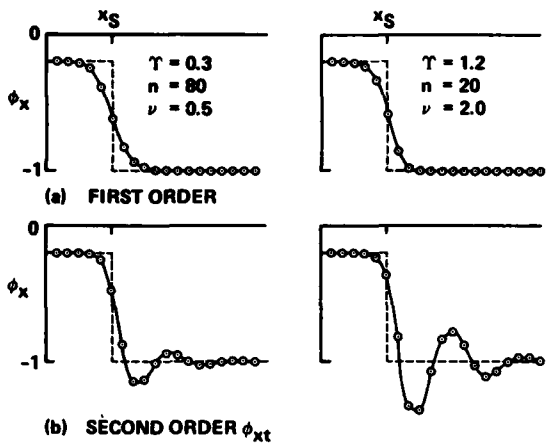


Fig. 14 Shock profiles for subsonic-to-subsonic case.

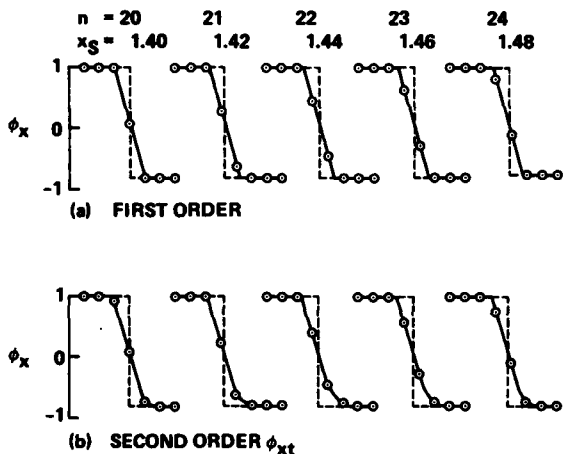


Fig. 15 Shock profiles for downstream-moving supersonic-to-subsonic case,  $\tau = 0.2$ ,  $\nu = 2.0$ .

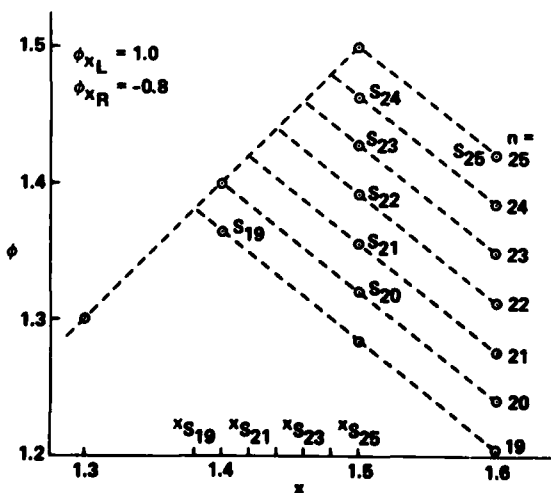


Fig. 16  $\phi$  versus  $x$  for downstream-moving, supersonic-to-subsonic case,  $\tau = 0.2$ ,  $\nu = 2.0$ .

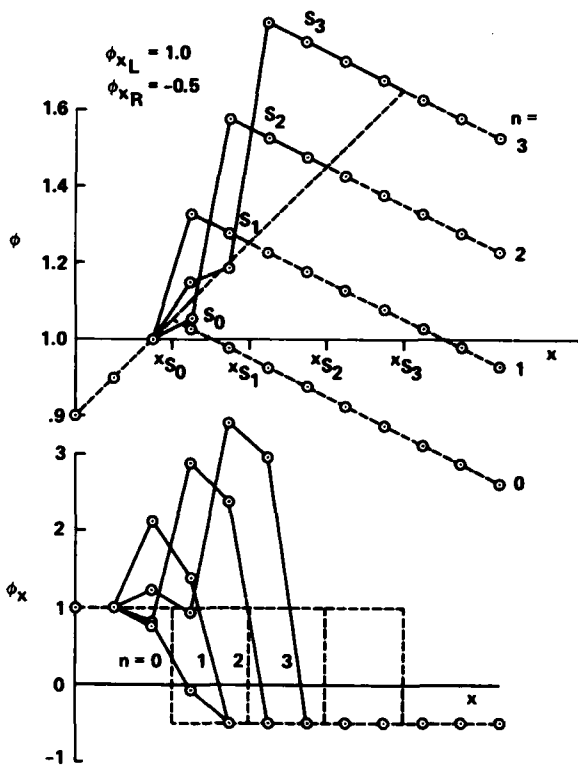
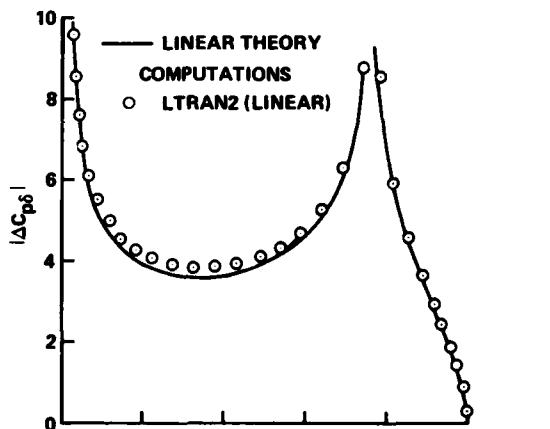


Fig. 17 First-order results for  $\tau = 2.0$ ,  $\nu = 8.0$ .



$$\Delta C_p = \delta_o |\Delta C_{p0}| \sin(\omega t - \phi C_p)$$

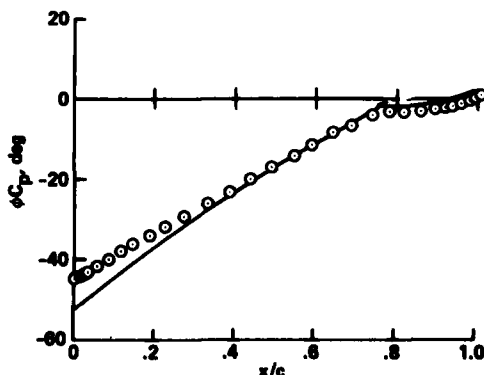


Fig. 18 Comparison of linear pressure coefficient differentials across an airfoil with oscillating trailing-edge flap,  $M_\infty = 0.80$ ,  $k = 0.128$ .

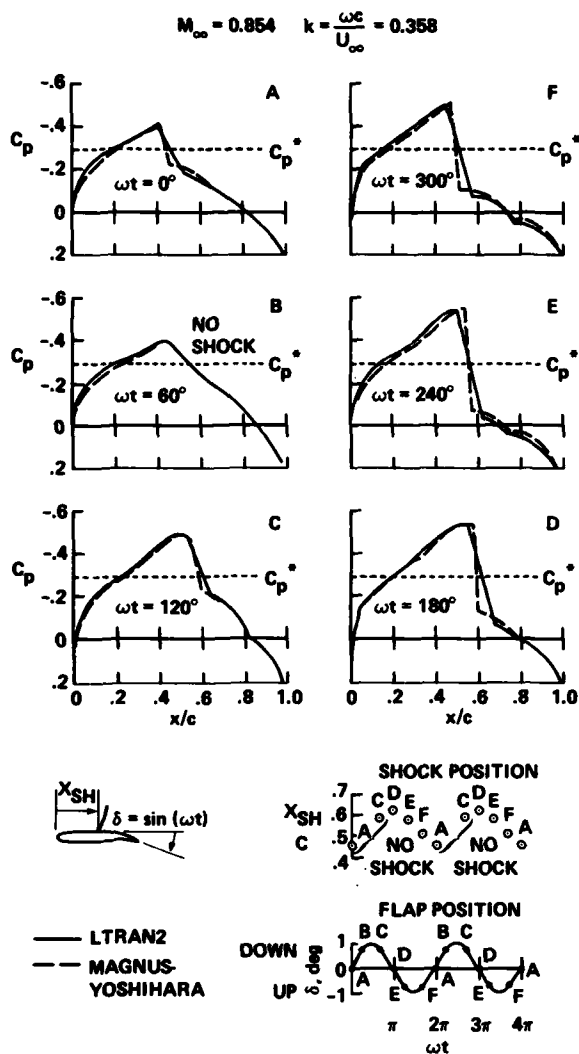


Fig. 19 Unsteady upper surface pressure coefficients for an NACA 64A006 airfoil with oscillating trailing-edge flap, Type B motion.

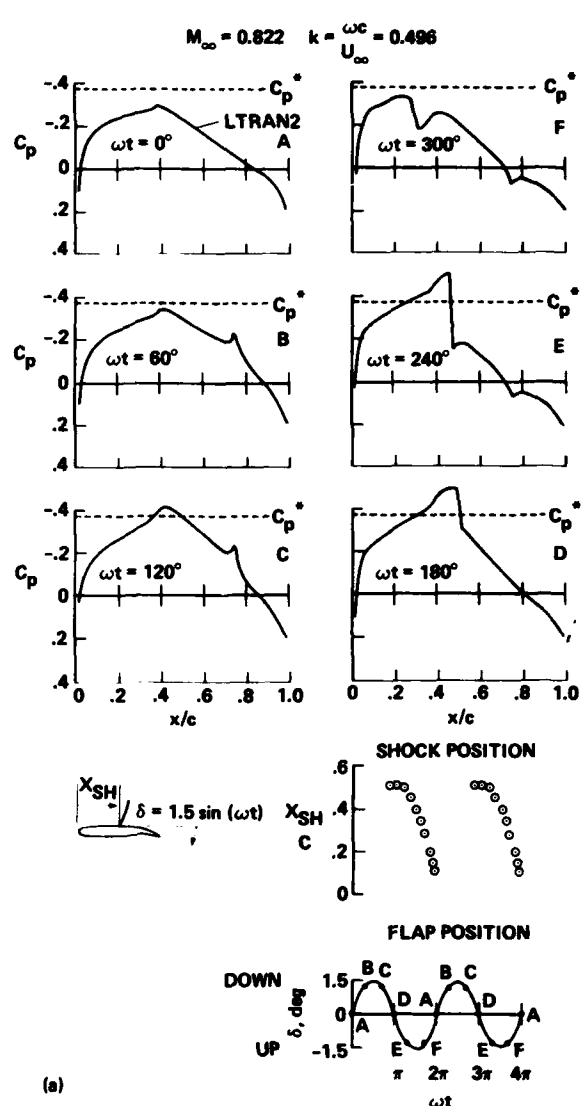
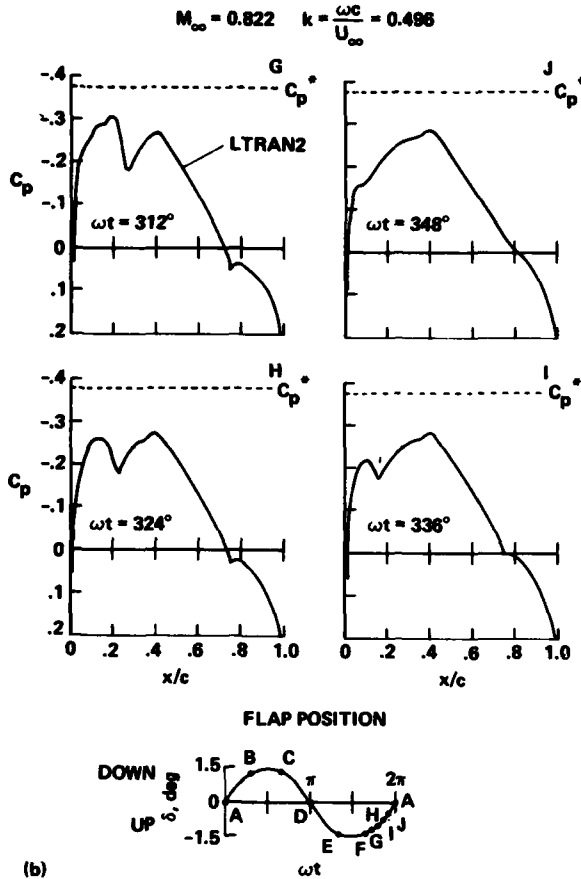


Fig. 20 Unsteady upper surface pressure coefficients for an NACA 64A006 airfoil with oscillating trailing-edge flap, Type C motion.



(b)

Fig. 20 Concluded.

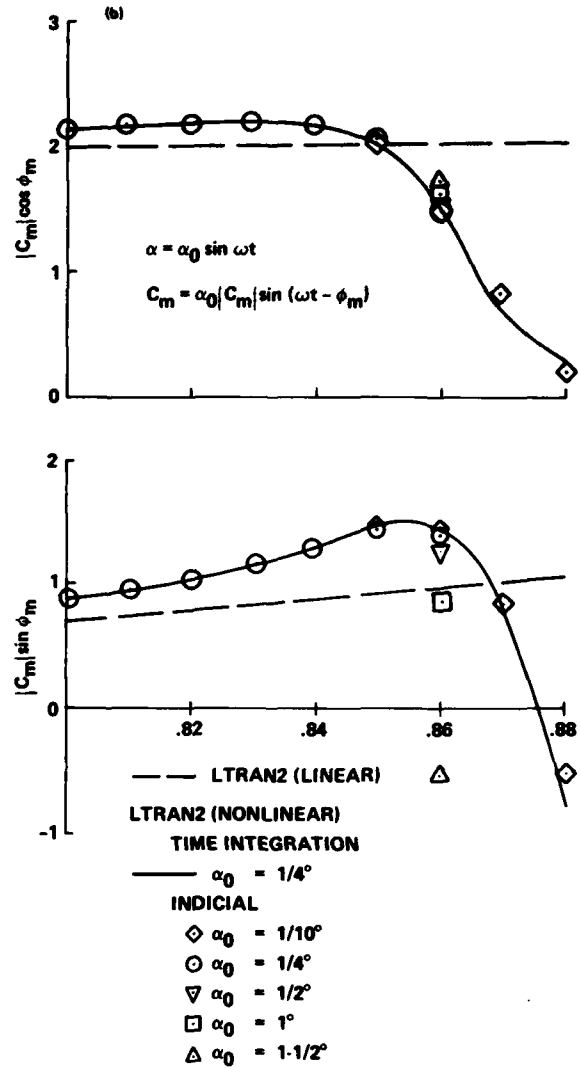
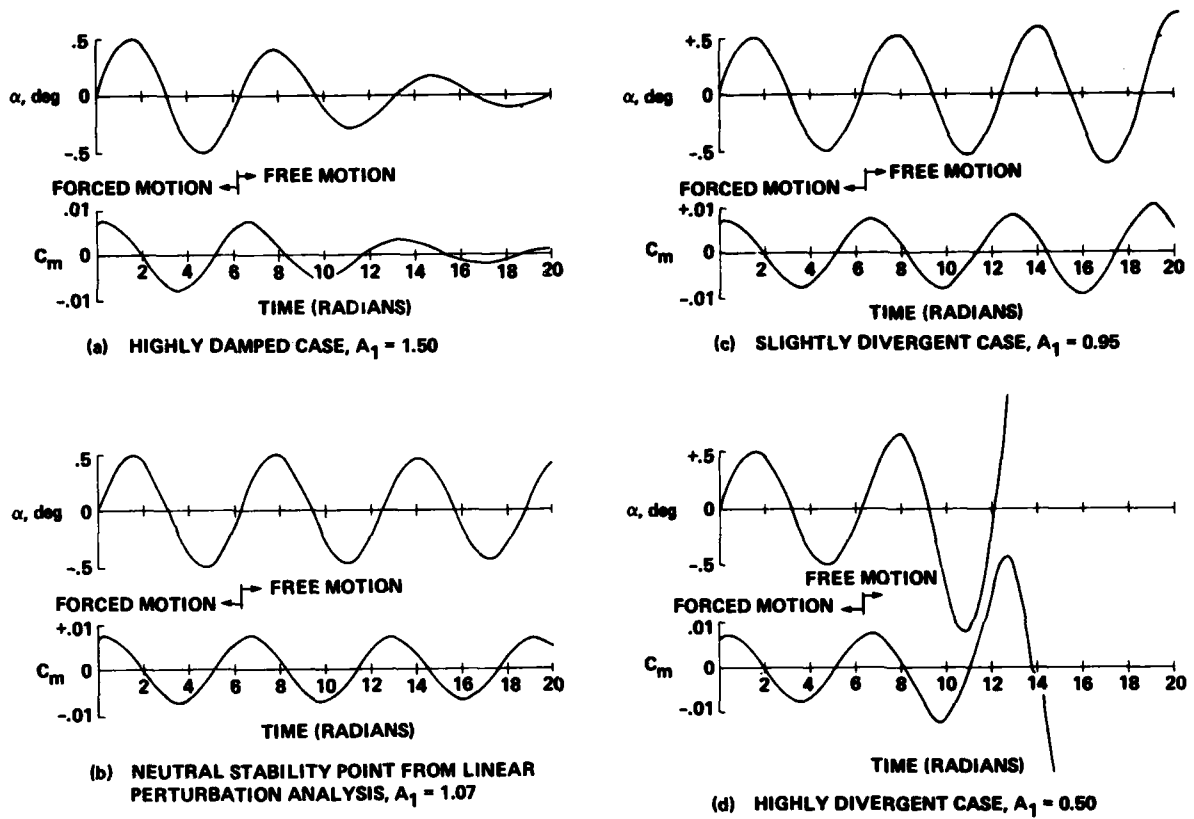
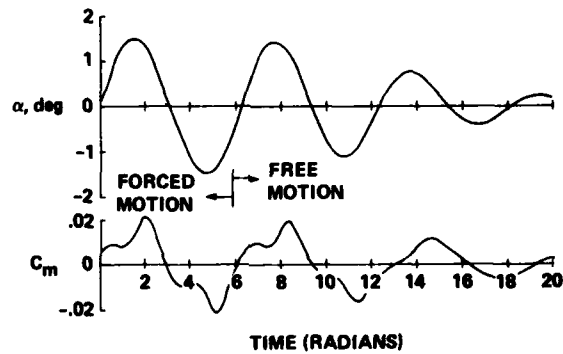


Fig. 21 Midchord moment coefficients versus free-stream Mach number for an oscillatory plunging NACA 64A006 airfoil  $\alpha = \alpha_0 \sin \omega t$ ,  $k = \omega c / U_\infty = 0.1$ ; indicial calculations.

Fig. 22 Constrained pitching oscillations,  $M_\infty = 0.88$ .Fig. 23 Constrained pitching oscillations,  $M_\infty = 0.87$ .



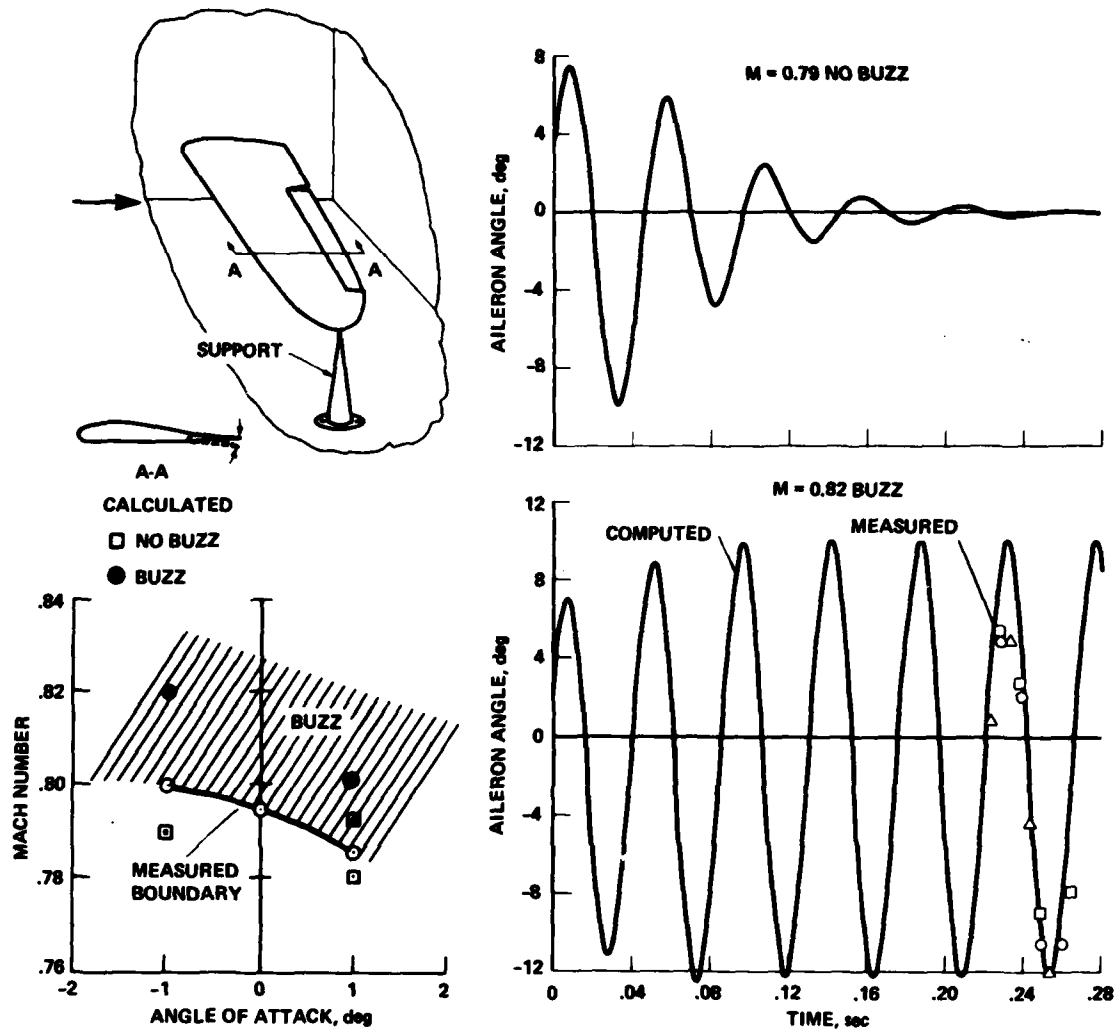


Fig. 24 Computed and measured characteristics of transonic aileron buzz; Reynolds-averaged Navier-Stokes computation for turbulent flow; from Steger and Bailey (Ref. 24).

LINEARISED METHODS IN  
SUPERSONIC FLOW

by

R. H. DOE

British Aerospace, Aircraft Group  
Weybridge-Bristol Division  
Filton, Bristol, England

SUMMARY

Following a brief statement of the linearised equations for supersonic potential flow the essential differences between subsonic and supersonic flows and the concept of the supersonic source are examined. Specialising the time dependence to oscillatory flow the generalised Green's Theorem for such flows is presented through which the integral equations forming the basis of the numerical methods are developed.

The second part of the paper outlines the numerical solution of the integral equations for lifting surfaces in particular those methods developed in British Aerospace. Some consideration is also given to the development of panel methods applicable to general configurations of wings and bodies.

1. INTRODUCTION

The purpose of this paper is to describe numerical methods, based on the linearised theory, for the prediction of unsteady airloads acting on vehicles travelling at supersonic speeds. It is not the intention to give a complete review of all available methods. For review material the reader is referred to papers cited by Ashley in the introduction to ref. 1. The emphasis will be placed on methods developed within British Aerospace with some comparison of the results with those of other workers. Some consideration is also given to the recent developments (elsewhere) of panel methods for bodies and wing-body combinations.

The detailed development of the linearised potential theory for supersonic aerodynamics is to be found in such texts as Ashley and Landahl (ref. 2), and the monographs of Ward (ref. 3) and Miles (ref. 4). In particular Miles book gives an appraisal of the conditions on Mach number, aspect ratio, thickness and amplitude of motion necessary for linear theory to apply and is primarily concerned with analytical methods of solution.

Numerical methods for finding solutions to the linearised equations are generally based on one or another integral equation statement of the problem. Section 2 of the present paper is therefore given over to a brief derivation of the basic integral equations which we seek to solve. In section 3 we deal with some of the methods of solution for lifting surfaces in isolation and in tandem. The final section looks briefly at the recent developments in panel methods for general wing-body configurations.

2. BASIC LINEARISED THEORY

We are concerned with the flight of a vehicle through an initially uniform fluid medium and the forces induced on the body by the resulting fluid motion. We assume the motion of the vehicle to consist of a mean steady translation through the fluid at speed  $U$  with small time-dependent excursions of the body surface from its mean position superposed. For a suitably 'streamlined' body whose surface slopes in the direction of flight are small the direct effects of viscosity and heat conduction within the fluid may be neglected. Furthermore any shock waves generated by the motion are assumed to be weak so that the flow may be taken to be irrotational and isentropic to a first approximation, at least.

The situation is illustrated in figure 1. A cartesian coordinate system  $(x, y, z)$  forms a frame of reference fixed at the mean position of some point in the body with the  $x$ -axis parallel to the undisturbed fluid flow. Points in space will be described by a position vector

$$\mathbf{R} = (x, y, z)$$

and the fluid motion by the vector velocity field  $\mathbf{Q}$ .

Under the assumption of irrotational flow there exists a scalar potential  $\Phi$  such that

$$\mathbf{Q} = \nabla \Phi \quad (1)$$

The assumption of isentropic flow of an initially uniform fluid implies a unique relationship between pressure and density

$$p/p_0 = (\rho/\rho_0)^\gamma \quad (2)$$

the sound speed,  $a$ , is given by

$$a^2 = \frac{dp}{d\rho} = \frac{\gamma p}{\rho} \quad (3)$$

and the following integral of the equations of motion exists (Bernoulli's equation)

$$\left(\frac{\rho}{\rho_0}\right)^{\gamma-1} = 1 - \frac{(\gamma-1)}{a_0^2} \left\{ \frac{\partial \Phi}{\partial t} + \frac{1}{2}(Q^2 - U^2) \right\} \quad (4)$$

### 2.1 The Linearised Equations

With the assumption that the presence of the body and its motion generates only small perturbations of the fluid properties we write

$$\Phi = U(x + \phi)$$

$$Q = U(\hat{e} + q) = U(\hat{e} + \nabla\phi) \quad (5)$$

where  $q$  is the non-dimensional perturbation velocity and  $\phi$  its potential. To first order then equation (4) becomes

$$\rho/\rho_0 = 1 - M^2 \left( \frac{1}{U} \phi_t + \phi_x \right) \quad (6)$$

where  $M$  is the freestream Mach number.

The continuity equation

$$\frac{\partial \rho}{\partial t} + \nabla \cdot (\rho Q) = 0 \quad (7)$$

becomes

$$-\frac{M^2}{U} \frac{\partial}{\partial t} \left( \phi_x + \frac{1}{U} \phi_t \right) + \nabla \cdot \left[ \nabla \phi - \hat{e} M^2 \left( \phi_x + \frac{1}{U} \phi_t \right) \right] = 0 \quad (8)$$

or, more usually,

$$(1-M^2) \phi_{xx} + \phi_{yy} + \phi_{zz} - 2 \frac{M^2}{U} \phi_{xt} - \frac{M^2}{U^2} \phi_{tt} = 0 \quad (9)$$

or

$$\nabla^2 \phi = \frac{1}{a_0^2} \frac{d^2}{dt^2} \phi \quad (10)$$

where

$$\frac{d}{dt} = \frac{\partial}{\partial t} + U \frac{\partial}{\partial x}$$

represents the time derivative following a particle travelling at the freestream velocity,  $U$ . This last form of the equation emphasises the fact that the physics of the linearised flow are precisely the same as in acoustic wave theory for a uniform medium. The first form, equation (8), is a law of conservation for the first order perturbation mass flow

$$m = \nabla \phi - \hat{e} M^2 \left( \phi_x + \frac{1}{U} \phi_t \right) \quad (11)$$

The expression for the pressure coefficient consistent with the present approximation is

$$C_p = \frac{p - p_\infty}{\frac{1}{2} \rho_\infty U^2} \approx -2(\phi_x + \frac{1}{U} \phi_t) \quad (12)$$

This expression is the correct first order approximation for points in the fluid away from the immediate vicinity of the body. It remains valid near the surface of wings, but should be augmented by the nonlinear terms

$$-(\phi_y^2 + \phi_z^2)$$

in the vicinity of slender bodies of revolution and the like (see, e.g. Ashley and Landahl, ref. 1).

#### Note

In later sections it will be convenient to introduce the alternative measure of time

$$T = Ut \quad (13)$$

which has the dimensions of length in common with the definitions of  $\phi$  and the cartesian components  $(x, y, z)$ . The unit of  $T$  is the distance travelled by particles in the freestream in unit time. The quantities  $\phi$ , and  $(x, y, z)$  may alternatively be regarded as having been non-dimensionalised with respect to the length unit  $l$  prior to setting  $T = Ut/l$ .

## 2.2 Supersonic versus Subsonic Flow

By consideration of the propagation of disturbances within the fluid implied by equation (10), and their convection relative to the body at freestream speed, the time taken for a disturbance wave front originating at the origin at time  $t = 0$  to just reach a field point  $R$  is determined by the solution of

$$(x - Ut)^2 = a_\infty^2 t^2 - r^2$$

$$\text{i.e.} \quad T^\pm \triangleq Ut^\pm = \frac{M}{M^2 - 1} (Mx \pm \sqrt{x^2 + (1 - M^2)r^2}) \quad (14)$$

where  $r = \sqrt{y^2 + z^2}$ . For outgoing waves we require that  $t > 0$ , whence for subsonic flow ( $M < 1$ ) only the one root

$$T = T^- = \frac{M}{1 - M^2} (R_\beta - Mx), \quad (15)$$

$$\text{where} \quad R_\beta = \sqrt{x^2 + (1 - M^2)r^2},$$

is meaningful. Disturbances will ultimately reach every point in the flow field.

In contrast, for supersonic flow ( $M > 1$ ) both roots are meaningful but only in a restricted, conical region of space.

$$T = T^\pm = \frac{M}{\beta^2} (Mx \pm R_\beta) \quad ; \quad x > \beta r \quad (16)$$

where

$$\beta = \sqrt{M^2 - 1}$$

$$R_\beta = \sqrt{x^2 - \beta^2 r^2}$$

No disturbance from the origin can reach points outside the rearward facing "Mach cone",  $x > \beta r$ .

This distinction between subsonic and supersonic flow is illustrated by the familiar diagrams in figure 2, and is of great utility in development of certain numerical methods.

For full accounts of the mechanisms of signal propagation refer to Garrick (ref. 5) and Das (ref. 6).

### 2.3 The Supersonic Source

The linearised equation for supersonic flow may be written symbolically as

$$\mathcal{L}_T\{\phi\} = 0 \quad (17)$$

where the operator on the left hand side is defined by

$$\begin{aligned} \mathcal{L}_T\{\phi\} &= \beta^2 \phi_{xx} + \phi_{yy} + \phi_{zz} - 2M^2 \phi_{xT} - M^2 \phi_{TT} \\ &= -M^2 \frac{\partial}{\partial T} (\phi_x + \phi_T) + \nabla \cdot (\nabla \phi - \hat{e} M^2 (\phi_x + \phi_T)) \end{aligned}$$

A fundamental solution to (17) is the perturbation potential field due to a source at the origin of time varying strength  $f(T)$

$$\begin{aligned} \phi = \phi_s(R) &= -\frac{1}{4\pi R_B} [f(T-T^+) + f(T-T^-)] \quad , \quad x > \beta r \\ &= 0 \quad , \quad \text{otherwise} \end{aligned} \quad (18)$$

The perturbation mass flux induced by the source inside the rearward facing Mach cone is

$$\underline{m} = \mathcal{L}\phi - \hat{e} M^2 \phi_T$$

where

$$\mathcal{L}\phi = \nabla \phi - \hat{e} M^2 \phi_x = (-\beta^2 \phi_x, \phi_y, \phi_z)$$

i.e.

$$\underline{m}_s = \frac{-\beta^2 R}{4\pi R_B^3} \left[ (f_+ + f_-) - \frac{M R_B}{\beta^2} (f'_+ - f'_-) \right] \quad (19)$$

Here we have written  $f_{\pm}$  for  $f(T-T^{\pm})$  and  $f'_{\pm}$  represents the derivative of  $f_{\pm}$  with respect to its argument.

In the immediate neighbourhood of the origin the flow is quasi-steady; the source strength is assumed to have changed by a negligible amount in the short time taken for disturbances to propagate through this region. Close to the origin then

$$\underline{m}_s = \frac{-\beta^2 R}{2\pi R_B^3} f(T) \quad (20)$$

This leads to an apparent paradox: we have claimed that equations (18, 19, 20) represent the flow due to a source and that the total mass flow emanating from that source at time  $T$  is  $f(T)$ . In the immediate neighbourhood of the source, however, equation (20) tells us that the mass flux vector is directed inward for  $f(T) > 0$ . The resolution of this paradox depends upon how equations (19, 20) should be interpreted at the Mach cone. A point source is an idealisation of the flow due to a continuous distribution of sources over a vanishingly small volume. An investigation of the flow due to such a volume distribution shows that there is a mass flux outflow between the Mach Cones emanating from the nose and tail of the distribution. This region becomes "invisible" as we allow the volume to shrink to zero. The total mass flux through an enclosing surface  $S$ ,

$$\int_S \underline{m} \cdot \hat{n} \, dS \quad , \quad (21)$$

is maintained constant during the limiting process. In the limit only the inflow due to re-expansion in the region behind the rear Mach cone remains visible as indicated by equation (20). The situation is illustrated in figure 3.

Taking the limit of zero volume first leads to a divergent integral with  $\underline{m}$  in (21) given by equation (20). It was to enable limiting processes of this kind to be taken through the integral sign that the concept of the "finite part integral" was introduced (see Ward, ref 3, or Heaslet and Lomax, ref. 7, where several alternate "recipes" are given for the evaluation of the finite part). The mass flux emanating from a point source can now be determined since

$$-\frac{1}{2\pi} \int_S \frac{\beta^2 R \cdot \hat{n}}{R_B^3} \, dS = 1$$

where the finite part of the integral is to be taken.

(22)

A second result of some utility is that total mass flux above (or below) a plane surface cutting through a source and inclined relative to the freestream at an angle less than the Mach angle,  $\sin^{-1} 1/M$  (see figure 4). The result is independent of the angle of inclination and is given by

$$-\frac{1}{2\pi} \int_{S_u} \frac{B^2 \mathcal{L} \cdot \hat{n}}{R_B^3} dS = 1/2 \quad (23)$$

where  $S_u$  is that portion of the enveloping surface above (or below) the 'cutting' plane. These results can be used to show that for a surface distribution of sources of density  $\sigma$

$$\hat{n} \cdot (\mathcal{M}_2 - \mathcal{M}_1) = \sigma$$

where  $\mathcal{M}_1$  and  $\mathcal{M}_2$  denote the mass fluxes on opposite sides of the surface and  $\hat{n}$  is the normal to the surface at this point directed from side 1 to side 2. Similarly the local surface density of (suitably orientated) doublets is given by the difference in the potential across the surface.

#### 2.4 Oscillatory Flow, Greens Theorem and an Integral Equation

The majority of numerical methods have been developed for a particular form of time dependence, namely, oscillatory motions. We shall therefore specialise our consideration to this class of solution. Note that more general time dependence may be treated through the use of the Fourier integral.

The velocity potential is assumed to have the form

$$\phi(\mathcal{R}, \tau) = \mathcal{R} \{ \varphi(\mathcal{R}) e^{i\omega\tau} \} = \mathcal{R} \{ \varphi e^{ik\tau} \} \quad (24)$$

where  $\omega$  and  $k = \frac{\omega}{U}$  are the circular and "reduced" frequency respectively. The complex amplitude of the potential satisfies

$$\mathcal{L}\{\varphi\} = 0 \quad (25)$$

where

$$\begin{aligned} \mathcal{L}\{\varphi\} &= -B^2 \varphi_{xx} + \varphi_{yy} + \varphi_{zz} - 2ikM^2 \varphi_{x\tau} + k^2 M^2 \varphi \\ &= -ikM^2 (\varphi_x + ik\varphi) + \nabla \cdot (\mathcal{L}\varphi - \mathcal{E} ikM^2 \varphi) \end{aligned}$$

The supersonic source is now represented by

$$\varphi = \varphi_s(\mathcal{R}) = -\frac{1}{2\pi R_B} e^{-ikM^2 x} \cos \frac{kM}{B^2} R_B \quad (26)$$

A generalised form of Green's Theorem which will enable the integration of equation (25) may be obtained by first noting that if  $\varphi$  is a solution of (25) then the function

$$\psi(\mathcal{R}) = \varphi(\mathcal{R}_0 - \mathcal{R}),$$

where  $\mathcal{R}_0$  is a fixed point, must satisfy the "adjoint" equation

$$\mathcal{L}'\{\psi\} \triangleq ikM^2 (\psi_x - ik\psi) + \nabla \cdot (\mathcal{L}\psi + \mathcal{E} ikM^2 \psi) = 0 \quad (27)$$

Forming a combination of (26) and (27) and integrating over a fluid volume  $V$  leads to the required result

$$\begin{aligned} \int_V [\varphi \mathcal{L}'\{\psi\} - \psi \mathcal{L}\{\varphi\}] \\ = \int_{S_V} [\psi (\mathcal{L}\varphi - \mathcal{E} ikM^2 \varphi) + \varphi (\mathcal{L}\psi + \mathcal{E} ikM^2 \psi)] \cdot \hat{n} dS_V \quad (28) \end{aligned}$$

where  $\hat{n}$  is the inward normal (pointing into the fluid) to the bounding surface,  $S_V$ .

Now take  $\varphi$  to be a solution of (25) and  $\psi$  to be the singular solution to (27) which corresponds to the potential at  $\mathcal{R}_0$  due to a source at  $\mathcal{R}$  i.e.

$$\psi_s(\mathcal{R}) = \varphi_s(\mathcal{R}_0 - \mathcal{R})$$

Note that  $\psi(\beta)$  is non-zero in the region for which

$$x_0 - x > \beta \sqrt{(y_0 - y)^2 + (z_0 - z)^2},$$

that is, in the forward facing Mach cone which defines the domain of dependence of  $\mathcal{R}_0$ . The volume of integration is bounded by the body surface, the Mach forecone from  $\mathcal{R}_0$ , and any surface upstream of the region of space influenced by the body. Evaluation of the surface integral involves the use of the finite part integrals (22) and (23). The result is

$$H(\mathcal{R}_0) \varphi(\mathcal{R}_0) = \frac{-1}{2\pi} \int_S e^{-ikM^2(x_0-x)} [G m_n - \varphi \hat{n} \cdot \mathbf{L}G] dS \quad (29)$$

Here we have identified

$$m_n = \hat{n} \cdot (\mathbf{L}\varphi - \hat{\mathbf{e}} ikM^2\varphi)$$

with the normal component of the perturbation mass flux at the body surface  $S$ . Other undefined terms are

$$G = \frac{1}{R_B} \cos \frac{kM}{B^2} R_B$$

where now

$$R_B = \sqrt{(x_0-x)^2 - \beta^2(y_0-y)^2 - \beta^2(z_0-z)^2}$$

and

$$H(\mathcal{R}_0) = \begin{cases} 1 & \text{in the fluid} \\ \frac{1}{2} & \text{in the surface } S \\ 0 & \text{inside the body} \end{cases}$$

Equation (29) may be interpreted in terms of surface singularity distributions. The term

$$e^{-ikM^2(x_0-x)} G m_n = \psi_S m_n$$

being identified with a source distribution of strength  $m_n$  and the remaining terms with a doublet distribution of strength  $\varphi$ . Note that  $m_n$  and  $\varphi$  are equal to the difference across the surface of normal mass flux and potential respectively ( $\varphi$  and hence  $m_n$  are identically zero inside the body).

In the particular case when  $\mathcal{R}_0$  lies in the body surface equation (29) may be regarded as an integral equation for  $\varphi$  if the normal mass flux has been prescribed through the boundary conditions. The equation may then be regarded as determining the necessary doublet distribution to ensure that  $\varphi$  is identically zero throughout the interior of the body given the surface source distribution of density  $m_n$ . This integral equation forms the basis of recent panel methods for the determination of supersonic flow around general wing-body combinations.

### 3. NUMERICAL METHODS FOR LIFTING SURFACES

In this section we shall be concerned with the flow around thin wing-like surfaces. In particular we are concerned with the effects of time dependent motions of the surface involving the bending and twisting of the wing camber surface. Within the linearised approximation the time-dependent perturbations are independent of and may be superposed on the mean steady flow. For the calculation of the unsteady components of the loads acting on the wing we need not consider the effects of steady wing thickness and camber.

Consider a thin wing whose surfaces lie close to a mean cylindrical surface with generators parallel to the freestream. (This means that not only is the wing thickness small but that the steady camber and the amplitude of unsteady motion are small also). Consistent with the linear theory conditions at the true wing surfaces are assumed to be the same as those existing on the upper and lower sides of the mean surface. In particular the boundary condition that the normal component of the fluid particle velocity relative to the true surface be zero is to be applied at the mean surface.

Applying the integral equation (29) to the mean surface of the wing and its wake we find,

$$\varphi(\mathcal{R}_0) = \frac{-1}{2\pi} \int_{S_u} e^{-ikM^2(x_0-x)} [G \Delta m_n - \Delta\varphi \hat{n} \cdot \mathbf{L}G] dS \quad (30)$$

where  $S_u$  is the 'upper' side of the mean surface and  $\hat{n}$  is directed from the lower to the upper side.  $\Delta m_n$  and  $\Delta\varphi$  represent the jump in normal mass flux and velocity potential respectively, across the mean surface.

Since we are dealing with a lifting surface the jump in normal mass flux is zero and equation (30) reduces to a trivial identity for  $\mathcal{L}_0$  on the mean surface.

A workable equation relating the flow velocity normal to the surface to the potential jump across it is obtained by differentiation

$$\begin{aligned} w(\mathcal{L}_0) &= \hat{n}_0 \cdot \nabla \varphi \\ &= \frac{1}{2\pi} \int_{\Sigma_u} e^{-ik\frac{M^2}{B^2}(x_0-x)} \hat{n}_0 \cdot \nabla (\hat{n} \cdot LQ) \Delta \varphi \, dS \quad (31)^* \end{aligned}$$

where  $\hat{n}_0$  is the unit normal to the mean surface at the point  $\mathcal{L}_0$ . Methods based on this equation are often referred to as "integrated potential" methods.

For planar wings, where the mean surface may be taken to be the plane  $z = 0$ , an alternative approach involving an integral equation with a simpler kernel than that in equation (31) may be developed utilising the antisymmetry of the flow with respect to  $z = 0$  and the restricted domains of influence and dependence of points in supersonic flow. Methods based on this approach are known as "integrated upwash" methods.

Referring to figure 5 consider the finite region  $\Sigma$  of the plane  $z = 0$  which lies in both the domain of influence and the domain of dependence of points on the wing mean surface. This region may or may not contain points in the wake; the part of the wake outside this region cannot affect the flow over the wing surface. The integral (29) may now be applied to the upper half space  $z > 0$ ; the flow in  $z < 0$  is to be determined by antisymmetry. The result is the same as if we had modelled the flow in the upper half space with a source distribution over the whole of the region  $\Sigma$ , imposing a condition corresponding to zero load on those parts of the region that lie outside the wing planform (the so called diaphragm regions). The source strength on the wing region is given by the prescribed upwash (which equals the component of mass-flux normal to the mean surface). The resulting equation is

$$\varphi(\mathcal{L}_0) = \frac{-1}{\pi} \int_{\Sigma_0} e^{-ik\frac{M^2}{B^2}(x_0-x)} Q \cdot w(\mathcal{L}) \, d\Sigma \quad (32)$$

where  $\Sigma_0$  is that part of  $\Sigma$  that lies within the domain of dependence of  $\mathcal{L}_0$  and the upwash,  $w$ , on the diaphragm regions is to be determined from the zero load condition. The load acting across the mean surface is given by

$$\begin{aligned} \Delta \varphi &= \mathcal{R} \{ l e^{ikt} \} \\ l &= -4 (\varphi_x + ik\varphi) \Big|_{z=0^+} \end{aligned}$$

where

The latter may be integrated for the case of zero load to give

$$\varphi = A(y) e^{-ikx}$$

where  $A(y)$  is determined from conditions existing at the upstream end of the region of zero load to give

$$\varphi = 0 \quad (33)$$

on the diaphragm outside the wake, and

$$\varphi = \varphi_{TE} e^{-ik(x-x_{TE})} \quad (34)$$

for points in the wake. (Equation (34) is also required for the wake region in the integrated potential formulation; the use of diaphragms outside the wing and its wake are, however, not required as  $\varphi$  is zero over such regions, and the domain of integration is correspondingly reduced).

It is also possible to derive an acceleration potential formulation equivalent to the integral equation of the subsonic kernel function methods, relating the upwash to the loads acting on wing (refs 8, 9, 10). Numerical methods employed in the solution of this integral equation, in common with subsonic methods, are usually of collocation type utilising sets of certain assumed loading distributions (modes).

---

\* The gradient operator  $\nabla_0$  is to be applied to  $\varphi$  as a function of  $\mathcal{L}_0$ . In taking it through the integral sign we have utilised the fact that  $\nabla_0 = -\nabla$ .



The coefficients attached to each distribution are determined by satisfying the integral equation only at an appropriate number of collocation points. There are difficulties with this approach connected both with the complexity of the kernel function and proper choice of loading modes for a given planform. The latter difficulty, in particular, is increased when the method is applied to more general configurations although Cunningham (ref. 11) has tackled the problem of interacting lifting surfaces.

Numerical methods for the solution of the integrated potential or integrated upwash formulations are generally based on 'finite element' techniques. The integration over the dependence domain is replaced by the sum of integrations over a set of simple elements. Over each elemental area the unknown is expressed as the sum of a few (often only one) simple functions. A variety of element shapes have been used such as squares (ref. 12), Mach or characteristic boxes (Box methods), and triangular or quadrilateral elements.

In the box methods, usually applied to the integrated upwash formulation, the dependence domain is divided up into a large number of equal sized elements. These elements are either rectangular, with diagonals parallel to the Mach lines (Mach boxes), or diamond shape with sides parallel to the Mach lines (figure 6). The upwash is generally assumed to be constant within each box. Examples of the Mach box technique are given in refs 13, 14 and 15 where the use of the diaphragm technique has been extended to cover general configurations of interfering surfaces. An example of the characteristic box method will be discussed in the following paragraphs.

The integrated potential formulation forms the basis of the method developed by Allen and Sadler (ref. 16), using characteristic elements, for planar wings and extended by Woodcock and York (ref. 17) to tandem wings.

Interesting recent developments by Appa and Jones based on the integrated potential formulation are reported in references 18 and 19. They work in terms of the reduced potential  $\bar{\phi} = \phi \cdot e^{-ikM^2x}$  and the corresponding modified upwash function, which eliminates the complex exponential term in equation (31). After integrating by parts with respect to  $x$  the problem is posed as an integral equation relating upwash to the potential gradient  $\bar{\phi}_x$ . The integral is then replaced by the sum of integrals over a set of quadrilateral elements (panels) covering the wing and wake planform(s), (figure 7). The method is applicable to general configurations of lifting surfaces.

### 3.1 A Characteristic Box Method

This method (ref. 20) was developed some 12 years ago for planar wings and is generally similar to that of Stark (ref. 21). This brief presentation differs in detail from that in reference 20 in order to be consistent with more recent, unpublished, extensions to tandem surfaces.

The integrated upwash formulation (31) for a planar wing, is written in terms of the characteristic coordinates

$$r = (x/\beta - y)/2\epsilon$$

where

$$s = (x/\beta + y)/2\epsilon$$

(35)

where  $\epsilon$  is identified with the semispan of an element in the characteristic box scheme; the boxes are defined by a lattice formed by the lines for which  $r$  and  $s$  are integer constants (figure 8). The upwash distribution over each box is taken to be constant equal to the mid-point value for boxes wholly on the wing and some suitable mean value for those wholly or partially off the wing. The potential, evaluated at the nodal points  $(m, n)$  of the lattice, is dependent only on the influence of those boxes in the region  $r \leq m$  and  $s \leq n$ .

For given lattice point we have then

$$\phi(m, n, \sigma^+) = \phi_{m,n} = \sum_{\mu=1}^m \sum_{\nu=1}^n S_{m-\mu, n-\nu} \omega_{\mu,\nu} \quad (36)$$

where the source influence coefficients  $S_{\mu,\nu}$  are given by

$$S_{\mu,\nu} = \frac{-\epsilon}{\pi} \int_{\mu}^{\mu+1} \int_{\nu}^{\nu+1} e^{-i\chi(r+s)} \cos \frac{2\chi}{M} \sqrt{rs} \frac{dr ds}{\sqrt{rs}} \quad (37)$$

with 
$$\chi = \frac{kM^2\epsilon}{\beta}$$

These integrals are evaluated following a procedure proposed by Zartarian and Hsu (ref. 22) whereby, after making the substitutions  $r = u^2$  and  $s = v^2$ , the inner integral is expressed in terms of the Fresnel integrals

$$C(z) - iS(z) = \frac{1}{\sqrt{2\pi}} \int_0^z \frac{e^{-it}}{\sqrt{t}} dt = \sqrt{\frac{z}{\pi}} \int_0^{\sqrt{z}} e^{-iu^2} du$$

The outer integral is evaluated numerically by Gaussian quadrature.

The problem is solved by following a systematic marching procedure working from the foremost point on the lattice along successive lines  $m = \text{constant}$ . At each step the upwash on every box in dependence domain save, possibly, that of the pivoted element itself is known. One of the following alternative conditions will apply

- (a) The pivotal element lies wholly on the wing; compute  $\Phi_{m,n}$  directly from (36)
- (b) The box lies wholly on a diaphragm region; solve (36) for  $w_{m,n}$  with  $\Phi_{m,n}$  given by the zero load conditions (33) or (34).
- (c) The box straddles a leading or side edge; compute a value  $w'$  for  $w_{m,n}$  as in (b) above. Determine a mean value for  $w_{m,n}$  by combining  $w'$  and the value of  $w$  on the wing weighted by the proportions of element area which lie off and on the wing respectively. Finally compute  $\Phi$  as in (a). A similar process applies at the trailing edge. Note that in this simple 'area-weighting' technique no account is taken of whether the edge is subsonic or supersonic.

Figure 9 illustrates results obtained with this method for an aspect ratio 2 rectangular wing at a freestream Mach number of 2. The "direct" generalised forces,  $Q_{ij}$ , are shown compared with analytic results obtained by Williams and Woodcock (ref. 23) for a set of increasingly complex deflection modes over a frequency range  $k = 0$  to 0.8 based on the root chord. The steady flow results ( $k = 0$ ) indicate errors of 1½% and 2% in the estimation of the lift,  $Q_{12}$ , and pitching moment,  $Q_{22}$ , respectively. In general it was found that the errors increased with increasing complexity of mode shape. An examination of the results shows that the discrepancy was predominantly in the magnitude  $|Q_{ij}|$  of the generalised forces, the differences in phase angle being typically 0.5°. The largest errors tend to occur for those deflection modes dependent on  $y^2$  indicating that a possible source lies in the treatment of the (subsonic) side edges.

In his method, Stark (ref. 21), employed a special technique for boxes cut by subsonic leading edges approximating the inverse square-root behaviour of the upwash in upstream part of the box at the leading edge. Stark's method, however, can only be applied to straight leading edges for a certain, discrete, set of Mach numbers dependent on the leading edge sweep.

A comparison of the results of the present method with exact conical flow theory for a cropped delta at Mach 1.054 in steady flow is shown in figure 10. It can be seen that there is an almost constant error in the present results (Stark's results are almost indistinguishable from the exact theory). This error leads to an overestimation of the of the lift force acting on the wing of some 3%.

A similar discrepancy exists in the comparison between the present method and that of Stark for the same wing oscillating in translation shown in figure 11.

Subsequent to the initial development of the present method it was discovered that a relatively minor modification to the definition of areas used in the leading edge weighting technique could produce results for wings with subsonic edges of greatly improved accuracy. The idea was derived from Evvard's equivalent diamond principle for steady flow over wings with subsonic edges. Considering the part of the wing covered by the element to be an isolated wing in an upwash field determined by alternative (b) above, Evvard's principle states that the potential at the rearmost point is obtained by applying the source integral to the area indicated in figure 12. The modification to the present method was simply to replace the wing area used in the weighting technique by that dictated by Evvard's principle. Results from the modified method are virtually indistinguishable from those of Stark. The method has the advantage of being applicable to wings of general planform at general supersonic Mach number.

### 3.2 An Extension to Interfering Tandem Surfaces

When one turns from the isolated planar wing to more general configurations the artificiality of using sources (as in the integrated upwash method) to represent the flow over the upper surface of each wing leads to certain conceptual difficulties in setting up the interference problem. Through the judicious use of diaphragms, however, there have been some impressive achievements (see, e.g. ref. 13).

In the present method an idea due to Fenain and Guiraud-Vallée (ref. 24) has been used to obtain an inverse form of the relationship (36). Equation (36) is a set of simultaneous equations relating the potential at the lattice points to the values of the upwash in each box.

Written in matrix form

$$\{\varphi_{m,n}\}' = [S_{m-\mu,n-\nu}] \{w_{\mu,\nu}\}$$

If the ordering of these equations follows the basic marching sequence then it is obvious that the coefficient matrix is a lower triangular matrix. The inverse relationship is

$$\{w_{m,n}\} = [D_{m-\mu,n-\nu}] \{\varphi_{\mu,\nu}\}$$

or

$$w_{m,n} = \sum_{\mu=1}^m \sum_{\nu=1}^n D_{m-\mu,n-\nu} \cdot \varphi_{\mu,\nu} \quad (38)$$

where

$$[D_{m-\mu,n-\nu}] = [S_{m-\mu,n-\nu}]^{-1}$$

can be obtained in a straightforward manner. (The cost is equal to the solution of (36) for one deformation mode).

Equation (38) is a discrete form of the integrated potential formulation enabling us to avoid the need to calculate the upwash in regions off the wing. The value of the potential is known in these regions from the zero load conditions (33, 34).

For the tandem surface problem we need to determine the upwash field in the plane ( $z = h$ ) of the second wing surface due to the potential distribution, on the upper surface of the first wing and its wake, and vice versa. Taking the  $z$  derivative of equation (32) and multiplying by  $\text{sign}(z)$  to account for the antisymmetry of the true flow field we obtain a relationship between the upwashes in the two planes. The resulting integral is discretised in the same manner as that for the potential by assuming constant upwash over the characteristic box elements of the first surface. Evaluating the result at the mid-points of boxes on the second surface (it is assumed that the lattices for the two surfaces coincide in plan-view) we obtain the form

$$w_{m,n}^{(2)} = w(m-\frac{1}{2}, n-\frac{1}{2}, h) = \sum_{\mu=1}^m \sum_{\nu=1}^n w_{\mu,\nu}^{(1)} W_{m-\mu,n-\nu} \quad (39)$$

The final step is to replace  $w_{\mu,\nu}^{(1)}$  through the relationship (38) to obtain

$$w_{m,n}^{(2)} = \sum_{\mu=1}^m \sum_{\nu=1}^n \varphi_{\mu,\nu}^{(1)} D_{m-\mu,n-\nu}^* \quad (40)$$

A similar relationship exists between the potential,  $\varphi_{\mu,\nu}^{(2)}$ , on the second surface and the upwash  $w_{m,n}^{(1)}$  on the first.

The solution process follows the same systematic march simultaneously in the two wing planes, each step involving the solution of, at most, a pair of simultaneous equations when the vertical separation is such that the two pivotal elements are mutually interfering. The treatment of boxes cut by planform edges is derived in a straightforward manner from that used in the planar wing method.

Results (supplied by the author's colleagues at B.Ae Warton) have been obtained using this method for the AGARD coplanar wing-tail configuration shown in figure 13, where the four, antisymmetric, mode shapes are also defined. The results at two Mach numbers,  $M = 1.2$  and  $3.0$ , for reduced frequencies  $k = 0$  and  $1.5$  were compared with those of Huttzell and Pollock, Schmid and Becker (taken from tables 5 and 7 of ref. 25), and a version of Woodcock's method (ref. 17). The general agreement between the methods is fair as illustrated by the polar plots of selected generalised forces in figures 14 and 15. Results were also obtained for the same configuration with the tail raised to  $z = 0.6$ . Again the general agreement between the methods is fair as illustrated in figures 16 and 17.

Also illustrated in figure 15 are results obtained by Jones and Appa (ref. 18) and Tseng and Morino (ref. 26). The generalised forces on the wing due to wing modes and on the tail due to tail modes obtained by these panel methods are in agreement with those obtained by the box methods. However, the interference effects, i.e. forces on the tail due to wing modes do not compare at all well. One suspects that  $k = 1.5$  is a rather severe test of these methods; it is also possible that the source of these discrepancies lies in the use of a rather small number of panels with the panel geometry unrelated to the Mach lines.

#### 4. METHODS FOR BODIES AND WING-BODY COMBINATIONS

For pointed, streamlined shapes whose dimensions in planes normal to the freestream are small compared with the length there has been a heavy reliance on slender body theory (e.g. Ward, ref. 3 and Miles, ref. 4). Applicable for low to moderate reduced frequencies based on body length, the part of the flow field which contributes to the transverse loads at a given  $x$  - station is obtained as a solution to the two-dimensional Laplace equation for the (incompressible) cross flow around the body section. For higher frequencies and transient flow problems Miles, ref. 4, shows that the correct equation for the crossflow is the two-dimensional wave equation

$$\phi_{yy} + \phi_{zz} = \frac{1}{a_0^2} \phi_{tt} = M^2 \phi_{\tau\tau}$$

He gives the solution for the lift acting on cones entering sharp-edged gusts.

In recent years some considerable effort has been expended on the development of numerical, panel methods for wing-body combinations in steady supersonic (and subsonic) flow. Rather less attention has been paid to the equivalent unsteady flow problem exceptions being the SOUSSA programs of Morino et al (ref. 27) and Woodcock's method (ref. 28) for isolated bodies. Both methods are aimed at the numerical solution of the integral equation (29) of section 2.

Woodcock specifies the boundary conditions in terms of the normal velocity component at the mean body surface, including the effects of the mean steady flow. The normal mass flux which is identified with local source strength, however, involves both the normal and tangential components of velocity. The resulting integral equation therefore involves both the potential and its tangential derivative at the surface. Woodcock solves this problem by approximating the tangential derivative by a finite difference quotient. The body is modelled as a polyhedron, the surface being made up of a set of flat facets. He then solves his equation for  $\phi$  by collocation using techniques similar to those used in his box method for tandem wings (ref. 17). Reference 28 contains an application to a complex fuselage with canopy at  $M = 1.225$ .

In contrast to Woodcock, Morino equates the normal mass flux to the surface normal velocity, the difference being of second order for bodies with small streamwise slopes. The body surface is divided into a set of quadrilateral elements within each of which the normal wash and surface potential are assumed constant. The true body surface within each element is approximated by a hyperboloidal paraboloid enabling analytic evaluation of the integrals over each panel in steady flow. For unsteady flow the integrands are replaced, locally, by a low order expansion in terms of frequency parameter in order to, again, achieve analytic evaluation of the panel influence coefficients. It is to be noted that Morino's formulation of the unsteady flow problem allows for more general motions than oscillatory flow. In practice this appears as a generalisation to complex values of frequency parameter, i.e. damped oscillatory flows.

A similar method to that of Morino employing higher order representations of the normal mass flux and potential distributions within a panel has been developed by Johnson et al at the Boeing Company. Their method appears to have been applied only to steady flows at supersonic speeds. However, it is worth noting that they give an alternative expression for the normal mass flux boundary condition in their work in subsonic oscillatory flow (ref. 29).

It is unfortunate that, as far as the author is aware, there are no published results for the unsteady flow about wing-body combinations, although, as previously mentioned, an example for an isolated body is given in ref. 28.

#### 5. CONCLUDING REMARKS

With regard to the results for interfering lifting surfaces quoted in section 3.2 it is noted that while the box methods are in qualitative agreement, the quantitative comparison can only be described as fair. Whether the accuracy of such methods is good enough for flutter or dynamic load prediction is dependent on the particular problem.

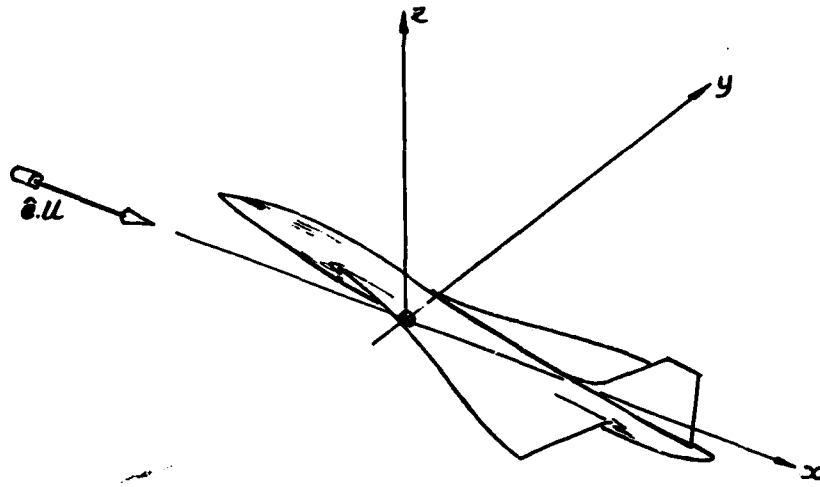
It should be remembered that these methods have been developed to obtain solutions to the same linearised statement of the unsteady flow problem. The question remains as to how closely the linear model represents the true flow; the paucity of experimental results leaves this question unresolved.

As to the development of panel methods for complex configurations, the lack of even qualitative agreement between the panel methods and box methods for certain interference forces leads one to suspect that much further work is required before they could be applied with confidence. (It is certain that the methods have developed beyond the point for which results have been quoted in this paper).

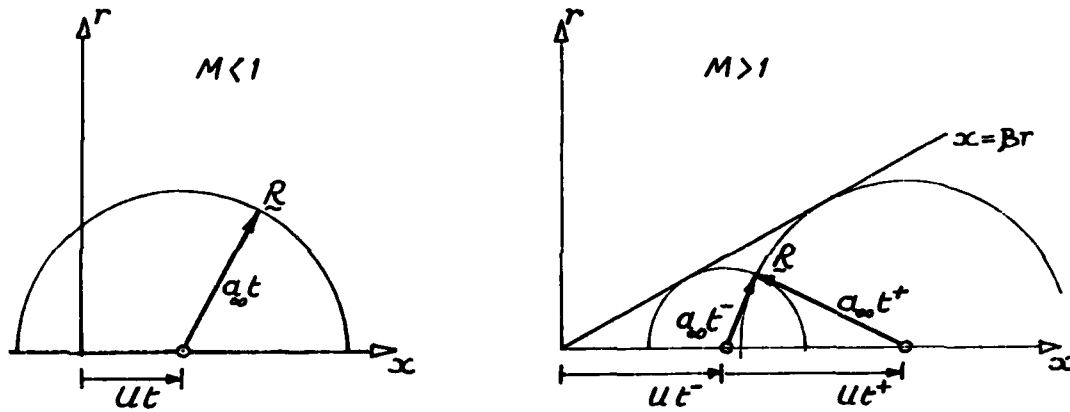
REFERENCES

1. Ashley, H.  
'Unsteady Subsonic and Supersonic Flow'  
AGARD Conference on Unsteady Aerodynamics,  
Ottawa, Canada, 1977 AGARD CP-227, Paper 1
2. Ashley, H, and Landahl, M. T.  
'Aerodynamics of Wings and Bodies'  
Addison - Wesley Publishing Co., 1965
3. Ward, G. N.  
'Linearised Theory of Steady High-Speed Flow'  
Cambridge University Press, 1955
4. Miles, J. W.  
'The Potential Theory or Unsteady Supersonic Flow'  
Cambridge University Press, 1959
5. Garrick, I. E.  
'Nonsteady Wing Characteristics', Section F,  
'Aerodynamic Components of Aircraft at High Speeds'  
Princeton University Press, 1957
6. Das, A.  
'Some Basic and New Aspects on the Disturbance Fields of  
Unsteady Singularities in Uniform Motion'  
AGARD Conference on Unsteady Aerodynamics,  
Ottawa, Canada, 1977 AGARD CP-227, Paper 6
7. Heaslet, M. A. and Lomax, H,  
'Supersonic and Transonic Small Perturbation Theory', Section  
D14.1, 'General Theory of High Speed Aerodynamics',  
Princeton University Press, 1954
8. Watkins, C. E. and Berman, J. H.,  
'On the Kernel Function of the Integral Equation Relating Lift  
and Downwash Distributions of Oscillating Wings in Supersonic  
Flow' NACA Rep. 1257, 1956
9. Richardson, J. R.  
'A Method for Calculating the Lifting Forces on Wings (Unsteady  
Subsonic and Supersonic Lifting-Surface Theory)'  
Brit. ARC A & M No. 3157, 1955
10. Cunningham, H. J.  
'Improved Numerical Procedure for Harmonically Deforming Lifting  
Surfaces from the Supersonic Kernel Function Method'  
AIAA Jour, Vol. 4, No. 11, Nov. 1966 pp 1961-1968
11. Cunningham, A. M. Jr.,  
'A Kernel Function Method for Computing Steady and Oscillatory  
Supersonic Aerodynamics with Interference',  
AIAA Paper No. 73-670, 1973
12. Pines, S., Dujundji, J., and Neuringer, J.  
'Aerodynamic Flutter Derivatives for a Flexible Wing with  
Supersonic and Subsonic Edges', Journal of the Aeronautical Sciences,  
Vol. 22. No. 10 Oct. 1955 pp 693-700.
13. Moore, M. T. and Andrew, L. V.  
'Application of the Supersonic Mach Box Method to Intersecting  
Planar Lifting Surfaces', 'Unsteady Aerodynamics for Advanced  
Configurations', Part IV.,  
FDL-TDR-64-152, 1965
14. Ii, J. M. and Rowe, W. S.,  
'Unsteady Aerodynamics of Non planar Wings and Wing - Tail  
Configurations of Elastic Flight Vehicles in Supersonic Flight'  
Jour, Aircraft Vol 10, No. 1. Jan 1973 pp 19-27

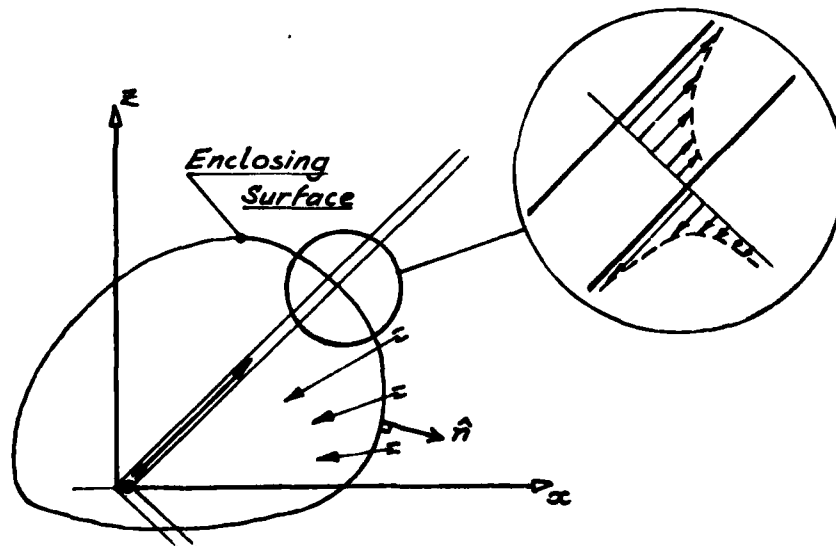
15. Chipham, R. R.  
'An Improved Mach-Box Approach for the Calculation of Supersonic Oscillatory Pressure Distributions', Proceedings AIAA/ASME/SAE 17th Structures, Structural Dynamics and Materials Conference, King of Prussia, Penn., pp.608-611
16. Allen, D. J and Sadler, D. S.  
'Oscillatory Aerodynamic Forces in Linearised Supersonic Flow for Arbitrary Frequencies, Planforms and Mach Numbers'.  
Brit. ARC R & M 3415, 1963.
17. Woodcock, D. L. and York, E. J.  
'A Supersonic Box Collocation Method for the Calculation of Unsteady Airforces of Tandem Surfaces', Proceedings of AGARD Symposium on Unsteady Aerodynamics for Aeroelastic Analyses of Interfering Surfaces. AGARD-CP-80-71, 1971
18. Jones, W. P. and Appa, K,  
'Unsteady Supersonic Aerodynamic Theory by the Method of Potential Gradient' AIAA Jour, Vol. 15, No. 1, Jan. 1977
19. Jones, W. P. and Appa K,  
'Unsteady Supersonic Aerodynamic Theory for Interfering Surfaces by the Method of Potential Gradient' NASA CR-2898, 1977
20. Doe, R. H.  
'A Numerical Method for the Calculation of Aerodynamic Forces on Wings Oscillating in Supersonic Flow'  
British Aircraft Corp. Filton Division Report AERO/SST/6091, Aug '69
21. Stark, V. J. E.  
'Calculation of Aerodynamic Forces on Two Oscillating Finite Wings at Low Supersonic Mach numbers" Saab Tech. Note TN.53, Feb. 1964
22. Zartarian, G and Hsu, P. T.  
'Theoretical Studies on the Prediction of Unsteady Supersonic Airloads on Elastic Wings' Parts I and II,  
USAF Wright Aeronautical Development Center, T.R. 56-97, 1956
23. Williams, D. E. and Woodcock, D. L.  
'Theoretical Derivatives for Rectangular Wings at Supersonic Speeds' R.A.E. Tech. Memo. Structures 610, Math 62.
24. Fenain, M. and Guiraud - Vallée, D.  
"Calcul Numérique des Ailes en Régime Supersonique Stationnaire ou Instationnaire", 1re Partie: Écoulement Stationnaire, 2e Partie: Écoulement Instationnaire,  
La Recherche Aérospatiale, No. 115 Nov-Dec 1966 pp.3-19, and No. 116, Jan-Feb. 1967 pp.22-23
25. Rodden, W. P.  
'A Comparison of Methods Used in Interfering Lifting Surface Theory' AGARD-R-643, 1976
26. Tseng, K. and Morino, L.  
'A New Unified Approach for Analysing Wing-Body-Tail Configurations with Control Surfaces' AIAA Paper No. 74-418, 1976.
27. Morino, L. and Tseng K.  
'Steady, Oscillatory and Unsteady, subsonic and supersonic Aerodynamics (SOUSSA) for Complex Aircraft Configurations' AGARD Conference on Unsteady Aerodynamics, Ottawa, Canada, 1977 AGARD CP-227. Paper 3
28. Woodcock, D. L.  
'The Theoretical Prediction of Steady and Unsteady Aerodynamic Loading on Arbitrary Bodies in Supersonic Flow'  
AGARD, Proceedings No. 204
29. Dusto, A. R., Epton, M. A. and Johnson, F. T.  
'Advanced Panel Type Influence Coefficient Methods Applied to Unsteady Three Dimensional Potential Flows'  
AIAA Paper 78-229, 1978



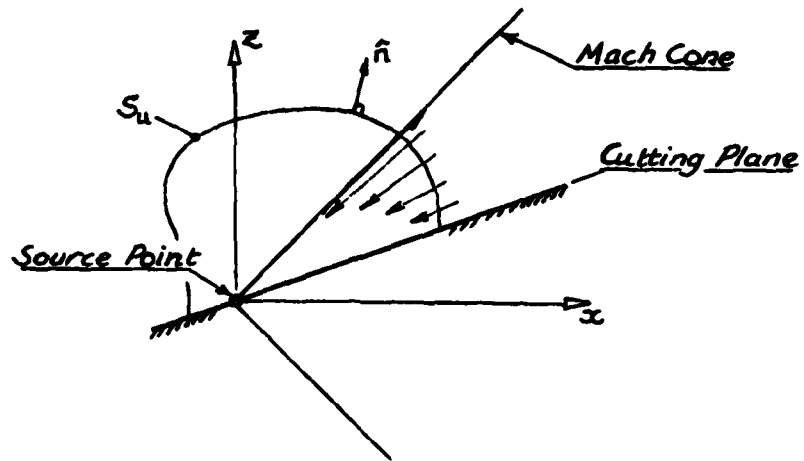
**Figure 1** Axis System for Aerodynamic Calculations



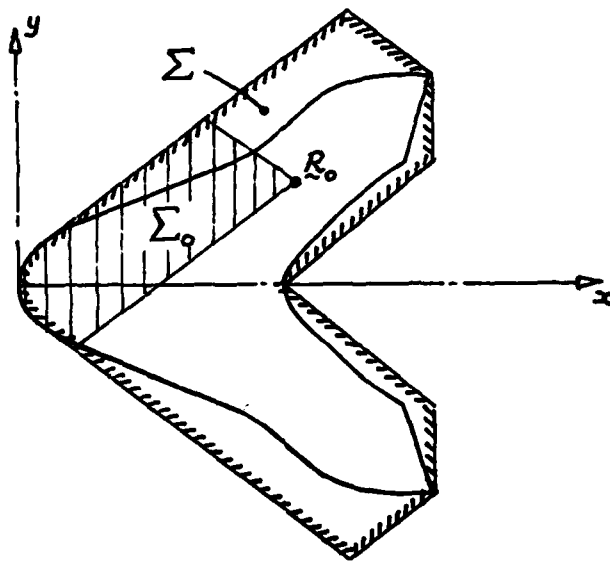
**Figure 2** Supersonic versus Subsonic Flow



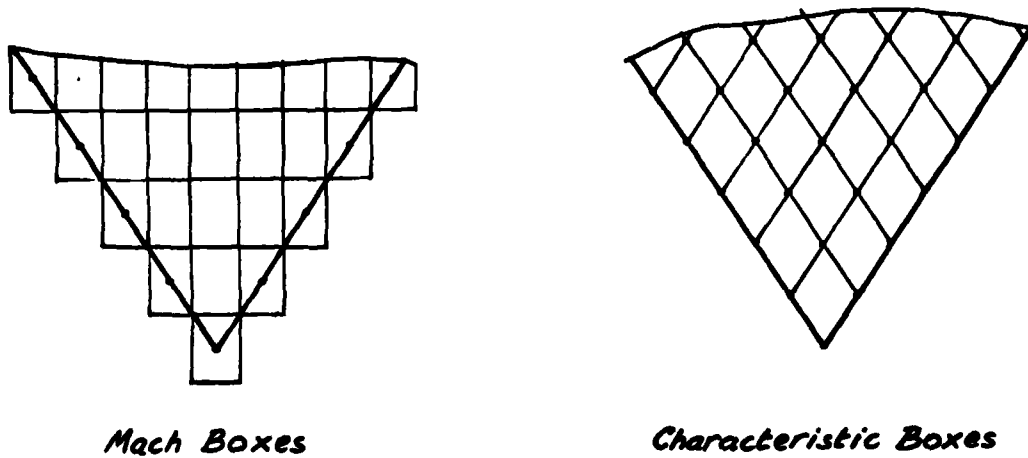
**Figure 3** Perturbation Mass Flow due to a Supersonic Source



**Figure 4** Supersonic Source 'Cut' by an Inclined Plane



**Figure 5** Planview of Wing and the Integration Regions  $\Sigma, \Sigma_0$



**Figure 6** Box Method Integration Schemes



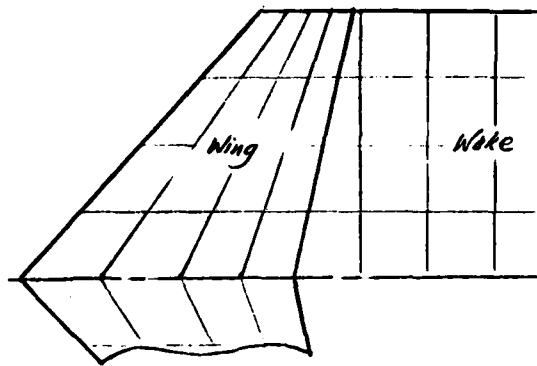


Figure 7 The Trapezoidal Finite Elements of Jones and Appa.

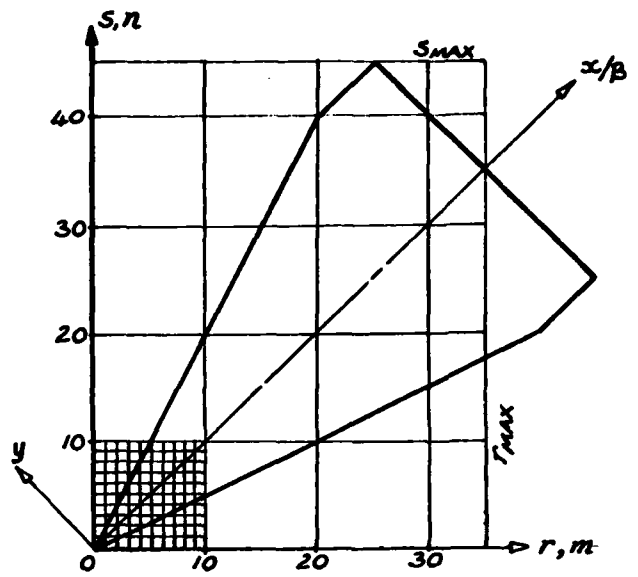


Figure 8 Calculation Grid for a Characteristic Box Method

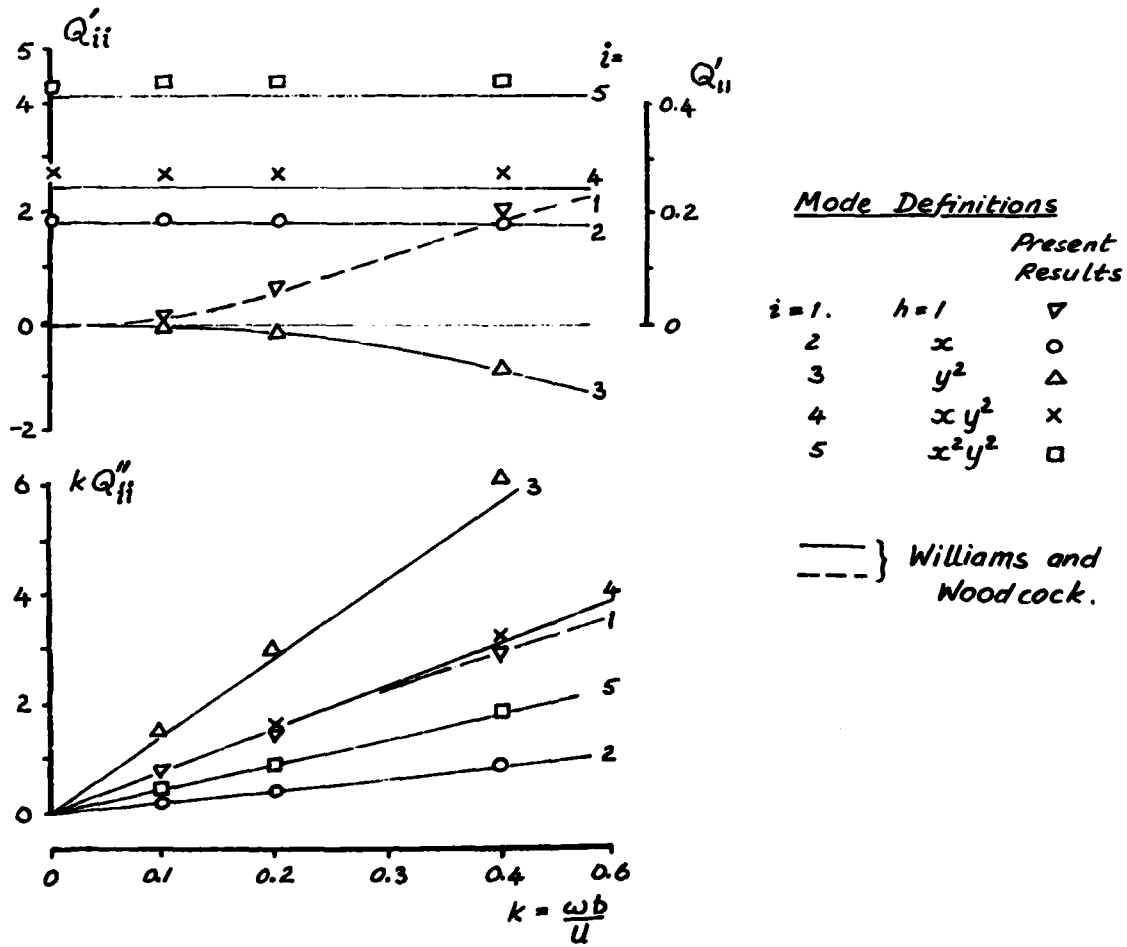
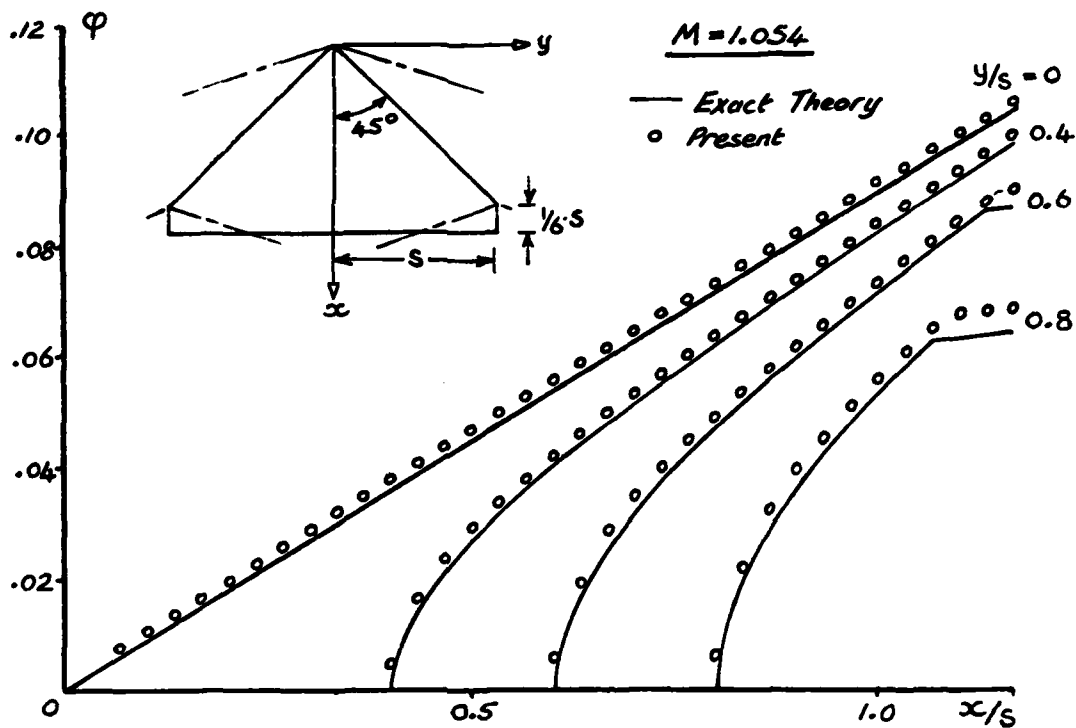
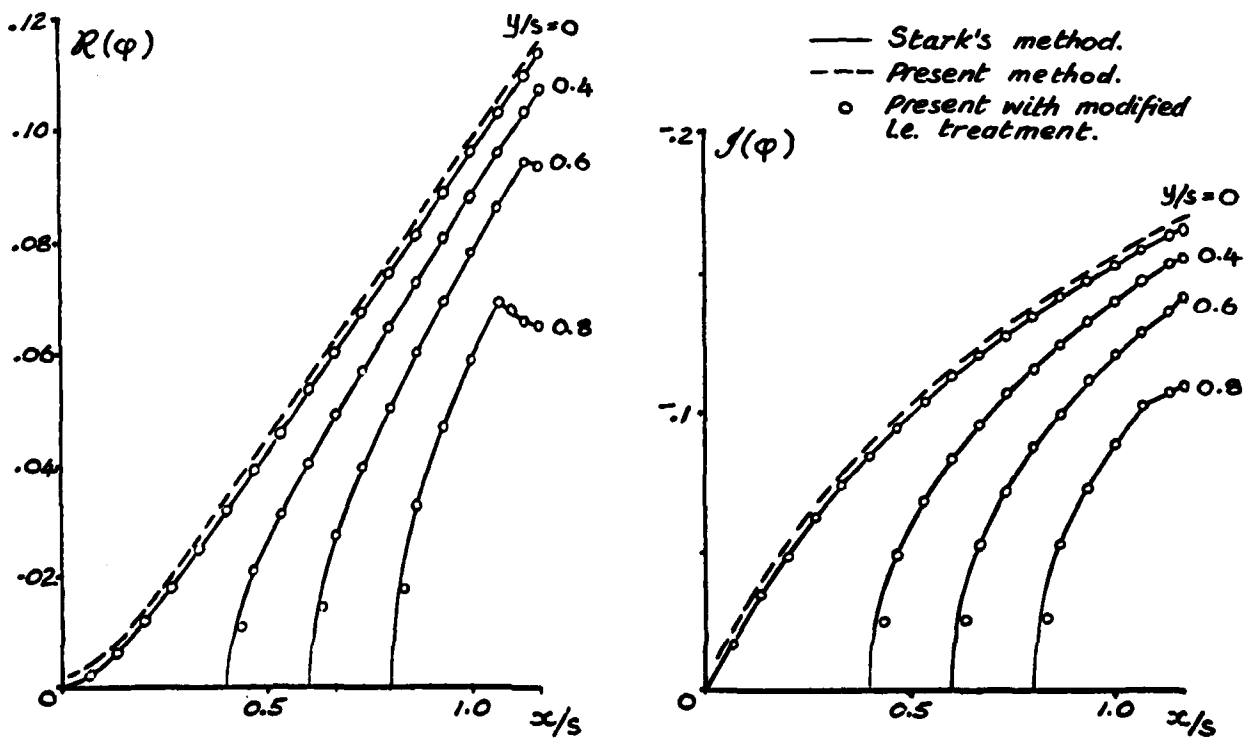


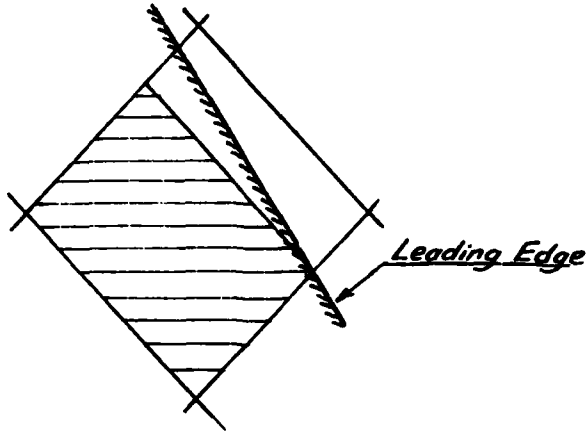
Figure 9 Generalised Forces Acting on an Aspect Ratio 2 Rectangular Wing at Mach 2



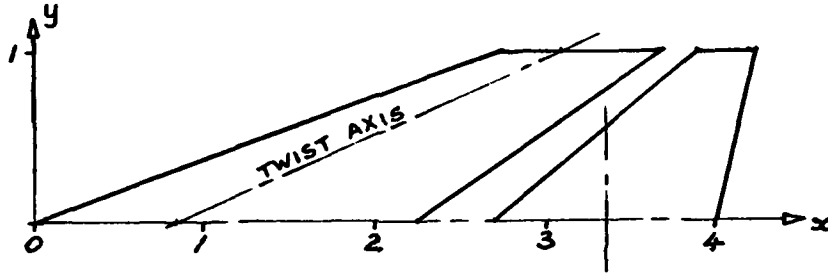
**Figure 10** Comparison of Results of Present Method with Exact Linear Theory for a Cropped Delta Wing



**Figure 11** Potential Distribution on a Cropped Delta Wing Oscillating in Translation at  $M = 1.054$ ,  $K = 0.9$



**Figure 12** Modified "Weighting Area" (shaded) used for boxes cut by a subsonic leading edge



**Figure 13** AGARD Wing - Horizontal Tail Configuration

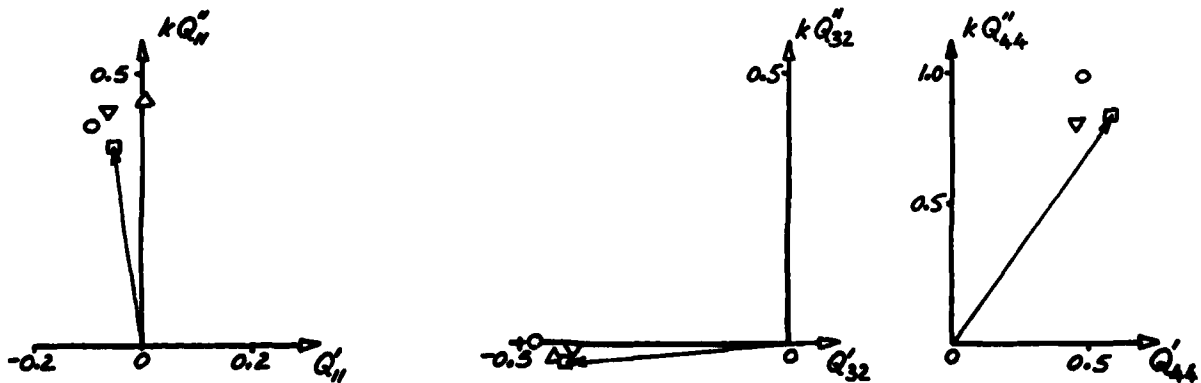
Deflection Mode Definitions:

Wing Modes:

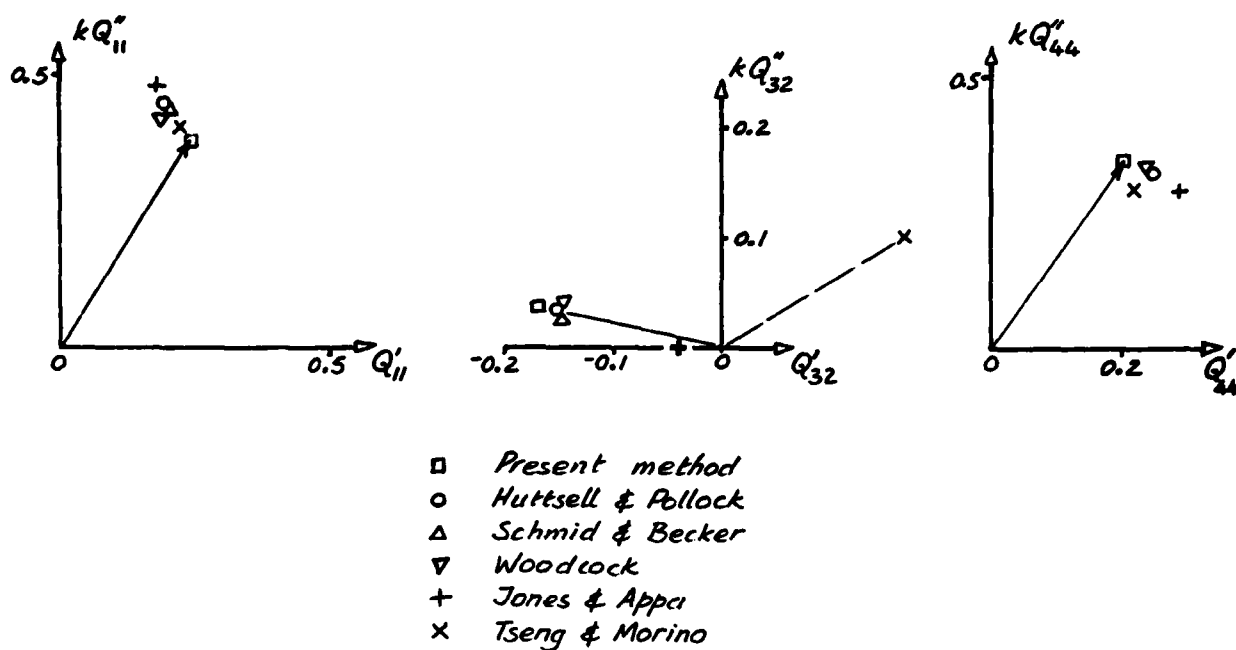
1.  $y(x - 2.25|y| - 0.85)$  ; wing twist
2.  $y|y|$  ; wing bending

Tail Modes:

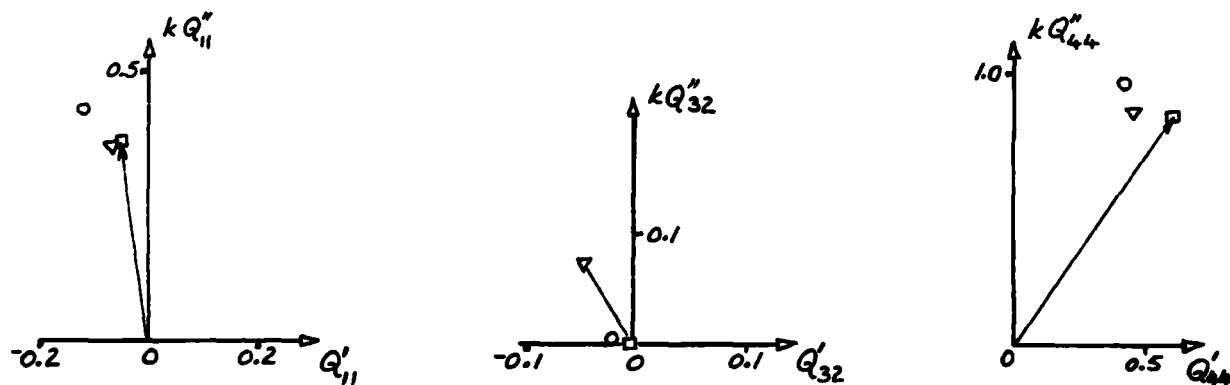
3.  $y$  ; tail roll
4.  $sgn(y) \cdot (x - 3.35)$  ; tail pitch



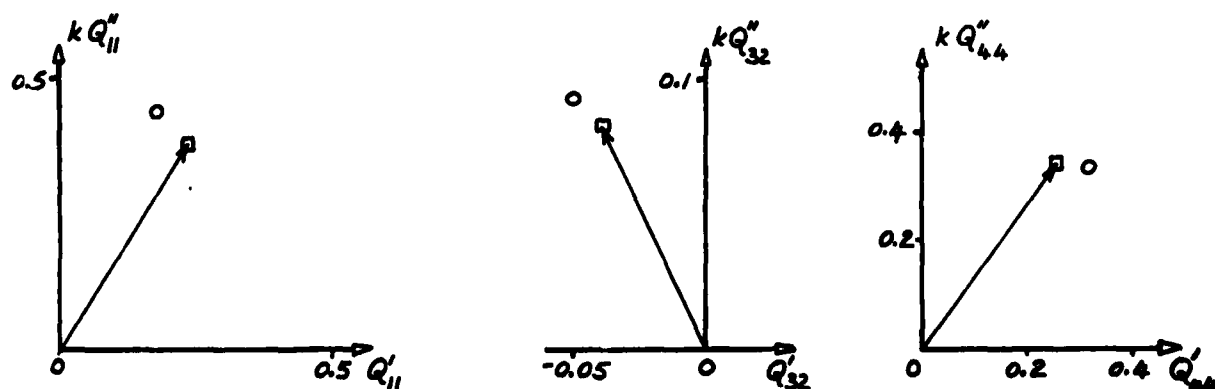
**Figure 14** Polar Plots of Selected Generalised Forces on the AGARD Wing-Tail Configuration,  $M = 1.2$ ,  $K = 1.5$   $Z_{tail} = 0$ .



**Figure 15** Polar Plots of Selected Generalised Forces on the AGARD Wing-Tail Configuration,  $M = 3.0$ ,  $K = 1.5$ ,  $Z_{tail} = 0$ .



**Figure 16** Polar Plots of Selected Generalised Forces on the AGARD Wing-Tail Configuration,  $M = 1.2$ ,  $K = 1.5$ ,  $Z_{tail} = 0.6$ .



**Figure 17** Polar Plots of Selected Generalised Forces on the AGARD Wing-Tail Configuration,  $M = 3.0$ ,  $K = 1.5$ ,  $Z_{tail} = 0.6$ .

## APPENDIX

## LIST OF PARTICIPANTS

<i>Name</i>	<i>Country</i>	<i>Firm/Institution/University</i>
ALLBRIDGE P.J.	United Kingdom	Aerodynamicist Westland Helicopters Ltd Yeovil, Somerset Tel: 935-5222 (434)
BOHN Dieter	Germany	Engineer Kraftwerk Union AG Wiesenstrasse 25 433 Mülheim Tel: 0208/456-1
BORLAND Christopher J.	USA	Sr. Specialist Engineer Boeing Co. P.O.B.3999 Seattle, Washington 98124 Tel: (206) 655-4145
BURT M.	United Kingdom	Dynamics Engineer British Aerospace (Aircraft Group) Warton Division, Warton Aerodrome Preston, Lancashire PR4 1AX Tel: 633-333
CHIOCCHIA Gianfranco	Italy	Assistant Professor Politecnico di Torino Corso Duca degli Abruzzi 24 10129 Torino Tel: 011-518 759 (518 374)
DAS A.	Germany	Professor Dr Institut f. Aerodynamik DFVLR 3300 Braunschweig Tel: 395-2440
DELAHAYE B.	France	Engineer SNECMA – Direction technique Centre de Villaroche 77550 Moissy Cramayel Tel: 437-91-23
DESOPPER André	France	Engineer ONERA 29 Avenue de la Division Leclerc 92320 Châtillon Tel: 657-11-60
DUPSLOFF Manfred	Germany	Dipl.-Engineer MTU Motoren- und Turbinen-Union Dachauerstr. 665 8 München Tel: 089/14891
EHRMANN Manfred	Germany	Aerodynamicist VFW – Fokker GmbH Hünefeldstr. 1-5 2800 Bremen 1 Tel: 538-33-61

A-2

<i>Name</i>	<i>Country</i>	<i>Firm/Institution/University</i>
FESEFELDT Klaus	Germany	Diplom-Physiker MBB – Hamburg Dept.HE 272 Hein-Sass Weg 2103 Hamburg 95 Tel: 747-5622
FIRCHAU W.	Germany	Dipl.-Math MBB – Hamburg Kreetslag 10 2103 Hamburg 95 Tel: 747-5819
GREEN M.J.	United Kingdom	Head of Dynamic Studies British Aerospace Woodford Stockport, Cheshire Tel: 061-439-5050
HALLIWELL D.G.	United Kingdom	Head of Flutter Research Rolls-Royce Ltd. P.O.B.31 Derby Tel: 42424 – Ext.1594
JUDITH Hans	Germany	Dipl.-Engineer Kraftwerk Union Wiesenstr.35 4330 Mülheim-Ruhr
HENSING P.C.	Netherlands	Scientific Staff Member Delft University of Technology Department of Aerospace Engineering Kluyverweg 1 2629 HS Delft Tel: 015-782-073
HORSTEN J.J.	Netherlands	Engineer National Aerospace Laboratory (NLR) Anthony Fokkerweg 2 Amsterdam Tel: 020-511 31 13
KANNEMANS H.	Netherlands	Engineer National Aerospace Laboratory (NLR) Anthony Fokkerweg 2 Amsterdam Tel: 020-511 31 13
KIENAPPEL K.	Germany	Engineer DFVLR – AVA Göttingen Bunsenstr.10 3400 Göttingen Tel: 0551-7091
KOHIYAR F.A.	United Kingdom	Deputy Section Leader Aerodynamics British Aerospace, Aircraft Group Kingston-Brough Div. Richmond Road Kingston-on-Thames, Surrey Tel: 01-546-7741 (158)

<i>Name</i>	<i>Country</i>	<i>Firm/Institution/University</i>
LANG D.C.	United Kingdom	Principal Aeroelastics Engineer British Aerospace, Aircraft Group Brough North Humberside HU15 1EQ Tel: 0482-66 71 21 (316)
LARROZE P.Y.	France	Engineer Neyrpic 75 rue General Mangin 38100 Grenoble Tel: (76) 96 48 30
MANTEGAZZA P.	Italy	Assistant Professor Istituto di Ingegneria Aerospaziale del Politecnico di Milano Via Golgi 40 20100 Milano Tel: 0039-2-236 43 08
MULAK P.	France	Engineer ONERA 29 Avenue de la Division Leclerc 92320 Châtillon Tel: 657 11 60 (2557)
NEWMAN H.T.	United Kingdom	Structural Dynamicist British Aerospace, Aircraft Group Kingston-Brough Division Richmond Road Kingston-on-Thames, Surrey Tel: 01-546-7741 (261)
POLZ Günther	Germany	Dipl.-Engineer MBB – München Unternehmensbereich Drehflügler u. Verkehr Postfach 80 11 69 8000 München 80 Tel: 089-6000 3658
RENAUD Jean	France	Research Coordinator Aerospatiale B.P.13 13722 Marignane Tel: (42) 89 90 22
ROTTOLI Giuseppe	Italy	Engineer Aeritalia Corso Marche 41 10146 Torino Tel: 333 26 85
ROUND D.F.	Germany	Aerodynamicist MBB – Hamburg Hamburger Flugzeugbau 2103 Hamburg 95 Tel: (040) 747 5470
RUSSO Anselmo	Italy	Dynamicist Cia Agusta Via Schiaparelli 8 20113 Gallarate

<i>Name</i>	<i>Country</i>	<i>Firm/Institution/University</i>
SALMOND D.J.	United Kingdom	Scientific Officer Royal Aircraft Establishment Farnborough, Hants Tel: 24461 (5111)
SCHMID H.	Germany	Aerodynamics Engineer MBB – München Airplane Division FE17 P.O.B.80 11 60 8000 München 80 Tel: 089/6000-4707
SCHNEIDER G.H.	Austria	Univ. Assistant Institut f. Gasdynamik u. Thermodynamik Techn. Universität Wien 1040 Wien Tel: 0222/65 87 31/492
SCHWARZE H.F.	Germany	Dr Engineer DFVLR Göttingen Bunsenstr.10 3400 Göttingen Tel: (0551) 709 22 95
SIDES Jacques	France	Engineer ONERA 29 Avenue de la Division Leclerc 92320 Châtillon Tel: 657-11-60 (24 35)
TURI Alberto	Italy	Aerodynamicist Agusta SpA Via Schiaparelli 8 20113 Gallarate
VACCA V.	Italy	Engineer Aeritalia SpA Pomigliano d'Arco (NA) Tel: 884 15 44
VAN GELDER P.A.	Netherlands	Engineer National Aerospace Laboratory (NLR) Anthony Fokkerweg 2 1059 CM Amsterdam Tel: 020-511 31 13
VAN KUIK G.A.M.	Netherlands	Engineer Delft University of Technology Department of Aerospace Engineering Kluyverweg 1 2629 HS Delft Tel: 015-785 170
VOSS Ralph	Germany	Dipl.-Physiker DFVLR Göttingen Bunsenstrasse 10 3400 Göttingen Tel: (0551) 709 22 95



<i>Name</i>	<i>Country</i>	<i>Firm/Institution/University</i>
VUILLET A.E.	France	Engineer SNIAS – Division Hélicoptère B.P.13 13722 Marignane Tel: (42) 89 90 22 (5133)
WOOD	United Kingdom	Project Supervisor, Aero Dept. Aircraft Research Association Manton Lane. Bedford MK41 7PF Tel: 50681

**REPORT DOCUMENTATION PAGE**

<b>1. Recipient's Reference</b>	<b>2. Originator's Reference</b>	<b>3. Further Reference</b>	<b>4. Security Classification of Document</b>								
	AGARD-R-679	ISBN 92-835-1364-9	UNCLASSIFIED								
<b>5. Originator</b>	Advisory Group for Aerospace Research and Development North Atlantic Treaty Organization 7 rue Ancelle, 92200 Neuilly sur Seine, France										
<b>6. Title</b>	SPECIAL COURSE ON UNSTEADY AERODYNAMICS										
<b>7. Presented at</b>	an AGARD Special Course at the von Kármán Institute, Rhode-St-Genèse, Belgium on 10-14 March 1980.										
<b>8. Author(s)/Editor(s)</b>	Various	<b>9. Date</b>	June 1980								
<b>10. Author's/Editor's Address</b>	Various	<b>11. Pages</b>	242								
<b>12. Distribution Statement</b>	This document is distributed in accordance with AGARD policies and regulations, which are outlined on the Outside Back Covers of all AGARD publications.										
<b>13. Keywords/Descriptors</b>	<table border="0"> <tr> <td>Aerodynamics</td> <td>Vibration</td> </tr> <tr> <td>Unsteady flow</td> <td>Flight control</td> </tr> <tr> <td>Flight characteristics</td> <td>Active control</td> </tr> <tr> <td>Flutter</td> <td></td> </tr> </table>			Aerodynamics	Vibration	Unsteady flow	Flight control	Flight characteristics	Active control	Flutter	
Aerodynamics	Vibration										
Unsteady flow	Flight control										
Flight characteristics	Active control										
Flutter											
<b>14. Abstract</b>	<p>Unsteady aerodynamics play an important role in aircraft response, aircraft loads, vibration environments and flight systems analysis; this role is becoming more significant with the advent of active control technology (ACT). For internal flows in engines, turbomachinery and helicopter rotors, unsteady aerodynamics are dominant features.</p> <p>The course provided a basic understanding of a range of related unsteady flow phenomena relevant to aeronautical applications, an awareness of the current state-of-the-art of prediction methods, and an appreciation of how unsteady aerodynamics are applied to contemporary practical problems.</p> <p>The course covered the following areas:</p> <ul style="list-style-type: none"> <li>+ a qualitative understanding of the character of unsteady flows at subsonic, transonic and supersonic speeds, including viscous effects for both attached and separated flows,</li> <li>+ an outline of the contexts in which unsteady aerodynamics are required for aircraft stability and control, flutter, aircraft dynamics response, ACT, turbomachinery vibration and helicopter rotor operation,</li> <li>+ a survey of the state-of-the-art of the current prediction methods with particular emphasis on recent developments in unsteady transonics, <i>and</i></li> <li>+ a description of contemporary experimental techniques and apparatus. ←</li> </ul> <p>The material assembled in this book was prepared under the combined sponsorship of the Fluid Dynamics Panel, the von Kármán Institute and the Consultant and Exchange Program of AGARD.</p>										

<p>AGARD Report No.679 Advisory Group for Aerospace Research and Development, NATO SPECIAL COURSE ON UNSTEADY AERODYNAMICS Published June 1980 242 pages</p> <p>Unsteady aerodynamics play an important role in aircraft response, aircraft loads, vibration environments and flight systems analysis; this role is becoming more significant with the advent of active control technology (ACT). For internal flows in engines, turbomachinery and helicopter rotors, unsteady aerodynamics are dominant features.</p> <p>The course provided a basic understanding of a range of related unsteady flow phenomena relevant to aeronautical applications, an awareness of the current</p> <p>P.T.O.</p>	<p>AGARD-R-679</p> <p>Aerodynamics Unsteady flow Flight characteristics Flutter Vibration Flight control Active control</p>	<p>AGARD Report No.679 Advisory Group for Aerospace Research and Development, NATO SPECIAL COURSE ON UNSTEADY AERODYNAMICS Published June 1980 242 pages</p> <p>Unsteady aerodynamics play an important role in aircraft response, aircraft loads, vibration environments and flight systems analysis; this role is becoming more significant with the advent of active control technology (ACT). For internal flows in engines, turbomachinery and helicopter rotors, unsteady aerodynamics are dominant features.</p> <p>The course provided a basic understanding of a range of related unsteady flow phenomena relevant to aeronautical applications, an awareness of the current</p> <p>P.T.O.</p>	<p>AGARD-R-679</p> <p>Aerodynamics Unsteady flow Flight characteristics Flutter Vibration Flight control Active control</p>
<p>AGARD Report No.679 Advisory Group for Aerospace Research and Development, NATO SPECIAL COURSE ON UNSTEADY AERODYNAMICS Published June 1980 242 pages</p> <p>Unsteady aerodynamics play an important role in aircraft response, aircraft loads, vibration environments and flight systems analysis; this role is becoming more significant with the advent of active control technology (ACT). For internal flows in engines, turbomachinery and helicopter rotors, unsteady aerodynamics are dominant features.</p> <p>The course provided a basic understanding of a range of related unsteady flow phenomena relevant to aeronautical applications, an awareness of the current</p> <p>P.T.O.</p>	<p>AGARD-R-679</p> <p>Aerodynamics Unsteady flow Flight characteristics Flutter Vibration Flight control Active control</p>	<p>AGARD Report No.679 Advisory Group for Aerospace Research and Development, NATO SPECIAL COURSE ON UNSTEADY AERODYNAMICS Published June 1980 242 pages</p> <p>Unsteady aerodynamics play an important role in aircraft response, aircraft loads, vibration environments and flight systems analysis; this role is becoming more significant with the advent of active control technology (ACT). For internal flows in engines, turbomachinery and helicopter rotors, unsteady aerodynamics are dominant features.</p> <p>The course provided a basic understanding of a range of related unsteady flow phenomena relevant to aeronautical applications, an awareness of the current</p> <p>P.T.O.</p>	<p>AGARD-R-679</p> <p>Aerodynamics Unsteady flow Flight characteristics Flutter Vibration Flight control Active control</p>

<p>state-of-the-art of prediction methods, and an appreciation of how unsteady aerodynamics are applied to contemporary practical problems.</p> <p>The course covered the following areas:</p> <ul style="list-style-type: none"> <li>- a qualitative understanding of the character of unsteady flows at subsonic, transonic and supersonic speeds, including viscous effects for both attached and separated flows.</li> <li>- an outline of the contexts in which unsteady aerodynamics are required for aircraft stability and control, flutter, aircraft dynamics response, ACT, turbomachinery vibration and helicopter rotor operation.</li> <li>- a survey of the state-of-the-art of the current prediction methods with particular emphasis on recent developments in unsteady transonics.</li> <li>- a description of contemporary experimental techniques and apparatus.</li> </ul> <p>The material assembled in this book was prepared under the combined sponsorship of the Fluid Dynamics Panel, the von Kármán Institute and the Consultant and Exchange Program of AGARD and was presented as an AGARD Special Course at the von Kármán Institute, Rhode-St-Genèse, Belgium on 10-14 March 1980.</p> <p>ISBN 92-835-1364-9</p>	<p>state-of-the-art of prediction methods, and an appreciation of how unsteady aerodynamics are applied to contemporary practical problems.</p> <p>The course covered the following areas:</p> <ul style="list-style-type: none"> <li>- a qualitative understanding of the character of unsteady flows at subsonic, transonic and supersonic speeds, including viscous effects for both attached and separated flows.</li> <li>- an outline of the contexts in which unsteady aerodynamics are required for aircraft stability and control, flutter, aircraft dynamics response, ACT, turbomachinery vibration and helicopter rotor operation.</li> <li>- a survey of the state-of-the-art of the current prediction methods with particular emphasis on recent developments in unsteady transonics.</li> <li>- a description of contemporary experimental techniques and apparatus.</li> </ul> <p>The material assembled in this book was prepared under the combined sponsorship of the Fluid Dynamics Panel, the von Kármán Institute and the Consultant and Exchange Program of AGARD and was presented as an AGARD Special Course at the von Kármán Institute, Rhode-St-Genèse, Belgium on 10-14 March 1980.</p> <p>ISBN 92-835-1364-9</p>
<p>state-of-the-art of prediction methods, and an appreciation of how unsteady aerodynamics are applied to contemporary practical problems.</p> <p>The course covered the following areas:</p> <ul style="list-style-type: none"> <li>- a qualitative understanding of the character of unsteady flows at subsonic, transonic and supersonic speeds, including viscous effects for both attached and separated flows.</li> <li>- an outline of the contexts in which unsteady aerodynamics are required for aircraft stability and control, flutter, aircraft dynamics response, ACT, turbomachinery vibration and helicopter rotor operation.</li> <li>- a survey of the state-of-the-art of the current prediction methods with particular emphasis on recent developments in unsteady transonics.</li> <li>- a description of contemporary experimental techniques and apparatus.</li> </ul> <p>The material assembled in this book was prepared under the combined sponsorship of the Fluid Dynamics Panel, the von Kármán Institute and the Consultant and Exchange Program of AGARD and was presented as an AGARD Special Course at the von Kármán Institute, Rhode-St-Genèse, Belgium on 10-14 March 1980.</p> <p>ISBN 92-835-1364-9</p>	<p>state-of-the-art of prediction methods, and an appreciation of how unsteady aerodynamics are applied to contemporary practical problems.</p> <p>The course covered the following areas:</p> <ul style="list-style-type: none"> <li>- a qualitative understanding of the character of unsteady flows at subsonic, transonic and supersonic speeds, including viscous effects for both attached and separated flows.</li> <li>- an outline of the contexts in which unsteady aerodynamics are required for aircraft stability and control, flutter, aircraft dynamics response, ACT, turbomachinery vibration and helicopter rotor operation.</li> <li>- a survey of the state-of-the-art of the current prediction methods with particular emphasis on recent developments in unsteady transonics.</li> <li>- a description of contemporary experimental techniques and apparatus.</li> </ul> <p>The material assembled in this book was prepared under the combined sponsorship of the Fluid Dynamics Panel, the von Kármán Institute and the Consultant and Exchange Program of AGARD and was presented as an AGARD Special Course at the von Kármán Institute, Rhode-St-Genèse, Belgium on 10-14 March 1980.</p> <p>ISBN 92-835-1364-9</p>